A STUDY OF WINDS AND WAVES

A thesis presented for the degree of
Doctor of Philosophy in Physics
in the University of Canterbury,
Christchurch, New Zealand.

by

N.J. CHERRY

1971

ACKNOWLEDGMENTS

I am grateful to my wife Gae for her patience and understanding, for punching the 1970 radar-wind data onto computer cards and helping in many other ways. I would like to thank Dr G. Austin for suggesting this line of research, Dr R.G.T. Bennett for his initial supervision and Dr G.J. Fraser for his help, guidance and supervision of the project over the past two years. Thanks also to Mrs Margaret Sewell for typing this manuscript and to Mr L. Hunter for processing and printing most of the photographs.

I am thankful for the financial support of the Physics Department, University of Canterbury, in the form of a Teaching Fellowship.

I also express my thanks to I.C.I. (Great Britain) for generously giving me a roll of 'Melinex' from which most of the superpressure balloons were made. Also to the personnel of Project GHOST for giving me balloon sealing tape and a heat seal iron. I am also thankful for their advice about balloons.

The project in its final form would have been impossible without the generous support of the New Zealand Meteorological Service in making available personnel, facilities and data. I am grateful to Dr J.F. de Lisle for his interest

and to Mr A. Ryan and Mr F. Borthwick and the staff of the Christchurch Meteorological Office for their help and advice. Also to Mr F. Collyer and his staff at the Meteorological Office at Hokitika for releasing superpressure balloons for me.

ABSTRACT

The project involved an observational program to study the lee waves produced over Canterbury due to the Southern Alps over the year 1970 using superpressure balloons and radar-wind/radiosonde balloons. The characteristics and performance of balloons (tetroons) and balloon systems were studied in detail. The data from the balloons was used to obtain a wave classification which may be used to predict the scale of wave motion from the radar-wind profile. It was also compared with solutions of two-, three- and exponential layer models to evaluate their applicability in predicting the wave motion. It was found that they gave a good correlation with observations when the atmosphere was approximated by layers but generally the airflow profiles were more complex and the layer theories at best predicted the scale of the wavelengths observed. The amplitudes of the waves were found to be mainly dependent on the resonance between the forcing periodicities of the mountains and the natural oscillations of the airflow.

P R E F A C E

The Aims of the Project

The aim has been to study lee waves and to understand them better by observations and their comparison with various theoretical models. The observations required some means of measuring the wave parameters. Superpressure balloons were decided to be the most appropriate source of data. When none were commercially available and very little practical details about their design, performance and characteristics could be found in the literature an additional objective was accepted. That of developing suitable balloons and balloon systems using the materials that were available and of determining the values of the parameters involved. The results of this work are in a paper that has been accepted by the Journal of Applied Meteorology for publication later this year.

The Outlay of the Thesis

The first chapter is introductory giving the aims of the project, the topographical and synoptic situations in Canterbury and a survey of the winds over Canterbury during 1970. Chapters 2, 3 and 4 deal with balloon theory, materials and systems respectively, as applied to the superpressure balloons used to obtain the main observational data and to

the materials that were available for their construction. Lee wave theory as used in the analysis of the observational results is mainly given in Chapter 5 and a summary of the characteristics of lee waves as given by the various theories based on the linearised wave equation and on observations is given in Chapter 6.

Chapter 7 discusses the analysis of the superpressure balloon and radiosonde data which is presented with the appropriate theoretical solutions in Chapter 8. The ascent rates and power spectra of selected radiosonde flights made during the period over which observations were made are found in Chapter 9. A summary of the conclusions is given in Chapter 10.

Two appendices include satellite photographs of some nor'west days and a discussion with examples of a numerical solution of the linearised wave equation.

Balloon profiles are contained in Appendix C and airflow profiles in Appendix D.

TABLE OF CONTENTS

Page

LIST OF FIGURES

LIST OF TABLES

C H A P T E R 1

INTRODUCTION

1. Aims of the Project

The main aims of the project were:

(a) To develop and understand a balloon system suitable for studying lee waves produced in the airflow over Canterbury.

(b) To undertake an observational programme to obtain data on the waves produced over Canterbury by the Southern Alps and Banks Peninsular in order to determine the conditions favourable for their production and the characteristics of the waves, such as their wavelength and amplitude, and to relate these to the airflow parameters.

(c) To understand the practical and theoretical aspects of atmospheric lee waves.

(d) To compare the experimental results with those obtained elsewhere and with the models based on solutions of the linearised wave equation, such as derived by Scorer et al, in order to determine its validity and their usefulness in predicting waves and wave characteristics over Canterbury.

(e) To undertake a survey of the winds over Canterbury over the period of a year, namely 1970, to determine the

frequency of occurrence of some of the conditions which produce waves.

2. Topographical Situation

The Southern Alps are a range of mountains lying approximately along a southwest-northeast line and presenting a barrier between 6000 and 12,000 feet high and 700 km long to the wind which is mainly from the westerly quarter. Upstream the nearest land mass is Australia, 3000 km away and downstream the flow is across the Canterbury Plains and the South Pacific Ocean except for Banks Peninsula. See Fig. 1.1. The Peninsula is only 25 km wide and its highest 'peak' is 3015'. It does not interrupt much of the flow and when the wind is from the northwest a balloon released from Hokitika will pass over the Alps and Banks Peninsula giving an opportunity to study the effect of a distinct secondary source on the primary wave train produced by the Alps.

The mountain ranges upstream of Canterbury show rather complex profiles (see balloon and mountain profiles in Chapter 8). For some wind directions they present some significant periodicities to the flow giving a chance to study the effect of periodic forcing on the airflow. The Torlesse and Puketeriki Ranges present quite steep faces to the Canterbury Plains rising from 1500' to 6000' in about 6 km. They lie approximately along the same SW-NE line. Behind

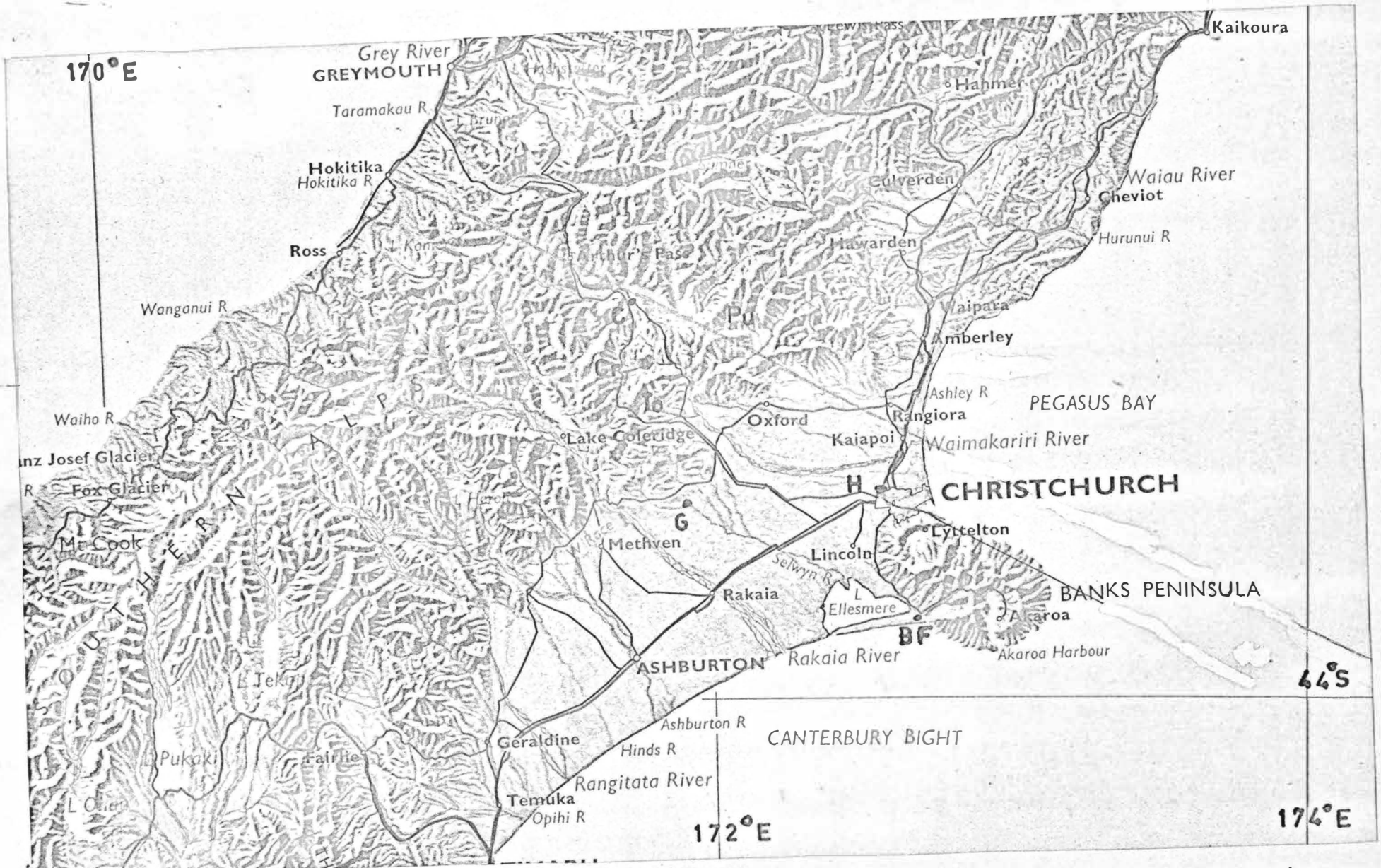

Fig 1.1: A map of the central area of the South Island of New Zealand showing the Southern Alps, the Canterbury Plains, Banks Peninsula and the balloon release sites. C: Cass, G: Glentunnel, H: Harewood and BF: Birdlings Flat. Mountain ranges Pu: Puketeraki, To: Torlesse and Cr: Craigieburn.

the Torlesse Range is the 7000' Craigieburn Range which lies along a north-south line.

Balloons were tracked using the New Zealand Meteorological Service's radar at Harewood (H on Fig. 1.1), from where the developmental balloons were released. The majority of the lee wave observational balloons were released for me by the Met. Service staff at Hokitika. A few initial balloons were released from Cass (C) to see if we could locate a balloon released from a site remote from the radar. These flew over the Puketeriki Range. One balloon was released from Glentunnel (G) (Balloon 19) by Mr P. Lamb, a masters student in Geography who was studying the interaction of the northwesterly wind with the surface. Six balloons were released by Miss Sue Watson and Mr Greg Opie, under my supervision, two from Harewood and four from Birdlings Flat (BF), as part of a B.Sc. Hons. research project to study the waves produced by Banks Peninsula.

3. Synoptic Situation

New Zealand is situated in the midlatitudes of the Southern Hemisphere and is subject to a westerly airflow. The weather is dominated by the progress of a complex system of depressions and anticyclones which pass from west to east resulting in a general oscillation of the surface wind between northwest and southwest. At higher levels the flow

is less complex, assuming a more smooth wave-like form of alternating troughs and ridges. The periodic structure of the wind over Canterbury is looked at in the next section.

The northwesterly situation, which is favourable for the production of waves, is usually associated with the movement of an anticyclone across northern New Zealand. Such a situation is shown by Fig. 1.2. This was how the northwester developed prior to the first balloons I released from Hokitika on 24 April 1970. The dashed lines show the less complicated structure of the 700 mb (approximately 3 km) isopleths.

The northwesterly airstream is enhanced by the presence of a depression to the southwest of the country and its associated cold front which intensifies the pressure gradient along the West Coast bringing NW stronger winds. As the front moves across the country it displaces the northwesterly airflow bringing southwesterlies behind it. On occasions the northwesterly will persist for several days and the direction remains quite constant through the troposphere and well into the stratosphere. On such occasions altocumulus lenticular wave clouds are usually evident much of the time except when a solid sheet of altocumulus is formed streaming back from some distance to the lee of the Alps. This is known as the nor'west arch. The arch is associated with the lee wave phenomena as it is quasi-stationary and has a wavelike structure in the cloud base.

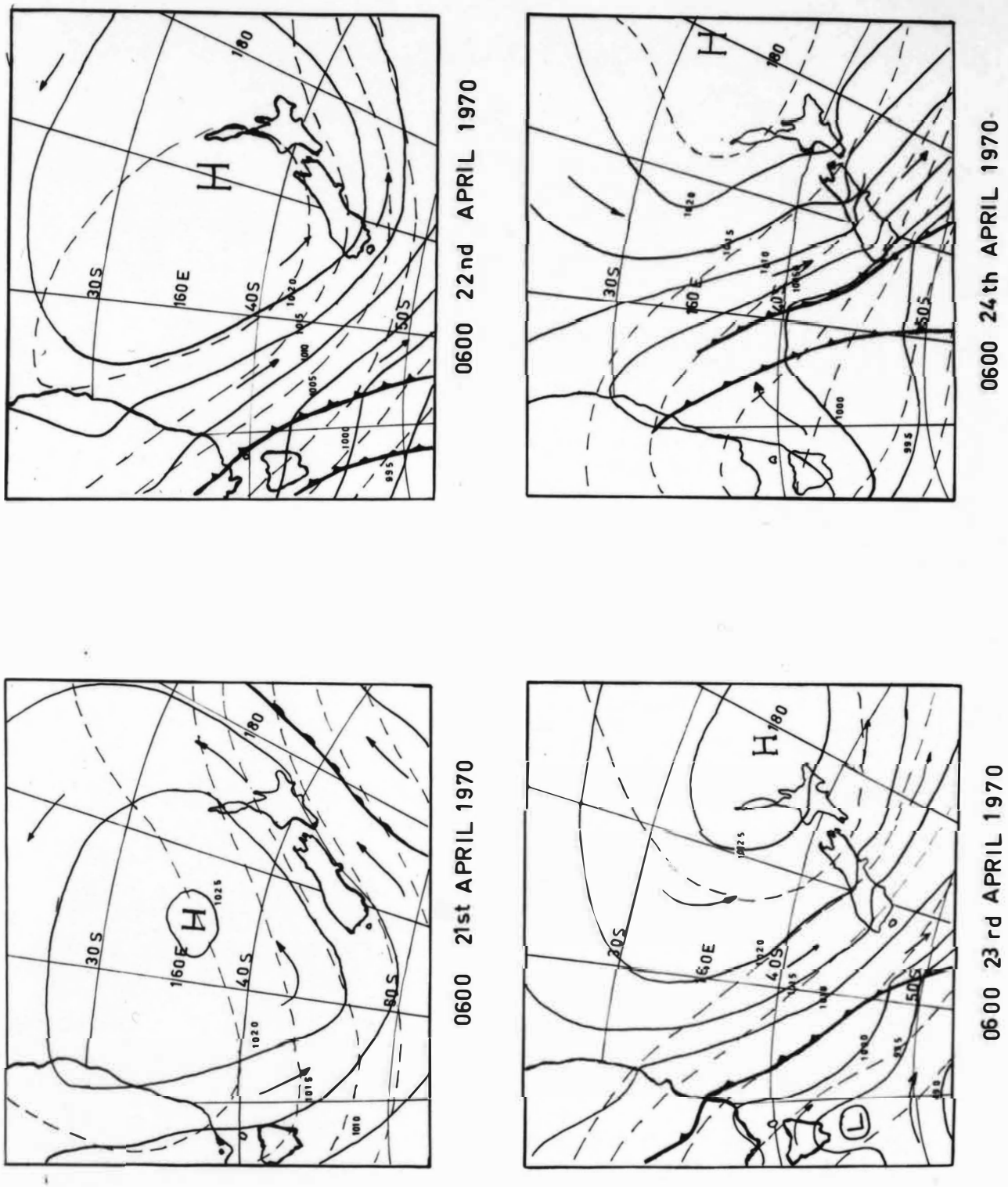

Fig 1.2: A typical synoptic situation which produces nor'westerly winds over New Zealand. The solid lines show the sea level isobars (mb) and the broken lines show the form of the 700 mb isopleths.

Sometimes it becomes chaotic and turbulent when the wind speed is high.

4. Survey of the winds over Canterbury during 1970

The midday radar/wind profile from Harewood was analysed for each day in 1970 to compute the mean tropospheric and stratospheric wind speeds and directions and the maximum tropospheric and stratospheric wind speeds. The distribution of the mean tropospheric wind direction for 1970 is given in Fig. 1.3. This shows that the wind is predominantly westerly with the distribution dropping off towards the north and south. There were no days when the wind was between 50^{o} and 110^{o}. There were 50 days when the wind was within 10^{o} of 310^{o} (the direction perpendicular to the mean direction of the Alps) and there were 122 days when the wind was within 30^{o} of 310^{o}. These were broken down and their monthly distribution is shown in Fig. 1.4. The shaded region indicates the number of days when the wind was within 10^{o} of 310^{o} and the unshaded region included the additional days when the wind was within 30^{o} of 310^{o}. This shows two peaks of the occurrence of nor'westers in February-March and August-September. It is commonly accepted that the best northwesterly period is February-March.

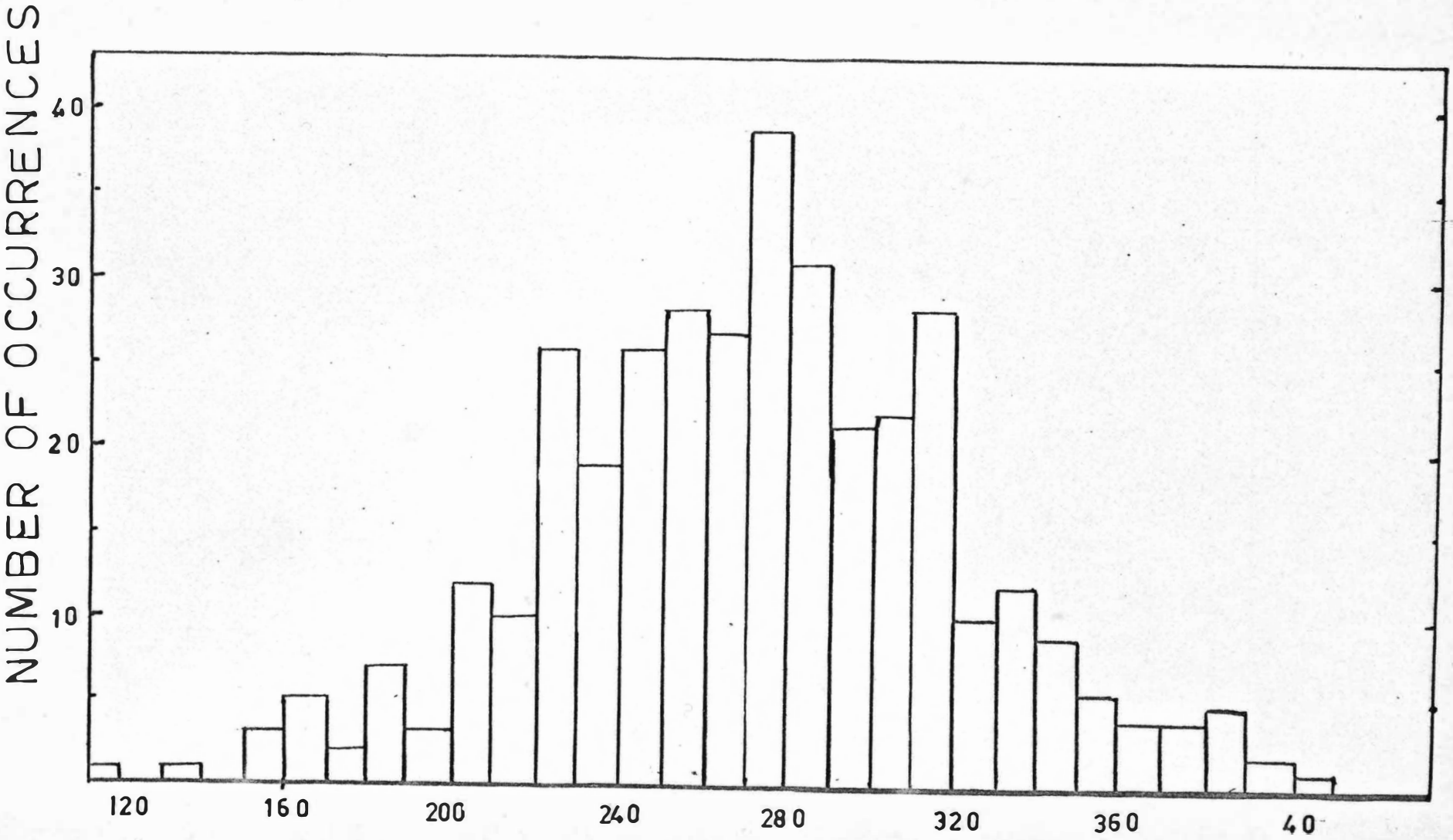

FIG 1.3: Distribution of the mean tropospheric wind direction during 1970.

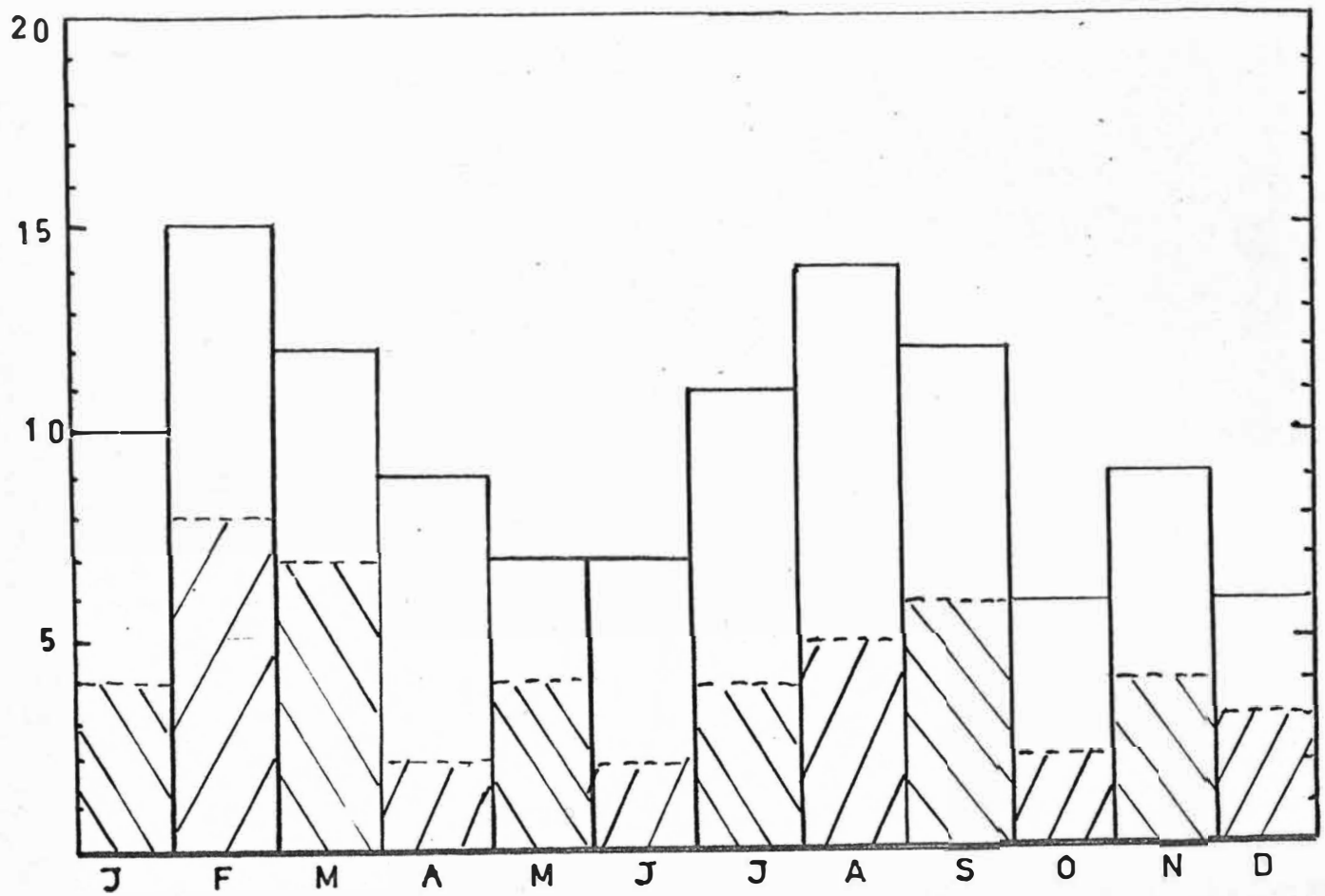

FIG 1.4: MONTHLY DISTRIBUTION OF NOR'WESTERS FOR 1970.

The distribution of the mean stratospheric wind is shown in Fig. 1.5. This shows a more uniform structure than the corresponding tropospheric direction with a slightly greater population in the middle of the range. The wind was within 30^{o} of west on 172 days in the troposphere and on 202 days in the stratosphere. This is a result of the smoother variation of the stratospheric wind. The power spectra of the mean wind directions in the troposphere and the stratosphere (Fig. 1.6, dashed line - troposphere, solid line - stratosphere) show some periodicity. The stratospheric spectrum is considerably smoother than the tropospheric spectrum indicating the more periodic structure of the tropospheric winds.

Fig. 1.7 shows the power spectra of the average (solid line) and maximum (broken line) tropospheric wind velocities. They both show marked periodicities. The three longest periods, 7.5, 4.8 and 3.5 days, appear in both (and in the spectrum of the maximum stratospheric wind velocity) with the 7.5 and 3.5 day periods having counterparts in the periodicities of the wind direction of 7 and 3.7 days. With the 15 and 2.3 day periods in Fig. 1.6 as well there is a very strong indication of a periodicity near 7 days. This is a result of the cyclonic flow in these latitudes. The passage of cyclones and anticyclones past New Zealand has been observed to have an approximately weekly cycle. When I

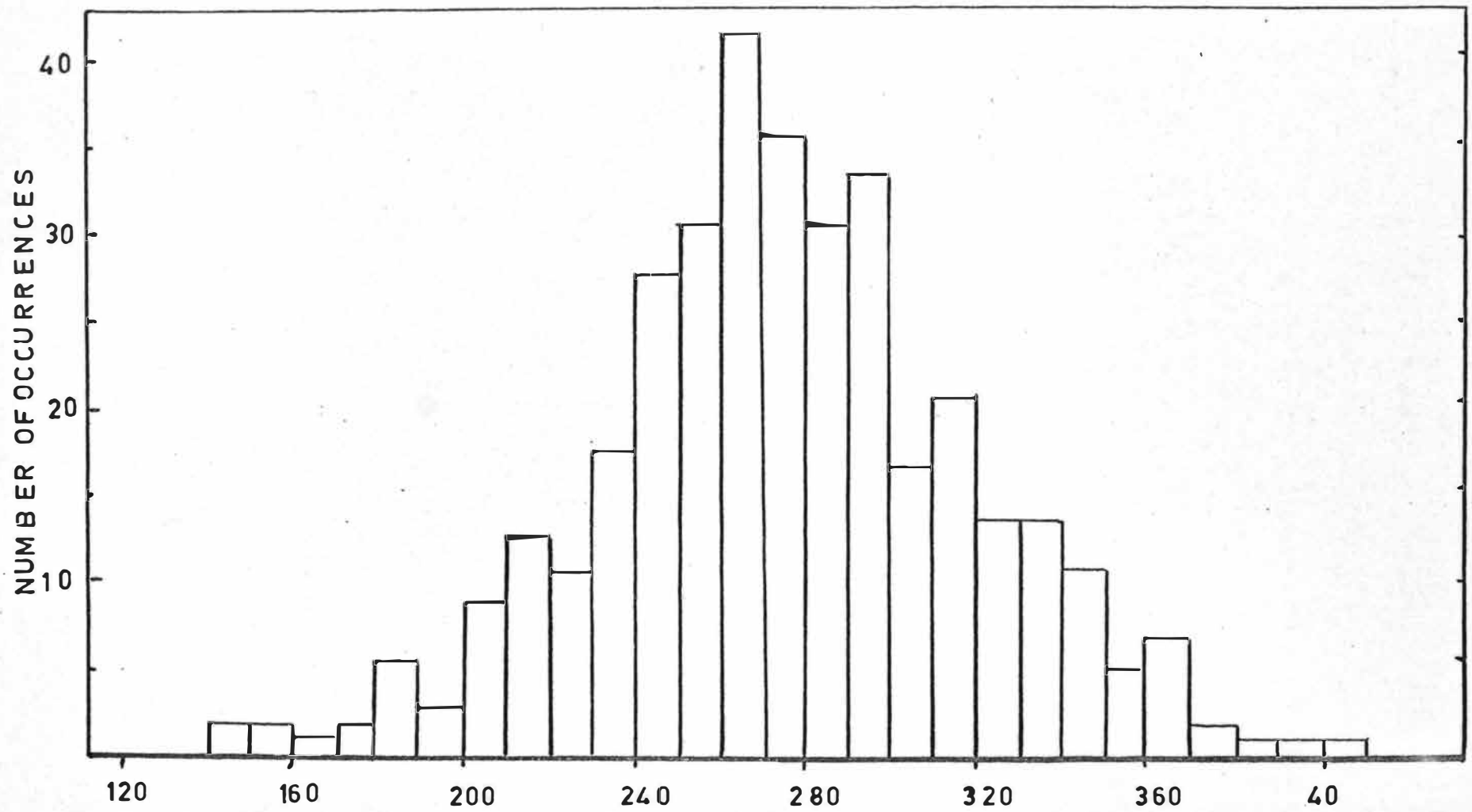

FIG 1.5 : DISTRIBUTION OF THE MEAN STRATOSPHERIC WIND DIRECTION DURING 1970.

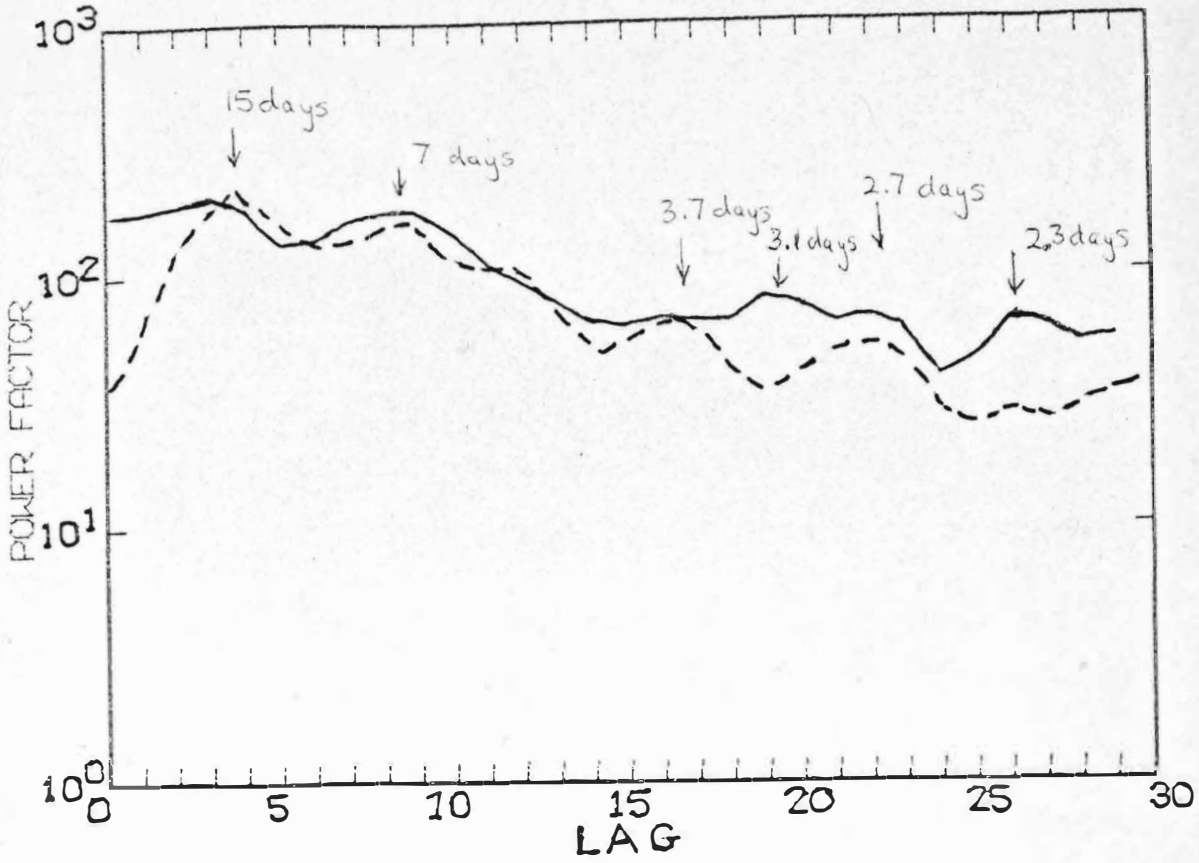

FIG 1.6: POWER SPECTRA OF THE MEAN TROPOSPHERIC (solid curve) AND STRATOSPHERIC (broken curve) WIND DIRECTIONS.

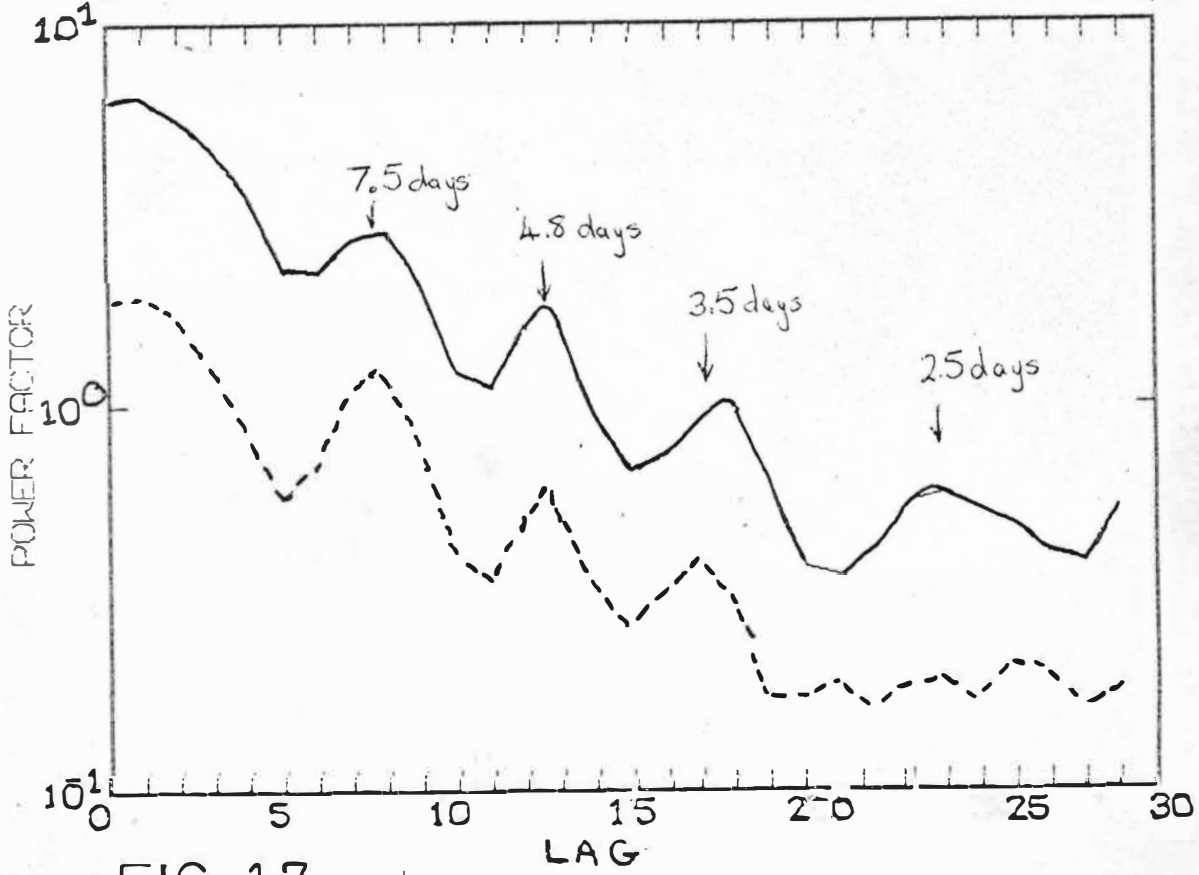

FIG 1.7: POWER SPECTRA OF THE AVERAGE (solid curve) AND MAXIMUM TROPOSPHERIC WIND SPEEDS. PERIOD = $\frac{60}{\text{LAG}}$ days

was at high school I noted one year that we had fine sunny conditions for every Sunday of the year except two although there was the usual seasonal weather variation overall. This periodicity can also be seen in the dates of Table 8.1 which records the dates of the superpressure balloon flights undertaken in this project, most of which were released under northwesterly conditions. For example: the 26th and 30th of March 1969, the 14th and 21st of January 1970, the 2nd and 30th of March 1970 and the 2nd, 15th and 22nd of July 1970.

Assuming that the wind direction varies as a smooth sinusoid between 200^{o} and 350^{o}, centred on 270^{o}, (this is the range which contains 88% of the population of the distribution given in Fig. 1.3) of period 7 days, then the wind direction will lie within 30^{o} of 310^{o} for an average of 2.25 days per cycle. This is 32.2% of the time compared to the 33.5% of the time observed during 1970.

5. An Empirical Wave Classification for North Canterbury based on the Wind Profile Characteristics

The superpressure balloons and satellite photographs were studied to find the days when large amplitude lee waves were formed over Canterbury. These were then tabulated (Table 1.1) with some of the wind speed parameters in order to determine the orders of magnitude of the characteristic velocities which result in large amplitude lee waves from the Southern Alps. The following parameters were used: The mean tropospheric wind direction D_t and speed U_t, the wind speed just above the ground (at about 300 m) U', the wind speed at the 800 mb standard level (approximately 2 km, about the height of the main mountain ranges upstream of Canterbury in nor'westerly conditions) U_m and the maximum tropospheric wind speed U_{max}.

Table 1.1: Days on which strong waves were observed over Canterbury on satellite photographs and in SPB flights, together with some wind profile parameters (in m sec^{-1}).

Date	D_t	U'	U_m	U_t	U_{max}	Wavelength (km)
5/3/69	290°	9	12	25	48	12.6
10/11/69	305°	9	12	18	37	12.2
21/1/70	298°	8	7	20	43	20.0
23/7/70	298°	12	22	22	39	noon 18.0 p.m. 16.9
4/8/70	287°	9	14	17	35	a.m. 11.3 p.m. 13.2
15/1/70	304°	8	15	21	37	a.m. 15.5 p.m. 11.3
25/12/70	308°	11	16	30	54	

This rather limited sample also suggests that the large waves formed have wavelengths within the range 10-20 km. This is consistent with casual observations of the cloud bands formed across the 60 km of the Canterbury plains between the Alps and Christchurch. These indicate that usually there are 5-7 bands and sometimes as many as 10 bands of lenticulars across the plains and in very strong nor'westerly conditions three have been observed, the third being almost directly overhead. The waves then mainly have a wavelength between about 8 and 12 km but may be as short as 6 km or as long as 30 km.

Table 1.1 suggests initial criteria for strong waves to be produced; that the mean tropospheric wind direction should be within 20° of about 310°, that U' should be greater than 8 mps, that U_t should exceed about 17 m sec^{-1} and that U_{max} should exceed approximately 35 mps.

A study of the airflow profiles over the year 1970 showed that these conditions were fulfilled at noon on 19 days, mainly during July, August and September. The midday radiosonde soundings from Harewood for the year were searched for evidence of waves and were classified according to the following scale:

A : very large amplitude waves, $\gtrsim$ 800 m

B : large amplitude waves, $\gtrsim$ 500 m

C : medium amplitude waves, $\gtrsim$ 200 m

D : small amplitude waves, $\lesssim$ 200 m

E : possibly waves present,

F : no evidence of waves.

(The orders of magnitude of the amplitudes were arrived at with reference to the methods outlined in Chapter 9.) These were tabulated and plotted against the various wind profile parameters to see whether any trends existed which could be used in a Wind Profile Wave Classification. Any classification derived in this way is only specifically applicable to this part of Canterbury because of the dependence of the wave train on the forcing of the mountains. The general form of the conclusions should be consistent with lee waves observed in other locations.

Since the forcing spectrum of the mountain is a function of the wind direction the main classification parameter was chosen to be the mean tropospheric wind direction. The magnitude of the waves produced over the year were plotted against this wind direction as functions of the 800 mb wind speed, in Fig. 1.8, the mean tropospheric wind speed, in Fig. 1.9, and the maximum tropospheric wind speed, in Fig. 1.10. A solid curve was drawn around the approximate boundary of the large amplitude waves. In Figs 1.8 and 1.9 a broken line was drawn near the boundary between no waves and weak waves. Not much significance can be given to this curve, based on the relatively small data sample, as no clearly distinct regions are evident. These curves may be used to give an indication of the scale of wave motion to be expected over Canterbury for the given conditions. Satisfying only one of the conditions is not sufficient to predict the formation of waves. If the wind speed at the level of the mountains is not strong enough, or the increase in velocity with height (indicated by the mean wind speed) is not sufficient, waves, especially large waves, will not be produced. Data from 11 days during 1969 on which there were strong waves was added to Figs 1.8 and 1.9. These points are indicated by a superscript '+'.

The angular positions of the mountain ranges upwind of Christchurch are shown on the diagrams. All the strong

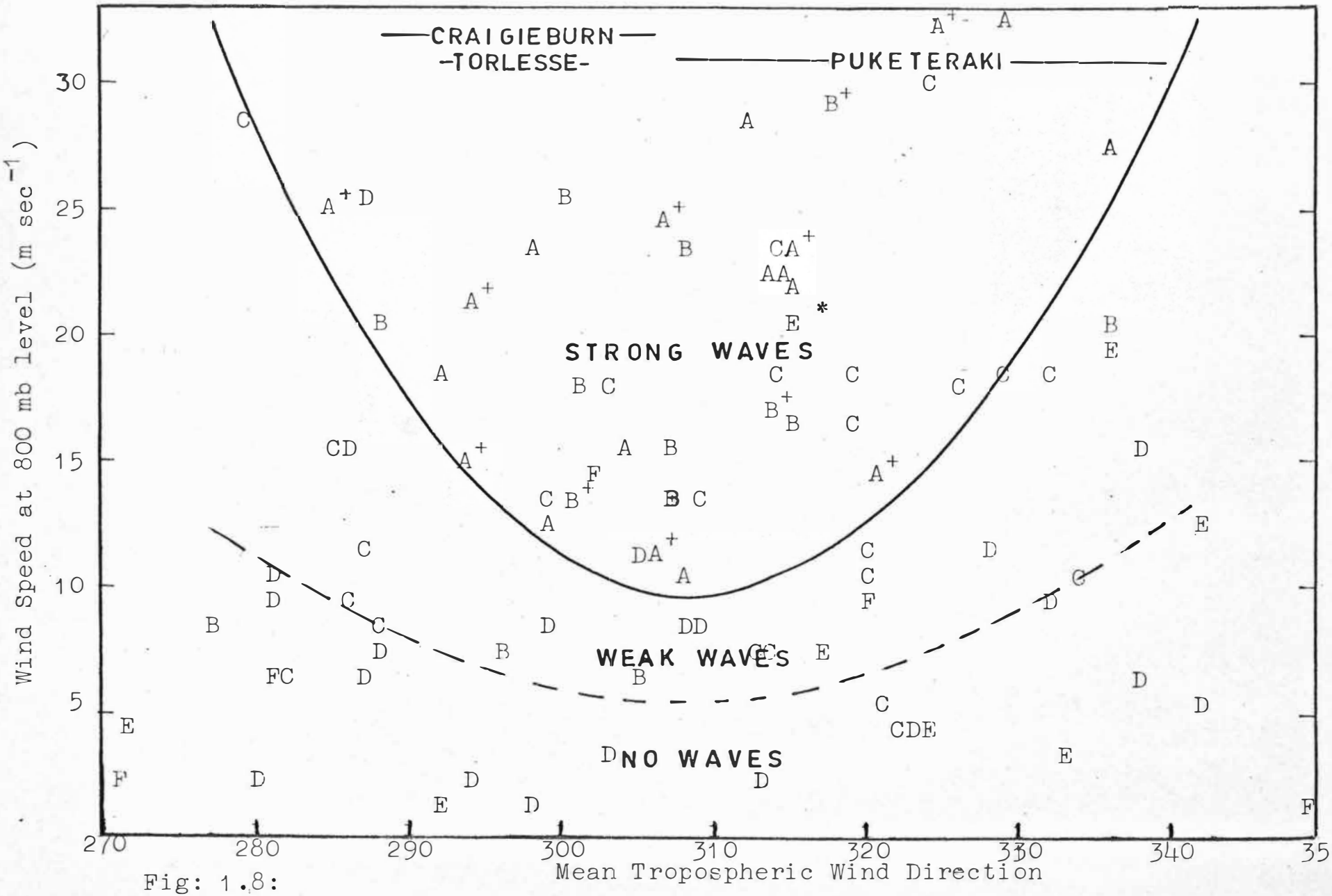

Fig: 1.8:

The Wave Classification as related to the mean tropospheric wind direction and the 800 mb wind speed. (800 mb is approximately at the level of the mountain ridges.) ('+': Data obtained from 1969)

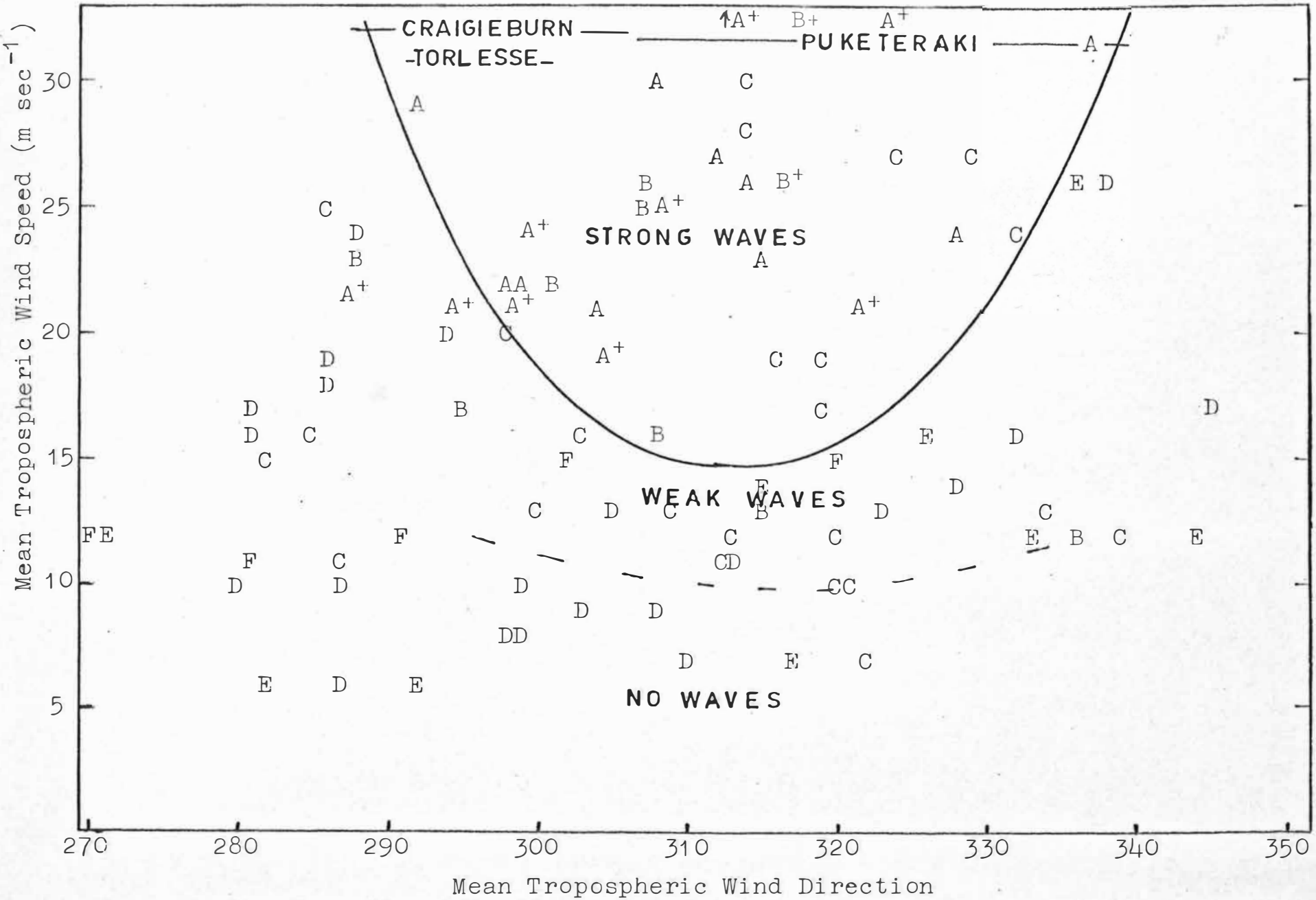

Fig 1.9: The Wave Classification related to the mean tropospheric wind direction and the mean tropospheric wind speed.

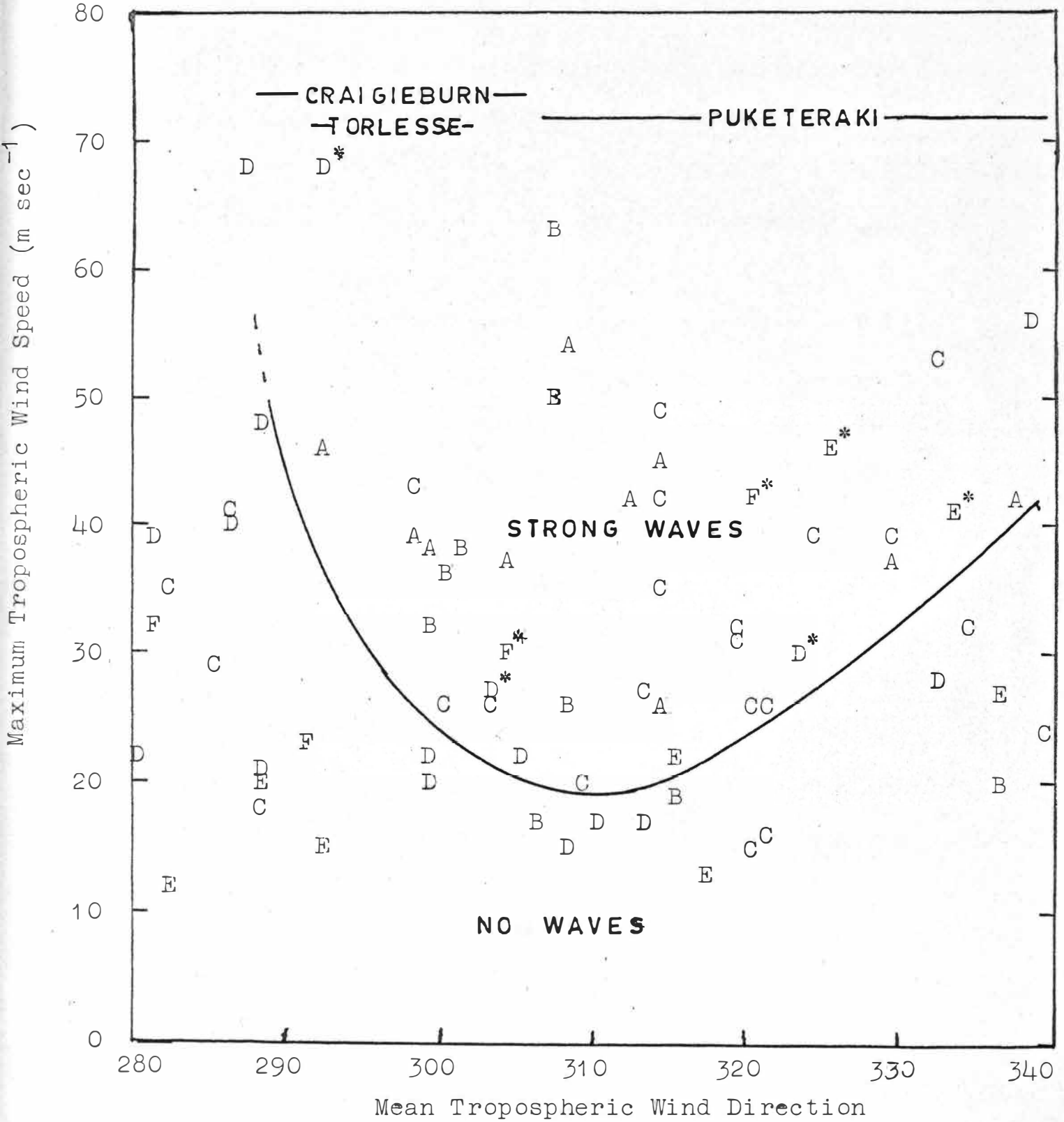

Fig: 1.10: The Wave Classification related to the mean tropospheric wind direction and the maximum tropospheric wind speed.

Note: * Indicates that one of the other parameters was subcritica

waves observed lie within the range covered by these mountains. The western end of the Craigieburn and Torlesse Ranges is bounded by the Rakaia Gorge. This seems to act as a cutoff to limit the production of waves to less than the usually observed 30^{o} of the direction perpendicular to mountain ridges.

An asterisk was used in the diagrams to indicate characters in a strong wave region which correspond to a day when one of the other conditions, particularly the low level wind speed, was not fulfilled.

The Wave Classification Diagrams

(a) Using the 800 mb Wind Speed (Fig. 1.8): The minimum critical velocity at this level, which is approximately at the height of the mountain ridges, for strong waves to be produced when the wind is close to the optimal direction is about 10 m sec^{-1}. This is consistent with the minimum critical velocities for other locations given in Table 6.1.

(b) Using the Mean Tropospheric Wind Speed (Fig. 1.9): Fig. 1.9 shows that for strong waves to be produced U_t was in excess of 15 m sec^{-1}. All the very strong waves occurred in association with mean tropospheric wind speeds in excess of 20 m sec^{-1}.

(c) Using the Maximum Tropospheric Wind Speed (Fig. 1.10): For large waves U_{max} was generally greater than 20-25 m sec^{-1}. The distribution was not as consistent as with the other two parameters in differentiating between the conditions resulting in waves. The maximum wind speed is not indicative of the general conditions in the troposphere.

The conditions near the ground where the distrubance is produced and the general conditions in the troposphere which allow the upward propagation of waves are more closely related to the low level wind speed and the average tropospheric wind speed.

Once the velocity criteria are fulfilled there is still the possibility that large amplitude lee waves may not result for a particular wind speed and direction because the forcing of the mountains for that particular direction may produce destructive interference in the lee wave train for the given wind speed.

The temperature lapse rate has an effect on the production of lee waves. Since a differentiation can be made by referring only to the wind speed profile it must have a secondary effect and may be neglected. This is convenient for forecasting the presence of waves over Canterbury since a radar wind sounding is made every six hours and radiosonde soundings are made only once every 24 hours for most of the year.

All large waves observed occurred when the wind direction was within the angular range of the three mountain ridges (290^{o}-340^{o}), the 800 mb wind speed was in excess of 10 mps and the mean tropospheric wind speed was greater than 20 m sec^{-1}.

C H A P T E R 2

BALLOON THEORY

1. Introduction

The importance of balloons as atmospheric sounding devices is shown by their extensive use by meteorologists throughout the world. Since the first successful balloon flight in 1783 a large body of information has been built up about the characteristics and performance of balloons so that now balloons are used in many different applications to obtain meteorological data.

Most commonly balloons are used for vertical soundings of the lower atmosphere. In this case an extensible latex rubber or neoprene is used, most commonly to determine the vertical wind profile and often to determine the temperature and humidity profiles using a radiosonde. This type of balloon will expand as it rises until it finally bursts.

Balloons are also used to make horizontal soundings, either to plot the global circulation as in Project GHOST, or to detect vertical perturbations in the horizontal airflow. Such a balloon requires a fixed maximum volume which determines its equilibrium displacement height. Constant volume balloons (C.V.B) or superpressure balloons have been described by Booker and Cooper (1965) and Lally (1967). This chapter summarises the theory of superpressure balloons.

2. Theory

A balloon rises because it is lighter than the air it displaces. If a balloon, volume V, has weight W and carries load W_L, so that the total weight is W, is filled with hydrogen, density ρ_{H_2}, then its free lift F_L is given by Archimedes' Principle:

i.e. Buoyancy force = weight of air displaced

= total weight of balloon + F_L

$$\rho_{air} V K = W_T + F_L \qquad (2.1)$$

where K is a factor dependent on the atmospheric pressure and temperature, and W_T is the total weight of the balloon and load including the weight of the hydrogen.

i.e. $$W_T = W + \rho_{H_2} V K$$

therefore $$F_L = (\rho_{air} - \rho_{H_2}) V K - W \qquad (2.2)$$

Now $$K = \frac{P}{760} \times \frac{273}{T}$$

where p is the atmospheric pressure in mm. of mercury and T is the absolute temperature.

Also ρ_{air} = 1293 gm/m^3 at S.T.P.

ρ_{H_2} = 89.9 gm/m^3 at S.T.P.

When the balloon moves it experiences a drag force D due to the air resistance on the balloon and its load will

increase as the velocity increases until it equals F_L and the vertical velocity becomes constant. Thus

$$F_L = 432.2\ (P/T)\ V - W - D \qquad (2.3)$$

where F_L, W, and D are in grams wt. and V is in m^3.

3. Equilibrium Level

From equation 2.3 it can be seen that F_L is positive, i.e. the balloon will rise, as long as:

$$432.2\ (P/T)\ V > W$$

If, however, the volume has a fixed maximum value V_e, then when the balloon reaches the volume V_e, in (2.3) V is fixed at V_e and since $\frac{(PV)}{(T)}$ is a constant the factor (P/T) becomes fixed. The balloon then, in the first instance, is confined to a constant density surface defined by $(P/T)_e$, since

$$P/T \propto \rho_{air}$$

When the balloon reaches this equilibrium level the net force becomes zero, i.e. $F_L = 0$.

Since $D = \frac{1}{2}\ \rho\ v^2\ C_D\ A^*$

where v is the vertical velocity and is zero at the equilibrium level (in static air), $\therefore$ D = 0.

Therefore, at equilibrium

$$W = 432.2\ (P/T)_e V_e \qquad (2.4)$$

To determine the equilibrium level for a balloon with total weight W (gms) and volume V (m^3) use:

$$(P/T)_e = \frac{W}{432.2\ V_e} \qquad (2.5)$$

The ratio (P/T) can be calculated as a function of height, assuming a model atmosphere as shown in Figure 2.1.

In practice the balloon will overshoot the equilibrium level and for a short time execute simple harmonic motion about it at the balloon's natural frequency (discussed later). This oscillation will be strongly damped by the drag force.

4. Superpressure and Supertemperature due to Free Lift

The gas inside the balloon is governed by the relation

$$(P/T)V = \text{constant} = (P/T)_o V_o = (P/T)_e V_e = (P/T)'_e V'_e \qquad (2.6)$$

Where the subscript 'o' applies to the values at the ground, 'e' applies to values at the equilibrium level. The prime refers to the value of the restricted volume at the

FIG 2.1

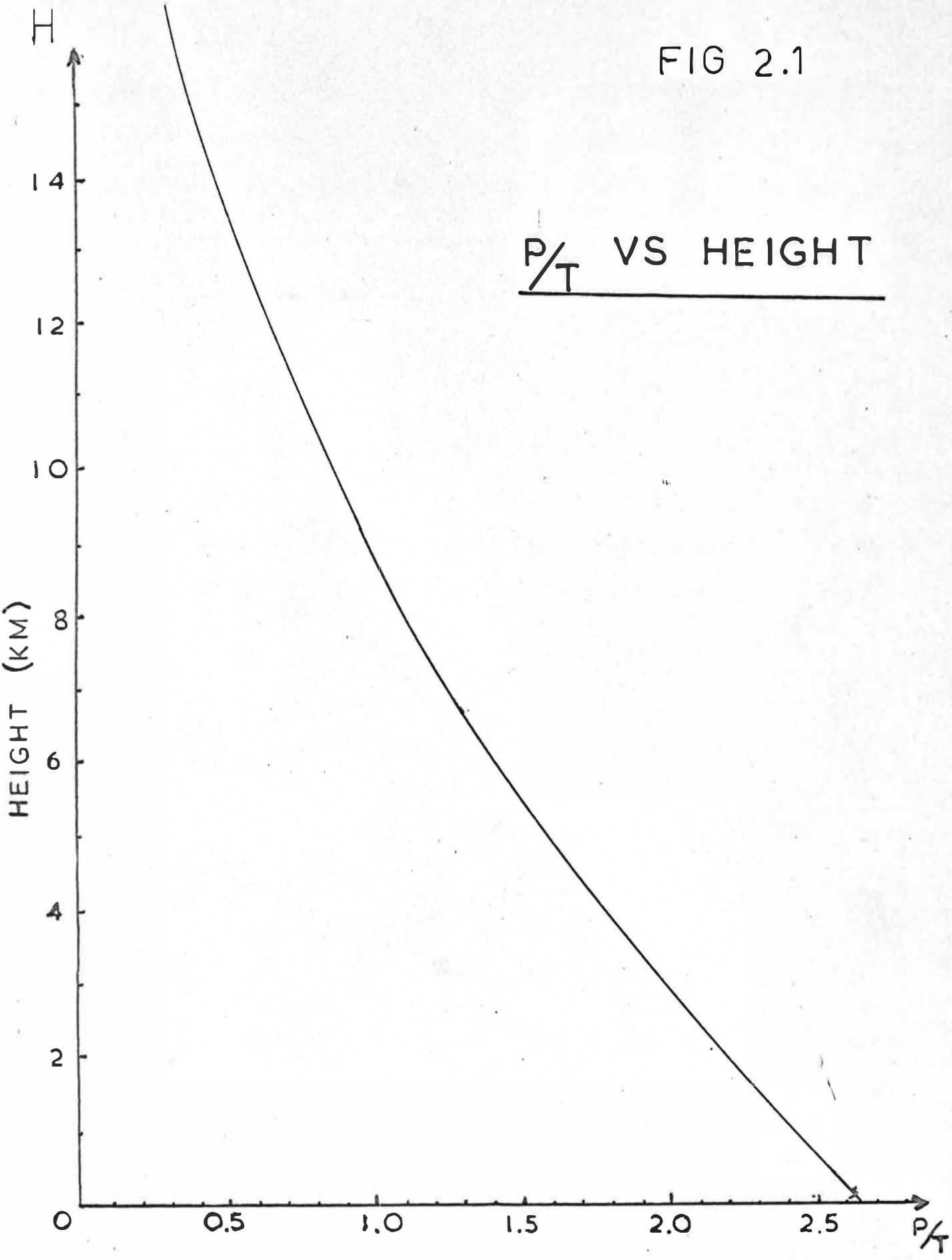
H
14
12
10
8
6
4
2
0
HEIGHT (KM)
0.5
1.0
1.5
2.0
2.5
P/T
P/T VS HEIGHT
PRESSURE (MM OF HG)
TEMPERATURE (°K)

equilibrium level and to the actual pressure and temperature inside the balloon, whereas the unprimed equilibrium level values refer to the balloon volume if unrestricted and to the ambient pressure and temperature.

From Archimedes' Principle:

$$V'_e = \frac{W}{432.2(P/T)_e} \qquad (2.7)$$

$$\text{and} \qquad V_o = \frac{W + F_L}{432.2(P/T)_o}$$

From (2.6) we see that the superpressure P_s and the supertemperature T_s are dependent variables, where

$$P_s = P'_e - P_e = \left[\frac{T'_e}{T_e}\frac{W + F_L}{W} - 1\right] P_e \qquad (2.8)$$

$$T_s = T'_e - T_e = \left[\frac{P'_e}{P_e}\frac{W + F_L}{W} - 1\right] T_e \qquad (2.9)$$

We also find that

$$P'_e = (P/T)_e \frac{W + F_L}{W} T'_e \qquad (2.10)$$

Assuming that $T_s = 0$, i.e. that all the heat generated by the compression of the excess gas is lost to the atmosphere, as is shown in the next chapter, then

$$T_e = T'_e$$

so from (2.8)

$$P_s = \frac{F_L}{W} P_e \qquad (2.11)$$

5. Supertemperature due to Infrared and Solar Radiation

A balloon in the atmosphere will be subject to infrared and solar radiation which it will tend to absorb, to a greater or lesser extent depending on the balloon material. This it will tend to reradiate, depending on its emission characteristics. Because the balloon will absorb more radiation than the surrounding air it will be at a higher temperature, i.e. there will be a supertemperature. This usually rises to a positive maximum during the day.

For high altitude balloons, above 20 km, it can be assumed that the balloon is in equilibrium with its radiation environment because there is little convection or conduction to the air. For balloons at lower levels, because of conduction of heat from the balloon to the air, its temperature will lie between the temperature calculated from radiative equilibrium and the ambient temperature.

(a) Infrared (blackbody) Radiation

Radiation from clouds and other objects, above, below and at the sides, is equal to the blackbody radiation from a source at the body's surface temperature.

If it is clear below the balloon will receive upward radiation from between 150 w/m^2 to 450 w/m^2 depending on the altitude and the air masses.

If it is clear above the balloon will receive varying intensities of radiation according to its altitude:

Above 15 km - - 10 w/m^2

10 to 15 km - - 20 w/m^2

Below 10 km - - 40 w/m^2

(b) Solar Radiation

At high levels the intensity of direct solar radiation is about 1400 w/m^2. At 16 km it is about 1200 w/m^2, and at 3 km it is about 1000 w/m^2. If there are clouds below the balloon the radiation reflected upward from them may be as high as 800 w/m^2.

At altitudes below 12 km, cirrus clouds rarely produce more than 10% reduction in incoming radiation.

For a polyester balloon the maximum solar heating at high altitudes (24 km) is about 20°C. A typical increase will be about 12°C. At lower altitudes an average temperature increase due to solar radiation will be 8 to 10°C.

Values of supertemperature for a polyester balloon have been calculated by Lally (1967), and are shown in Figure 2.2.

FIG 2.2:
SUPERTEMPERATURE VS HEIGHT

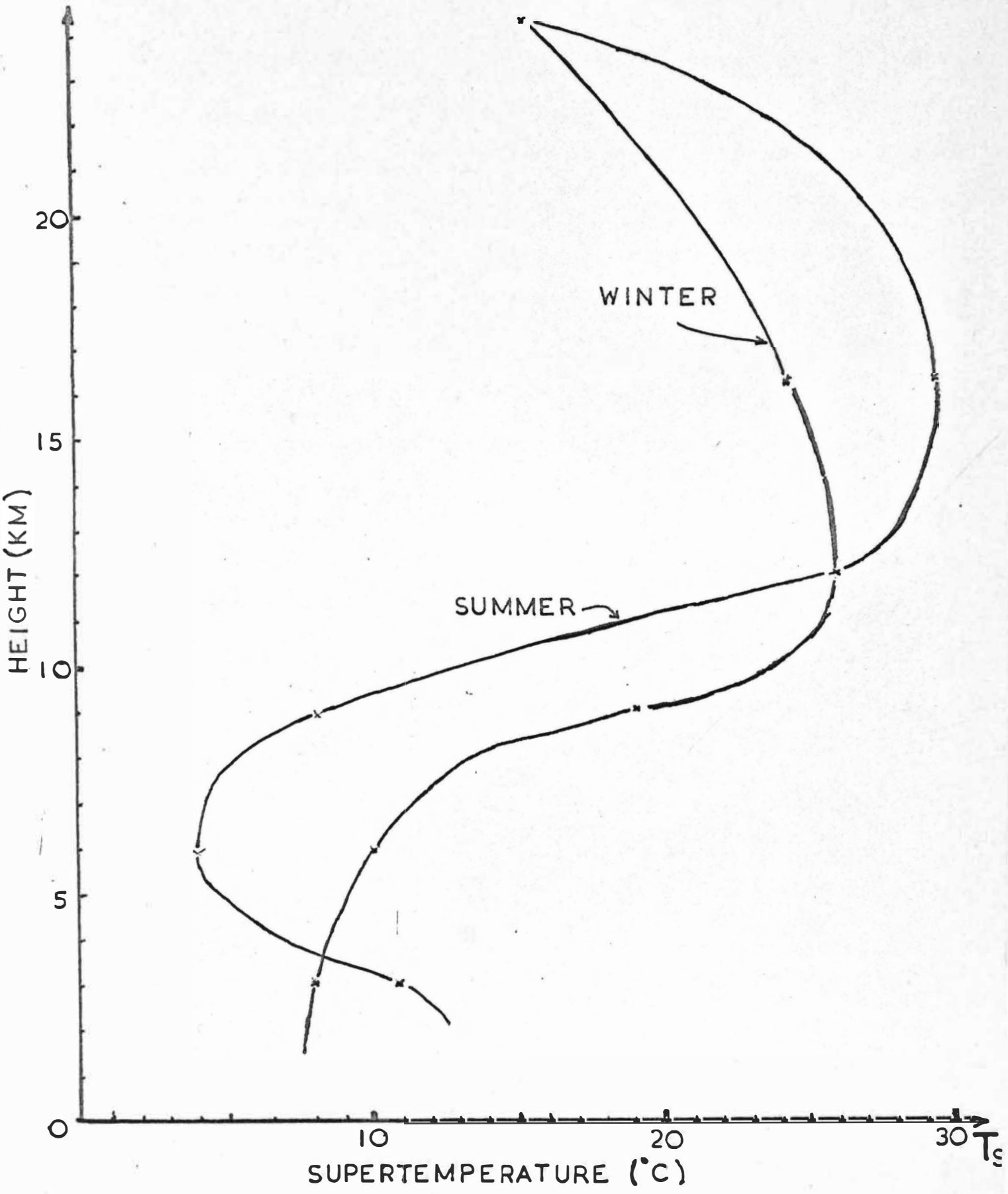

FOR A POLYESTER BALLOON IN TEMPERATE WINTER AND TEMPERATE SUMMER. (LALLY '67)

The supertemperature of a polyethylene balloon is lower than that of a polyester balloon however, since it absorbs only 6% of the infrared radiation whereas polyester is almost black. Lally's calculations apply to long duration balloons that are in thermal equilibrium with the atmosphere and can be considered as maximum supertemperatures for short duration flights during which the balloon will heat up somewhat less. This gives a maximum supertemperature above the tropopause of 30°C or about 14% and an average supertemperature below the tropopause of about 10°C or about 4%.

6. The Constant Volume Balloon as a Tracer of Air Motion

It was suggested by Angell and Pack (1961, 1962) that superpressured constant volume balloons provide a first approximation to the 3-D airflow. They say that the chief evidence for this lies in a combined qualitative and quantitative comparison of the balloon's oscillations in the vertical at different times of the day and under varying stability conditions.

Since the balloon seeks to follow a constant density surface it is free to follow the horizontal movement of the air under the influence of the horizontal drag force, but it resists vertical motions to an extent governed by the relation between the vertical drag force and the restoring force which is proportional to the difference in density

from that at the natural level. Booker and Cooper (1965) simulated the trajectory of a pillow shaped balloon in a sinusoidal airflow, using a computer. The programme considered the elastic stretching of the superpressure balloon with varying superpressure. Twentyfive different combinations of wind speed and amplitudes covering all the usual lee wave conditions were looked at. The balloon and parcel of air were assumed to start at the same point and to move downstream at the same rate. The result is shown in Figure 2.3.

The results show that the balloon will underestimate the amplitude and indicate the position of the maxima and minima too far upstream.

Vergeiner and Lilly (1970) attempted to confirm Booker and Cooper's computations by considering the following equation of motion for the balloon:

$$\underset{\text{(weight)}}{-M \ddot{z}_B - M g} + \underset{\text{(lift)}}{\rho V g} + \underset{\text{(drag)}}{C_D A (V_A - V_B) |V_A - V_B|} = 0 \qquad (2.12)$$

where M = total mass of the balloon and load, gms,

V = volume of the balloon, m^3,

A = cross sectional area of the balloon, m^2,

C_D = drag coefficient,

ρ = density of the ambient air, gm/m^3,

z_B = height of the balloon as a function of time, m,

FIG 2.3: COMPARISON OF AIR PARCEL AND BALLOON TRAJECTORIES.

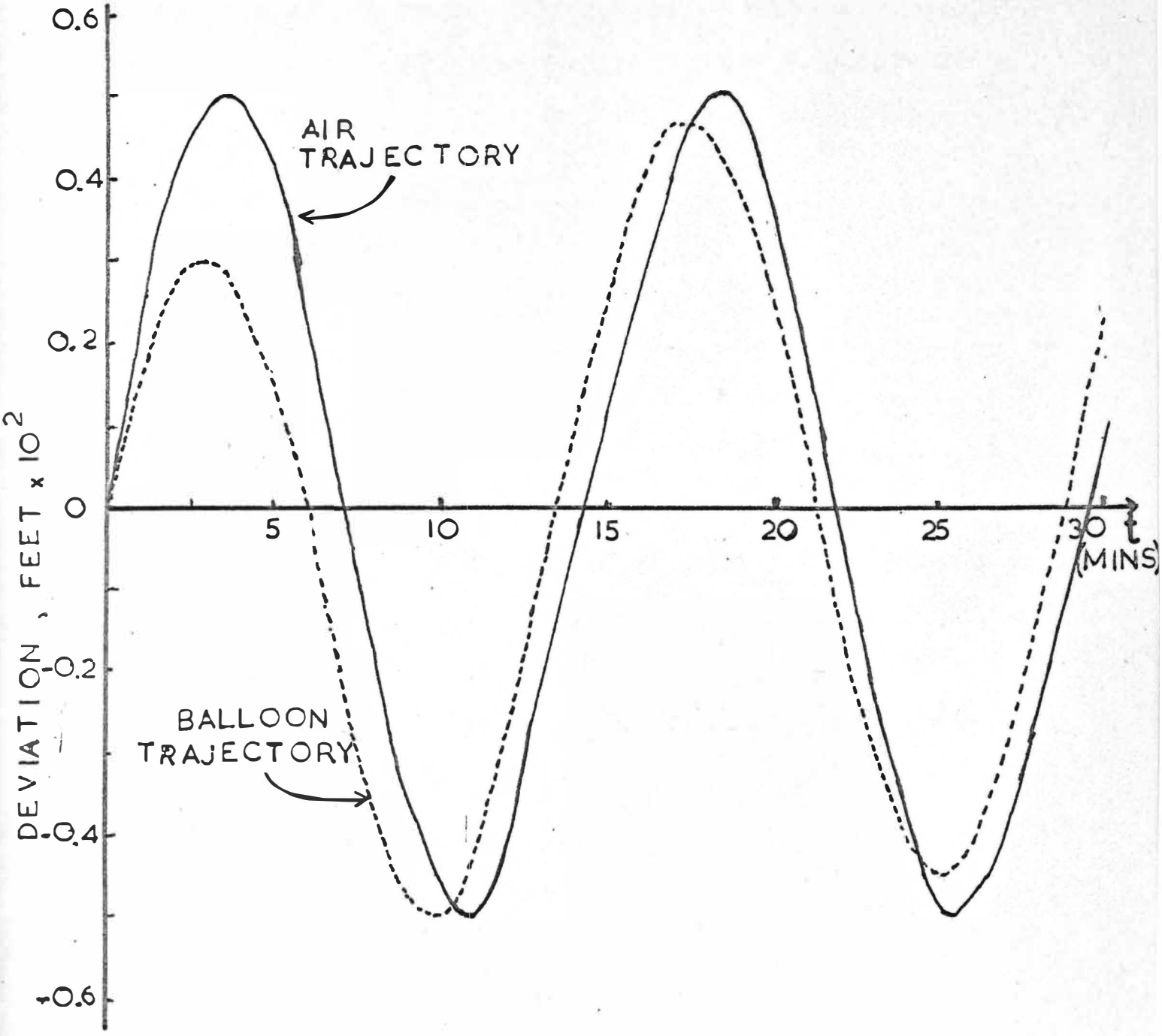

AIR PARCEL AND RESULTING BALLOON TRAJECTORIES FOR A WAVE OF 6 N MILE WAVELENGTH, 1000 FT AMPLITUDE AND 30 KT HORIZONTAL WIND SPEED, FOR A POLYESTER PILLOW.

$V_B = \dot{z}_B$ = vertical velocity of the balloon, mps,

V_A = vertical velocity of the air, mps.

At the equilibrium level the weight of the balloon equals the weight of the air displaced $V\rho_e g$, the subscript 'e' referring to the equilibrium level. Therefore the 'weight' and the 'lift' terms may be replaced by $g\ V\ (\rho-\rho_e)$. Then

$$\frac{M}{C_D\ A\ \bar{\rho}}\ \ddot{z}_B - g\ V\ (\rho-\rho_e) = (V_A-V_B)\ |V_A-V_B| \qquad (2.13)$$

Now $(\rho-\rho_e)$ is a function of height,

viz. $\rho-\rho_e = -10^{-4}\ k\ (z_B-z_e)$

where $k = 2.5$ gm/m^3/m at the ground ($z = 0$)

and $k = 1.8$ gm/m^3/m at 10 km.

Equation (13) becomes

$$C_1\ \ddot{z}_B + C_2\ (z_B-z_e) = (V_A-V_B)\ |V_A-V_B| \qquad (2.14)$$

where $$C_1 = \frac{M}{\bar{\rho}\ C_D\ A} \qquad (2.15)$$

and $$C_2 = \frac{g\ V\ k\ 10^{-4}}{C_D\ A}$$

This gives the period of the free oscillation as:

$$\tau = 2\pi\sqrt{\frac{c_1}{c_2}} \qquad (2.16)$$

For a tetroon with a side of 1.996 m at 10 km the period of free oscillation of the balloon is 3 minutes, which is uncomfortably close to lee wave periods, but the oscillation is strongly damped by the drag force due to the air resistance.

Vergeiner and Lilly used the equation in the form:

$$\frac{d}{dt}(z_A - z_B) = \begin{cases} +\sqrt{+ \text{ left-hand side}} & \text{if L.H.S.} > 0 \\ -\sqrt{- \text{ left-hand side}} & \text{if L.H.S.} < 0 \end{cases} \qquad (2.17)$$

Equation (2.17) was integrated to compute the "true" vertical displacements of the air z_A using the observed balloon track z_B.

Lally (1967) derived an expression for the natural period of oscillation of the balloon in terms of the atmospheric pressure and temperature, viz.

$$\tau = 2\pi\sqrt{\frac{T}{g\left(\frac{\partial T}{\partial z} - \frac{T}{p}\frac{\partial p}{\partial z}\right)}} \text{ seconds} \qquad (2.18)$$

Now $$\frac{\partial p}{\partial z} = -3.48 \times 10^{-3} \frac{\rho}{T} g \quad \text{nt/m}^2\text{/m}$$

therefore $$\tau = 2\pi \sqrt{\frac{T}{g\left(\frac{\partial T}{\partial z} + 3.342 \times 10^{-1}\right)}} \text{ secs} \quad (2.19)$$

For an isothermal atmosphere:

$$\tau = 10.86\ T \text{ secs} \quad (2.20)$$

where T is the absolute temperature.

An adiabatic lapse rate ($\frac{\partial T}{\partial z} = -10^{-2}\ ^{o}C/m$) will increase the period by approximately 15%.

7. Drag Coefficient and Ascent Rate

The drag force on a body moving through a viscous fluid is proportional to the kinetic energy of the body and the effective area of the body.

$$\text{i.e. } D = \tfrac{1}{2} \rho v^2 C_D A^* \quad (2.21)$$

where
- D is the drag force in nt,
- ρ is the density of the fluid in kgm/m^3,
- v is the velocity of the body through the fluid in m/sec,
- C_D is the drag coefficient,
- A^* is the effective area of the body, in m^2.

A balloon rising through the atmosphere, assumed static, will be subjected to an upward lifting force F_L in equilibrium with the drag force. The vertical velocity or

ascent rate is defined by this equilibrium relation.

$$\text{i.e.} \qquad F_L = \tfrac{1}{2} \rho v^2 C_D A^* \text{ nts} \qquad (2.22)$$

The values of the drag coefficient and resulting ascent rates for particular balloon systems are given in the next chapter.

8. Superpressure and Ascent Rate

This will be considered as two cases.

(a) Balloons with gas release valves

For balloons with gas release valves the superpressure will be constant at the value determined by the setting of the valve. As the balloon ascends the gas inside the balloon will expand and outgas through the valve decreasing the free lift as the volume of the balloon is constant and as the balloon ascends it displaces air with decreasing density. An expression for the ascent rate may be derived by substituting equation (2.21) into equation (2.3), noting that equation (2.3) is expressed in gms wt. and equation (2.21) in newtons.

Thus $$(432.2\,(P/T)V - W)\, g \times 10^{-3} = \tfrac{1}{2} \rho v^2 C_D A^* \qquad (2.23)$$

and using $$(P/T) = K \rho \qquad (2.24)$$

where $$K = 2.15 \frac{\text{mm of Hg}/^{\circ}\text{K}}{\text{kgm}/\text{m}^3}$$

then $$v = \sqrt{\frac{2\,g\,(931\,V - W/\rho)}{C_D\,A^* \times 10^3}} \qquad (2.25)$$

It can be seen that in equation (2.25) the only variable for a particular balloon is the density of the atmosphere $\rho(z)$ so as ρ decreases the ascent rate v will decrease until at the equilibrium level it becomes zero.

For a tetroon with length of side (L) of 1.966 m filled with hydrogen, with a gas release valve attached, the initial ascent rate will be approximately 3.6 mps. or 215 m/min.

(b) Balloons with a fixed amount of lifting gas weighed off to give a particular superpressure at the equilibrium height

In this case the balloon will not be filled with lifting gas when it is released but the gas will be free to expand as the balloon ascends and the atmospheric pressure decreases, until it reaches its equilibrium height where it has filled its volume which is fixed at V_e. Again, the ascent rate may be derived from equation (2.23) but since the balloon is free to expand during the ascension the factor (PV/T) is constant, from the gas laws, while the effective area of the balloon, A*, is increasing as the balloon expands.

Thus $$v = \sqrt{\frac{2\,g\,(432.2\,(P/T)\,V - W)}{C_D(A^*\rho) \times 10^3}} \qquad (2.26)$$

where all the parameters on the right hand side are constant except A* and ρ, A* increasing with height and ρ decreasing with height, so that the factor $(A^*\rho)$ is essentially constant with height so that the ascent rate will be constant. This has been observed on actual balloon flights.

The superpressure for a particular balloon is given by equation (2.11):

i.e. $$p_s = \frac{F_L}{W} p_e \qquad (2.11)$$

and the free lift of a balloon is given by equation (2.22):

i.e. $$F_L = \tfrac{1}{2} \rho v^2 C_D A^* (nt) \qquad (2.22)$$

However, F_L in (1.11) is in grams wt., therefore converting (2.22)

$$F_L = (\tfrac{1}{2} \rho v^2 C_D A^*/g) \times 10^3 \text{ gm.wt.}$$

Substituting:

$$p_s = (\tfrac{1}{2} \rho v^2 C_D A^* p_e/gW) \times 10^3 \qquad (2.27)$$

For a particular balloon W, g, C_D, p_e and (ρA^*) are constant, therefore let

$$K_B = (\tfrac{1}{2} p_e C_D A^* \rho/gW) \times 10^3 \qquad (2.28)$$

Hence

$$p_s = K_B v^2 \qquad (2.29)$$

The maximum value of superpressure allowed will be determined by the strength of the balloon materials and the construction. This maximum value of superpressure will determine the maximum ascent rate attainable within the set limits of safety, i.e.

$$\max (v) = \sqrt{\frac{\max (p_s)}{K_B}} \qquad (2.30)$$

CHAPTER 3

CHARACTERISTICS AND PROPERTIES OF BALLOON MATERIALS

1. Introduction

Different types of balloons obviously require materials with different properties. For example, a vertical sounding balloon needs to be extensible so that rubber or neoprene is used, whereas a horizontal sounding balloon needs to be inextensible so that a plastic such as polyethylene or polyester is used. This chapter only considers horizontal sounding balloons so discusses only the properties of the plastics available, viz.:

(i) Polyethylene: Low density polyethylene only is discussed and is referred to as polythene.

(ii) Polyethylene Terephthalate: Manufactured by I.C.I. as 'Melinex' and Du Pont as 'Mylar'. 'Melinex' type S and 'Mylar' type A are referred to as polyester.

Ideally a constant volume superpressure balloon should have the following properties:

(a) A very large modulus of elasticity, in the order of 10^9 nt/m^2, so that it maintains a constant volume for reasonable values of superpressure.

(b) Be transparent to all radiation so that the balloon will be at the same temperature as the surrounding air.

(c) Be impermeable to oxygen, nitrogen, hydrogen, helium and water vapour so that there is no loss of lifting gas and no increase in the balloon's weight due to the inward diffusion of the atmospheric gases.

(d) Be able to be sealed readily with a seal strength equal to the strength of the balloon material itself.

(e) Be plastic at room temperatures for ease of manufacture and so that it does not crack when folded for packing and transportation. Lally (1967) also suggests that it is desirable that the balloon be 'glassy' at the floating altitude so that it will shatter if struck by an aircraft.

2. Structural Properties

(a) Polythene

The properties of a given polythene depend primarily on two factors, its average molecular weight and its density, both of which may be controlled in the polymerisation process. Polythene has a molecular structure consisting of long chain polymers containing 600 - 4000 Methylene groups per molecule.

e.g. $\ldots - CH_2 - CH_2 - CH_2 - CH_2 - \ldots$

They also contain less than 1% olefinic and other groups. There appears to be less than one olefinic bond per molecule.

In an unstressed state most of the molecules can be considered to be in partially curled configurations. The molecules continually change their shape executing micro-Brownian motion, but this is entirely random so there is no discernable motion.

Upon the application of moderate stresses the process becomes stress-biased in that the net motion of the molecules will then result in an orientation in the direction of the stress. When the load is removed the diffusion process is again random, thus it is an elastic or plastic process.

A permanent change of molecular configuration requires higher stress levels, causing a breaking up of complete chain entanglements.

At room temperature polythene is a partially amorphous partially crystalline material in the unstressed state, but on the application of a strain a first order transition involving increased crystallisation occurs. Lowering the temperature can also cause this transition. The crystallisation is time dependent, the rate being proportional to the stress magnitude.

Below about $-80^{\circ}C$ a second order transition takes place in which intrinsic properties, such as heat capacity and thermal expansion, suddenly change and the material becomes "brittle" or "glassy".

The macroscopic results of these properties are essentially shown by four types of deformation:

(a) An instantaneous shift of chain segments from the local potential energy minimum. (The initial elastic response.)

(b) A diffusion of the chain segments by the mechanism of micro-Brownian movement in the stress direction. (The retarded elastic or plastic response.)

(c) A breaking down of the chain entanglements under stress. (Irreversible creep.)

(d) An increased crystallisation caused by the increased molecular attraction due to (b).

(b) Polyester

Polyester has plastic properties like polythene but it has a larger modulus of elasticity and higher tensile strength. Structurally instead of the Methylene chain polymer it has a polyethylene terephthalate polymer. Also it has a more complicated manufacturing process than polythene and some other plastic films.

The polymer is first extruded through a slot die as a continuous sheet, after which it is cooled rapidly to prevent it from crystallising. At the next stage the film is heated and drawn in two directions at right angles. This has the effect of arranging the molecules in a systematic pattern so that they lie in the plane of the film but in no

particular direction in that plane, thus giving the film its greater strength. Because the film is stressed equally in two directions at right angles it has uniform properties in both longitudinal and transverse directions. Some manufacturers produce polyester with greater longitudinal strength for particular applications.

3. Mechanical Properties

Table 3.1: Mechanical properties of polythene and polyester.

Property	Units	Polythene	Polyester
Ultimate Tensile Strength	nt/m^2	6.9×10^6	1.722×10^8
Tensile Modulus	nt/m^2	1.184×10^8	37.9×10^8
Ultimate Elongation	%	300 - 600	60 - 110
Stress to produce 5% Elongation	nt/m^2	4.6×10^6	1.0×10^8
Initial Tearing Strength	gm/mil	[illegible]	600
Propagating Tearing Strength (Elmendorf)	gm/mil	100 - 300	15
Bursting Strength (Mullen (1 mil)	nt/m^2	$6.9\text{-}8.3 \times 10^4$	41.3×10^4
Density	gm/cc	0.92	1.395
Folding Endurance	cycles	65 - 575	10^5

(a) Elasticity

Figure 3.1 shows the graph of the applied force vs the resulting extension of a 1 m long sample of 3 mil polythene (Cherry (1969)). Since the sample is 1 m long the extension is equal to the strain. This sample shows typical plastic behaviour and is indicative of the performance of both polythene and polyester.

FIG 3.1:
APPLIED FORCE VS EXTENSION

FOR A POLYETHYLENE SAMPLE, 1 METRE LONG, 0.1 METRE WIDE, 3 MIL THICK.

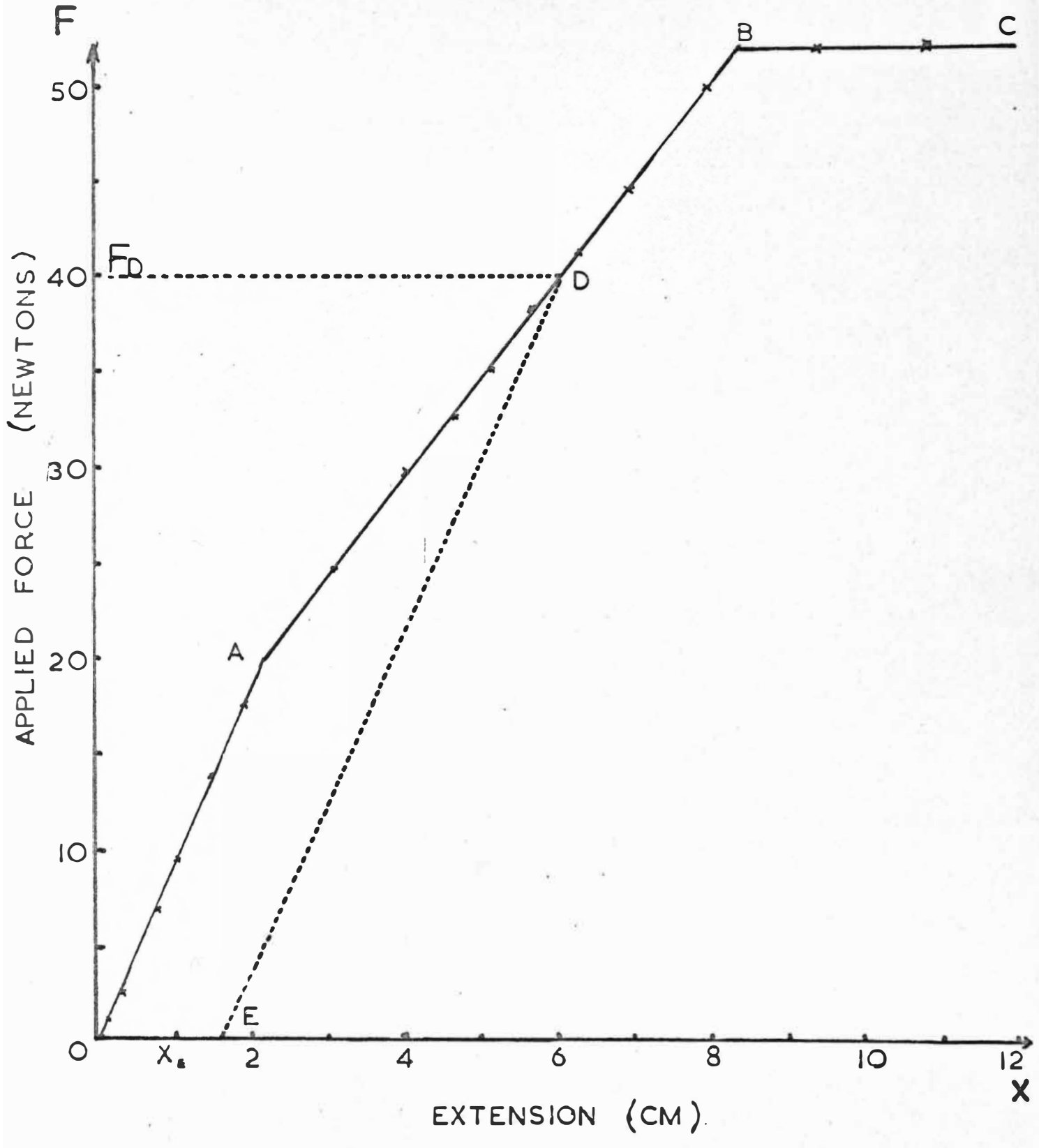

OA is the elastic region corresponding to (a) above in the section on structure.

AB is the constrained plastic region corresponding to (b) above.

BC is the fully plastic region, corresponding to irreversible creep as in (c) above.

A sample taken up to D and released, will unload elastically along DE and arrive at E in a state of self-stress. If reloaded immediately it can stand a load F_D without further plastic deformation.

For the elastic region OA we can define a tensile (Young's) modulus Y:

$$Y = \frac{\text{stress}}{\text{strain}} = \frac{\Delta F/A}{\Delta x/x} = \frac{F}{x}\frac{x}{A} \qquad (3.1)$$

where F is the applied force (nt),

A is the cross-sectional area (m^2),

x is the length of the sample (m),

Δx is the extension due to F (m).

From Fig. 3.1

$Y = 1.184 \times 10^8$ nt/m^2 for polythene,

or $Y = 1.72 \times 10^4$ psi.

From table 1 it can be seen that the tensile modulus of Polyester is about 32 times greater than this, i.e.:

$Y = 37.9 \times 10^8$ nt/m^2 for polyester,

or $Y = 55 \times 10^4$ psi.

Also from fig. 3.1 it can be seen that the maximum stress for the elastic region for polythene is:

$$\sigma_m = \frac{F_m}{A} = 2.63 \times 10^6 \text{ nt/m}^2 \qquad (3.2)$$

(b) Creep

For a plastic substance it is not true that the same stress produces the same strain no matter how long the stress is applied. The plastic will glide, in time, under a constant stress. Plastic glide is a form of flow like liquid flow except that the atomic movements are crystallographically organised, and occur as creep at constant stress.

The slowness of the creep suggests that it is a thermally activated process, and in fact, creep rates at a given stress usually increase by a factor of 2 or 3 for each 10^{o}K temperature rise.

For polyester the creep is very small for normal stresses but for polythene the creep is an important factor.

(c) Creep in Polythene

Assuming the incompressibility of plastic (Alexander 1967) then

$$l\ w\ t = l_o w_o t_o = \text{constant}$$

where 'o' refers to the initial unstressed state. The stress is

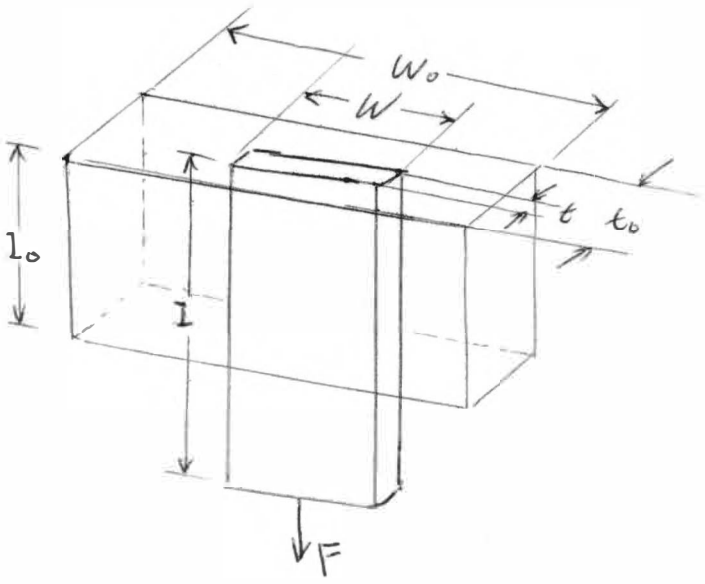

$$\sigma = \frac{F}{A} = \frac{F}{wt} = \frac{F}{A_o}\lambda \quad (3.3)$$

where $\lambda = \frac{l}{l_o}$

Fig. 3.2 shows the extension, $\Delta l = l - l_o$, vs time for a sample of polythene 1 m long initially. (Uniaxial Creep) Temperature = 33°C.

Figure 3.3 shows the extension vs time under biaxial stress, n = 1, of a sample initially 1 m long at 33°C. n is the ratio of the stresses in the two perpendicular axial directions.

Conclusions:

Initially there is an elastic-plastic deformation which is quite quick, and in the order of 15 - 30 minutes it settles down to a slow creep rate C_r,

with uniaxial stress $C_r = 1.65 \times 10^{-3}$ m/hr

with biaxial stress $C_r = 8.25 \times 10^{-4}$ m/hr

for a stress of 4.2×10^6 nt/m^2.

As a function of stress $C_r = 2.33^{4/3} \times 10^{-12}$ m/hr uniaxial stress

and $C_r = 1.15^{3/2} \times 10^{-13}$ m/hr biaxial stress.

FIG 3.2 : EXTENSION VS TIME

FOR A 1 M. LONG SAMPLE OF POLYETHYLENE UNDER UNIAXIAL STRESS. (TEMPERATURE 33 °C)

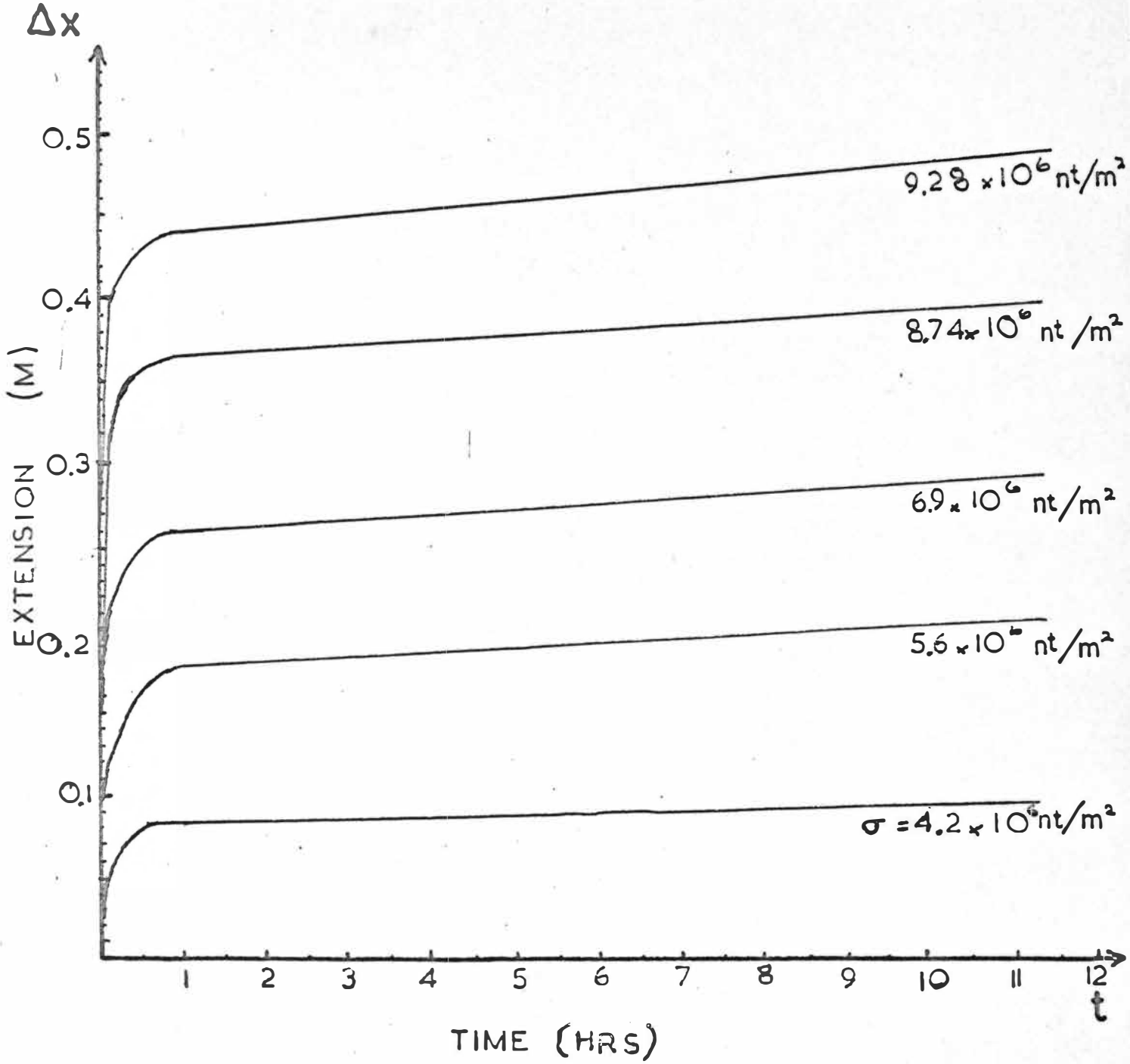

ALEXANDER H. JAN'67 : AFCRL-67-0075 SPECIAL REPORT Nº 57, PROCEEDINGS, 4 TH AFCRL SCIENTIFIC BALLOON SYMPOSIUM III. P 19. CREEP CHARACTERISTICS OF POLYETHYLENE FILM.

FIG 3.3:
EXTENSION VS TIME

FOR A 1 M. LONG SAMPLE OF POLYETHYLENE UNDER BIAXIAL STRESS. (TEMPERATURE 33°C) EQUAL STRESSES.

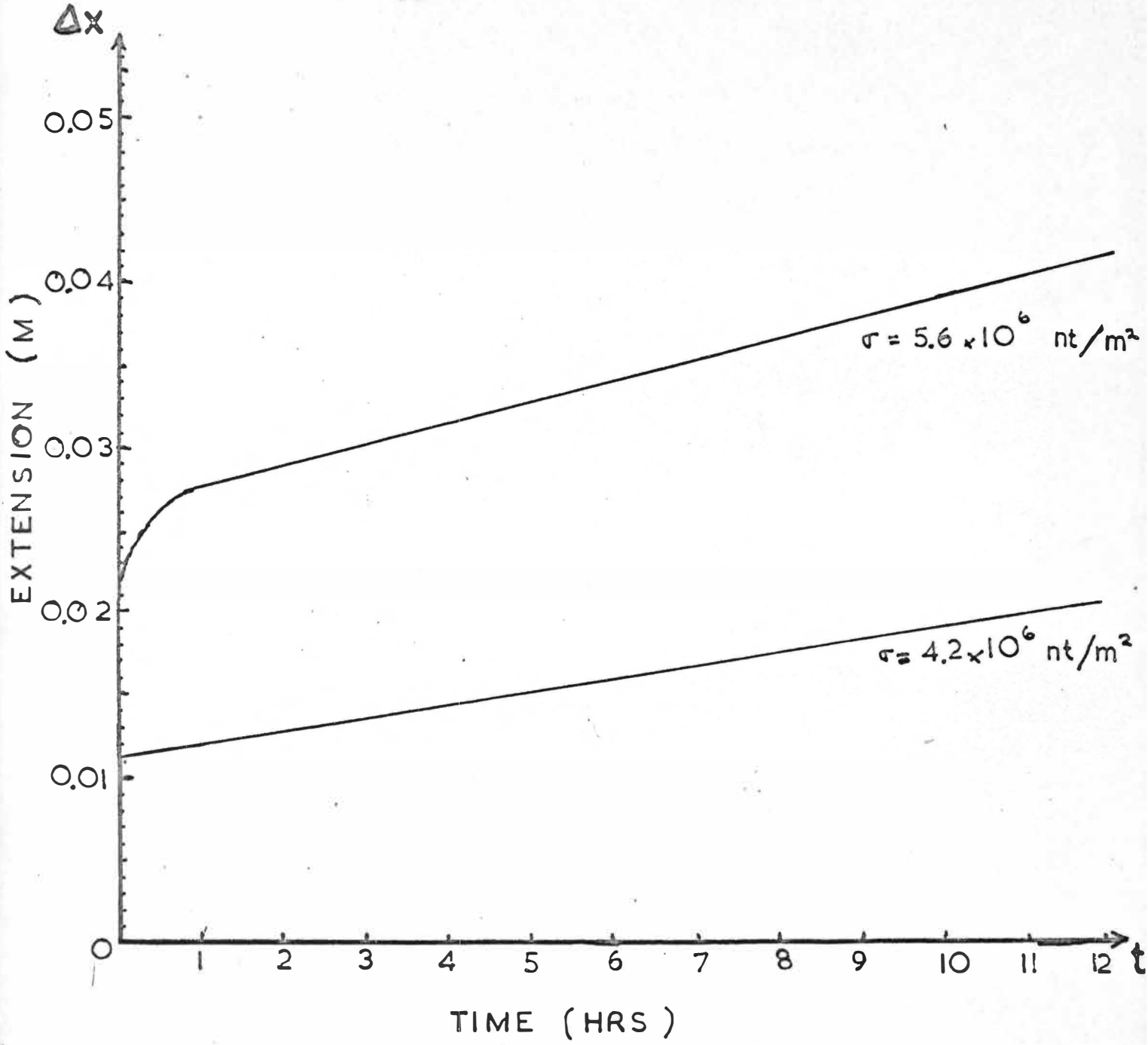

(ALEXANDER H., JAN '67.)

(d) Relation between Superpressure and Film Stress

For a spherical balloon with radius r metres at a superpressure of p_s nt/m^2, the surface tension T nt/m may be defined as the work done in isothermally stretching the balloon film by 1 m^2.

Let the superpressure increase by dp_s resulting in the radius increasing from r to r + dr.

Work done by the superpressure $W_p = p_s \, 4\pi r^2 \, dr$

(neglecting 2nd order terms)

Work done on the surface $W_s = T \, d(4\pi r^2)$

$$W_s = 8 \pi T \, r dr$$

Equating $W_p = W_s$ gives

$$p_s = \frac{2T}{r} \quad \text{for a spherical balloon.} \qquad (3.4)$$

For a nonspherical balloon this can be generalised to:

$$p_s = T \left(\frac{1}{r_1} + \frac{1}{r_2} \right) \qquad (3.5)$$

where r_1 and r_2 are the radii of curvature of the surface in perpendicular planes.

Considering an arbitrary cross-section of the surface, width w metres and thickness t metres, with surface tension T and stress σ.

Now T = Force per unit length of cross-section

$$= \frac{F}{w} \text{ nt/m}$$

$$\text{or} \quad F = w\,T\,nt$$

$$\therefore \sigma = \frac{F}{A} = \frac{wT}{wt} = \frac{T}{t} \quad nt/m^2 \tag{3.6}$$

Therefore the stress for a given superpressure will be given by

$$\sigma = \frac{p_s}{t\left(\frac{1}{r_1} + \frac{1}{r_2}\right)} \tag{3.7}$$

Hence in common balloon units:

$$\sigma = \frac{5.25\,p_s}{t\left(\frac{1}{r_1} + \frac{1}{r_2}\right)} \times 10^6 \tag{3.8}$$

$$\text{or} \quad p_s = 1.905\,\sigma\,t\,(r_1+r_2)/r_1r_2 \times 10^{-7} \tag{3.9}$$

where σ is the stress in nt/m^2,

p_s is the superpressure in mm of Hg,

t is the thickness of the balloon film in mils,

r_1, r_2 are the radii of curvature in m in two perpendicular planes.

Since the surface tension is proportional to the radii of curvature of the surface the maximum stress will occur where the factor r_1r_2 is greatest. For a sphere $r_1 = r_2 = r$, therefore;

$$\sigma = \frac{5.25\,r\,p_s \times 10^6}{2\,t} \tag{3.10}$$

over the whole surface of the sphere. For a tetroon the maximum stress occurs at the centre of each of the triangular faces where the curvature has a radius of the order of L, the length of the side of the tetroon. Thus $r_1 = r_2 = L$. Therefore the maximum stress in the surface of the tetroon is given by

$$\sigma_{max} = \frac{5.25\ L\ p_s \times 10^6}{2\ t}$$

and the maximum superpressure allowed (3.11)

$$p_s\ max = 3.81\ (t/L)\ \sigma_{max} \times 10^{-7}$$

For example: For an L = 2m tetroon this gives a maximum superpressure for:

(a) A 3 mil polythene film:

p_s max = 1.5 mm for the elastic region,

and p_s max = 3.75 mm for the plastic region.

(b) A 1 mil polyester film:

p_s max = 19.1 mm for 5% elongation,

and p_s max = 32.8 mm for ultimate yielding.

(e) <u>The Effect on the Volume, Stress and Superpressure of a Forced Change in Height</u>

If a balloon is forced by the airflow to fly above its equilibrium height the two major factors need to be considered:

(a) The decrease in atmospheric pressure will cause an increase in the differential pressure across the balloon film, increasing the superpressure and the film stress. If this increase is large enough the balloon will burst.

(b) The increase in stress will tend to stretch the balloon (elastically or plastically depending on the magnitude of the stress) increasing its volume, thus decreasing the increased superpressure.

(f) Superpressure and Volume Perturbations

Let the balloon, assumed to be made out of an elastic material, have volume V at its equilibrium level where the ambient pressure is p_e and the internal balloon pressure is p'_e. Then the superpressure is:

$$p_s = p'_e - p_e \tag{3.12}$$

If the balloon is forced to rise the ambient atmospheric pressure will drop to $(p_e - \Delta p)$ resulting in an increase in the balloon's volume ΔV and changing the internal pressure of the balloon to p'_{ep}. Thus the new superpressure will be:

$$p'_s = p'_{ep} - (p_e - \Delta p) \tag{3.13}$$

From the gas laws:

$$p'_e V = p'_{ep} (V + \Delta V) \tag{3.14}$$

Substituting for p'_e and p'_{ep} from (3.12) and (3.14) in (3.13)

$$p'_s = p_s + \Delta p - (\Delta V/(V+\Delta V))\, p'_e \qquad (3.15)$$

Thus the increase in superpressure Δp_s is:

$$\Delta p_s = p'_s - p_s$$

so from (3.15)

$$\Delta p_s = \Delta p - (\Delta V/(V+\Delta V))\, p'_e \qquad (3.16)$$

If the volume is fixed, i.e. $\Delta V = 0$, then (3.16) gives

$$\Delta p_s = \Delta p$$

as expected. If however, there is an increase in the volume then the resulting increase in superpressure is less than Δp.

(g) Stress and Volume Perturbations

If the stress of the balloon film σ, increases by $\Delta\sigma$, then the balloon, in the elastic region, will expand elastically giving a change in the linear dimension L of ΔL, and a change in the volume V of ΔV. The volume of the balloon will be of the form

$$V = K L^3 \qquad (3.17)$$

where $K = \frac{4}{3}\pi$ for a sphere and L is the radius of the sphere,

and K = 0.177 for a tetroon and L is the length of the side. Thus the increased volume will be:

$$V + \Delta V = K(L + \Delta L)^3$$

From (3.1) $$Y = \frac{\Delta\sigma}{\Delta x/x} \qquad (3.1)$$

$$\therefore \quad \Delta L = \frac{\Delta\sigma L}{Y} \qquad (3.18)$$

$$\therefore \quad V + \Delta V = K L^3 \left(1 + \frac{\Delta\sigma}{Y}\right)^3$$

so that

$$\Delta V = V\left(\frac{3\Delta\sigma}{Y} + 3\left(\frac{\Delta\sigma}{Y}\right)^2 + \left(\frac{\Delta\sigma}{Y}\right)^3\right) \qquad (3.19)$$

For polythene Y is about 10^8 nt/m^2 and stress is about 10^6 nt/m^2. Thus the factor $(\Delta\sigma/Y)$ is of the order of 10^{-2} and for polyester it is of the order of 10^{-3} so that the second and third order terms may be neglected.

Therefore

$$\Delta V = 3\,V\,\frac{\Delta\sigma}{Y} \qquad (3.20)$$

is a good approximation to (3.19).

(h) <u>Stress, Volume and Superpressure Perturbations</u>

There are three equations which relate perturbations in stress, volume and superpressure to each other, viz:

From (2.11)

$$\Delta\sigma = C\,Y\,\Delta\,p_s \qquad (3.21)$$

where

$$C = \frac{2.625\ L}{Y\ t} \times 10^6 \quad (m/nt/m^2\text{-mil}) \tag{3.22}$$

From (3.16)

$$\Delta p_s = \Delta p - \frac{\Delta V}{V + \Delta V} p'_e \tag{3.16}$$

and from (3.20)

$$\Delta V = 3\ V \frac{\Delta\sigma}{Y} \tag{3.20}$$

Substituting from (3.21)

$$\Delta V = 3\ C\ V\ \Delta\ p_s \tag{3.23}$$

Using (3.20) and (3.21) to eliminate ΔV and $\Delta\sigma$ from (3.16) an expression for the increase in superpressure due to an increase in height (resulting in a drop in the ambient pressure of Δp) which takes into account the elasticity of the balloon is obtained:

$$\Delta p_s = -\frac{1}{6C} + \frac{\Delta p - p'_e}{2} \pm \sqrt{\frac{1}{36C^2} + \frac{(\Delta p + p'_e)}{6C} + \frac{(\Delta p - p'_e)^2}{4}} \tag{3.24}$$

and the increase in stress:

$$\Delta\sigma = -\frac{Y}{6} + \frac{CY}{2}(\Delta p - p'_e) \pm \sqrt{\left(\frac{Y}{6}\right)^2 + \frac{C^2Y^2}{6}(\Delta p + p'_e) + \frac{C^2Y^2}{4}(\Delta p - p'_e)^2} \tag{3.25}$$

Once Δp_s or $\Delta\sigma$ has been calculated the other two factors may be calculated from (3.16), (3.21) and (3.23). For example:

If a tetroon whose equilibrium height is 12 km (p_e = 145 mm) is displaced upwards by the airflow through a height of 1 km (Δp = 20 mm) then:

(a) For a 3 mil polythene balloon with an equilibrium superpressure of 3 mm, L = 3.3 m:

$$\Delta p_s = 3.1 \text{ mm}$$

$$\Delta \rho = 5.35 \times 10^6 \text{ nt/m}^2$$

$$\Delta V = 0.179 \text{ m}^3$$

This stress increases the stress at the centre of the tetroons' faces beyond the elastic limit. However, if the balloon is taped (see section on balloon volume) it can be seen from Fig. 4.1 that the volume vs superpressure curve will still be linear so the balloon as a whole will react elastically. Hence a polythene balloon would be able to withstand a 1 km displacement at 12 km without going beyond its effective elastic region.

(b) for a 1 mil polyester balloon with an equilibrium superpressure of 10 mm, L = 2 m:

$$\Delta p_s = 12.7 \text{ mm}$$

$$\Delta \sigma = 46.3 \times 10^6 \text{ nt/m}^2$$

$$\Delta V = 0.075 \text{ m}^3$$

This stress is well within the elastic region for polyester,

so a polyester balloon can easily withstand the increased pressure due to a 1 km displacement from a natural equilibrium height of 12 km.

4. Thermal Properties

The supertemperature of a balloon due to the absorption of radiation by the balloon film has already been considered. This section considers the effect of the thermal properties of the plastic film which have an effect on the stress, volume and superpressure of the balloon and thus its equilibrium height and its overall performance.

Table 3.2: Thermal properties of Polythene and Polyester.

Property	Units	Polythene	Polyester
Specific Heat	Cal/gm/^{o}C	0.55	0.315
Thermal Conductivity	$\frac{\text{cal-mil}}{\text{sec-}^{o}\text{C-m}^{2}}$	3.15×10^{3}	0.353×10^{3}
Coefficient of Expansion	$^{o}\text{C}^{-1}$	22×10^{-5}	2.7×10^{-5}
Melting Point	^{o}C		265
Service Temperature	^{o}C		-60 - 150
Heat Seal Temperature	^{o}C		230

Table 3.3: Properties of Hydrogen and Helium

Gas	Molecular Weight	Specific Heats*			
		C_v	C_p	$C_p - C_v$	$\frac{C_p}{C_v}$
Hydrogen	1.008	4.88	6.87	1.99	1.41
Helium	4.003	2.98	4.97	1.99	1.67

*Unit of specific heats is cal/mole-^{o}C.

(a) Heat Capacity of a Balloon

The heat capacity of a balloon C_b will be the sum of the heat capacity of the plastic film and the heat capacity of the lifting gas, i.e.

$$C_b = m_f s_f + n\, C_v \quad \text{cal}/^{o}\text{C} \qquad (3.26)$$

where m_f = mass of the plastic film in grams,

s_f = specific heat of the plastic film in cal/gm,

n = number of moles of lifting gas in the balloon

= mass of the lifting gas/molecular weight,

C_v = specific heat of constant volume of the lifting gas.

For example for L = 2m tetroons using hydrogen as the lifting gas:

C_b = 575 cal/^{o}C for 3 mil polythene

and C_b = 444 cal/^{o}C for 1 mil polyester.

In each case the hydrogen contributes 311 cal/^{o}C.

(b) Temperature Response of a Balloon to changes in the Ambient Temperature

A change in the ambient temperature at a given level will be very slow but for a balloon rising through the atmosphere to its equilibrium height the ambient temperature will be changing continuously over a large range of temperatures. This will cause a differential temperature across the plastic film and will result in a flow of heat through the film from the gas inside the balloon to the air outside.

Consider the balloon and gas to be at the same temperature T_o ^{o}K for the initial condition, as will be the case as a balloon is released from the ground. Let the balloon experience a change in the ambient temperature at a rate of $\frac{dT}{dt}1$ ^{o}K/sec which results in the temperature of the lifting gas changing at a rate of $\frac{dT}{dt}2$ ^{o}K/sec. After a time Δt the temperature outside and inside the balloon respectively will be:

$$T_1 = T_o + \frac{dT}{dt}1 \, \Delta t \qquad (3.27)$$

and

$$T_2 = T_o + \frac{dT}{dt}2 \, \Delta t \qquad (3.28)$$

resulting in a differential temperature

$$T_1 - T_2 = \left(\frac{dT}{dt}1 - \frac{dT}{dt}2\right) \Delta t \qquad (3.29)$$

This will cause a flow of heat ΔQ, given by:

$$\Delta Q = \frac{K\ A\ (T_1 - T_2)}{dx}\ \Delta t \qquad (3.30)$$

where ΔQ = heat flow in cals,

K = thermal conductivity of the plastic film in cal-mil/sec-^{o}K-m^2.

dx = thickness of the balloon film in mils.

This heat loss may also be expressed in terms of the temperature change of the lifting gas, viz.:

$$\Delta Q = n\ C_v\ \Delta\ T_2\ \Delta\ t \qquad (3.31)$$

where n = number of moles of lifting gas,

C_v = specific heat of constant volume of the lifting gas,

and ΔT_2 = the resulting change in T_2, the temperature inside the balloon.

Hence from (3.28)

$$\Delta T_2 = \frac{dT}{dt}2\ \Delta t \qquad (3.32)$$

Equating (3.30) and (3.31) and substituting from (3.32)

$$\frac{dT_2}{dt^2} = C_t\ \frac{(T_1 - T_2)}{\Delta t} \qquad (3.33)$$

where

$$C_t = \frac{K\ A}{n\ C_v\ dx} \qquad (3.34)$$

Therefore from (3.29) and (3.33)

$$\frac{dT_2}{dt} = -\frac{C_t}{1 + C_t}\frac{dT_1}{dt} \qquad (3.35)$$

And from (3.29) and (3.35) the resulting differential temperature is:

$$T_1 - T_2 = \frac{1}{C_t + 1}\frac{dT_1}{dt}\,\Delta t \qquad (3.36)$$

It can be seen from (3.34) that C_t is a function of n which for a sealed balloon (i.e. one without a gas release valve) is constant so that C_t is then a constant for a particular balloon. However, if a gas release valve is fitted n will decrease as the gas outgases but will become constant after the valve has closed off near the equilibrium level. During the ascent in this case n will be a function of density, and thus the ratio (P/T). viz.:

$$n = k\,(P/T)\,V \qquad (3.37)$$

where V is the volume of the balloon in m^3

and k = 32.18 mole-$^oK/m^3$-mm for hydrogen,

and k = 16.05 mole-$^oK/m^3$-mm for helium.

Thus C_t becomes

$$C_t = \frac{K\,A}{k\,(P/T)\,V\,C_v\,dx} \qquad (3.38)$$

For example: An L = 2m tetroon of 1 mil polyester using hydrogen as the lifting gas and carrying 180 gm load will have an equilibrium level of about 12.5 km.

(a) If it has a fixed amount of lifting gas such that the equilibrium superpressure is 10 mm, then it will have a volume of 0.417 m^3 on the ground where (P/T) = 2.64 (U.S. Std.Atm.1966).

Hence n = 35.3 moles and C_t = 14.2.

Assuming an ascent rate of 3 m/sec and a temperature lapse rate of 7°K/km, then:

$$\frac{dT}{dt}_1 = 2.1 \times 10^{-3} \ ^\circ K/sec$$

Therefore $$\frac{dT}{dt}_2 = 1.935 \times 10^{-3} \ ^\circ K/sec$$

which will lead to a supertemperature at 10 km of 0.42°K.

(b) If the balloon is filled at the ground and fitted with a gas release valve then at the ground C_t = 4.17 and at 10 km C_t = 12.2. Assuming that C_t increases uniformly, the supertemperature can be calculated from the mean value $\overline{C}_t$ = 8.185. For the same ascent rate and lapse rate as in (a) above this gives a value for the supertemperature at 10 km of 0.7°K.

In both cases it can be seen that the resulting supertemperature is negligible.

(c) Response Time for Heat Loss from a Balloon

In situations such as when the lifting gas is compressed to form the superpressure, the balloon gas is at a higher temperature than the ambient air and not in equilibrium with it. Thus heat is lost from the balloon gas through the plastic film. A consideration of the rate of heat loss from the balloon leads to an expression for the supertemperature resulting from the compression of the gas, as a function of time.

The excess heat energy of the balloon gas Q is:

$$Q = n C_v (T_g - T_a) \qquad (3.39)$$

where n is the number of moles of lifting gas,

C_v is the specific heat of constant volume of the lifting gas,

T_a is the ambient air temperature, assumed constant,

and T_g is the initial temperature of the balloon gas just after it has been heated. The heating is assumed to be instantaneous.

If T(t) is the internal temperature of the balloon as a function of time t, t being the time after the heating occurred, then the excess heat at time t is:

$$Q(t) = n C_v (T(t) - T_a) \qquad (3.40)$$

Therefore the rate of heat loss is:

$$\frac{dQ(t)}{dt} = n C_v \frac{dT(t)}{dt} \qquad (3.41)$$

Now the rate of heat loss is governed by the conductivity of the plastic film, viz.:

$$\frac{dQ(t)}{dt} = \frac{K A (T(t) - T_a)}{dx} \qquad (3.42)$$

where K is the thermal conductivity of the plastic film,

A is the surface area of the balloon,

and dx is the thickness of the plastic film.

Equating (3.41) and (3.42)

$$\frac{dT(t)}{dt} + C_t T(t) = C_t T_a \qquad (3.43)$$

where

$$C_t = \frac{K A}{n C_v dx}$$

Solving (3.43) for T(t) gives:

$$T(t) = T_a + (T_g - T_a) e^{-C_t t} \ ^oK \qquad (3.44)$$

Thus the supertemperature resulting from this heating, as a function of time after the heating occurred is:

$$T_s(t) = (T_g - T_a) e^{-C_t t} \ ^oK \qquad (3.45)$$

Hence the time taken for the supertemperature to decrease to $T_s(t)$ is:

$$t = \frac{1}{C_t} \ln \frac{(T_g - T_a)}{(T_s(t))} \text{ secs} \qquad (3.46)$$

Hence the time taken for the supertemperature to decrease

(a) To one half its original value is:

$$t_{\frac{1}{2}} = \frac{0.693}{C_t} \text{ secs} \qquad (3.47)$$

(b) to 10% of its initial value is:

$$t(10\%) = \frac{2.303}{C_t} \text{ secs} \qquad (3.48)$$

(c) to 1% of its initial value is:

$$t(1\%) = \frac{23.03}{C_t} \text{ secs} \qquad (3.49)$$

For example: For an L = 2m, 1 mil polyester tetroon (C_t = 14.2) the supertemperature produced by the compression of the lifting gas should not exceed 30^{o}K. Therefore from (3.49) it can be seen that the supertemperature will be down to 0.3^{o}K in 1.62 secs.

Since the compression of the gas will take place over a longer period than this there will be no significant build up of supertemperature due to this cause although there will be a supertemperature due to the absorption of infrared radiation as discussed previously.

(d) Changes in Volume due to Changes in Temperature

If a length of material L experiences a change in temperature ΔT, then it will experience a change in length ΔL given by:

$$\Delta L = \alpha L \Delta T \qquad (3.50)$$

where α is the linear coefficient of expansion of the material. The volume will be of the form:

$$V = K L^3 \tag{3.17}$$

Hence

$$V + \Delta V = K (L + \alpha L \Delta T)^3$$

therefore

$$\Delta V = K L^3 (3\alpha\Delta T + 3\alpha^2(\Delta T)^2 + \alpha^2(\Delta T)^3) \tag{3.51}$$

Since α is very small the second and third order terms may be neglected. Thus a good approximation to the change in volume is:

$$\Delta V = 3 \alpha V \Delta T \tag{3.52}$$

For example: (a) an L = 2m, 3 mil polythene tetroon will experience a change in volume of -0.033 m^3 of 2.4% in ascending to 4 km.

(b) An L = 2m, 1 mil polyester tetroon will experience a change of volume of -0.008 or 0.57% in ascending through the troposphere.

For polyester, at least, this decrease is negligible.

5. Permeability and Diffusion Rate

An important consideration when choosing a material for balloon construction is the permeability of the material for the gases involved. It is not sufficient for the material to have a low permeability for hydrogen or helium but it must also have an even lower permeability for oxygen and nitrogen.

The rate at which a gas diffuses through a plastic film is given by:

$$\text{Rate of loss of gas} = \frac{\delta p A}{t} \quad m^3/hr \qquad (3.53)$$

and

$$\%\ \text{Rate of loss of gas} = 100\ \frac{\delta p A}{V t} \quad \%/hr \qquad (3.54)$$

where δ is the permeability of the film in $\frac{m^3 - mil}{m^2\text{-(mm of Hg)-hr}}$

p is the partial thickness of the film in mils,

t is the thickness of the film in mils,

A is the area in m^2,

and V is the volume in m^3.

Table 3.4: Permeability of Polythene and Polyester for various gases at 25°C. (Lally, 1967).

	H_2	He	O_2	N_2
Polythene	12.22×10^{-7}	10.26×10^{-7}	7.78×10^{-7}	2.78×10^{-7}
Polyester	0.99×10^{-7}	1.45×10^{-7}	0.495×10^{-8}	0.792×10^{-9}

The permeability, and hence the diffusion rate, is very dependent on temperature. The permeability drops off by a factor of approximately 1.5 per $10^{o}C$, i.e. it will drop off by a factor of approximately 25.6 due to the $80^{o}C$ drop in temperature in ascending through the troposphere.

C H A P T E R 4

BALLOONS AND BALLOON SYSTEMS

1. Introduction

In commencing this project I was restricted to the use of the only available materials, polythene and cellotape. My initial systems as a result were rather simple and crude, and resulted in the development of the tandem system which was designed to overcome the limitations set by the low strength of the polythene. Later, after I.C.I. had given me some polyester, I was able to construct stronger balloons. This chapter outlines some of the practical aspects involved in the development of the balloons and systems such as the volumes and drag coefficients of tetroons which had to be determined empirically. Also described are the balloon systems and an indication is given of their various performances, capabilities and limitations.

2. Balloon Shapes and Volumes

(a) Sphere: The optimum shape is of course the sphere since it has the largest volume to surface area ratio, but for a balloon other considerations are important, viz. ease of manufacture and strength. A sphere is difficult to construct from a flat sheet of plastic since it must be built

up from many segments and hence has many seams.

Volume of a sphere = $\frac{4}{3} \pi r^3$

Area of a sphere = $4 \pi r^2$

where r = the radius of the sphere.

(b) Cylinder or Pillow: A pillow is a cylinder with its ends sealed with straight seams.

Volume of a Cylinder = $\pi r^2 l$

Surface Area of a Cylinder = $2 \pi r l + 2 \pi r^2$

Volume of a Pillow = $\pi r^2 l'$

Surface Area of a Pillow = $2 \pi r l$

where r is the radius of the cylinder or pillow

l is the length of the cylinder or pillow

and l' is the modified length of the pillow to allow for the shaped ends.

A pillow is easier to construct than a cylinder because all its seams are straight but its volume is slightly smaller for the same length because of the shape of the ends.

(c) Tetroon: A tetroon is a tetrahedral balloon with four equilateral triangular faces whose sides have length L. It is constructed from a rectangular piece of plastic film of length 2L and width 0.866L. The two short edges are joined together, then the other two edges are sealed at right angles to each other.

Volume of a tetrahedron = $\frac{1}{3}$ B h

where B is the area of the base of the tetrahedron

and h is the altitude of the tetrahedron.

Area of one side = B = $\frac{1}{2}$ L . $\frac{\sqrt{3}}{2}$ L

= $\frac{\sqrt{3}}{4}$ L^2

therefore the surface area of a tetrahedron, and thus the surface area of a tetroon = 4B = $\sqrt{3}$ L^2.

The altitude of the tetrahedron is:

$$h = (L^2 - \tfrac{1}{3} L^2)^{\frac{1}{2}} = \sqrt{\tfrac{2}{3}}\, L$$

therefore

Volume of a tetrahedron = 0.118 L^3.

Because a tetroon is made of plastic it does not retain a perfectly tetrahedral shape, but rather it distorts to accommodate a somewhat larger volume of gas. I determined the actual volume of a tetroon by three methods:

(1) By weighing a polythene balloon filled with carbon dioxide giving:

Volume of a tetroon = (0.177 ± 7%)L^3

(2) By weighing a polythene balloon filled with water giving:

Volume of a tetroon = (0.177 ± 2%) L^3

(3) By weighing off a polyester balloon filled with hydrogen giving:

Volume of a tetroon = $(0.176 \pm 0.2\%)\ L^3$

In the light of the above results the following expression for the volume of a tetroon was used:

$$V = 0.177\ L^3 \qquad (4.1)$$

The actual volume is dependent on the superpressure. Fig. 4.1 shows some curves of the volume of a polythene balloon as a function of superpressure. It can be seen that polythene cannot sustain even a small superpressure without large increases in volume. This is improved somewhat by taping the balloon. As long as the superpressure is less than about 10 mm of Hg this expansion can be used to advantage, as is seen in the section on stress, volume and superpressure perturbations, in the detection of vertical perturbations in airflows since the expansion reduces the restoring force towards the equilibrium level so that the balloon tends to follow the airflow very closely. The stretching of the plastic may lead to instabilities in the equilibrium height which in regular wave patterns will not be important, (Vergeiner and Lilly, 1970) and in hydraulic jump situations is to advantage.

Polyester, on the other hand, is extremely strong and undergoes very little expansion, as can be seen from Fig. 4.2. The increase in volume with superpressure is less than 2.2% up to about 75 mm of Hg so that for all polyester

FIG 4.1:
SUPERPRESSURE VS VOLUME

FOR AN L = 2.108 POLYETHYLENE TETROON USING CO_2, ADJUSTED BY 0.1 M TO ALLOW FOR STRETCHING DUE TO THE WEIGHT OF CO_2 ON THE BOTTOM FACE.

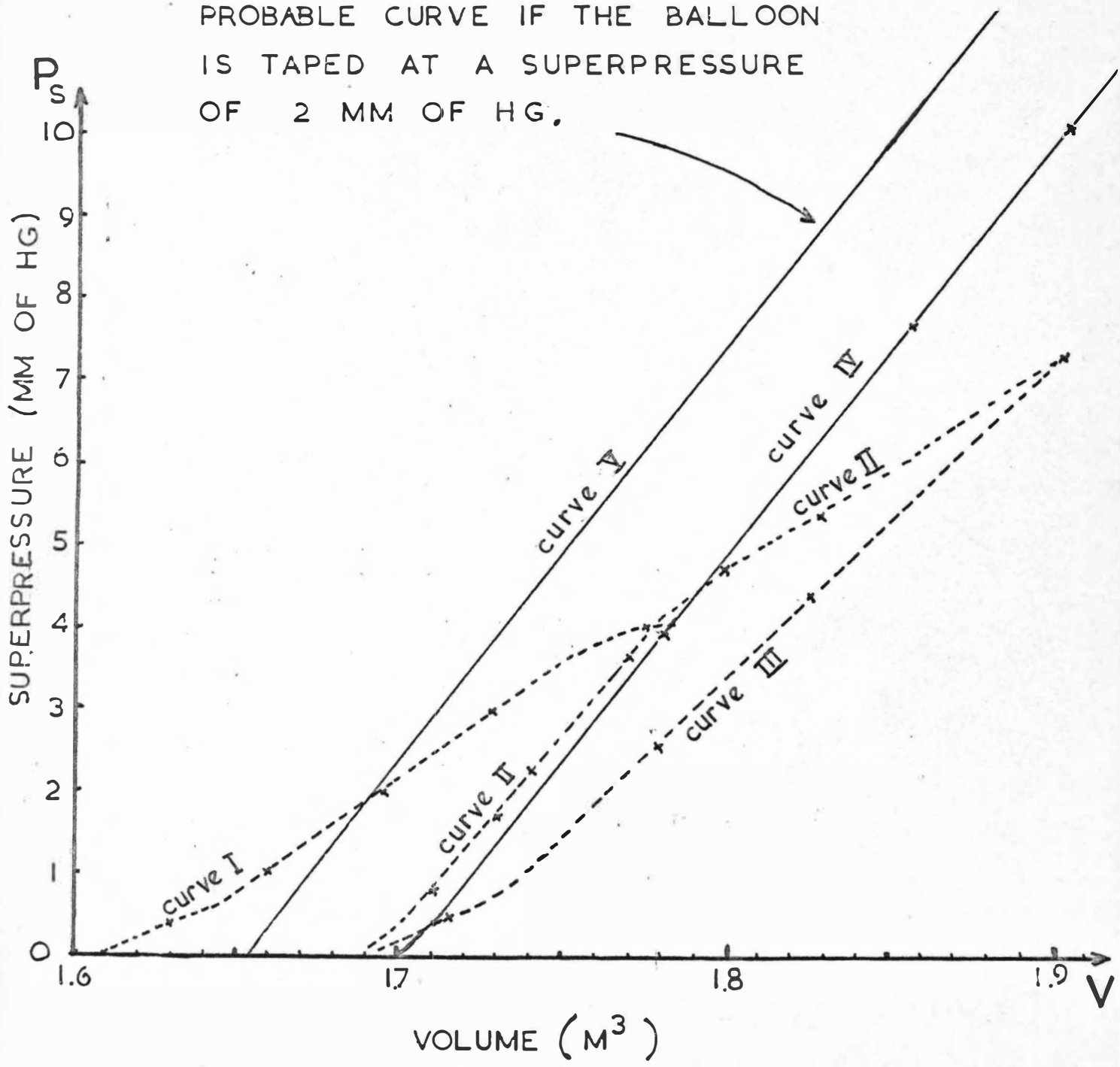

FIG 4.2:
SUPERPRESSURE VS % VOLUMETRIC DEFORMATION FOR A POLYESTER TETROON.

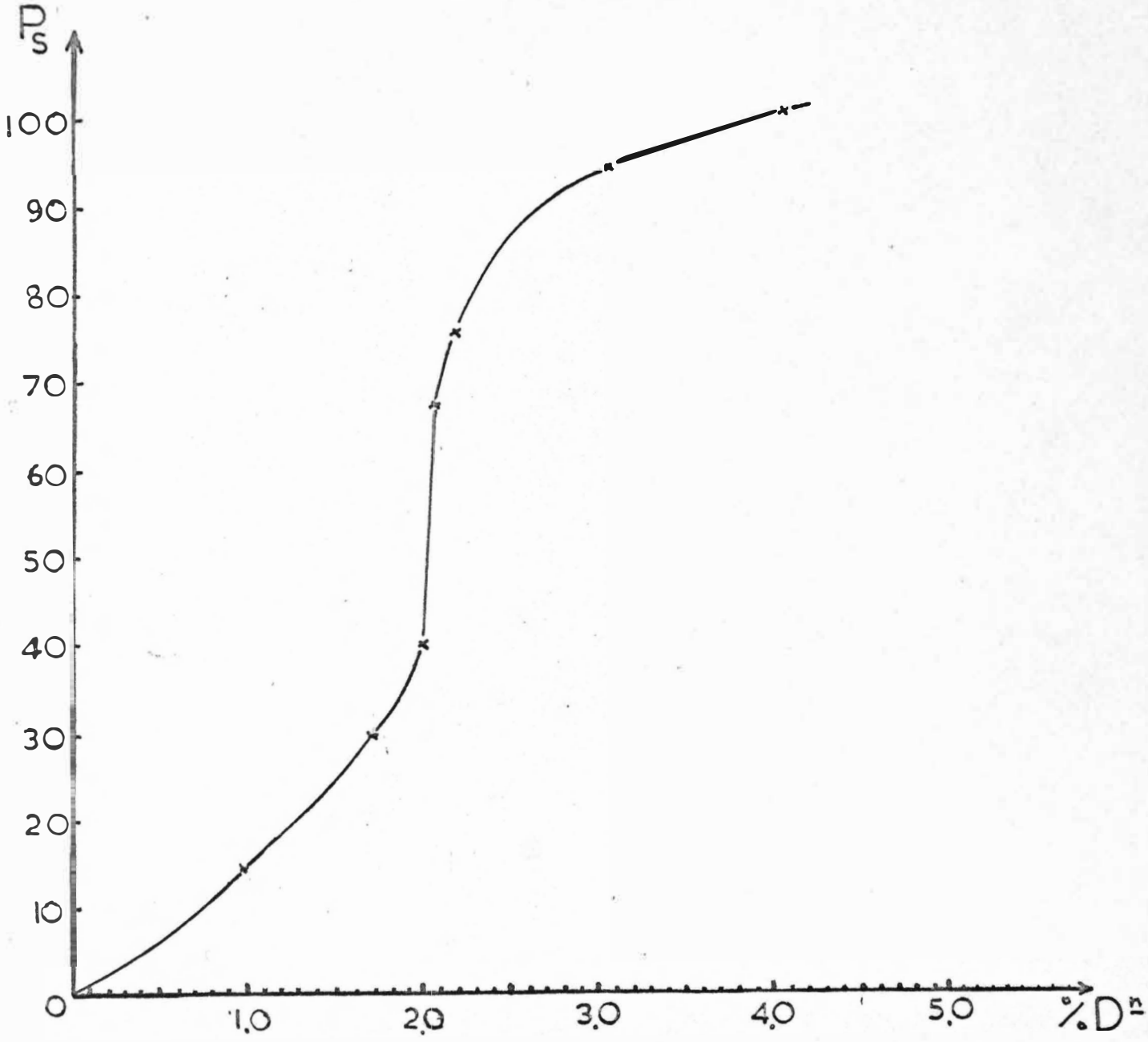

tetroons the volume can be taken as given by (4.1). See also the section on volume perturbations due to increased stress.

Table 4.1: A comparison of the surface area enclosing a volume of 1 m^3 for various balloon shapes.

Shape	Volume Formula	Area/($1m^3$)
Sphere	$\frac{4}{3}\pi r^3$	4.83 m^2
Tetrahedron	0.118 L^3	7.15 m^2
Tetroon	0.177 L^3	5.48 m^2

Note: The tetroon is only 13.5% less efficient than a sphere.

3. Balloon Systems

Introduction: Constant volume, superpressure balloons have been used quite successfully for lee wave studies so are the obvious choice of balloon for this project. With a knowledge of their response to the fluctuations of the airflow the actual streamline of an air particle can be fairly accurately determined. Since none was commercially available a suitable balloon or balloon system had to be developed. The requirements of the system were:

(a) A fast ascent rate so that the balloon would clear the ground quickly and avoid obstructions, ascend quickly through clouds and the icing layer to minimise the build up

of ice on the balloon and reach its equilibrium level as soon as possible. This would facilitate early radar acquisition and minimise the uncertainty of the balloon's position since the main release sites, Hokitika, Cass and Birdlings Flat, are some distance from the radar and lie behind hills or mountains. Hokitika, the most used release site, is situated upstream of the Southern Alps, 153 km away from the radar. The height of the mountains together with the curvature of the earth means that the balloon must be above 3.5 km before it can be sighted.

(b) A balloon that would have a fixed maximum volume to give a stable equilibrium height while still being capable of following the motions of the airflow.

Development

For a balloon to rise it must be able to expand, and for it to stay at an equilibrium level the volume must be constant. To obtain this in practice four main systems suggested themselves:

(a) An extensible balloon inside an inextensible envelope.

(b) An inextensible balloon which is strong enough to accommodate the superpressure of the lifting gas.

(c) A tandem system consisting of a lifting balloon (liftoon) with high lift towing a constant volume

balloon containing enough gas to give it zero lift or small enough lift that the gas can be contained as a superpressure by the balloon.

(d) A balloon with a gas release valve which would allow the balloon to be filled at the ground to give the required lift, then release the gas as the pressure tended to build up and close off just below the equilibrium level to maintain a super-pressure for stability.

(a) An extensible balloon inside an inextensible envelope:

This was tried using 1" square mesh nylon netting to construct a spherical envelope 1.67 m in diameter which enclosed a 500 gm rubber balloon (Balloon 1). The balloon burst at 7.7 km, probably due to a puncture caused by the roughness of the nylon netting. To overcome this 5 mil polythene was used as the envelope (Balloon 2). This also burst because the polythene was not strong enough to contain the superpressure resulting from the 500 gms of lift required to obtain an ascent rate of 3 m/sec. It became obvious some time later that this amount of lift would have resulted in a superpressure of about 118 mm of Hg, which would stress the polythene well beyond its elastic limit. With more knowledge this system would have worked but the greater efficiency of the later systems meant that it was not tried again.

(b) An inextensible balloon strong enough to contain the superpressure of the lifting gas (free balloon):

Initially only polythene was available so polythene tetroons were constructed and used successfully. However, the low tensile modulus and low tensile strength set the upper limit of the superpressure of a taped tetroon at 10 mm. This results in a maximum ascent rate of about 0.7 m/sec (Balloons 6 and 7).

Later I.C.I. (Great Britain) generously gave me a roll of 'Melinex' (referred to as polyester). Polyester has an ultimate tensile strength twentyfive times that of polythene. The ultimate tensile strength is the factor that limits the maximum superpressure that a balloon of a given size and thickness can contain and thus the maximum ascent rate attainable for a free balloon. Given the ultimate tensile strength the maximum superpressure can be calculated from equation (3.9).

For an L = 1m, 1 mil polyester tetroon equation (3.9) gives a value of 65.5 mm as the maximum superpressure. In carrying out a destruction test on a similar balloon I found that it burst at 62 mm, which is in good agreement with the result predicted by equation (3.9).

The maximum superpressure can then be substituted into equation (3.30) to give the maximum attainable ascent rate. However the constant K_B in (2.30) which is defined by (2.28),

must be modified to include the drag on the radar reflector. This is done by letting:

$$C_D A^* = C_{Dt} A_t^* + C_{Dr} A_r^* \qquad (4.2)$$

where C_{Dt} and C_{Dr} are the drag coefficients and A_t^* and A_r^* are the effective areas of the tetroon and radar reflector respectively. The drag coefficient of the radar reflector is taken as one, and its effective area as the area of square middle section which gives:

$$C_{Dr} A_r^* = 0.274 \qquad (4.3)$$

where A_r^* is in m^2.

For example:

(i) For an L = 2m, 1 mil polyester tetroon equation (3.9) mentioned above gives 33 mm as the maximum superpressure. From equation (2.11) an L = 2m tetroon with 90 gm of free lift has a superpressure at its equilibrium height of 30 mm. This amount of free lift will, from (2.30), together with the modification made in equations (4.2) and (4.3) result in an ascent rate of about 1.89 m/sec. Neglecting the radar reflector gives an ascent rate of about 2.06 m/sec, an increase of 8%, which is not negligible.

(ii) For an L = 1.32 m, 1 mil polyester tetroon with an equilibrium level of 5 km, the maximum superpressure is 50 mm, which is taken as 40 mm for safety. This allows a free lift of about 28 gm which results in an ascent rate of about

0.93 m/sec. Neglecting the radar reflector gives an ascent rate of about 1.1 m/sec, an increase of 18.5%.

In example (i) above the balloon will have an equilibrium height of about 12 km. Ascending at 1.9 m/sec it would take the balloon about 105 mins to reach its equilibrium height. In example (ii) above it will take the balloon about 90 mins to ascend to its equilibrium height of 5 km. In each case the length of the time taken means that the balloon's effectiveness is reduced considerably. If the balloons were released from Hokitika the first would be able to be sighted soon enough for the uncertainty in its position to be small, but it would not ascend to its equilibrium level until well to the lee of the mountains. The second would be approximately over the last range of mountains by the time it reached its equilibrium height but the uncertainty in its position for acquisition would be large as it would be at least 50 km from Hokitika and be in the region where there are large permanent echoes.

These examples show that a free balloon does not have a high enough ascent rate for the applications of the project.

An alternative method is to lift a constant volume balloon with small or zero lift to altitude by some external means. For example: (a) Using an aircraft: This method was used by Booker, Cooper, Hart and Cook (1968). However, it was too expensive for this project.

(b) Using a Tug Balloon: Another balloon can be used to lift the constant volume balloon to altitude if there is some way of separating them. Wooldridge and Lester (1969) and Booker and Cooper (1965) used this method separating the balloons with a fuse. Booker and Cooper used cotton cord soaked in saltpetre.

(c) Tandem System:

To gain a faster ascent rate and to overcome the problem of the superpressure resulting from the free lift required I decided to use two balloons in tandem. One balloon was an extensible rubber balloon (liftoon) with a large free lift. The other was a constant volume superpressure balloon with its lift carefully measured to give a containable superpressure. A reasonable free lift was given to lift the balloon to its equilibrium height as it was released below this for safety. These two balloons were to be released below the constant volume balloon's equilibrium height by some device, thus obtaining a fast ascent rate and a containable superpressure.

Although simple in principle, a major difficulty needed to be overcome: the development of a reliable release mechanism to separate the balloons. The two main possibilities were a timing device or a pressure sensitive device.

(i) Timing Device: A mechanical timing device could have been used but it would have worked out difficult to make and

expensive in the long run. I experimented with potassium nitrate fuses and found that if the ascent rate was known the balloons could be released by the fuse to within 100 m of the desired height for an ascent rate of the order of 3 m/sec. This form of release was unsuitable for my particular application as many of the balloons for this project were released in rain and almost all had to pass through cloud before release, thus giving a high probability of the fuse being extinguished.

Since the balloons are mainly pressure sensitive and since the atmospheric pressure falls off in a known way a pressure sensitive device lends itself to this application.

(ii) Pressure Trigger: The expansion of an aneroid capsule with decreased pressure was used to withdraw a pin from a spring loaded rod from which the constant volume balloon was suspended. The capsule was mounted in such a way that the expansion required to trigger the mechanism could be varied to vary the height of release. The pressure trigger was then set to release at a particular pressure height using a vacuum chamber.

See Figure 4.3 for the drawing of the pressure trigger.

The following table gives an indication of the reliability of the pressure trigger. H_R and H'_R are the actual and calibrated release heights respectively.

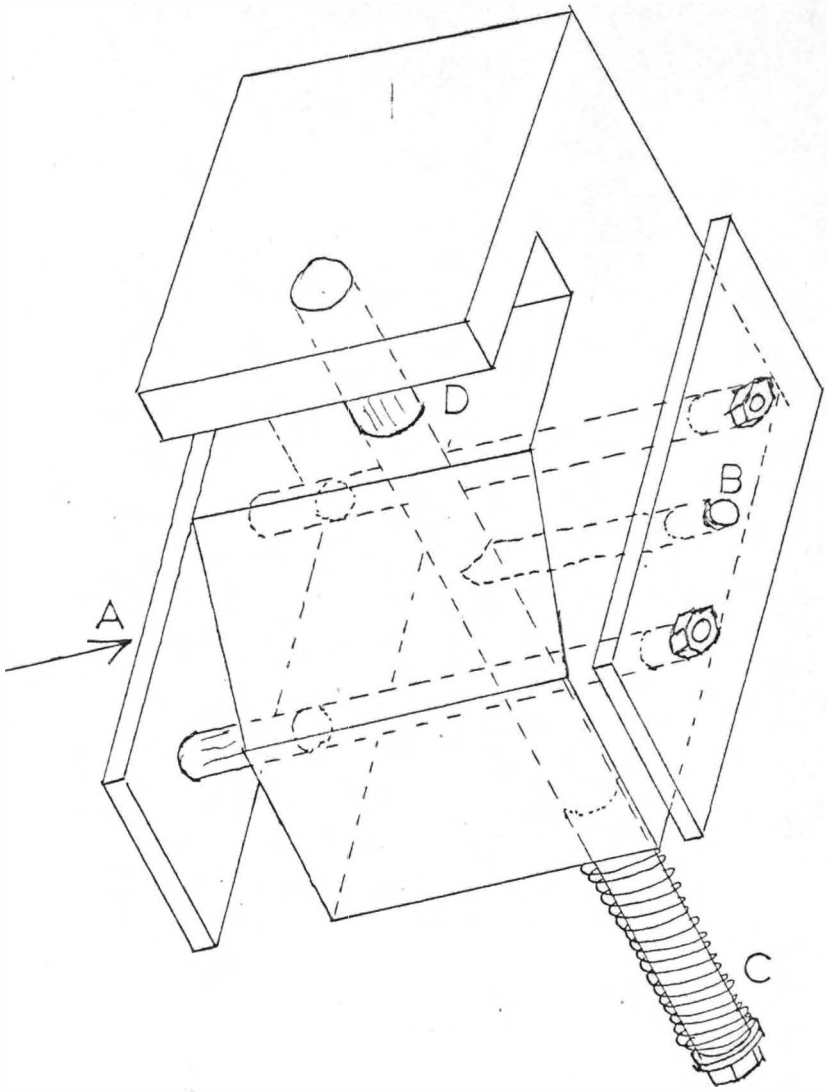

FIG 4.3: PRESSURE TRIGGER.

As the balloon ascends the aneroid capsule which is situated to the left of this element expands until it presses on the left hand plate at A. This withdraws the pin B which releases the spring loaded rod C which drops the balloon tether from the rod in slot D.

Table 4.2: Comparison of actual and calibrated release heights for the aneroid capsule pressure trigger.

Balloon Number	H'_R(km)	H_R(km)	Comments
5	3.4	3.4	Good
8	5.0	4.9	Good
9	2.0	1.69	Southerly gale. Freezing level 300 m. C.V.B. froze.
10	2.75	3.33	Good
11	3.7	3.65	Good
12	3.2	2.75	Good
14	10.0	10.3	Good
15	10.0	15.0	Pressure trigger failed to release. Probably froze.
16	9.0	11.5	Released too late.
13	9.5	9.7	Good
24	7.6	7.5	Good
25	9.5	9.66	Good
26	9.0	9.0	Good
27	9.5	18.5	Pressure trigger failed to release.

Of the 14 flights which used the tandem system 10 released successfully within the height tolerance of 500 m, i.e. 71% reliability.

Possible causes of failure of the pressure trigger to release at the required height:

(a) The pressure trigger may drop the constant volume balloon too low due to the buffeting of turbulence although this is unlikely as there is a retaining spring in the release pin assembly. If a balloon is released too low it does not necessarily mean a wasted flight as it should still rise to its equilibrium level, though at a considerably slower rate. Useful information may still be obtained.

(b) The pressure may not release at all if the mechanism is frozen and coated with ice, as appears to be the case for Balloons 15 and 27 which ascended until their liftoons burst. This was largely overcome on Balloons 23-26 by coating the pressure trigger with a silicon based oil.

(c) Some aneroid capsules were found to have leaks. If the leak had gone unnoticed it could have caused the pressure trigger not to release.

(iii) Difficulties in the use of the tandem system:

It was found to be very difficult to release a tandem system out in the open in high winds. I have done this on occasions on my own, but at the cost of several burst balloons. It is possible for a person to release a tandem system on their own if there is adequate shelter. I released several balloons from Cass by filling them in the Railways Dept. goods shed, opening the large doors at the

downwind end of the shed and running the wind while trying to release the two balloons smoothly - fun!

The large number of components increased the possibility of failure, increased the total drag and increased the possibility of failure due to icing, either of the pressure trigger mechanism or by the build up of ice on the components of the system. After the failure of the first balloon from Cass (Balloon 13) I calculated that it would take only a layer of ice about 0.3 mm thick on the top surfaces of the balloons alone to absorb 1000 gms of free lift. Mr V.E. Lally of Project GHOST suggested the use of a spray-on silicon based polish (Johnson's "Pledge") to shed water from the balloons to reduce the build up of ice. Every balloon since then has been sprayed with "Pledge".

(iv) Description of the Tandem System:

A complete tandem system consisted of a liftoon (lifting balloon), a parachute, a pressure trigger, a constant volume balloon and a corner radar reflector. Some aspects of the liftoon, C.V.B. and pressure trigger have already been mentioned but some additional practical details are mentioned below.

Liftoon: The liftoon was a rubber or neoprene balloon which was used to provide the lift required to gain a fast ascent rate. Care was taken to ensure that the volume of

gas put into a particular balloon would not result in it bursting below the release level. If this happened the pressure trigger and parachute would still be attached to the C.V.B. and, being somewhat heavier than the free lift, would cause the balloon to descend. With some lower balloons I used a 100 gm rubber balloon with about 800 gms of lift which resulted in an ascent rate of approximately 3 m/sec. For the majority of balloons, since they were to release at about 10 km, I used a 500 gm rubber balloon with 900-1000 gms of free lift. These had an ascent rate of about 4 m/sec. For some of the Cass balloons I used 650 gm neoprene balloons with about 3000 gms of lift resulting in ascent rate of the order of 8 m/sec.

Parachute: A plastic and cellotape parachute was attached to the pressure trigger for safety to support it as it fell after the liftoon had burst. It reduced the descent rate to about 1 m/sec. Initially the parachute was tied in series, with the liftoon above and the pressure trigger below. This meant that the strings and joints of the parachute had to withstand the total tension due to the lift of the liftoon directly onto the pressure trigger. The parachute was then tied to the top of the pressure trigger and a string at the top of it looped around the release rod with the tether from the C.V.B. so that the parachute flew in a closed attitude so as not to cause increased drag.

The pressure trigger and constant volume balloon are described in detail above.

Radar Reflector: The function of the balloon target or reflector is to return echo signals back to the ground equipment from which the pulses are transmitted. The maximum range obtainable is limited by the intensity of the response and the accuracy of the measurements depends to a large extent on the echo being steady. Thus the reflector needs to be an efficient reflector of the wavelength used and its efficiency should not vary greatly with the angle of incidence. Also it should be light and have little drag.

If the echo cross-section is σ, intensity of incident radiation I_o and the distance to the receiver is r then the intensity of the echo is:

$$I = \frac{I_o \sigma}{4\pi r^2} \qquad (4.4)$$

Passive Corner Reflector: This consists of three planes, one of which is square and is intended to remain horizontal in flight. Underneath the square right angle triangular sections are fixed along the diagonals so as to form four corners. When the top of the reflector is horizontal the efficiency of the reflector is a maximum for beams at an elevation of 35^o. For long range acquisition another four triangular sections are attached to the top to give a larger cross-section and to ensure that there is a reflection from

the target even when the balloon is at low elevations and the top flat plane only would be presented to the incident beam. In this case for the ordinary reflector the reflection would be zero. I have found with the complete reflector that a balloon can be acquired close to the radar horizon and tracked until it is over the opposite horizon.

(d) Valved Balloon:

Many of the problems associated with the tandem system were overcome by the addition of a gas release valve to the constant volume balloon. This enabled the C.V.B. to be completely filled at the ground to give maximum lift, then allowed the gas to escape as the pressure tended to build up during the balloon's ascent to its equilibrium level. The valve was designed to close if the superpressure reached a certain minimum level to maintain the superpressure at this level for stability.

This system had several advantages, not the least being the dispensing with the liftoon. Other advantages were cost, ease of manufacture, ease of handling and increased reliability. It was quite possible for one person to release a valved balloon in windy conditions even if there was very little shelter.

Initially the system could not be used because a suitable valve was not available. However, I developed a very simple, cheap, reliable, easy to make valve which makes

possible a system with far more overall efficiency than the tandem system. The valve consisted of a spring loaded ping pong ball seated into the end of a $1\frac{1}{8}$" diameter turned aluminium rod with cross-section as shown in Figure 4.4. A good seal between the ball and the rod was obtained by spreading a thin layer of silicon rubber around the lip of the rod and seating the ball in while the rubber was still unset. Silicon rubber does not harden appreciably over the normal range of atmospheric temperatures.

The opposite end of the valve was threaded to screw straight onto the balloon filler valve. Valves made in this way weighed less than 20 gm. The release pressure, which was the final superpressure, was set by adjusting the tension of the spring which was made out of very fine wire. The lightness of the ping pong ball compared with the tension of the spring meant that the valve's operation was virtually independent of attitude. To ensure that the gas could escape fast enough so that the superpressure did not build up during the ascent I connect a balloon to a manometer and the compressed air supply in the lab. No appreciable increase in superpressure was observed for very fast flow rates.

Advantages of the Valved Balloon: This system has several advantages over the tandem system although the maximum ascent rate is limited by the size of the balloon. For

FIG 4.4: CROSS-SECTION THROUGH A GAS RELEASE VALVE.

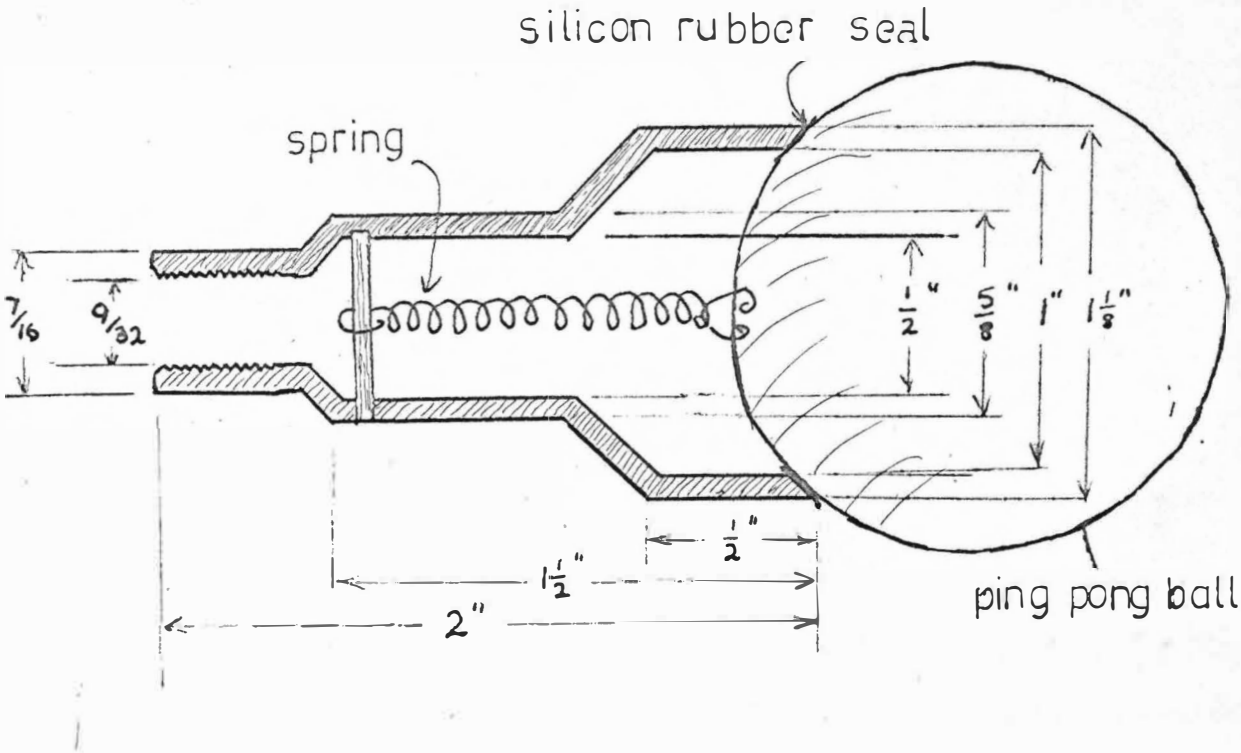

SCALE 1.5 : 1

A GAS RELEASE VALVE FOR A CONSTANT VOLUME SUPER PRESSURE BALLOON.

balloons of ordinary size however, a sufficiently large ascent rate is attained. The following are some of the main advantages:

(a) The valve is easier to manufacture than the pressure trigger and the materials are more readily available.

(b) The number of balloons required is reduced, reducing the cost, the drag and the difficulties in filling and releasing the system in open, windy conditions.

(c) The valve eliminates the necessity of weighing off the C.V.B. accurately. This eliminates one of the possible causes of a balloon bursting, viz. too high a superpressure resulting from excess lifting gas.

(d) The possibility of failure due to icing is reduced as there is no release mechanism to freeze up. To stop the valve from freezing up it was coated with a silicon based oil. During the ascent through clouds the balloon will either be outgassing, which will tend to keep water out of the valve, or the valve will be closed. The valve should only be closed if the balloon has already reached its equilibrium height, after which the valve should remain closed, hence icing will not affect it.

(e) There is a large reduction in the amount of gas required.

(f) The total drag for the same amount of lift is less because there are fewer components.

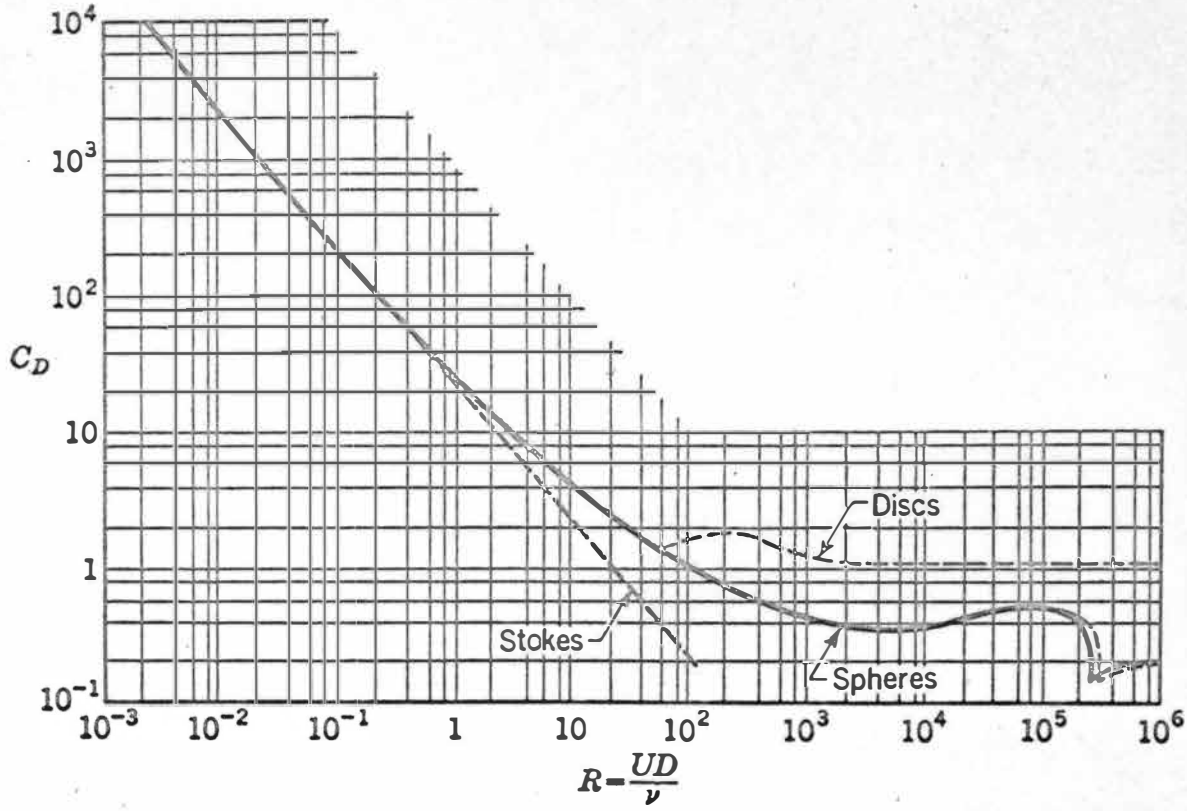

FIG 4.5: DRAG COEFFICIENT OF A SPHERE (STREETER 1962)

4. Drag Coefficients

In determining the ascent rate of a particular balloon or balloon system it is essential to know the drag coefficient of the balloon or the system. It is also important to show that the drag of the constant volume balloon is large so that it follows the movement of the airflow closely.

The drag coefficient is not a constant for a particular shape but rather is a function of the balloon's velocity and size and also of the air's characteristics such as density and viscosity. Thus it is convenient to determine the drag coefficients of the various balloons and balloon systems as a function of Reynold's Number.

(a) Drag Coefficient of a Spherical Balloon:

The drag coefficient of a sphere as a function of Reynold's Number is very well known and is given in Figure 4.5, (Streeter, 1962). Balloons such as liftoons do not maintain perfectly spherical shapes but are elongated in the vertical due to the lift of the gas inside and the weight of the load attached to their bottom. A good approximation to the drag on the liftoon can be found by taking the drag coefficient as that of a sphere and the effective area as the actual cross-sectional area of the liftoon.

(b) Drag Coefficient of a Tetroon:

The shape of a tetroon makes it very difficult to determine its drag coefficient theoretically. When it is

full it becomes somewhat rounded due to the distortion of the plastic so that its shape is approximately spherical and its drag coefficient should lie between that of a sphere and that of a perfect tetrahedron. The only accurate way that I could get an indication of the drag coefficient of a tetroon was to determine it experimentally.

I coated a plastic tetroon with plaster of paris to make a solid model. The Mechanical Engineering Dept., University of Canterbury, generously allowed me to use their wind tunnel to determine the drag vs velocity curves for this model in two orientations. From these I calculated the drag coefficients. The results are given in Figures 4.6 and 4.7 as a function of Reynold's Number. The effective area is taken as the actual cross-sectional area of the tetroon, i.e. $A_t^* = 0.433\ L^2$.

(c) Drag Coefficient of a Corner Radar Reflector:

The drag of the radar reflector may be taken as the drag of a flat plate with an effective area equal to the actual area of the flat square middle section of the reflector. Thus the drag coefficient is taken as one and the effective area, by measurement, is 0.274 m^2. i.e.

$$C_{Dr}\ A_r^* = 0.274 \qquad (4.5)$$

where A_r^* is in m^2.

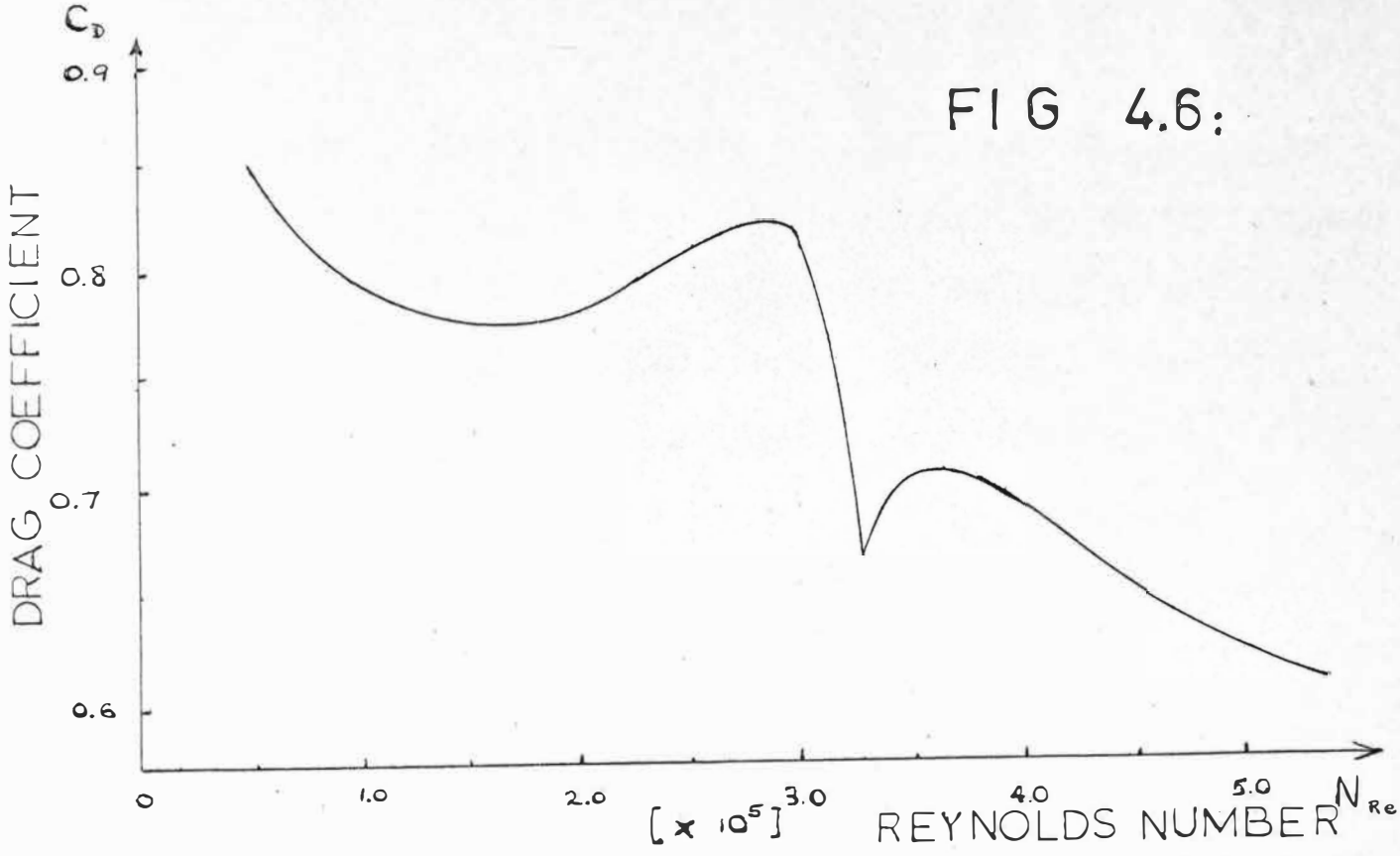

FIG 4.6:

DRAG COEFFICIENT FOR A TETROON ASCENDING APEX DOWN.

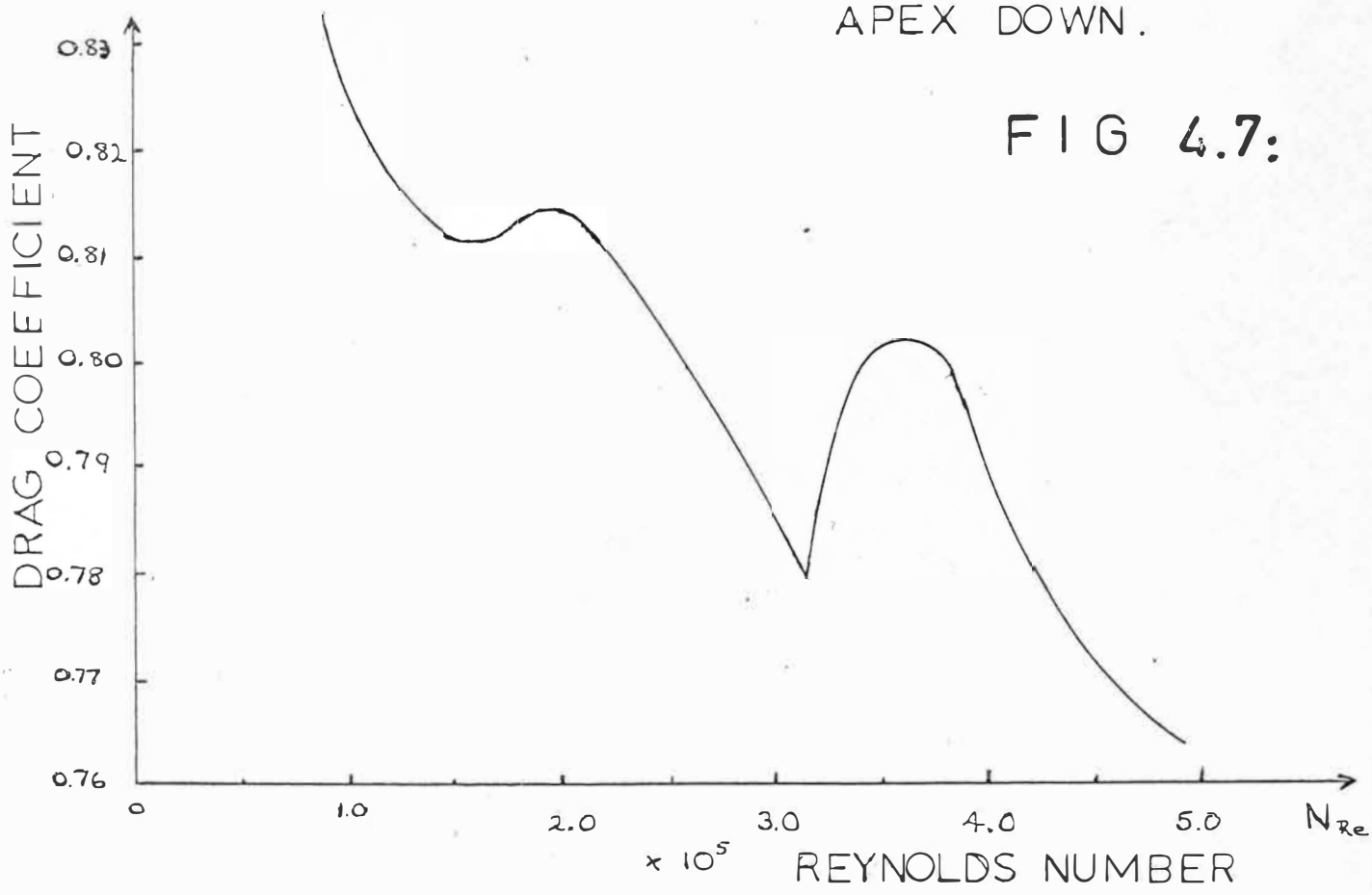

FIG 4.7:

DRAG COEFFICIENT FOR A TETROON ASCENDING APEX UP.

(d) Drag Coefficient of a Tandem System:

Because of the turbulent flow past each of the components in the tandem system the total drag will not be equal to the sum of the drag on each of the individual components. There will be shielding of the lower components by the higher components, mainly the liftoon. The amount of shielding will vary with size and velocity and hence Reynold's Number. Thus the drag coefficient is best determined experimentally. This I have done using data from 16 tandem systems. The results are shown in Figure 4.8, where Reynold's Number was calculated from:

$$N_{Re} = \frac{\rho \, v \, D}{\eta} \qquad (4.6)$$

where ρ is the atmospheric density at the ground, in kgm/m^3,

v is the initial ascent rate averaged over about the first 10 minutes of the recorded flight, in m/sec,

D is the diameter of the liftoon at the ground in m, calculated from its lift,

and η is the viscosity of the air for the temperature of the particular flight, in M.K.S. units.

An indication of the magnitude of the shielding can be gained from the following example:

A tandem system consisting of a 500 gm liftoon with 1000 gm of lift, towing an L = 1.7 m tetroon with 20 gm of

FIG 4.8: DRAG COEFFICIENT OF A TANDEM BALLOON SYSTEM.

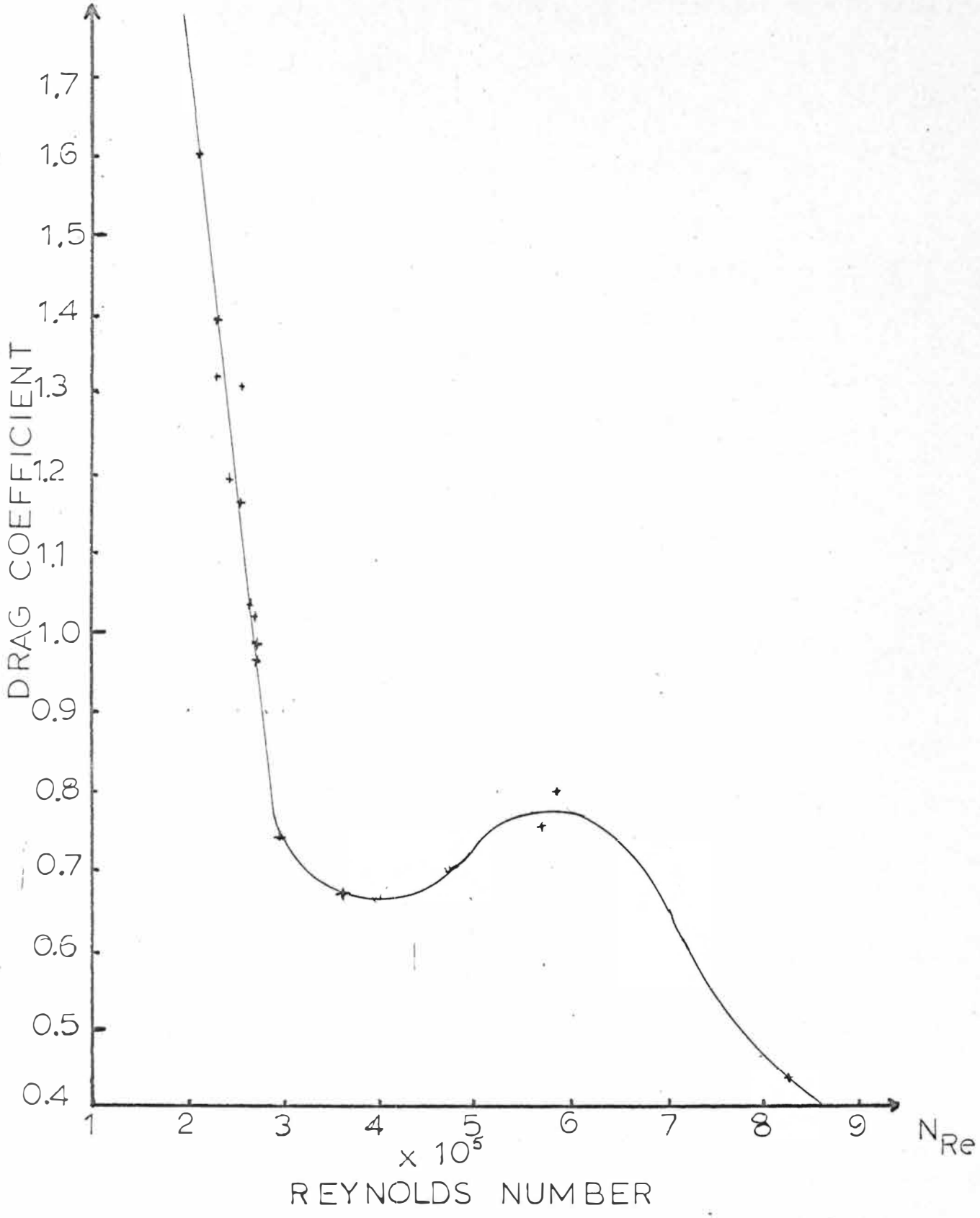

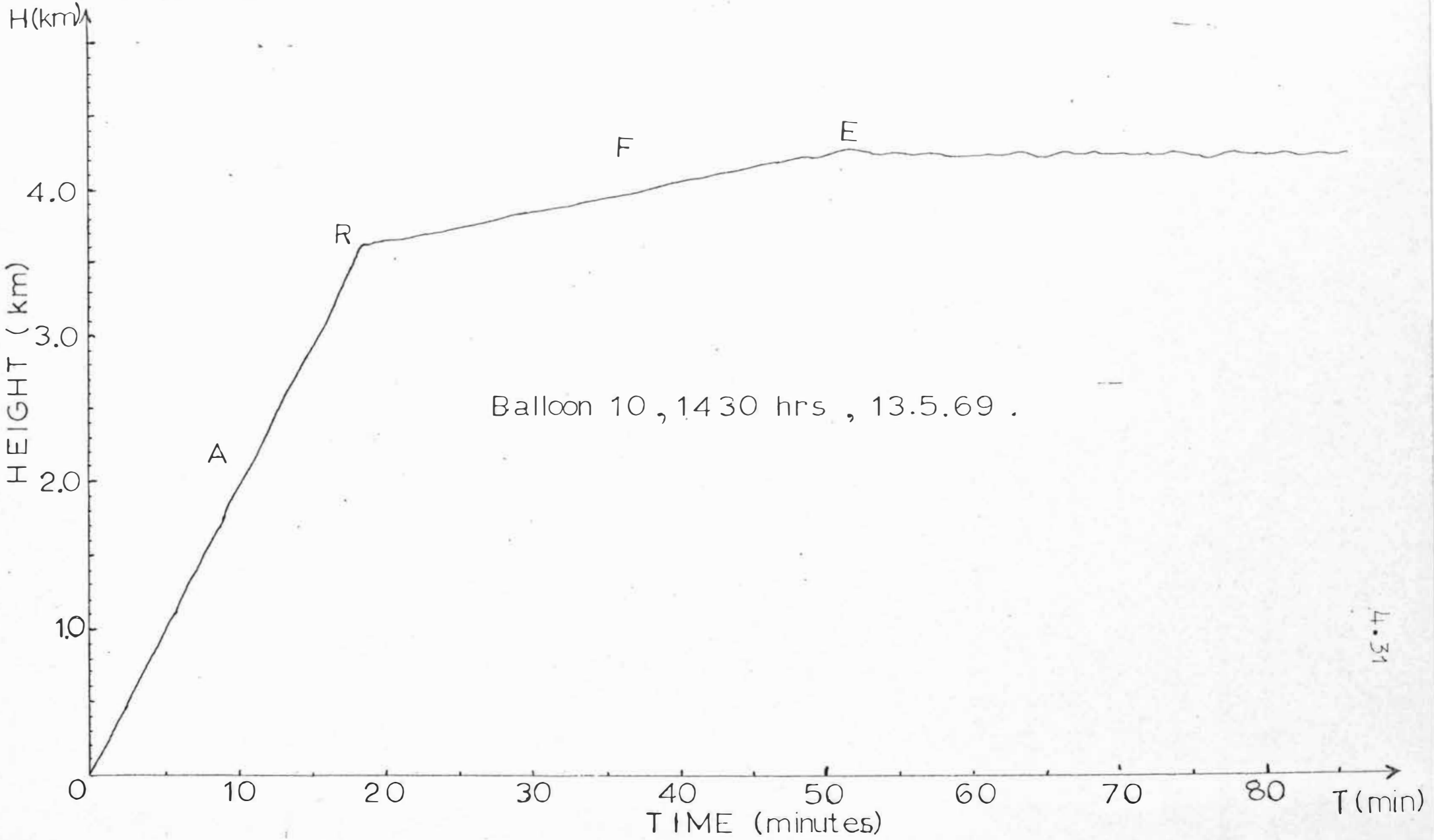

FIG 4.9: A typical tandem balloon system. Region A: Balloon under tow, $\bar{v}$ = 3.1 m/sec Released by the pressure trigger at point R. Region R: Ascending under its own lift (23gm). At point E it reaches its equilibrium level 52 minutes after release.

lift and a standard corner reflector attached, will have an ascent rate of approximately 4 m/sec. This was calculated using the experimentally determined curve for the drag coefficient of the tandem system as a whole, Figure 4.8. Considering the drag on the system to be due to the sum of the drag on the individual components as calculated from the empirically determined drag coefficients and assuming a drag equation of the form:

$$F_L = \tfrac{1}{2} \rho v^2 C_D A^*$$

where

$$C_D A^* = C_{Dt} A^*_t + C_{Dl} A^*_l + C_{Dr} A^*_r$$

where 't' refers to the tetroon, 'l' to the liftoon and 'r' to the radar reflector. In this case I found that it requires about 1500 gms of lift to attain the same ascent rate of 4 m/sec. This means that the shielding of the liftoon reduces the total drag by about 33%.

5. Ascent Rates of Tetroons and the Tandem System

Expressions for the ascent rates of balloons are given in sections (vii) and (viii) in Chapter 2. In general the ascent rate is governed by an equation such as (2.22), i.e.

$$F_L = \tfrac{1}{2} \rho v^2 C_D A^* \qquad (2.22)$$

For particular types of balloons equations such as (2.25)

and (2.26) can be used. These equations show that the square of the ascent rate is proportional to the density of the air ρ, the drag coefficient of the balloon C_D and the effective area of the balloon A*.

The atmospheric density varies approximately in a known way. Assuming an atmospheric as given by the U.S. Standard Atmosphere, 1966, the density may be given by:

$$\rho = 0.465 \frac{P}{T} \qquad (4.7)$$

where P is the atmospheric pressure in mm of Hg,

and T is the atmospheric temperature in ^{o}K.

The drag coefficients for the various balloons and systems are given above as a function of Reynold's Number, the effective area being defined in each case.

The free lift is variable and limited by the liftoon for a tandem system, constant and fixed by the maximum superpressure allowed for a sealed tetroon and is variable and limited by the size of the balloon for the valved tetroon.

In order to compare the performance of each of these systems ascent rates were calculated, the results being shown in Figure 4.10, and in table 4.3.

The following methods of calculation were used:

(a) Ascent Rates of Tandem Systems: The data for tandem systems could be divided into three groups depending on the size of the liftoon. The values of free lift and

resulting ascent rate for each size of liftoon were averaged and are shown in Table 4.3 below.

Table 4.3: Ascent rates of various tandem balloons for given weights of liftoon, as derived from actual balloon flights.

Weight of Liftoon (gm)	Free Lift of System (gm)	Ascent Rate (m/sec)
100	680	3.23
500	766	3.12
650	2700	5.25

For free lifts greater than about 750 gms in liftoons to lift balloons to heights above about 8 km it is advisable to use a 500 gm balloon as the possibility of it bursting before the release level is almost negligible.

(b) Ascent Rates of Valved Tetroons: The ascent rate of a valved tetroon is derived from equation (2.25), viz.:

$$v = \sqrt{\frac{2\,g\,(931\,V - W/\rho)}{C_D\,A^* \times 10^3}} \qquad (2.25)$$

where the volume of the tetroon V, is given by (4.1):

$$V = 0.177\,L^3 \qquad (4.1)$$

The weight of the balloon W includes the weight of the

balloon materials plus the weight of the load (in grams). For 1 mil polyester the weight of the balloon W_B is given by:

$$W_B = 57\ L^2 + 15\ L + 38 \qquad (4.8)$$

The load includes the radar reflector and the valve, which together may weigh up to 200 gm. I chose, for the purpose of comparison, a typical value of 180 gm. Hence:

$$W = 57\ L^2 + 15\ L + 218\ (gm) \qquad (4.9)$$

I used the values of density as given by the U.S. Standard Atmosphere 1966. The term $C_D\ A^*$ was expanded to include the drag of the radar reflector using (4.5). i.e.:

$$C_D\ A^* = C_{Dt} A^*_t + 0.274 \qquad (4.10)$$

where

$$A^*_t = 0.433\ L^2 \qquad (4.11)$$

The drag coefficient of the tetroon as a function of Reynold's Number is shown in Figure 4.6. This I approximated by a three valued function:

$$\overline{C}_D = 0.79 \text{ for L less than or equal to 1.5 m,}$$

$$\overline{C}_D = 0.65 \text{ for L between 1.5 m and 2.0 m,} \qquad (4.12)$$

$$\overline{C}_D = 0.60 \text{ for L greater than or equal to 2.0 m.}$$

I wrote a computer programme to calculate the ascent rates and the times taken to reach the various heights, for

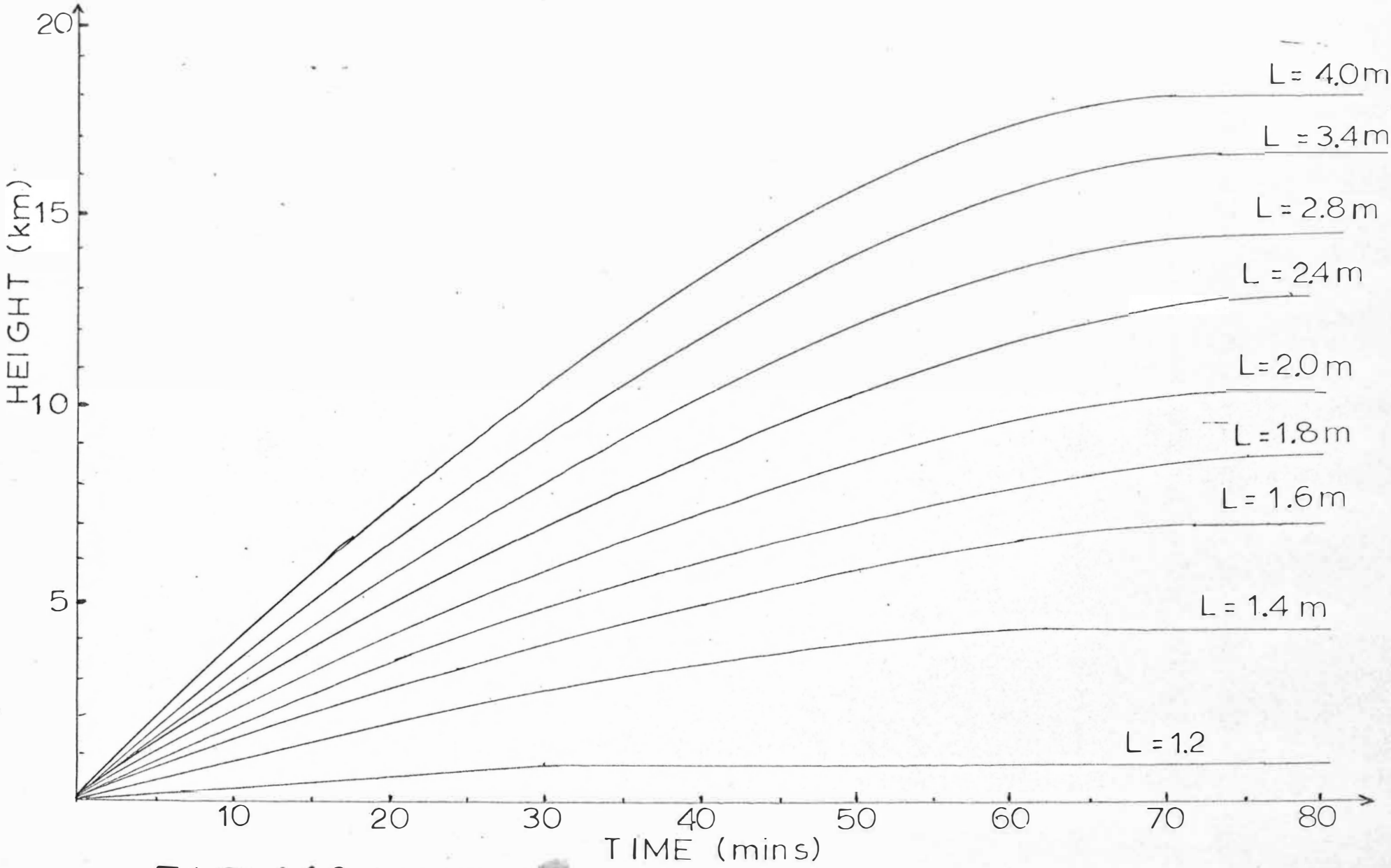

FIG 4.10: HEIGHT VS TIME CURVES FOR TETROONS OF VARIOUS SIZES USING 1 mil POLYESTER AND A LOAD OF 180 gm.

balloons of various sizes, using equations (4.1) to (4.12) and (2.25). The results were graphed and are shown in Figure 4.10.

(c) Ascent Rates of Sealed Tetroons: The ascent rate of a sealed tetroon is dependent on the amount of free lift the balloon is given when it is being weighed off. The maximum amount of free lift is limited by the maximum stress that the balloon material can stand. Hence the maximum ascent rate is given by (2.30), viz.:

$$\max (v) = \sqrt{\frac{\max (p_s)}{K_B}} \qquad (2.30)$$

where K_B is a constant for a particular balloon given by (2.28).

$$K_B = (\tfrac{1}{2} p_e C_D A^* \rho / g W) \times 10^3 \qquad (2.28)$$

I chose, for the purposes of comparison, 1 mil polyester as the balloon material. The maximum allowable superpressure is given by (3.11), viz.:

$$\max (p_s) = 3.18 (t/L) \sigma_{max} \times 10^{-7} \qquad (3.11)$$

where for polyester

$$\sigma_{max} = 1.722 \times 10^8 \ \text{nt/m}^2$$

Hence for 1 mil polyester

$$\max (p_s) = \frac{65.6}{L} \ \text{mm of Hg.} \qquad (4.13)$$

where L is the length of the side of the tetroon in metres. For safety (see Chapter 3, iii(b)) I take

$$\max (p_s) = \frac{40}{L} \text{ mm of Hg} \qquad (4.14)$$

Since A* and ρ both vary with height although their product remains approximately constant, as shown by the observed balloon ascents, I chose the values of these quantities at the equilibrium level as an indication of the overall mean ascent rate. Now ρ is given by (4.7), A* is given by (4.11), and W is given by (2.5). C_D is assumed to have a constant value of 0.63. Substituting these and (4.14) into (2.30) gives:

$$v = 21.75 \left(\left(\frac{P}{T}\right)_e T_e \right)^{-\frac{1}{2}} \qquad (4.15)$$

The equilibrium level P/T ratio is found for a particular sized balloon with a particular overall weight from (2.5) and the temperature at the equilibrium level (T_e) is found from the U.S. Standard Atmosphere 1966 to be given by

$$T = 288.15 - 6.55\ H\ (^{o}K) \qquad (4.16)$$

for H less than or equal to 11 km, where H is the height in km, and for H greater than 11 km

$$T = 216.65\ (^{o}K)$$

Some representative values of equilibrium height, mean

ascent rate and time taken to reach the equilibrium level are given in Table 4.4 for balloons of various sizes with a range of loads. Figure 4.11 shows the graphs of the curves of the time taken to reach the equilibrium height vs the size of the tetroon for a load of 180 gm, for tetroons with and without gas release valves, and for a tandem system with a 100 gm liftoon with 700 gm of lift. Larger balloons will not be shielded by the liftoon as much as smaller balloons so that the overall drag of the tandem system will be more than allowed for. Curve IV in figure 4.11 is included to approximate a more realistic curve for the tandem system, being derived by considering the drag of the system to be equal to the sum of the drag of the individual components, neglecting any shielding effects.

6. Conclusions

The tandem system works well in getting the constant volume balloons quickly to their equilibrium levels although there is a reasonable possibility of failure (approximately 30%) because of the large number of elements involved and the effect of icing on each of them, particularly the pressure trigger. Also they are difficult to release in windy conditions, especially if a large filling shed is not available.

Table 4.4: Equilibrium height for sealed tetroons, mean ascent rate, and time taken to ascend to the equilibrium level from sea level for various representative loads and tetroon sizes. H_e (km), $\bar{v}$ (m/sec), T (sec).

L (m)		Loads (grams) 40	60	80	100	120	140	160	180	200
1.2	H_e	6.42	5.46	4.59	3.80	3.00	2.25	1.56	1.92	0.31
	$\bar{v}$	1.20	1.12	1.05	1.00	0.95	0.91	0.87	0.84	0.80
	T	89.6	81.4	72.6	63.4	52.6	41.4	30.0	18.3	6.4
1.4	H_e	8.92	8.22	7.51	6.82	6.17	5.57	5.01	4.48	4.00
	$\bar{v}$	1.43	1.36	1.29	1.23	1.17	1.13	1.10	1.05	1.01
	T	104	101	97.2	92.6	87.6	82.4	77.0	71.4	65.8
1.6	H_e	10.7	10.2	9.60	9.08	8.60	8.14	7.66	7.19	6.73
	$\bar{v}$	1.66	1.58	1.51	1.45	1.40	1.35	1.30	1.25	1.22
	T	108	107	106	104	103	101	98.2	95.1	92.0
1.8	H_e	12.3	11.8	11.3	10.8	10.4	10.0	9.61	9.24	8.89
	$\bar{v}$	1.83	1.77	1.72	1.67	1.61	1.65	1.51	1.47	1.43
	T	111	111	109	108	108	107	106	105	104
2.0	H_e	13.5	13.1	12.7	12.3	11.9	11.6	11.2	10.9	10.6
	$\bar{v}$	1.99	1.94	1.89	1.84	1.79	1.75	1.71	1.68	1.63
	T	113	113	112	111	111	110	109	108	108
2.2	H_e	14.6	14.2	13.9	13.5	13.2	12.9	12.6	12.3	12.0
	$\bar{v}$	2.14	2.09	2.04	2.00	1.95	1.91	1.87	1.83	1.80
	T	114	114	113	113	113	112	112	111	111
2.4	H_e	15.6	15.3	14.9	14.6	14.3	14.0	13.8	13.5	13.2
	$\bar{v}$	2.29	2.24	2.19	2.14	2.10	2.06	1.99	1.99	1.96
	T	114	114	114	114	114	113	113	113	113
2.6	H_e	16.5	16.1	15.9	15.6	15.3	15.1	14.8	14.6	14.3
	$\bar{v}$	2.42	2.37	2.33	2.29	2.25	2.21	2.17	2.14	2.11
	T	113	113	113	113	113	113	113	113	113

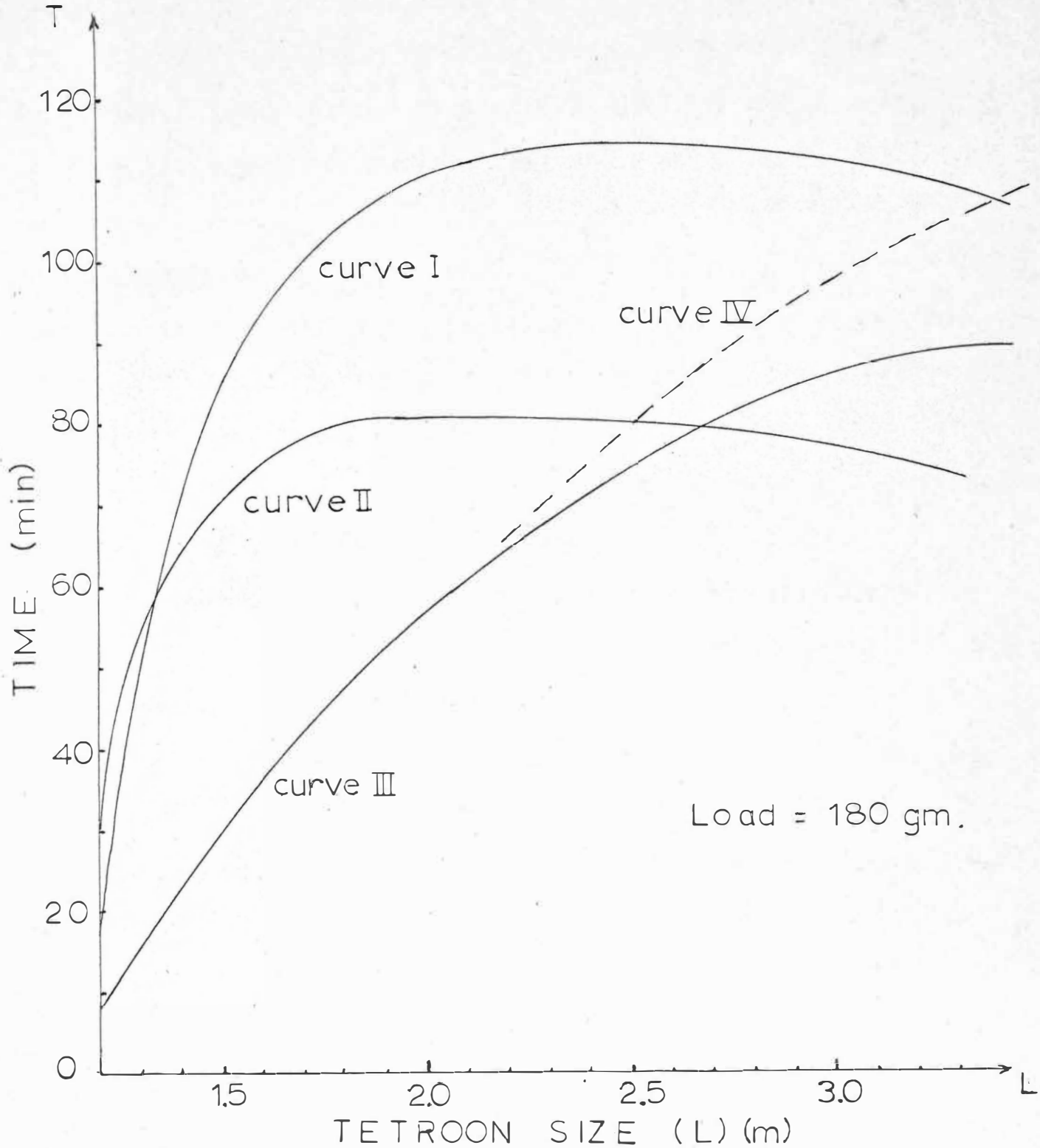

FIG 4.11: COMPARISON OF THE TIME TAKEN BY THE THREE SYSTEMS TO GET TETROONS OF VARIOUS SIZES TO THEIR EQUILIBRIUM HEIGHTS. Curve I : SEALED TETROONS Curve II : VALVED TETROONS. Curve III : TANDEM SYSTEM. Curve IV: TANDEM SYSTEM MODIFIED TO ALLOW FOR DECREASED SHIELDING.

Tetroons on their own make good constant volume balloons if made out of a strong material such as polyester as they are easy to make, having only three straight seams, and are only 13.5% less efficient than a sphere with respect to volume to surface area ratio. However, their ascent rate is restricted by the strength of the balloon material to values which, for most practical purposes, are too low, except for low level balloons (up to 4 km with loads greater than 200 gm) and for long duration balloons such as used by Project GHOST.

The addition of a gas release valve which allows the lifting gas to escape as the balloon ascends, keeping the superpressure at a predetermined level and closing when the pressure tends to drop below this level as the balloon approaches its equilibrium level, allows the balloon to be filled completely before release. This results in an increased mean ascent rate and reduces the time taken by a tetroon of any size, with a load of 180 gms, to reach its equilibrium level in a maximum of 80 minutes. The tetroon on its own has fewer things that can go wrong, reducing the possibility of failure. In my project the failure rate for valved tetroons has been less than 5%. This coupled with the ease of filling and releasing makes the valved tetroon system the most reliable and efficient balloon system for this project.

C H A P T E R 5

LEE WAVE THEORY

1. Introduction

Since the work of Lyra and Queney in the 1940's an extensive literature has been built up on the theoretical aspects of lee waves. This may be divided into three sections. The basis of the division is rather arbitrary but it simplifies the discussion.

(a) Linear Theory: Including the work of such authors as Queney, Lyra, Scorer, Corby, Sawyer, Wallington, Doos, Yih, Danielson, Bleck and many others. It is mainly characterised by the use of the linearised wave equation, derived using the perturbation method, and its application through the use of simplified models to the atmosphere in order to obtain the characteristics of atmospheric lee waves.

(b) Nonlinear Theory: Including the work of Long, Miles, Crapper, et al. It is characterised by their use of the nonlinear wave equations in the problems of fluid flows over obstacles of various shapes in order to obtain analytic solutions. These solutions are compared with the flow in tanks in simulation experiments and to the flow of air over mountains.

(c) Numerical Theory: The above two sections have in common the search for analytic solutions of the wave equations. These must necessarily involve severe restrictions or simplifications. With the availability of high speed computers it has been possible to solve the linear wave equation numerically for arbitrary wind and mountain profiles. Authors employing this method include Krishnamurti, Pekelis, Lin, Apelt, et al.

Because of the abundance of material a detailed consideration of it all is not practical nor is it necessary here. A good background can be gained from Yih (1965), from the WMO technical note 34,(1960) by Queney et al., and from the reviews by Corby (1954) and Krishnamurti (1964). As the observations undertaken in this project lend themselves to a comparison with the linearised theories only these are discussed in more detail, particularly those that are used in this project. The next chapter discusses the characteristics of atmospheric lee waves as derived from the linearised theory and observational programmes.

2. Historical Background

Lord Rayleigh (1883) observed that a small obstacle, such as a fishing line, when moved slowly through still water, or held stationary in flowing water, produces a surface which is covered with "a beautiful wave-pattern fixed

relatively to the obstacle". He noted further that the waves on the upstream side had a shorter wavelength than those downstream (as for the doppler effect) and that they are propagating at the velocity of the water since they are stationary with respect to the obstacle. Thompson had shown that there was a minimum velocity (about 23 cm sec^{-1}) below which waves were not formed. The same effect was produced when the end of a stick was held just on the surface of the water or if the surface was depressed by blowing on it. Thus by assuming a stream function of the form:

$$\psi = c\,z - \Sigma\,\alpha\, e^{-kz} \cos(kx + \varepsilon)$$

for a surface which is depressed at the point x = 0 by a positive line of pressure, when x is large and positive the disturbance is of the form

$$\frac{2\,\pi \sin k_1 x}{k_2 - k_1}$$

and when x is large and negative it has the form

$$\frac{2\,\pi \sin k_2 x}{k_2 - k_1}$$

where k_1 and k_2 are the downstream and upstream wave numbers respectively ($k_1 < k_2$) and where $k_1 k_2 = \frac{g\rho}{T}$ and $k_1 + k_2 = \frac{\rho c^2}{T}$ where ρ is the fluid density, T the capillary tension, and g gravity and c the fluid velocity.

Lord Kelvin (1886) showed that water flowing over an obstacle will be depressed at the surface, in the same way as the positive pressure used by Lord Rayleigh, hence the resulting wave pattern should be of the same form. However, when Lord Kelvin, after observing the waves in the wake of a boat, derived expressions for the surface of a channel, he found waves downstream only with a fast exponential decay on the upstream side of the obstacle. His initial solution contains waves on both sides of the obstacle but he imposes a condition of no waves upstream to obtain what he calls "the practical solution".

It is now generally assumed that there are waves downstream only.

A closely related controversy, called the problem of the upper boundary, has existed over the choice of the sign of the radical obtained in the two layer solution.

Lyra and Queney were two of the first workers to consider the problem of atmospheric lee waves. Lyra (1940, 1943) for simplicity considered a uniform airstream and a rectangular mountain profile. The waves he obtained were unrealistic in that they increased in amplitude indefinitely with height. It was found that they were mainly caused by the steepness of the sides of his mountain. Queney (1947) considered the flow of a uniform airstream over a bell shaped mountain as a special case of his general theory of

adiabatic perturbations in a stratified rotating fluid. His solutions include waves whose wavelengths are less than about 2 km and greater than about 200 km. This does not account for the majority of lee waves which are observed to have wavelengths between about 2 and 30 km. Also the amplitude of his waves increased with height.

Scorer (1949) used the perturbation method to derive a linearised wave equation which included the effect of rotation. This was neglected by restricting the solution to wavelengths less than about 50 km. For wavelengths greater than about 100 km the coriolis force starts to have an effect.

3. Validity of the Perturbation Technique

In the perturbation derivation of the linearised wave equation it is assumed that the flow is inviscid, isentropic and laminar. The displacements and perturbations are assumed to be small so that second order perturbation terms can be neglected.

Viscosity acts only to damp the waves. This damping is very small as can be seen by the persistence of lee wave trains over hundreds of kilometers as observed on satellite photographs. For example Doos (1962) and Fritz (1965).

The assumption that the flow is isentropic means neglecting the effect of radiation and condensation.

Radiation effects will be small over distances in the order of 100 km. Sometimes there is little or no condensation in a wave train as shown by the complete absence of clouds. More often there are a few altocumulus lenticulars about but these are often small compared to the overall scale so will have little effect on the waves. When there are many clouds about the perturbation theory will be more approximate. When there is a complete sheet of cloud the effects of condensation can be included by the use of the wet-bulb potential temperature in the stability β_1 (defined by (5.10)).

Since as yet there is no satisfactory theory of turbulent flow only laminar flow can be studied at all fully theoretically. Turbulent flows have been studied empirically as in the work of Forchtgott (1949), Gerbier and Berenger (1960), Harrison (1965), Georgii (1969), Pao (1969) and Hall and Pao (1969).

The assumptions of small displacements and perturbations hold quite well if the height of a mountain is small compared to its width (Corby, 1954). They do not hold for the case of the standing eddy although here the eddy can be considered as modifying the lowest stream line as the flow above the eddy is laminar. Scorer (1969) showed that even for large amplitude waves the airflow is still described well by the simplified linear wave equation as long as the

slope of the streamlines is small.

Over the scale of Queney's waves the earth's rotation cannot be neglected by for waves of wavelength less than 50 km as considered by Scorer rotation can be neglected because the scale of motion is small.

4. Linearised Wave Equation

The equation describing the flow of a fluid over an obstacle may be derived by considering the effect of the obstacle as introducing a perturbation to the fluid parameters in the momentum, continuity equations and the equation of constant entropy. Neglecting viscosity the linearised equations of motion in two dimensions (x,z) are:

$$\bar{\rho}\, U\, u_x + \bar{\rho}\, U'\, w = - p_x \qquad (5.1)$$

$$\bar{\rho}\, U\, w_x = - p_z - g\, \rho \qquad (5.2)$$

where $\bar{\rho}$ and U are the density and horizontal velocity of the undisturbed flow respectively. The prime indicates differentiation with respect to z and the subscripts indicate partial differentiation. u, w, ρ and p are the horizontal and vertical velocity perturbations and the density and p pressure perturbations respectively. The linearised continuity equation is

$$\bar{\rho}\, (u_x + w_z) + U\, \rho_x + \bar{\rho}'\, w = 0 \qquad (5.3)$$

Neglecting heat conduction the linearised equation of constant entropy is:

$$U\,p_x + w\,\bar{p}' - c^2\,(U\,\rho_x + w\,\bar{\rho}') = 0 \qquad (5.4)$$

where c is the speed of sound. Elimination of ρ_x from (5.3) and (5.4) gives

$$c^2\,\bar{\rho}\,(u_x + w_z) + U\,p_x + w\,\bar{p}' = 0 \qquad (5.5)$$

Elimination of p_x from (5.1) and (5.5) then gives

$$\bar{\rho}\,(c^2 - U^2)\,u_x = -\,(c^2\,\bar{\rho}\,w_z + (\bar{p}' - \bar{\rho}\,U')\,w) \qquad (5.6)$$

Substituting for ρ_x in the equation resulting from the elimination of p from (5.1) and (5.2) gives

$$(\bar{\rho}Uu_x)' + \frac{g}{U}\,\bar{\rho}u_x = \bar{\rho}Uw_{xx} - \frac{g}{U}\,(\bar{\rho}w)_z - (\bar{\rho}U'w)_z \qquad (5.7)$$

Equations (5.6) and (5.7) relate u and w in terms of the parameters of the undisturbed flow. Elimination of u between (5.6) and (5.7) and replacing $\bar{p}'$ by $-g\bar{\rho}$ yields the linearised wave equation

$$M(z)\,\frac{\partial^2 w}{\partial x^2} + \frac{\partial^2 w}{\partial z^2} - A(z)\,w_z + B(z)\,w = 0 \qquad (5.8)$$

an ecliptic partial differential equation where

$$M(z) = 1 - \frac{U^2}{c^2}$$

$$A(z) = \beta - \frac{2\,U\,U'}{c^2 - U^2} \qquad (5.9)$$

$$B(z) = \frac{g\,\beta_1}{U^2} - \frac{U''}{U} + \frac{U'}{U}\left(\beta_1 - \frac{g}{c^2}\right)$$

where $\beta = \frac{\overline{\rho}'}{\overline{\rho}}$ and $\beta_1 = \beta - \frac{g}{c^2}$ (5.10)

$$= \frac{1}{\theta}\frac{d\theta}{dT} = \frac{1}{T}(\gamma_a - \gamma)$$

Several terms in A and B are neglected because in the atmosphere $U\,U' \ll c^2$, $U^2 \ll c^2$ and $U' \ll g$. If the last term in B(z) is neglected Eq. (5.8) is the same as derived by Scorer (1949) and others.

If ζ is the displacement of a streamline from its undistrubed level, (5.8) can be transformed to an equation for ζ by making use of the linearised equation

$$U\,\zeta_x = w \qquad (5.11)$$

And if we assume that the variation of ζ in the horizontal direction is harmonic with wave number k, i.e.

$$\zeta = \zeta(z)\,e^{ikx} \qquad (5.12)$$

then (5.8) can be written

$$\zeta'' + \left(\frac{2U'}{U} - \beta\right)\zeta'(z) + \left(\frac{g\,\beta_1}{U^2} - k^2\right)\zeta(z) = 0 \qquad (5.13)$$

These wave equations are often further simplified by assuming that M(z) = 1 and either A(z) (β) is small or the

equations are transformed using an integrating factor of the form

$$W = w \left(\frac{\rho}{\rho_o}\right)^{\frac{1}{2}} \qquad (5.14)$$

The wave equations may be solved generally for arbitrary airflow and mountain profiles, as done by Krishnamurti (1964) and Pekelis (1969), or they may be solved by assuming the coefficients are constant across layers in the atmosphere and applying the boundary and interface conditions (see two layer theory below). Doos (1961) showed that if B(z) decreased exponentially the wave equation transforms to a Bessel equation which may be solved analytically in terms of Bessel functions. Danielson and Bleck (1970) obtained more generality by using a layer model in which B(z) changed exponentially within each of the layers.

In practice there are occasions when the atmosphere forms clearly defined layers or an exponential form and on these occasions the appropriate theory may be applied. In general however, the atmosphere does not exhibit this convenience but is rather more complex such that only a qualitative evaluation of wave characteristics may be gained, by a consideration of the analytical or mathematical theories. Only the numerical methods can be expected to give any accurate solutions for the general case.

5. Two Layer Theory (Scorer's Theory)

Scorer (1949, 1953, 1954, 1955 and 1956 and in papers in partnership with other people) has examined in depth the properties of a two layer atmosphere favourable for the production of lee waves and the characteristics of such waves. Considering a simplified wave equation

$$w'' + (l^2 - k^2)\, w = 0 \qquad (5.15)$$

where l is known as the Scorer parameter where

$$l^2 = \frac{g\beta_1}{U^2} - \frac{U''}{U} \quad (km^{-2}) \qquad (5.16)$$

Taking a two layer model where l^2 is taken as a constant in each of the layers, the interface being at height h (km). Letting w die away at large z and choosing w to have the form

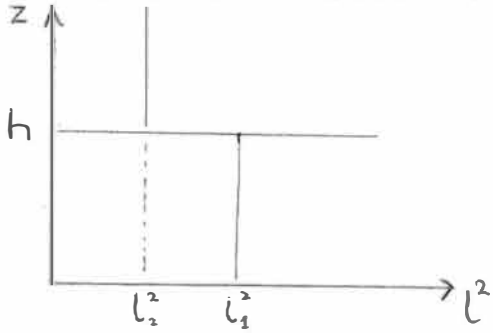

Fig. 5.1

$$w_1 = A\, e^{\mu_1 z} + B\, e^{-\mu_1 z} \qquad (5.17)$$

and $$w_2 = C\, e^{-\mu_2 z} \qquad (5.18)$$

neglecting the horizontal variation of w(x,z) which has been assumed to be proportional to e^{ikx} as this does not affect the vertical variation of w (w(z)). Now equations of the form of (5.17) are solutions of (5.15) if

$$\mu_1, \mu_2 = \pm (k^2 - l^2)^{\frac{1}{2}} \qquad (5.19)$$

Applying the lower boundary condition w(0) = 0, from (5.17) we have that A = -B.

Now $(k^2 - l^2)^{\frac{1}{2}}$ is to be positive for k > 1 if the displacement is to remain finite at infinite height. Queney and Lyra, and most later workers in the field took the radical to be

$$- i (l^2 - k^2)^{\frac{1}{2}}$$

whereas Scorer took it to be

$$+ i (l^2 - k^2)^{\frac{1}{2}}.$$

The controversy was resolved by Crapper (1959), who following the mathematical formalism of Rayleigh, showed that the former was true. Corby and Sawyer (1958) showed that Scorer's choice actually leads to upstream waves not lee waves.

From w continuous across the interface, $\mu_1 \neq \mu_2$, therefore C = A and

$$e^{\mu_1 h} + e^{-\mu_1 h} = e^{-\mu_2 h} \qquad (5.20)$$

and from w_z continuous across the interface

$$\mu_1 (e^{\mu_1 h} - e^{-\mu_1 h}) = - \mu_2 e^{-\mu_2 h} \qquad (5.21)$$

Substituting (5.21) into (5.20) gives

$$\tanh \mu_1 h = - \frac{\mu_1}{\mu_2} \qquad (5.22)$$

where $\mu_1 = (k^2 - l_1^2)^{\frac{1}{2}}$ and $\mu_2 = (k^2 - l_2^2)^{\frac{1}{2}}$. Eq. (5.22) is the same as that derived by Scorer, except for the minus sign. There are no solutions of (5.22) for $l_2 > l_1$ for real values of k. If $l_2 > l_1$ there are solutions for complex values of k. There is also no solution for $k > l_1$ but there may be discrete lee waves for values of k for $l_1 > k > l_2$. Then substituting into (5.22)

$$\mu_1 = -i \nu_1 = -i (l_1^2 - k^2)^{\frac{1}{2}}$$

(choosing the negative radical for the reasons given above) gives

$$\tan \nu_1 h = - \frac{\nu_1}{\mu_2} \qquad (5.23)$$

An obvious solution of the interface equation is $\nu_1 = 0$, i.e. $l_1^2 = k^2$. However, this is not a practical solution of the wave equation:

$$w'' + (l^2 - k^2) = 0$$

for it means that in the lower layer $w'' = 0$, which is hardly ever true in practice. Therefore $\nu_1 = 0$ is not a solution. Equation (5.23) has solutions only if

$$(l_1^2 - l_2^2)^{\frac{1}{2}} h > (2n + \tfrac{1}{2})\pi \qquad (5.24)$$

If there are solutions for n = 0,1,2,...,N-1, there are N discrete waves. Eq. (5.23) may be solved numerically for values of k which result in waves of wavelength $\frac{2\pi}{k}$.

6. Bounded Two Layer Atmosphere

If at any level the component of the wind velocity parallel to the flow across the mountain goes to zero then there will usually be no waves above this level (Gerbier and Berenjer, 1960). If U goes to zero in general l^2 becomes extremely large or infinite. This implies reflection of waves at this level trapping the waves. The introduction of a rigid boundary at this level will then have no effect on the waves. However, the introduction of a rigid boundary at some finite height will have some effect on the solution of the wave equation as it is solved according to the given boundary conditions.

The general form of w(z) which is a solution of the wave equation (5.15) is given by (5.17). Hence taking the two layer atmosphere as defined in the unbounded two layer theory, except with a rigid boundary at height H and choosing w(z) to have the following forms in each of the two layers:

$$w_1(z) = A\, e^{\mu_1 z} + B\, e^{-\mu_1 z} \tag{5.25}$$

and $$w_2(z) = C\, e^{\mu_2 z} + D\, e^{-\mu_2 z} \tag{5.26}$$

From the lower boundary condition that $w_1(0) = 0$, $B = -A$.
From the upper boundary condition that $w_2(H) = 0$

$$D = - C\, e^{2\mu_2 H}$$

The continuity of w and w' at the interface gives

$$A\,(e^{\mu_1 h} - e^{-\mu_1 h}) = C\,(e^{\mu_2 h} - e^{\mu_2(2H-h)}) \tag{5.27}$$

and

$$\mu_1 A\,(e^{\mu_1 h} + e^{-\mu_1 h}) = \mu_2 C\,(e^{\mu_2 h} + e^{\mu_2(2H-h)}) \tag{5.28}$$

Eq. (5.27) divided by (5.28) gives the interface equation

$$\frac{\mu_2}{\mu_1} \tanh(\mu_1 h) = \frac{e^{\mu_2 h} - e^{\mu_2(2H-h)}}{e^{\mu_2 h} + e^{\mu_2(2H-h)}} \tag{5.29}$$

or $$\frac{\tanh(\mu_1 h)}{\mu_1} = \frac{\tanh(\mu_2(h-H))}{\mu_2} \tag{5.30}$$

When $H \to \infty$ $\tanh(\mu_2(h-H)) \to -1$. Thus when $l_1^2 > k^2 > l_2^2$ and as the boundary goes to infinity (5.30) approaches eq. (5.23), the unbounded case.

If we now consider $k^2 < l_2^2, l_1^2$, both μ_1 and μ_2 are imaginary. Eq. (5.30) contains only real terms and may have solutions in the range. It must be noted that such

solutions give a sinusoidal variation of $w_2(z)$ and so are only practicable in the bounded case to ensure that there is zero energy at great height. A suitable level for the boundary would be where U = 0 and/or where l^2 is very large. l^2 often becomes large in the stratosphere near the tropopause. The effect of the introduction of a boundary at such a height is looked at in the consideration of particular balloons.

Corby and Sawyer (1958) found that the introduction of a rigid boundary at about the tropopause introduced a long wavelength component which had a maximum amplitude high in the troposphere. It did not affect the lower wavelength component predicted by the unbounded theory very much as its amplitude was very small at the level of the boundary. Fig. 5.2 shows the graphical solution of the case considered by Corby and Sawyer, namely, $l_1^2 = 4.0$ km^{-2}, $l_2^2 = 0.3$ km^{-2}, h = 1.0 km and H = 11.0 km. It shows that there is one solution for $k^2 < l_2^2$ giving rise to the long wavelength component.

It is of interest to see what the effect of varying the height of the boundary is. Fig. 5.3 show the results of a numerical solution of wavelengths from (5.30) for the above case, where the height of the boundary is raised from 2 km to 20 km. It is seen that the first resonance mode decreases in wavelength extremely rapidly as the boundary

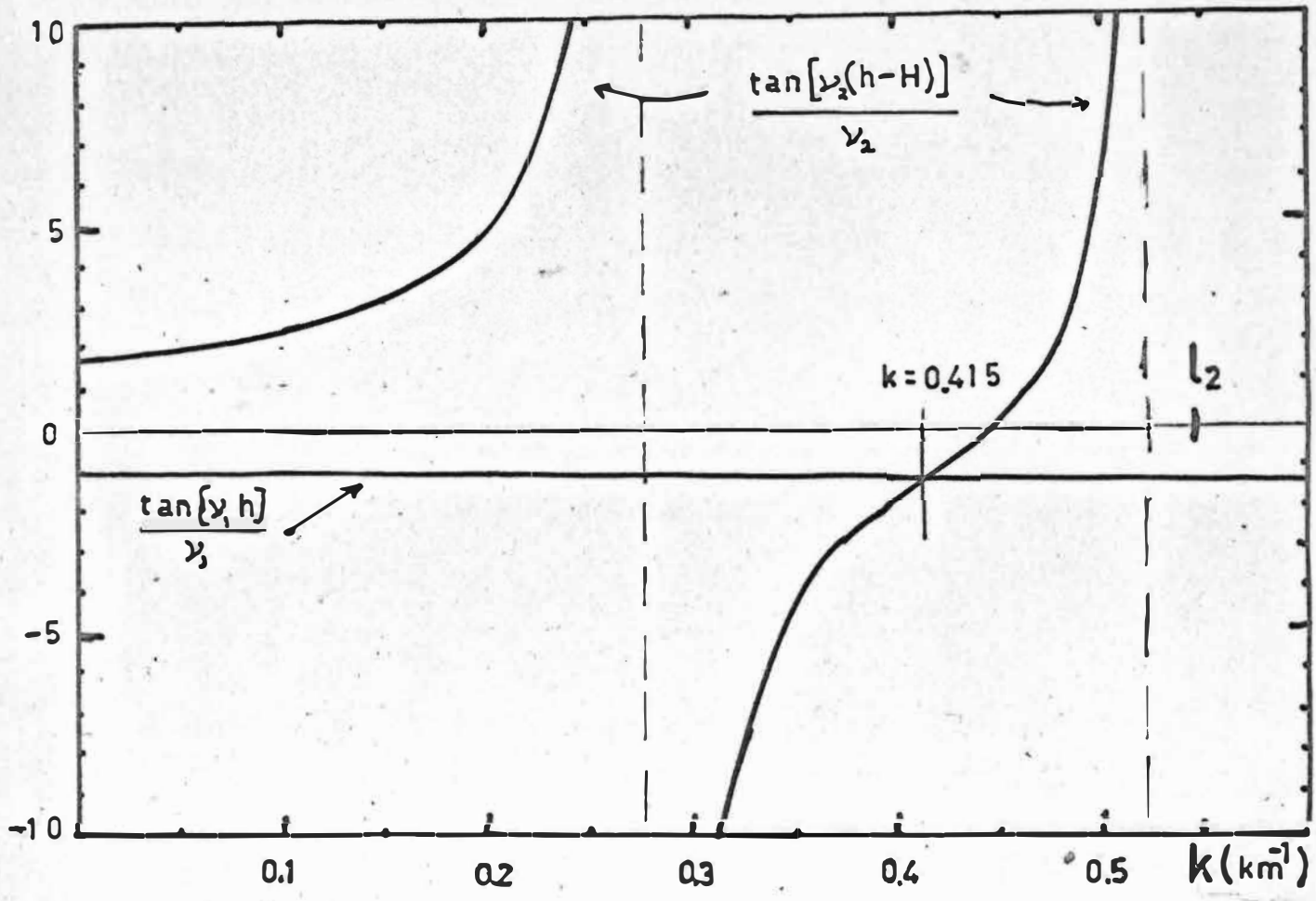

FIG 5.2: Graphical solution of the case considered by Corby and Sawyer (1958)

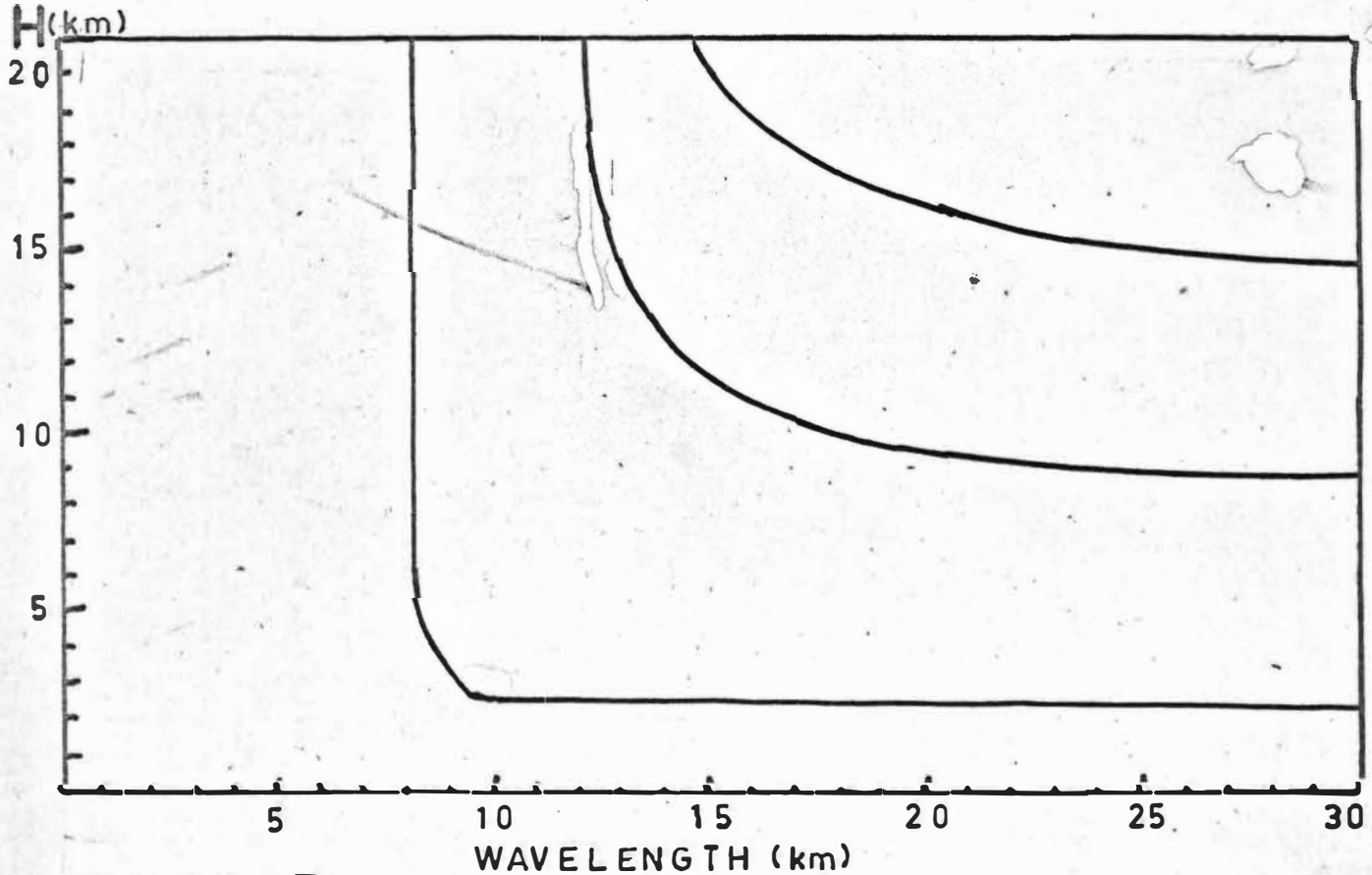

FIG 5.3: The effect of the boundary height om the wavelength in the bounded two layer model. ($l_1^2 = 4\,km^{-2}, l_2^2 = 0.3\,km^{-2}, h = 1\,km$)

is raised above 2 km and approaches the 8.25 km wavelength of the unbounded solution. As the height of the boundary increases further more resonance modes appear whose wavelengths drop quickly with increasing H to be asymptotic to a wavelength of approximately 12.2 km. There will be an infinite number of discrete modes for infinite H so again we see that H must be finite to give a practicable solution.

7. Three Layer Model (After Berkshire (1969))

If the two layers in the above theory correspond to the troposphere and stratosphere we would expect that since the stratosphere is in general more stable than the troposphere ($l_2^2 > l_1^2$) there will be no lee waves as there are no real values of k which satisfy (5.23). However, in practice waves are observed under such conditions, i.e. when the troposphere/stratosphere are considered as two layers, the stratosphere being more stable than the troposphere. Berkshire showed that the solution for the displacement $\varsigma(x,z)$ in the general case includes an integral term which is a function of k, namely

$$\text{Real} \int_0^\infty e^{ik(x-\xi)} \frac{F(k,z)}{F(k,0)} \, dk \qquad (5.31)$$

where the F(k,z) is a function which is a solution of the wave equation for the given boundary conditions. For most values of k F(k,0) is large but for some values of k, it is

very small. Such values of k contribute considerably to the integral and to the displacement, i.e. they correspond to the wavenumbers of lee waves that exist for the given conditions.

Berkshire (1969) derived an expression for F(k,0) for a three layer model in which $l_2 = 0$. This is rather restrictive so for more flexability the following general expression has been derived for F(k,0). The so-called Amplitude Factor is $F(k,0)^{-1}$, where

$$|F(k,0)|^2 = 1 + \frac{\sin^2(\mu_1 h_1)}{\mu_1^2}\left[(l_2^2 - l_1^2) + (l_3^2 - l_2^2) \times \left\{\frac{\mu_1}{\mu_2}\sin(\mu_2 h)\cot(\mu_1 h_1) + \cos(\mu_2 h)\right\}^2\right] \quad (5.32)$$

By solving (5.32) numerically for the range of k under interest a wave number spectrum is obtained which is in many ways analogous to a filter response curve in electronics. It gives an indication of the response of the three layer atmosphere to the various values of k.

8. Exponential Troposphere Model (Doos' Method)

If the l^2 profile can be approximated by an exponential of the form

$$B(z)^* = B_0 e^{-\lambda z} + B_1 \quad (5.33)$$

the wave equation (5.15) can be transformed by changing the independent variable to

$$\eta = \beta e^{-\frac{\lambda z}{2}} \tag{5.34}$$

where

$$\beta = 2\frac{\sqrt{B_0}}{\lambda} \tag{5.35}$$

Eq. (5.15) becomes

$$\eta^2 \frac{d^2 w}{dz^2} + \eta \frac{dw}{dz} + \left[\eta^2 - \frac{4}{\lambda^2}(k^2 - B_1)\right] w = 0 \tag{5.36}$$

which is a Bessel equation having solutions

$$w = A J_\nu (\beta e^{-\frac{\lambda z}{2}}) + B Y_\nu (\beta e^{-\frac{\lambda z}{2}}) \tag{5.37}$$

for $k \geqslant k_0 = \sqrt{B_1}$

where $$\nu = \frac{2}{\lambda}\sqrt{k^2 - B_1} \tag{5.38}$$

and

$$w = C J_{i\mu} (\beta e^{-\frac{\lambda z}{2}}) + D J_{-i\mu} (\beta e^{-\frac{\lambda z}{2}}) \tag{5.39}$$

where

$$\mu = \frac{2}{\lambda}\sqrt{B_1 - k^2} \qquad k < k_0 = \sqrt{B_1} \tag{5.40}$$

since Bessel functions of the second kind (Y) approach $-\infty$ when the argument tends to zero ($z \to \infty$) we must put B = 0 to fulfil the upper boundary condition that the wave amplitude goes to zero at great heights. Generally B_1 is close to zero so for real wave numbers we can neglect the second form of the equation.

For a single bell shaped mountain ridge, height h and half width a,

$$\zeta(x,z) = F(z)\ \mathrm{Re} \int_{k_0}^{\infty} e^{-ak}\, e^{ikx}\, \frac{J_\nu(\beta\, e^{-\frac{\lambda z}{2}})}{J_\nu(\beta)}\, dk \qquad (5.41)$$

$$\text{where } F(z) = \frac{U(0)}{U(z)}\, ab\, \exp\left\{\frac{g-R\gamma}{2RT_o}\, z\right\} \qquad (5.42)$$

$$\text{and } \frac{g-R\gamma}{2RT_o} = \frac{34.2 + \frac{dT}{dz}}{2\, T_o(z)}\ \mathrm{km}^{-1} \qquad (5.43)$$

where T_o is the temperature of the undisturbed flow. Doos shows, and it can be seen by applying the same reasoning used in the three layer theory, to (5.41), that the allowable waves are given by the solutions ν_n of

$$J_{\nu_n}(\beta) = 0 \qquad (5.44)$$

Then from (5.38)

$$k_n = (B_1 + (\frac{\lambda \nu_n}{2})^2)^{\frac{1}{2}} \qquad (5.45)$$

The amplitudes are then given by

$$A_n = \lambda\pi ab\, \frac{U(0)}{U(z)}\, \exp\left\{\frac{g-R\gamma}{2RT_o}\, z - a\, k_n\right\} \times \frac{\sqrt{k_n^2 - B_1}}{k_n} \qquad (5.46)$$

$$\times \left[\frac{J_\nu(\beta\, e^{-\frac{\lambda z}{2}})}{\frac{d}{d}\, J_\nu(\beta)}\right]_{\nu=\nu_n}$$

This method does not take account of the stability of the stratosphere and the trapping that can occur due to the increase in ℓ^2.

9. Corby's Mean Tropospheric Wavelength

Corby (1957) discovered an empirical relationship which related the mean tropospheric wavelength, $\bar{\lambda}$, linearly to the mean tropospheric wind speed, $\bar{U}$. Fritz (1965) used this expression to compare it with the lee wavelengths observed in satellite data. Namely

$$\bar{\lambda} = 2\pi \left(\frac{g\bar{\beta}_1}{\bar{U}^2}\right)^{\frac{1}{2}} \tag{5.47}$$

where $\bar{\beta}_1$ is the mean value of β_1 in the troposphere.

10. Parcel Method

If a parcel of air is displaced vertically from its natural level and released it will tend to oscillate about its natural level at the "Vaisala-Brunt" frequency the period of which is given by

$$\tau(z) = \frac{2\pi T(z)}{g(\gamma_a - \gamma(z))} \tag{5.48}$$

and $$\lambda = U(z)\,\tau(z)$$

where γ_a and $\gamma(z)$ are the dry adiabatic and actual lapse rates of the airflow. Wavelengths derived from this method would be expected to be very approximate since for a wave with a finite amplitude T, τ and U vary across the height of one oscillation so will introduce considerable complexity.

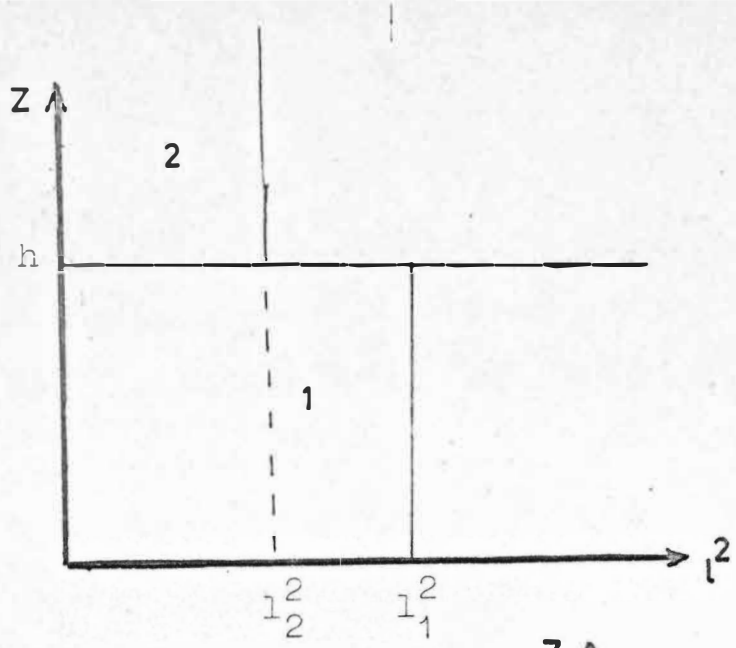

(a) Two layer Model

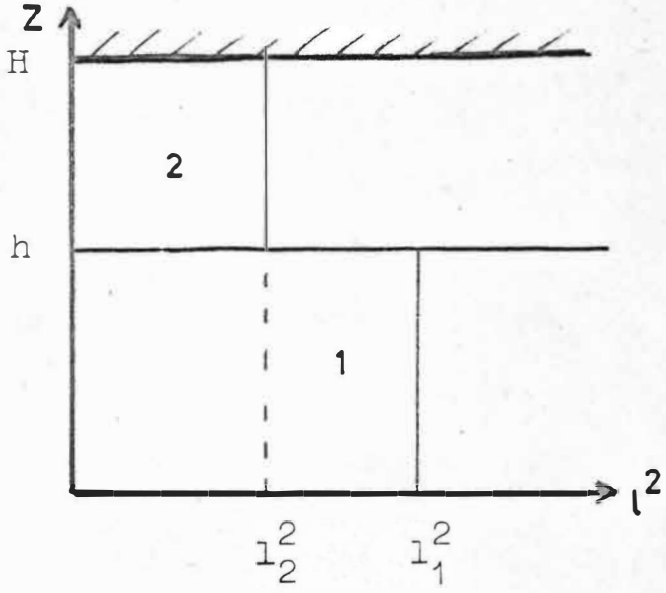

(b) Bounded Two Layer Model

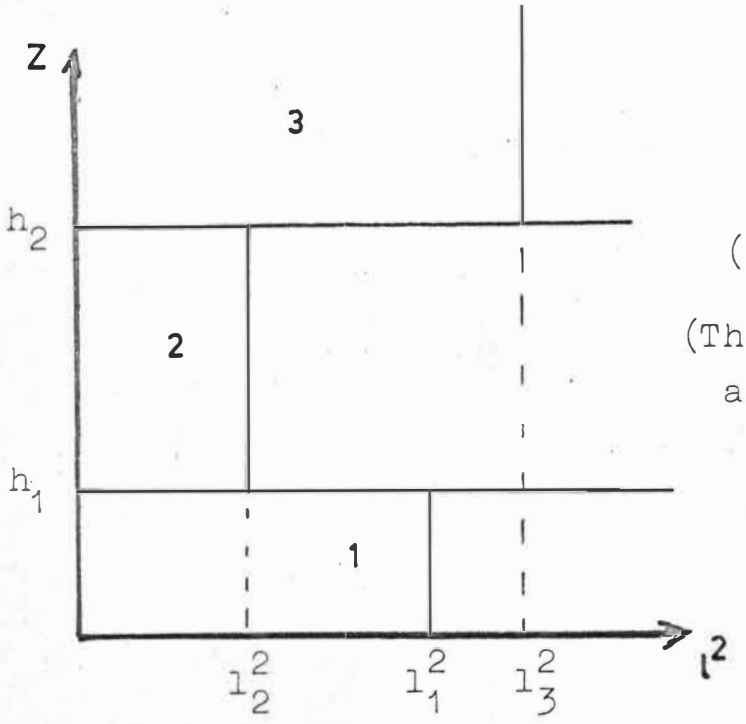

(c) Three Layer Model

(The l^2 parameters are arbitary.)

FIG5.4: CONSTANT l^2 LAYER MODELS.

C H A P T E R 6

LEE WAVE CHARACTERISTICS

Rather than including an extensive literature survey which would just present the work done by other people I have tried to extract from the literature a summary of the theoretical and observational conditions which favour the production of lee waves. I have tried to relate the theory and observations, to explain the various aspects in physical terms and where possible to evaluate the parameters and to apply them to the situation here in Canterbury. This, hopefully, will enable me to understand what is happening and also to interpret the results of my balloon flights adequately and accurately.

1. Conditions Favourable for Lee Wave Production

A consideration of a simple two layer atmosphere gives an indication of the type of conditions which must be satisfied in order that waves can exist. Scorer (1949) showed that for there to be discrete wave solutions in a two layer atmosphere the top layer must be less stable than the lower $l_2^2 < l_1^2$ (Eq. (5.2)). There often exists an adiabatically mixed layer at the ground for which $l^2 = 0$. Waves have still been observed under such conditions. Scorer (1951)

showed that for lee waves which have a maximum amplitude in the lower layers of the atmosphere, $l^2 > k^2$ in a fairly deep layer low down, but $l^2 < k^2$ in a deep layer above. This must be true for w" in (5.15) must change sign at least once since w = 0 at the ground and at some great height, and for waves to exist w is non-zero in between. Hence a criteria which I have called the 'Scorer Criteria' can be stated as "for lee waves to occur l^2 must reach a maximum low in the troposphere and then decrease upwards". This was first stated by Scorer. This criteria is usually fulfilled in the troposphere when waves are observed. See for example Doos (1962), Colquhoun (1967) and Wooldridge and Lester (1969). It is also evident from the results of this project.

The actual conditions which fulfil the Scorer Criteria can be derived from (5.16), namely

$$l^2 = \frac{g\,\beta_1}{U^2} - \frac{U''}{U} \qquad (5.16)$$

Neglecting the effect of the wind shear

(i) For l^2 a maximum low in the troposphere: This occurs if U is small and/or β_1 is large. β_1 is large if the lapse rate is small. Often in Canterbury U near the ground is less than 2-3 m sec^{-1} which makes l^2 greater than 20 km^{-2} or even greater than 50 km^{-2} on some occasions.

(ii) For l^2 to decrease above this level: This may be caused by the lapse rate decreasing and tending towards the dry adiabatic lapse rate. Or, as is usually the case, it is caused by an increase in the horizontal wind speed with height. It may be seen by consideration of the airflow profiles in Chapter 7 that usually the lapse rate is approximately constant at about 6-8^{o}K/km and the variation in l^2 in the troposphere is mainly due to changes in the wind speed.

(iii) An additional factor must be considered for flow across mountain ranges (long ridges); that is the angle of the flow to the direction perpendicular to the ridge. Gerbier and Gerenger (1960) found that by far the most pronounced effects were produced when the wind flow was within 30^{o} of the direction. This is also mentioned by Alaka (1960) et al. Also for good waves the wind direction should remain approximately constant with height. If at any level the direction of the wind becomes parallel to the ridge Gerbier and Gerenger found that wave lift usually disappears above this level. They also found that the wind speed must exceed some minimum value before waves will be set up. This is discussed further below.

For a complex set of mountain ranges, such as the Southern Alps (New Zealand) it is very difficult to apply the first part of (iii) above as there are directions other

than the direction perpendicular to the main ranges for which the spacing of the ridges is in resonance with the natural frequencies of the airflow. This occurred on 12/5/71 for example. The mean tropospheric wind was northerly and although the perpendicular direction to the main ranges is Northwesterly, large amplitude standing lee waves were observed visually. Their wavelength was about 20 km.

2. Critical Velocity Conditions

It has been found empirically that the horizontal wind speed is one of the most important factors in the consideration of standing lee waves. It is not only important because of its role in the l^2 parameter but because it is observed that unless the wind exceeds some minimum critical velocity or if it exceeds some maximum critical velocity at some level under given conditions there are no standing lee waves.

A first order explanation for this can be seen by noting that the waves in a standing wave train are actually propagating upstream at exactly the downstream wind speed. It can be reasoned that if the wind velocity is too low or too high there will be no discrete wave produced that has the corresponding velocity so the disturbance will tend to propagate upstream or be carried away downstream by the wind.

(a) Minimum Critical Velocity

The observations of several authors seem to imply that this minimum velocity is dependent on the height of the mountain under consideration. For example the approximate minimum wind speeds required at the mountain height for waves to exist for various mountain ranges are given in Table 6.1.

Table 6.1: A comparison between the approximate minimum wind speed required for waves to be produced and the heights of the mountains producing them.

Author	Mountains	Height(m)	Velocity ($m\ sec^{-1}$)
Booker(1965)	Allegheny	300	5.0
Pilsbury(1955)	In the United Kingdom	600	7.5
Manely(1945)	Pennines	800	8.0
Larsson(1954)	Jamtland		10.0
Gerbier and Berenger(1960)	French Alps	1,400	10.0
Jenkins and Knutter(1953)	Sierra Nevada	2,000?	12.5

The existence of such a velocity is reasonable also from the point of view that wave would not be expected to result from a mountain if the time taken to traverse the mountain was

large compared to the period of the natural oscillation of the air. Corby and Wallington (1956) show that the condition for maximum amplitude of waves occurs when the critical conditions are just satisfied.

(b) Critical Velocity Conditions from the Two Layer Theory

One particular day last winter looked as though it would be a good wave day as it had a very strong upward wind gradient such that the wind was in excess of 150 knots at 7 km. However, there was no evidence of waves whatsoever. This prompted me to look for a critical maximum velocity. A study of the two layer theory revealed the relation between the velocities in the two layers (assumed constant) for an isothermal atmosphere. The interface equation (5.23) has at least one solution if, from (5.24)

$$(l_1^2 - l_2^2)^{\frac{1}{2}} h > \frac{\pi}{2} \qquad (6.1)$$

where l^2 is defined by (5.16). For an isothermal atmosphere in the absence of wind shear

$$\beta_1 = \text{const} = \frac{\gamma_a}{T} = \frac{10}{T} \text{ km}^{-1} \quad \text{and} \quad l^2 = \frac{10^5}{T U^2} \text{ km}^{-2} \qquad (6.2)$$

where T is the absolute temperature and U is the horizontal wind speed in m sec^{-1}. Substituting (6.2) into (6.1) an expression for the critical condition for lee waves in terms of the velocities, the temperature and the height of the

interface:

$$\frac{1}{U_1^2} - \frac{1}{U_2^2} = \frac{\pi^2 T}{4 \times 10^5 h^2} \qquad (6.3)$$

For a given temperature and interface height two critical velocities can be derived from (6.3).

(i) The maximum velocity in the lower layer for waves to be produced, for a given velocity in the upper layer. Assuming that the interface is above the mountain height this velocity is then the maximum velocity at the mountain height for which standing waves can exist.

(ii) The minimum velocity in the upper layer which will support waves for a particular velocity in the lower layer. This must always be greater than the velocity in the lower layer for (6.1) to hold.

If the particular velocities are outside these critical velocities the inequality (6.1) is not realised so there are no waves. Eq. (6.3) has been plotted in Fig. 6.1 for $T = 260^{\circ}K$, approximately the average temperature of the troposphere, for various values of the interface height. It is clear that the interface height limits the maximum value of U in the lower layer ($U_{1\ max}$) and for a particular value of h, $U_{1\ max}$ tends to a limiting value no matter how great the velocity in the upper layer is. This limiting value can be used as an indication of the maximum wind speed allowed at the mountain level for lee waves to exist in an

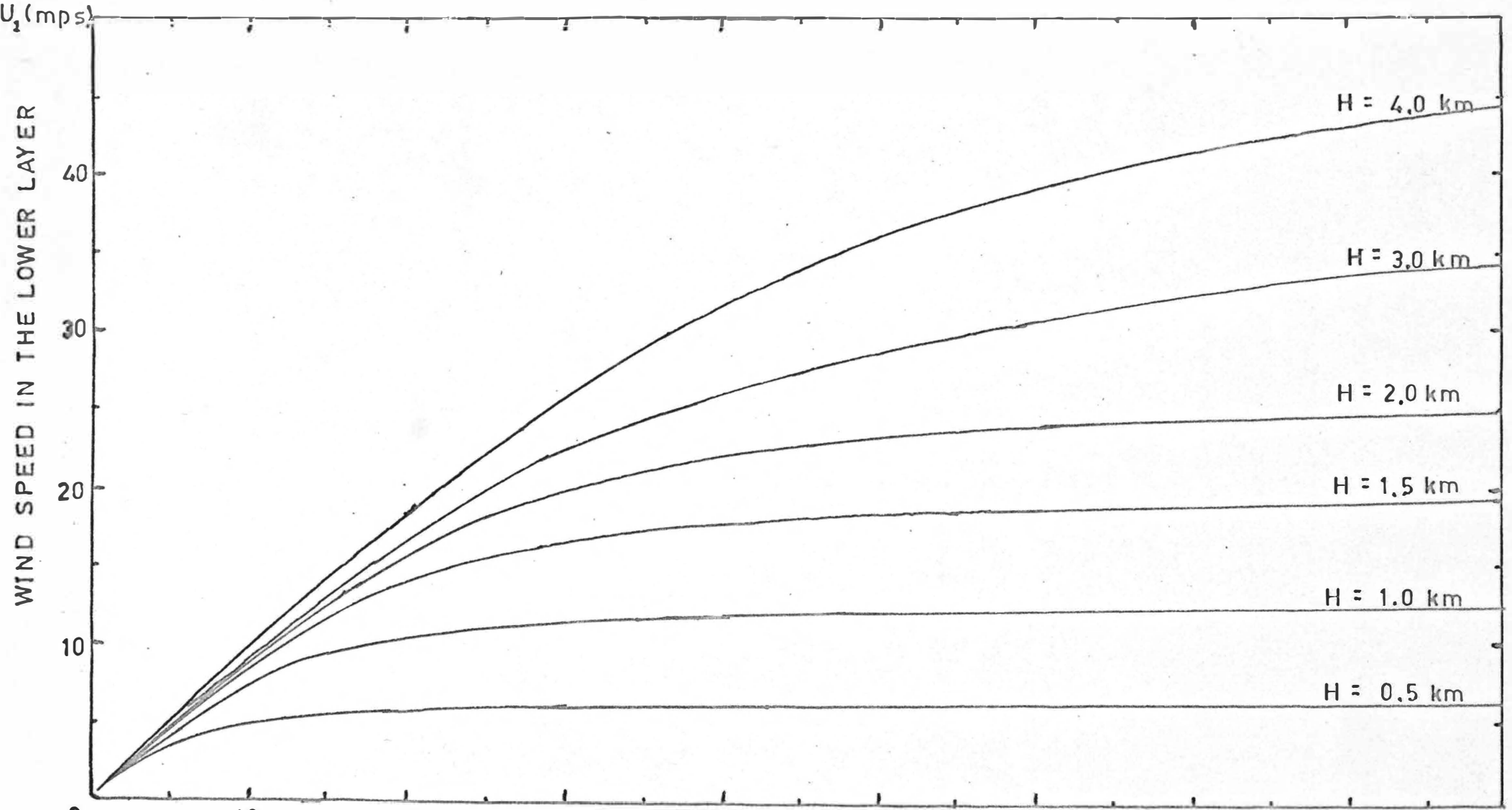

FIG 6.1: CRITICAL CURVES FOR THE WIND SPEEDS IN A TWO LAYER ISOTHERMAL ATMOSPHERE ($T = 260^{\circ}$ K)

isothermal atmosphere. It is shown below that the limiting value is not very sensitive to changes in temperature so can probably be used as an approximation to the maximum wind speed for waves in a more general atmosphere.

For example: In Canterbury the interface height is often about 1 km and the average velocity in the upper layer seldom exceeds 40 m sec^{-1}. For h = 1 km, assuming an isothermal atmosphere T = 260°K, this theory predicts a maximum wind speed in the lower layer for waves to exist of 11.8 m sec^{-1}. If T = 300°K the critical velocity is about 11.2 m sec^{-1}. This is in general agreement with Förchtgott's classification. In his terms wind speeds greater than $U_{1\ max}$ result in rotor streaming rather than wave streaming. However his observations do not show a minimum velocity in the upper layers, greater than U_1, for which waves do not exist, but rather a critical velocity, which is a function of height, which if exceeded at any level results in rotor streaming, i.e. turbulent flow, about and above that level.

A lower critical value of the velocity across the mountains below which no waves can exist cannot be obtained from (6.1) as in the two layer theory the smaller U_1, the greater is the left hand side of (6.1), which increases the possibility of the existence of waves.

3. Förchtgott's Wave Classification

Förchtgott (1949, 1952), a gliding instructor, made extensive observations of the airflows over mountains in Bohemia using gliders and both visual and photographic observations of clouds. He developed the following empirical classification:

(a) Undisturbed Streaming: This occurs when the winds are light. Each streamline executes a single wave over the mountain then returns quickly to its natural height.

(b) Standing Eddy Streaming: This occurs with slightly stronger winds which increase slowly with height. A standing eddy occurs just in the lee of the mountain.

(c) Wave Streaming: With still stronger winds and a marked increase in wind velocity with height the standing eddy disappears and lee waves develop in association with a stationary system of vortices having approximately horizontal axes. Turbulence is associated with the vortices (rotors). The waves die out away from the ridge both horizontally and vertically. He did not find waves down to the ground in practice. (Corby (1954) comments that the existence of these closed vortices does not seem conclusive as the existence of so-called rotors would be provided by the wind shear in the wave system. The turbulence too could be accounted for by the wind shear, which would be intensified in the crests and troughs of the waves.)

(d) Rotor Streaming: With very strong wind that exists in a layer of restricted vertical extent, the wave train breaks down to form a very turbulent flow. Förchtgott says that this will take place when the layer falls to about 1½ times the height of the ridge.

These types of flow are summarised in Fig. 6.2 which shows the critical curve that Förchtgott found empirically from his observations. As he had observed turbulent flow beneath the level of the mountain ridge he draws a horizontal line at the height of the mountain below which there is chaotic flow. This line intersects the critical curve at C, dividing the region above the curve into standing eddy and wave streaming and the area below the curve into rotor streaming.

It can be seen from the diagram that for Canterbury where the waves are produced by mountains about 1.5 to 2.0 km high have maximum wind speed at the level of the mountains of about 15 m sec^{-1}. This is of the same order as that predicted by the two layer theory, depending on the height of the interface. Thus observations done elsewhere suggest that the Southern Alps should produce lee waves when the wind at the level of the mountain ridge lies in the range of approximately 10 mps to 15 mps.

To obtain the type of streaming at any level from Fig. 6.2 the right hand height axis is used together with the velocity at that height on the bottom axis.

FiG 6.2

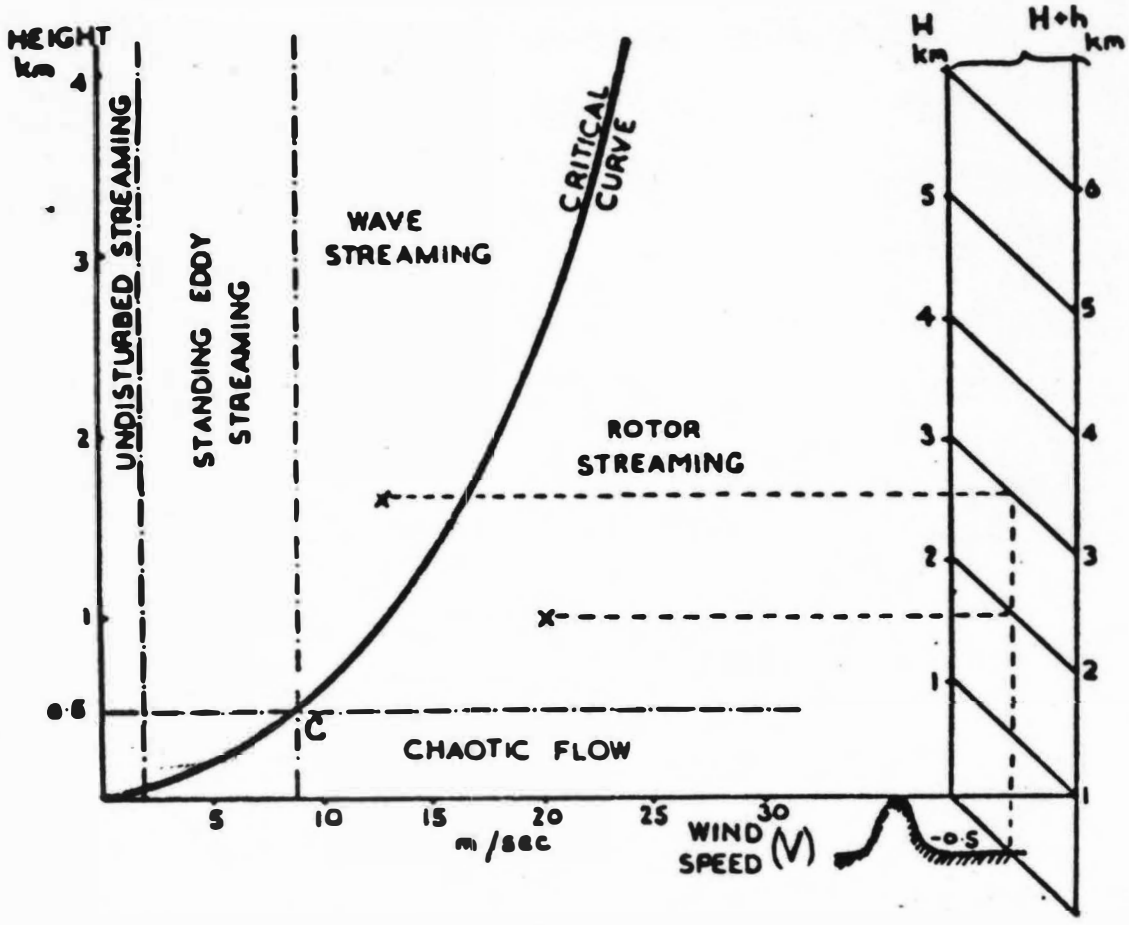

Diagram for determining type of mountain airflow (after Förchtgott).

4. Harrison's Mountain Wave Index

Harrison studied lee waves as a source of severe CAT for jet aircraft at high altitudes over the American Rockies. He notes that statistics show that at mid-latitudes aircraft experience a higher incidence of turbulence at 35,000 feet than at 25,000 feet. This may be due to the trapping of waves by the tropopause causing an intensification of turbulence at the level of the tropopause. The empirical index he used to predict the occurrence of waves at turbojet levels involves the differential sea level pressure across the mountains and the maximum wind speed between 15,000 and 20,000 feet. The critical curves are shown in Fig. 6.3.

5. Lee Wave Wavelengths

The wavelength of a wave is a function of the horizontal wind speed and the restoring forces, or the stability. This can be seen by considering the Scorer parameter on which the wavelength is very dependent. Or it can be seen simply from the parcel theory in which the wavelength is the product of the wind speed and the period of the natural oscillation of the parcel of air. This period is related to the inverse of the temperature gradient and thus the stability.

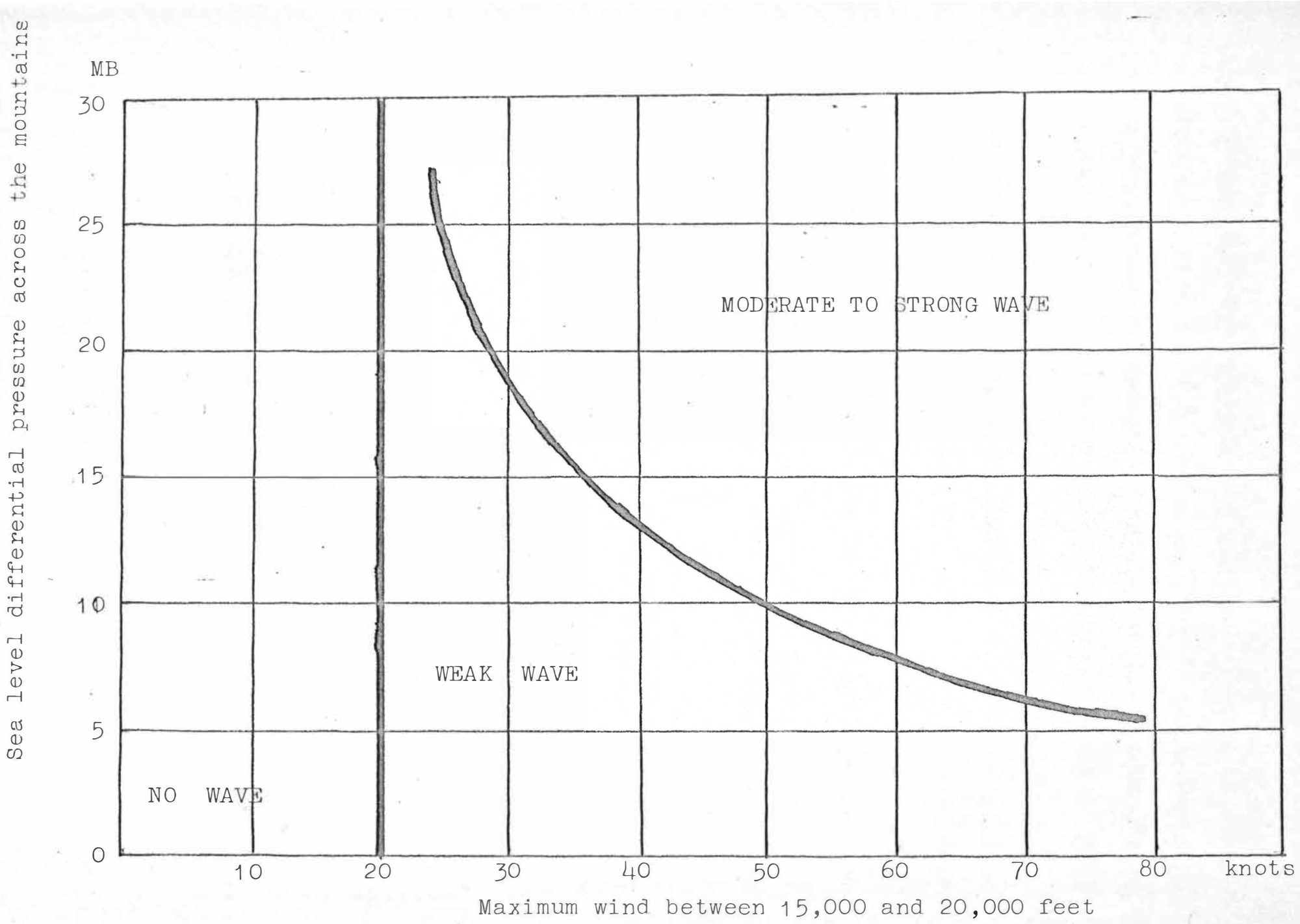

Fig 6.3: Harrison's Wave Index (UAL forcasting nonogram).

Observations (Larsson, 1954) show that lee wave wavelengths generally lie in the range 5-25 km with a majority around 8-10 km. Shorter wavelengths are often observed in the power spectra of constant volume balloon flights and in the cloud structure. (These are not to be confused with billow waves which lie approximately along the direction of the wind rather than perpendicular to it as is the case for lee waves.) Their amplitudes are usually quite small compared to the other waves that are present. Sometimes wavelengths as long as 40-60 km are observed. For example in the power spectra of balloon flights of Wooldridge and Lester (1969) and in some of the balloon flights in this project. Observations of short wavelength waves using balloons are usually limited by the tracking radar accuracy and sampling time. Reiter et al. (1965) observed an extremely long (325 km) wave in the Tiros V photographs.

The various layer or exponential theories give the wavelengths of the waves that are solutions of the wave or interface equation for the given boundary conditions. These may only be expected to be accurate to the extent that the atmosphere is approximated by layers of constant l^2 or an exponential decrease in l^2. The unbounded and bounded two layer theories give wavelengths which generally lie within the outer range given by Larsson. The three layer theory gives a wavenumber spectrum which usually has a continuum of

possible wave numbers for small k which drops off so that above wavenumbers of about 0.7-0.8 km^{-1} (~ 8 km) the amplitude factor is very small. However, 'resonance' peaks of various intensities often occur in this spectrum for wavenumbers as large as about 3 km^{-1} (about 2 km) corresponding to possible lee wave modes.

It is seen in the analysis of the balloon flights in Chapter 7 that the bounded two layer theory gives the same values of wavelengths as the unbounded two layer theory for the short wavelengths and the rigid upper boundary results in the introduction of longer wavelength components as found by Corby and Sawyer (1958). These longer wavelengths are very close to the long wavelengths given by the three layer theory when the boundary is placed at the level where there is a large increase in l^2.

Doos' Bessel function solution for the exponential troposphere gives a wide range of solutions from wavelengths less than 1 km to greater than 200 km. This wide range is perhaps not usual but is possibly due to conditions here in Canterbury such as the föhn wind which results in high lapse rates. The examples that Doos looks at give wavelengths in the range 5.9-26.0 km. The very unstable troposphere ($l^2 < 1$ km^{-2} throughout) experienced here on occasions results in the wider range of wavelengths. For wavelengths greater than about 50-60 km the coriolis force

cannot be neglected. Thus long wavelengths are not valid solutions of the simplified wave equation used by Doos. In Doos' solution usually only the principal and sometimes the second wavelength have non-negligible amplitudes. This agrees with Scorer's choice of the principal wavelength only.

6. Effect on the Wavelength of Variations of the Two Layer Parameters

As for the critical velocity conditions discussed earlier in this chapter I have been rather interested to find out how the wavelength varies with the variation of the Scorer parameters and the interface height. To do this I solved equations (5.23) and (5.30) numerically for a range of the parameters which is mainly applicable to the data obtained in this project. Figures 6.4 and 6.5 show the variations in wavelength for h = 0.5 km to 2.0 km respectively, plotted against the Scorer parameter in the lower layer. Curves for a range of values of the Scorer parameter in the upper layer are shown on each figure.

They show that an increase in l_1^2 results in a decrease in the wavelength and, especially for higher values of h, it results in the introduction of multiple resonance modes which start at longer wavelengths than the initial modes and decrease with increasing l_1^2 to approach the principal mode.

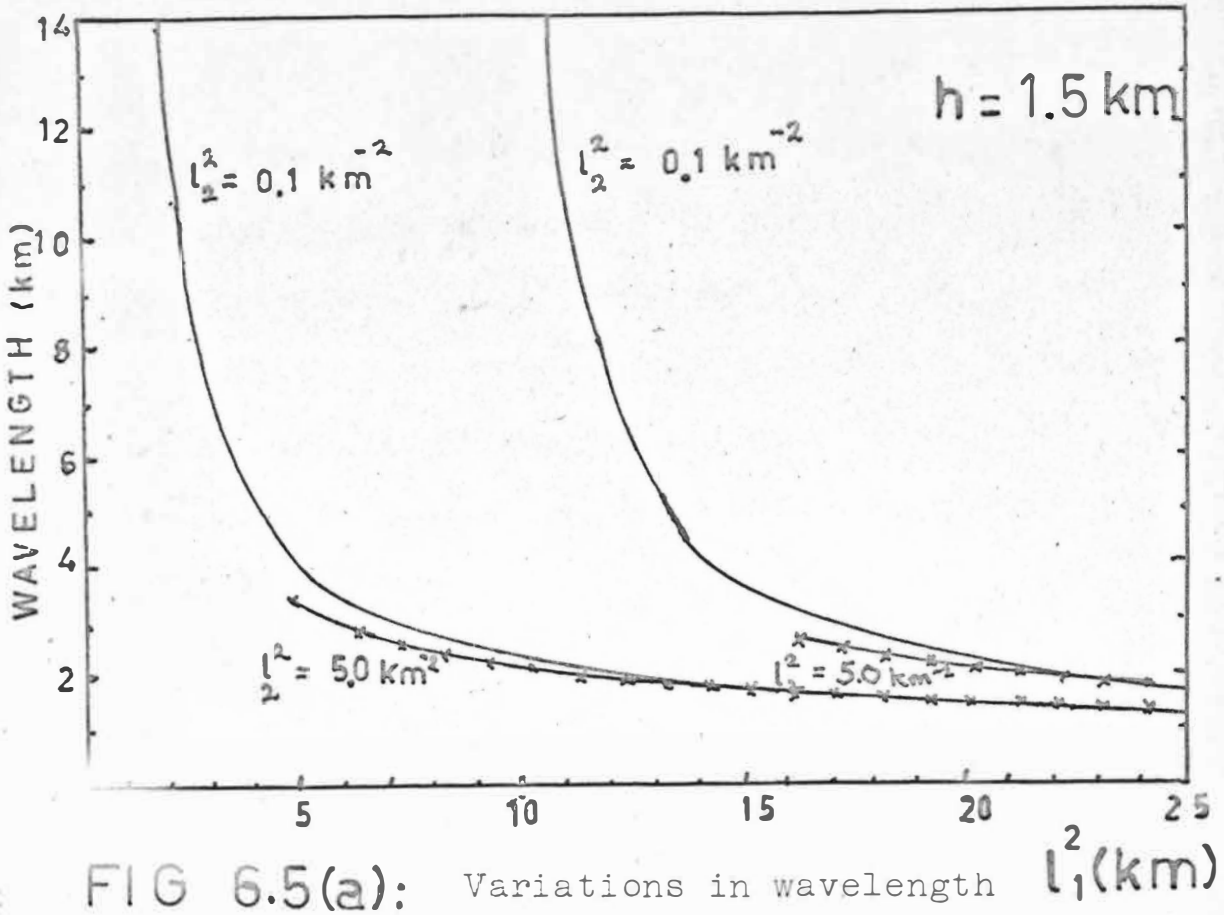

FIG 6.5(a): Variations in wavelength as related to the twp layer theory parameters for h= 1.5km

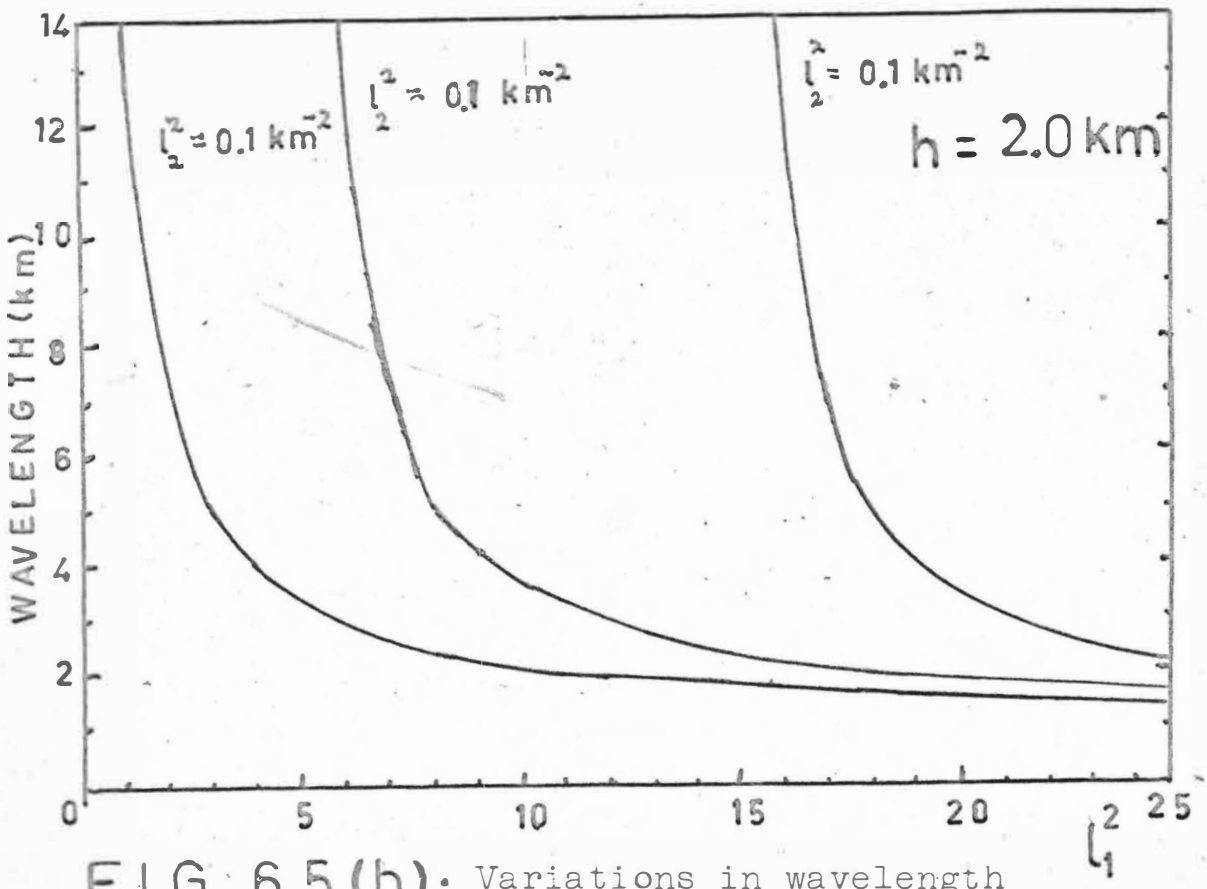

FIG 6.5(b): Variations in wavelength as related to the two layer theory parameters for h= 2.0km

Table 6.2: Showing the variation in wavelength (km) as a function of l_2^2 for various interface heights. ($l_1^2 = 20.0$ km^{-2})

l_2^2	h = 0.5	h = 1.0	h = 1.5		h = 2.0		
0.1	3.24	1.71	2.33	1.54	3.63	1.80	1.48
0.5	3.17	1.70	2.33	1.54	3.58	1.80	1.48
0.9	3.10	1.70	2.32	1.54	3.53	1.80	1.48
1.3	3.04	1.70	2.31	1.54	3.48	1.80	1.48
1.7	2.97	1.70	2.30	1.54	3.43	1.80	1.48
2.1	2.91	1.70	2.29	1.54	3.38	1.80	1.48
2.3	2.88	1.70	2.28	1.54	3.35	1.79	1.48
5.0	2.52	1.68	2.21	1.53		1.78	1.48

Table 6.3: Showing the variation in wavelength (km) as a function of l_2^2 (km^{-2}) for various interface heights h (km) for $l_1^2 = 5.0$ km^{-2}

l_2^2	h = 0.5	h = 1.0	h = 1.5	h = 2.0
0.1	*	6.37	3.94	3.41
0.3	*	5.85	3.90	3.40
1.3	*	4.81	3.76	3.35
2.3	*	4.13	3.61	3.30
3.0	*	3.45	3.24	3.24

*The inequality (6.1) is not satisfied so there are no wave solutions.

Tables 6.2 and 6.3 show the variation in wavelength for constant l_1^2 (5.0 km^{-2}, and 20.0 km^{-2}), for a range of l_2^2 and h. It is evident that the wavelength is not very sensitive to variations in l_2^2 when it is small with respect to l_1^2 or h and it decreases with increasing l_2^2. Increases in the thickness of the lower layer (h) also result in a decrease in the wavelength and as mentioned above, for higher values of l_1^2, it results in the introduction of multiple modes. It is interesting to note that in Table 6.3 as l_2^2 increases the wavelengths for all the interface heights approach approximately the same value of 3.24 km.

7. Effect of the Layer Parameters on the Solutions of the Three Layer Model

As an example the mean values of the parameters were chosen to be:

$$l_1^2 = 25\ km^{-2},\quad l_2^2 = 2\ km^{-2},\quad l_3^2 = 5\ km^{-2},$$

$$h_1 = 1.6\ km,\qquad h_2 = 15\ km$$

The wavenumber spectrum for this case is shown in Fig. 6.6(a). It contains resonance peaks corresponding to wavelengths of 10.0, 6.77, 5.57, 5.14, 4.70 and 4.50 km. By varying each of the parameters in turn, holding the rest at their mean value, the spectra in Figs 6.6(b) to 6.6(f) were

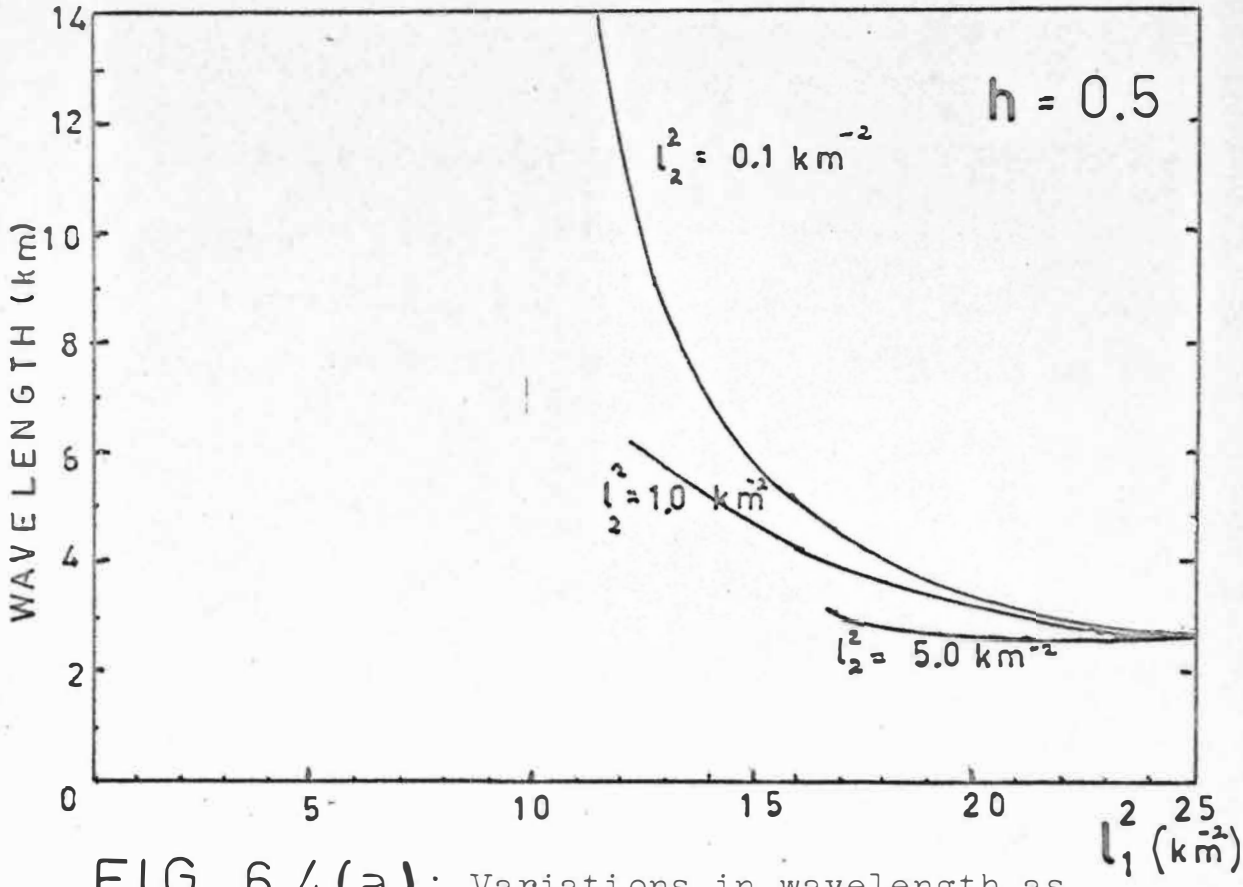

FIG 6.4(a): Variations in wavelength as related to the two layer theory parameters for h = 0.5km

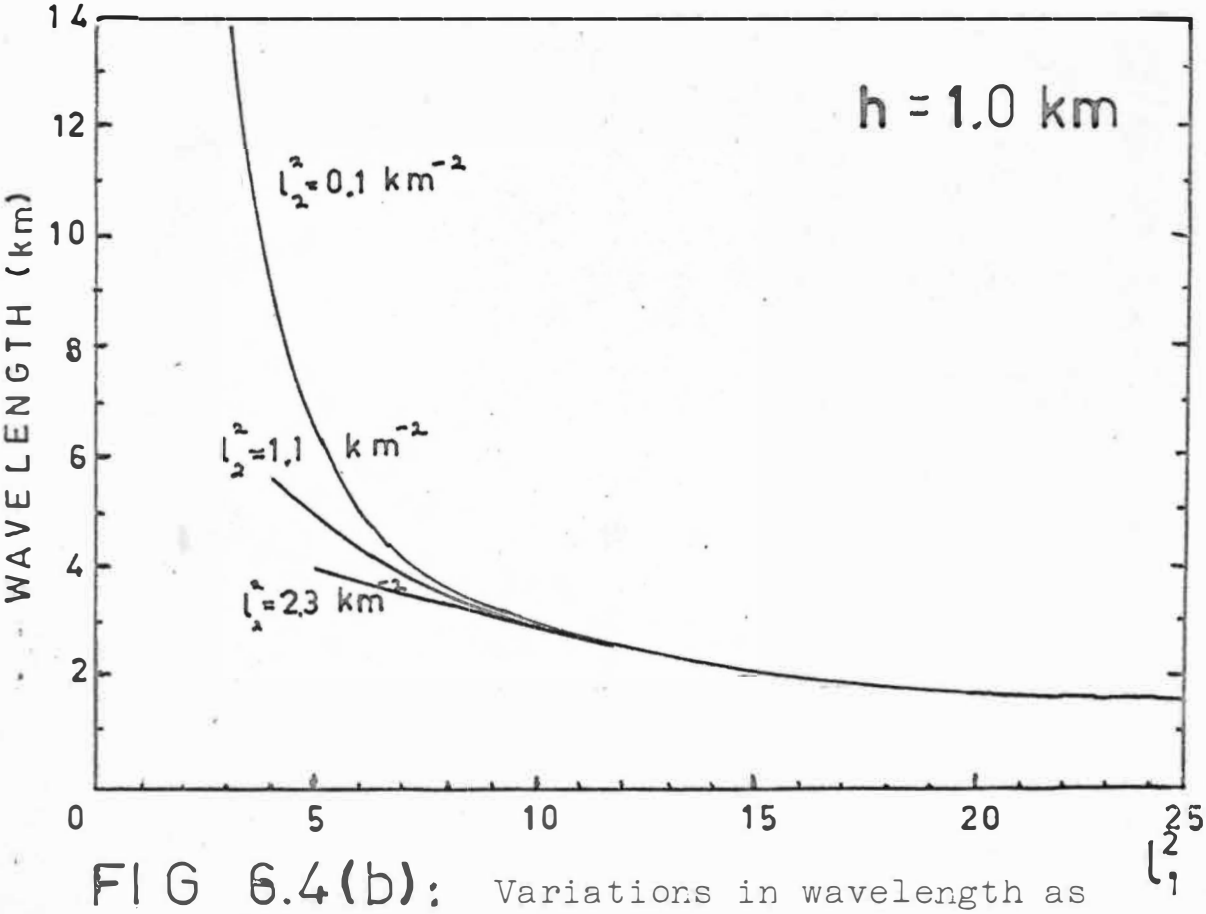

FIG 6.4(b): Variations in wavelength as related to the two layer theory parameters for h = 1.0 km

FIG 6.6: INVESTIGATING THE EFFECT OF THE PARAMETERS ON THE THREE LAYER SOLUTION.

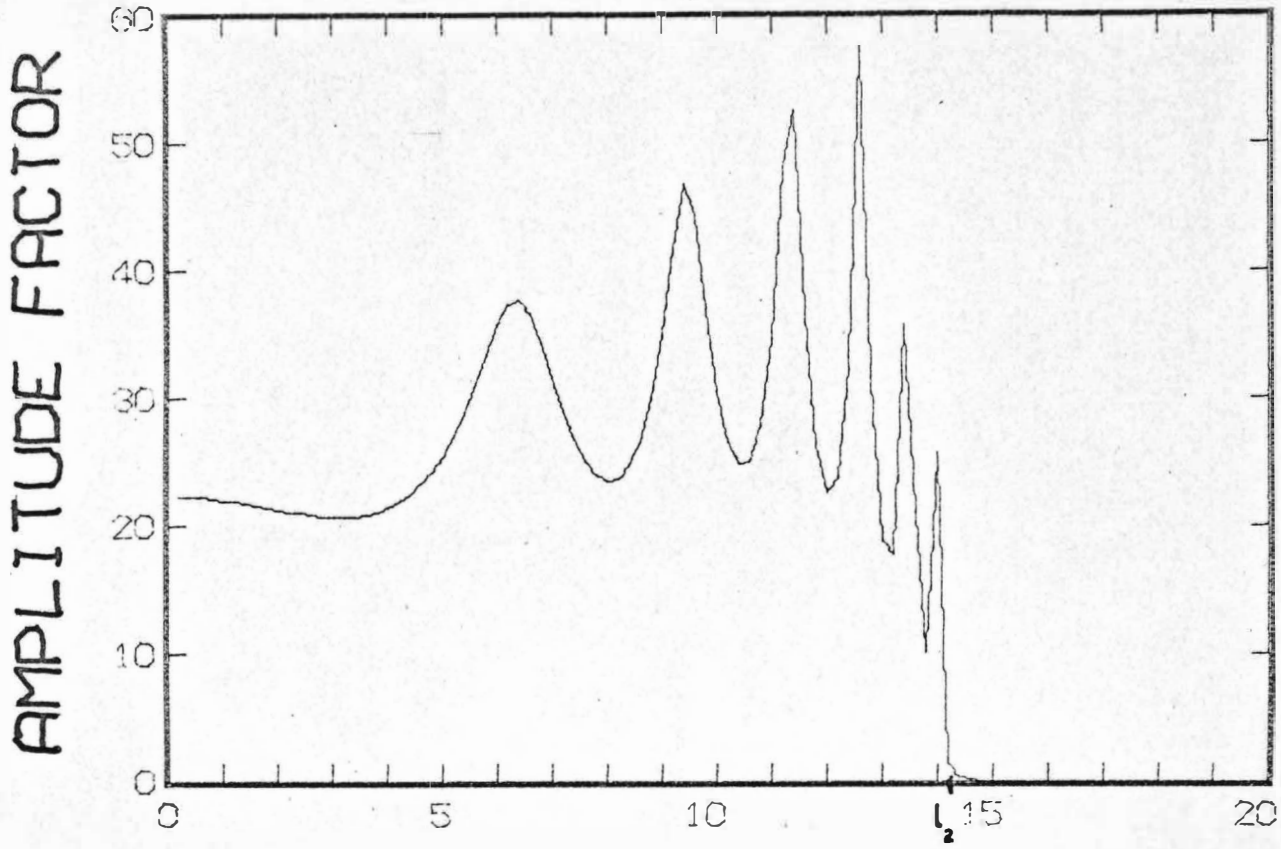

FIG 6.6(a): The mean state.

$l_1^2 = 25\,km^{-2}$ $l_2^2 = 2\,km^{-2}$ $l_3^2 = 5\,km^{-2}$

$h_1 = 1.6\,km$ $h_2 = 15.0\,km$

The mean state for an example of the effect of each of the layer parameters on the three layer solution.

FIG 6.6(b): VARYING l_1^2

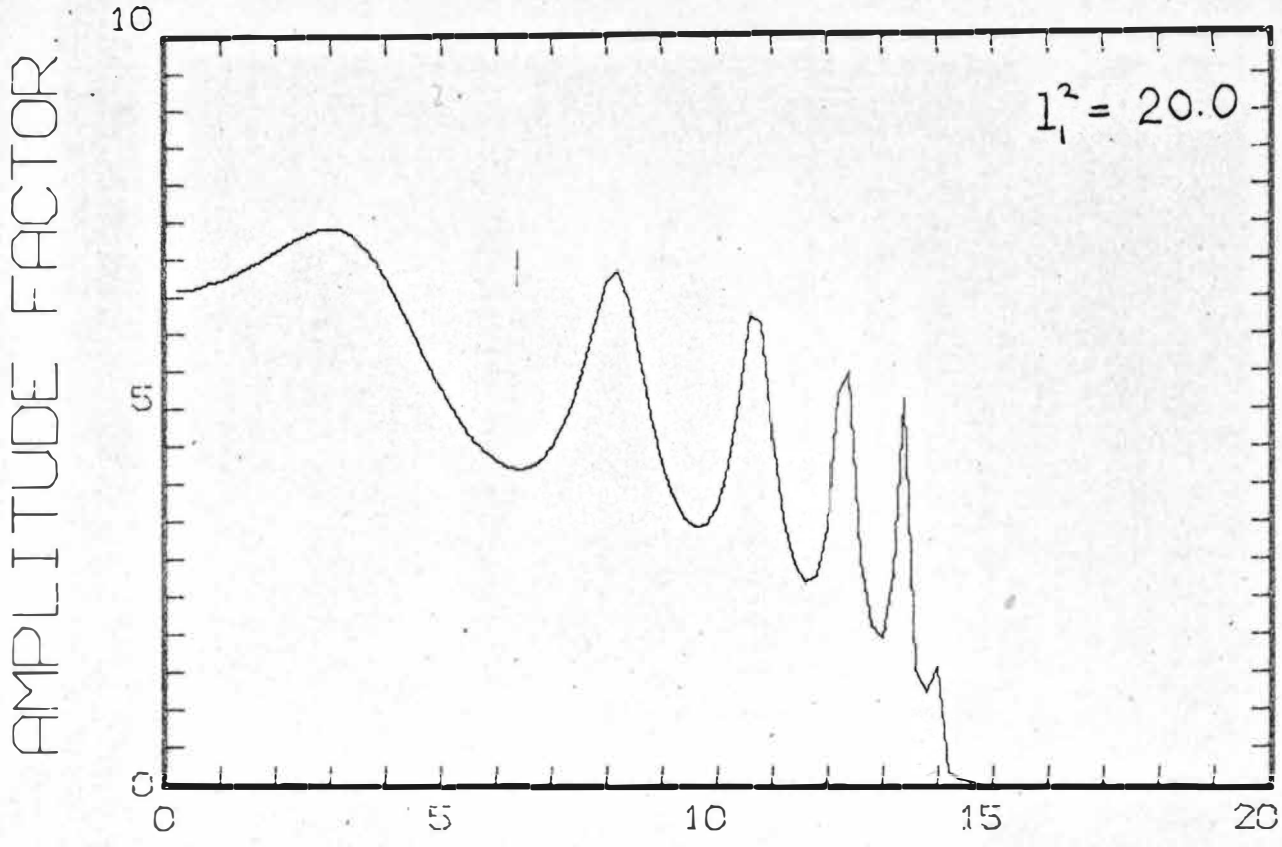

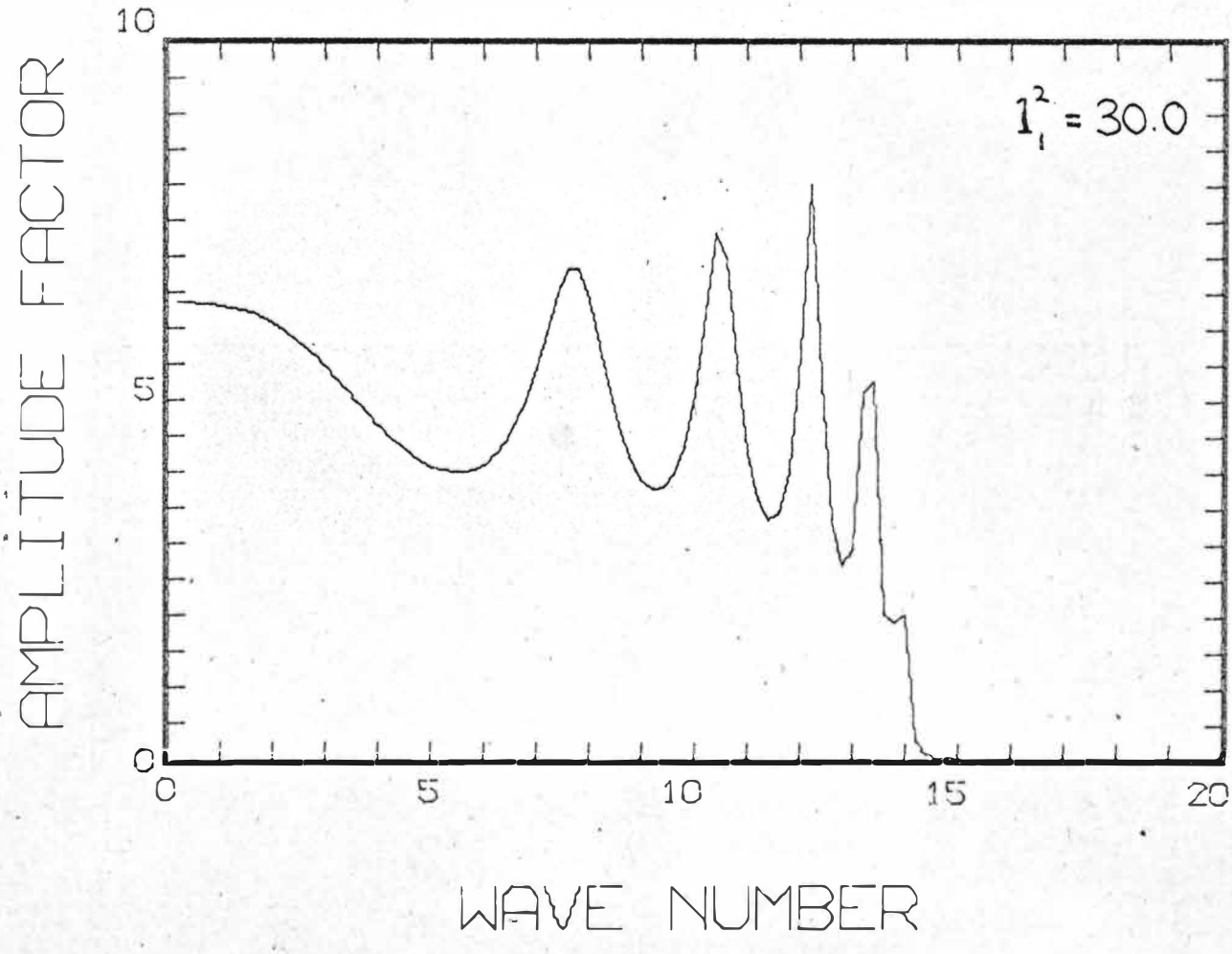

FIG 6.6(c): VARYING l_2^2

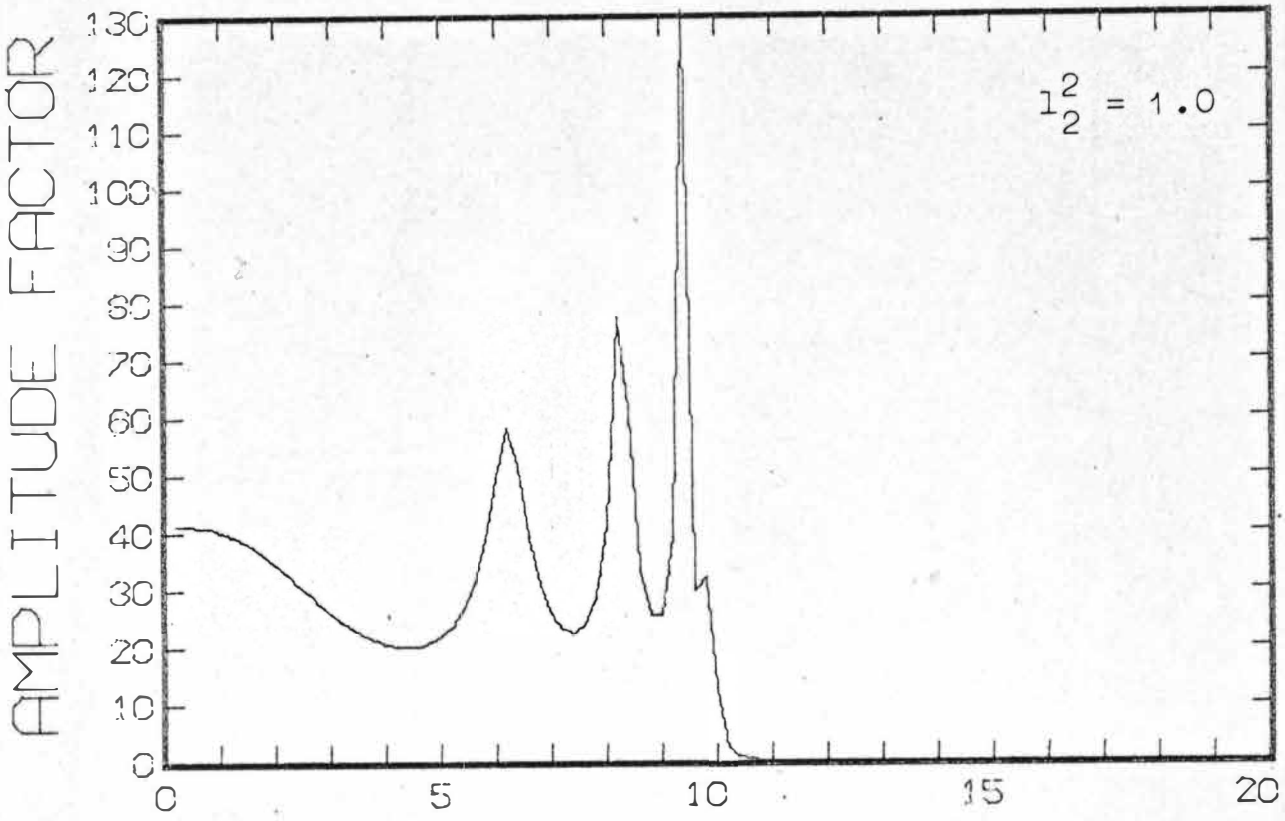

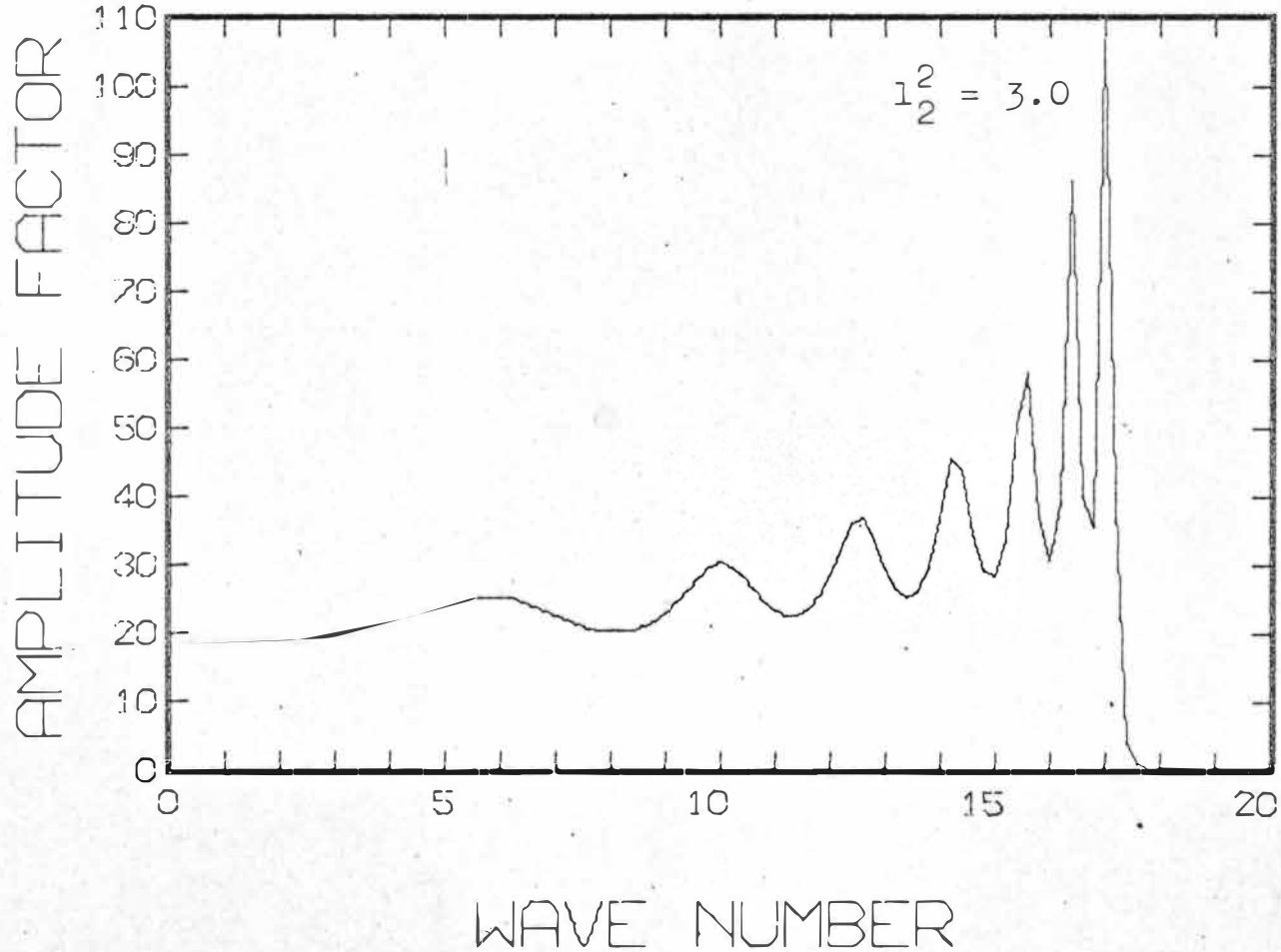

FIG 6.6 (d): VARYING l_3^2

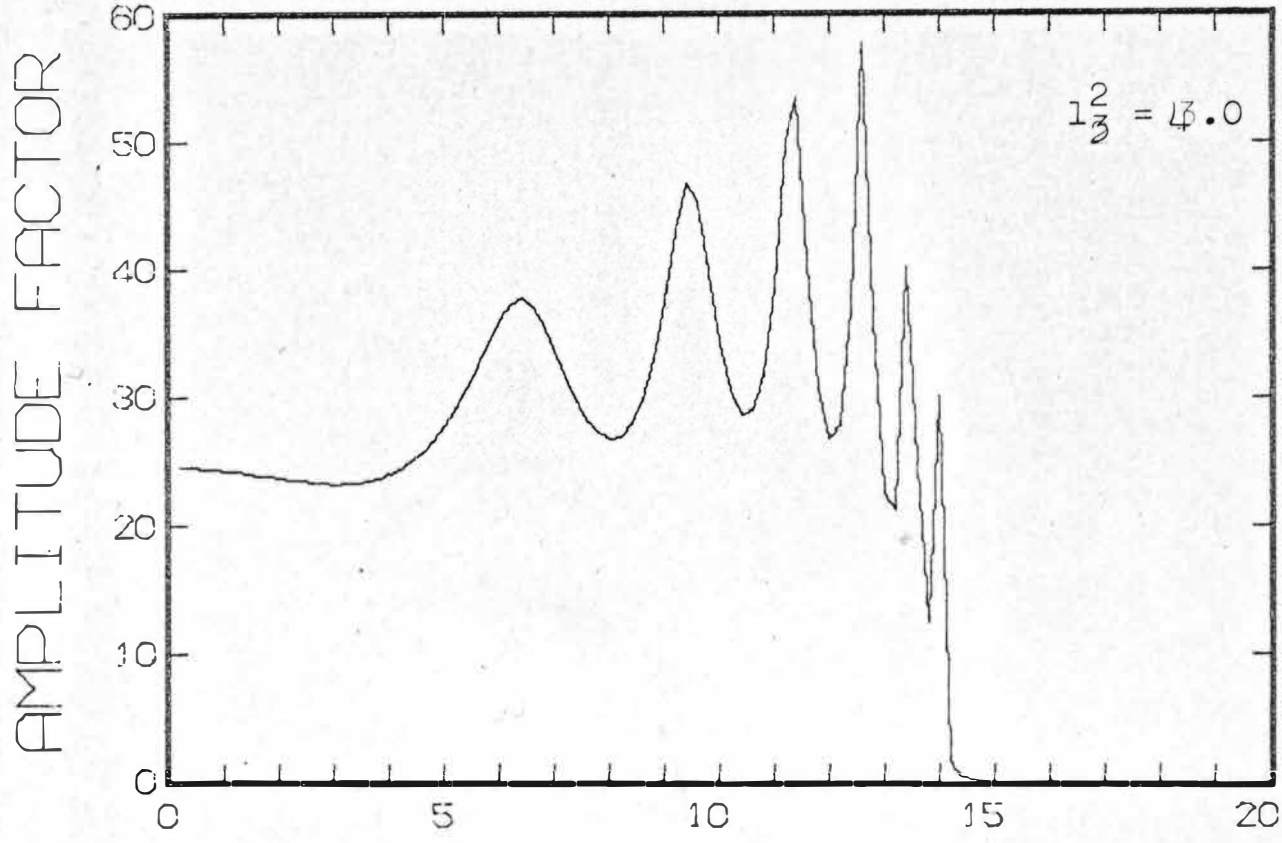

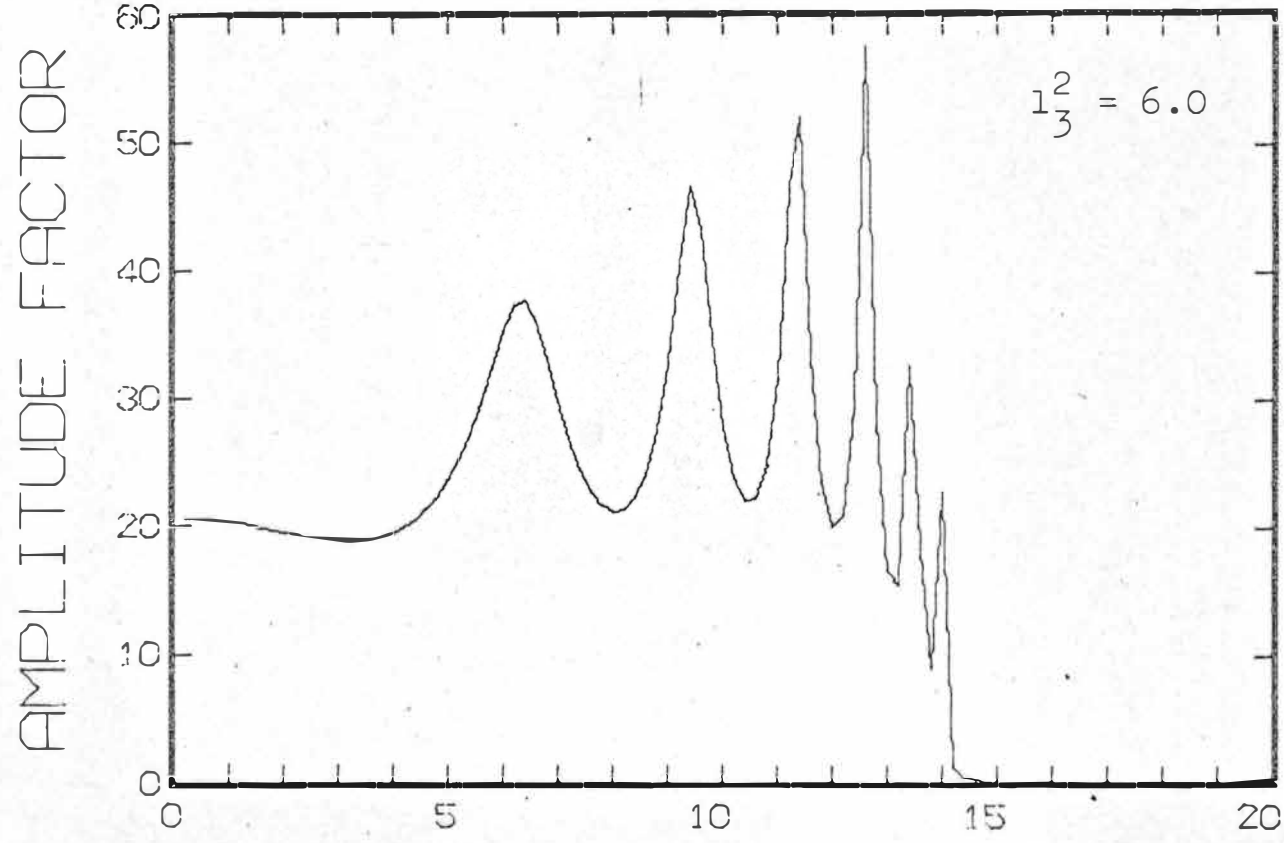

FIG 6.6(e): VARYING h_1

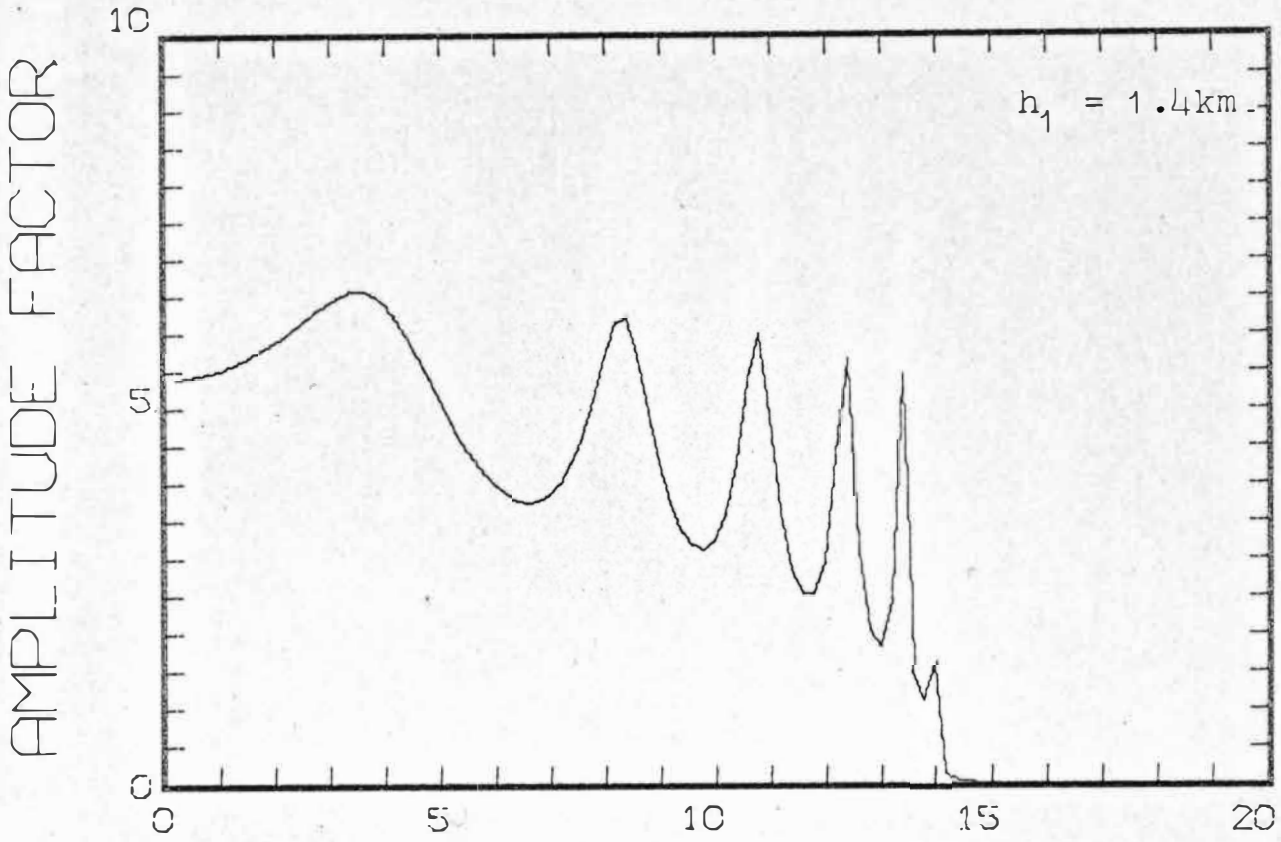

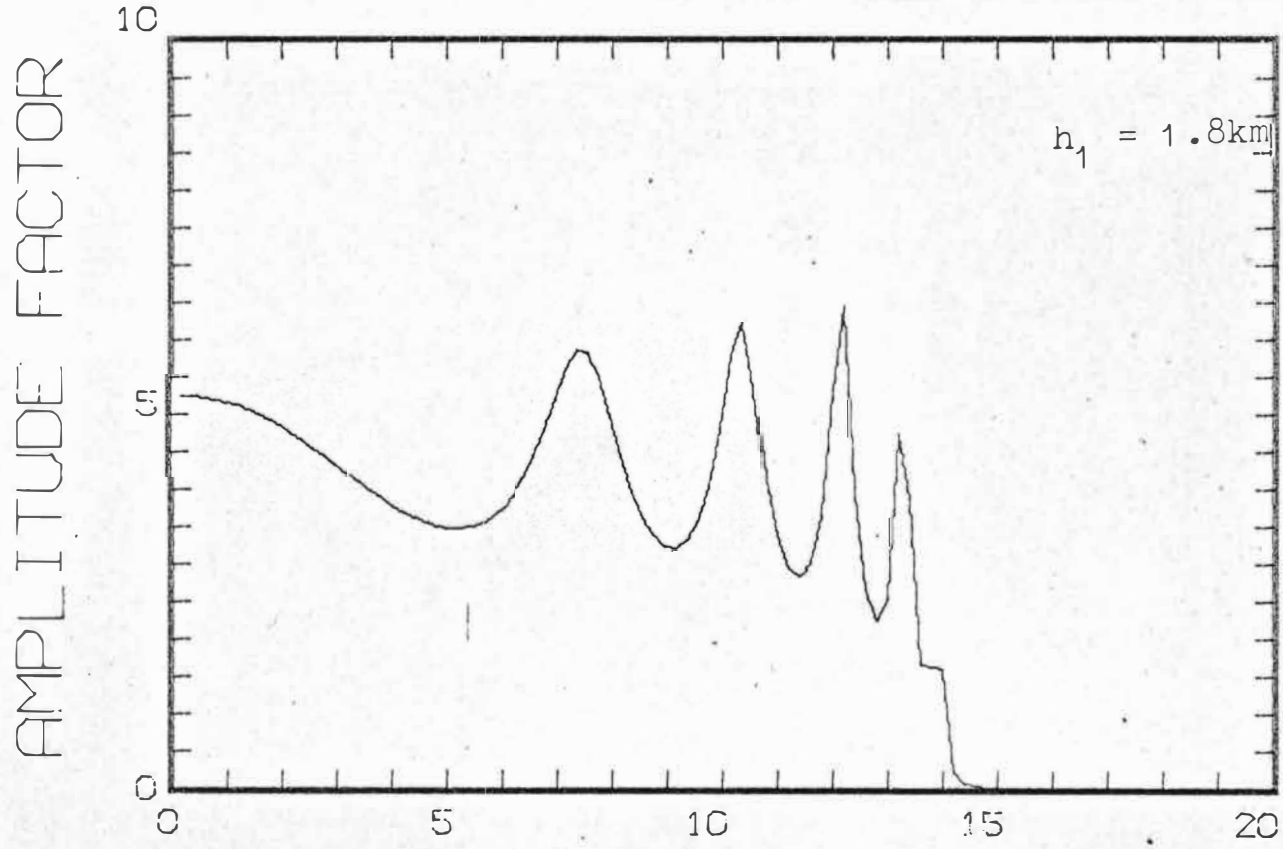

FIG 6.6(f): VARYING h_2

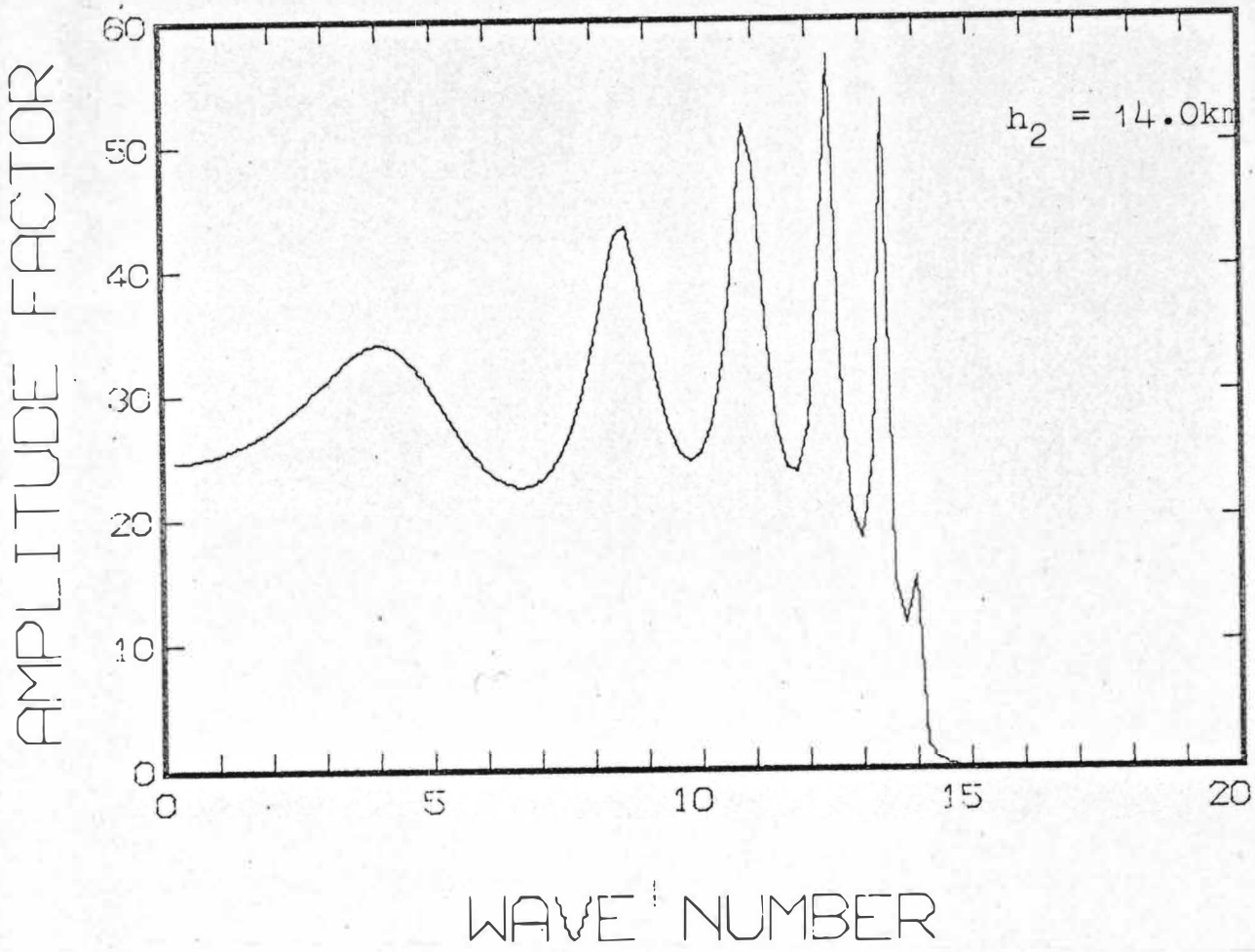

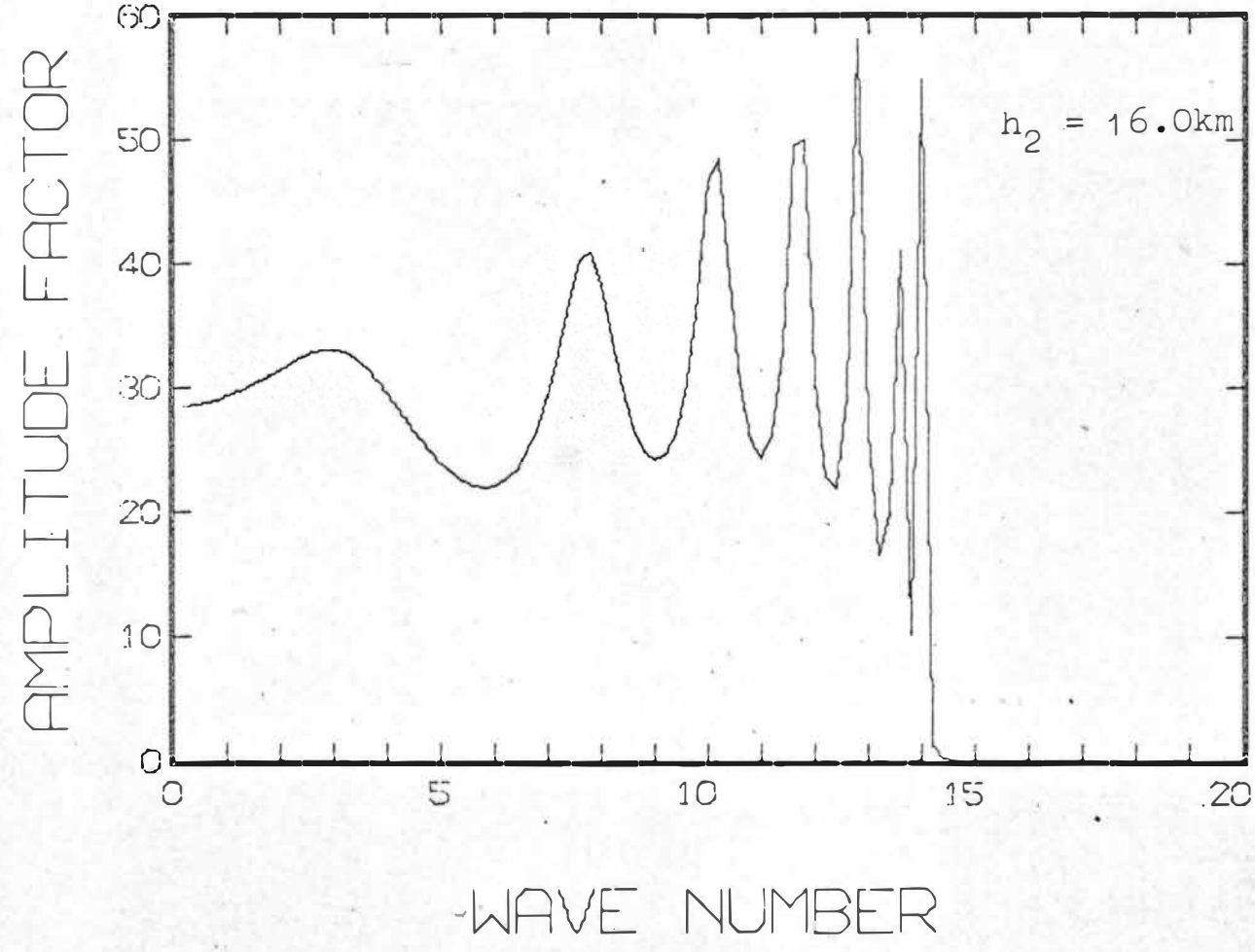

obtained. Fig 6.6(b), varying l_1^2: The amplitude factor decreases away from the mean case. Increasing l_1^2 from 20 to 30 km^{-2} leaves the short wavelengths (large k) relatively unchanged and decreases the longer wavelengths. For example the longest wavelength decreases from 21 km to 10.0 km and then to 8.11 km for l_1^2 = 30 km^{-2}. The rate of decrease in wavelength of this component falls off quickly with increasing l_1^2.

Fig. 6.6(c), varying l_2^2: $k=l_2$ was found to correspond to a cutoff, that is there were no significant waves in this case for wave numbers greater than l_2. Inspection of other wave number spectra used in the theoretical analysis of the SPB data show that resonance peaks do exist for $k > l_2$. Thus l_2 can be seen to be the cutoff of the 'modulated continuum' and for wave numbers greater than l_2 resonance peaks are relatively isolated corresponding to the discrete mode solutions of the two layer theories. For example: The k spectrum for 1200 26/4/70 for l_1^2 = 3.8 km^{-2}, l_2^2 = 0.4 km^{-2}, l_3^3 = 5.2 km^{-2}, h_1 = 5.2 km and h_2 = 10.6 km, shows a slight peak in the continuum (λ = 19.9 km) for k less than $k = l_2 = 0.63$ and two very strong resonance peaks corresponding to wavelengths of 5.72 and 3.0 km with little peaks at 3.88 and 3.2 km. The two layer theory gives the three middle wavelengths and the bounded two layer theory has these three plus the long 19.9 km wavelength solution.

The 3 km wavelength corresponding to k = 2.1 (k^2 = 4.4) lies in the range of $k^2 > l_1^2$ for which there are no two layer solutions. For the three layer solution this value of k lies in a range where the amplitude factor is imaginary. Eq. (5.32) shows that this generally occurs when μ_1^2 is negative, i.e. when $k^2 > l_1^2$. Solutions of k which correspond to imaginary amplitude factors are 'leaky' resonance modes (Danielson and Bleck, 1970) which lead to dampening for positive values of x, i.e. in the lee of the mountains.

Fig. 6.6(d), varying l_3^2: Varying l_3^2 by this small amount has no effect on the wavelengths but the increase in l_3^2 results in a reduction of the amplitude factor of the continuum, heightening the resonance effect of the peaks.

Fig. 6.6(e), varying h_1: A comparison of Fig. 6.6(b) with 6.6(e) shows that changing the height of the interface has almost exactly the same effect as changing the l^2 parameter in the bottom layer. The wavelength changes inversely proportionally to h_1.

Fig. 6.6(f), varying h_2: Increasing the upper interface height decreases the wavelengths. The effect is greatest on the long wavelengths and decreases towards the cutoff wave number. Changes in this interface height affects the relative intensities of the resonance peaks. This is analogous to changing the height of the rigid upper boundary in the bounded two layer theory. However the three layer

theory gives more information about the relative intensities of the various resonance modes than just their wavelengths. Expansion of the two layer theories to include solutions for the amplitudes of the wave components would provide this information as a function of height.

The overall results are consistent with the two layer and bounded two layer theories in that the wavelength varies inversely as l^2 and h_1 vary. The height of the upper interface has a marked effect on the intensities of the resonance modes, particularly in this case for the short wavelength modes.

8. Lee Wave Amplitudes

The amplitude of a lee wave is taken as half the distance between the levels of maximum and minimum displacement. Commonly observed amplitudes range from a few tens of metres to about 500 m. Under some situations amplitudes as great as 1,000 m have been observed (Sierra Wave Project, Holmboe and Kleiforth, (1957)). For example they report a wave with an amplitude of 850 m at the 3 km level on 16/2/52. Vergeiner and Lilly (1970) report a wave of the same amplitude over Denver on 1/3/67.

Amplitudes for lee waves can be obtained from the various layer or exponential troposphere theories but they correspond to the amplitude that would result in such an

'idealised' atmosphere from the appropriate analytic shape chosen for the mountain. However, mountains and airflows are seldom, if ever, 'ideal'. Usually there is an irregular variation of l^2 with height and the mountain shape is rather complex. For example Wooldridge and Lester (1969) found that there was a very poor correlation between the amplitudes predicted by the simple two layer theory and the amplitudes observed on their balloon flights.

The results of a project undertaken by two final year honours students (Susan Watson and G. Opie) show conclusively that the frequencies of forced oscillations over the hills are at present in constant level balloons at heights up to 10 km. (These results are presented in the following chapters.)

Corby and Sawyer (1958) demonstrate the dependence of the amplitude on the size and shape of the mountain. Thus the dominating factor determining the amplitude of lee waves is the resonance between the airflow and the mountain. If there are any natural frequencies of the airflow that are in resonance or close to resonance with the frequencies at which the airflow is forced to oscillate over the mountain then these frequencies will in general result in large amplitude lee waves. Thus very short wavelengths (high frequencies) will not be observed to have large amplitudes as hills and mountains that are of such size as to produce a

significant disturbance of the airflow will not usually contain significant small scale periodicities.

The importance of this resonance effect can be seen from Corby and Sawyer (1958) who considered the effect of the size and shape of a single mountain (demonstrated below). The effect of periodicities due to several ranges of mountains can be seen by considering each range as an independent generator of lee waves. The waves produced by each mountain in succession will be superimposed in the airflow. If the waves produced by one mountain are in phase with the waves produced by another mountain downstream of the first, reinforcement will take place. If they are out of phase cancellation takes place (Scorer, 1961).

Scorer and the majority of authors have taken the principle wavelength as the only one with a significant amplitude. Some of my power spectra of constant level balloon flights show shorter wavelengths with greater power factors than some longer wavelength(s). This may be explained in terms of the resonance of the mountain with the shorter wavelength and to a lesser extent with the longer wavelength. The general scale of mountains however favours longer wavelengths in the range 5-25 km.

9. Factors Affecting Lee Wave Amplitudes

Scorer (1949) derived an expression for the displacement of a streamline from its undisturbed level after it has been forced to flow over a ridge of height h and half-width b,

$$\zeta_z = -2\pi h b e^{-kb}(U_1/U_z)\phi_{z,k}\,(\phi_{1,k}/k)^{-1} \sin kx \qquad (6.4)$$

where k is the lee-wave number, U is the horizontal wind speed and ϕ satisfies the wave equation (5.15).

(a) Effect of Mountain Size and Shape: To consider the effect of mountain shape consider a mountain of constant height and variable width. Varying b shows a pronounced maximum in the mountain factor for $b = k^{-1}$. This is resonance with the shape of the mountain. Allowing both the height and width of the mountain to vary in the same ratio the height of the mountain is found to dominate until $b = 2k^{-1}$ after which there is a sharp decrease in the wave amplitude. Corby and Wallington (1956) mention for example that when a mountain exceeds $b = 2k^{-1}$ by a factor of four, which could be expected to produce larger waves, the contribution of mountain factor to the amplitude is decreased by 1/27

(b) Effect of Wind Speed: The amplitude is proportional to U_1/U_z. We know from Scorer's theory that for waves to exist U must generally increase with height. Therefore it can be seen that the larger the wind speed at the surface

(U_1) and the smaller the increase in speed with height, the greater will be the amplitude of the waves. Other factors such as the angle of the wind to the ridge and the minimum velocity at the hill tops are mentioned elsewhere. The critical wind speeds are discussed in Section 2 of this chapter.

(c) Effect of the l^2 profile: Since the variation of the stream function is proportional to the variation of l^2 its effect is considered by noting the effect of variations in l^2 with height and in time. Scorer (1953) shows that at high levels gradual changes in l^2 result in the vertical velocity decreasing or increasing as the l^2 parameter increases or decreases with height. This can be seen by considering that l^2 in the absence of wind shear is proportional to the stability. Thus a decrease in l^2 implies a decrease in stability and the restoring forces resulting in an increase in vertical velocity and vice versa. Thus the variation of l^2 is inversely proportional to the wavelength. This is consistent with observations that show a predominance of short wavelengths low in the troposphere where l^2 is large and a predominance of long wavelengths high in the troposphere where the stability is low. Because of this differential variation of wavelengths with l^2 and height a simple relationship between l^2 and the amplitude of the waves is not obtainable.

In terms of the two layer theory as proposed by Scorer (1949) there is a change in the form of the disturbance (stream function) across the interface. Below the interface $l^2 > k^2$ and the disturbance is periodic in terms of cos and sine. Above the interface $l^2 < k^2$ and the disturbance decreases exponentially. This in general means that the form of the disturbance changes as l^2 decreases below k^2. This obviously happens at different heights for different wavelengths. The longer the wavelength the higher the level.

Corby and Wallington (1956) found that it was impossible to find how the maximum amplitude of a given wave varied in terms of the l^2 parameters but it was possible in terms of the difference between them (L^2), i.e. $L^2 = l_1^2 - l_2^2$. They found that large amplitude waves resulted from a large decrease in l^2 (large L^2) and a small value of l^2 in the upper layer and that the largest amplitude waves occur when the critical conditions are just fulfilled.

The effect of variations of l^2 in time can be seen by the effect they have in the light of the above comments. For example if the stability in the lower layer is gradually increasing in time such that from a condition of no waves the critical conditions are just fulfilled then at such a time large amplitude waves may be set up.

(d) Additional Factors: Each mountain may be considered as an independent generator of lee waves for which section (a) above applies. Wave train produced by successive mountains are superimposed on the airstream as it travels across the mountains. If the wave from one mountain is in phase with the wave produced by a mountain downstream of it there will be reinforcement. If they are out of phase there will be cancellation. This effect was observed by Gerbier and Berenger (1960) in their experimental study of lee waves in the French Alps. These mountain resonance effects can account for the predominance of shorter wavelengths over longer wavelengths in actual airflows on some occasions. Booker (1965), for example, found that maximum amplitudes occurred for wavelengths of 6 n mi. This corresponded to the spacing between the two ranges producing the waves.

Gerbier and Berenger also mention that their observations showed that a mountain range or large mountain mass has more influence than an isolated hill or peak. The steeper the lee slope the larger the waves or eddies that are produced. The best waves are produced by ridges which are concave towards the wind, than by straight ridges, and ridges that are convex towards the wind produce the smallest effects.

To Summarise:

Shorter wavelength waves have maximum amplitudes in the lower, more stable layers of the atmosphere and negligible amplitudes high in the troposphere so are relatively unaffected by conditions in the stratosphere and changes in the upper boundary conditions. They require only small obstacles for good resonance. They sometimes occur high in the troposphere where there is a sharp decrease in the wind speed with height, sometimes in association with small rotors (Gerbier and Berenger (1960)).

Longer wavelength waves have their maximum amplitudes higher in the atmosphere in the less stable layers. Thus they are very dependent on conditions in the stratosphere, the increase in l^2 near the tropopause and the upper boundary conditions. They are in resonance with larger mountains and ridges.

For an actual complex set of mountain ranges it is very difficult to obtain a theoretical value of the amplitudes of the waves produced. It should be found though, that the amplitude of the waves is very sensitive to the periodic forcing of the mounting disturbance. Both from the resonance between the airflow and an individual mountain's size and shape and between the airflow and periodicities introduced by successive mountain ranges and/or peaks.

10. Diurnal and Semidiurnal Variations

Booker (1965) studied the semi-diurnal variations of leewaves experimentally and Scorer (1952,1953). His (1952) comments are based on observations of the behaviour of lee waves in the evening by Roper (1952).

Booker found that the amplitude reached a maximum during the midmorning (about 1000 hrs) and a minimum in the early afternoon (about 1400 hrs) with a secondary maximum in the late afternoon (about 1800 hrs). The wavelengths observed showed a maximum near midday. They then decreased until in the evening they were about half the daytime maximum. These are in agreement with Gerbier and Berenger (1961) and with the theoretical results of Scorer (1953) who showed that the wavelength should vary as the thickness of the adiabatic layer at the surface.

The amplitude variation shows the effect of the resonance with the mountain periodicities. As the wavelength increases it passes the natural wavelength of the mountains with the corresponding maximum in the amplitude. The further increase in the wavelength takes the airflow out of resonance with the ground, decreasing the amplitude. During the afternoon as the wavelength decreases again it passes through the resonance effect again. The smaller amplitude maximum during the afternoon is probably due to a deepened adiabatic surface layer.

11. Effect of Adiabatic Layers

Adiabatic layers are important because in the absence of wind shear when the temperature decreases adiabatically β_1 and thus l^2 are zero. One might initially think that because the adiabatic region is unstable and not stratified this would mean that there will be no waves above such a level. However, an adiabatic layer is sometimes observed near the ground when waves are observed in the middle troposphere. Corby and Wallington (1966) show that the main effect of an adiabatically mixed layer near the ground is to reduce the amplitude of the waves and to increase their wavelength. If the layer is too thick the waves will disappear altogether. Berkshire (1969) investigated the effect of a neutrally stable ($l^2 = 0$) layer in the middle troposphere on the propagation of waves into the stratosphere using a three layer model. He concluded that there can be significant radiation of waves into the stratosphere through such a layer provided that the lower layer is sufficiently stable. In some situations a type of resonance occurs and the waves produced are more pronounced than the corresponding case of uniform stratification. This depends critically on the airflow parameters and the layer thicknesses.

I have grave doubts about the validity of these conclusions. Berkshire's results are based on a consideration of an amplitude factor which is derived from the linearised

wave equation. Because of the extremely low stability in an adiabatic layer a disturbance results in turbulence rather than a laminar flow. Also the small restoring forces involved are likely to result in very large perturbation velocities. Both of these factors are at variance with the assumptions made in the derivation of the linearised wave equation. Scorer (1953) showed that if l^2 was zero in some middle layer the flow over a mountain would produce a disturbance which was not laminar. Therefore perturbation theory does not hold and Berkshire's assumption that the flow in the case when $l_2 = 0$ is described by the linearised wave equation is incorrect.

When l^2 goes to zero the amplitudes derived from Doos' method become impractically large. This is in agreement with Scorer's (1953) result that there is an inverse relation between the amplitude and l^2. Amplitudes greatly in excess of 1 km often result from this. Obviously the assumption that perturbations are small does not hold so that the perturbation derivation breaks down. The amplitudes thus obtained are practically and theoretically unreliable.

CHAPTER 7

BALLOON DATA AND THEORETICAL ANALYSIS

- An Introduction to the Data Given in Chapter 8

1. Introduction

The major source of data was superpressure balloons released from Harewood (Christchurch Airport), Hokitika, Cass and Birdlings Flat under suitable northwesterly and southwesterly conditions, mainly between January and November 1970. Two of the developmental balloons released in March 1969 were also used. Wind velocity and temperature profiles were obtained from the Meteorological Office for Harewood. A radiosonde/radar wind balloon was released from there at midday every day of the year and at midnight during the summer while Operation Deep Freeze were flying to Antarctica. From these balloons the l^2 profiles for the days of interest were calculated. Constant and exponential layer fits to this profile provided the parameters for use in the two layer (2L), bounded two layer (2LB), three layer (3L) and exponential layer (EXP) solutions. The wavelengths that are solutions of each of these theories for the given profiles are compared with the wavelengths of the oscillations in the SPB (superpressure balloon) and radiosonde (RAD) flights. All wavelengths are given in km.

Wavelengths calculated from the parcel theory (Section 5.10) at the balloon's equilibrium height are given where appropriate. The mean tropospheric wind direction D_t from the radar wind radiosonde balloon is also given to be compared with the direction perpendicular to the mean direction of the mountain ranges in the Southern Alps (310^o) and with the mean direction of the wind as given by the SPB (D_b). Data was also collected from satellite photographs when they were available. Some of these are given in Appendix A.

Calculations were done with the aid of an IBM 360/44 computer and many of the graphs were drawn on the IBM 1620/27 plotter in the University of Canterbury Computer Centre.

2. Power Spectra

The power spectra were calculated after the method of Blackman and Tukey (1958), p.52. This included prewhitening, scaling to give zero mean, taking the finite cosine fourier transform of the autocovariance function, then correcting for the prewhitening and the scaling to the mean.

The power spectra thus obtained were used to determine whether there were any regular periodicities in the balloon and mountain profiles and to give their wavelengths.

It is important to determine whether any particular peak in the power spectra has significance. This is dependent on the equivalent number of degrees of freedom for each point of the spectrum, which is equal to twice the number of points in the series over which the spectrum is taken divided by the maximum number of lags in the spectrum,

$$\text{i.e.} \qquad k_f = \frac{2N}{M} \tag{7.1}$$

The average number of points in each flight was about 300 so that using 30 lags gave an equivalent number of degrees of 20 with 80% confidence that the true value lies between 0.62 and 1.42 of the estimate calculated (see table 7.1). The average number of points for a balloon in altitude was about 200. Therefore there were about 13 degrees of freedom giving 80% confidence between 0.54 and 1.54 of the computed value. If the power spectrum was taken over less than 100 points, 20 lags were used so that the 80% confidence range say for 70 points, 7 degrees of freedom, was between 0.37 and 1.75 of the calculated value. For example Fig. 7.1 shows the power spectrum of balloon 1503 during its descent through the troposphere. It consisted of 110 points so there are about 7 equivalent degrees of freedom. The error bars indicate the range of 80% confidence. It is seen that at this level of confidence even the apparently strong peak has very little significance.

FIG 7.1(a):

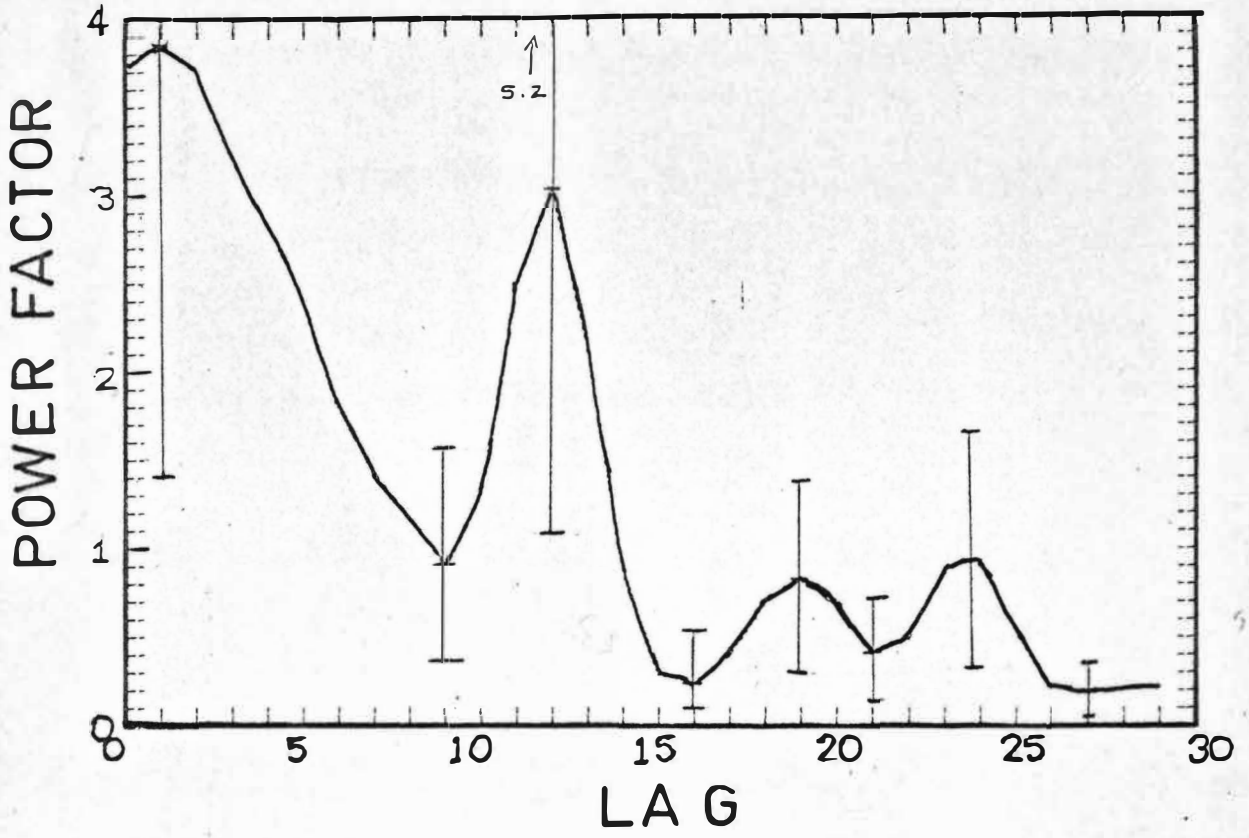
POWER FACTOR
4
3
2
1
0
5.2
0
5
10
15
20
25
30
LAG

(b)

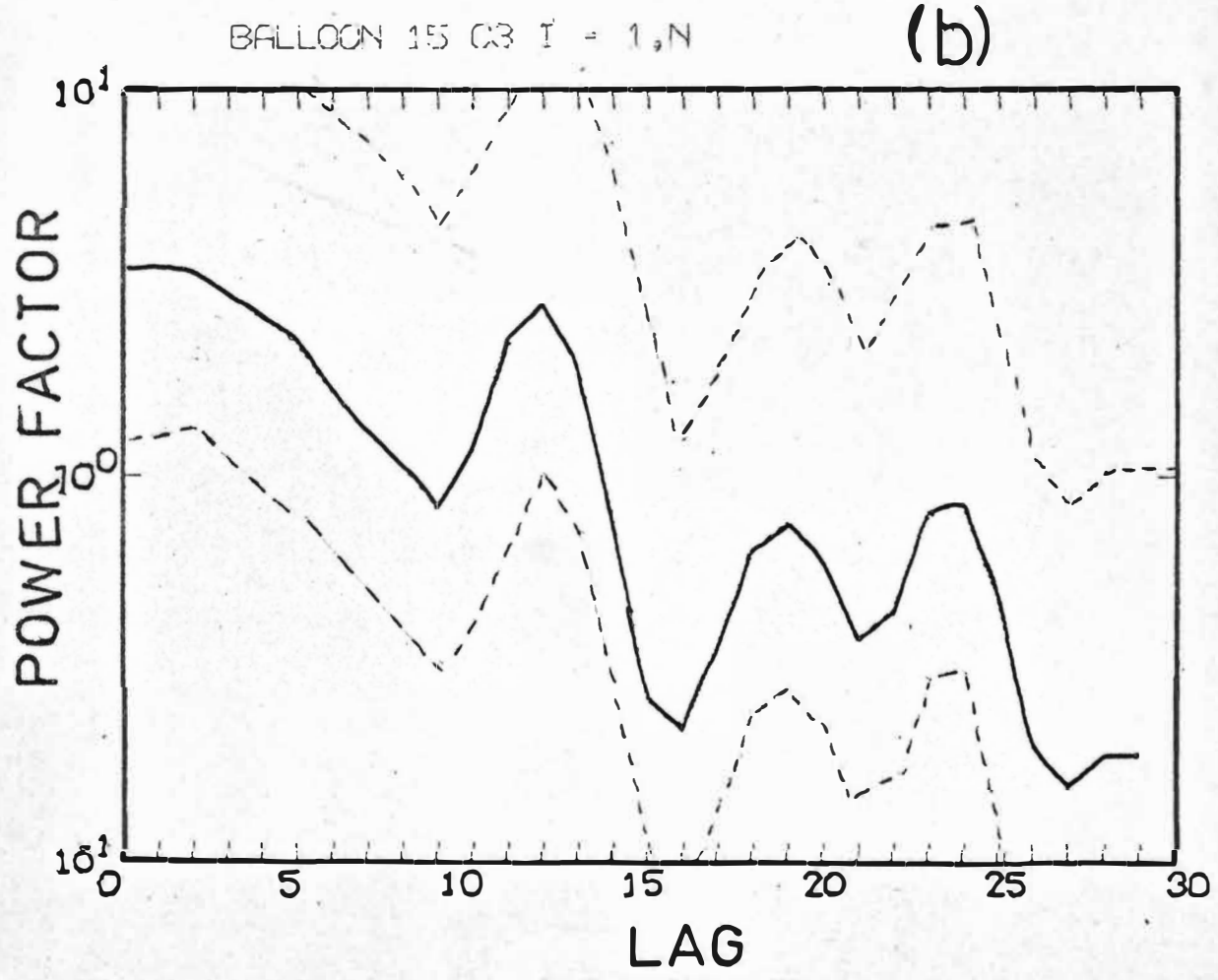
BALLOON 15 C3 I = 1,N
POWER FACTOR
10^1
10^0
10^{-1}
0
5
10
15
20
25
30
LAG

Table 7.1: The proportions of the computed values over the 80% confidence range for various numbers of degrees of freedom (k_f). The figures in brackets are the $\log_{10}$ of the factors. (From Blackman and Tukey, 1958).

k	Exceeded by 90% of all values	Exceeded by 10% of all values
1	0.016 (-1.80)	2.71 (0.43)
2	0.10 (-1.00)	2.30 (0.36)
3	0.19 (-0.72)	2.08 (0.32)
4	0.26 (-0.58)	1.94 (0.29)
5	0.32 (-0.49)	1.85 (0.27)
10	0.49 (-0.31)	1.60 (0.20)
20	0.62 (-0.21)	1.42 (0.15)
30	0.69 (-0.16)	1.34 (0.13)
40	0.73 (-0.14)	1.30 (0.11)
50	0.75 (-0.12)	1.26 (0.10)

Fig. 7.2 shows the power spectrum of balloon 45H12 between the alps and Banks Peninsula, on a log scale. Since the confidence range is given by multiplicative factors, on the log scale they are additive and all of the same length. Thus on a log scale the confidence range is independent of the power factor, as can be seen also from Fig. 7.1(b). The balloon shows clearly waves of the order of 10 km with a shorter wavelength superimposed on it. These the power spectrum shows positively to be 12 km and 2 km.

3. Analysis of SPB Data

The range, elevation, azimuth and time were taken manually from the visual display of the radar which had a minimum sampling interval of 0.5 mins. From these the position of the balloon relative to the release position and its velocity components were computed for each time interval. The power spectrum of the vertical velocity of the balloon was calculated and gave an indication of the presence and periods of waves over portions of the flights that were of interest. From the periods the wavelengths were calculated using the mean horizontal velocity of the balloon over the section being analysed.

The profiles of the mountains flown over were scaled to give zero mean and similarly analysed for spacial periodicities which might be in, or near to, resonance with a

FIG 7.2: POWER SPECTRUM OF A BALLOON SHOWING THE REGION OF 80% SIGNIFICANCE.

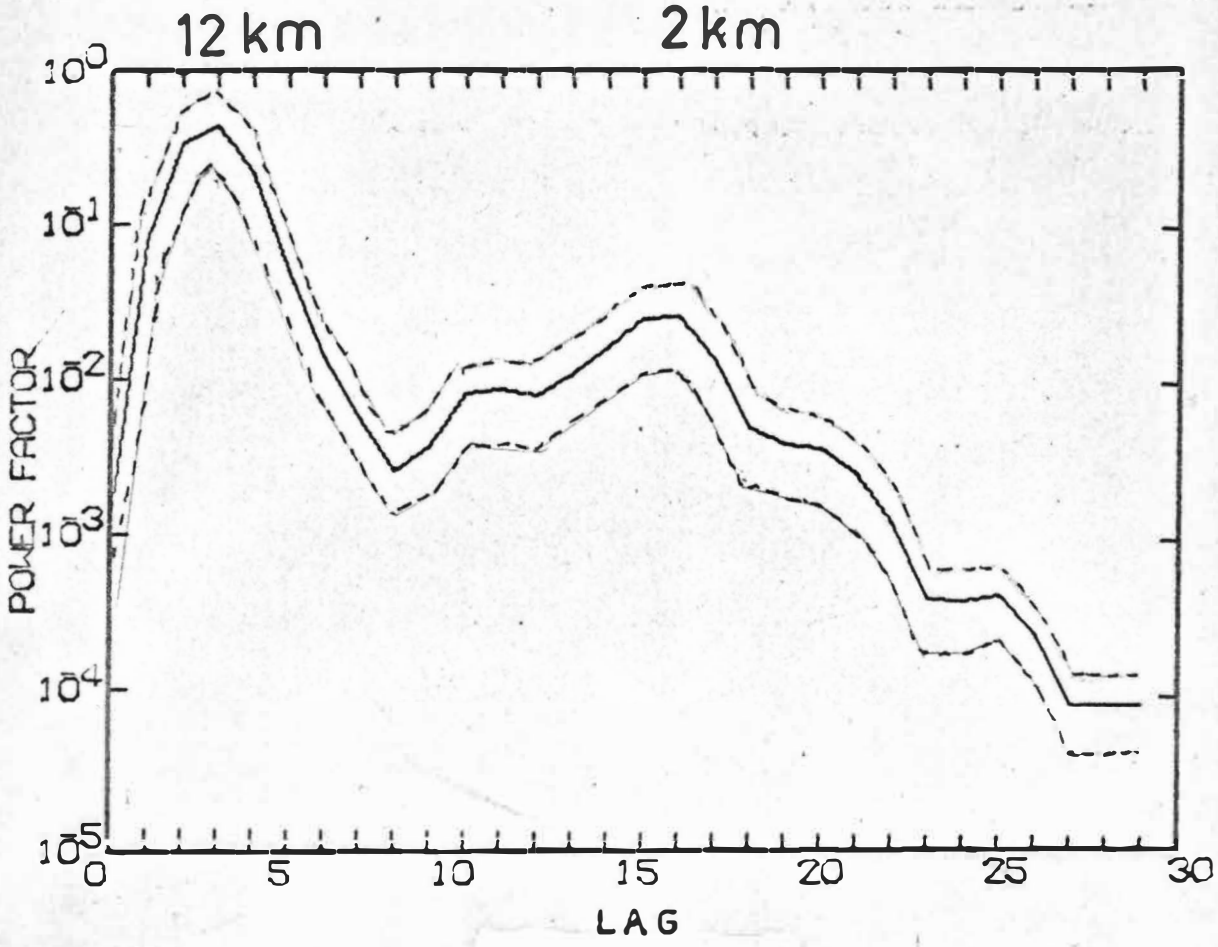

BALLOON 45 H12, BETWEEN THE ALPS AND BANKS PEN.

natural oscillation of the airflow. They also show if there was any regular forcing of the airflow.

Large oscillations of the radar were observed for low elevations over the hills and mountains. These give large echoes when within the radar beam which has a beam divergence of about 2.7^{o}. Thus because of the relative intensities of the echoes the radar often tracked with the balloon in the range gate but indicating a lower elevation than that of the balloon. When large mountain echoes were within the range gate the radar locked onto the mountain because it gave the largest return. This almost always happened for balloons flying across the Craigieburn, Torlesse and Puketeraki ranges below 6 km, and sometimes when they were higher.

The height of the balloon was adjusted for the curvature of the earth and atmospheric ducting of the radar beam using the standard correction factors. Namely:

$$\text{Curvature correction:} \quad + \frac{(\text{Range})^2}{12714}$$

$$\text{Ducting correction:} \quad - \frac{(\text{Range})^2}{68000} \qquad (7.2)$$

$$\text{Total correction:} \quad + 6.74364 \times 10^{-5} \times (\text{Range})^2$$

where the range is in km.

Inspection of balloons 36, 37 and 43 which were tracked out to ranges of about 100 km shows an essentially constant

equilibrium height within about 300 m with a tendency to be low by about this amount at long ranges. Assuming that this was not due to gas leakage but to the radar tracking. The height correction at 100 km is 674 m. Hence the height would be almost constant if the correction was increased by 44%. This difference is small compared to the actual height of the balloon being 5% for an average height of 6 km and as the difference increases smoothly to this amount for the purposes of this analysis it may be neglected.

4. Analysis of Radiosonde and Radar Wind Data

The heights of the heights of the radiosonde at half minute intervals, and thus the ascent rate, were calculated from the pressure and temperature using the following hydrostatic equation.

$$h_{i+1} - h_i = - \frac{(T_{i+1} - T_i)}{0.068330} \ln \left(\frac{P_{i+1}}{P_i}\right) \qquad (7.3)$$

where h is the height in km and T is the absolute temperature. The heights given by (7.3) were compared to the heights given by the radar tracking the balloon on several occasions and found to be in very good agreement. Table 7.2 gives the heights of a radiosonde balloon as obtained from the radiosonde using (7.3) and from the radar.

Table 7.2: Comparison of Heights derived from the hydrostatic equation using radiosonde data and heights obtained from the radar tracking the radiosonde. Balloon released at 1100 hrs, 14/1/70.

Time (min)	Radiosonde Heights (km)	Radar Wind Heights (km)	Difference (m)	% Diff.
5.0	1.39	1.5	-110	-7.5
10.0	2.86	2.9	- 40	-1.4
15.0	4.23	4.3	- 70	-1.64
20.0	5.78	5.8	- 20	-0.35
30.0	8.60	8.6	0	0.0
40.0	12.01	12.1	- 90	-0.75
50.0	15.20	15.6	-400	-0.60
60.0	18.93	19.4	-470	-2.44
70.0	23.01	23.5	-490	-2.10
76.0	26.11	26.3	-190	-0.73

It can be seen that the trend was to underestimate the height by an average percentage difference of 1.93%.

To obtain information about the vertical motion of the airflow as the radiosonde ascended, as an indication of the presence of waves, it was assumed that the actual ascent rate of the balloon relative to the air around it varied smoothly with height. This variation was approximated by an

exponential fitted to the derived ascent rate. The vertical velocity of the airflow was then assumed to be the difference between the ascent rate of the radiosonde and this smooth exponential variation. Periodicities in this derived vertical velocity profile were found by power spectrum analysis. Assuming that the wavefronts of the individual wave components are vertical, then since the waves are quasi-stationary, the time taken for a balloon to traverse one wavelength of a component in the horizontal direction is the period of that component (Fig. 7.3). Thus the horizontal wavelengths of the waves can be found by the product of the mean horizontal wind speed and the period of the vertical oscillation of the radiosonde balloon. If the wavefronts are not vertical wavelengths derived in this way can be considered as indicative of the general scale of wavelengths in the airflow traversed by the radiosonde balloon.

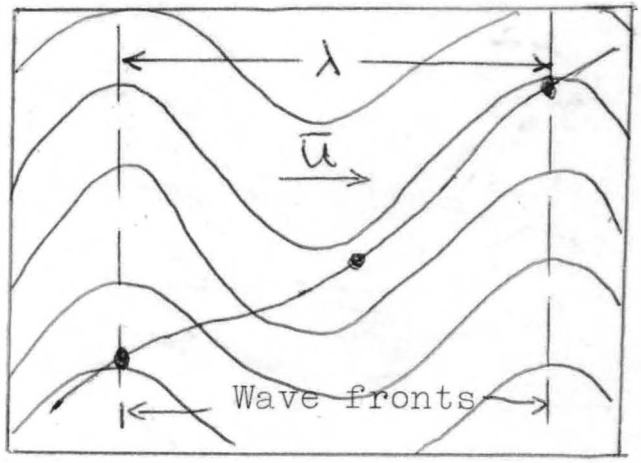

Fig. 7.3

The Scorer parameter (l^2) was calculated from the airflow parameters and plotted against height in order to make constant l^2 and exponential l^2 layer approximations. The exponential fit was done within the program by fitting the average straight line to the natural log of l^2, between

the ground and the tropopause. If l^2 went to zero at some level below the tropopause the fit was made up to this level. (Then $B_1 = 0$.) The programme then continued and found the zeros of the Bessel equation (5.44) and calculated the wavelengths of the solutions using (5.45). The fitted exponential is shown superimposed on the l^2 profile for each of the days studied. Sometimes the stable layer near the ground, which is indicated only by the first few points in the radiosonde ascent profiles does not affect the exponential fit much so it is essentially ignored. This stable layer has a marked effect on the solution of the wave equation in the two and three layer theories. On one or two occasions when this happened another profile was fitted giving more weight to the points near the ground. It is found that it makes a considerable difference to the possible solutions.

On several days because of high wind speeds and large lapse rates the Scorer parameter remains less than 1 km^{-2} throughout the whole troposphere. This gives very small values for λ in the exponential layer such that (5.45) gives extremely small wavenumbers and wavelengths greater than 1000 km result. For such wavelengths the Coriolis force cannot be neglected so they are not valid solutions of the simplified wave equation. For this reason wavelengths greater than about 50 km were neglected. There are no real

solutions for the wavenumber in the exponential theory when l^2 generally increases with height through the troposphere.

Since the SPB flights extended over periods of several hours it was assumed that the wave patterns observed were quasi-stationary (stationary with respect to the mountains) in order to compare the balloon wavelengths with the wavelengths that are solutions of the various theoretical approximations. On the majority of the occasions this was probably quite a good assumption as the main power spectra used are those of the portions of the flights to the lee of the mountains alone. This usually lasted for up to two hours during which time the wind velocity and temperature profiles would not change very much. This is borne out by casual observations of the movement, or lack of movement, of wave clouds and by time-lapse films of wave clouds.

5. Difficulties Encountered

A major drawback has been the lack of upper wind and temperature data upstream of the mountains in the undisturbed flow. The only radar wind/radiosonde soundings taken the central or northern parts of the South Island are from Harewood Airport, Christchurch, which is in the disturbed northwesterly flow. Very soon after balloons are released from Harewood under northwest winds they pass over Banks Peninsula. The Peninsula is known to produce quite large

vertical velocities under some such conditions (Farkas, 1958). This was also evident in some of the radiosondes analysed for this project. The effect of the disturbance of the airflow was overcome as much as possible by smoothing the data twice with weights 0.125, 0.20, 0.35, 0.20, 0.125 and by averaging over 2 minute intervals corresponding to layers between 500 and 800 m thick.

Harewood is a considerable distance from the alps and is subject to low level coastal winds which are often north-easterly, while a nor'wester is blowing at higher altitudes. Thus readings taken at Harewood at the low levels may not be representative of the undisturbed conditions upstream of the alps. This was overcome as much as possible by extrapolating the velocity profile from the nor'westerly flow above the coastal winds, down to ground level. An indication of the mean surface wind along the central west coast of the South Island can be gained from the mean pressure gradient across this region using the geostrophic wind equation:

$$\bar{U}_g \sim 8.25 \times 10^2 \frac{\Delta p}{\Delta y} \qquad (7.3)$$

where $\bar{U}_g$ is in mps when the pressure gradient is in mb/km. The scale factor between $\bar{U}_g$ and the pressure gradient includes the angular velocity component of the earth's rotation at these latitudes and the sea level atmospheric density, taken from the U.S. Standard Atmosphere to be

1.226 km/m^3.

6. Comments on the Theoretical Analysis

The two layer wavelengths are the solutions of the interface equations (5.23) and (5.30), found numerically. The bounded two layer atmosphere can have several solutions over and above the unbounded two layer atmosphere, which are dependent on the height of the boundary. For some boundary heights there are a multiplicity of solutions near a certain wavelength which tend asymptotically to that wavelength as the boundary height is increased slightly. Where in the analysis of the bounded two layer theory a cluster of such solutions appear an attempt has been made to give the asymptotic solution.

The three layer solution was obtained by inspection of the wave number spectrum for the given layer approximation. Wavelengths were calculated from the wavenumbers of the resonance peaks as described in section 5.7. This gave in general only wavelengths longer than about 4-5 km, corresponding to wave numbers less than l_2. Sometimes very small peaks were observed for short wavelengths but these had very small amplitudes compared to the peaks corresponding to the longer wavelengths. On many days very high stabilities (in excess of 50 or 100 km^{-2}) were found in the top layer, as on 5/3/69. The effect of increasing the value of l_3^2 from 50

to 100 to 200 km^{-2} was investigated. The results are tabulated below (Table 7.3).

Table 7.3: To investigate the effect of large stability in the top layer of a three layer atmosphere. Profiles based on 5/3/69. l_1^2 = 0.7 km^{-2}, l_2^2 = 0.2 km^{-2}, h_1 = 6.5 km and h_2 = 21.0 km.

l_3^2 (km^{-2})	Wavelengths (km) (amplitude factor)	
50.0	18.7 (4.2)	15.0 (0.95)
100.0	18.5 (3.0)	14.8 (0.70)
200.0	18.5 (2.2)	14.8 (0.40)

Once the l_3^2 is large (50 km^{-2}) increases in it have very little effect on the wavelengths of the solution. Increases in l_3^2 result in decreases in the amplitude factor. Thus if the value of l^2 exceeds 50 km^{-2} in the top layer it was usually set equal to 100.0 km^{-2} in order to obtain the wavelengths of the solution, unless there was a well defined limit in l_3^2 less than 100 km^{-2}.

The effect of changing l^2 in the bottom layer over the range of possible choices was investigated and the resulting wavelengths set out in Table 7.4. The amplitude factor was found to decrease with the increase in l_1^2.

Table 7.4: To investigate the effect of the choice of l_1^2 on the wavelengths in the three layer solution for 1200 hrs on 16/6/70. $l_2^2 = 0.8\ km^{-2}$, $l_3^3 = 1.5\ km^{-2}$, $h_1 = 0.8$ km, $h_2 = 11.0$ km.

l_1^2 (km^{-2})	Wavelengths (km)
8.0	10.42 7.68 4.63
10.0	10.15 7.59 4.63
12.0	10.03 7.59

Increases in l_1^2 in the order of 50% in this case decreases the wavelength by a far smaller amount (approximately 4% for the long wavelength and approximately 1.2% for the shorter wavelength). For $l_1^2 = 12\ km^{-2}$ the amplitude factor of the 4.63 km wavelength is too small for it to be detected visually.

Both wavelengths and amplitudes were calculated for the exponential layer. It should be noted that the amplitude was calculated (eq. (5.46)) from factors derived from both the observed temperature and velocity profiles and the exponential fit to the l^2 profile. Thus it can be expected to be accurate when the exponential fits the l^2 profile exactly. Otherwise it is only accurate to within the accuracy of the fit.

As mentioned in Section 6.8 the amplitude of a particular wave component is very dependent not only on the airflow characteristics but on the degree of resonance between the mountain size and shape and the characteristic wavelengths of the airflow. Thus here the amplitude is used only as an indication of the response of the airflow with height to the particular wavelengths. The calculation involves the height and half width of the mountain exciting the waves. These were taken as 2.0 and 4.0 km respectively which are approximately the values for the Torlesse and Puketeraki Ranges which are the last ranges before the plains. They both lie approximately along the same SW-NE line so that if the wind is coming from the north of NW the balloon would probably pass over the Torlesse Range and if the wind was from the south of NW the balloon would probably pass over the Puketeraki Range.

7. Effect of Smoothing and Averaging on EXP

The problem of obtaining the parameters of the undisturbed airflow from a balloon released in the disturbed flow prompted a study of the effect of smoothing and averaging. Smoothing was done using weights 0.125, 0.200, 0.350, 0.200 and 0.125, which were stored in an array called WEI.

Using a radiosonde released at 0000 hours on 25/12/70 the temperature and horizontal wind speed were smoothed once

using WEI and the following parameters were derived for the exponential fitted to the l^2 profile as defined in Eq. (5.33).

$B_o = 0.9529$ $B_1 = 0.0$ $\lambda = 0.6106$ and $\beta = 3.1976$

The solution of the eq. (5.44) with these parameters was

Wavelength = 37.48 km

By smoothing again using WEI the parameters of the fitted exponential were:

$B_o = 0.9587$ $B_1 = 0.0$ $\lambda = 0.6488$ and $\beta = 3.0182$

The solution of eq.(5.44) with these parameters was

Wavelength = 43.55 km.

Hence small changes in the parameters of the fitted exponential such as caused by various amounts of smoothing result in considerably larger changes in the wavelength.

Using a radiosonde released at 1200 hours on 25/4/70 the airflow parameters were averaged over 3, 4, and 5 points. The results of this are shown in Table 7.5.

Table 7.5: The effect of averaging over 3, 4 and 5 values of the airflow parameters on the resulting solution of the exponential layer model.

Number of points Averaged over =	3	4	5
Wavelengths	64.00	48.69	47.55
	6.90	6.68	6.60
	3.54	3.49	3.45
	2.32	2.28	2.25
	1.67	1.65	1.64
	1.26	1.26	1.24
	0.97	0.97	0.96

As the number of values averaged over (i.e. as the thickness of the layers considered) is increased, the wavelengths tend to decrease asymptotically to some limit for each component. This limit was assumed to be the solution for the undisturbed airflow. Since this was closely approached when averaging over four values this amount of averaging was chosen in order to retain resolution in the l^2 profile to which layers for the model solutions were fitted.

C H A P T E R 8

COMPARISON OF DATA AND THEORETICAL SOLUTIONS

1. Introduction

The data is presented in the form of a table of wavelengths derived from the power spectra of the SPB's and of the radiosonde ascents and wavelengths that are solutions of the two layer, bounded two layer, three layer and exponential layer theories for the particular approximations to the l^2 profile. The wavelengths of periodicities in the mountain profile are also tabulated. Other information such as wavelengths of waves from satellite photographs, the mean tropospheric wind direction, the wavelength given by the parcel theory and the wind speed at the height of the mountain ridge is provided where available and applicable. This form of presentation of the data was chosen mainly for efficiency in comparison and to condense the copious volume of diagrams of power spectra and wave number spectra to a practical size.

2. Data used in Two and Three Layer Approximations

The l^2 profile was plotted out on a larger scale than is shown in the profile summary presented here. These plots were used to determine the best two and three layer approximations to the observed l^2 profile. On many

occasions three layers were clearly defined and could be approximated quite well. On other occasions there were no distinct layers and sometimes there was more than one possibility for choosing three layers. In table 8.1 for profiles with more than one possible three layer structure all the possibilities are given.

Table 8.1: Two and Three layer approximation parameters.

Time	Date		l_1^2	l_2^2	l_3^2	h_1	h_2(H)	Layer Fit
1200	5/3/69	(a)	0.7	0.2	50.0	6.5	21.0	Fair
		(b)	0.7	0.2	100.0	6.5	21.0	"
		(c)	0.7	0.2	200.0	6.5	21.0	"
1200	26/3/69	(a)	50.0	2.0	10.3	2.5	20.2	Fair
		(b)	50.0	2.0	100.0	2.5	29.2	Ambiguous
0000	14.1.70		0.4	0.1	100.0	5.0	18.5	Good
1200	14/1/70		11.0	0.7	100.0	1.2	19.0	Good
0000	21/1/70		3.0	24.0	0.8	1.7	3.2	Good
1200	21/1/70		40.0	0.2	50.0	0.7	19.0	Fair
1200	2/3/70	(a)	4.7	0.35	2.7	1.6	13.0	Fair
		(b)	4.7	0.40	50.0	1.6	17.5	Ambiguous
1200	30/3/70	(a)	0.2	10.0	40.0	17.0	21.5	Fair though ambiguous
		(b)	0.5	0.2	40.0	4.0	21.5	
1200	24/4/70		1.5	0.5	4.5	6.8	17.5	Poor
1200	25/4/70		10.0	1.0	50.0	2.6	19.5	Fair
1200	26/4/70	(a)	6.0	3.8	0.4	1.7	5.2	Ambiguous
		(b)	3.8	0.4	1.0	5.2	10.6	

Table 8.1 (contd):

Time	Date		l_1^2	l_2^2	l_3^2	h_1	h_2(H)	Layer Fit
1200	4/6/70	(a)	8.0	1.0	8.3	1.0	20.5	Quite good
		(b)	1.1	0.2	1.3	6.0	10.0	Ambiguous
1200	16/6/70		8.0	0.8	1.5	0.8	11.0	Poor
1200	18/6/70		10.0	1.0	30.0	1.0	22.0	Fair
1200	2/7/70		10.0	1.0	1.5	0.8	11.0	Poor
1200	15/7/70	(a)	1.8	0.2	2.4	5.6	9.5	Fair
		(b)	1.0	2.4	36.0	9.5	18.0	Ambiguous
1200	23/7/70		2.0	0.5	7.0	0.6	12.0	Poor
1200	4/8/70		4.0	0.5	3.0	1.5	16.0	Fair
1200	13/8/70		15.0	1.0	60.0	0.8	21.0	Good
0000	15/10/70		10.0	0.2	1.0	0.8	11.0	Good
1200	15/10/70		0.7	0.5	50.0	4.5	20.5	Good
1200	2/11/70		1.0	2.0	70.0	7.5	16.0	Good
1200	18/11/70		1.0	0.2	60.0	8.3	20.0	Good

On several of the days the l^2 profile showed an increase at about the tropopause or just above of 0.5 to 5.0 km^{-2}. Several km above this again there was a rapid increase in l^2 to greater than 50 km^{-2}. This was one of the sources of ambiguity in the choice of the layer approximations. The effect of choosing the first increase as the third layer compared with choosing the second larger increase was

looked at in connection with the radiosonde 1200 2/3/70. Each was found to give essentially the same wavelengths with an addition mode appearing in the middle of the range for the second choice. This was suggested by the results obtained in Section 6.7.

The wind speed at the level of the mountain ridge ($\sim$ 2 km) $\bar{U}_m$ is given. It is only an approximate value because it was taken off the radar wind profile at Harewood.

3. List of Abbreviations and Symbols Used

In the data summary the following symbols are used for convenience in the tables.

- 2L - The unbounded two layer model
- 2LB - The bounded two layer model
- 3L - The three layer model
- EXP - The exponential layer model (Doos)
- RAD - The wavelengths obtained from the radiosonde ascent rate
- MOUNT - The wavelengths of periodicities in the mountain profile
- SPB - The superpressure balloon and its detected wavelengths
- BALLOON - Used when a balloon other than a SPB was used
- TROPO - Refers to the troposphere
- STRATO - Refers to the stratosphere

ASC - Refers to the ascent portion of a flight

O.M. - Refers to a part of a flight over the mountains

DESC - Refers to the descent portion of a flight

LEE - Refers to the part of the flight to the lee of the mountains

IN ALT - Refers to the part of the flight when the SPB was in or near its equilibrium altitude

W.F. - Refers to the whole flight

E.H. = The SPB's equilibrium height

$\bar{\lambda}_p$ = The mean wavelength given by the parcel theory. The height considered may be given as a subscript.

$\bar{\lambda}_s$ = The mean wavelength as measured off a satellite photograph.

D_t = Mean tropospheric wind direction found by averaging over the wind directions given for the troposphere by the radar/wind sounding.

D_s = Mean stratospheric wind direction obtained from the radar/wind sounding.

D_b = The mean direction of the SPB flight.

D_{PERP} = The direction perpendicular to the mean direction of the mountains in the southern alps, $\simeq 310^{o}$.

* - Indicates that long wavelengths were given as solutions of the particular model which are too long for Coriolis force to be neglected and so are not valid solutions.

+ - Indicates that an attempt has been made to give the asymptotic solution of a cluster of modes in the bounded two layer theory.

( ) - Indicates wavelengths that have perhaps doubtful significance when taken from the power spectrum.

____ - (Underlining) Indicates strong peaks on the power spectrum which are well above suspicion.

The terms 'long', 'medium' and 'short' wavelengths are used in a very relative sense. Generally they refer to wavelengths greater than 10 km, between 5 and 10 km and less than 5 km respectively.

Note: All wavelengths are given in km.

The balloons are designated by a number followed by a letter(s) and a number.

The initial number refers to the number of the balloon, the letter or letters refer to the release point (H : Hokitika, C : Cass) and the absence of a letter refers to a balloon released from Harewood. Where 'Pro' is used it refers to a balloon released in connection with the Honours Part III project of Miss S. Watson and Mr G. Opie.

The final number refers to toe sequence number of the particular release point or project.

Balloon profiles may be found in Appendix C and airflow profiles in appendix D

4. Superpressure Balloon and Theoretical Data

Balloon 3: Released: Harewood, 1400 5/3/69 (Tandem)

2L	2LB	3L	EXP	MOUNT	RAD	SPB ASC	SPB IN ALT
	18.18	18.5	25.19	60.0	(26.8)		
		15.0					
8.5	8.5		9.74	8.6	8.1	9.5	
					(5.75)	5.01	4.4
					(3.49)	3.51	3.5
					(2.37)		
					2.01	2.07	
					1.68		

$\overline{U}_g$ = 20.2 mps $U_m \sim$ 12 mps

D_t = 290° E.H. = 6.5 km

D_b = 301° $\lambda_{p\ 6.5} \approx$ 15 km

EXP: Good fit in the troposphere.

Satellite: A pass at 0930 5/3/69 shows waves to the lee of the South Island with an average wavelength of λ_s = 12.6 km.

Comment: Good waves are shown in the SPB profile as it ascended upstream of Banks Peninsula with a wavelength of about 9.5 km. This wavelength, together with the long wavelength in the radiosonde spectrum are the solutions of EXP which had a good fit in the troposphere. The layer theories also show a medium and a long wavelength but

shorter than those observed. λ_p was not observed. The amplitude at about 7 km as given by EXP is 750 m whereas the actual amplitude was about 100 m.

Reference to table 9.1 shows that the 8.1 km wavelength observed in RAD had a significant amplitude. This wavelength is very close to that predicted by the 2L and 2LB models. The 2.4 km wavelength in RAD was found to have an amplitude of approximately 60 m.

Balloon 5: Released: Harewood, 1430 26/3/69 (Tandem)

2L	2LB	3L	EXP	MOUNT	RAD	SPB IN ALT
	13.91	13.9	14.72			
	10.10	10.1				
	7.02	7.0	6.29			
	5.85	5.82			5.30	
	5.23	5.24				
	4.85	4.83	3.88		3.32	3.7
		4.62	2.76			
	4.50	4.50	2.11		1.90	2.1
1.60	1.60		1.67			
1.20	1.20		1.35		(1.26)	1.4
			1.09		(0.97)	

D_t = 260° E.H. = 6.7 km

D_b = 257° $\lambda_{p6.5}$ = 10.9 km

EXP: Quite a good fit although l^2 is underestimated low in the troposphere and overestimated in the middle troposphere.
Comment: This developmental tandem balloon system worked ideally showing the ascent under lift, slower ascent under its own lift and settling into its equilibrium level. Although the balloon oscillations in altitude are small the power spectrum shows three strong peaks. These have corresponding, though shorter wavelengths in RAD. The observed wavelengths are in very good agreement with EXP which also predicts a small amplitude at the SPB's equilibrium level. A small amplitude would be expected because D_t is 260°, 50° off the DPERP. The layers for the two layer model were quite well defined but there was no distinct increase in l^2 into the third layer so l_3 and h_2 were only approximate.

There was very little wind up to about 3 km. The large stability near the ground caused by this would account for the absence of long wavelengths.

Balloon 14C2: Released: Cass, 0830 14/1/70 (Tandem)

0000 Radiosonde:

2L	2LB	3L	EXP	MOUNT	RAD	SPB IN ALT
	30.17	31.4	51.5			(97.0)
13.87	13.88	13.65	14.8	15.0	14.4	(15.0)
				8.6		(8.8)
					(6.3)	(6.9)
				(4.4)	(4.6)	4.4
				(3.4)	(3.5)	
2.405	2.405			(2.2)	(2.5)	

D_t = 280° $\lambda_{p\ 10} \simeq$ 42 km $\overline{U}_m$ = 12 mps

D_b = 280° E.H. $\simeq$ 10 km $\overline{U}_g$ = 12 mps

EXP: A good fit in the troposphere. Amplitude at 10 km $\simeq$ 1.6 km.

1200 Radiosonde:

2L	2LB	3L	EXP	MOUNT	RAD	SPB IN ALT
			58.0			(97.0)
	13.46	13.65		15.0	16.0	(15.0)
	9.61	9.52	9.23			
	9.09			8.6		(8.8)
	8.26	8.26				
	7.68	7.66			(6.53)	(6.9)
			4.44	4.4		4.4
				3.4	3.14	
	2.41	2.41		2.2	2.14	

$D_t = 273^o$ $D_s = 277^o$

E.H. $\simeq$ 10 km

EXP: The fit is quite good in the middle and upper troposphere but it underestimates l^2 near the ground.

Satellite: At 1050 14/1/70 $\lambda_s \simeq 17.3$ km

At 1058 14/1/70 $\lambda_s = 14.8$ km

At 1300 14/1/70 $\lambda_s \simeq 23$ km

$\therefore \overline{\lambda}_s \simeq 16$ km

Comment: Since the flight took place during the morning both the 0000 and 1200 hour radiosondes were used. There is a good correlation between the mountain wavelengths and the 0000 RAD and the SPB. There is quite a good correlation between 2L and the shortest wavelength of RAD in both cases but it fails to predict the longer wavelengths that were present, probably because it neglects the trapping effect of the increase in l^2 in the stratosphere. The exponential fit to the midnight l^2 profile is good and EXP predicts the scale of the wavelengths observed. It is not a one-to-one comparison as the very long wavelengths predicted by EXP are very sensitive to the parameters of the fitted exponential and so their uncertainty is very dependent on the accuracy of the fit. The long wavelength suggested by the power spectrum of the SPB was evident in the satellite photograph of the cloud pattern, and there is a corresponding long wave solution in all of the models.

Balloon 1503: Released: Cass, 0832 21/1/70 (Tandem)

2L	2LB	3L	EXP	MOUNT	RAD	SPB DESC
	21.13	20.93	37.5		20.2	
	15.05	14.95	13.3	15.0		(13.0)
			7.63	8.6		6.36
			4.97	4.4		4.77
				3.4		3.50
					2.7	2.63
				2.2	(2.2)	2.0
1.21	1.21				1.7	

D_t = 298° D_s = 334°

D_b = 301° $\bar{U}_m$ = 7 mps

EXP: It is a good average fit but underestimates l^2 near the ground.

Satellite: A photograph taken during the late morning of 21/1/70 shows a wavelength of about 20 km as observed in RAD also.

Comment: Allowing for the accuracy of the fit there is quite a good correspondence between SPB and EXP. There was a relatively well defined surface layer and stable upper layer. 2LB and 3L predict the long waves and the short wave. The longest wave was observed by the satellite and RAD.

Balloon 18: Released: Harewood, 1400 2/3/70 (Free tetroon)

2L	2LB	3L	EXP	RAD	SPB IN ALT
			*		
			38.9		
			31.2		
	27.1	27.3	25.6		
			21.75		
			18.68		
	12.0	12.1	16.24		
	11.4			(9.0)	
3.95	3.95			(3.60)	
				(2.46)	
				1.46	1.73
				1.2	1.26
					0.46

D_t = 222° $\quad\quad$ $\bar{\lambda}_{p1.2}$ = 3 km

D_b = 243° $\quad\quad$ $\bar{U}_m$ = 12 mps

EXP: Not a very good fit below 4 km. It neglects a stable layer.

Comment: This was a very low level balloon and the wind speed at this level was about 4 - 5 mps. There are obvious short wavelength waves and these were evident in the power spectrum. There also appears to be a longer wave present which had a wavelength of about 18 km. Because EXP does

not take into account the stable (slightly) layer near the ground the solutions all have long wavelengths. The low level balloon did not experience any long waves but the radiosonde, which ascended to about 27 km, did. Thus there were other longer waves present in the airflow at higher levels. 2L and 2LB predict the 3.9 km wavelength in RAD. The l^2 profile lent itself to two possible three layer approximations. The solution shown here corresponds to (a) in Table 8.1. It was found that taking the higher, more stable region as the third layer did not change the wavelengths already given but introduced another at 10.5 km wavelength, perhaps corresponding to the 9.0 km seen in RAD.

Balloon 19: Released: Glentunnel, 1530 30/3/70

(A rising radiosonde balloon)

2L	2LB	3L	EXP *	RAD	BALLOON TROPO	BALLOON STRATO
			45.3			
			36.3			
			29.8			
	25.9	26.2	25.1			~29
			21.3			
			18.2			
	15.7+	15.6				
12.5	12.5	12.6		12.4		
						7.3
					(4.77)	4.3
				3.96	(3.45)	3.18
					2.7	2.58
				2.42	2.3	

D_t = 312° D_s = 287°

D_b = 308° $\bar{U}_m$ = 25 mps

EXP: Quite a good fit in the troposphere.

Comment: The balloon ascended to 16 km and power spectra were taken of the tropospheric and the stratospheric sections. The stratospheric spectrum shows significant peaks for all the given wavelengths and the tropospheric spectrum shows a marked absence of long wavelength waves and

significant peaks only for the two shortest waves shown. The midday profile shows small values of l^2 throughout the troposphere. This results in the absence of short waves in the models. There is quite a good correlation between the long wavelengths in the theoretical solutions and the balloons. These are mainly associated with the upper air conditions which do not change as quickly as the conditions near the ground which, if they resulted in increasing stability during the afternoon, would account for the presence of the short waves.

Balloon 24H2: Released: Hokitika, 0832 24/4/70 (Tandem

25H3: Released: Hokitika, 1332 24/4/70 (Tandem)

26H4: Released: Hokitika, 1940 24/4/70 (Tandem)

Since there was only a midday radiosonde flight the one profile had to be used for all three balloons.

2L	2LB	3L	EXP	RAD
	31.5	31.4	23.0	18.3
	12.4	12.56	14.62	
	9.4	9.4	9.8	
6.72	6.72	6.68		(6.12)
5.43	5.43			(4.07)
				2.93
				2.16
				(1.53)

$D_t = 300^o$ $\bar{U}_g = 13.4$ mps

$D_s = 265^o$ $\bar{U}_m = 20$ mps

EXP: It is not a good fit. There are no well defined layers to fit the 2L or 3L models.

24H2			25H3			26H4	
MOUNT	SPB W.F.	SPB DESC	MOUNT	SPB O.M.	SPB DESC	MOUNT	SPB ASC
		30		30	30		
12.0						(15)	
			8.5				8.5
6.0			5.0	6.8		5.5	
		4.7	4.0			4.0	
	3.22	3.5		3.4	3.4	3.35	
(2.5)	2.4	2.8	(2.4)	2.8	2.8	(2.7)	2.9
(2.2)		2.0	(2.1)	2.0		(2.24)	2.1

Comments:

24H2: The SPB was released too high by the pressure trigger in the tandem system. The long (30 km) wavelength is a solution of the 2LB and 3L models. There is no correlation between the models and the balloon for shorter wavelengths due to the complex variation of l^2 with height.

25H3: There was a marked decrease in the amplitude factor in the power spectra of the 30 and 2.8 km waves in the descent stage compared to the high altitude part over the mountains. There was a noticeable increase in the 3.4 km component lower down. This suggests, in line with the

bounded two layer theory and the decrease in l^2 at high levels, that longer wavelengths predominate at high levels and shorter wavelengths at low levels. The 30 km wave can be seen in the balloon profile over the mountains and it has an amplitude of about 300 m. Also it is evident in the descent stages of both 24H2 and 25H3. EXP gives an amplitude of about 450 m for the long wave component at about 10 km.

26H4: The balloon profile shows a slow ascent through the stratosphere from 10 to 16 km. Its velocity profile follows approximately that of the midday radiosonde flight showing that the velocity conditions in the stratosphere did not change very much over the day. There are no obvious waves in the balloon profile. This is supported by the power spectrum although there is one peak at about 8.5 km. The amplitudes given by EXP were not encountered by the balloons which is not surprising since the exponential does not fit the l^2 profile very well at all.

Balloon 27H5: Released: Hokitika 1329 26/4/70 (Tandem)

2L	2LB	3L	EXP	MOUNT	RAD	SPB ASC	SPB DESC
			*				
	19.89	19.9	18.18				
			14.87		14.1		
			12.56				
			10.80	10.0		(9.7)	
			9.43				
5.71	5.71	5.72		5.43			
3.88	3.88	3.88			4.25	(4.2)	(3.65)
3.36	3.36	3.20		3.30			
		3.0		2.45	2.23	(2.2)	(1.78)

$D_t = 280^o$ $D_s = 316^o$

$\bar{U}_m = 6$ mps

EXP: Not a good fit.

Comment: The SPB was carried too high before it was released. There were no marked waves in the profile and the power spectra show very little periodicity. The midday radiosonde showed significant oscillations. The descent stage of the SPB shows a curve which may be due to a long wavelength wave. The layer profiles chosen give very strong resonance peaks in the 3L k-spectrum which are probably due to the over simplification of the profiles.

The velocity profile shows that the wind was almost constant at about 6 mps up to 5 km. If this was true over the mountains then conditions were almost certainly sub-critical and no waves would result (as observed). Förcht-gott's classification gives a minimum critical velocity for waves to be produced for mountains of the scale of the Southern Alps of about 13 mps. An increase in l^2 between 3 and 5 km due to a slight decrease in the wind speed would tend to reduce the upward propagation of waves.

Balloon 31H6, 32Pro3: Released: Hokitika 1300 4/6/70 (Valved)
Harewood 1900 4/6/70 (Valved)

2L	2LB	3L	EXP	RAD	31H6 MOUNT	31H6 SPB	32Pro3 MOUNT	32Pro3 SPB
			84.9					
	27.0	27.0	24.6	(25.0)				
	10.75	10.7	14.0		12			11
	8.27	8.25	9.28					
	7.20	7.13						
	6.66	6.68	6.58					
3.48	3.48				3.3	(4.6)	4.4	4.22
				(2.3)	(2.65)	2.2	2.3	2.3
						1.95	1.6	(1.7)
				(1.47)		1.50		(1.3)

$E.H._{31} \simeq 8.0$ km
$\bar{U}_g = 13.1$ mps

$E.H._{32} \simeq 6.3$ km
$\bar{U}_m = 14$ mps

$D_t = 341^o$ $\quad$ $D_s = 300^o$

$D_{b31} = 309^o$ $\quad$ $D_{b32} = 318^o$

EXP: Not a good fit.

Parcel Theory: Between 5 and 8 km the parcel theory gives wavelengths that increase from 6.7 to 16 km. At about 6 km, the E.H. of 32Pro3, it gives a wavelength of 8 km. This was not observed in the balloon profiles.

Comment: The l^2 profile lent itself to be divided into three layers in two ways, shown in Table 8.1. The results above are the solutions using (a). By considering only the l^2 profile in the middle and upper troposphere (b) the following solutions were obtained:

2L	2LB	3L
10.43	11.94	10.5
6.61	6.99	6.62
6.26		

These are close to the values given in the middle range for profile (a). It may be inferred then that the short wave solutions from (a) result from the stable layer (or the interface above the stable layer) and that the long wave solutions result from the stable upper layer. Although EXP is not a good fit it gives the same scale of solutions as the constant layer theories.

The 11 km wavelength in 32Pro3 was close to the solutions given by the layer theories for both profiles. This wave was most likely excited by the Alps. The lack of excitation in the middle range may account for the lack of observed waves in this range.

Inspection of the balloon profile of 31H6 shows a long wave oscillation above the mountains at 8 km with a wavelength of about 25-30 km. Its presence is substantiated by the 25 km peak in RAD. A wavelength in this range was a solution of 2LB, 3L and EXP.

The 11 km wavelength in the profile of 32Pro3 is evident in its ascent but it is absent from the spectrum of the profile over Banks Peninsula due to the distrubance of the airflow by the Peninsula. The periodicities in the Peninsula all appear in the balloon profile above it.

Balloon 34H7: Released: Hokitika 1300 16/6/70 (Valved)

2L	2LB	3L	EXP	MOUNT	RAD	SPB ASC	SPB LEE
			70.6				
			31.7				
			20.0	20.0		21.7	
			14.4				13.0
	10.0	10.0	11.0				
			8.6	8.0			
	7.54	7.55	6.8		5.9	5.8	
4.05	4.05	4.10		3.7	4.1	3.95	3.95
				2.2	2.05	2.6	2.29
					1.54	1.8	1.74

D_t = 281° $\quad\quad$ $\lambda_{p6.5}$ = 11 km

D_b = 279° $\quad\quad$ E.H. ≃ 9.2 km

$\bar{U}_g$ = 5.3 mps $\quad\quad$ $\bar{U}_m$ = 11 mps.

EXP: Not an accurate fit but a good average fit.

Satellite: At 0919 16/6/70 $\bar{\lambda}_s$ = 10.4 km

At 1551 16/6/70 $\bar{\lambda}_s$ = 14.8 km

Comment: The satellite photographs indicate that the principal wavelength increased from about 10 km at midmorning to about 15 km in the later afternoon. This is consistent with the SPB flight which gave a mean wavelength of about 13 km at the 6-7 km level. This wavelength was not observed

in the ascent stage over the mountains so it must be the result of the response of the airflow to the distrubance of the mountains. It was not a forced wavelength so must be a natural wavelength.

The layer theories predict wavelengths of the scale of those observed. EXP predicts the long and middle wavelengths quite well but fails to provide the short wavelengths. This was probably because it neglected the ground layer, which even though it is quite shallow, affects the waves considerably.

Balloon 35H8: Released: Hokitika 1300 28/6/70 (valved)

2L	2LB	3L	EXP	MOUNT	RAD	SPB
	14.26		12.0			
	9.48	9.66				
	8.79^{+}					
	7.50	7.48				
	6.57			6.67	6.9	7.42
2.87	2.87			3.75	3.22	4.3
					1.42	2.2
					1.21	1.86

$D_t = 339^{o}$ $\quad D_b = 327^{o}$

E.H. = 8 km $\quad \overline{U}_g = 15.7$ mps

$\overline{U}_m = 8$ mps

EXP: The average exponential fitted to the whole troposphere did not fit very well so another exponential was fitted between the ground and about 6 km. The solution of the equation for this profile is given above.

Satellite: At 1000 28/6/70 $\bar{\lambda}_s$ = 19.5 km.

Comment: It appears that the balloon was lifted by the air stream to such a level that the lifting/superpressure gas was lost and it became negatively buoyant. For the valve setting of about 30 mm this would have required a displacement of about 800 m at 8 km. It appears from the SPB profile that, allowing for the missing data, such a displacement was quite possible. The amplitude of the rather noisy oscillations near the end of the flight was about 650 m.

The l^2 profile shows a general decrease from the ground up to 10 km due to the general increase in wind speed through the troposphere. The mean tropospheric wind direction measured at Harewood, above the coastal nor'easterlies, was about 330°. This is almost perpendicular to the direction of the ridge of the Torlesse Range over which the balloon passed. Thus the criteria for good waves were satisfied and large amplitude waves were observed.

Balloon 36H9, 37H10: Released Hokitika 0700 and 1300 2/7/70 (valved)

2L	2LB	3L	EXP	MOUNT	36H9 O.M.	LEE	37H10 MOUNT	IN ALT
			29.1					
	19.21	14.4	14.6	15.0	18.5	13.0	15.0	
	10.29	9.44	9.39					9.8
	8.11	7.85		8.3			8.3	
		6.98	6.67					
	6.63	6.54		4.8	4.0		4.8	4.9
3.52	3.52	'3.32'		3.3		3.67	3.3	3.50
					2.94	2.65		
				2.45	(2.38)		2.45	
					(1.91)		(1.91)	

$D_t = 279^o$ $D_s = 294^o$

$E.H._{36} = 8.2$ km $E.H._{37} = 8.0$ km

$\bar{\lambda}_{p8.0} \simeq 14.5$ km $\bar{U}_g = 8.8$ mps

$\bar{U}_m = 6$ mps

EXP: Not a good fit, but follows the general decrease in l^2.

Satellite: At 0930 2/7/70 $\bar{\lambda}_s \simeq 9.5$ km to the north of the South Island.

Comment: Both balloons show a predominant wavelength around 3.5 - 4 km which is that predicted by the two layer theory. These waves would have been excited by the 3.3 km mountain wavelength. The 2LB, 3L and EXP give solutions for

middle and long wavelengths some of which are close to those observed. There is quite a good correlation between the mountain wavelengths and the balloon wavelengths.

Balloon 37 which was released just after the midday radiosonde shows a good agreement between its wavelengths and 2LB (and thus to 3L and 2L) which are solutions based on the midday profile. The exception, 4.9 km, is very close to the 4.8 km forcing wavelength of the mountains.

The amplitudes of the waves are significant just to the lee of the mountains. This is to be expected for the waves that are just a response to the forcing of the mountain. The amplitude given by EXP shows a nodal surface for the 14.6 km component near the 8 km level and an amplitude of about 130 m for the 9.4 km component. This is approximately that which was observed. The two layer theory is inadequate because it fails to predict the longer wavelengths that were observed. The three layer and bounded two layer solutions are better. The variation between 2LB and 3L is due to the complete trapping caused by the upper boundary in 2LB which is not caused by the slight increase in l^2 as allowed for by 3L.

Balloons 38Pro4, 39Pro5: Released Birdlings Flat 1300 and 1530 15/7/70 (valved)

2L	2LB	3L(a)	3L(b)	38Pro4 MOUNT	38Pro4 SPB	39Pro5 MOUNT	39Pro5 SPB
			24.2	12.0	12.0		
			8.97			8.5	
			7.25		7.83		7.3
6.76	6.76	6.77	6.5				
5.03	5.04	5.03	5.28				
4.80	4.87			4.6	4.0	4.2	4.3
				2.8	3.1	3.3	
				2.2	2.27	2.15	2.43
					(1.64)		(1.79)

$D_t = 215^o$ $\quad D_{b38} = 204^o$

$E.H._{38} = 6.0$ km $\quad D_{b39} = 213^o$

EXP: The 1^2 profile generally increased through the troposphere so there was no exponential solution.

Comment: It is interesting to note that for profile (a) (see Table 8.1) the three constant layer theories all gave the same solutions. This was initially thought to be due to the low stability in the upper layer which did not introduce trapping for any long wavelengths. However, even the introduction of a rigid boundary does not show up any long wavelength modes. This is consistent with Fig. 5.3 which

shows that for the case chosen there were no long waves for boundary heights less than 9 km. Case 31(b) was looked at because there was a very stable layer above the original third layer. The upper interface was chosen at 18 km where the first rapid increase in l^2 occurred. If the interface had been taken at 20.5 km where the major increase in l^2 occurred the only effect on the solutions would have been to reduce the long wavelength to 17.2 km.

Balloon 38Pro4 shows significant waves at about 6 km with amplitudes of about 400 m. Balloon 39Pro5 did not reach its equilibrium height before tracking was terminated. Hence the wavelengths given are the mean wavelengths over the height range 3-7 km.

Balloons 41Pro7, 42Pro8: Released: Birdlings Flat 1930 and 2025 23/7/70 (valved)

2L	2LB	3L	EXP	RAD	41Pro7 MOUNT	41Pro7 SPB	42Pro8 MOUNT	42Pro8 SPB
	No Solutions		31.5					
		(19.0)		19.0				20.6
			13.1					
		8.1				8.3		8.24
		6.68			6.1		5.5	5.2
				4.9	4.0	4.65		
								3.3
				2.45	(2.6)	2.8	(2.6)	2.5
					(2.22)	(2.22)	(2.22)	
				(1.75)		(1.12)		

$D_t = 298^o$ $D_s = 265^o$

$E.H._{41} = 10$ km $E.H._{42} = 8$ km

EXP: Not an accurate fit but a good average fit.

Satellite: At 1016, 23/7/70 $\bar{\lambda}_s$ 15.6 km

At 1200, 23/7/70 Mid. N.Z. $\bar{\lambda}_s$ 20 km

Mid. Sth.Is. $\bar{\lambda}_s$ 18 km

At 1606, 23/7/70 North Is. $\bar{\lambda}_s$ 14.1 km

Kaikouras Sth.Is. $\bar{\lambda}_s$ 16.9 km

South of Sth.Is. $\bar{\lambda}_s$ 12.7 km.

Comment: Both of these balloons were released from Birdlings Flat under westerly conditions so that they flew across the southern part of Banks Peninsula. The satellite photographs (see Appendix A) show that there was a lot of wave activity to the lee of New Zealand on this day. They show that the wavelengths generally increased during the morning to about 20 km at midday then decreased again during the afternoon. They followed the same sort of variation as the mean tropospheric wind speed above Harewood which was 17.3 mps at 0600, 21.4 mps at 1200 and 17.2 mps at 1800 hours.

The l^2 profile shows a general decrease up to about 7 km above which it increases into the stratosphere to peak at about 16 km.

Both of the balloons exhibit the characteristic ascent of valved SPB's with significant waves at their equilibrium heights. The wavelengths of 42Pro8 (8 km) are generally longer than those of 41Pro7 (10 km). This is consistent with the increase in l^2 from about 0.2 km^{-2} at 8 km to 0.5 km^{-2} at 10 km. 3L predicts the medium and long wavelengths quite well but shows a complete lack of short waves. The l^2 difference between the bottom and middle regions is too small for there to be two layer solutions.

Balloon 43H11: Released Hokitika 0730 4/8/70 (valved)

2L	2LB	3L	EXP	RAD	MOUNT	SPB IN ALT
	23.36		42.8	(32.2)		22.4
		14.3	12.6			
	11.3	10.5				
	9.28	9.1		10.5		8.39
4.69	4.69		6.72	(5.45)		4.47
				3.0		(3.36)
				(2.0)		2.69

D_t = 287° D_b = 299°

D_s = 276° E.H. = 4.3 km

$\overline{\lambda}_p$ = 9 km

$\overline{U}_g$ = 13.1 mps $\overline{U}_m$ = 11 mps

(There were no significant periodicities in the power spectrum of the mountain profile.)

Satellite: At 0901, 4/8/70 $\overline{\lambda}_s \sim 11$ km and at 1550 4/8/70 $\overline{\lambda}_s \sim 13$ km. These waves appear to be over the mountains with an altocumulus sheet (the nor'west arch) to the lee of the mountains.

Comment: Inspection of the balloon profile shows that any waves that were present had small amplitudes. RAD and SPB gave wavelengths of about the same scale. Application of the Scorer Criteria to the l^2 profile implies that since l^2

decreased with height, U increased with height, there should be good waves present. The additional criterion that the direction of the wind be within 30° of the direction perpendicular to the mountain ridge should also be applied. D_t at midday was 287°, 33° off the perpendicular direction and the mean stratospheric wind direction was even further around to the west at 276°. The balloon flight indicates however, that during the early morning the wind direction at about 4.3 km was 299°, only 11° off the perpendicular direction. Hence the lack of wave activity must be associated with the random nature of the mountains. Any wave trains produced by particular mountains are nullified by all the other wave trains produced by other mountains and ridges.

There is a good correlation between the SPB and RAD. SPB shows four significant wavelengths, particularly the long (22 km) wave. RAD shows very little activity throughout the troposphere and only two peaks in the power spectrum with any significance. The decreased activity would have been due to the changing of the wind direction towards the west during the morning.

The wavelengths observed agree quite well with 2L and 2LB but again the bounded two layer theory is more realistic because it predicts the longer wavelengths that were present. EXP was a good average fit through the troposphere and has solutions which are of the same order as those observed. It lacks the short waves.

Balloon 44: Released: Harewood 0930 13/8/70 (Valved)

2L	2LB	3L	EXP	RAD	SPB IN ALT
			*		
	17.6	23.3	17.5		
	12.7	11.2			
	10.0				10.5
	9.0	9.4			
	8.0		8.6		
	6.6^{+}			6.96	
2.39	2.39			(3.16)	3.16
				(1.88)	2.25
				1.55	(1.66)
				1.30	(1.37)

$D_t = 342^{o}$ $D_b = 351^{o}$

E.H. = 3.4 km $\bar{U}_g = 26.3$ $\bar{U}_m = 20$ mps

Parcel Theory: Between 3 and 3.7 km the parcel theory gives an average wavelength of about 16 km.

EXP: Quite a good fit except near the ground.

Comment: This was a day when the wind was well round to the north of west but wave clouds were present over Canterbury so I decided to release a balloon from Harewood. The separation of the wave clouds was about 10 km, the long wavelength observed by the SPB. None of the middle of longer long waves were present but it was surprising that any were

present at all considering the wind direction. The short wavelengths evident in RAD and SPB show a marked similarity.

Balloon 45H12: Released Hokitika 0700 15/10/70 (Valved)

Balloon and Mountain Data:

MOUNT (Alps)	SPB (Alps - B.P.†)	MOUNT (B.P.)	SPB (Lee of B.P.)
	12.0	12.0	11.0
8.5			
5.5		6.0	
4.0		3.8	4.4
	3.1	(3.5)	
		2.6	2.36
	2.0	2.1	1.8
	(1.23)		1.5

D_b = 311° E.H. = 4.0 km

†B.P.: Banks Peninsula

Theoretical Results:

0000 15/10/70					1200 15/10/70				
2L	2LB	3L	EXP	RAD	2L	2LB	3L	EXP	RAD
	19.8	19.6	19.2	18.4				29.5*	(36.0)
			7.5	6.0		15.6	15.7	15.0	
3.67	3.67			3.3		10.9	10.8		
				1.9		9.38	9.4		
				(1.6)	8.7	8.7	8.7		3.8
									1.8
$\bar{\lambda}_p \simeq$ 10 km					$D_t = 309^o$ $\bar{\lambda}_p \simeq$ 10 km				
					$\bar{U}_m$ = 10 mps				

EXP: A good fit in both cases. There was a very stable layer in the stratosphere by midday.

Satellite: At 0910 15/10/70 to the south of the South Island $\lambda_s \sim 15.5$ km. At 1620 15/10/70 there were well developed waves over Canterbury, $\lambda_s \sim 11.3$ km.

Comment: This was probably the best balloon of the project in that it demonstrated so many things. It was at quite a low level so the fluctuations in the radar over the mountains were quite large. It was lost due to the ground echo from the Craigieburn and Torlesse Ranges, which is a pity because the region where the first wave would have been produced was lost. The SPB profile shows a well developed

system of waves to the lee of the Alps, with an amplitude of approximately 150-200 m and with a predominant wavelength between 11 and 12 km. (12 km from the power spectrum.) It is evident that a shorter wave (2.0 km) was superimposed onto this longer wave. The long wavelength wave train produced a cloud pattern which was photographed by the satellite and gave a wavelength very close to that given by the SBP.

In addition the balloon also passed over Banks Peninsula and the effects of this secondary source of waves can be seen in the SPB profile. The irregularities produced by the Peninsula appear to disrupt the smoother waves at a point 30 km downstream from the first hill in the Peninsula. This gives an angle of propagation of 7.6^{o} to the horizontal. If the disturbance was carried downstream at the mean wind velocity up to the level of the SPB the vertical propagation velocity was about 1.6 mps. This would appear to be a reasonable velocity for internal gravity waves.

The principal 12 km wavelength is the natural oscillation that results from the airflow incident on the Southern Alps. When this disturbed airstream flows across Banks Peninsula it is in resonance with the ground disturbance but the resulting natural oscillation has a wavelength of 11 km. This is the wavelength that is the solution of the layer profiles derived from a radiosonde which ascended through the distrubed flow. Thus the Peninsula is presented with an

airflow with a different l^2 profile than that presented to the Alps with a resulting difference in the natural wavelengths.

The proximity of these two wavelengths suggests that the smoothed and averaged profile used is not too different from that upstream of the Alps. The 15.6 km wave given by 2LB and 3L was probably out of resonance with the mountains so was not produced. It did not appear in the power spectrum of the mountain profile.

There was a good correlation between the theoretical solutions for the midnight profile and the radiosonde wavelengths which had very strong peaks on the power spectrum.

The parcel theory gave a wavelength close to that which was observed.

There was a considerable difference between the profile of the 0000 radiosonde and the 1200 radiosonde. The solutions obtained from these profiles show very different wavelengths. The SPB released at 0700 was then flying in an airstream with characteristics somewhere between them. Since the "midday" radiosonde was actually released at 1100 and the SPB flight was over the Peninsula at about 1000, the "midday" profile was most appropriate.

Balloon 46H13: Released: Hokitika 1230 2/11/70 (Valved)

2L	2LB	3L	MOUNT (Alps)	RAD	SPB
No Solutions		17.4	15.0	(14.0)	
		9.17			11.0
		7.0	8.6		
		6.01			
		5.04	4.6	4.2	
			3.16		3.7
			2.5	(1.91)	2.36
				1.32	1.37

D_t = 293° D_b = 301°

E.H. = 4.3 km $\overline{\lambda}_p \sim$ 9.4 km

$\overline{U}_g$ = 14.3 mps $\overline{U}_m$ = 11 mps

Comment: The balloon profile shows a marked increase in height between the time when the balloon was lost due to the ground returns from the mountains and the time it was relocated. This may in part be due to the signal from the mountains causing the radar to give a lower elevation than that of the balloon. The height difference is too large for it to be solely due to this. It could indicate a large primary wave just to the lee of the Alps or there may have been an undular hydraluic jump present such as observed over Colorado by Vergeiner and Lilly, 1970. In either of these

cases the balloon would tend to return to its natural equilibrium density level and underestimate the size of the wave or jump.

The unstable conditions required for a jump were not associated by large wind velocities. It was about 17 mps at these levels. They may have been associated with the very low stability throughout the troposphere as indicated by the very low values of l^2.

Another possibility is that the balloon was carried down by the air as it descended in the lee of the mountains then returned to its equilibrium level under its own lift.

Because l^2 increased with height there were no 2L, 2LB or EXP solutions. The three layer solution gives medium and long waves with a complete absence of short waves. The short wave oscillations in the SPB profile were probably due to the Alps and Banks Peninsula.

Balloon 47H14: Released: Hokitika 1156 18/11/70 (Valved)

2L	2LB	3L	EXP	MOUNT	RAD	SPB
			*			
			32.9			
	24.5	24.2				29.6
	15.8	15.7	15.7	(15.0)	11.4	
8.35	8.35		9.42	8.6		
6.67	6.67					5.37
				3.3	(3.3)	(3.69)
				(2.7)		2.81
				2.28	2.42	

D_t = 299° D_s = 299°

E.H. = 10 km λ_p = 18 km

$\overline{U}_g$ = 19.6 mps $\overline{U}_m$ = 11 mps

EXP: A very good fit through the troposphere except for the point just above the ground.

Comment: l^2 is very small up to about 14 km which is why there are no short wavelength theoretical solutions. There is an obvious long wavelength of about 30 km and an amplitude of about 150 m. This is a multiple of the 15 km wavelength in the mountains. The amplitude given by EXP for the 32.4 km component at about 10 km is very close to that observed. The layer theories could at best be

described as predicting the scale of the motion but they lack the short wavelength components. It may be that these short wavelengths are submultiples of the longer wavelengths that are picked up by the power spectrum analysis. In which case the theories may be considered more reliable than initially indicated.

CHAPTER 9

RADIOSONDE DATA

1. Introduction

Radiosonde/radar wind balloon flights were the source of the temperature and horizontal wind velocity profiles. As discussed in Chapter 7 the raw radiosonde data was analysed for temperature and pressure at half minute intervals. Using these in the hydrostatic equation 7.3 the height and ascent rate of the balloon were calculated. By assuming that the ascent rate varied smoothly as an exponential the fluctuations of the ascent rate about this exponential were taken as a measure of the vertical motion of the airflow. Corby (1957) studied radiosonde data in order to find evidence of atmospheric gravity waves. He found that information derived from radiosondes was useful in the study of lee waves.

On several occasions I was prevented from releasing an SPB when a wave situation was set up. On such occasions data about the waves in the airflow could be obtained from the daily midday radiosonde flight.

The periods of the waves were obtained from the power spectrum of the perturbations from the fitted smooth variation in the ascent rate. Inspection of the ascent rate profile revealed heights where the perturbations in the

ascent rate were maximum. An attempt was made to relate the scale of the oscillations producing the maximum to the lag (period) of the resonance peaks in the power spectrum, aided by a comparison with an SPB flight if there was one at about the time of the radiosonde. From this lag the approximate wavelength was calculated using

$$L \simeq \frac{1.8\ \bar{U}}{(\text{lag})} \qquad (9.1)$$

where L is the wavelength in km and $\bar{U}$ is the mean tropospheric or stratospheric wind speed (in mps) depending on the height at which the maximum occurred. The maximum amplitude of this wave was then calculated using, from Corby (1957)

$$A_{max} \simeq \frac{w_{max}\ L}{2\ \pi\ U} \qquad (9.2)$$

where w_{max} and U are the maximum perturbation velocity and the horizontal wind speed in mps at the level of the maximum. When A_{max} is in m (9.2) becomes

$$A_{max} \simeq 159.3\ \frac{w_{max}\ L}{U} \qquad (9.3)$$

For Example: The balloon 0000 14/1/70 shows a maximum perturbation velocity at about 12 km of 5.1 mps. This was at the tropopause. Thus the mean wind speed was taken as the mean speed over the whole flight, 22.6 mps. These quite large scale oscillations were assumed to be related to the strong peak in the power spectrum at Lag = 2.4. Thus the

approximate wavelength of the wave was assumed to be, from (9.1), 17 km. Using (9.2) gives the displacement of the wave at this level of 306 m, where the wind speed was 45 mps. A secondary maximum of about 1.2 mps low in the troposphere at 3.2 km was produced by some smaller scale oscillations. Assuming that these correspond to the peak in the power spectrum at 11 lags an amplitude of about 46 m is given, since the wind speed at this level was approximately 19 mps and the mean tropospheric wind speed was 28 mps. If it had been due to the peak at 8 lags the wavelength would have been 6.3 km and the amplitude about 63 m. In both cases the amplitude is quite small.

2. Ascent Rate Profiles and Power Spectra

The following figures are the profiles from a selection of radiosonde balloons released over the period January 1970 to March 1971, except for the first in Fig. 9.1 which was released at 1200 hours on 5/3/69. Due to truncation errors in the plotting subroutines the scaled grid often is smaller than the centre line grid. This has been allowed for in reading off the values of U by reference to the original computer printout.

3. Discussion of the Profiles

Most of the profiles show a tendency for the ascent rate to increase with height. This was to be expected since the ascent is described by an equation of the form

$$F_L = \tfrac{1}{2} \rho v^2 C_A A^* \qquad (2.22)$$

Since the radiosonde balloon is approximately spherical the effective area may be given by

$$A^* = 4 \pi \left(\frac{3V}{4\pi}\right)^{\frac{2}{3}} \qquad (9.4)$$

And since the ambient density ρ is proportional to the ratio of the pressure to the temperature, and the ratio $\frac{P V}{T}$ is constant, the ascent rate may be expressed as

$$v = \left[\frac{F_L}{2 \pi \left(\frac{3}{4}\right)^{\frac{2}{3}} \rho C_D \left(\frac{V_o}{\rho}\right)^{\frac{2}{3}}} \right]^{\frac{1}{2}} \qquad (9.5)$$

The free lift F_L, the drag coefficient C_D, and the density and volume of the balloon at the ground ρ_o and V_o are all constant. Eq. (9.5) may then be written as

$$v = K \rho^{-\frac{1}{6}} \qquad (9.6)$$

Hence as ρ decreases as the balloon ascends the ascent rate will increase. Initially the perturbation velocity of the airflow, as derived from the ascent rate, was calculated by taking the difference between the observed ascent rate and

a velocity of the form of (9.6) when K was determined by the initial conditions. However, this was insensitive to variations from the ideal situation, such as gas leakage from the balloon, which cause the mean ascent rate to be less than that calculated. Therefore it was decided to use an exponential fit, which on most occasions approximated the mean rate of ascent very well. For balloons that went very high, greater than 30 km, the mean ascent rate usually increased above this fitted exponential.

4. Analysis of Waves Evident in the Profiles

The results of the analysis for the maximum displacements and vertical velocities, with the corresponding wavelengths as derived using the equations and assumptions stated in section 9.1, are presented in Table 9.1 below. Where there were two alternative wavelengths which may have been producing the maximum and when one could not be rejected with reference to an associated SPB flight both are given in the table.

Table 9.1: Table of the Height, maximum vertical velocity (w_{max}) and maximum amplitude (A_{max}) for an approximate wavelength L as derived from the ascent profile and power spectrum of the ascent of radiosonde balloons released from Harewood.

Time	Date	Height (km)	w_{max} (mps)	A_{max} (m)	L (km)
1200	5/3/69	2.5	3.0	61	2.4
		15.0	9.0	455	8.1
0000	14/1/70	12.0	4.0	202	14.4
1200	14/1/70	6.0	-1.0	-18.6	3.1
		6.0	-1.0	-12.7	2.1
0000	21/1/70	3.0	1.8	169	1.8
		3.0	1.8	122	1.3
		9.0	6.0	472	15.0
1200	21/1/70	5.8	2.0	41	2.7
		5.8	2.0	26	1.7
		16.2	2.8	294	11.3
0000	27/1/70	3.5	1.0	35	1.0
		13.7	2.7	46	1.3
		13.7	2.7	23	0.7
1200	2/3/70	0.4	2.8	643	2.5
		0.4	2.8	383	1.5
		17.0	2.9	208	3.6
1200	24/4/70	2.0	3.4	68	2.9
		17.0	2.0	77	4.0
1200	25/4/70	6.0	5.3	83	1.6
		14.5	6.0	1100	11.5
1200	26/4/70	8.5	2.9	75	3.8
1200	4/6/70	No significant waves			
1200	16/6/70	2.3	3.0	71	2.0
		17.0	2.5	107	5.9
1200	28/6/70	11.5	9.2	433	6.5

Table 9.1 (contd):

Time	Date	Height (km)	w_{max} (mps)	A_{max} (m)	L (km)
1200	2/7/70	16.0	3.0	112	5.5
1200	23/7/70	3.5	4.0	79	2.5
		10.0	4.5	414	19.1
1200	4/8/70	3.0	1.0	21	2.0
		13.5	2.5	83	5.5
		25.0	11.0	728	10.5
0000	15/10/70	2.3	1.0	34	3.2
		14.0	2.0	217	18.4
1200	15/10/70	2.0	2.0	44	1.8
		16.0	2.0	43	2.2
1200	2/11/70	3.0	3.0	142	4.2
		8.0	6.0	73	1.4
1200	18/11/70	7.0	2.0	62	3.3
		15.0	4.0	479	11.4
1200	7/12/70	2.8	2.0	124	3.9
		15.0	4.0	148	9.4
1200	24/2/71	2.7	8.0	1390	23.0
		13.0	-2.0	-40	5.3
1200	15/3/71	12.0	3.0	35	2.7

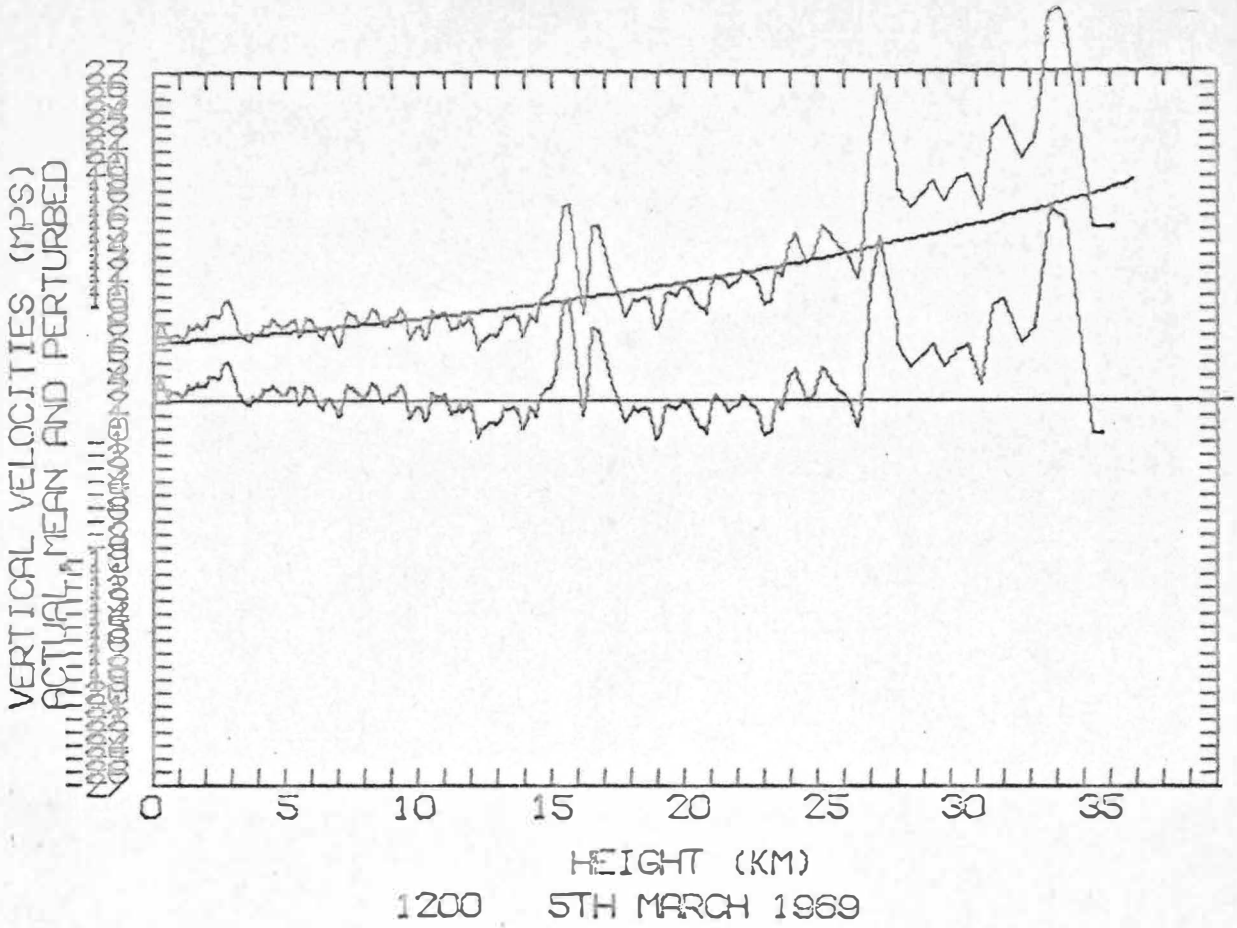
VERTICAL VELOCITIES (MPS)
ACTUAL, MEAN AND PERTURBED
0
5
10
15
20
25
30
35
HEIGHT (KM)
1200 5TH MARCH 1969

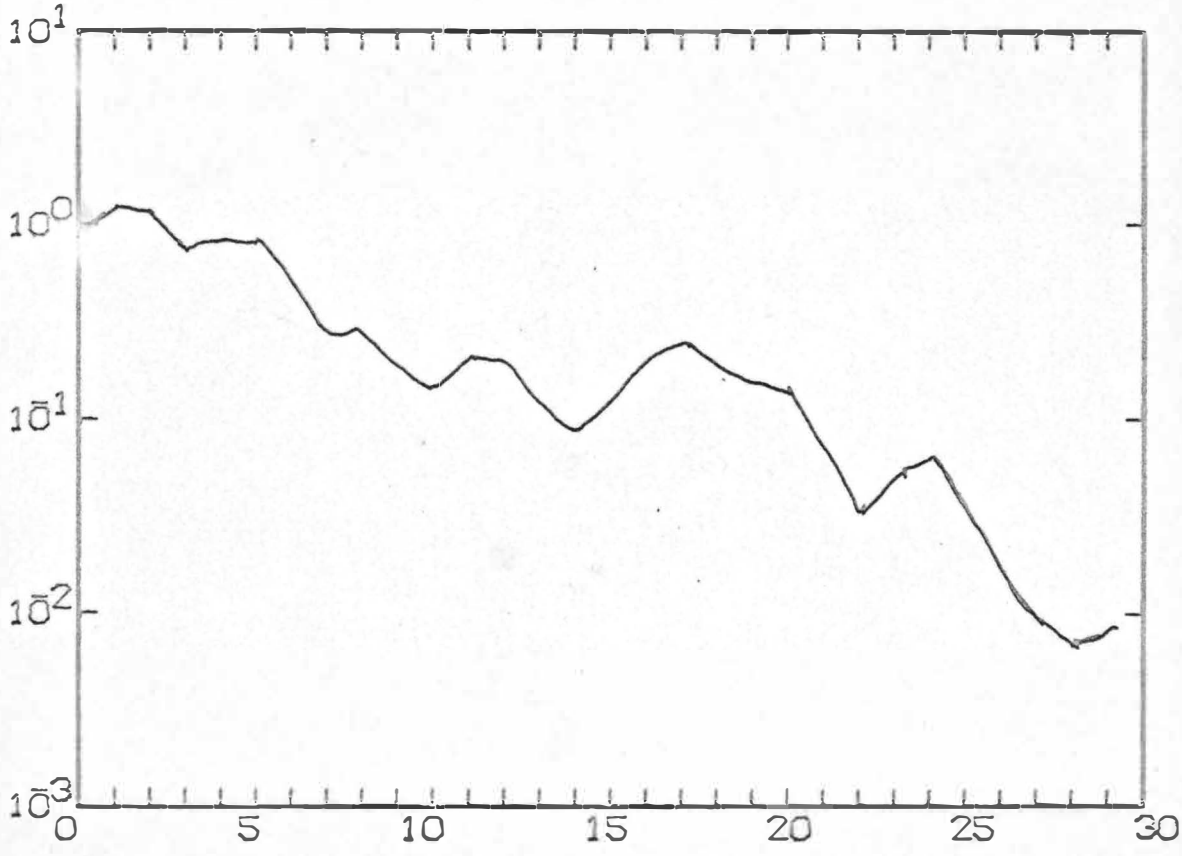
10^{1}
10^{0}
10^{-1}
10^{-2}
10^{-3}
0
5
10
15
20
25
30

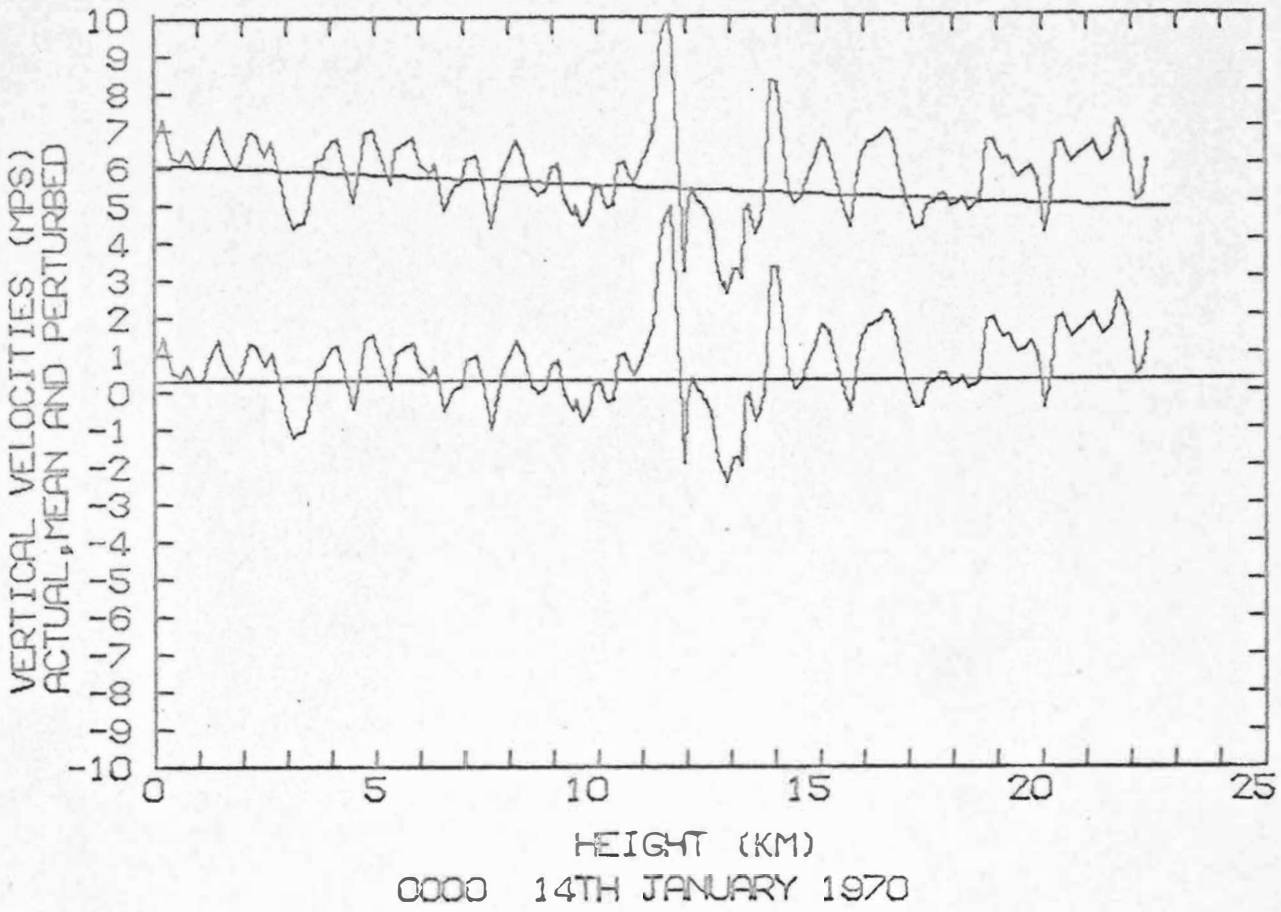
VERTICAL VELOCITIES (MPS)
ACTUAL, MEAN AND PERTURBED
10
9
8
7
6
5
4
3
2
1
0
-1
-2
-3
-4
-5
-6
-7
-8
-9
-10
0
5
10
15
20
25
HEIGHT (KM)
0000 14TH JANUARY 1970

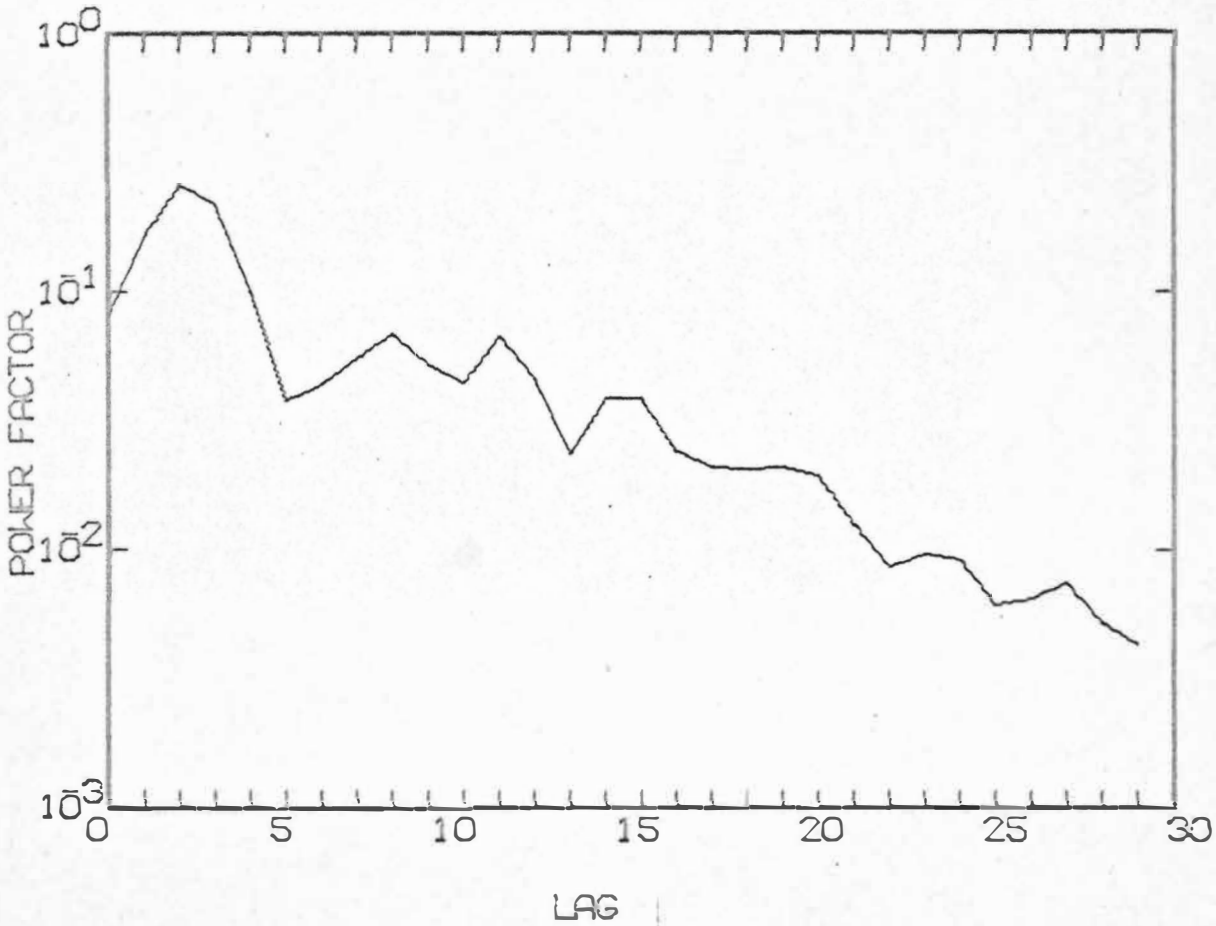
POWER FACTOR
10^0
10^1
10^2
10^3
0
5
10
15
20
25
30
LAG

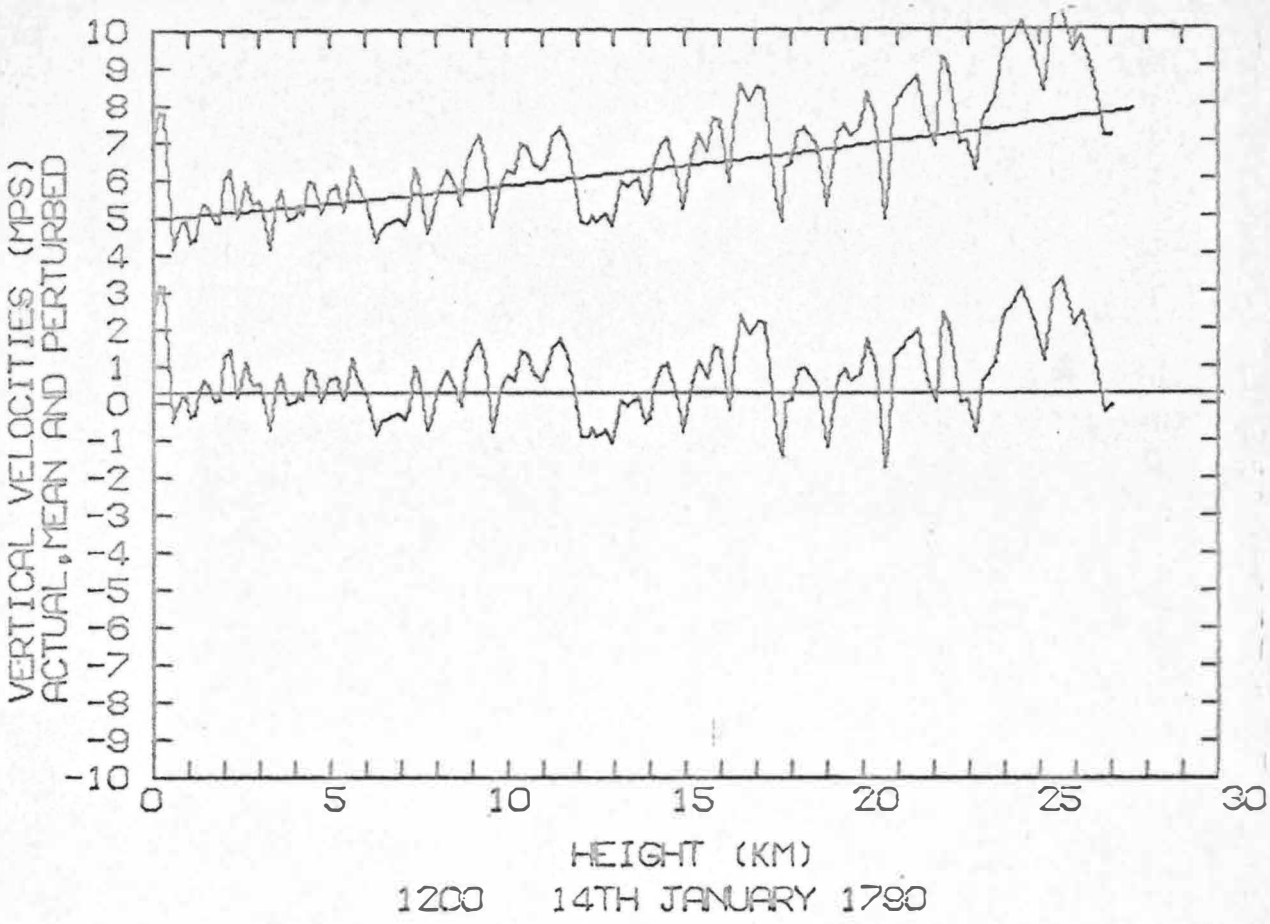
VERTICAL VELOCITIES (MPS)
ACTUAL, MEAN AND PERTURBED
10
9
8
7
6
5
4
3
2
1
0
-1
-2
-3
-4
-5
-6
-7
-8
-9
-10
0
5
10
15
20
25
30
HEIGHT (KM)
1200 14TH JANUARY 1780

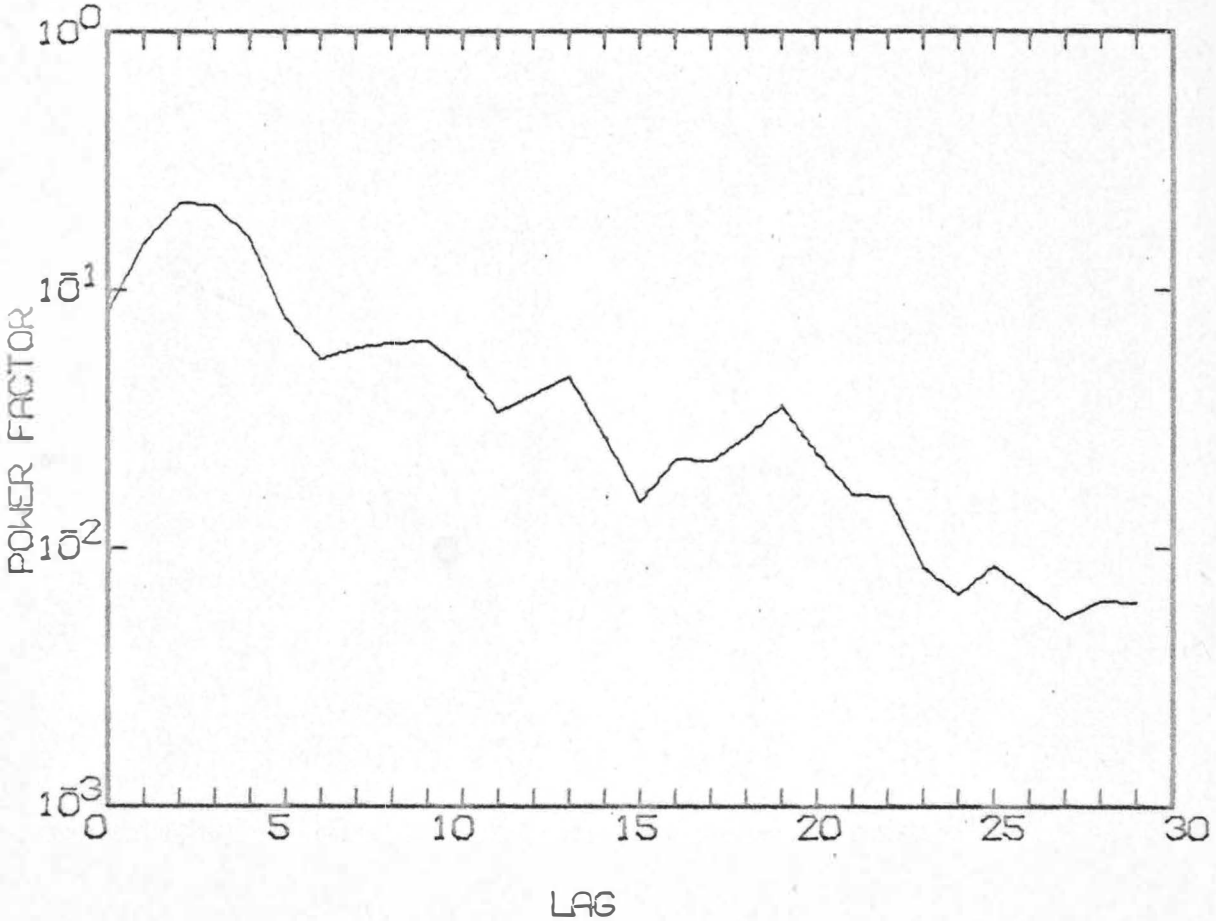
POWER FACTOR
10^0
10^{-1}
10^{-2}
10^{-3}
0
5
10
15
20
25
30
LAG

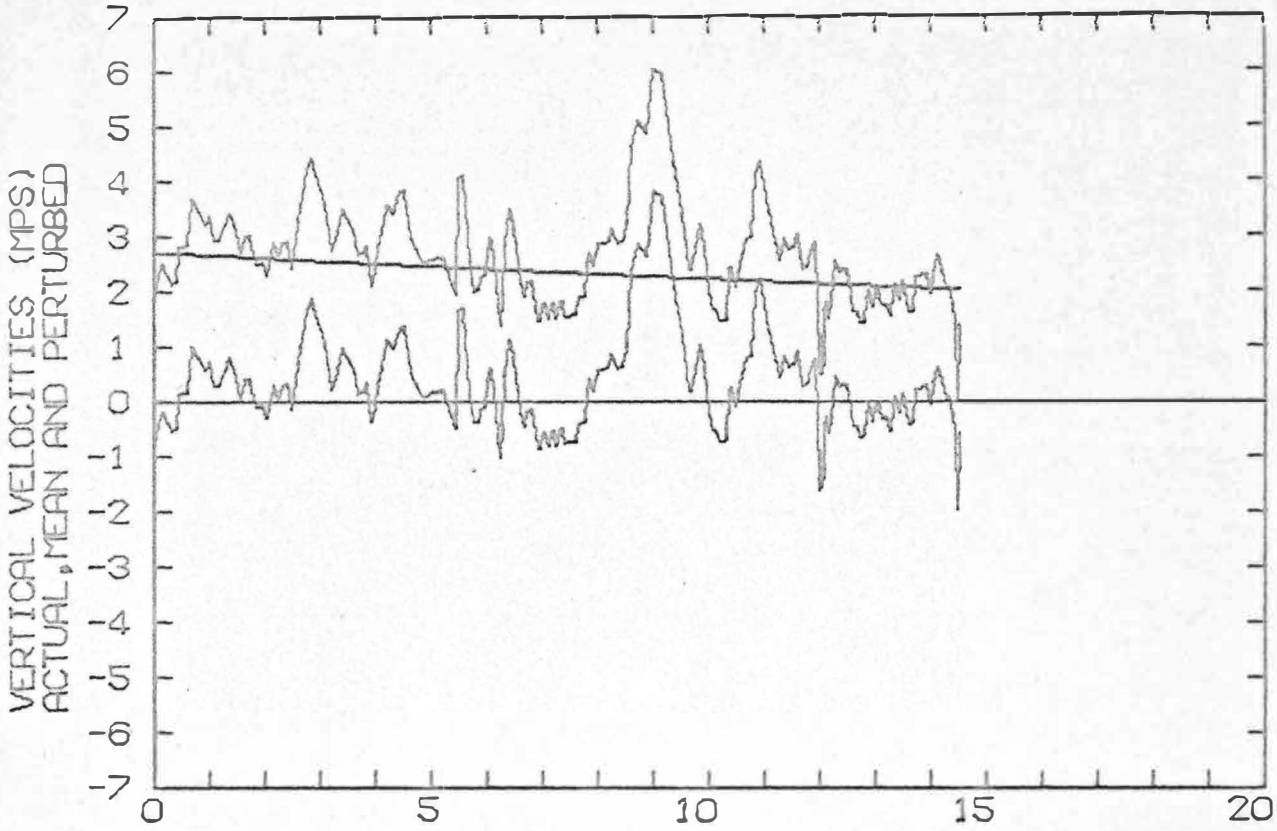
VERTICAL VELOCITIES (MPS)
ACTUAL, MEAN AND PERTURBED
7
6
5
4
3
2
1
0
-1
-2
-3
-4
-5
-6
-7
0
5
10
15
20
HEIGHT (KM)
0000 21ST JANUARY 1970

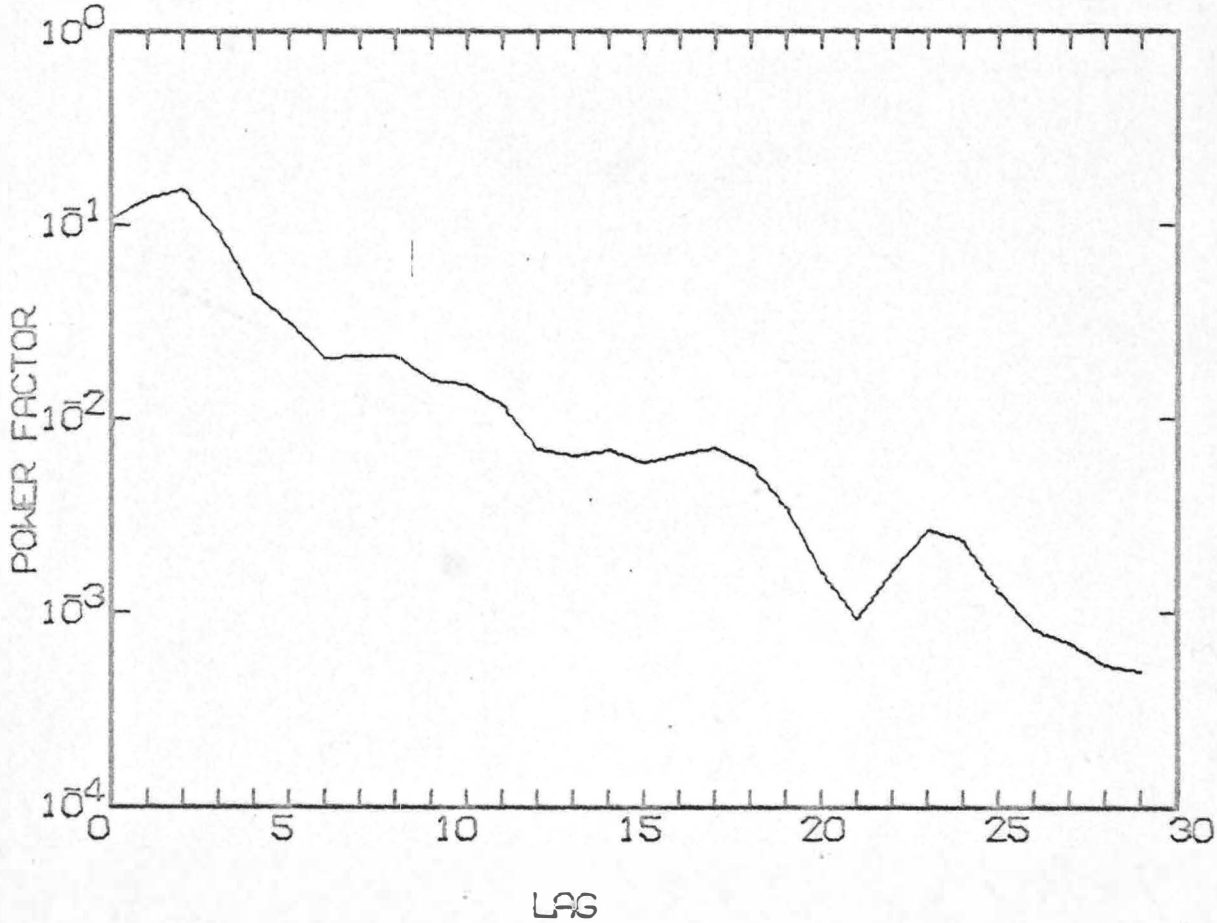
POWER FACTOR
10^0
10^1
10^2
10^3
10^4
0
5
10
15
20
25
30
LAG

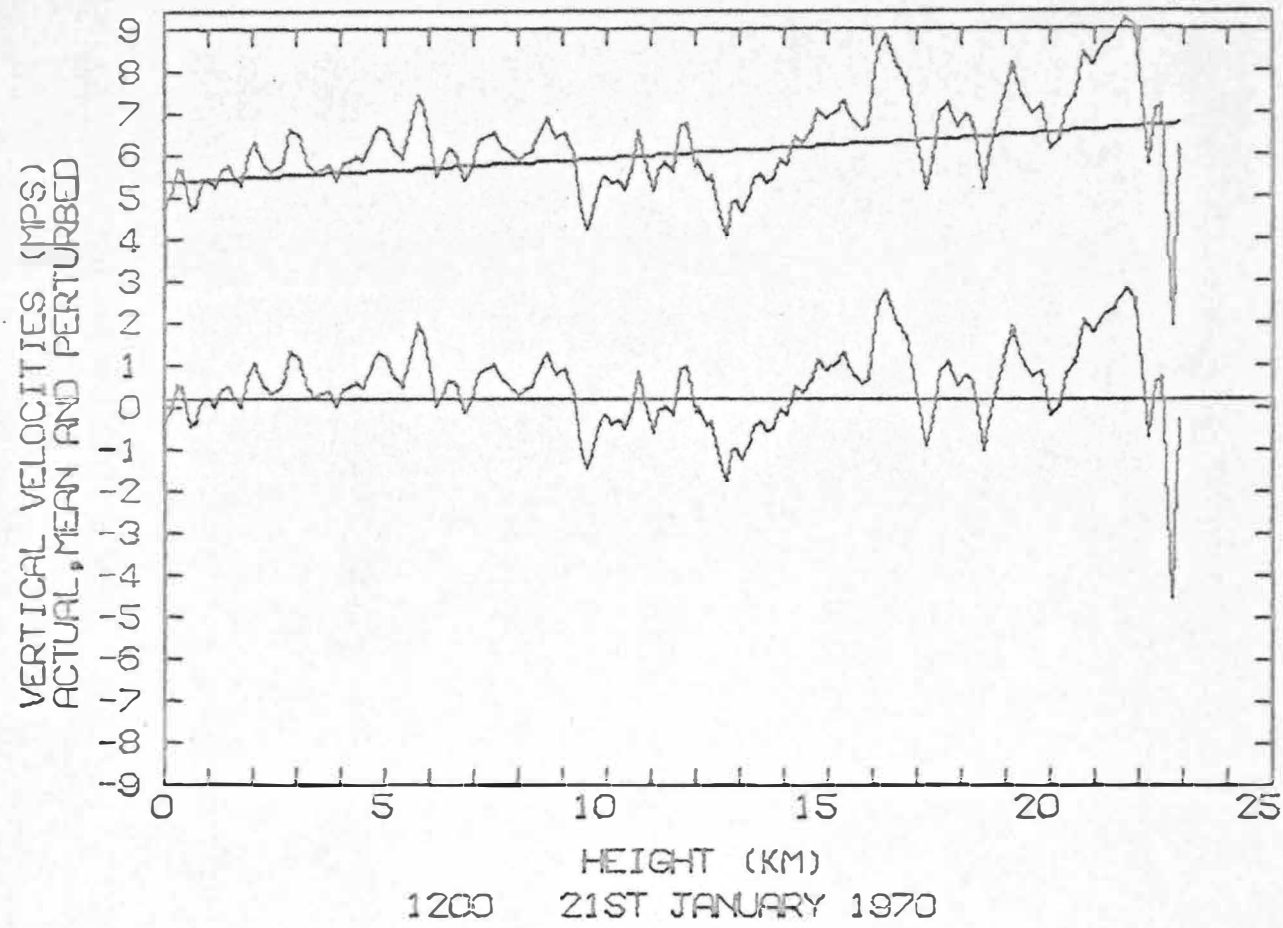
VERTICAL VELOCITIES (MPS)
ACTUAL, MEAN AND PERTURBED
-9 -8 -7 -6 -5 -4 -3 -2 -1 0 1 2 3 4 5 6 7 8 9
0 5 10 15 20 25
HEIGHT (KM)
1200 21ST JANUARY 1970

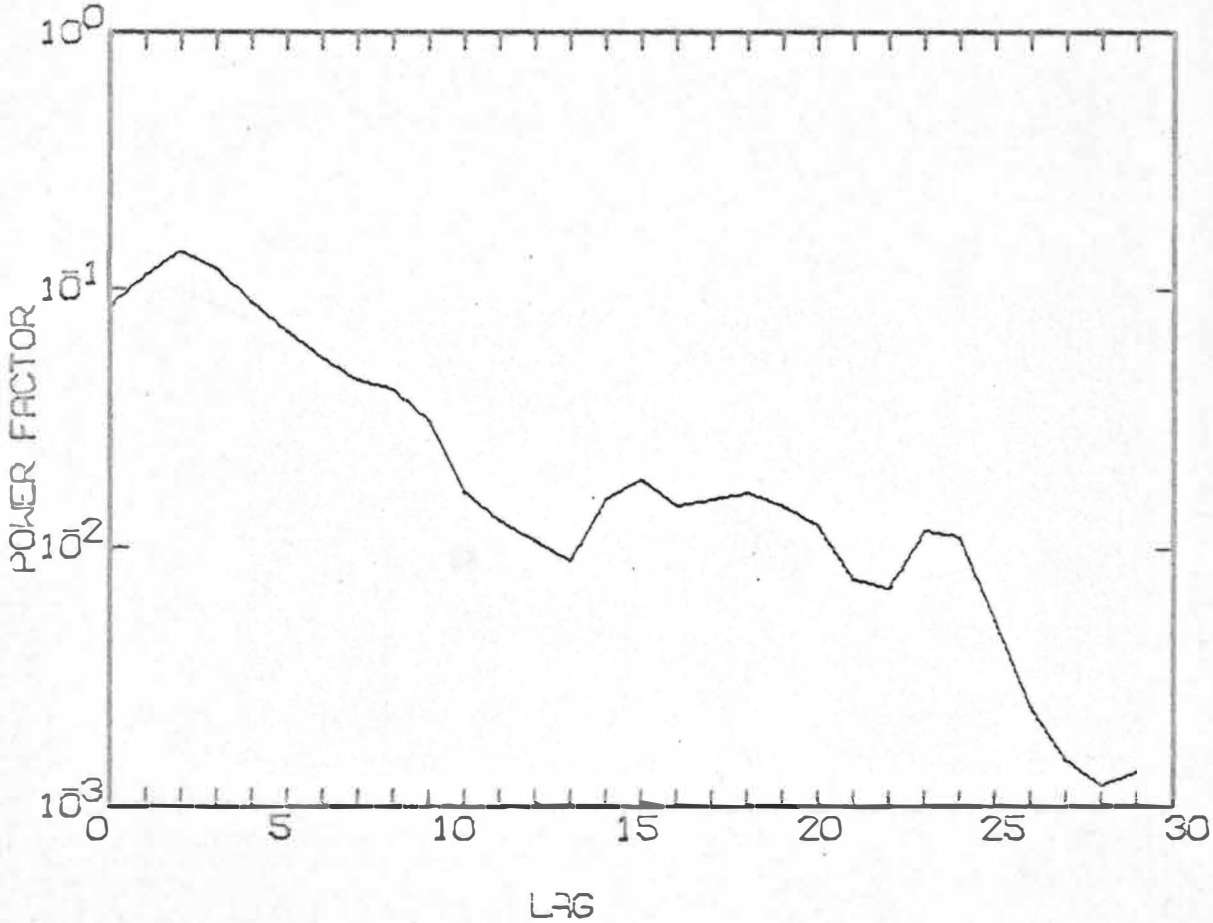
10^0
10^1
10^2
10^3
POWER FACTOR
0 5 10 15 20 25 30
LAG

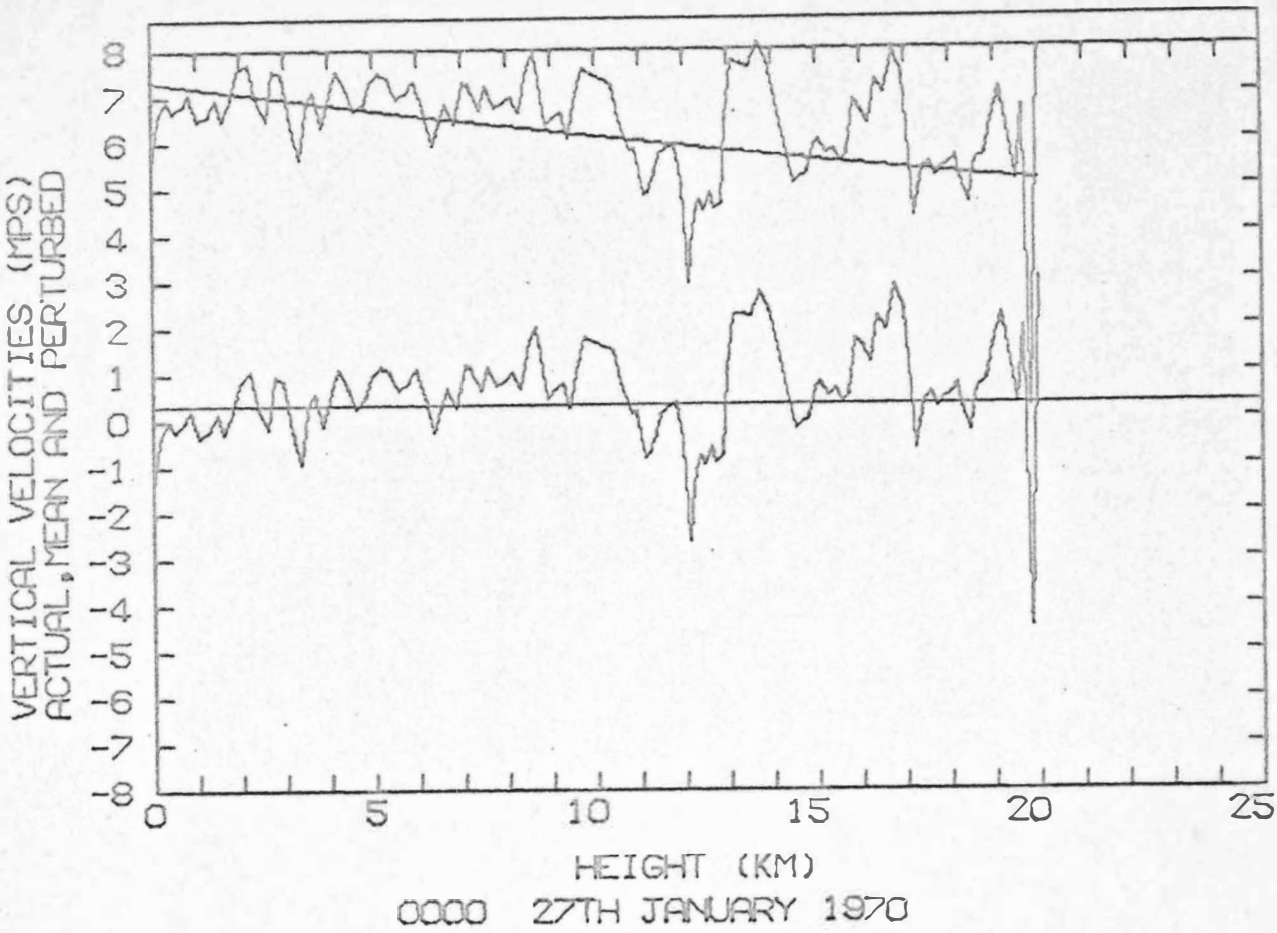
VERTICAL VELOCITIES (MPS)
ACTUAL, MEAN AND PERTURBED
8
7
6
5
4
3
2
1
0
-1
-2
-3
-4
-5
-6
-7
-8
0
5
10
15
20
25
HEIGHT (KM)
0000 27TH JANUARY 1970

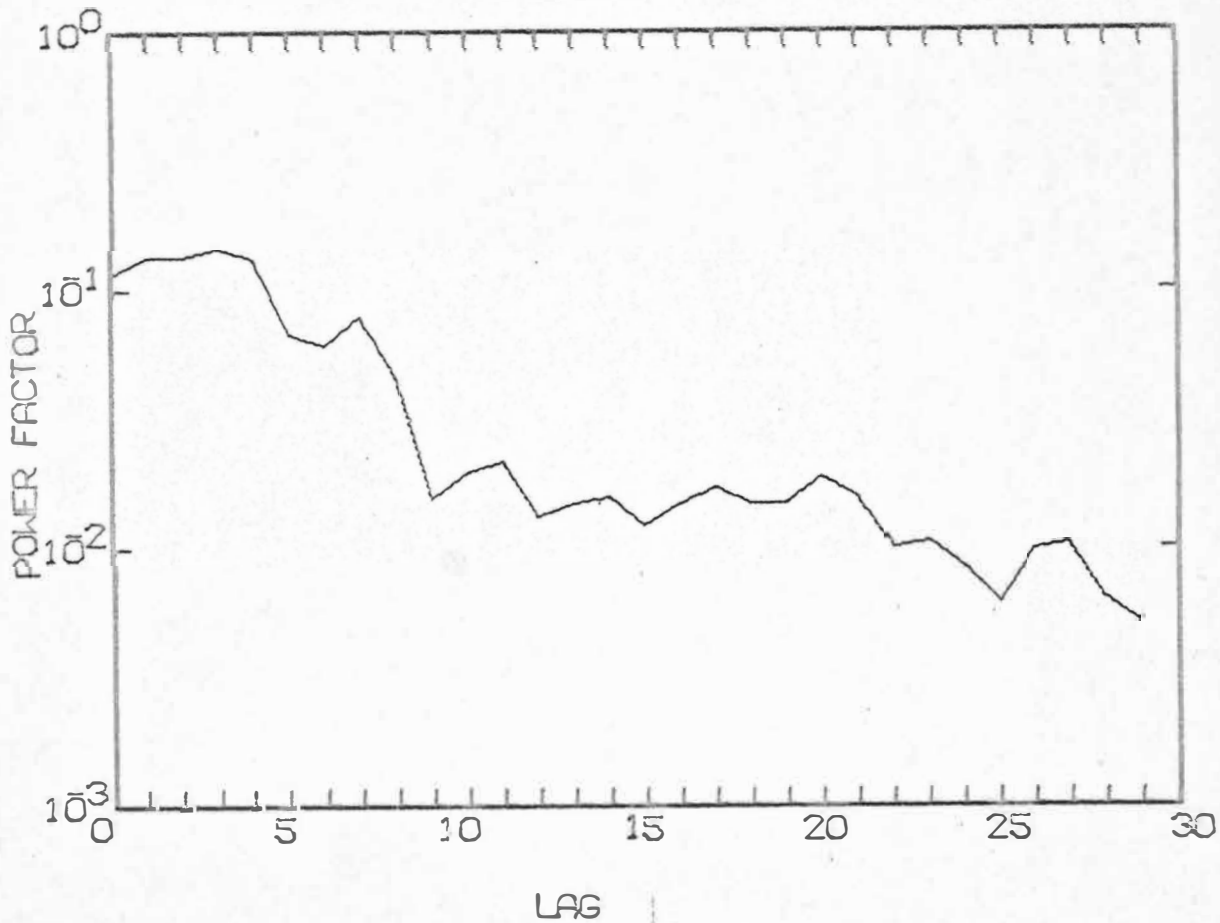
10^0
10^{-1}
10^{-2}
10^{-3}
POWER FACTOR
0
5
10
15
20
25
30
LAG

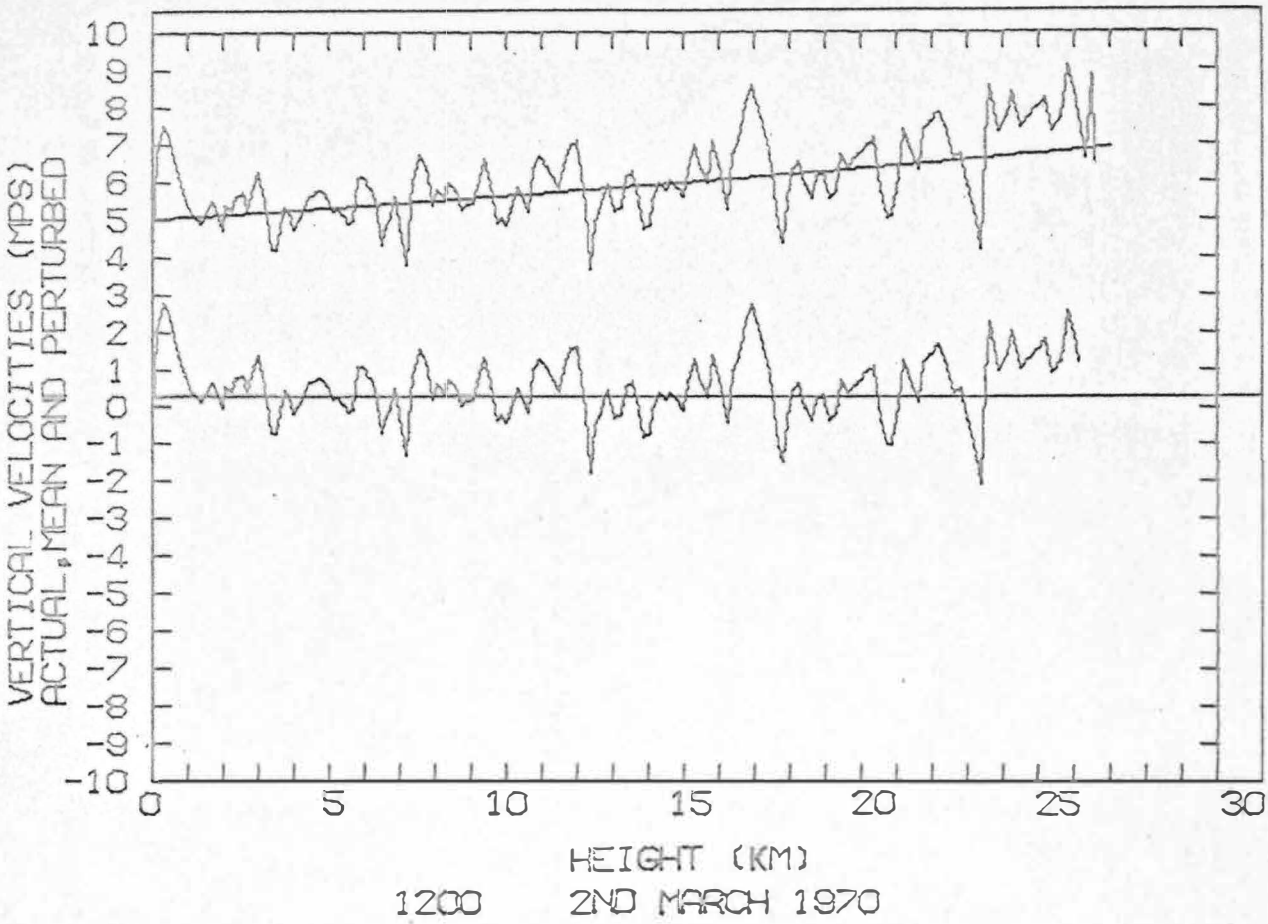
VERTICAL VELOCITIES (MPS)
ACTUAL, MEAN AND PERTURBED
10
9
8
7
6
5
4
3
2
1
0
-1
-2
-3
-4
-5
-6
-7
-8
-9
-10
0
5
10
15
20
25
30
HEIGHT (KM)
1200 2ND MARCH 1970

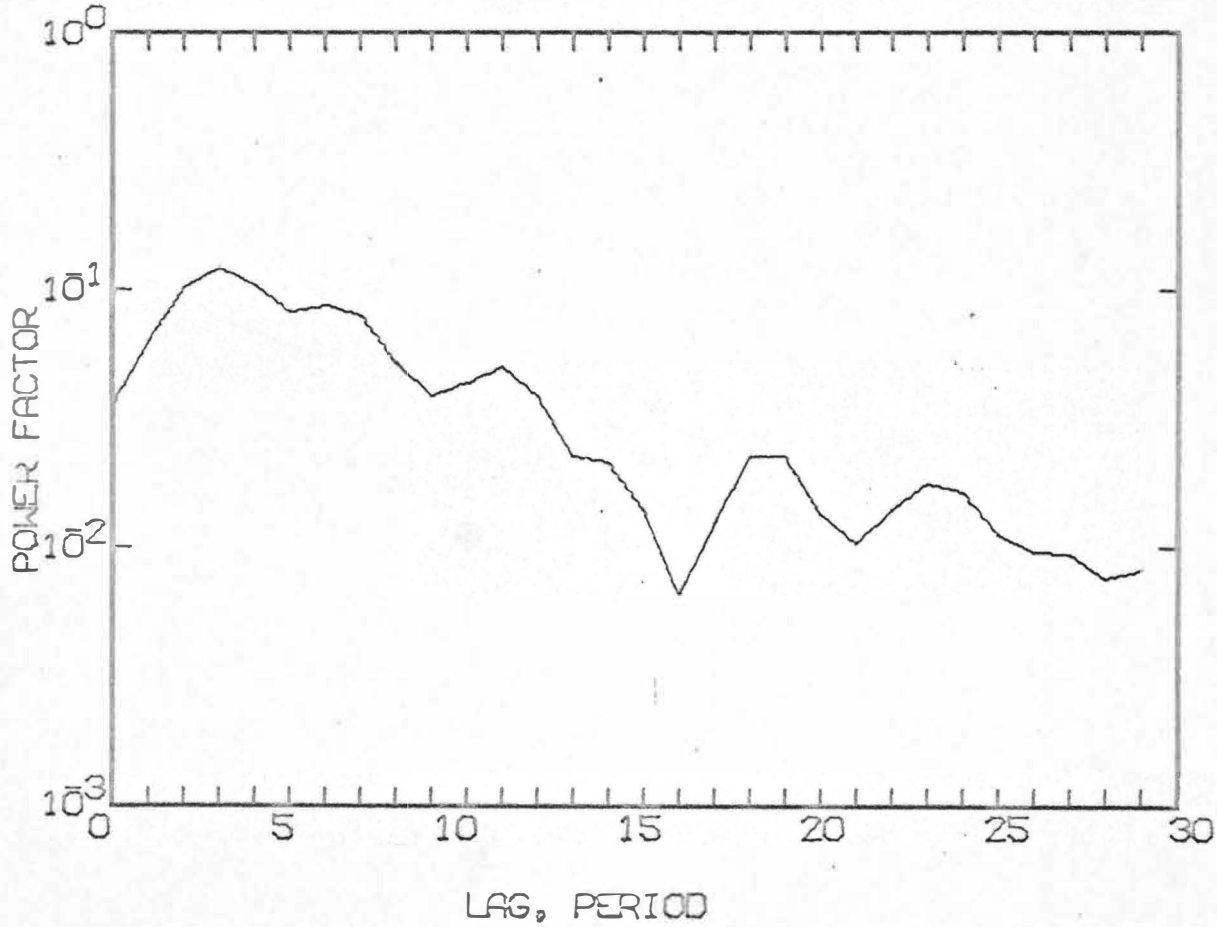
10^0
10^1
10^2
10^3
POWER FACTOR
0
5
10
15
20
25
30
LAG, PERIOD

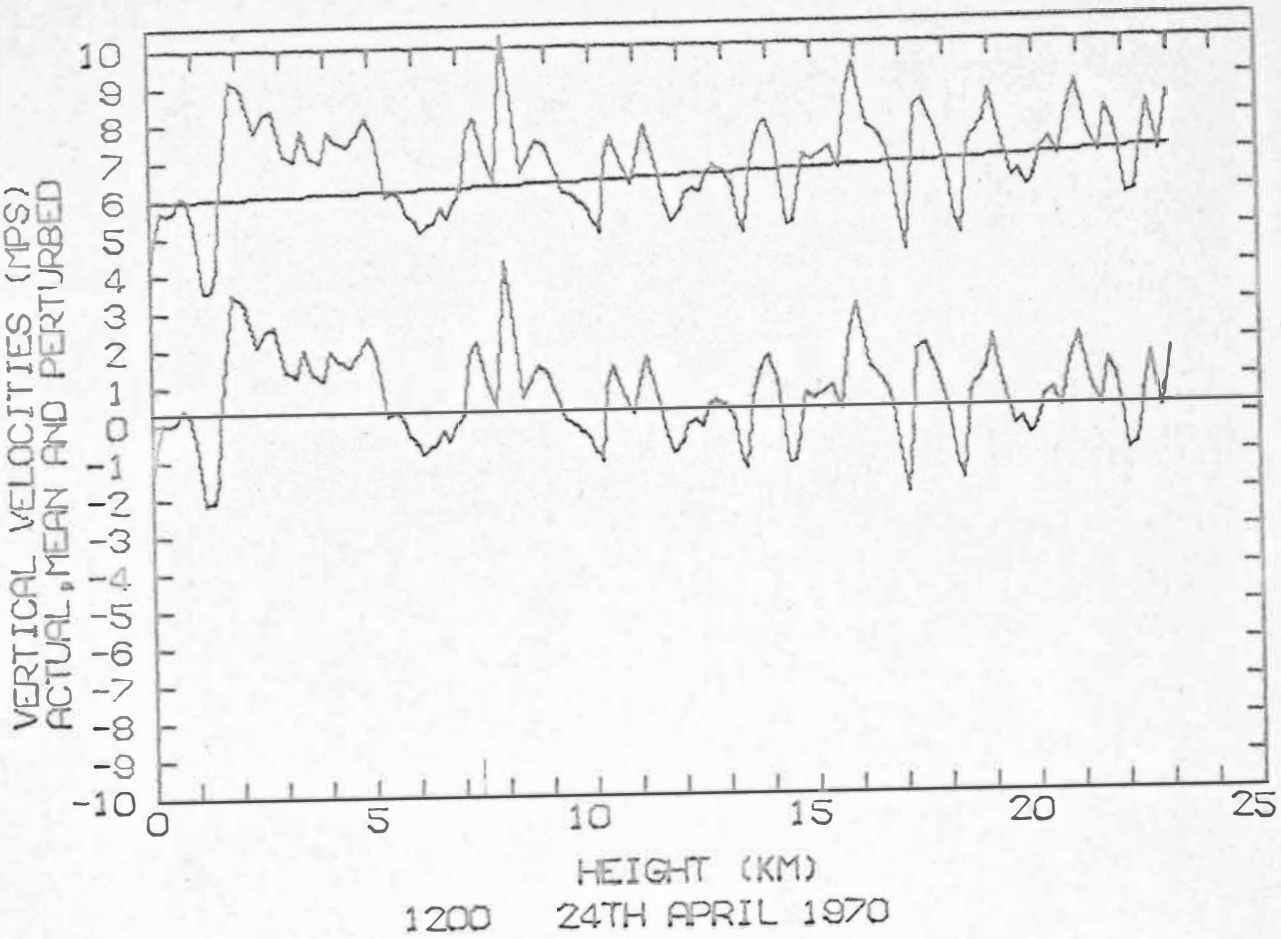
VERTICAL VELOCITIES (MPS)
ACTUAL, MEAN AND PERTURBED
10
8
6
4
2
0
-2
-4
-6
-8
-10
0
5
10
15
20
25
HEIGHT (KM)
1200 24TH APRIL 1970

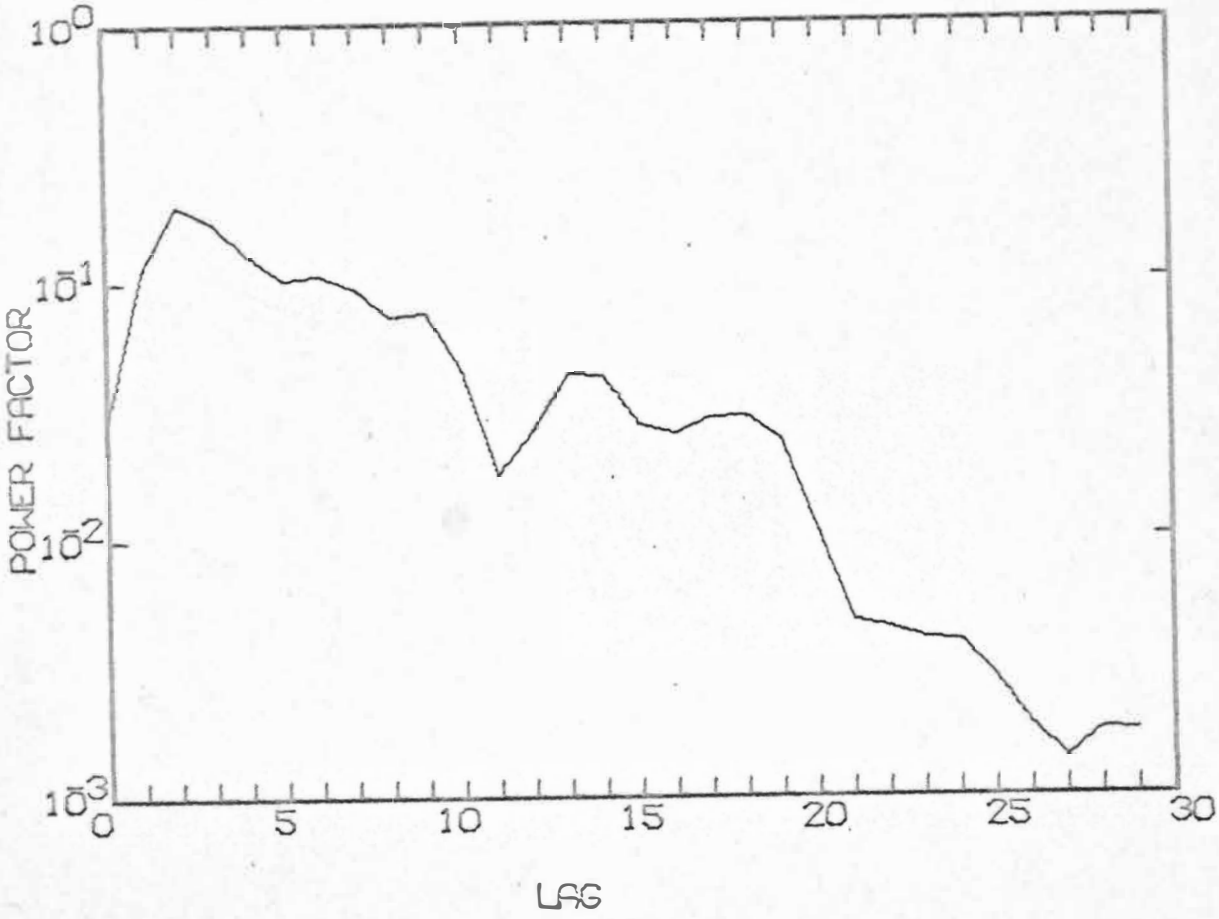
10^0
10^1
10^2
10^3
POWER FACTOR
0
5
10
15
20
25
30
LAG

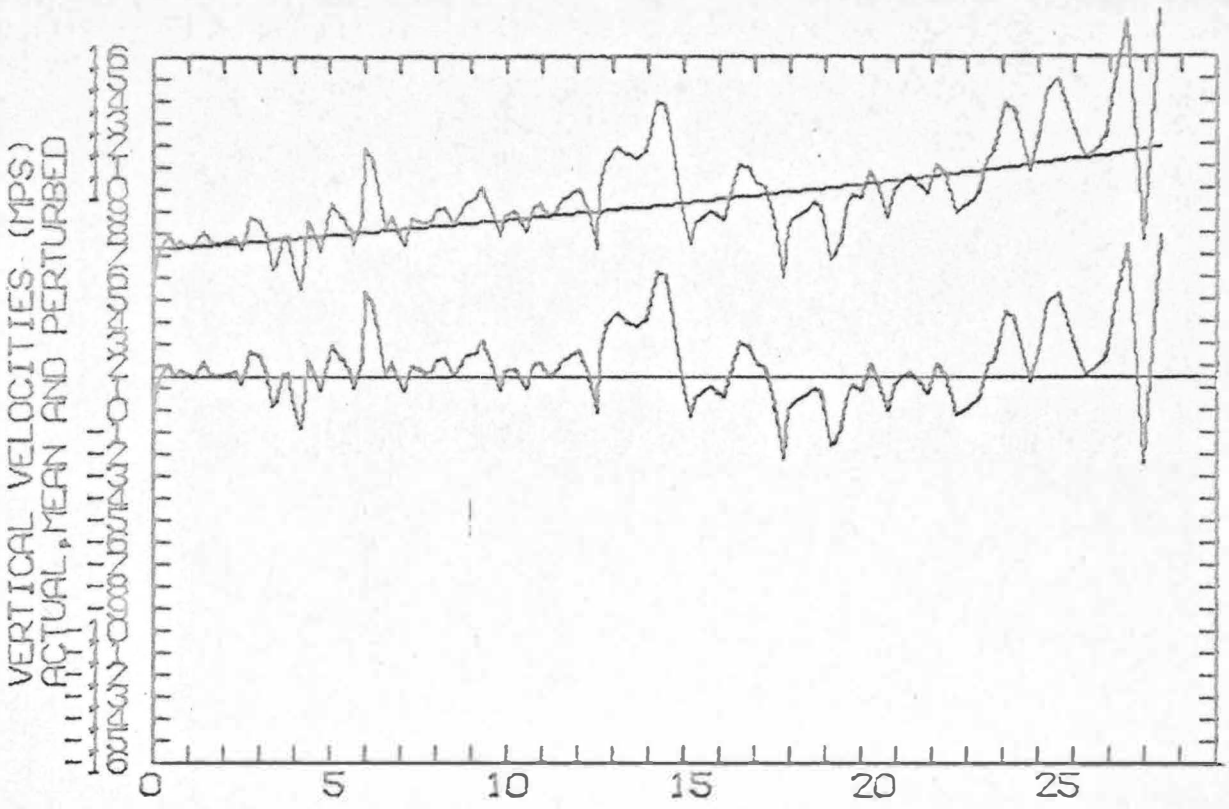

1200 25TH APRIL 1970

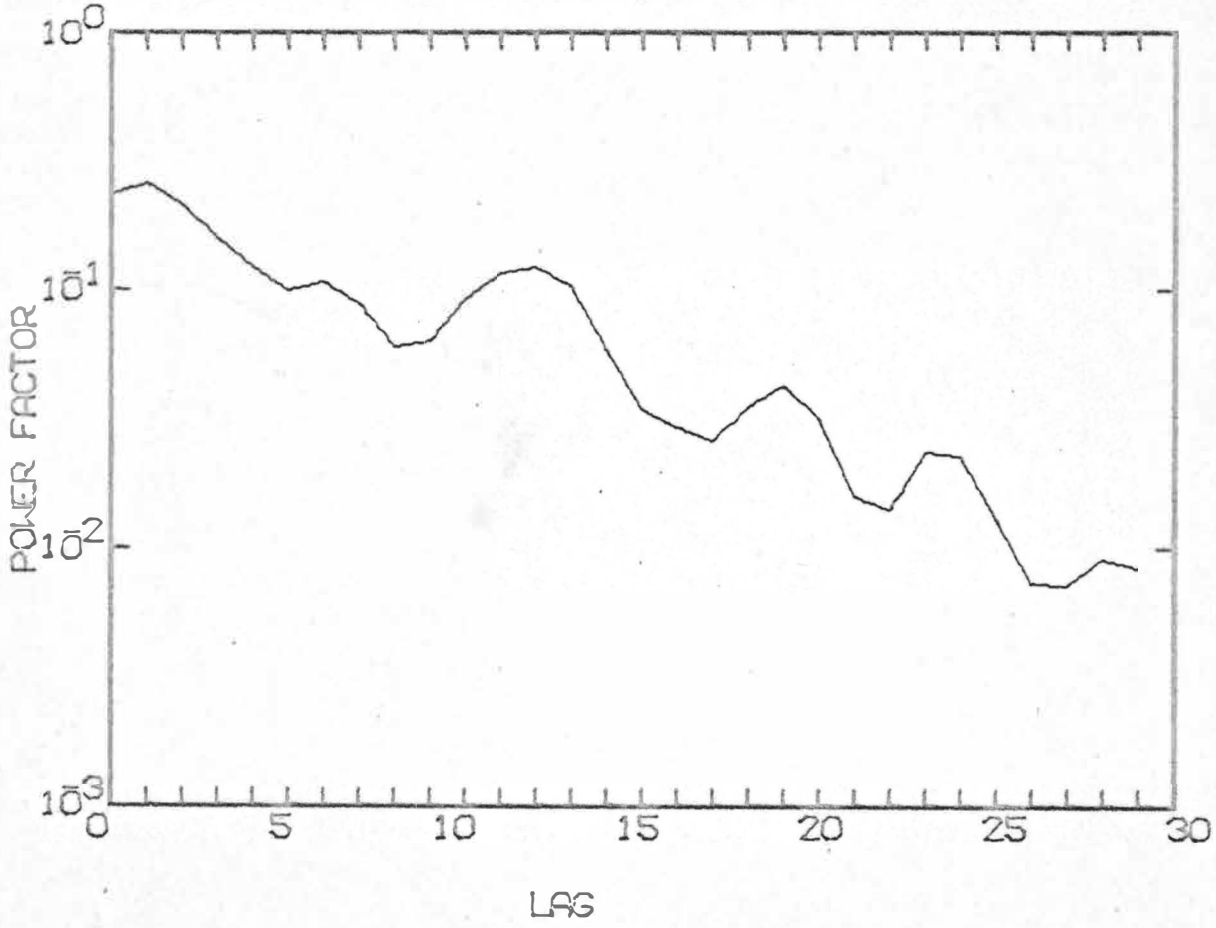

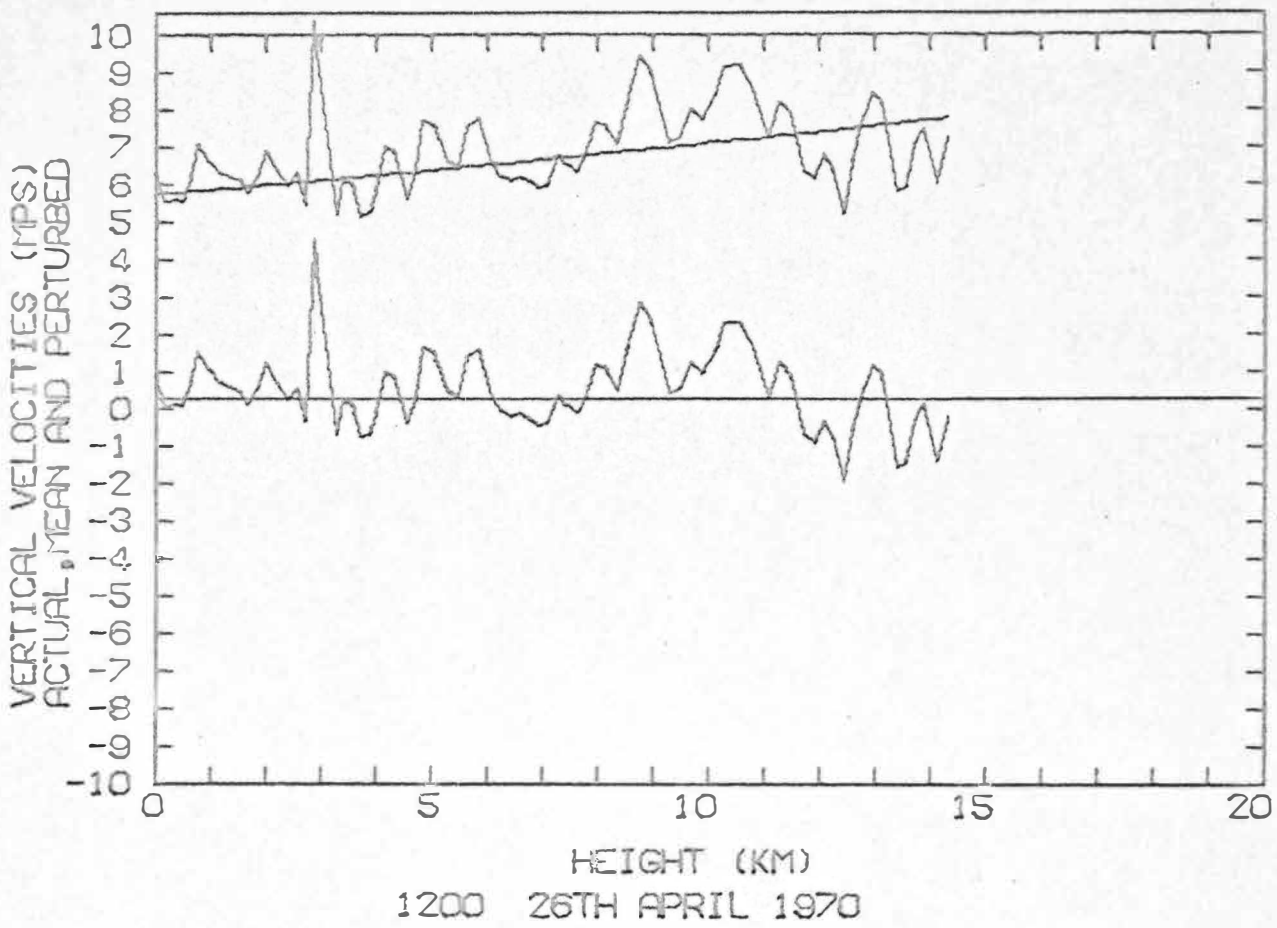
VERTICAL VELOCITIES (MPS)
ACTUAL, MEAN AND PERTURBED
10
9
8
7
6
5
4
3
2
1
0
-1
-2
-3
-4
-5
-6
-7
-8
-9
-10
0
5
10
15
20
HEIGHT (KM)
1200 26TH APRIL 1970

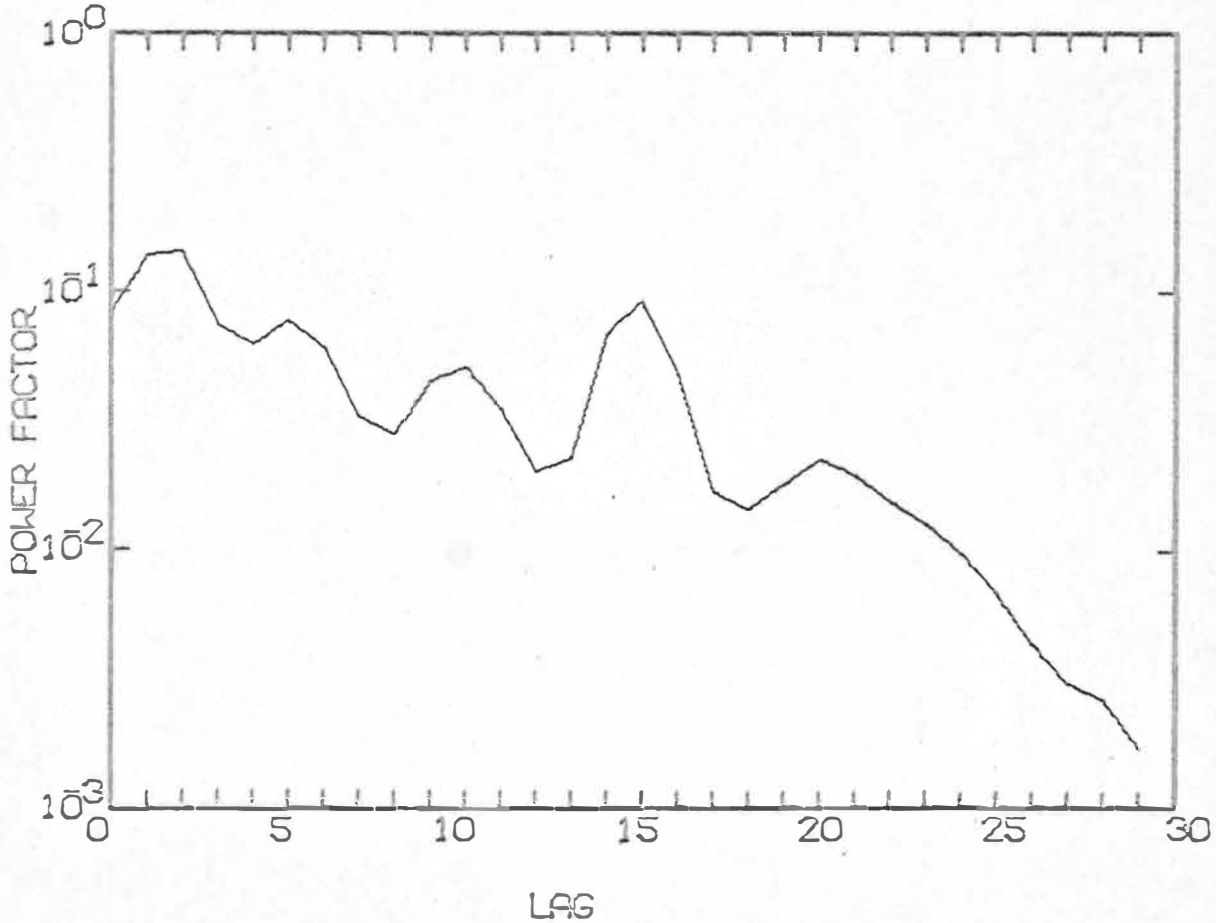
POWER FACTOR
10^0
10^1
10^2
10^3
0
5
10
15
20
25
30
LAG

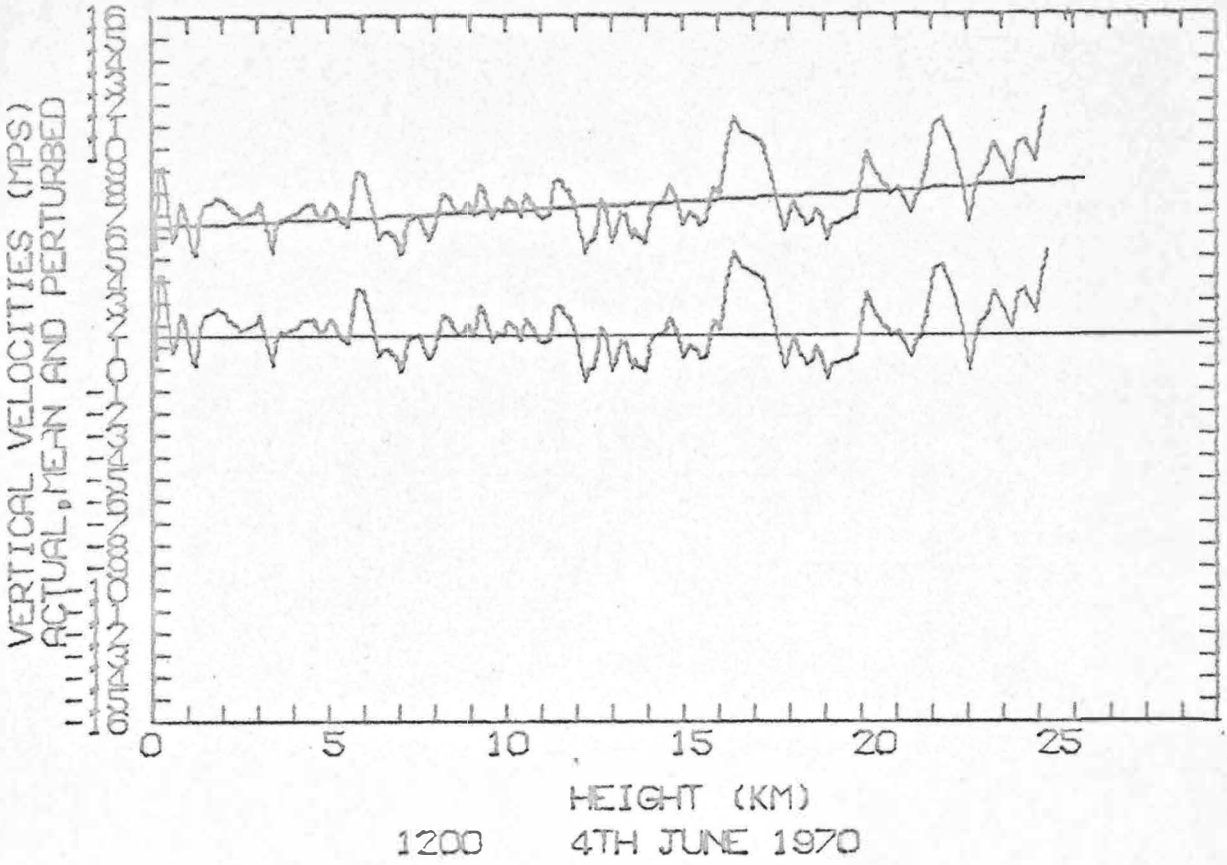
VERTICAL VELOCITIES (MPS)
ACTUAL, MEAN AND PERTURBED
0
5
10
15
20
25
HEIGHT (KM)
1200 4TH JUNE 1970

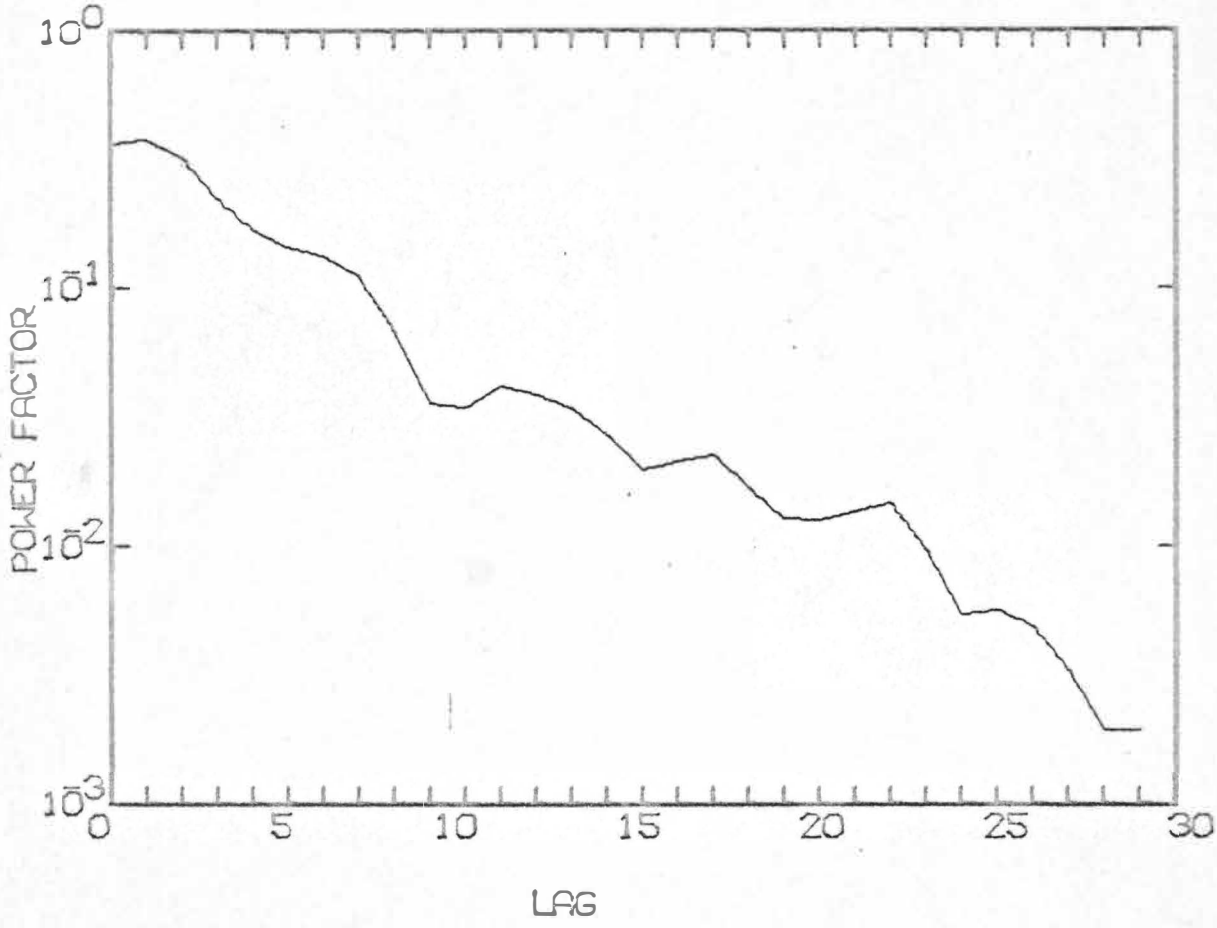
10^0
10^1
10^2
10^3
POWER FACTOR
0
5
10
15
20
25
30
LAG

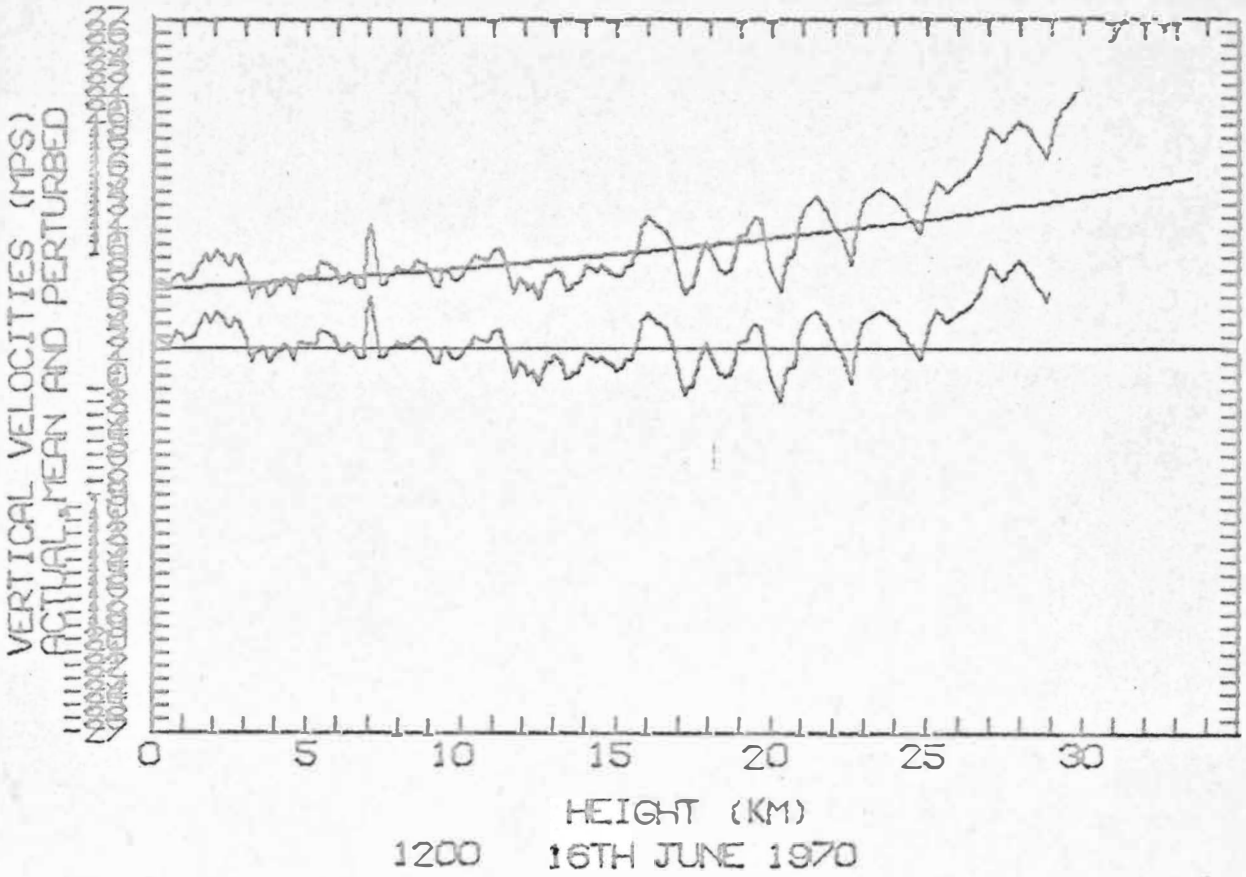

1200 16TH JUNE 1970

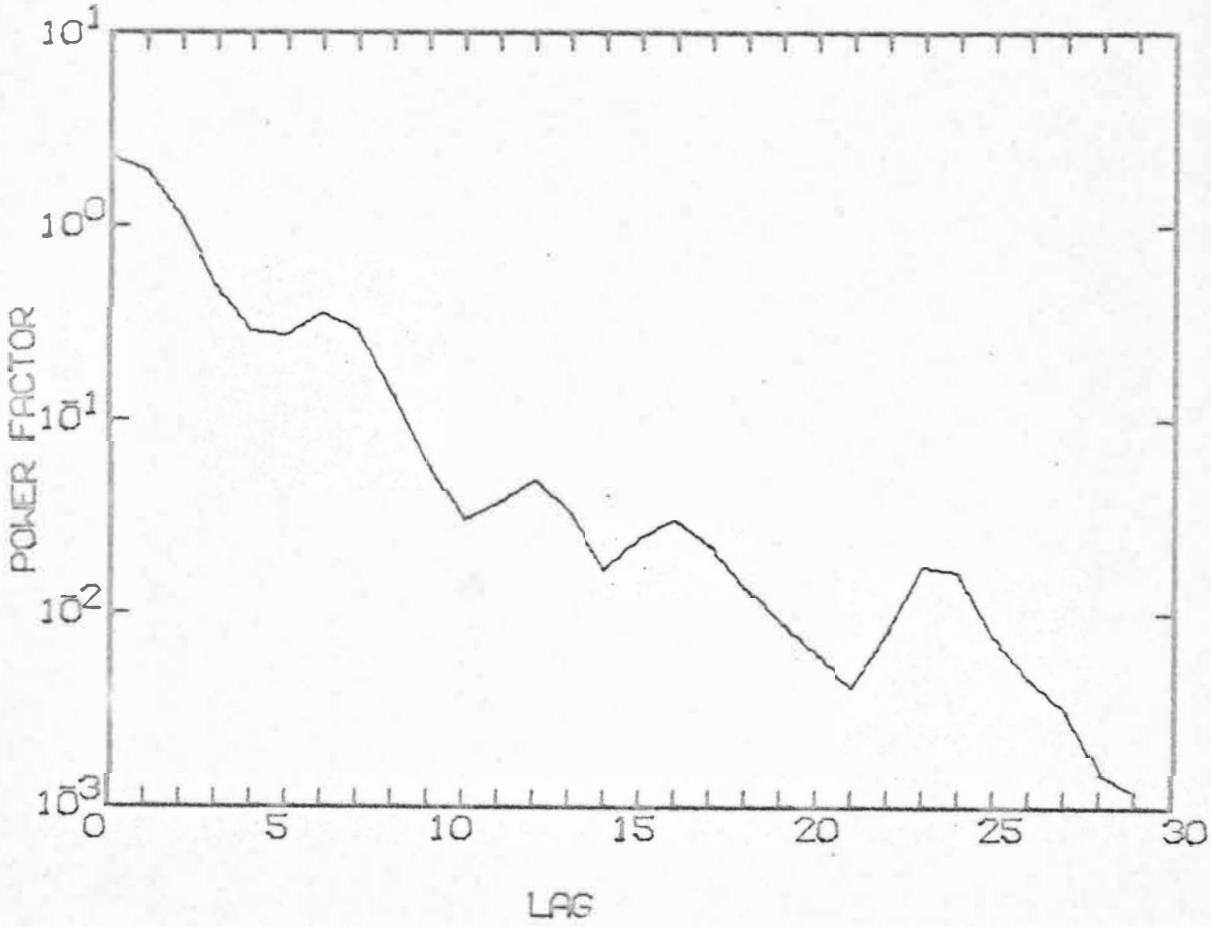

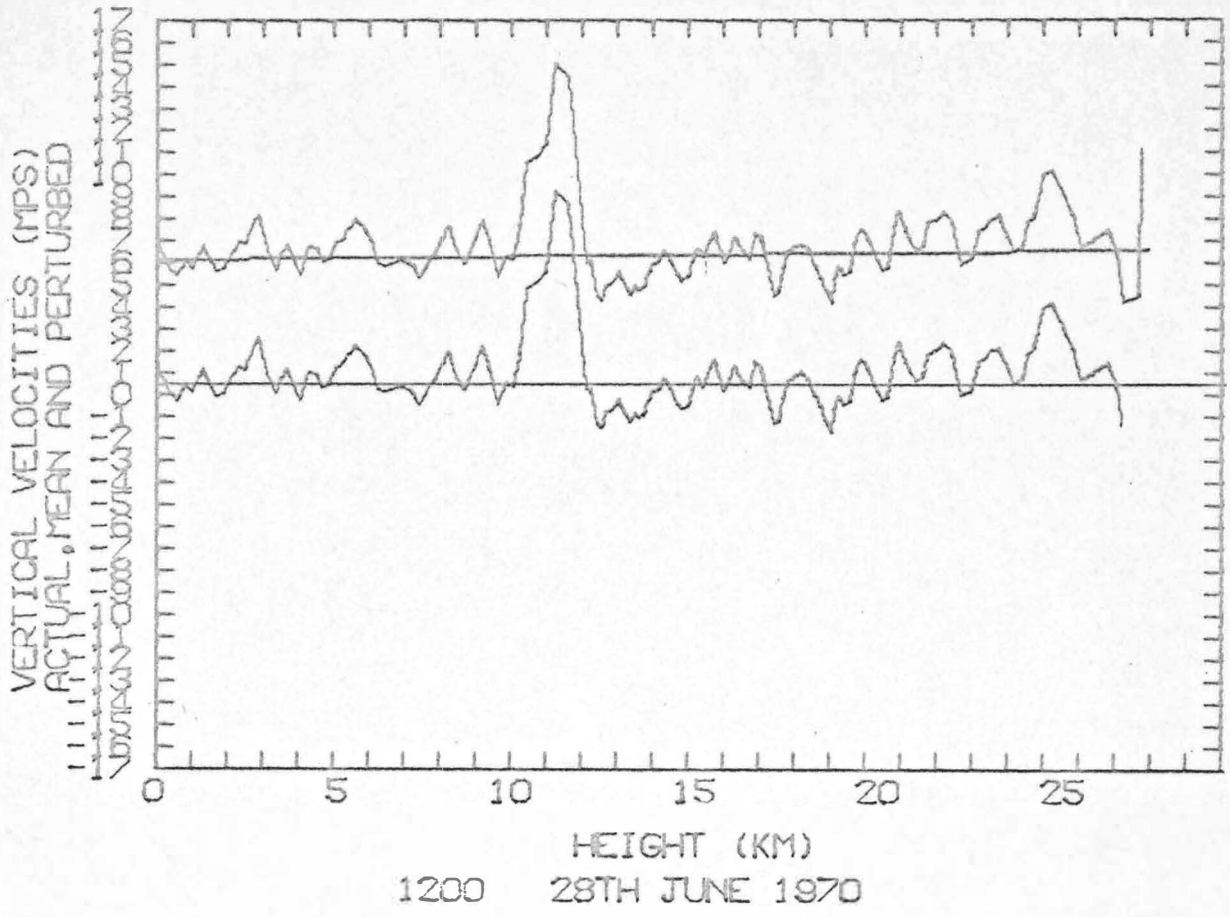

1200 28TH JUNE 1970

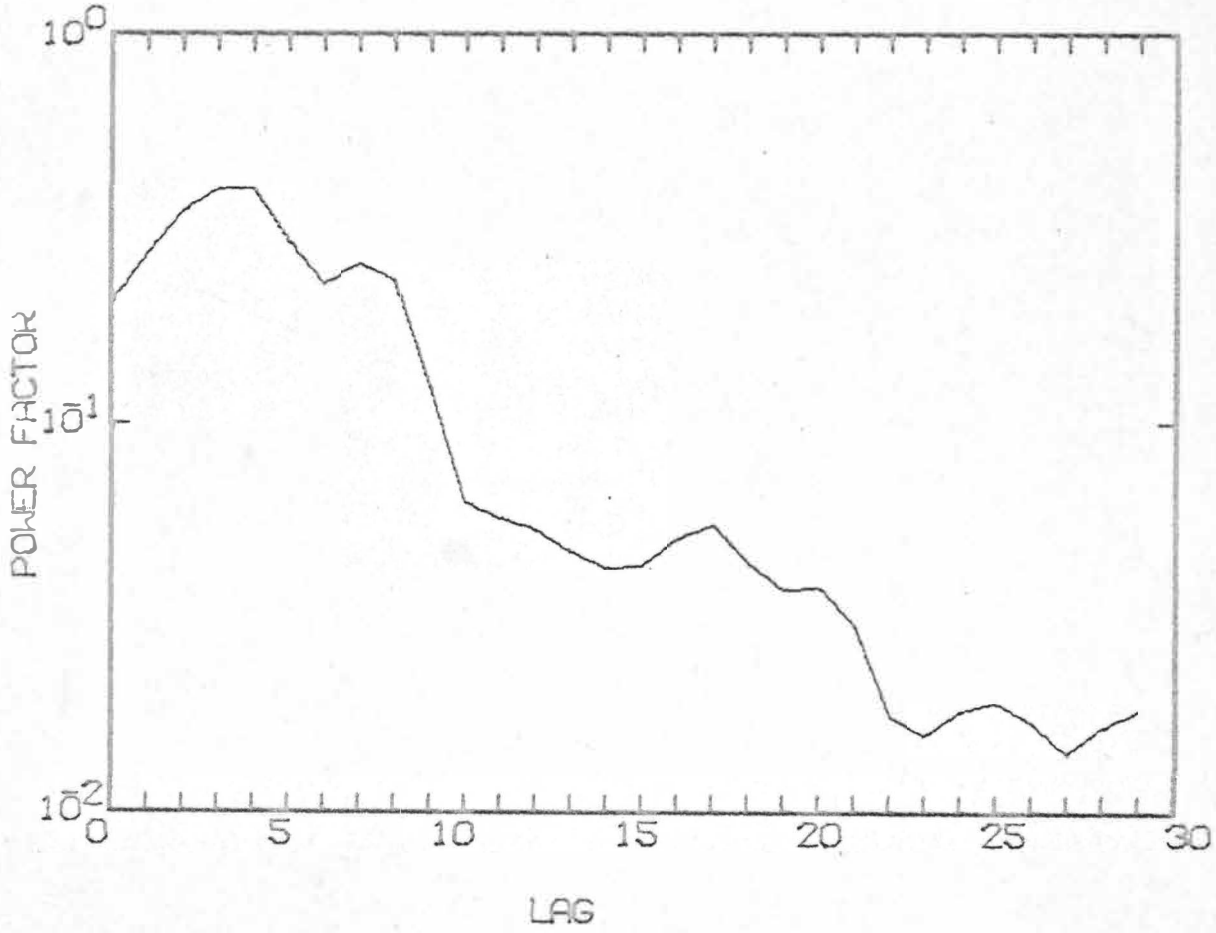

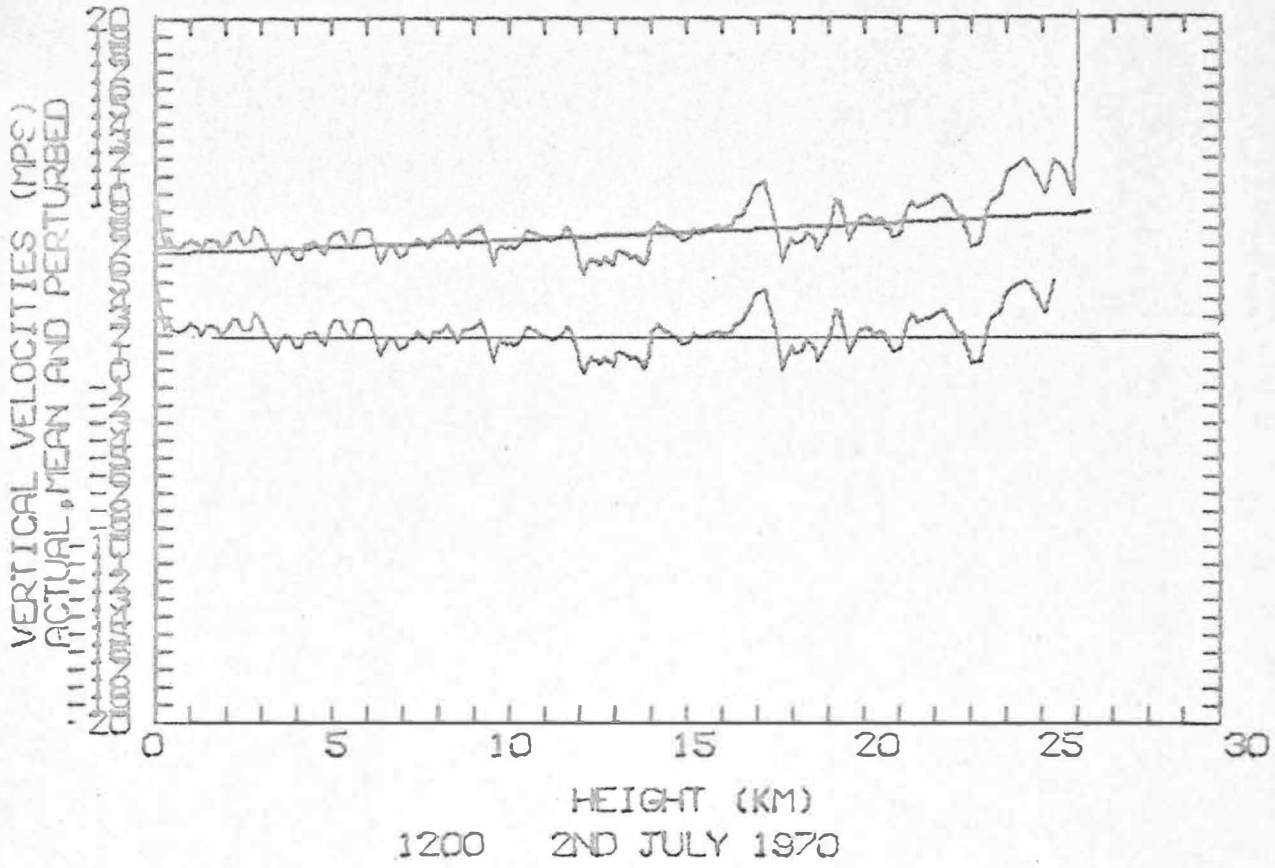
VERTICAL VELOCITIES (MPS)
ACTUAL, MEAN AND PERTURBED
0
5
10
15
20
25
30
HEIGHT (KM)
1200 2ND JULY 1970

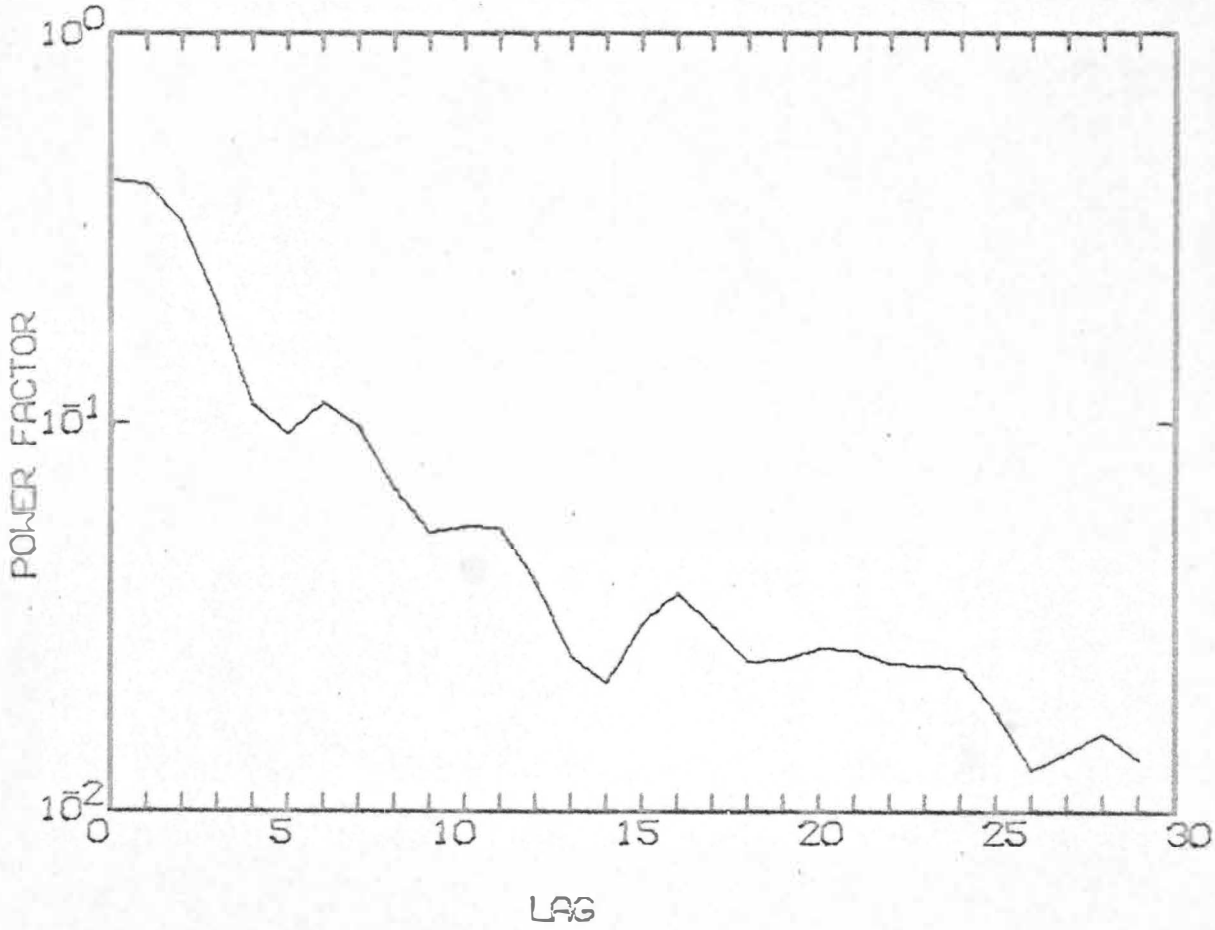
POWER FACTOR
10^0
10^1
10^2
0
5
10
15
20
25
30
LAG

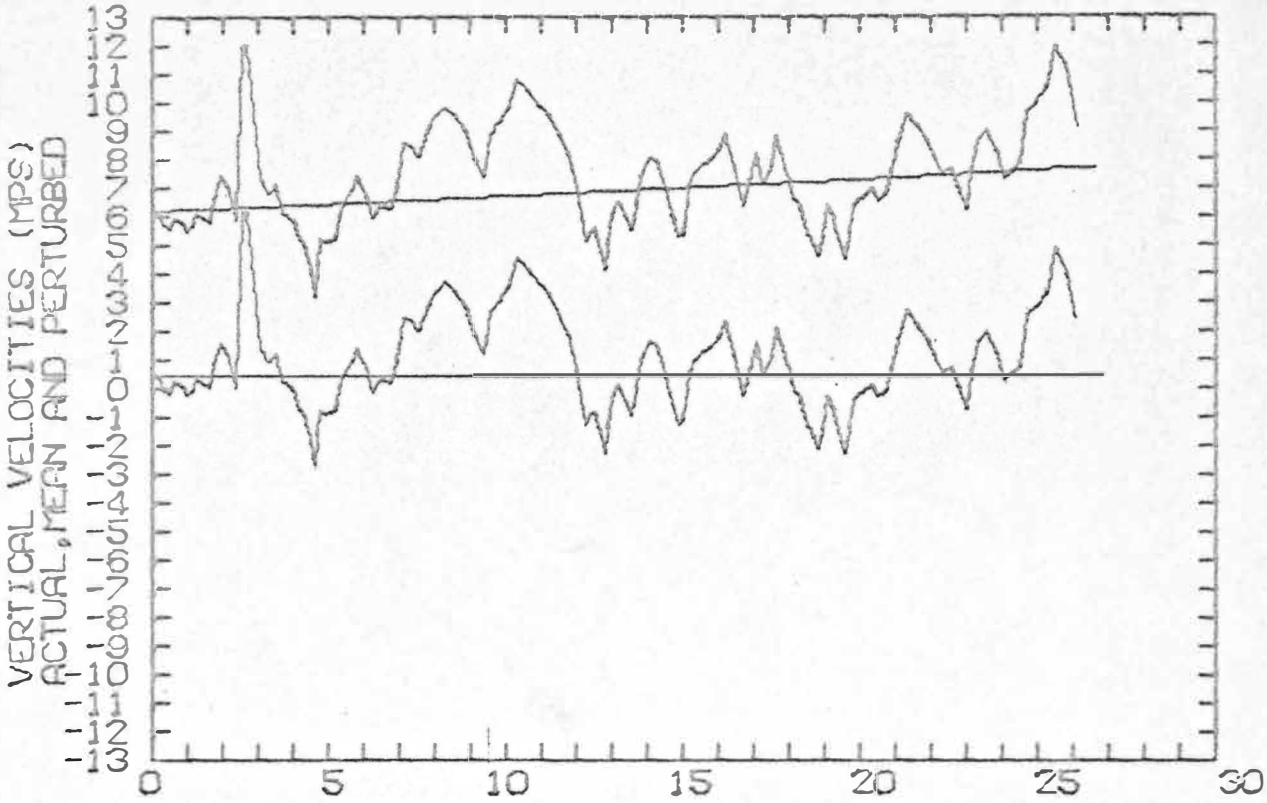
VERTICAL VELOCITIES (MPS)
ACTUAL, MEAN AND PERTURBED
-13
-12
-11
-10
-9
-8
-7
-6
-5
-4
-3
-2
-1
0
1
2
3
0
5
10
15
20
25
30
HEIGHT (KM)
1200 23RD JULY 1970

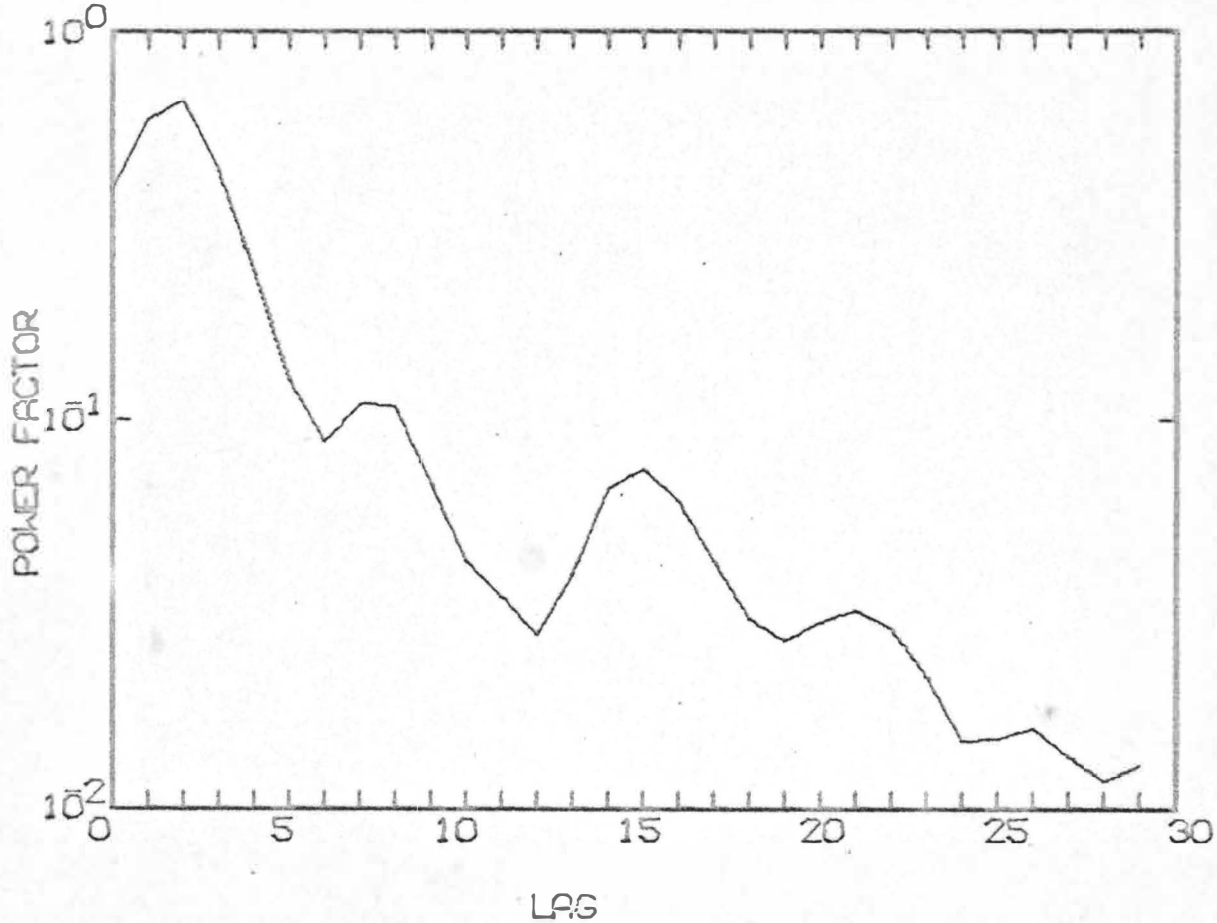
10^0
10^1
10^2
POWER FACTOR
0
5
10
15
20
25
30
LAG

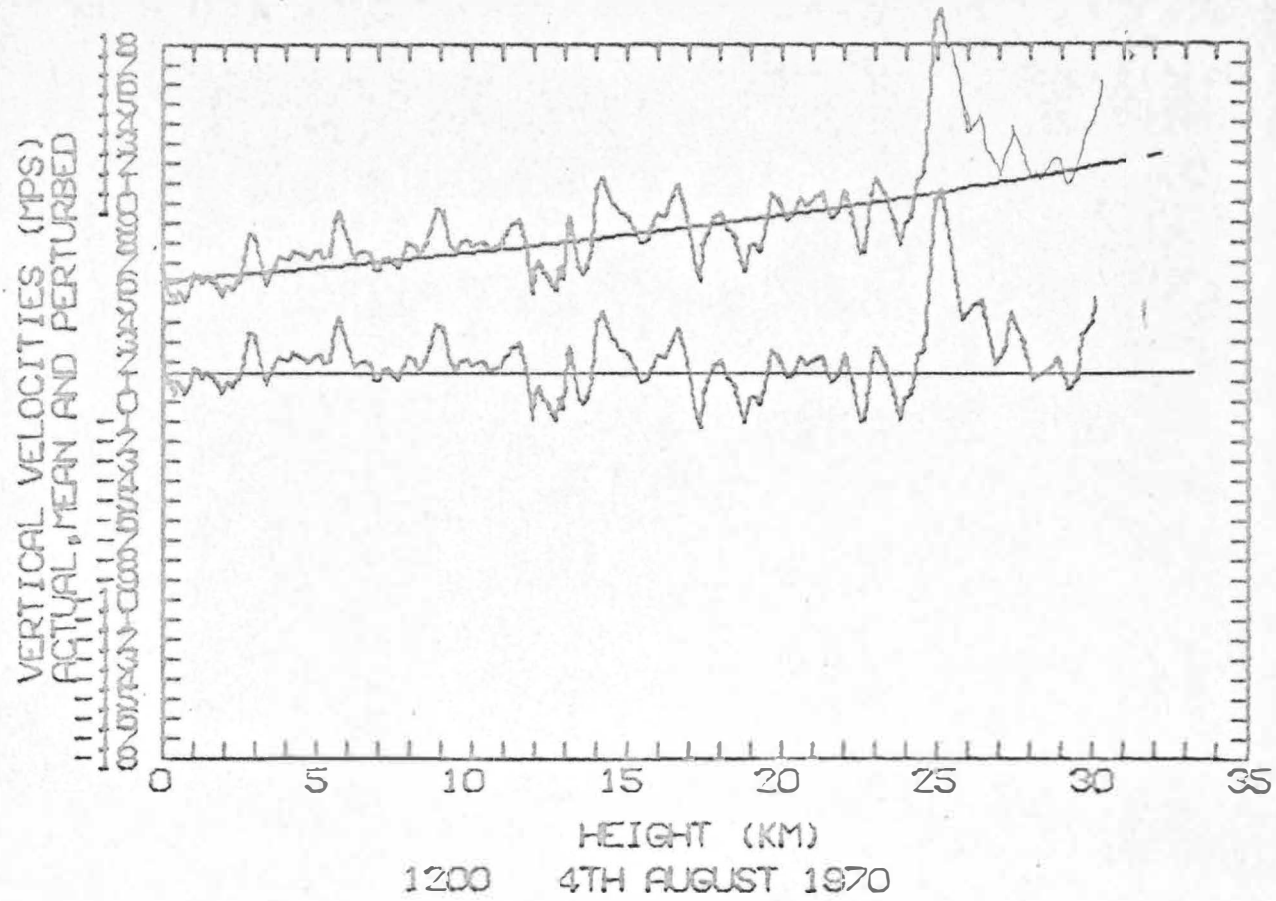
VERTICAL VELOCITIES (MPS)
ACTUAL, MEAN AND PERTURBED
0
5
10
15
20
25
30
35
HEIGHT (KM)
1200 4TH AUGUST 1970

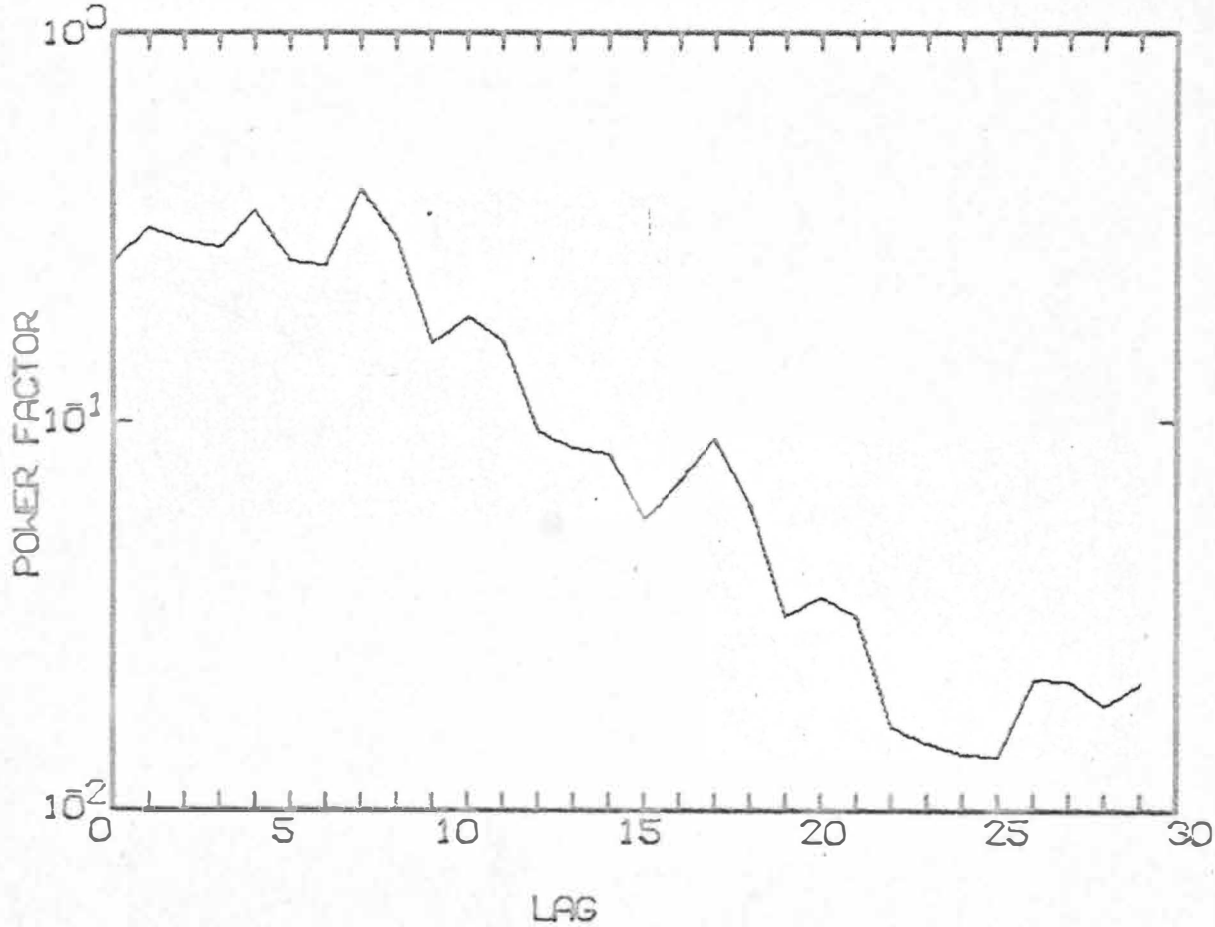
10^0
10^1
10^2
POWER FACTOR
0
5
10
15
20
25
30
LAG

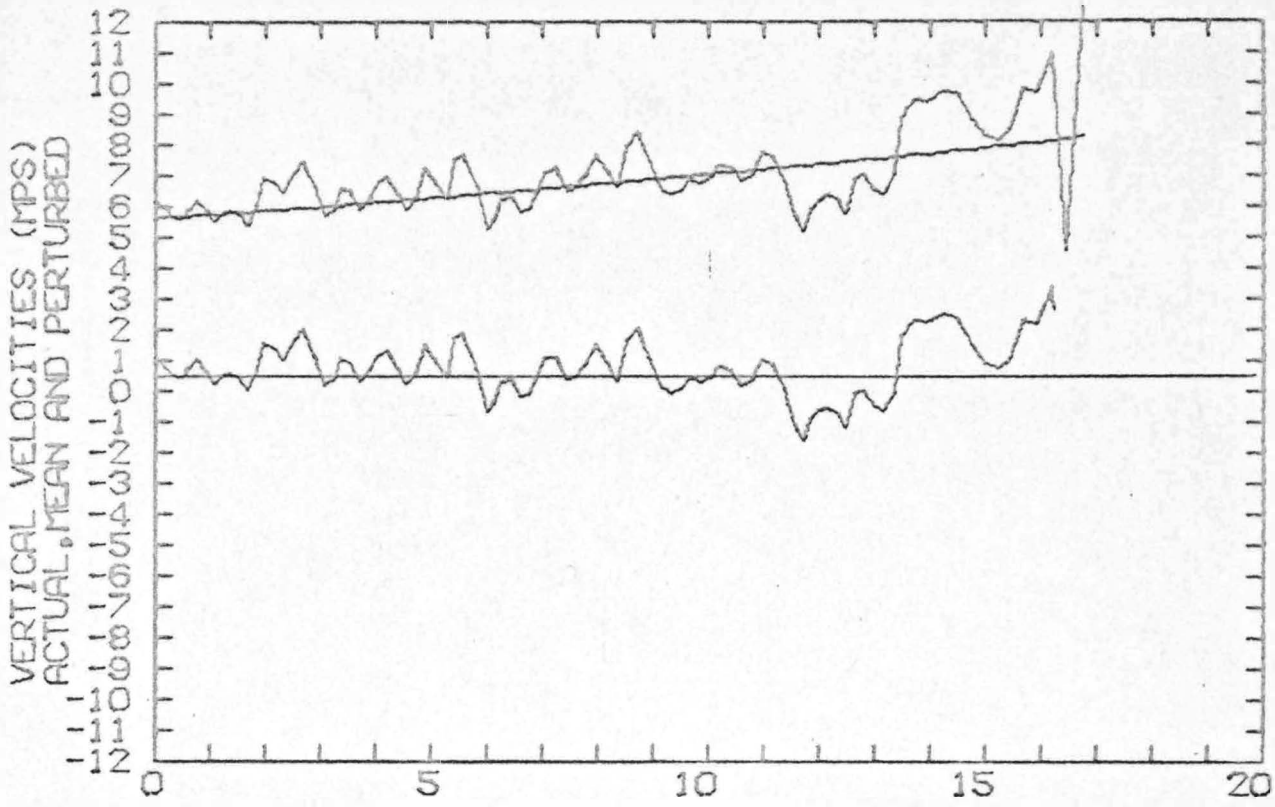
VERTICAL VELOCITIES (MPS)
ACTUAL, MEAN AND PERTURBED
12
11
10
9
8
7
6
5
4
3
2
1
0
-1
-2
-3
-4
-5
-6
-7
-8
-9
-10
-11
-12
0
5
10
15
20
HEIGHT (KM)
0000 15TH OCTOBER 1970

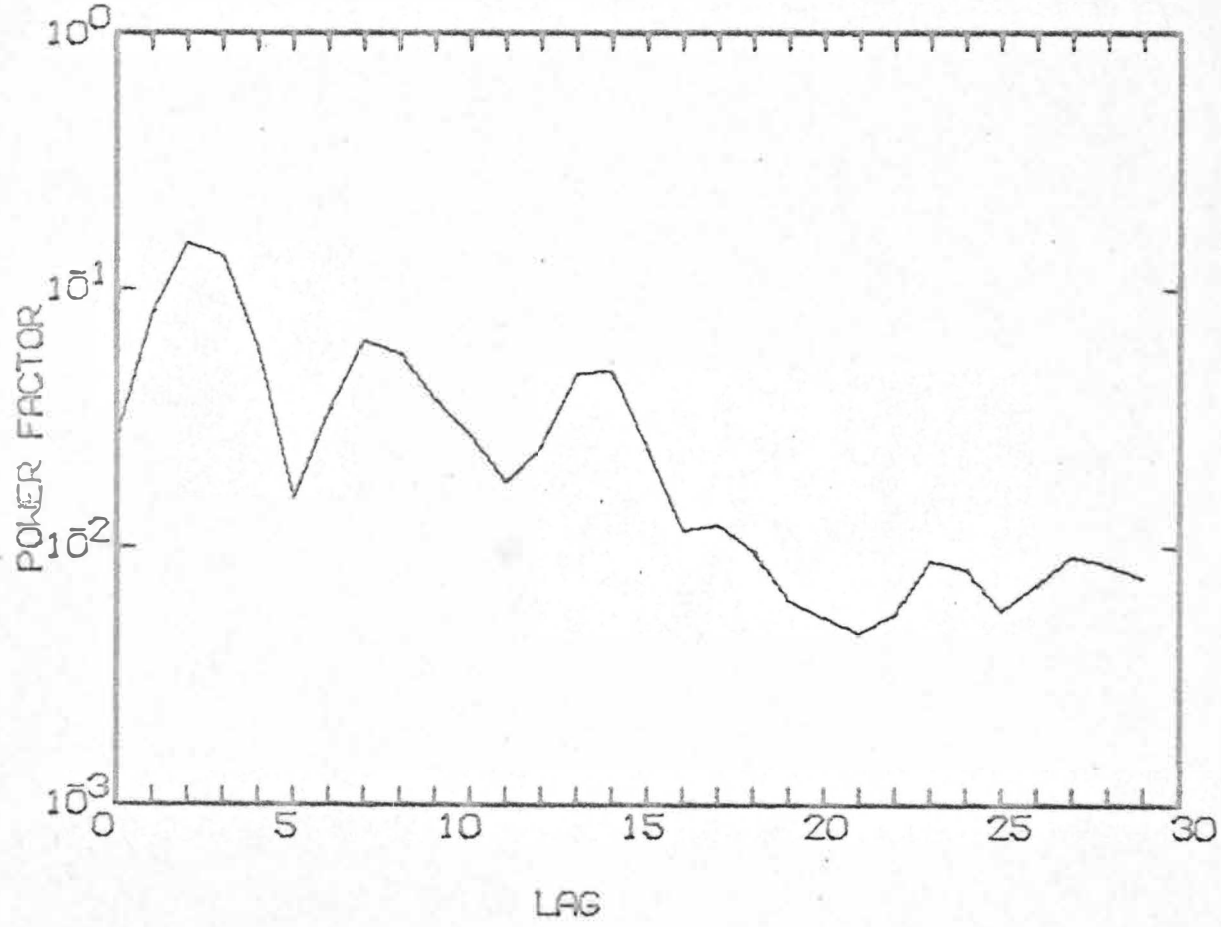
POWER FACTOR
10^0
10^1
10^2
10^3
0
5
10
15
20
25
30
LAG

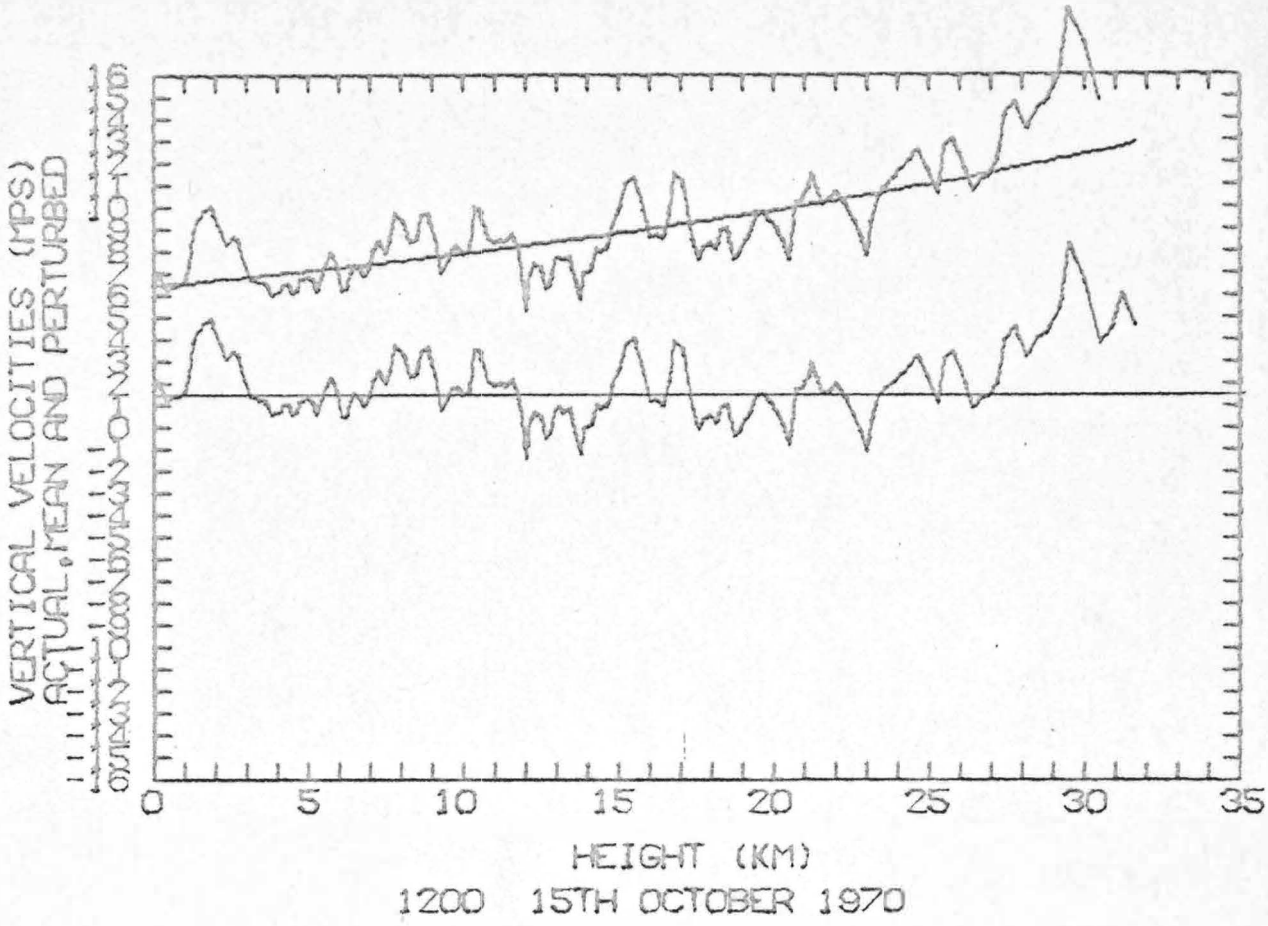
VERTICAL VELOCITIES (MPS)
ACTUAL, MEAN AND PERTURBED
0
5
10
15
20
25
30
35
HEIGHT (KM)
1200 15TH OCTOBER 1970

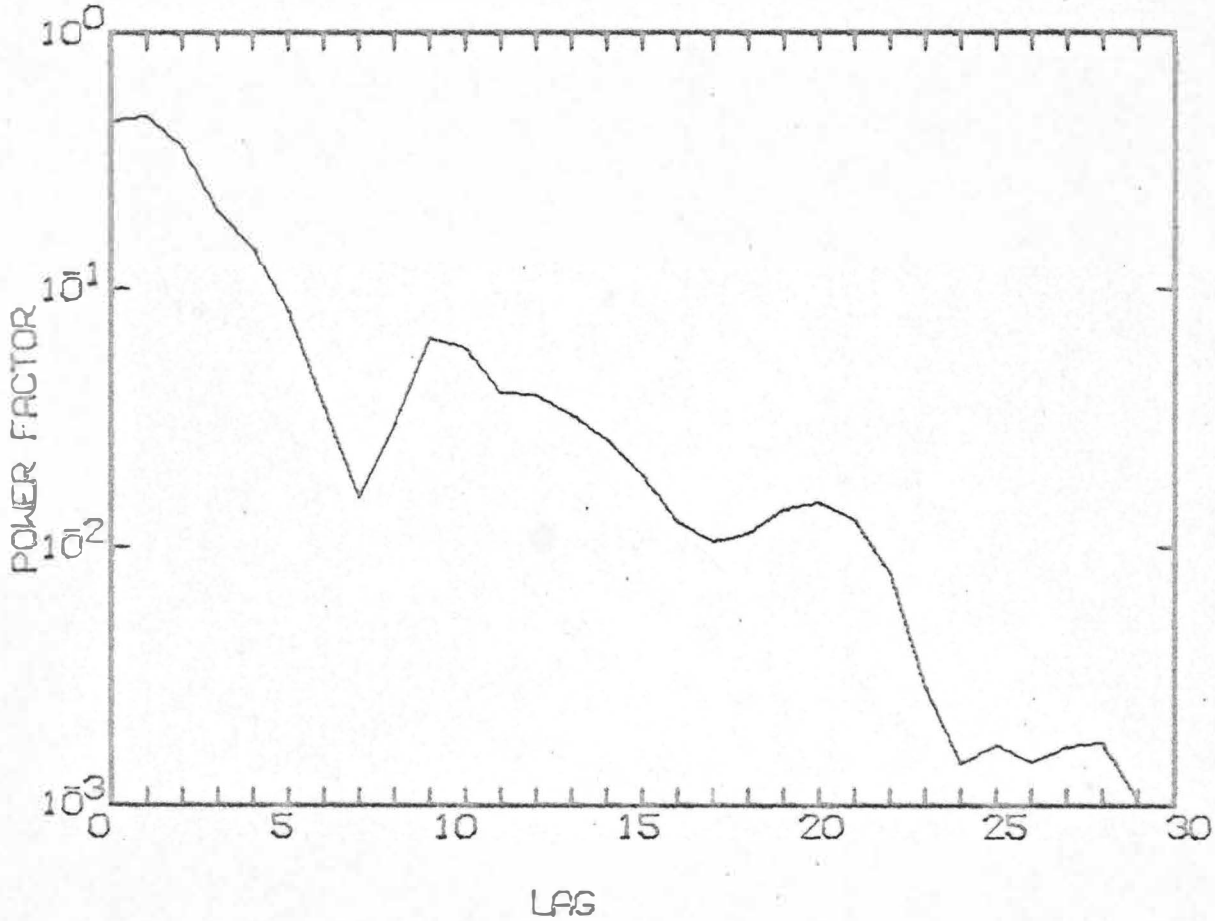
10^0
10^{-1}
10^{-2}
10^{-3}
POWER FACTOR
0
5
10
15
20
25
30
LAG

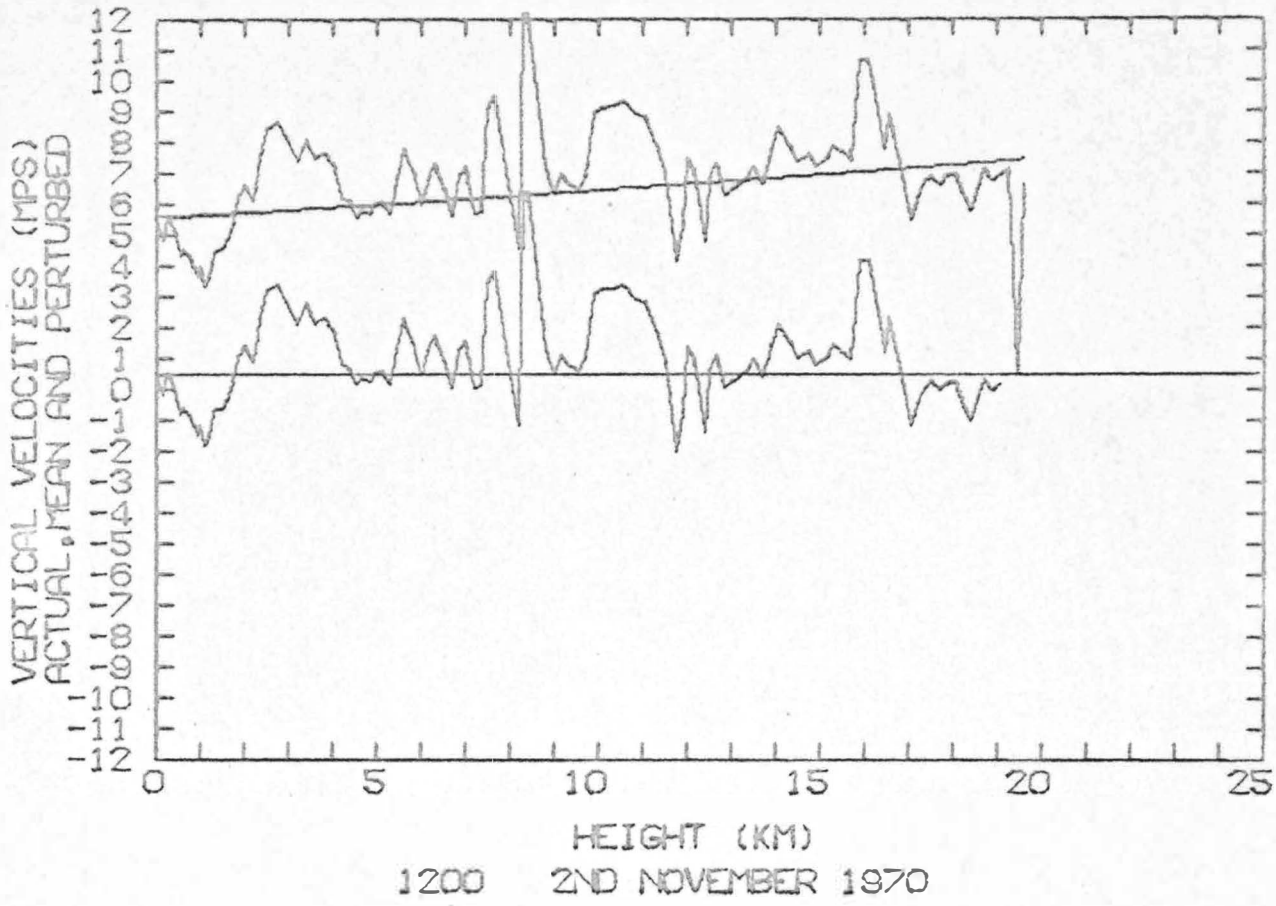
VERTICAL VELOCITIES (MPS)
ACTUAL, MEAN AND PERTURBED
12
11
10
9
8
7
6
5
4
3
2
1
0
-1
-2
-3
-4
-5
-6
-7
-8
-9
-10
-11
-12
0
5
10
15
20
25
HEIGHT (KM)
1200 2ND NOVEMBER 1970

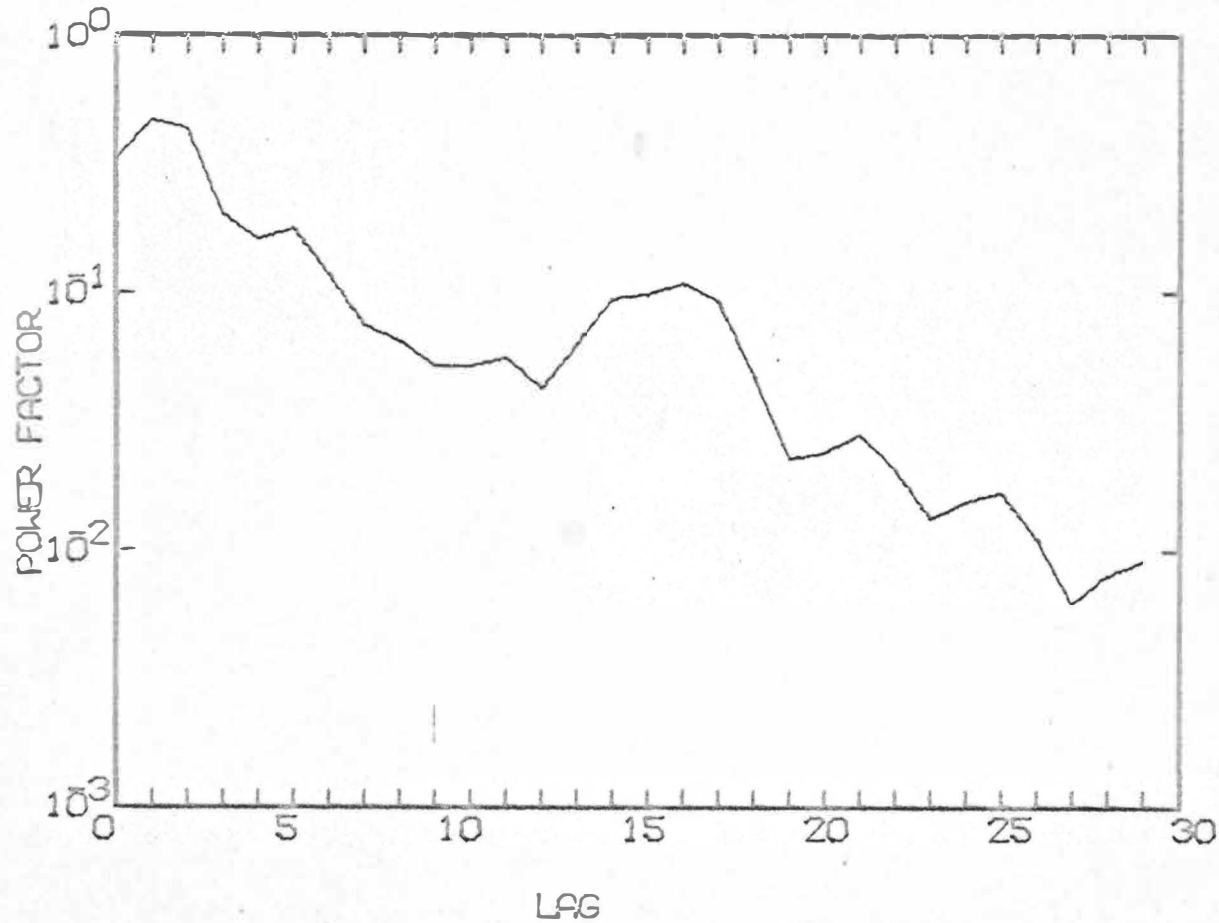
10^0
10^1
10^2
10^3
POWER FACTOR
0
5
10
15
20
25
30
LAG

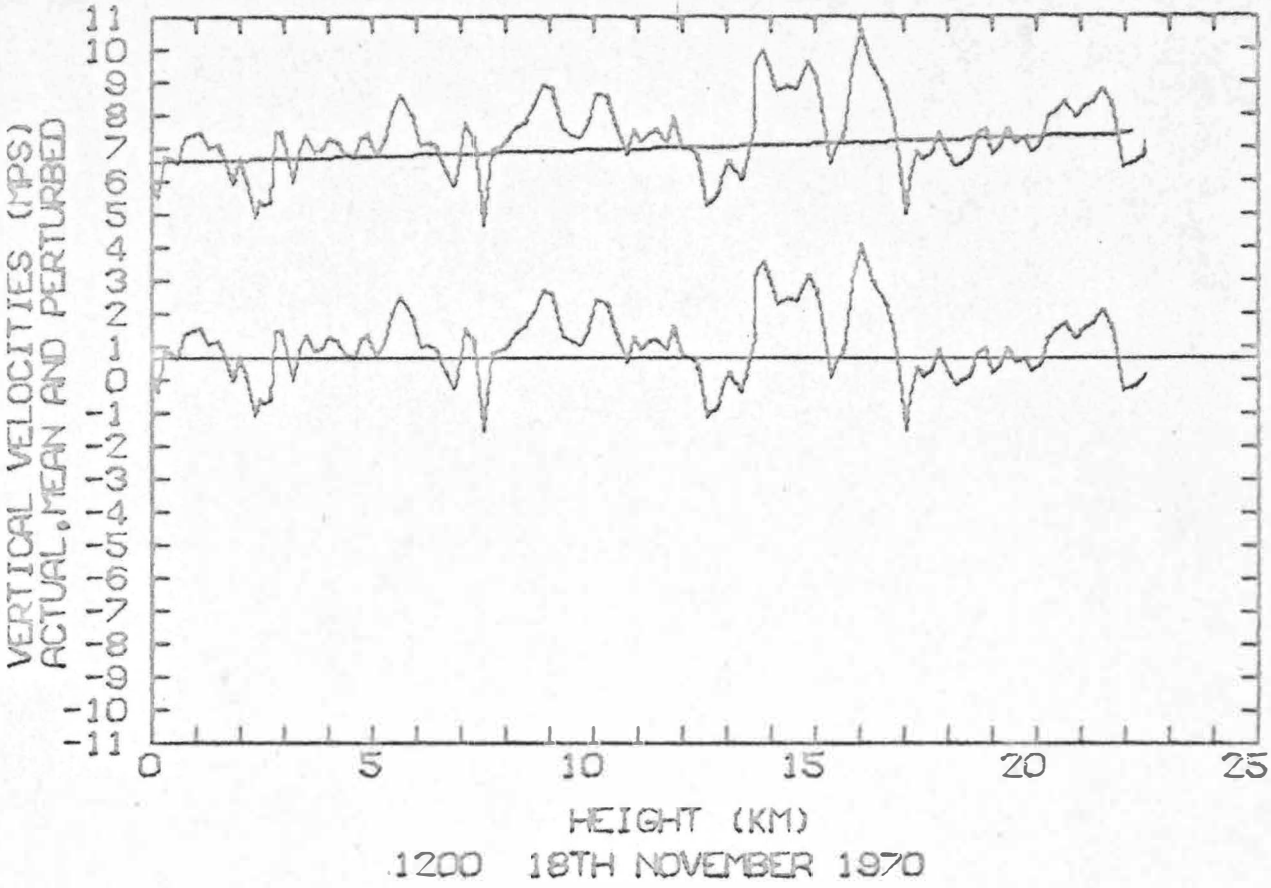
VERTICAL VELOCITIES (MPS)
ACTUAL, MEAN AND PERTURBED
11
10
9
8
7
6
5
4
3
2
1
0
-1
-2
-3
-4
-5
-6
-7
-8
-9
-10
-11
0
5
10
15
20
25
HEIGHT (KM)
1200 18TH NOVEMBER 1970

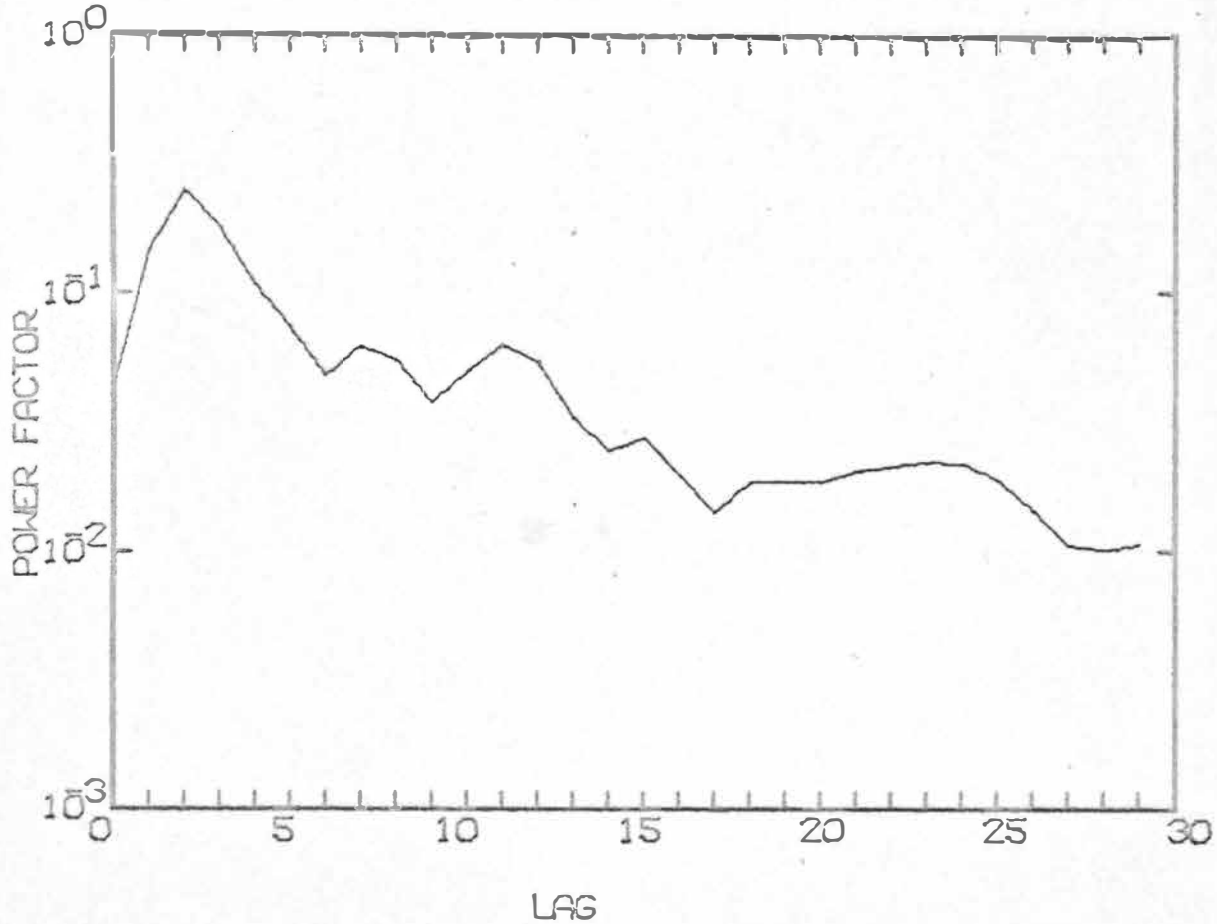
10^0
10^1
10^2
10^3
POWER FACTOR
0
5
10
15
20
25
30
LAG

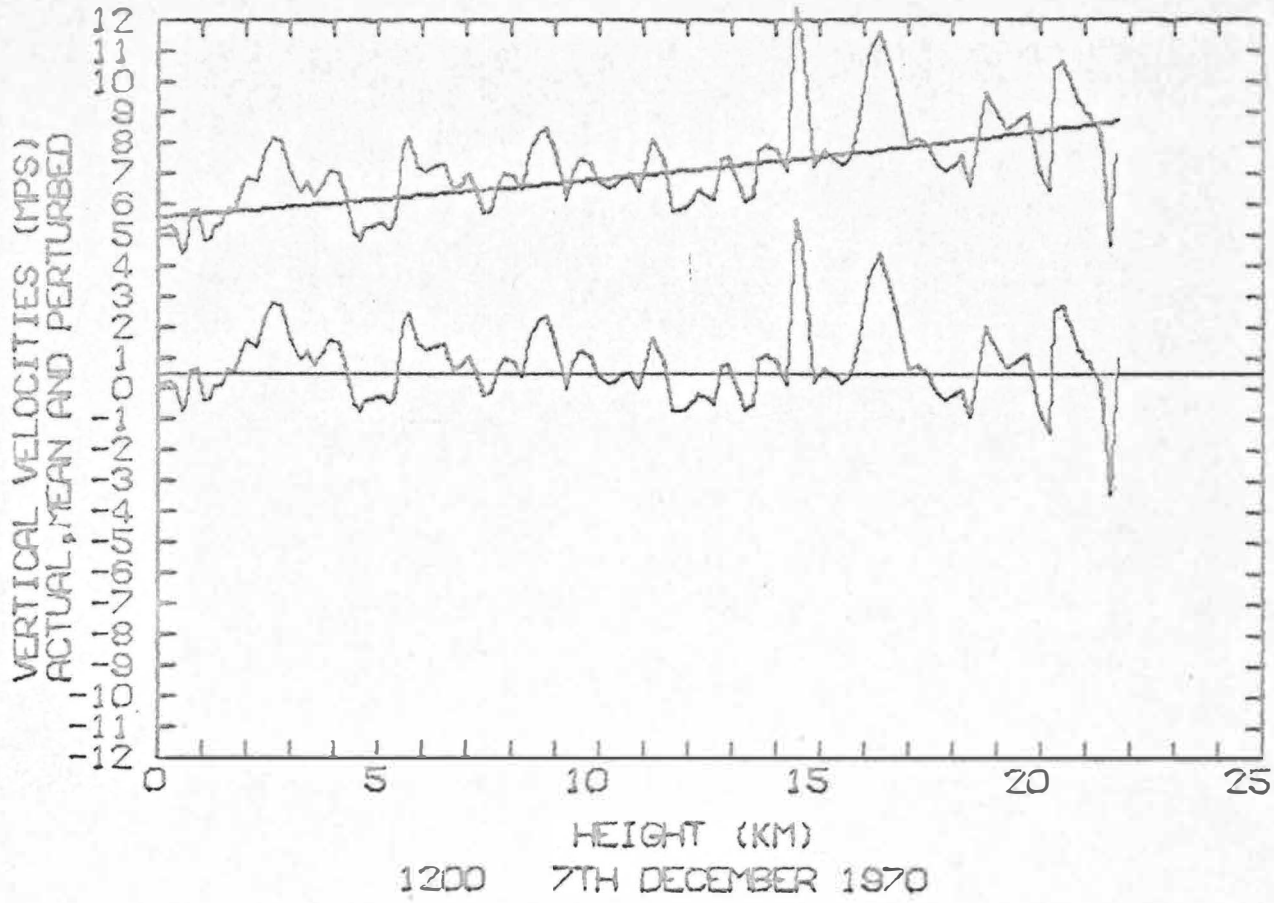
VERTICAL VELOCITIES (MPS)
ACTUAL, MEAN AND PERTURBED
12
11
10
9
8
7
6
5
4
3
2
1
0
-1
-2
-3
-4
-5
-6
-7
-8
-9
-10
-11
-12
0
5
10
15
20
25
HEIGHT (KM)
1200 7TH DECEMBER 1970

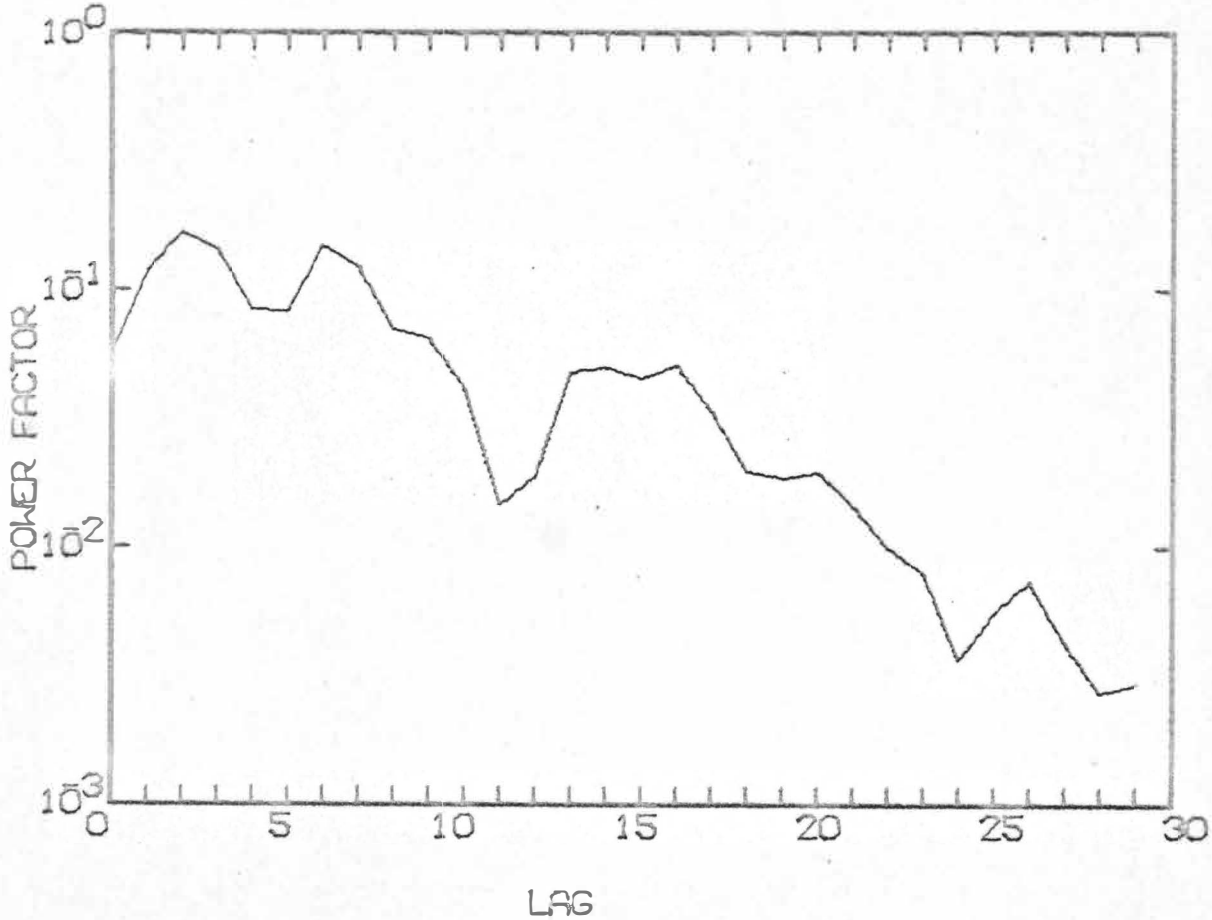
10^0
10^1
10^2
10^3
POWER FACTOR
0
5
10
15
20
25
30
LAG

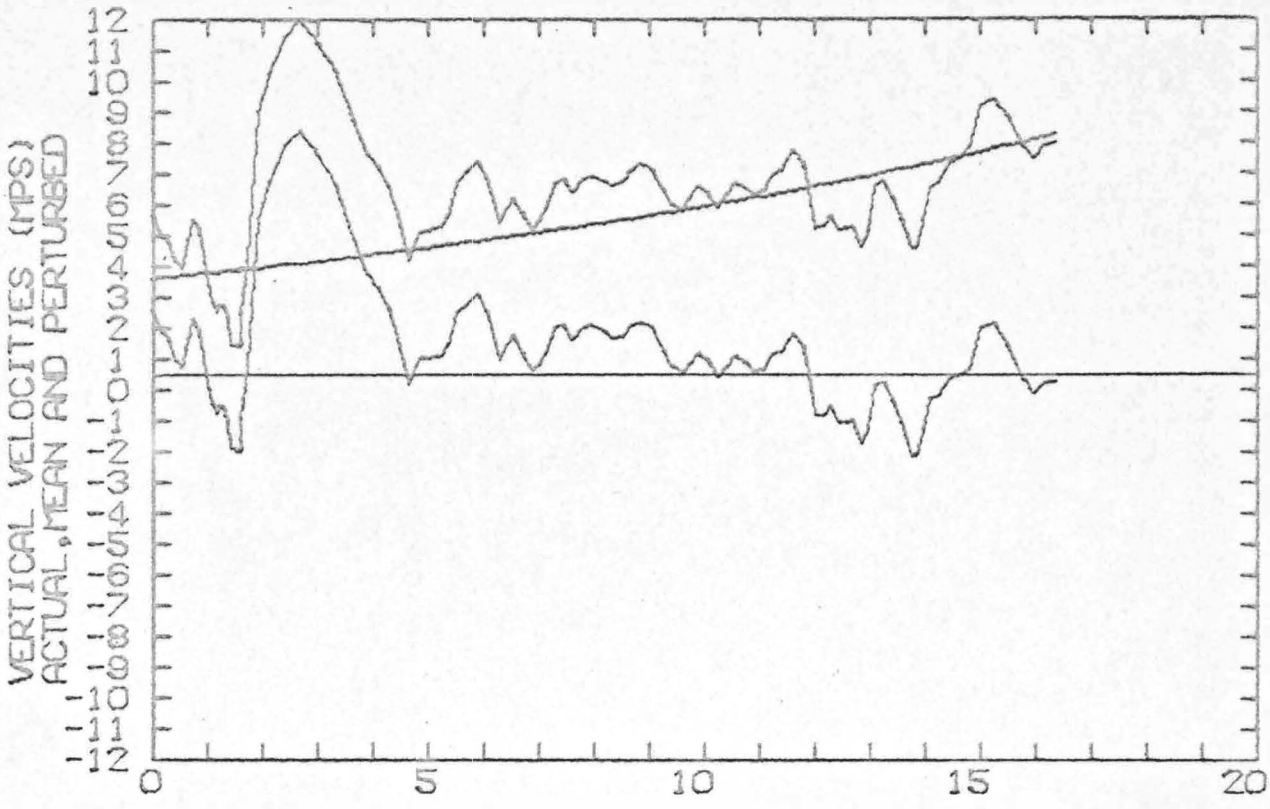

1200 24TH FEBRUARY 1971

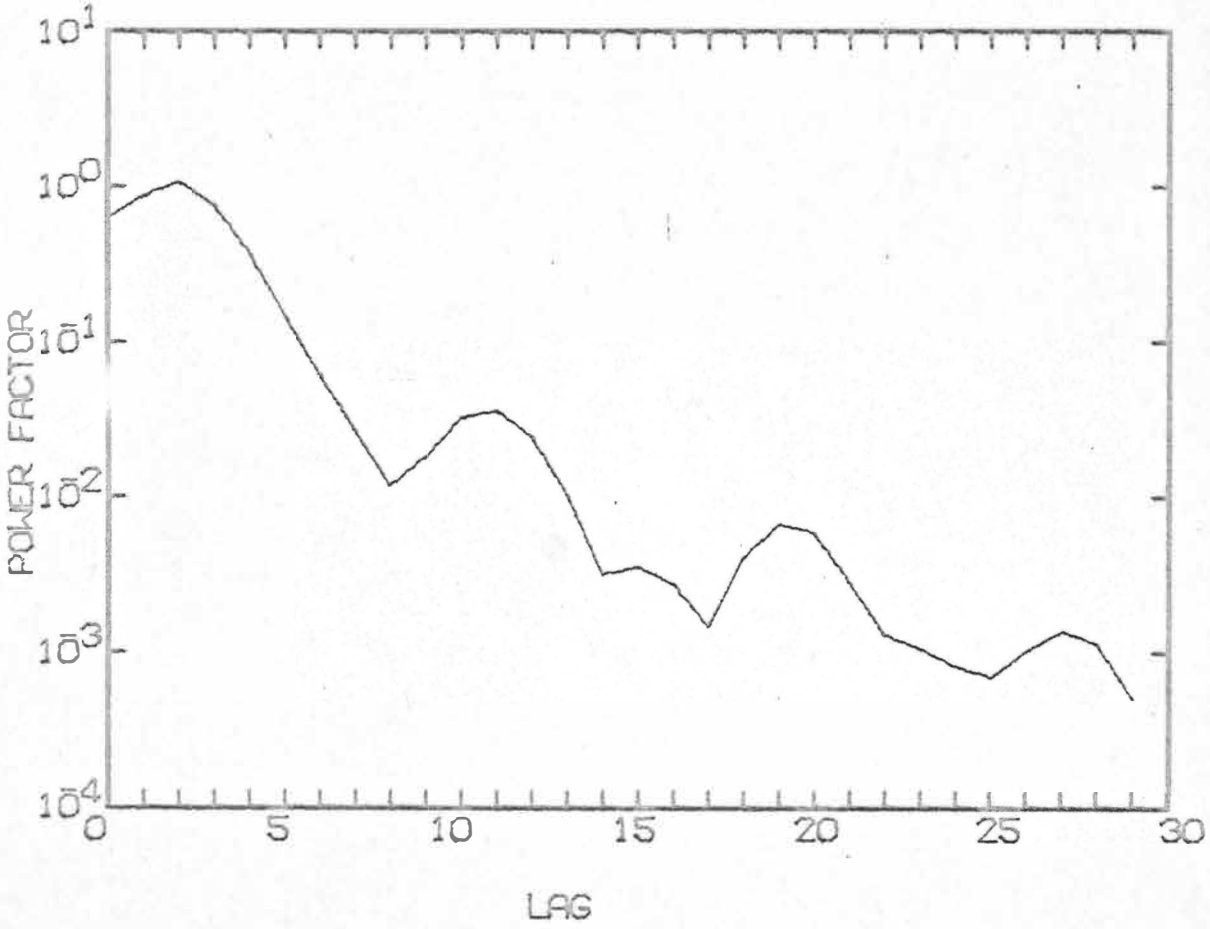

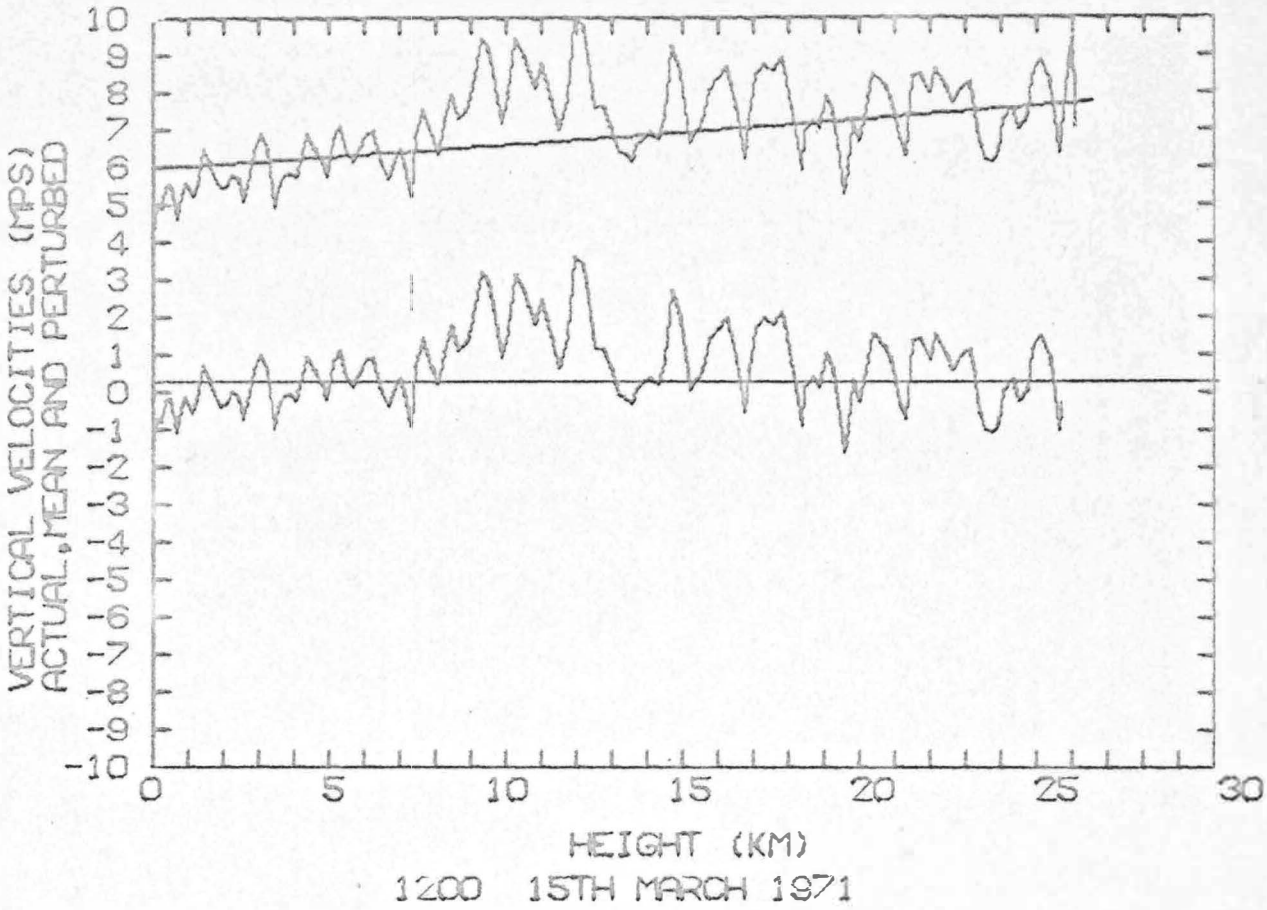
VERTICAL VELOCITIES (MPS)
ACTUAL, MEAN AND PERTURBED
10
9
8
7
6
5
4
3
2
1
0
-1
-2
-3
-4
-5
-6
-7
-8
-9
-10
0
5
10
15
20
25
30
HEIGHT (KM)
1200 15TH MARCH 1971

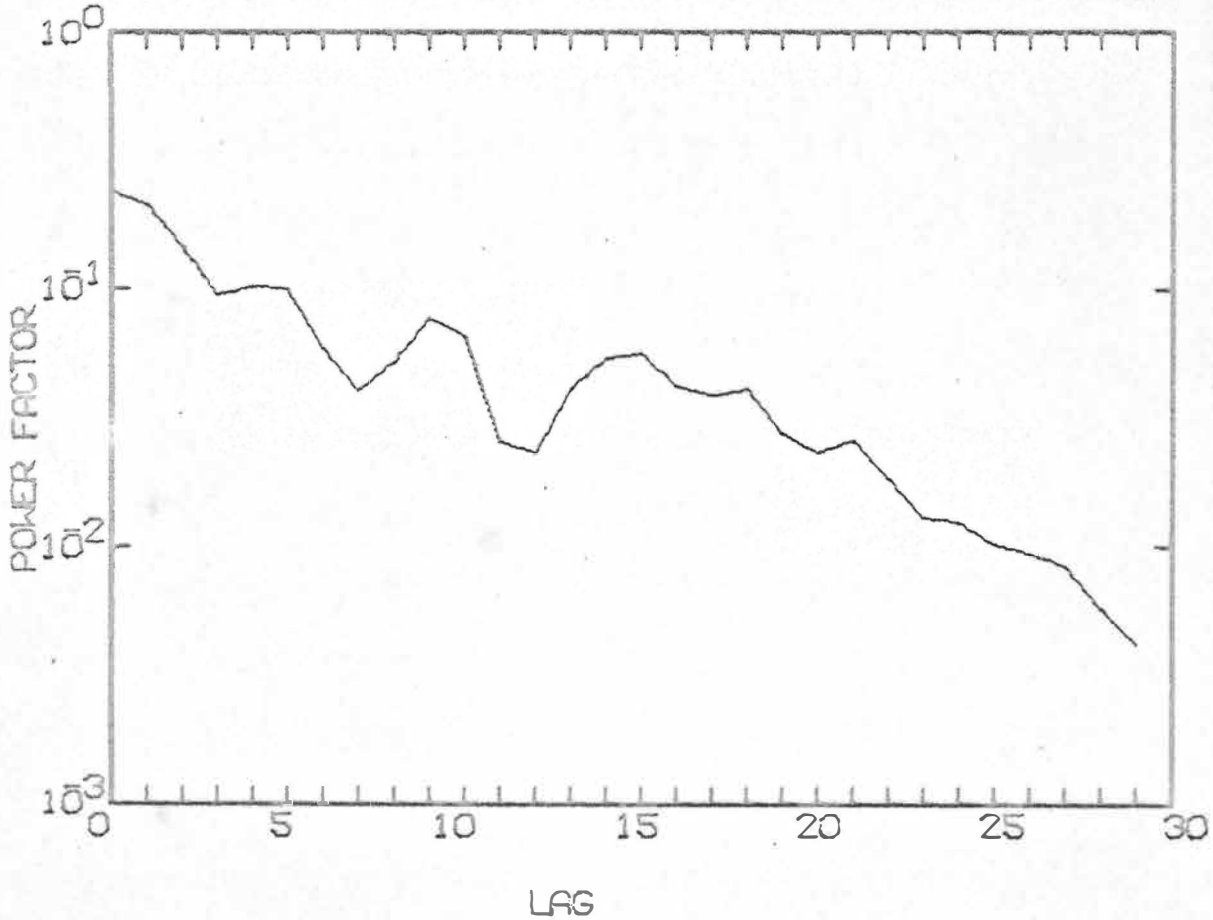
10^0
10^{-1}
10^{-2}
10^{-3}
POWER FACTOR
0
5
10
15
20
25
30
LAG

5. Discussion of the Results

It should be noted that these results are not considered to be exact but rather that the wavelengths given are approximately those in the airflow traversed by the radiosonde balloon. The maximum amplitudes may be considered as indicative of the scale of the amplitudes of the waves in the airflow, subject to accuracy of the choice of the wavelength of the wave producing the maximum.

There is a difference between some of the wavelengths given by RAD in Chapter 8 and those given above. This arises because the wavelengths in RAD were derived from the period of the peaks in the power spectra using only the mean tropospheric wind speed, based on the assumption that the majority of lee waves will only have significant amplitudes in the troposphere. The assumption may tend to break down for some long wavelentth components which reach a maximum in the stratosphere but since where long wavelengths exist the wind speed tends to be high it may be assumed that the long waves will be in a region where the wind speed is of the same order as that in the troposphere and the scale of their wavelengths will be predicted by the use of the mean tropospheric wind speed.

It was found in Chapter 8 that the wavelengths given by RAD were of the same order generally as those found in the SPB profile with differences arising because of the

separation of the flights in time and the different terrain flown over. Differences in the relative intensities of the peaks in the power spectra for the waves being compared were expected because the various wave components reach their maximum amplitudes at different levels. Thus the SPB flying at a certain level may not have given significance to a wave that had a maximum at a considerably different height.

Table 9.1 shows that generally the maxima observed low in the troposphere were due to short wavelength waves which often had amplitudes less than 100 m. On some occasions, for example 0000 21/1/70, 1200 2/3/70 and 1200 2/11/70 short wavelengths were observed to have amplitudes greater than 100 to 200 m. Of the days shown one day only 24/2/71 was there a large amplitude long wavelength wave observed near the ground. The velocity profile shows that the wind was light on the ground and increased rapidly at first (this may have been due to the effect of the wave on the balloon making the sounding) then steadily up to more than 40 mps at 10 km. The mean tropospheric wind direction was 326°, 16° off the direction perpendicular to the Alps. Also the distance between the Puketeraki range and some 3000' foot hills over which the airflow would have passed upstream of Harewood is about 22 km. Thus the wave in the airflow was in resonance with the mountain profile. These

factors, in line with the 'Scorer criteria' and airflow/ mountain resonance, are indicative of large amplitude waves such as were observed.

The majority of the balloons show a long wavelength maximum amplitude in the high troposphere or in the stratosphere consistent with the low values of l^2 at these levels.

6. Discussion of Particular Balloons

(The associated SPB is given in brackets where applicable.)

1200 5/3/69: (B3) The small amplitude short wave was associated with a slightly stable layer ($l^2 \simeq 1$ km^{-2}) near the ground and the medium wavelength maximum occurred just below a very stable stratospheric layer.

0000 14/1/70: This maximum occurred where l^2 initially increased in the stratosphere, several km below a very stable layer.

1200 14/1/70: (14C2) No particular maxima were evident so the maximum vertical velocity in the middle troposphere was looked at and found not to have a significant amplitude. The increase in the oscillations in the stratosphere seems to indicate a medium to long wavelength wave. There is a strong long wave peak in the power spectrum showing that there was some regular long wave oscillation present.

0000 21/1/70: (15C3) The short wave maximum low in the troposphere occurred in a very stable layer. The large amplitude oscillation at 9 km occurred just below the tropopause. Above the tropopause the disturbance died away very quickly.

1200 21/1/70: (15C3) The low level maximum occurred in a slightly stable region and the high level maximum occurred just below a very stable stratospheric layer.

0000 21/1/70: There were no large vertical velocities observed and the maxima picked out resulted in small amplitudes showing that there were no significant waves present. The velocity profile shows that the wind speed was less than about 5 mps up to 3 km resulting in a stable layer up to this level which is above the level of the mountains. Thus no significant waves would be expected in the light of the Förchtgott classification and the general theoretical indications of the effect of l^2.

1200 2/3/70: (18) The results suggest significant short waves low in the troposphere such as observed by balloon 18. The slight maximum at 17 km does not appear to be associated with a long wavelength. An approximate calculation suggested that the amplitude was about 200 m. The majority of the oscillations were considerably smaller than this. Thus, as indicated by the power spectrum, there appears to be no

significant waves high in the atmosphere.

The balloons on 24, 25 and 26 April 1970 show only short wavelength waves with quite small amplitudes except for the 11.5 km wave on the 25th. This had a very large amplitude at the level of the maximum but it died away quickly with height. Consideration of the l^2 profile suggests that conditions were suitable for a large amplitude wave at about this level. l^2 decreased from a stable layer near the ground to be quite small between 10 and 12 km. Between 14 and 15 km, where the maximum occurred it increases considerably prior to the major increase into the very stable layer in the high stratosphere. Thus the disturbance would be expected to propagate up and the long wave component might be expected to be trapped below the stable layer, as observed.

The balloon on 4 June shows no significant waves in the power spectrum and only small oscillations in the ascent rate. The horizontal wind velocity was small near the ground and decreased between 2 and 4 km which would tend to inhibit the upward propagation of waves.

The rest of the balloons show the same sort of results as those discussed above. The balloon on 4/8/70 is worthy of note. It shows three distinct scales of oscillation which have maximum amplitudes at different heights proportional to the wavelength. The results imply a large

amplitude wave in the stratosphere. The l^2 profile does not show the very stable stratospheric layer which is usually observed.

C H A P T E R 1 0

CONCLUSIONS

The combination of favourable topography and the prevailing winds from the westerly quarter makes Canterbury an ideal place for the formation of lee waves. The year 1970 was different from usual in the frequency and character of the nor'westerly conditions. The results obtained show only a small number of medium and large amplitude waves which, if taken as being a general indication of conditions would give a mistaken impression of the situation in Canterbury under northwesterly conditions.

It is fitting in concluding to consider whether, or to what extent, the initial aims as set out in the first chapter were fulfilled.

1(a). Balloons and Balloon Systems

Tetroons were made and tested and their parameters measured. They were successfully used in tandem and valved systems to obtain data on lee waves over Canterbury. The information about the characteristics and performance of tetroons and balloon systems was found to be of enough interest to be accepted for publication in the Journal of Applied Meteorology.

A strong plastic material was found to be preferrable in the construction of superpressure balloons although polyethylene was used successfully in tandem systems and could be used with valves if the balloons were taped and were not subjected to large displacements from their equilibrium levels. The elasticity of polythene to some extent compensates for the decrease in the ambient pressure in an upward displacement so that the increase in superpressure is reduced.

The tandem system was found generally to ascend faster than the equivalent valved tetroon as the lift was not limited by the SPB. It has the disadvantage that it is dependent on the pressure trigger which may fail to release if it ices up. The valved balloons were more convenient to fill and release than a tandem system, particularly when little shelter was available for releases in high winds. On several occasions valved balloons lost altitude after a large upward displacement from their equilibrium level when the change in ambient pressure exceeded the operation pressure of the valves.

1(b). <u>On the Use of Radiosondes in Obtaining Data on Lee Waves</u>

Although several approximations and assumptions were used in order to analyse the radiosonde data for periodic perturbations the results given are in good agreement with

SPB flights at about the same time and they provide a considerable amount of added information about the vertical structure of the lee wave train. The results discussed in Chapters 8 and 9 show a generally good correlation between the waves found in the airflow by the radiosonde and the characteristics of waves as given by the constant l^2 layer models and solutions. The midday radiosonde flight is a ready source of lee wave data as well as the temperature and horizontal wind velocity profiles.

There is a considerable advantage in the use of a radiosonde over the use of an SPB because of the proximity in time between the l^2 profile and the wave characteristics. The time interval between the SPB flight and the nearest radiosonde was a major factor in the comparison of practical and theoretical results.

The two different types of balloon, SPB and radiosonde, were found to be complementary both giving useful information about the wave characteristics of the airflow from different points of view. The SPB generally provided information about the waves present at a given level and how they varied in the horizontal direction. The radiosonde gave information about the vertical structure of the lee wave train .

2. Observational Programme

Twenty two balloons released during 1970 were found to be suitable for a comparison with the solutions of the various theoretical layer models. The number and nature of the flights were limited by the weather. Over the year there were very few strong, deep, persistent nor'westers that resulted in the formation of large amplitude lee waves, usually characteristic of Canterbury. There was no shortage of nor'westers; as the survey showed, they occurred with great regularity. The wind was within 30^{o} of 310^{o} on 122 days. On very few occasions did they last long enough or have the right airflow characteristics for the production of good waves. The l^2 profiles in Chapter 8 show a surprising number in which l^2 was less than one throughout the whole troposphere. Even when the velocity profile looked good for waves the lapse rate was very high and close to the dry adiabatic lapse rate resulting in very low stability. Inspection of the results of the radiosondes for such days from Table 9.1 shows that the short wave maxima occurring low in the troposphere had very small amplitudes and that significant long wavelength waves were found in the stratosphere at the level where l^2 began to increase upwards into a very stable layer. This suggests that on the days when the stability was low throughout the troposphere the gravity

wave energy propagated freely through the troposphere until it was trapped beneath the stable stratospheric layer where the energy was absorbed by a long wavelength mode. Unfortunately this occurred above the level of the SPB flights in this project. For this reason also the radiosondes have proved useful.

3. Measured and Calculated Characteristics of Lee Waves

A summary is given of the characteristics of lee waves as given by the layer theories and as derived from observations. The theoretical considerations were restricted to a study of the layer models and their solutions of the linearised wave equation. The effects of variations of the layer and airflow parameters on the solutions given by the constant l^2 two layer, bounded two layer and three layer models. Solutions of the wave equation for an exponential layer model were also obtained.

Certain critical velocities are found to limit the formation of lee waves. A minimum velocity of the airflow across the mountain must be attained before waves form in the lee. This is observed to be a function of the mountain height and varies from about 8 mps for hills 800' high to about 12.5 mps for mountains 2000' above the ground to their lee. Such a minimum velocity can be derived for the lower layer in the two layer theory, given the other parameters,

in order for there to be a solution of the interface equation. It is also observed that if the wind speed exceeds some value standing lee waves cannot exist and turbulence results. This velocity cannot be derived from the layer theories but may be obtained from Förchtgott's classification.

The characteristics of an airflow which favours the production of waves may be derived from the two layer theory by a consideration of the conditions required for there to be a solution of the wave equation (or the interface equation). This was called the 'Scorer Criteria' and consists of the conditions that l^2 must decrease with height from some maximum low in the troposphere and the wind must pass over the mountain ridge within 30^o of the perpendicular to its direction. This, it was found, was fulfilled for good tropospheric waves. E.G. Balloons 14C2, 31H6, 32Pro3, 41Pro7, 42Pro8, and 45H12.

Varying the parameters in the two layer model showed that the wavelength varied inversely to l_1^2, l_2^2 and the interface height h, but for some values of h as it is increased longer wavelength modes become solutions for some large values of l_1^2.

An obvious simplification involved in the two layer model is the complete neglect of the stratosphere. Two

layer tropospheric/stratospheric models have no analytical solutions for real wavenumbers. The effect of the stratosphere can be included by extending to a three layer model. Such a model gives no simple analytic solutions but the resonant values of the wavenumber can be obtained from a wave number spectrum of the so-called amplitude factor. (The validity of this method of obtaining a solution for the wavelengths is shown by a comparison with the bounded two layer theory.)

It is found that the effect of including a stable layer in the stratosphere is to introduce resonance modes at longer wavelengths than $\frac{2\pi}{l_2}$, which are not solutions of the two layer theory. It was found in an example that the wavelengths that are solutions of the three layer model vary inversely as the variations in the layer parameters. The stability (l^2) in the upper layer and the height of the upper interface had a marked effect on the amplitude factor of the resonant modes with wave numbers less than l_2. There is a considerable difference between the amplitude factor for wave numbers less than l_2 and that for wave numbers greater than l_2. The former gave broad resonance peaks and the latter, when they appeared, were intense narrow peaks corresponding to discrete modes as found in the unbounded and bounded two layer models. Often these discrete modes

did not appear in the three layer k-spectrum because their width was less than the increment in k used in the calculation.

4. Comparison of Experimental and Theoretical Results

(a) It was not expected, nor was it found, that the actual excitation wavelengths in the mountain profile should appear in the airflow to the lee of the mountains but rather that the mountain wavelengths near to resonance with the natural wavelengths of the airflow will excite those natural wavelengths to an extent governed by the degree of resonance. In balloons 34H7, 36H9, 41Pro7 and others evidence was found of wavelengths close to those in the mountain profile that did not persist in the airflow to the lee of the mountains. There were also other waves present to the lee that were close to the solutions of the natural waves from the layer theories.

(b) Wavelength Correlation between Balloons and Model Solutions: Discussion of each of the balloons is given with the results in Chapter 8. A trend was evident that the extent to which the theories predicted the observed wavelengths depended very strongly on the accuracy of the fitted layers. Differences were observed due to the time interval between the SPB flight and the radiosonde flight from which the l^2 profile was calculated. To give an overall view a

comparison in general terms between the observed wavelengths and the model solutions is given in the Table 10.1 below. Broadly defined terms are used to describe the correlation or fit. In descending order of correlation they are: Good, Fair, Scale, Poor and No. Scale is used to indicate that they theory gave solutions that were of the same scale as those observed. Often the variation of l^2 was not exponential but it showed a general decrease which the exponential fitted followed in an average manner. This was termed a 'Mean' fit.

Table 10.1: A comparison between the observed wavelengths and the theoretical wavelengths that were solutions of the layer models with reference to the accuracy of the extent to which the model approximated the observed profile.

		Constant l^2 Layers			Exponential l^2 layers		
Time	Date	Fit	Wavelength Correlation SPB	RAD	Fit	Wavelength correlation SPB	RAD
1200	5/3/69	Fair	Fair	Fair	Good	Good	Good
1200	26/3/69	Fair	Poor	Fair	Fair	Fair	Good
0000	14/1/70	Good	Poor	Good	Good	Good	Good
1200	14/1/70	Good	Scale	Fair	Fair	Fair	Poor
1200	21/1/70	Fair	Fair	Fair	Mean	Good	Poor
1200	2/3/70	Fair	No	Fair	Poor	No	No
1200	30/3/70	Fair	No	Fair	Fair	Poor	No
1200	24/4/70	Poor	Scale	Fair	Poor	Scale	No

Table 10.1 (contd):

Time	Date		Constant l^2 layers Fit	Wavelength Correlation SPB	Wavelength Correlation RAD	Exponential l^2 layers Fit	Wavelength Correlation SPB	Wavelength Correlation RAD
1200	26/4/70		Poor	Poor	Poor	Poor	Poor	Poor
1200	4/6/70	(a)	Fair	Scale	Scale	Poor	No	Poor
		(b)	Fair	Scale	Poor			
1200	16/6/70		Poor	Scale	Scale	Mean	No	No
1200	28/6/70		Fair	Scale	Fair	Mean	No	No
1200	2/7/70		Poor	Fair		Mean		Scale
1200	15/7/70	(a)	Fair	Scale		-		
		(b)	Fair	Scale		-		
1200	23/7/70		Poor	(3L)Scale	(3L)Scale	Mean	No	No
1200	4/8/70		Fair	Scale	Scale	Good	Scale	Scale
1200	13/8/70		Good	Scale	Fair	Fair	Poor	No
0000	15/10/70		Good	Scale	Good	Good	Poor	Scale
1200	15/10/70		Good	Good	No	Good	Poor	Scale
1200	2/11/70		Good	Poor	Scale	-		
1200	18/11/70		Good	Scale	Poor	Good	Poor	Poor

(Note: The dash under EXP indicates that l^2 on the average increased through the troposphere so EXP gives no solutions.)

The variation of l^2 with height was only simple enough on a few days to be approximated well by simple layer models. In general the l^2 profile was rather more complex.

The unbounded two layer model suffered most in this regard and it failed to give solutions close to those waves observed on all but a few occasions. It always showed an absence of the longer wavelengths observed. The dependence of the solutions on the accuracy of the layer fits is evident in Table 10.1. For the constant l^2 layer models their correlation with RAD is better than with the SPB's due to the time difference. When there was a good layer fit the bounded two layer model and the three layer model generally gave a good, fair or scale correlation with the observed wavelengths. If the fit was fair the resulting solutions showed a fair correlation or at least they predicted waves of the same scale as those observed. Some of the wavelengths predicted when there was a good fit were not observed because they were not excited by the mountain. Thus a conclusion which may seem self-evident is that when the atmosphere has three layer characteristics the bounded two layer and the three layer predict quite well the natural wavelengths of the airflow but they will only be produced if they are close to resonance with the mountain.

The exponential layer model (after Doos, 1961) shows the same dependency on the accuracy of the fit to the l^2 profile. Poor fits result in poor or no correlation. Good fits, depending on how good they are, result in good or scale correlations and mean fits can give poor results or good results. The reverse trend is shown by EXP in that there was generally a better correlation between it and the SPB's than between EXP and RAD. This would arise because EXP considers only the variation of l^2 in the troposphere and so cannot be expected to describe wave conditions in the stratosphere. Since most of the SPB's in this project flew in the troposphere and the radiosonde balloons flew through both the troposphere and the stratosphere the observed difference in correlations are explicable. The exponential model is useful to predict the wavelengths of waves in the troposphere when l^2 decreases approximately exponentially.

An interesting feature of the model solutions was the inter-relationship between the three layer solutions and the bounded and unbounded two layer solutions. Even when the value of l^2 in the upper layer was small, as for 26/3/69 (5), 2/3/70 (18) and 26/4/70 (27H5), the solutions were essentially the same. This gives justification to the assumption made in the three layer model that the values of k which correspond to peaks in the wave number spectrum correspond to resonant mades of waves. It also illustrates

the trapping effect of the stable upper layer (since it is equivalent to a rigid boundary) which is completely neglected by the unbounded two layer theory.

The solutions of the bounded two layer theory contained the solutions of both the two layer and three layer models.

The parcel theory was shown in every case to be completely inadequate to describe the waves in the airflow. It could only be expected to be realistic in an atmosphere in which the lapse rate and the horizontal wind speed were constant with height. A situation like this occurred on 2/3/70 when the wind was almost constant at about 17 mps between 3 and 12 km and the lapse rate was almost constant at 7.7^{o}C/km. Since the temperature decreased from 273 ^{o}K to 210^{o}K over this height range the mean wavelength given by the parcel theory was 11.3 km. A periodicity corresponding to a wavelength of 9 km was observed in the radiosonde flight.

The wavelength given by the mean parameters as described in section 5.9 was found to give wavelengths that were far longer than those observed by the balloons and satellite photographs.

(c) A Comparison of the Amplitudes Observed and Given by EXP: The following comments are applicable to the amplitudes as given by the other analytical solutions of the layer models except perhaps 2L in some respects but it was found to be convenient to calculate the amplitude as

given by EXP in the programme which solved the Bessel function form of the wave equation. These amplitudes are shown with the airflow profiles in Chapter 8. The amplitude profile usually shows a wave-like variation with height for several of the wavelengths that are solutions of the equation. Quite commonly two or three nodal surfaces are indicated in the troposphere. The calculations were terminated at the tropopause because the theory is only applicable to the troposphere as above this level l^2 does not vary exponentially so the linearised wave equation does not transform to a Bessel equation such as used in the troposphere.

The amplitudes given by the theory bear little relationship to the observed wavelengths as they are calculated by assuming an idealised mountains. For a complex range of mountains such as the Southern Alps this is completely unrealistic. The importance of the forcing of the mountain is shown very clearly by the SPB's. On the days when the layer models were applied with some success the natural waves that were solutions of the model which were not close to a forcing wavelength in the mountain profile were not in general found in the airflow to the lee of the mountain. Often the forcing wavelengths did not appear in the SPB profile showing that they were not near to a natural wavelength of the airflow.

5. Survey of the Winds over Canterbury during 1970

The survey was carried out using the midday radar wind balloon sounding from Harewood and showed that there were significant periodicities in the wind directions in the troposphere and stratosphere and in the wind speeds. The mean flow in both the troposphere and the stratosphere was centred on the westerly direction because New Zealand is situated in the mid-latitude zonal westerlies.

The monthly distribution of the occurrence of nor'westers over the year showed two maxima separated by six months. These were in February-March and in August-September and correspond to the equinoxes.

A periodicity of period approximately 7 days, with multiples and submultiples of 7 days, was found in the power spectra, along with several other shorter periods. This was caused by the passage of cyclones and anticyclones across the country in the low troposphere which at higher levels correspond to the roughs and ridges of smoother planetary waves.

6. An Empirical Wave Classification for Predicting the Occurrence of Waves over North Canterbury from the Radar-wind Profile

A means of predicting the scale and occurrence of lee waves over Christchurch and North Canterbury using the radar

wind profile from Harewood was derived using the profiles from radiosonde released at midday from Harewood during 1970. The parameters used in the prediction are the mean tropospheric wind direction and speed and the wind speed at the 800 mb standard level. These are available every six hours from a radar wind sounding balloon. Thus an up to date check can be made on the conditions likely to be experienced in the approach of aircraft to land at Christchurch International Airport (Harewood) during Nor'westerly winds.

The prediction is made by plotting these wind speeds against the mean tropospheric wind direction on diagrams such as shown in Figures 1.8 and 1.9. The position of the point plotted relative to the critical curves gives an indication of the scale of wave motion likely to be present in the airflow.

All large waves observed were produced when the wind over Christchurch had flowed over the Craigieburn and Torlesse or the Puketeraki mountain ranges, that is, when the mean tropospheric wind direction was between 290^{o} and 340^{o}. In addition the wind speed at the 800 mb level was in excess of 10 m sec^{-1} and the mean tropospheric wind speed was greater than 15 m sec^{-1}. The very large waves occurred in association with mean tropospheric wind speeds in excess of 20 m sec^{-1}. The critical velocities increase as the wind

direction varies away from 310°. In all cases the 800 mb wind speed was exceeded by the mean tropospheric wind speed. Thus the method is consistent with the 'Scorer Criteria'. The wind direction must be within less than 30° of the direction perpendicular to the mean direction of the Alps and the velocity must increase with height resulting in a decrease in l^2 with height.

APPENDIX A

Satellite Photographs of Selected Nor'west Days

The following photographs were taken by the ESSA 6, ESSA 8, ITOS 1 and Nimbus 3 satellites on northwest days over the period November 1969 to October 1970. The approximate position and extent of the Southern Alps is shown by a blue line extending from about 174°E, 41°S to 168°E, 45°S.

Fig. A.1: 0857 10/11/69 The mean tropospheric wind direction was 305°. Large amplitude waves were evident in the midday radiosonde profile from Harewood (172°32'E, 43°29'S). The photograph shows a gap in the clouds to the lee of the Alps over North Canterbury and an arch. Waves with an approximate wavelength of 12 km were evident in the south of the South Island.

Fig. A.2: 0858 14/1/70 Waves were evident to the lee of the North Island and to the North of the South Island of wavelength about 15 km. Balloon 14C2 was released from Cass at 0830 and a wavelength of 15 km was found in the power spectrum of the flight to the lee of the mountains and in the mountain profile.

Fig. A.3: 1210 14/1/70 This was taken later on the same day as the above photograph. Because of an altitude error it was not gridded. The cross shown corresponds to the centre of the original photograph which was at 176.6°E, 41.05°S, which is about Castlepoint on the SE coast of the North Island. The large waves were being produced by the Tararua and Ruahine Ranges. The wavelength was about 23 km. The midday radiosonde from Harewood showed a 20 km wavelength.

Fig. A.4: 0919 16/6/70 Waves were visible over the mountains in the North and South Islands and to the lee of the Tararua and Ruahine Ranges. The wavelength of the waves to the north of the South Island was about 10 km. An interesting feature is the cloud vortex to the SE of the South Island indicating a depression.

Fig. A.5: 0959 28/6/70 The mean tropospheric wind direction was 339° at midday, fairly well round to the north as is indicated by the clouds in the photograph. Note the break in the clouds to the lee of the Southern Alps and the arch even with the wind well away from the north west.

Fig. A.6: 1200 23/7/70 The picture was not gridded because of a height error. Good waves were produced to the lee of the Tararua and Ruahine Ranges (wavelength about 20 km) and in the lee of the north of the South Island, probably from the Kaikouras. Of interest to the glider

pilots who wish to attain a long distance record flight is the wave form extending across Cook Strait. There was an interesting decrease in wavelength towards the north in the waves to the lee of the North Island. Relative positions can be seen by referring to the next Figure which is a photograph taken four hours later.

Fig. A.7: 1600 23/7/70 Waves are evident over the Southern Alps and over and to the lee of the North Island. These latter waves had a wavelength of approximately 14 km. Hence it has decreased from the 20 km observed at midday.

Fig. A.8: 1532 4/8/70 Extensive waves are evident over and to the lee of the South Island. The wavelength in the middle of the South Island was about 13 km.

Fig. A.9: 1625 15/10/70 Waves are evident between North Canterbury and the central North Island. The major wavelength present was about 11 km. Balloon 45H12 was released from Hokitika at 0700 and experienced large waves of between 11 and 12 km.

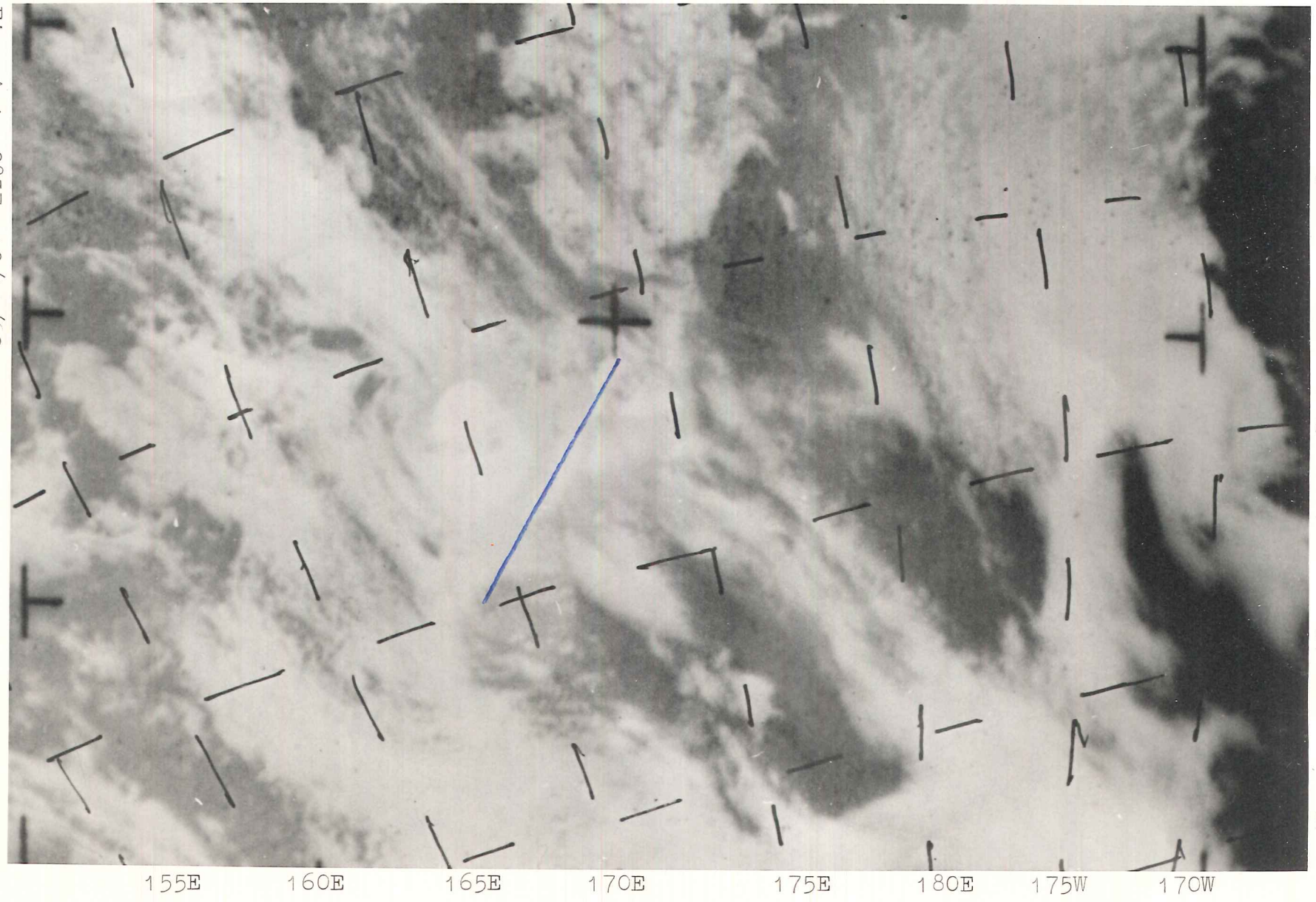

Fig: A.1: 0857 10/11/69

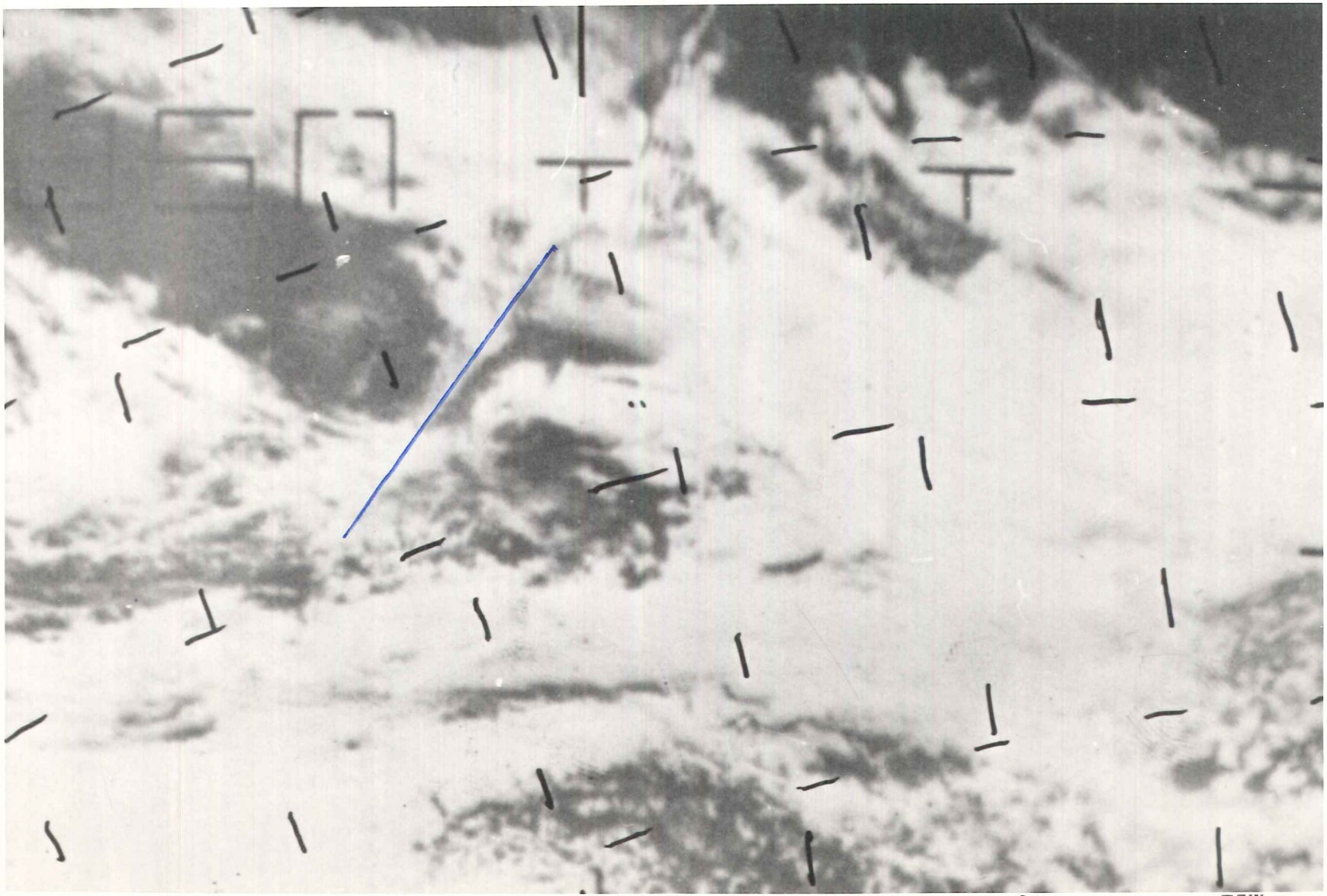

Fig A.2: 0858 14/1/70

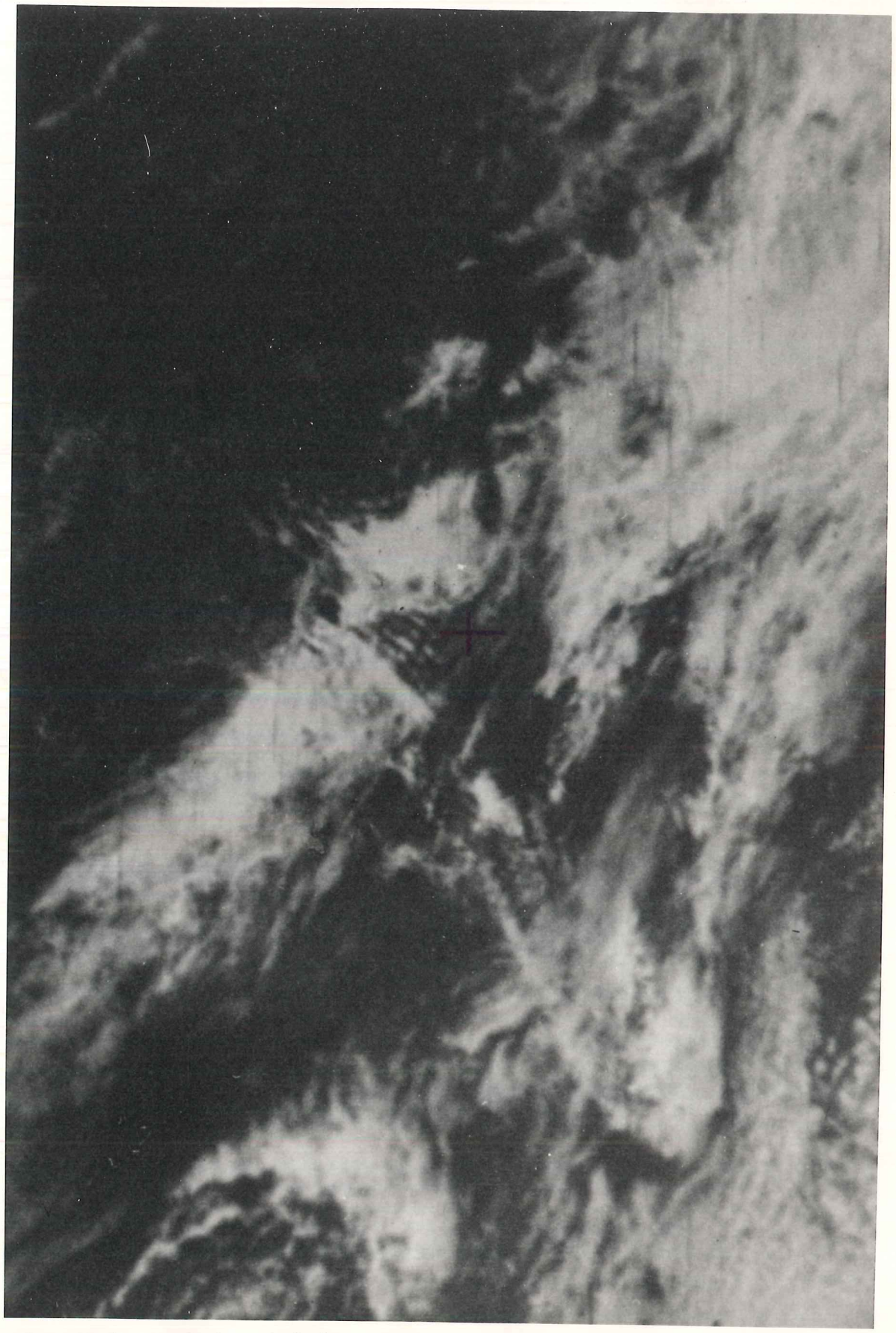

Fig A.3: 1210 14/1/70

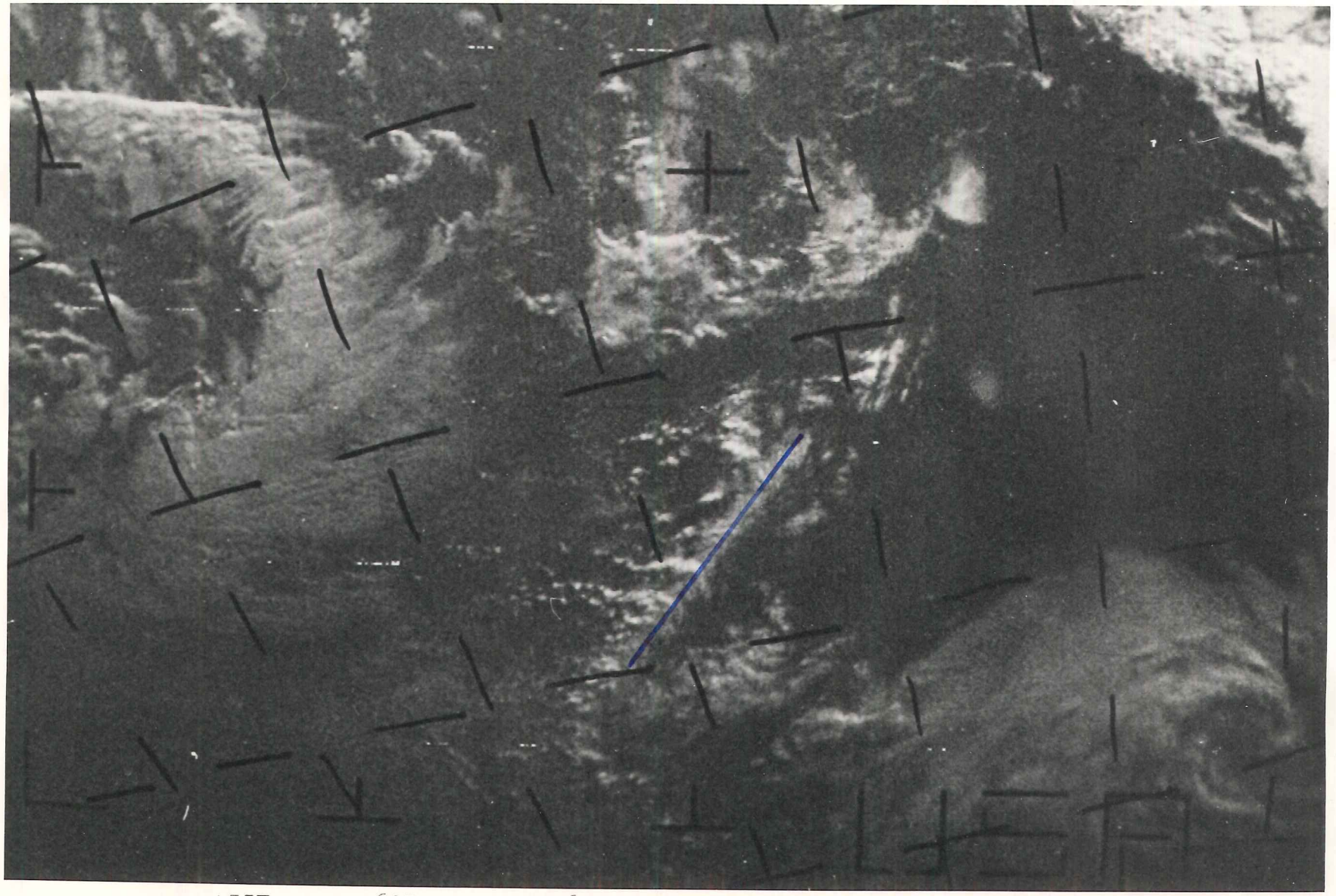

Fig A.4: 0919 16/6/70

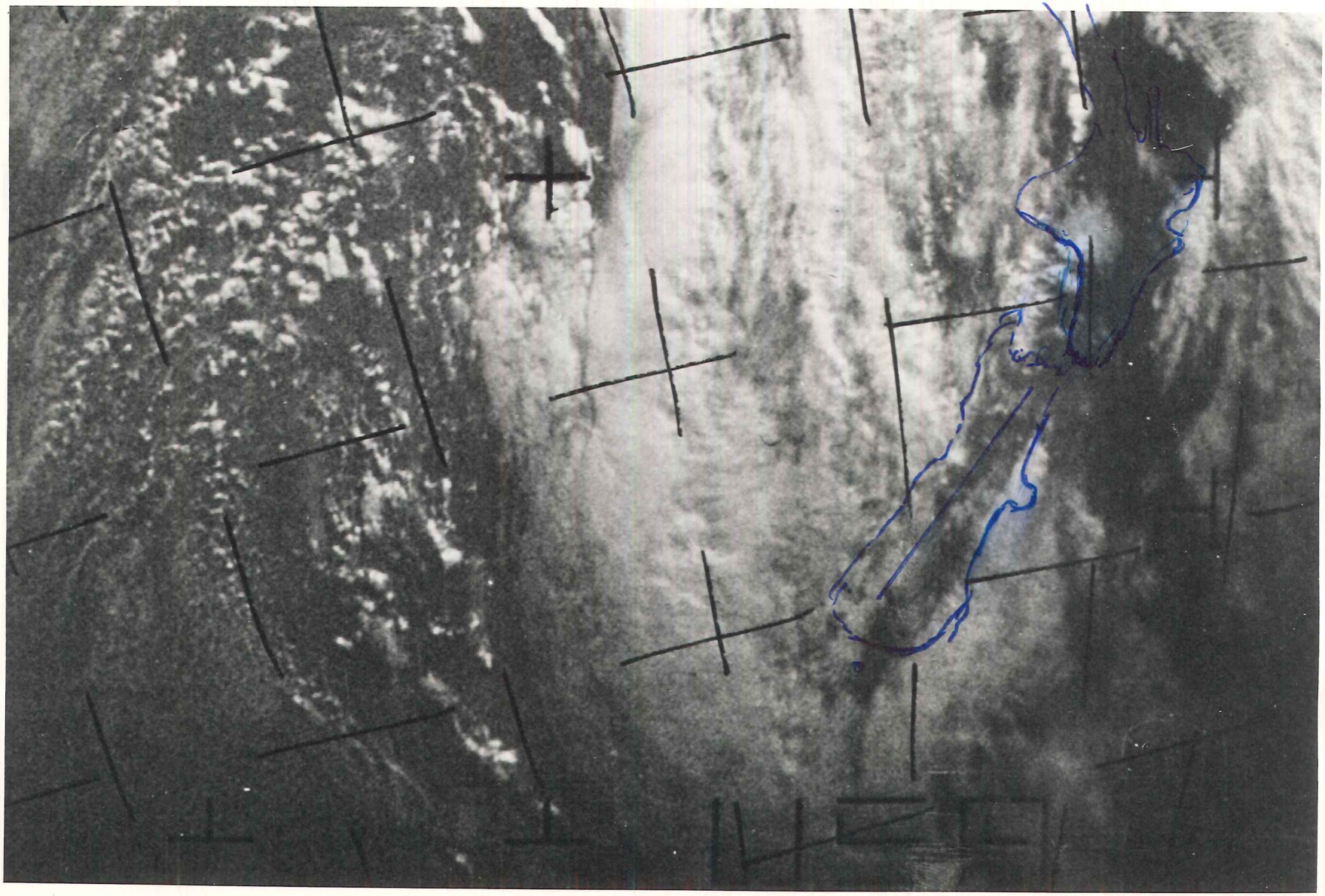

Fig A.5: 0959 28/6/70

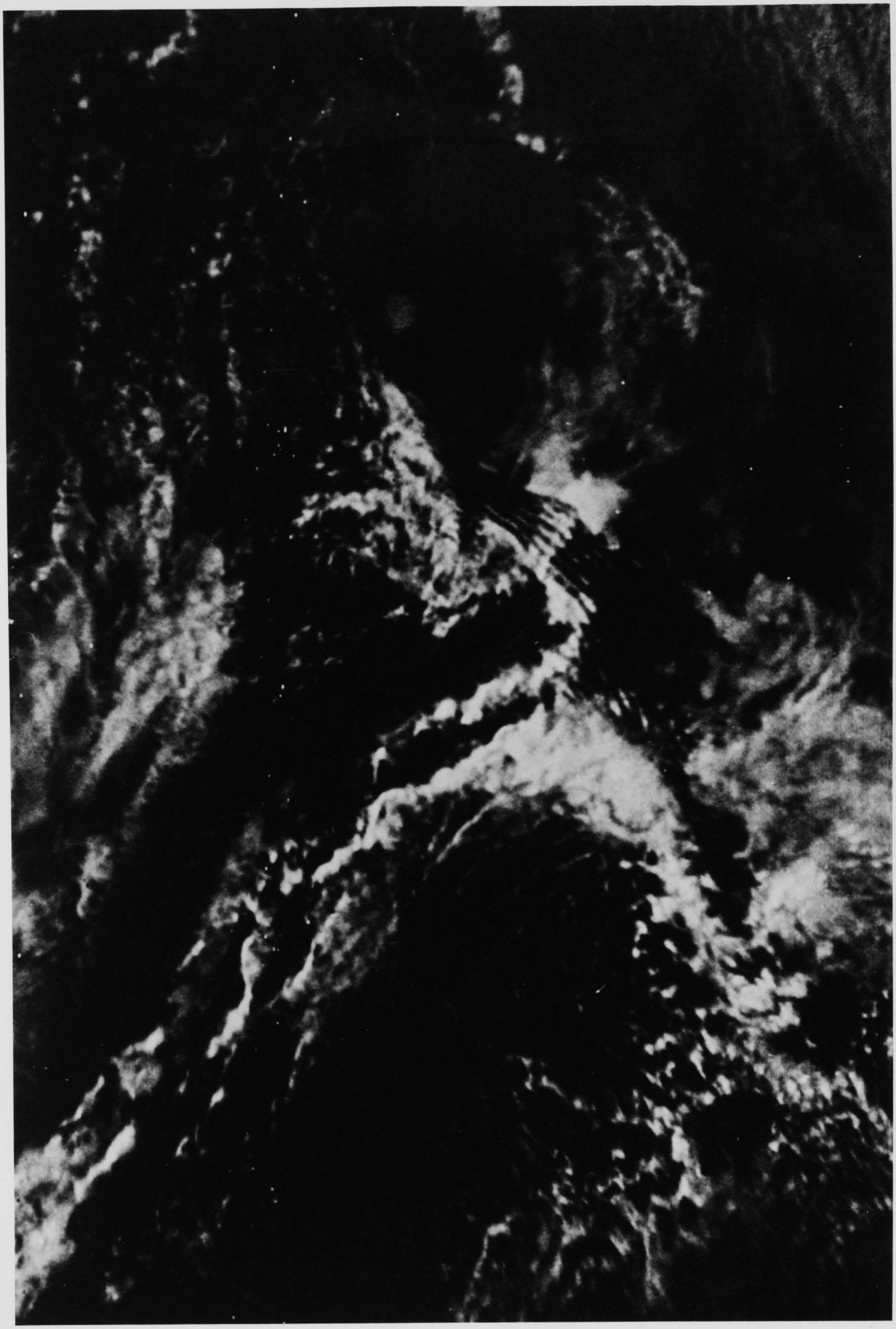

Fig A.6: 1200 23/7/70

Fig A.7: 1600 23/7/70

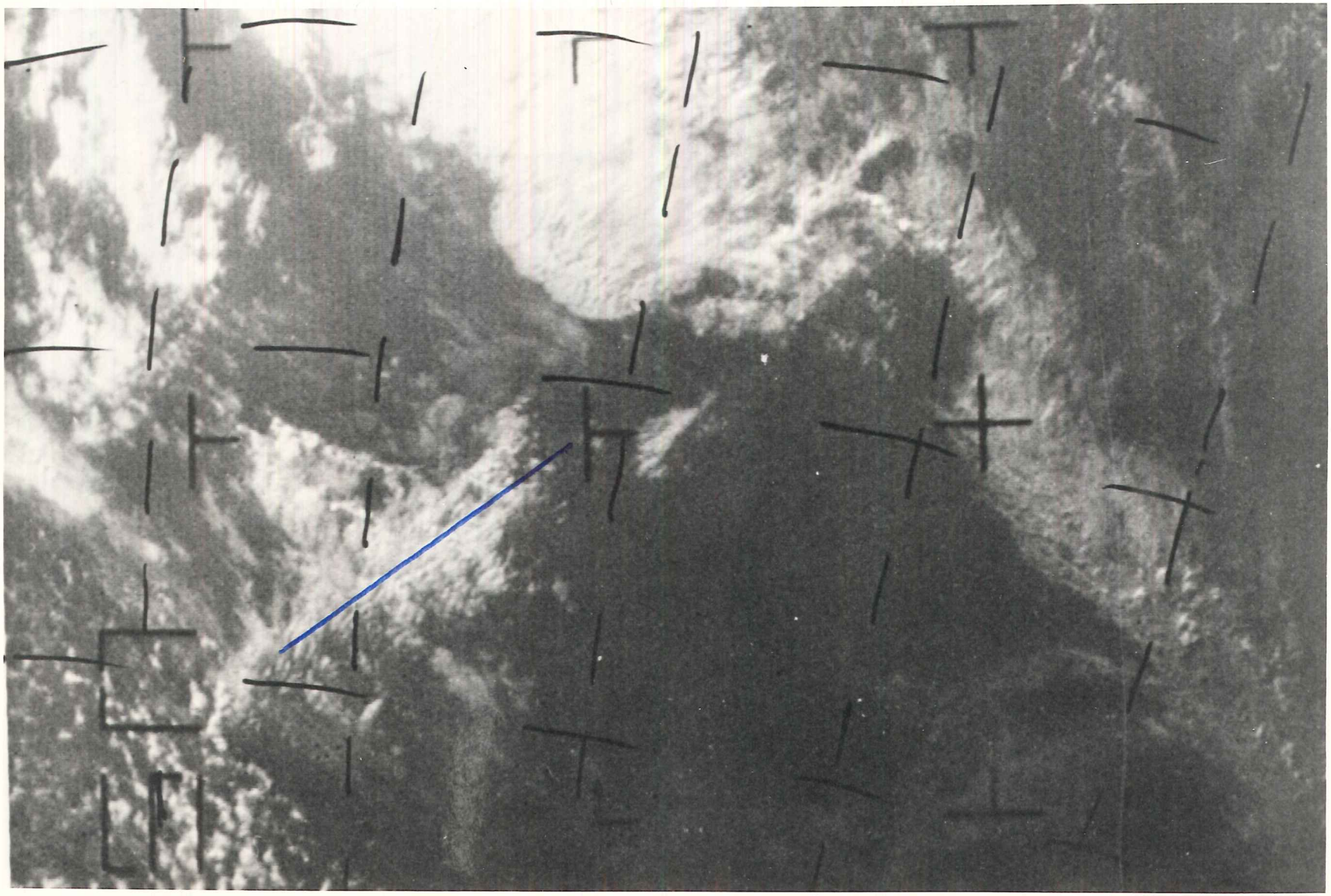

Fig A.8: 1532 4/8/70

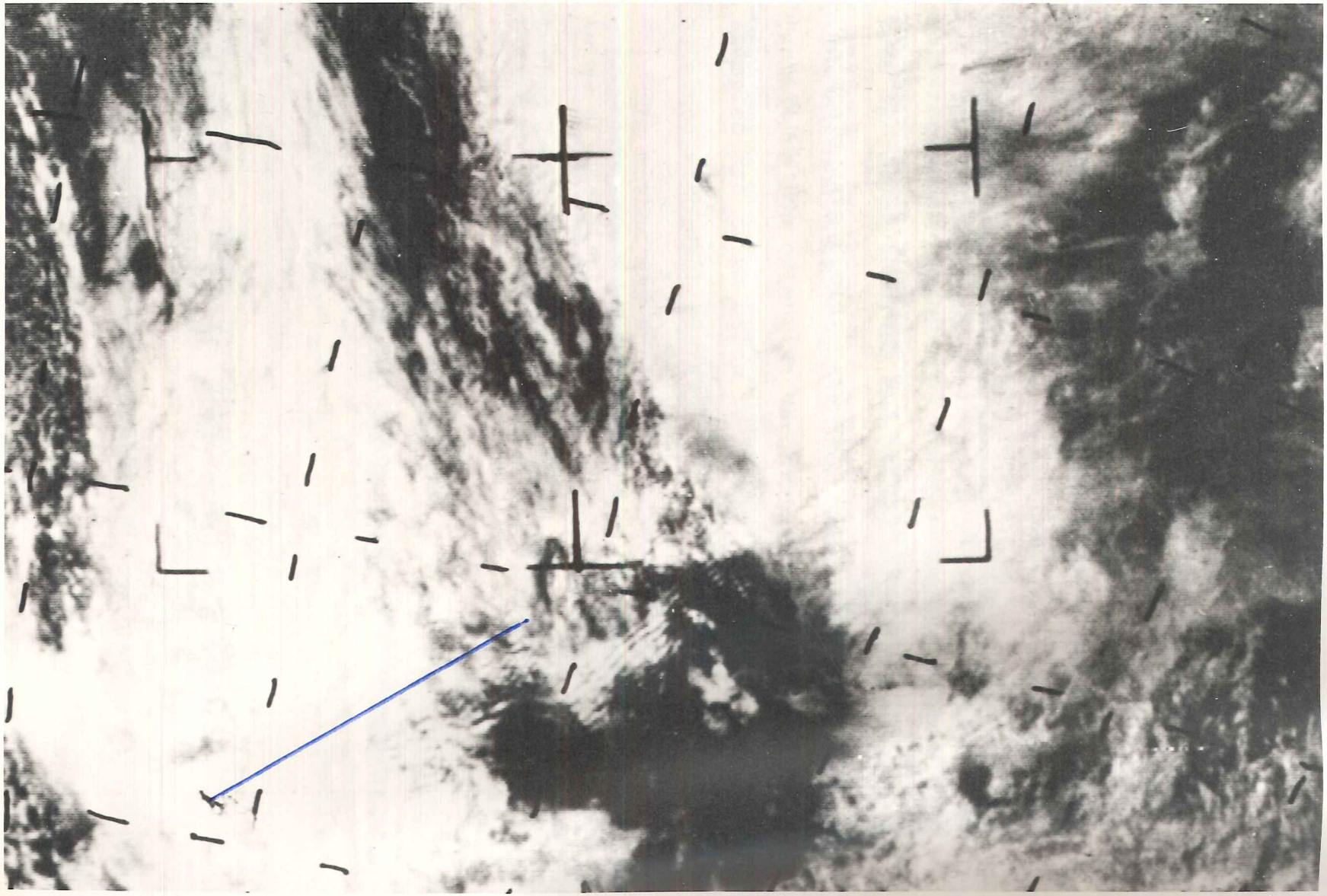

Fig A.9: 1625 15/10/70

APPENDIX B

A Numerical Method for Solving the Wave Equation

The following method was used to obtain solutions to the wave equation with arbitrary wind and mountain profiles. Initially it was intended to make wide use of this type of solution as it is far less restrictive in its assumptions than the layer theories and provides a visual solution for the whole wave field. However, due to limited computing facilities its extensive use was impracticable. Some examples are given below to illustrate the type of solution obtained with what was available.

The method was applied to solve the wave equation in terms of the displacement of the streamline from its undisturbed level (ζ), namely

$$M(z)\frac{\partial^2\zeta}{\partial x^2} + \frac{\partial^2\zeta}{\partial z^2} + A(z)\frac{\partial\zeta}{\partial z} + B(z)\zeta = 0 \qquad (B.1)$$

$M(z)$ is very close to unity low in the atmosphere.

$$A(z) = 2\frac{U'}{U} - \beta$$

and (B.2)

$$B(z) = \frac{g\beta_1}{U^2} - \frac{U'}{U}\left(\frac{M'(z)}{M(z)} - \frac{g}{c^2}\right) - 2\frac{U'^2}{c^2}$$

which is approximately $B(z) = \frac{g\beta_1}{U^2}$.

The finite difference form of (B.1) for a point (i,j) corresponding to (x,z) on a square grid of spacing Δ is

$$\frac{1}{\Delta^2}\left[D(i\pm1,j) + D(i,j\pm1) - 4D(i,j)\right] + \frac{A(z)}{2\Delta}\left[D(i,j+1) - D(i,j-1)\right]$$

$$+ B(z)\, D(i,j) = 0 \qquad \text{(B.3)}$$

Hence the approximate relationship between the displacement at any point and the displacements at the points around it as given by the finite difference form of the wave equation is

$$D(i,j) = \frac{1}{\frac{4}{\Delta^2} - B(z)} \left\{\frac{1}{\Delta^2}\left[D(i\pm1,j) + D(i,j\pm1)\right] + \frac{A(z)}{2\Delta}\left[D(i,j+1) - D(i,j-1)\right]\right\} \qquad \text{(B.4)}$$

Boundary conditions: It was assumed that the displacement is zero far upstream and far downstream from the mountain. The heights of the mountain profile were fed into the j = 1 row of the D array based on the assumption that the lower streamline follows the mountain profile. The simplest upper boundary condition was to assume that the displacement is zero at some large height. It was suggested by Pekelis (1969) that this boundary condition could be justifiably used if the boundary was above 40-60 km. A rigid upper boundary is probably a good approximation if the boundary corresponds to the interface at the base of the very stable stratospheric layer which is often observed, as was the case

for the bounded two layer theory. (For this reason the upper boundary was placed at 20 km.) Each calculation of D over the whole array is known as an iteration. Initially all the displacements were assumed to be zero except the lower boundary. The values of D may then be calculated using (B.4). The effect of the mountain will enter the displacement array as calculations are done for D in the region of the mountain. After successive iterations if the method is convergent the values of D over the array will settle down and approach the solution of the wave equation (B.1).

If the value of the displacement at the point (i,j) for the k^{th} iteration is D'(i,j) then in the $(k+1)^{th}$ iteration the displacement at this point, D(i,j), as calculated from (B.4), differs from the previously calculated value by R, the residual.

$$R = D(i,j) - D'(i,j)$$

Therefore

$$R = \frac{1}{4-B(z)} \left\{ \frac{1}{\Delta^2} [D(i\pm1,j) + D(i,j\pm1)] + \frac{A(z)}{2\Delta} [D(i,j+1) - D(i,j-1)] - (4 - B(z))\, D'(i,j) \right\} \quad (B.5)$$

The new value of D(i,j) in each iteration may be found by calculating the residual and adding it to the previously calculated D(i,j), i.e.

$$D(i,j) = D'(i,j) + R \quad (B.6)$$

This is in the form of a Gauss-Seidel Iteration.

The method may converge faster if a greater proportion of R is added to give the new value of D(i,j), i.e.

$$D(i,j) = D'(i,j) + \omega R \qquad (B.7)$$

where ω is known as the relaxation parameter and lies approximately in the range $1 < \omega < 2$. (B.7) is in the form of an Extrapolated Liebmann iteration.

The simple method outlined above was sometimes found to be unstable, particularly in the region of the mountain. This instability was removed by the use of a more complex residual formulation taking the residual at a point as a linear combination of the residuals at the point and the four points around it. Let

$$\begin{aligned} C_0(z) &= \frac{4}{\Delta^2} - B(z) \\ C_1(z) &= \frac{1}{\Delta^2 C_0(z)} \\ C_2(z) &= \left(\frac{1}{\Delta^2} - \frac{A(z)}{2\Delta}\right) / C_0(z) \\ \text{and} \qquad C_3(z) &= \left(\frac{1}{\Delta^2} + \frac{A(z)}{2\Delta}\right) / C_0(z) \end{aligned} \qquad (B.8)$$

which are the coefficients of the D's in the expansion of the right hand side of (B.4). The residual is taken as

$$R = \frac{[R_{i,j} + C_1(j)(R_{i+1,j}+R_{i-1,j}) + C_2(j-1)R_{i,j-1} + C_3(j+1)R_{i,j+1}]}{1.0 + 2C_1(j)^2 + C_2(j-1)^2 + C_3(j+1)^2} \quad (B.9)$$

where the single point residuals have the form

$$R_{i,j} = C_1(j)\,[D(i+1,j) + D(i-1,j)] + C_2(j)\,D(i,j-1) + C_3(j)\,D(i,j+1) \quad (B.10)$$

An accuracy parameter (RMS) was used to give an indication of the convergence of the solution for successive iterations. It was defined as the square root of the ratio of the sum of the squares of the residuals to the sum of the squares of the displacements.

Example: Choosing the profiles used by Scorer (1949) Eq. (B.1) was solved numerically using the one and five residual formulas in Eqs (B.5) and (B.9,10), with $\Delta = 0.5$ km, i = 1,100 and j = 1,40.

Investigating the use of the single residual formula for this example showed that the RMS error increased after 10 iterations for $\omega \geq 1.2$. Fig. B.1 shows the RMS error of the single residual form after 10 iterations for a range of ω. The minimum was 0.139 for $\omega = 0.7$ and the rate of convergence was down to 4×10^{-3}/iteration.

The calculation times for this array were 2.2 sec/iteration for the single point residual form and 5.1 sec/iteration for the five residual form. Hence the latter took 2.3 times longer to calculate but the RMS error was down by a factor of 5.5 making it more efficient to this stage. It was found to be more efficient overall.

Taking $\omega = 1.6$ and using the five residual form it was found that after 100 iterations the RMS error was 2.22×10^{-3} (Fig. B.2) and after 200 iterations it was 0.83×10^{-3}. The calculation took about 17 mins. The rate of convergence is shown in Fig. B.3. It was about 7.7×10^{-5}/iteration after 100 iterations and about 5.3×10^{6}/iteration after 200 iterations. The solution is shown in Fig. B.4. It shows that the disturbance was significant above the mountain but it died away quickly downstream. Waves were evident in the numerical printout but they had very small amplitudes (about 3 m). Their wavelength was about 5.25 km compared to about 5.8 as given by Scorer. Their amplitude was increasing with each iteration at the rate of about 0.5 m/10 iterations after 200 iterations.

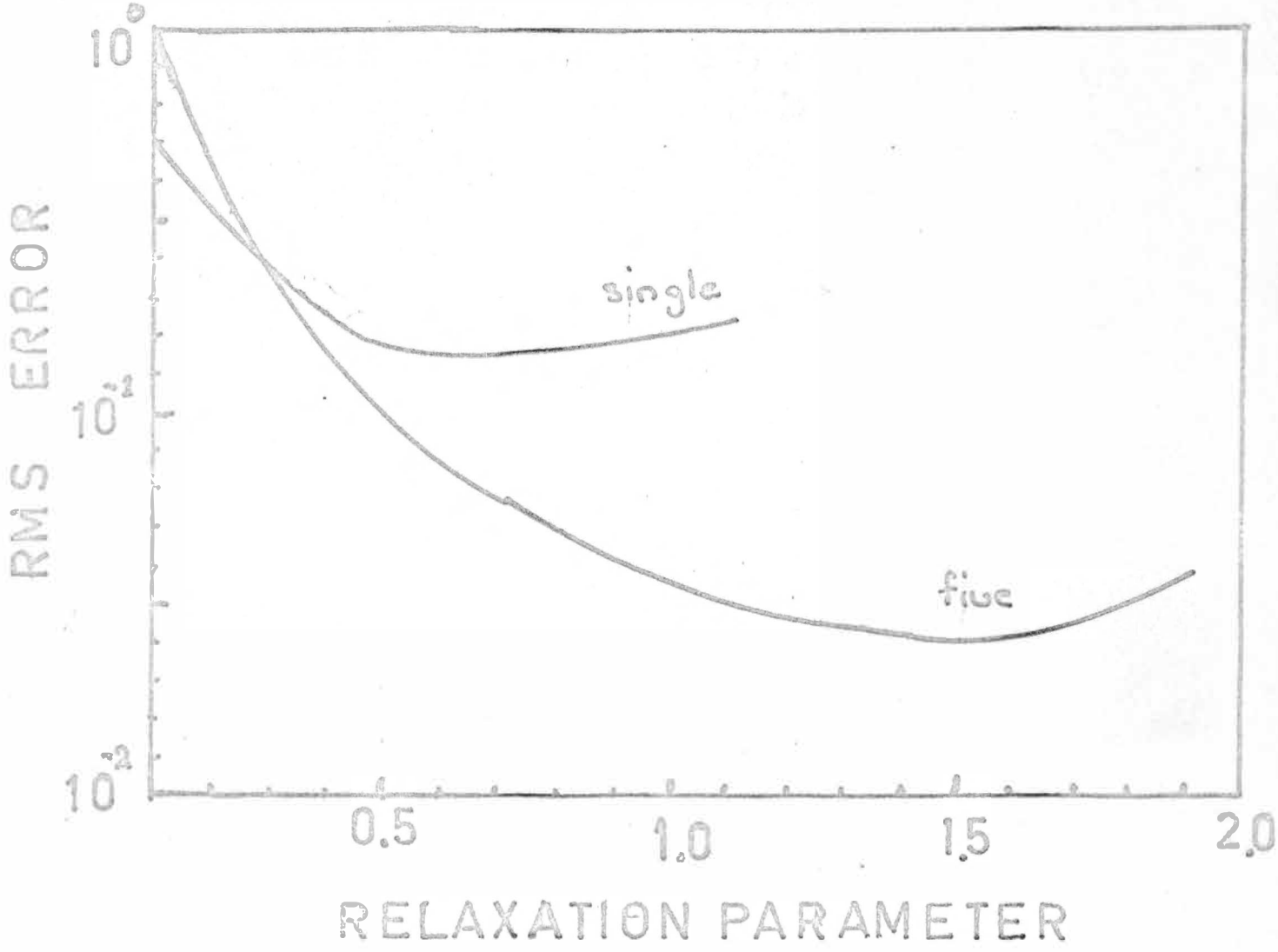

FIG B.1 : Single and five residual RMS errors as a function of the relaxation parameter.

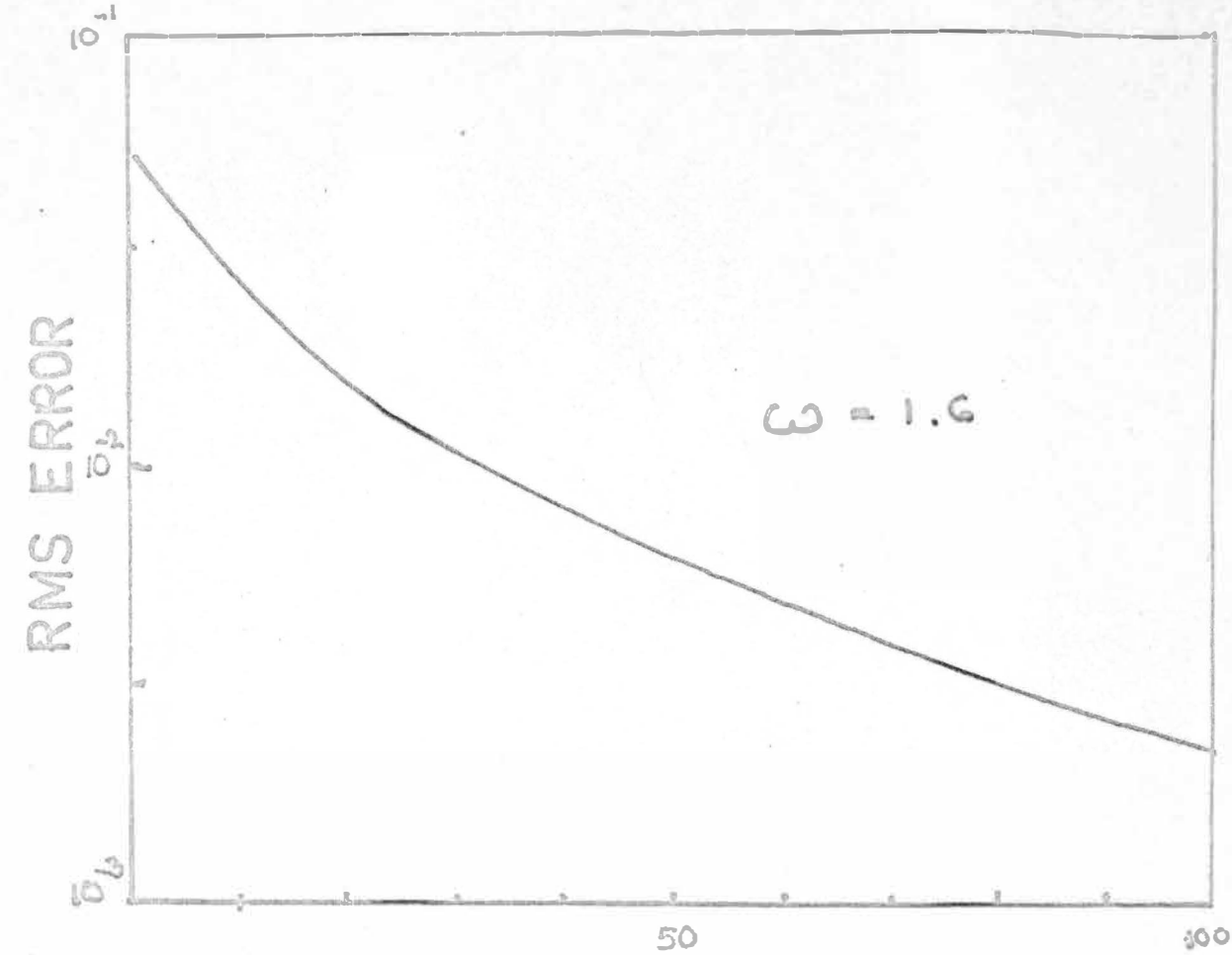

FIG B.2:
NUMBER OF ITERATIONS

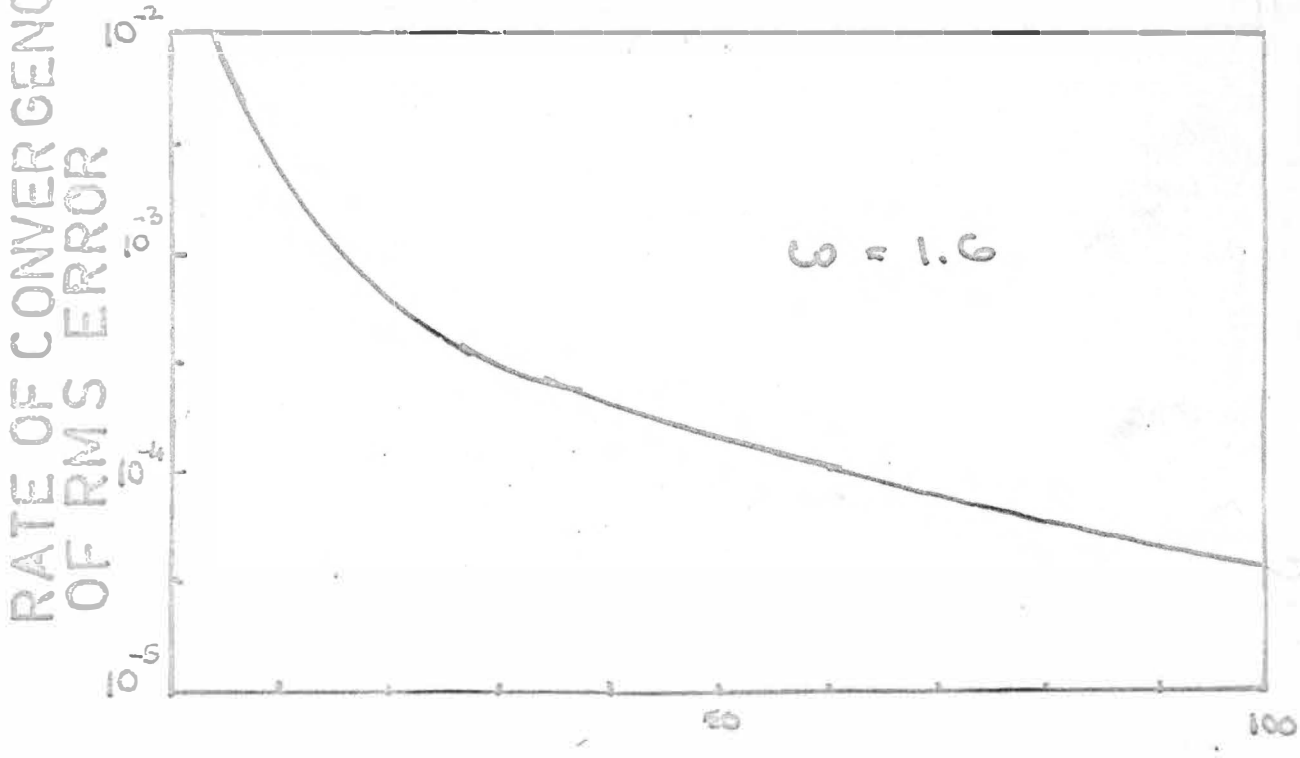

NUMBER OF ITERATIONS

FIG B.3:

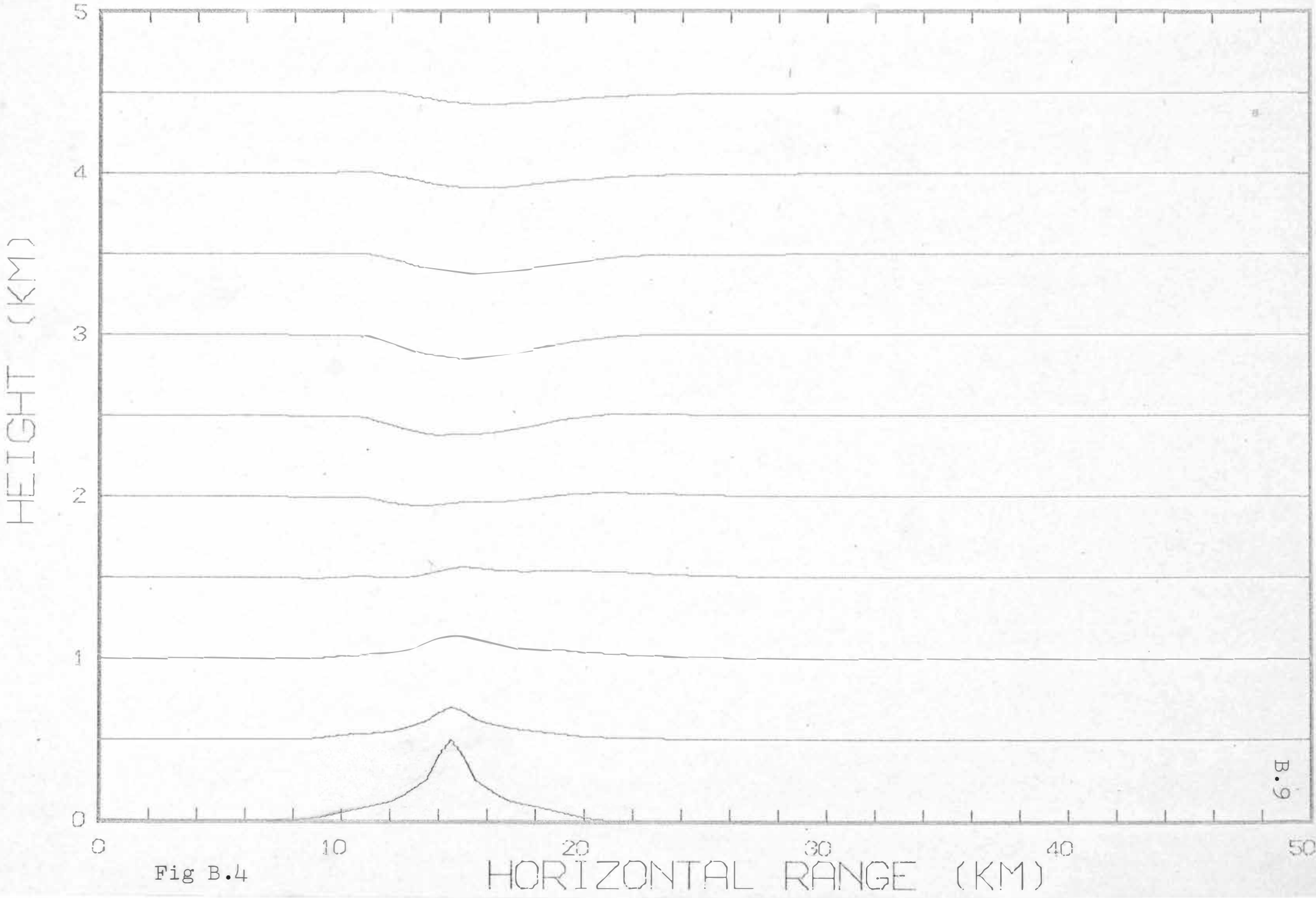

Fig B.4

Appendix C

Balloon profile diagrams:-

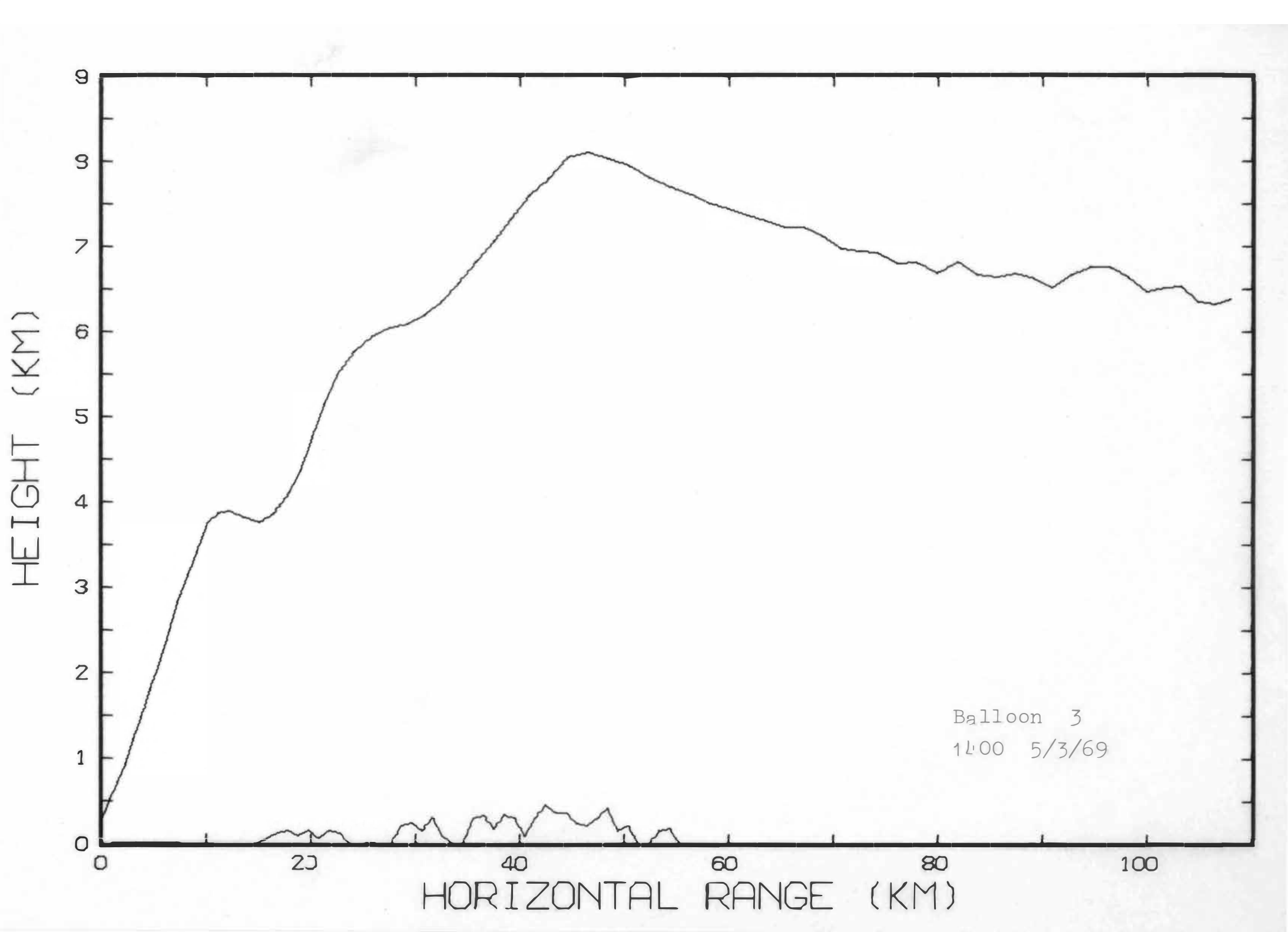
HEIGHT (KM)
0
1
2
3
4
5
6
7
8
9
0
20
40
60
80
100
HORIZONTAL RANGE (KM)
Balloon 3
1400 5/3/69

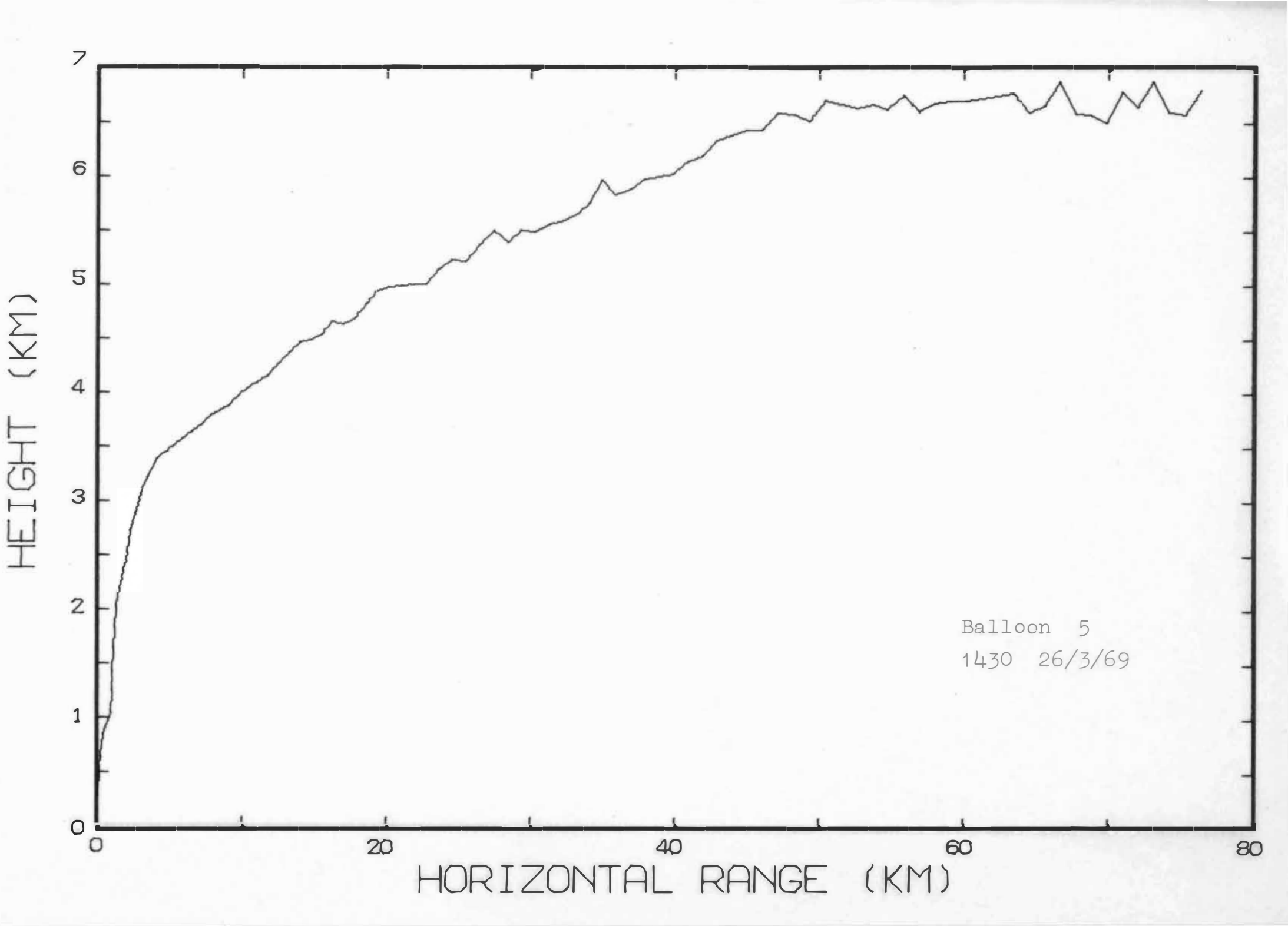
HEIGHT (KM)
0
1
2
3
4
5
6
7
0
20
40
60
80
HORIZONTAL RANGE (KM)
Balloon 5
1430 26/3/69

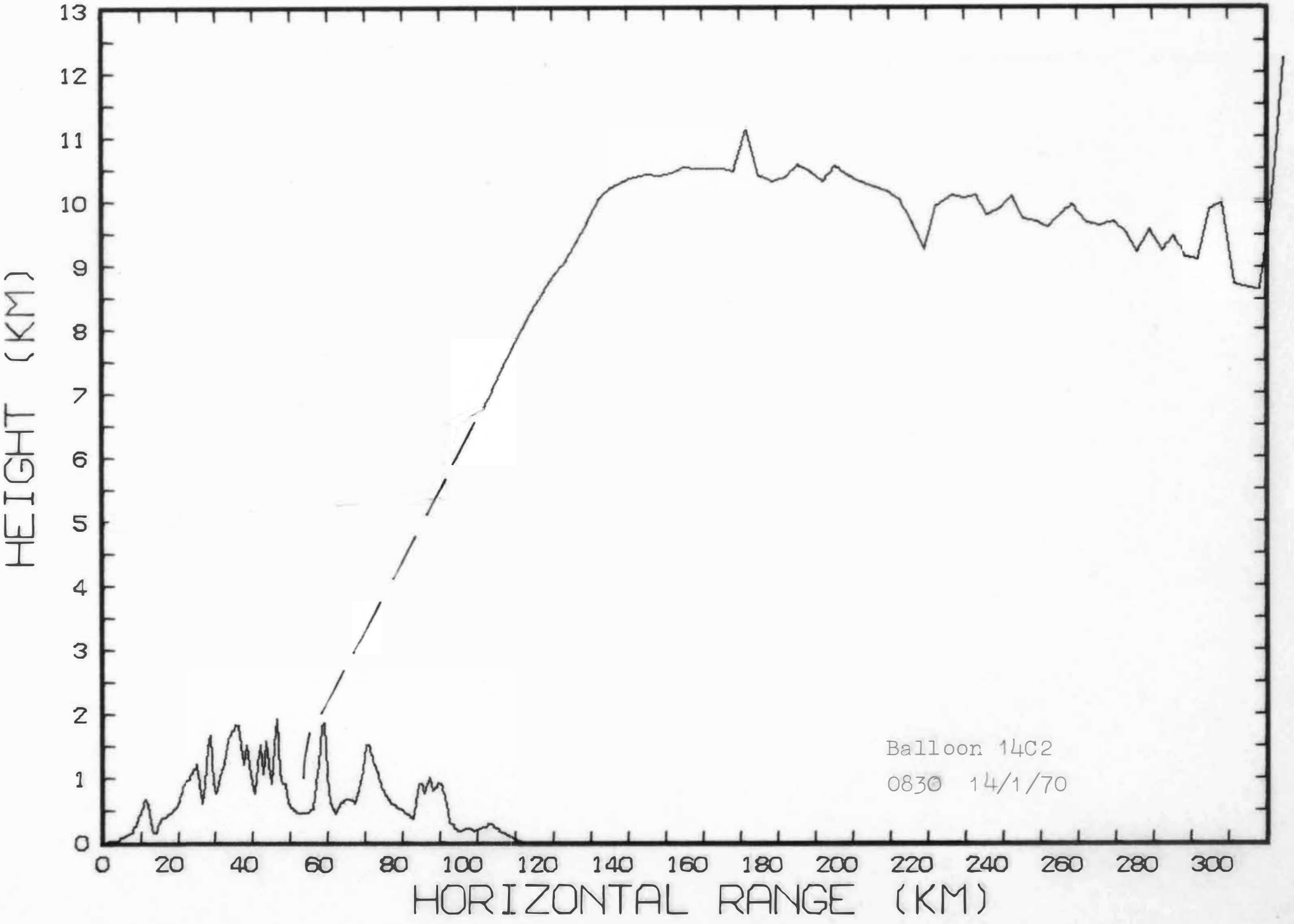
HEIGHT (KM)
0
1
2
3
4
5
6
7
8
9
10
11
12
13
0
20
40
60
80
100
120
140
160
180
200
220
240
260
280
300
HORIZONTAL RANGE (KM)
Balloon 14C2
0830 14/1/70

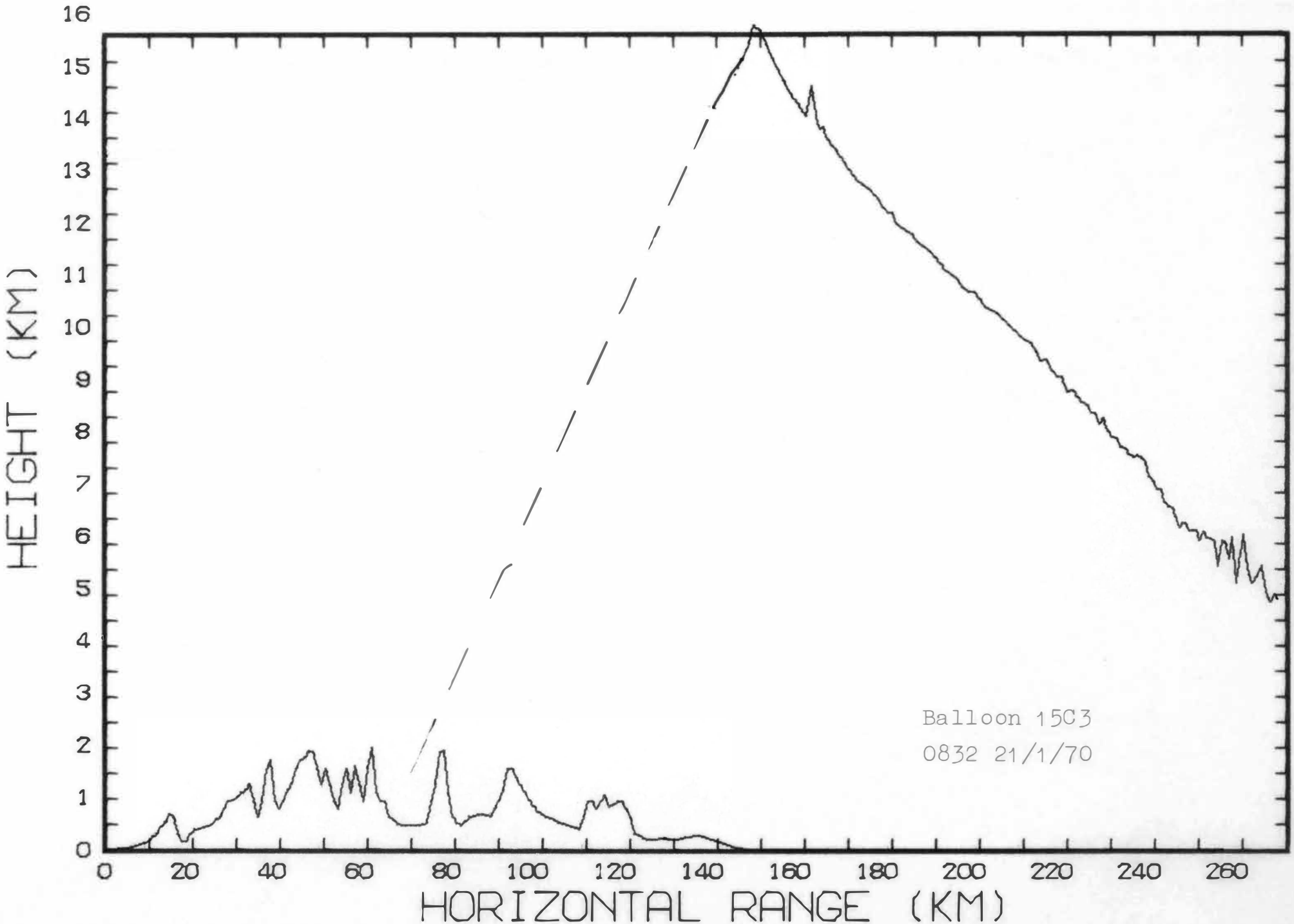
HEIGHT (KM)
0
1
2
3
4
5
6
7
8
9
10
11
12
13
14
15
16
0
20
40
60
80
100
120
140
160
180
200
220
240
260
HORIZONTAL RANGE (KM)
Balloon 15C3
0832 21/1/70

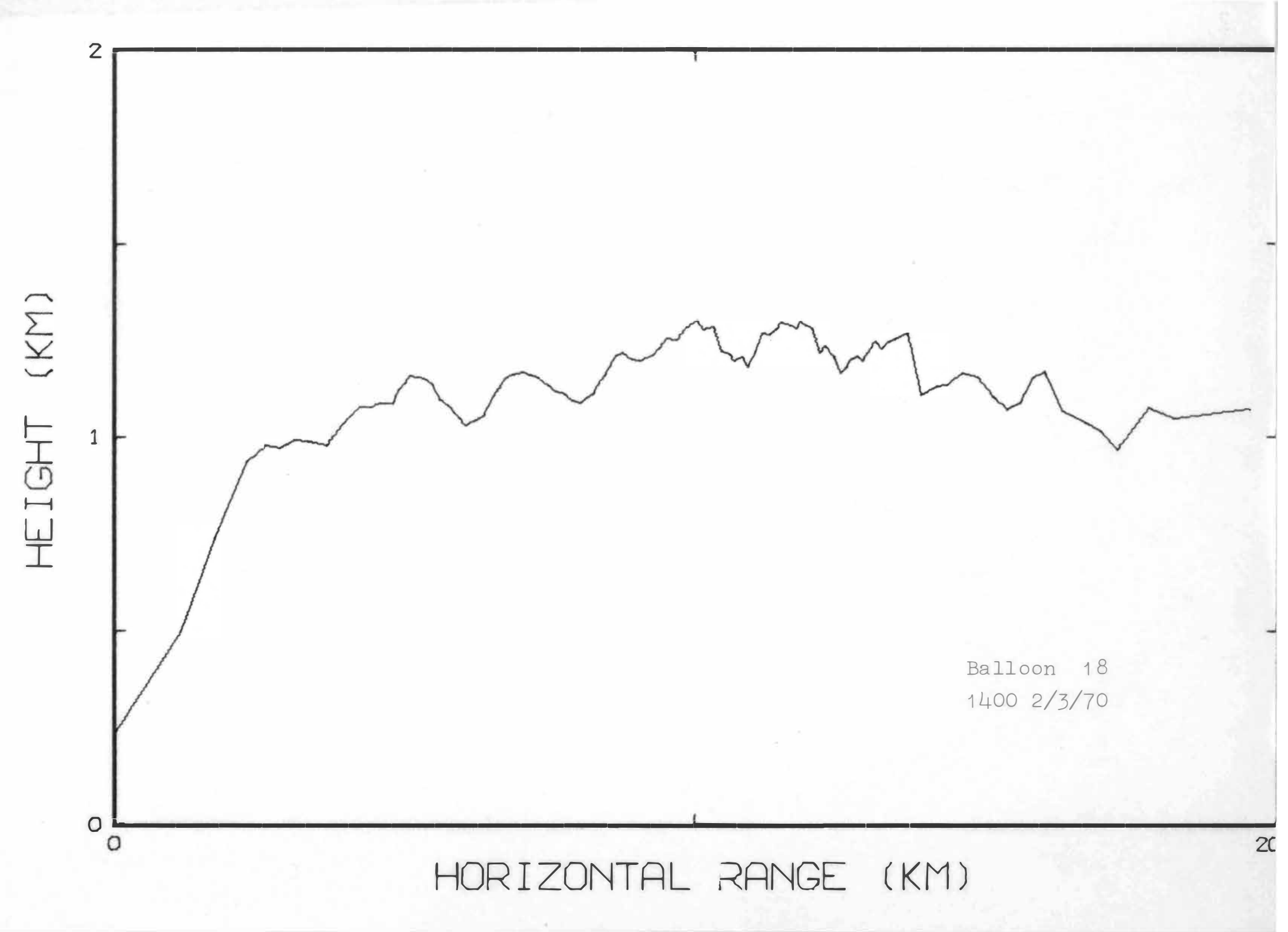
2
1
0
HEIGHT (KM)
0
20
HORIZONTAL RANGE (KM)
Balloon 18
1400 2/3/70

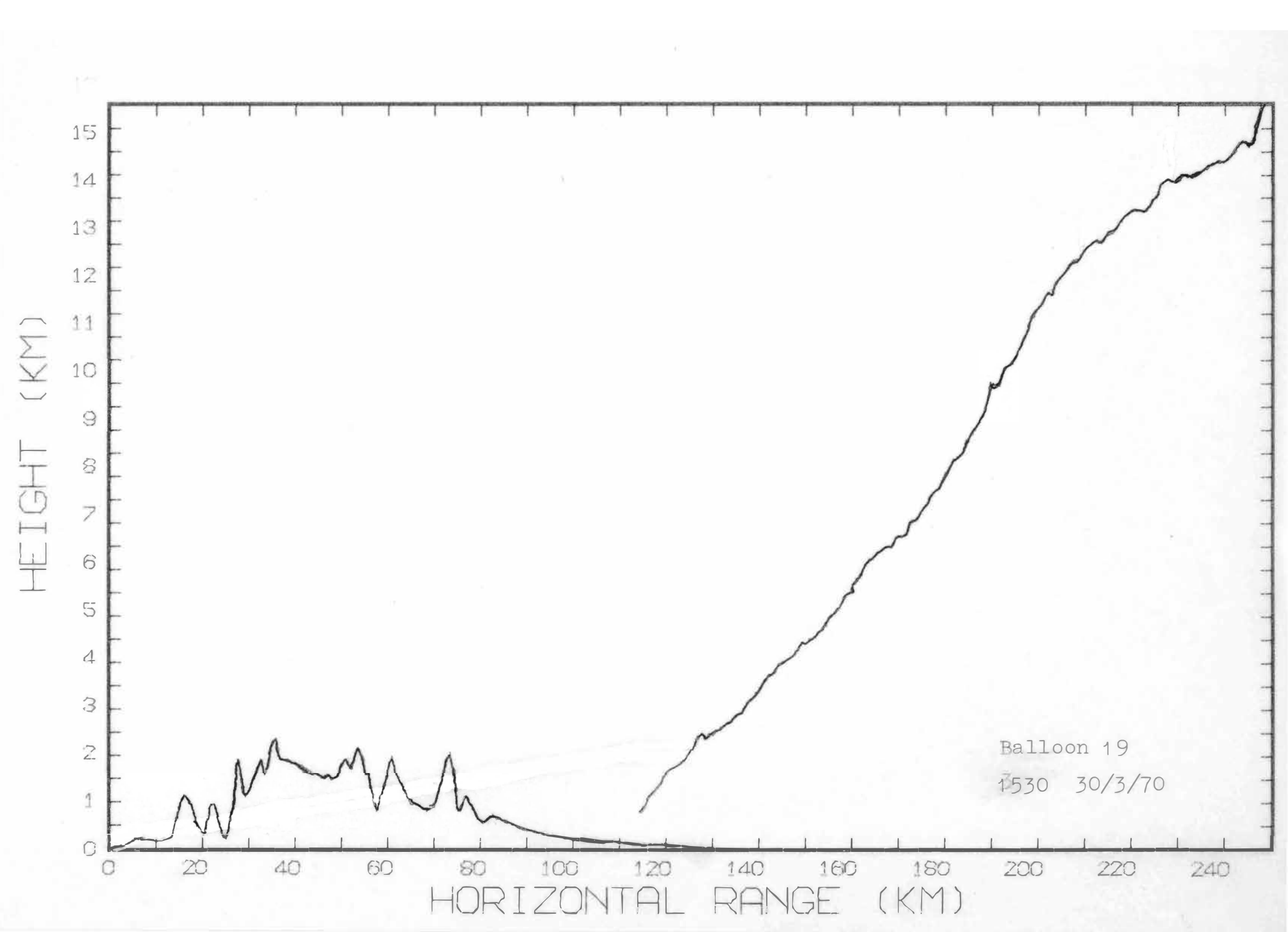
HEIGHT (KM)
0
1
2
3
4
5
6
7
8
9
10
11
12
13
14
15
0
20
40
60
80
100
120
140
160
180
200
220
240
HORIZONTAL RANGE (KM)
Balloon 19
1530 30/3/70

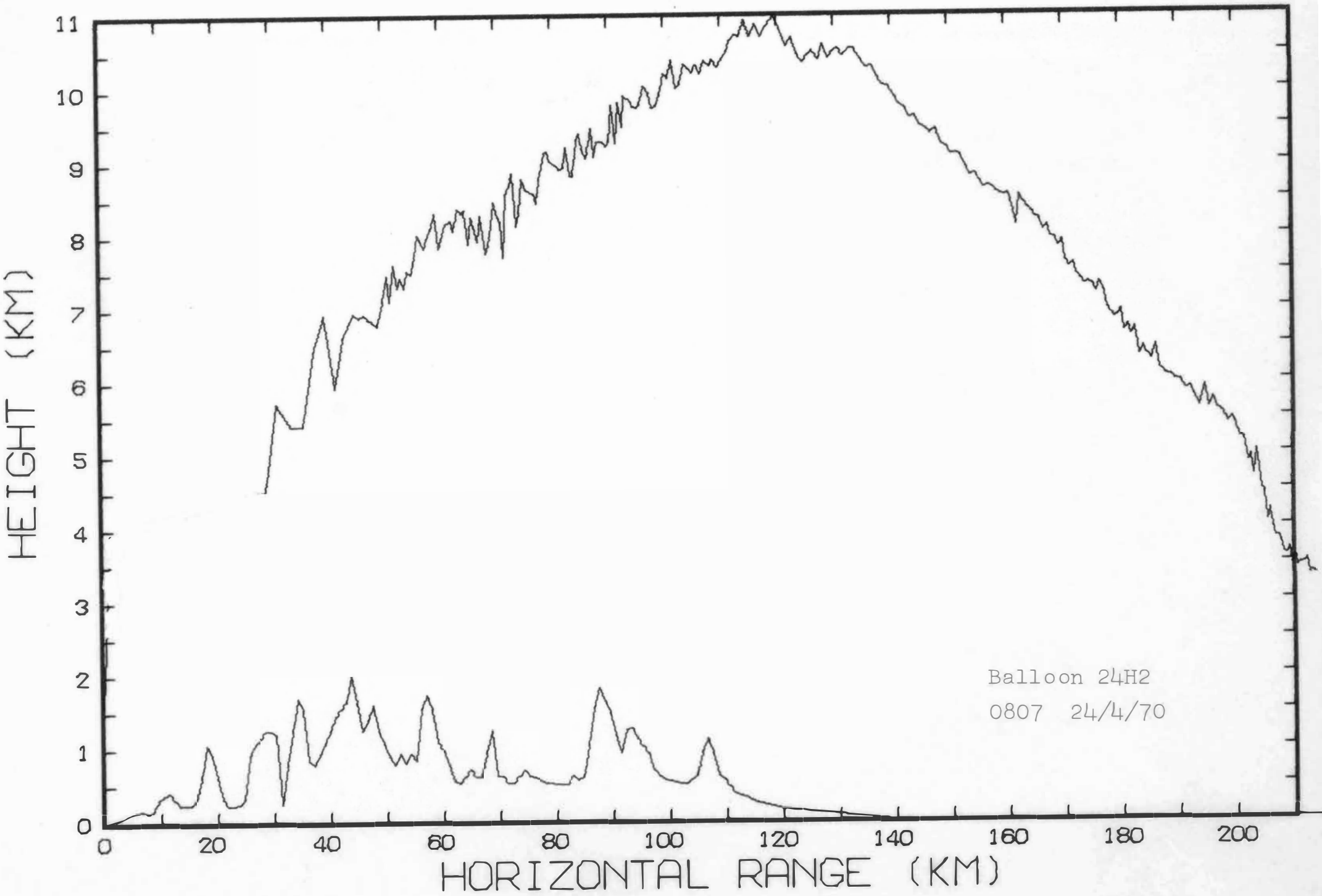
HEIGHT (KM)
HORIZONTAL RANGE (KM)
0
1
2
3
4
5
6
7
8
9
10
11
0
20
40
60
80
100
120
140
160
180
200
Balloon 24H2
0807 24/4/70

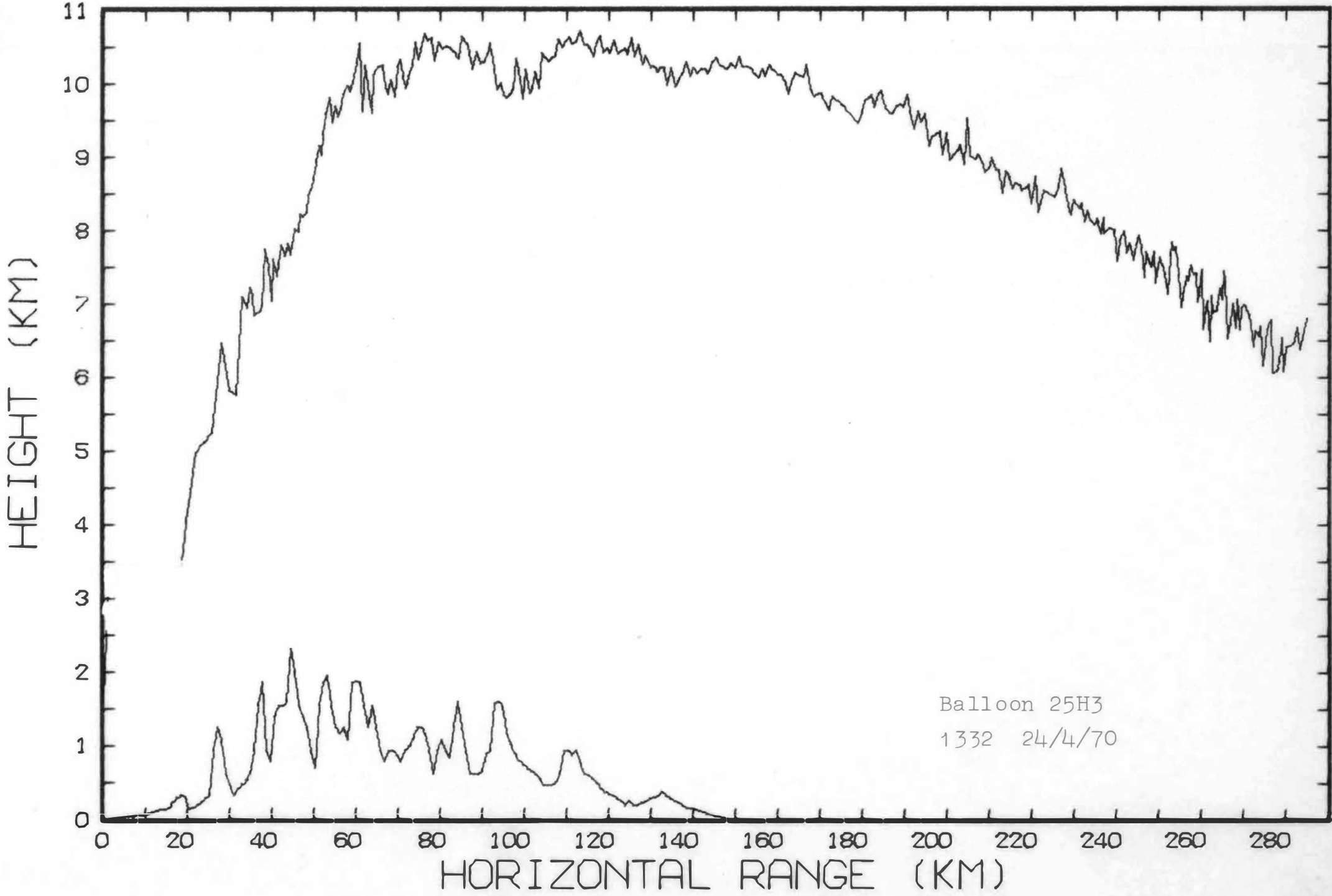
HEIGHT (KM)
HORIZONTAL RANGE (KM)
0
1
2
3
4
5
6
7
8
9
10
11
0
20
40
60
80
100
120
140
160
180
200
220
240
260
280
Balloon 25H3
1332 24/4/70

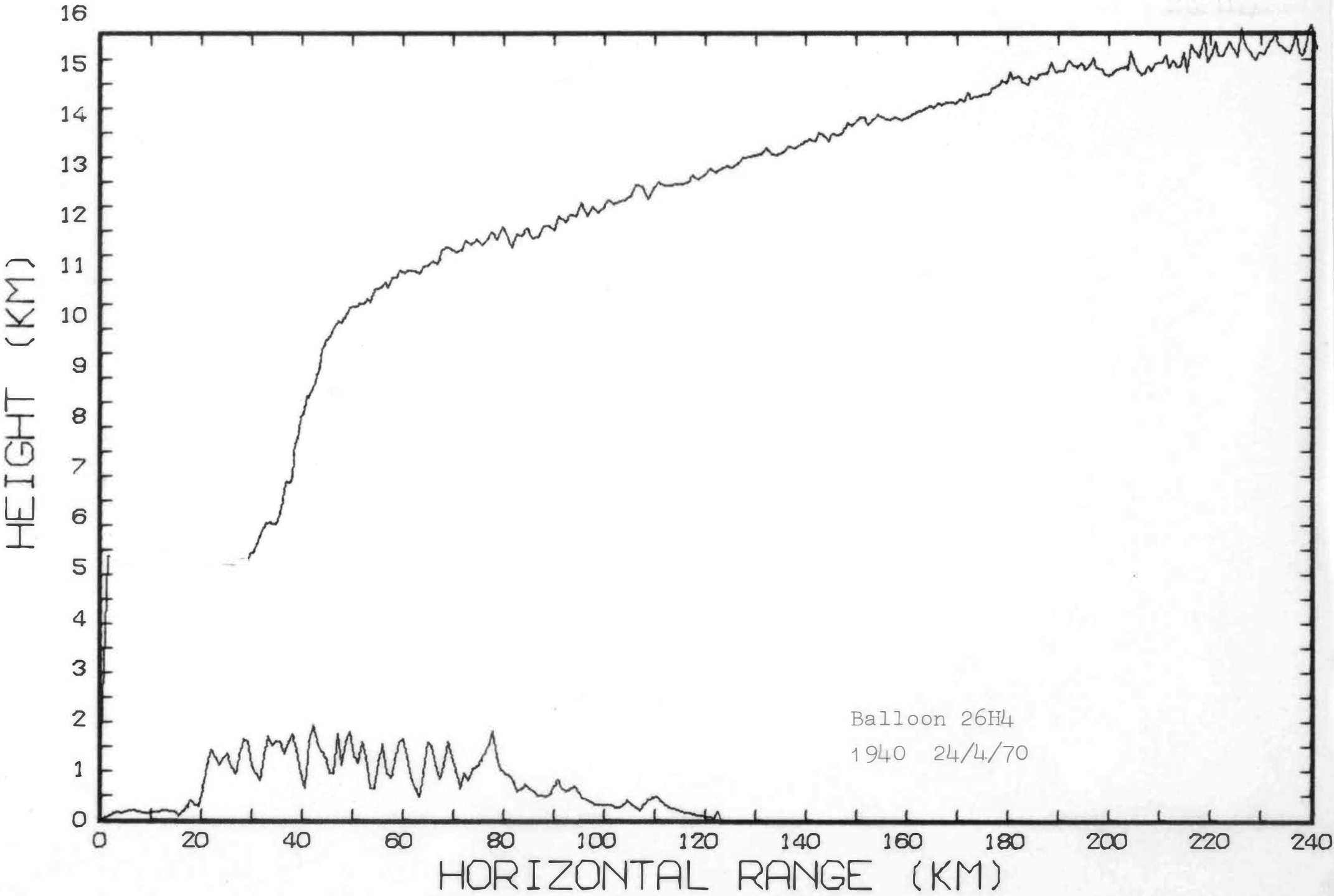
HEIGHT (KM)
0
1
2
3
4
5
6
7
8
9
10
11
12
13
14
15
16
0
20
40
60
80
100
120
140
160
180
200
220
240
HORIZONTAL RANGE (KM)
Balloon 26H4
1940 24/4/70

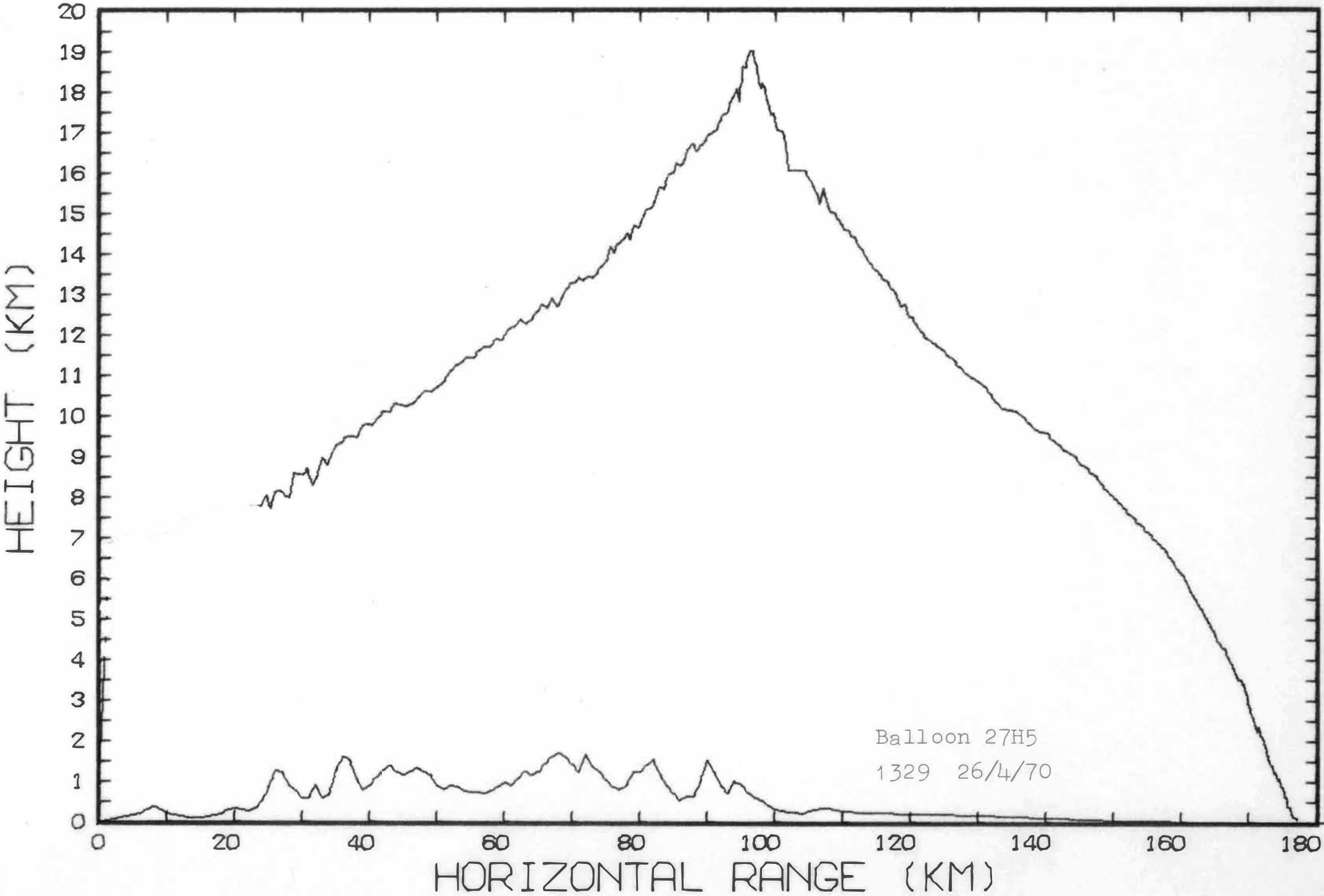
HEIGHT (KM)
0
1
2
3
4
5
6
7
8
9
10
11
12
13
14
15
16
17
18
19
20
0
20
40
60
80
100
120
140
160
180
HORIZONTAL RANGE (KM)
Balloon 27H5
1329 26/4/70

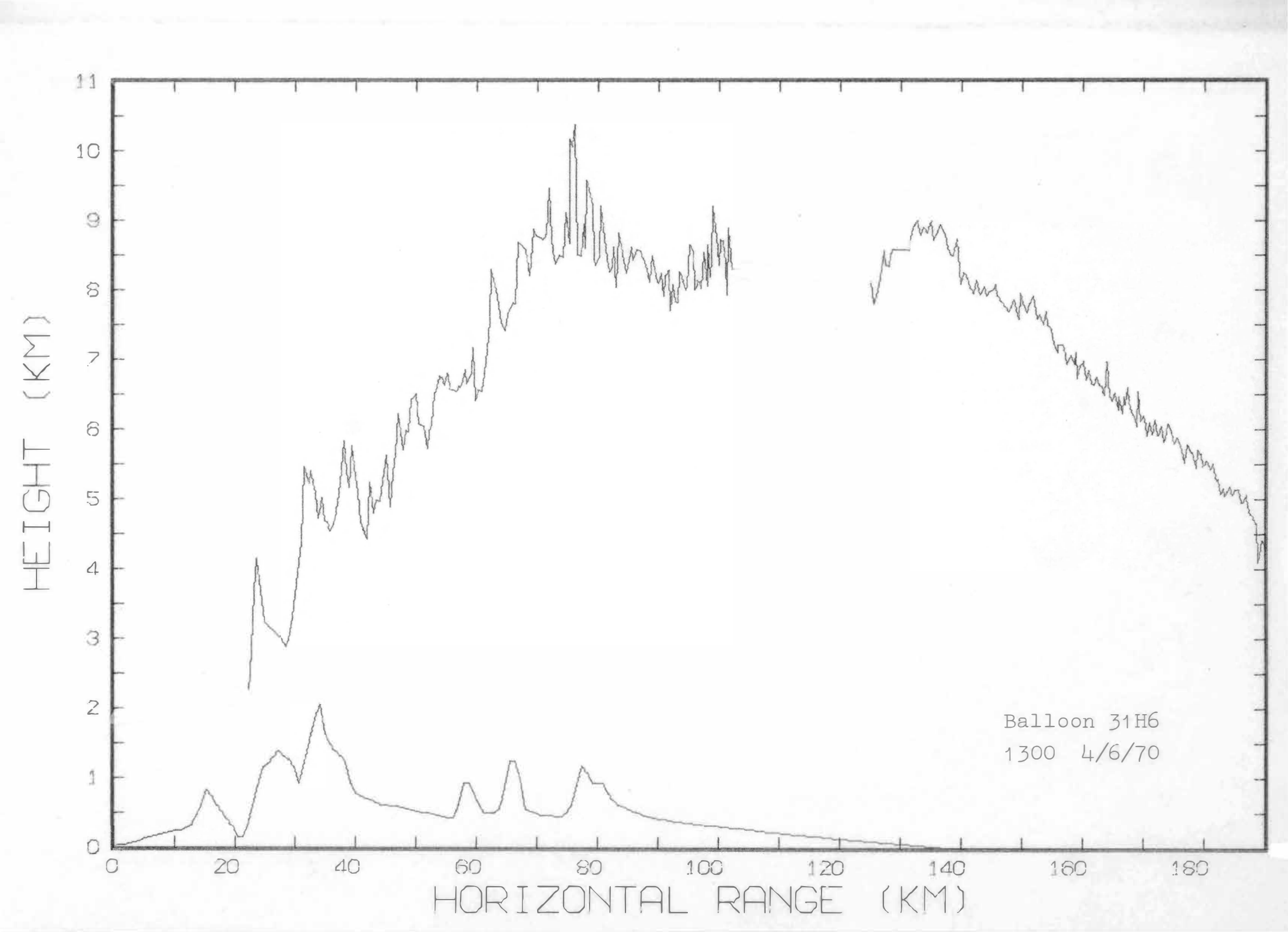
HEIGHT (KM)
HORIZONTAL RANGE (KM)
0
1
2
3
4
5
6
7
8
9
10
11
0
20
40
60
80
100
120
140
160
180
Balloon 31H6
1300 4/6/70

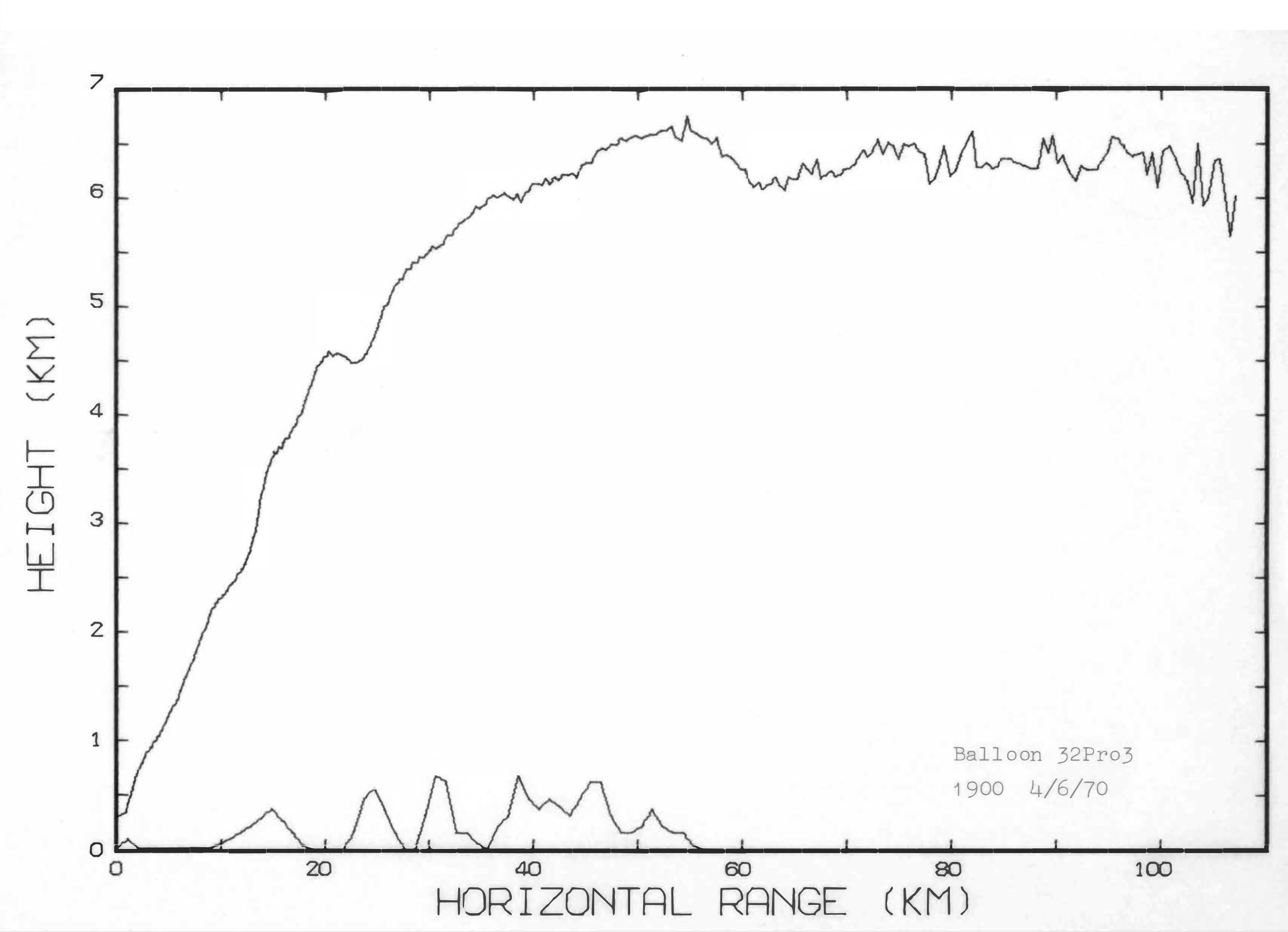
HEIGHT (KM)
0
1
2
3
4
5
6
7
0
20
40
60
80
100
HORIZONTAL RANGE (KM)
Balloon 32Pro3
1900 4/6/70

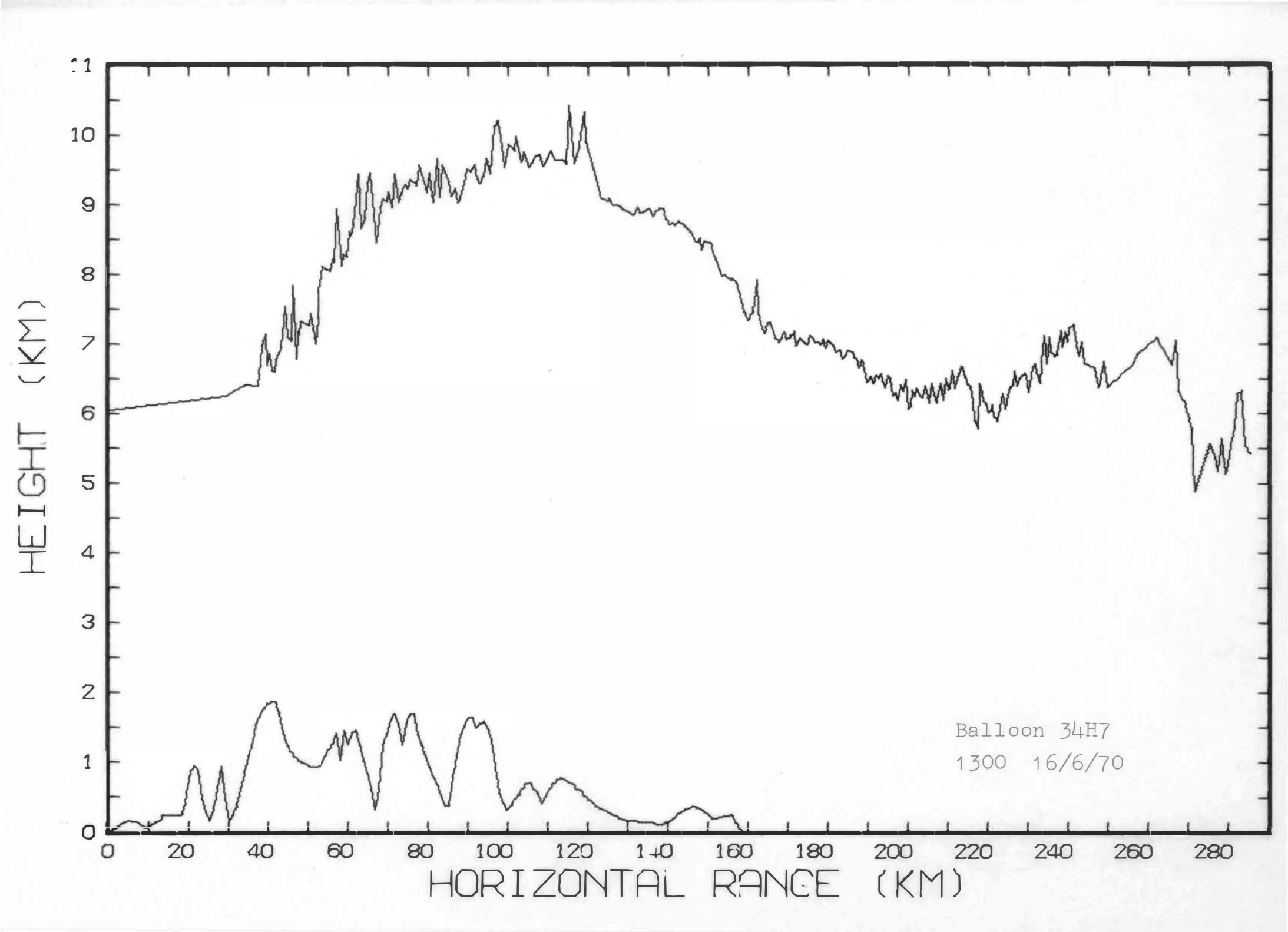
11
10
9
8
7
6
5
4
3
2
1
0
HEIGHT (KM)
0
20
40
60
80
100
120
140
160
180
200
220
240
260
280
HORIZONTAL RANGE (KM)
Balloon 34H7
1300 16/6/70

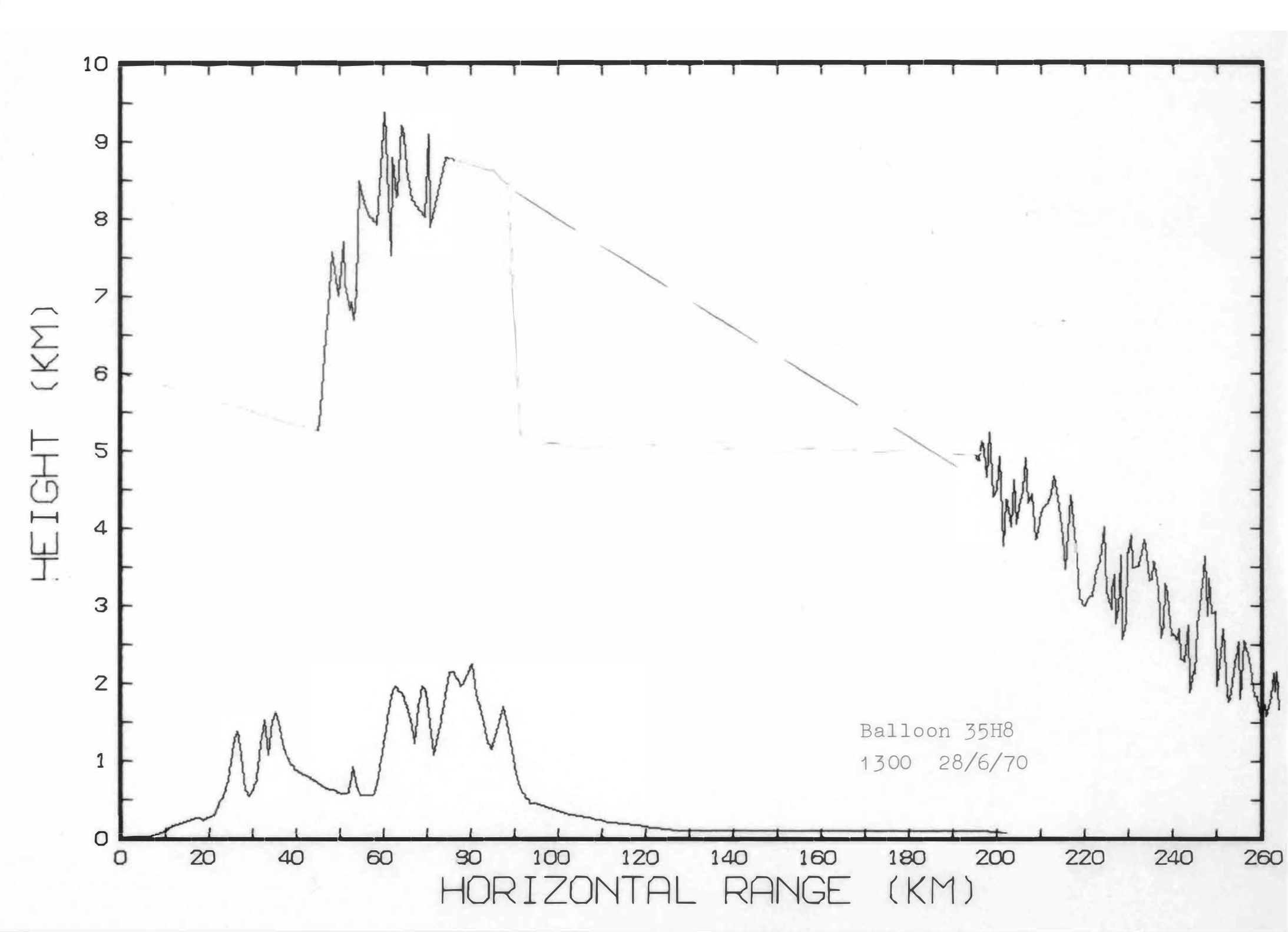
HEIGHT (KM)
0
1
2
3
4
5
6
7
8
9
10
0
20
40
60
90
100
120
140
160
180
200
220
240
260
HORIZONTAL RANGE (KM)
Balloon 35H8
1300 28/6/70

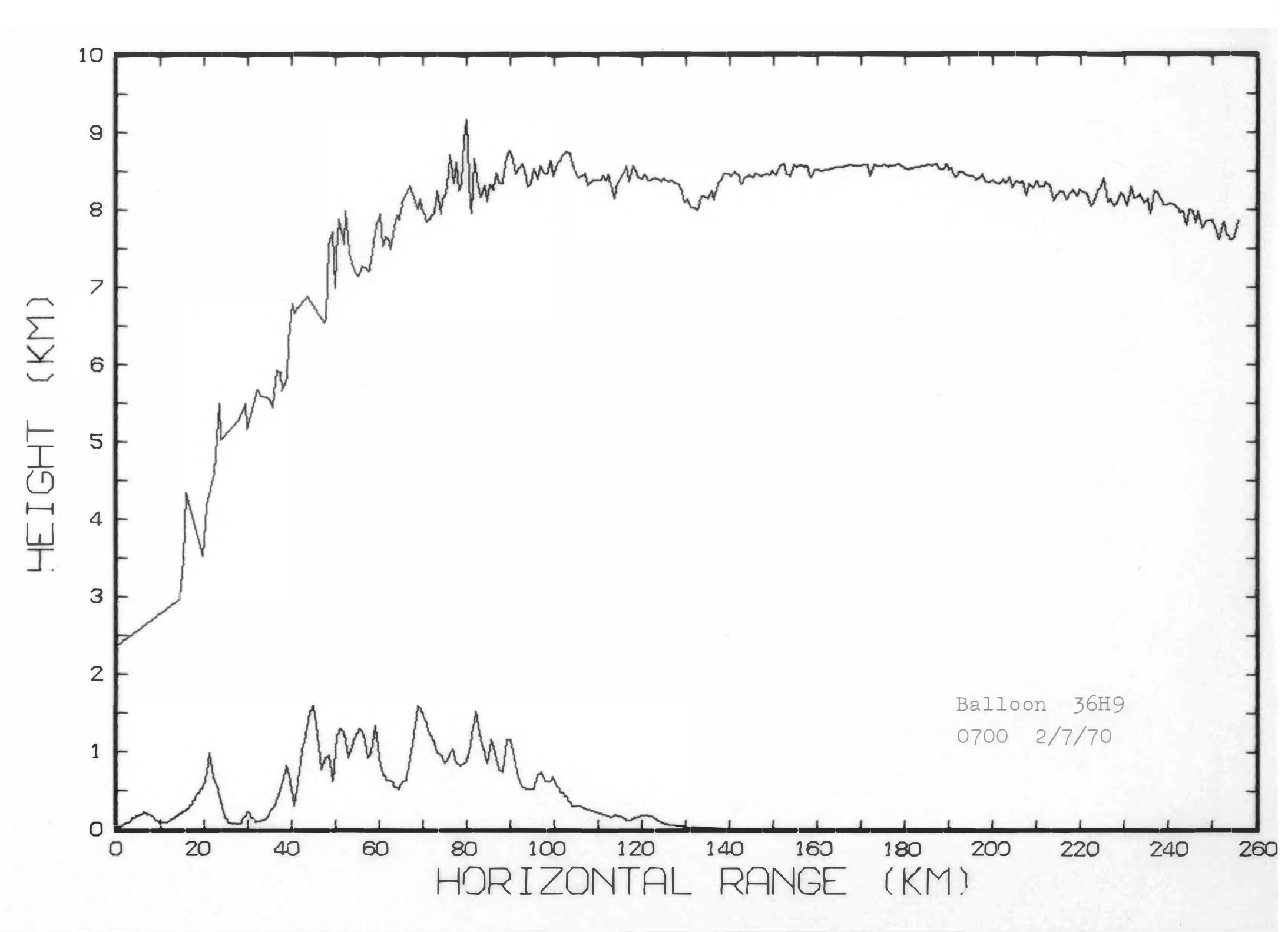
HEIGHT (KM)
0
1
2
3
4
5
6
7
8
9
10
0
20
40
60
80
100
120
140
160
180
200
220
240
260
HORIZONTAL RANGE (KM)
Balloon 36H9
0700 2/7/70

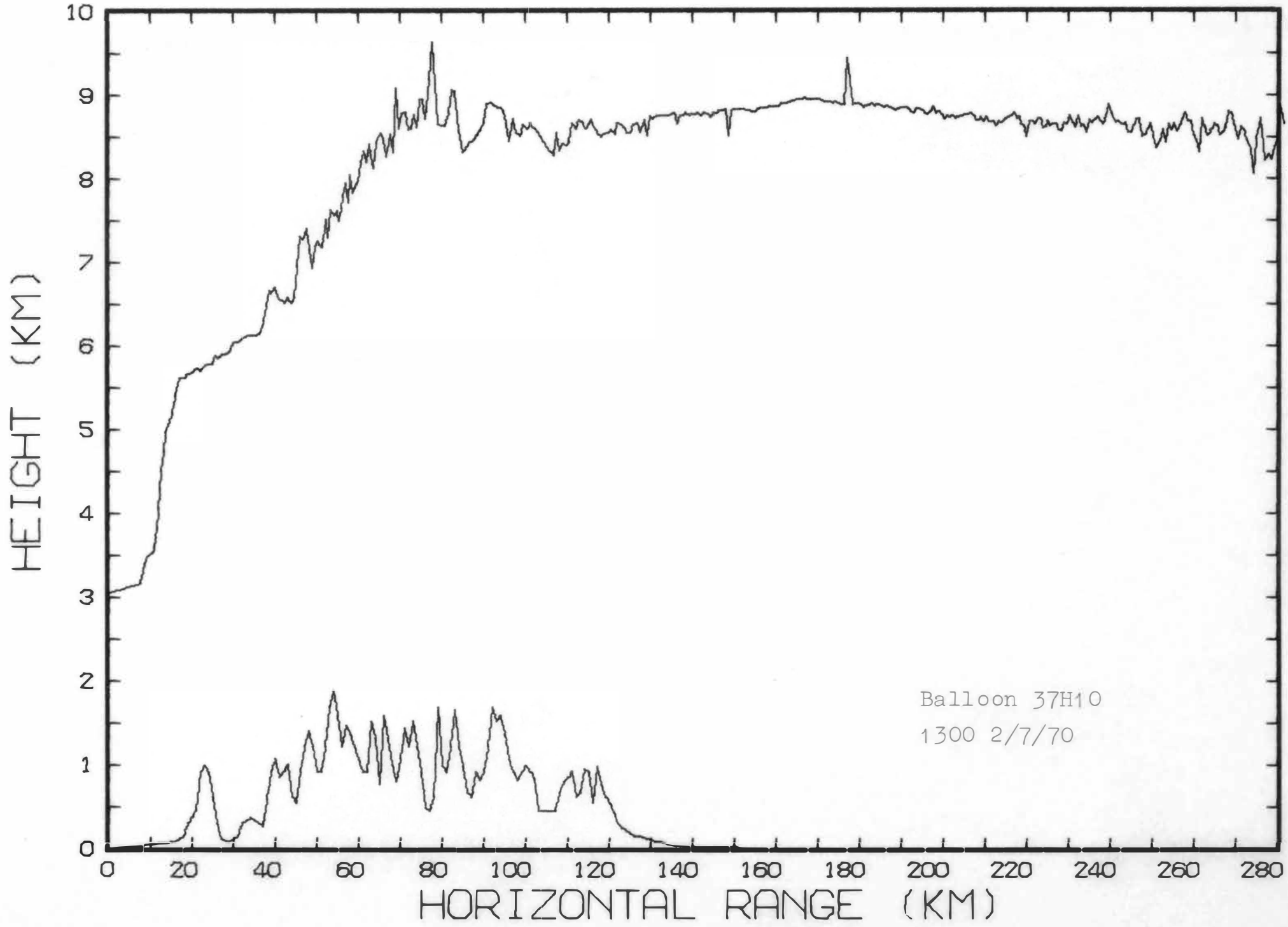
HEIGHT (KM)
HORIZONTAL RANGE (KM)
0
1
2
3
4
5
6
7
8
9
10
0
20
40
60
80
100
120
140
160
180
200
220
240
260
280
Balloon 37H10
1300 2/7/70

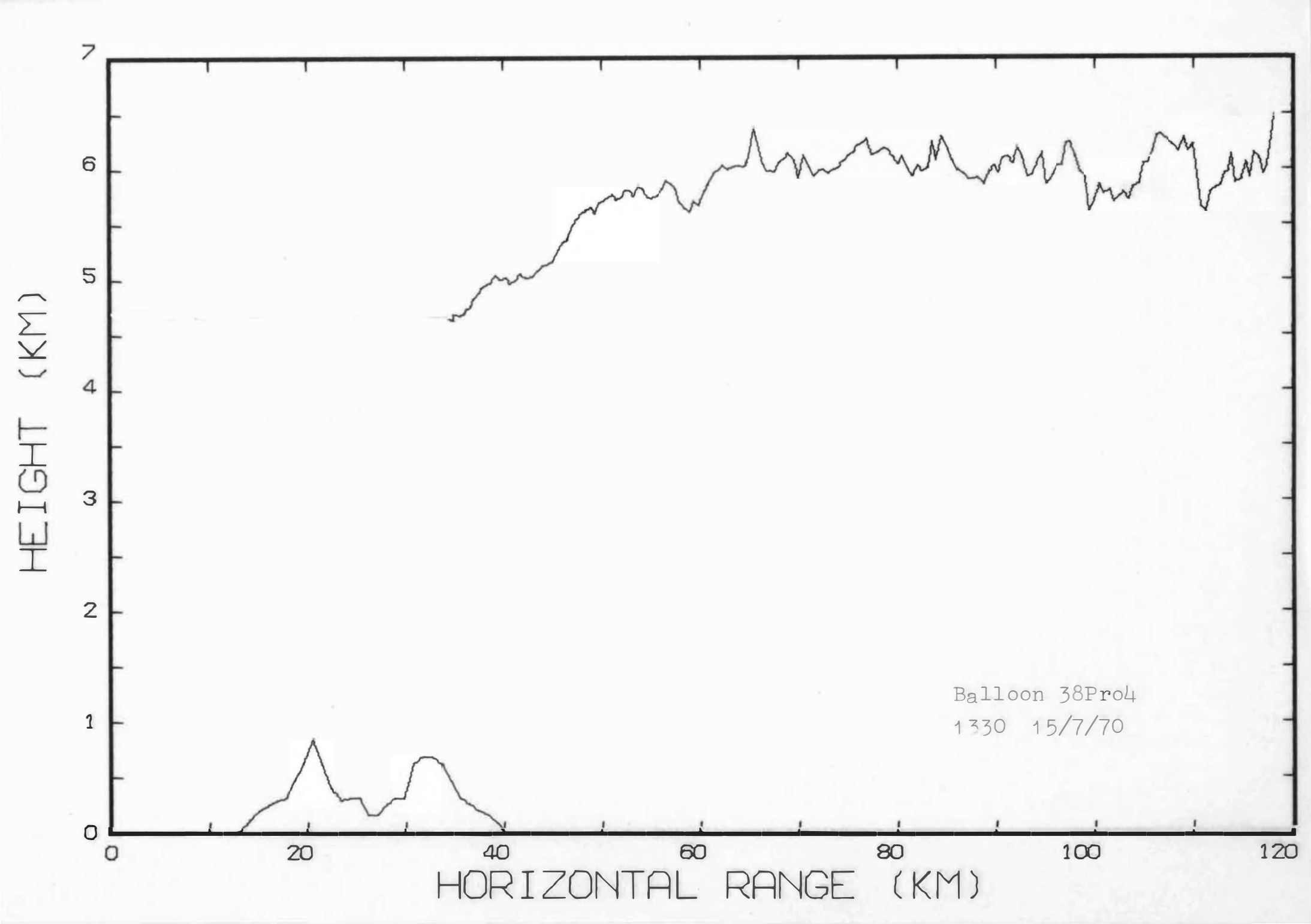
HEIGHT (KM)
0
1
2
3
4
5
6
7
0
20
40
60
80
100
120
HORIZONTAL RANGE (KM)
Balloon 38Pro4
1330 15/7/70

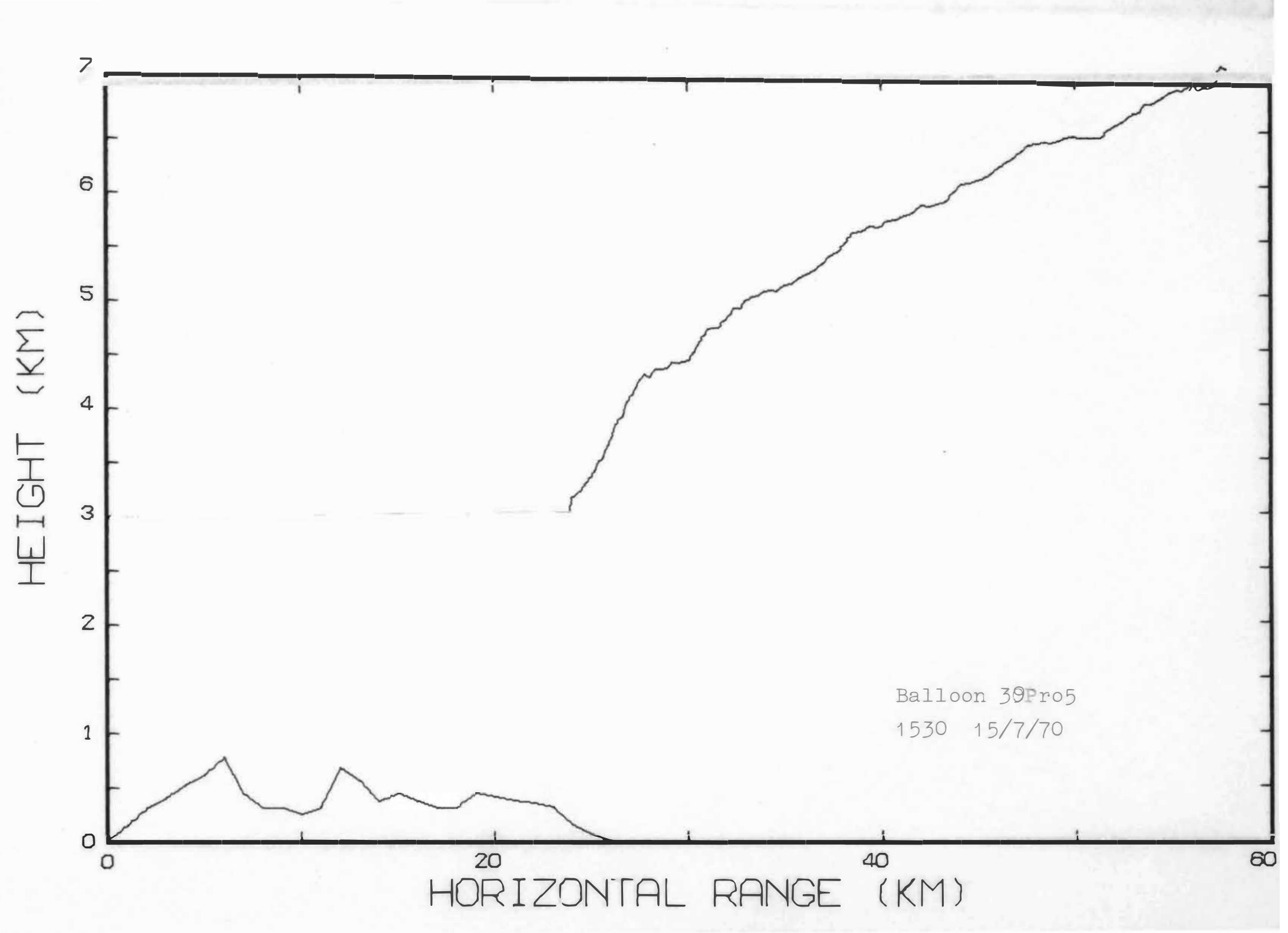
HEIGHT (KM)
0
1
2
3
4
5
6
7
0
20
40
60
HORIZONTAL RANGE (KM)
Balloon 39Pro5
1530 15/7/70

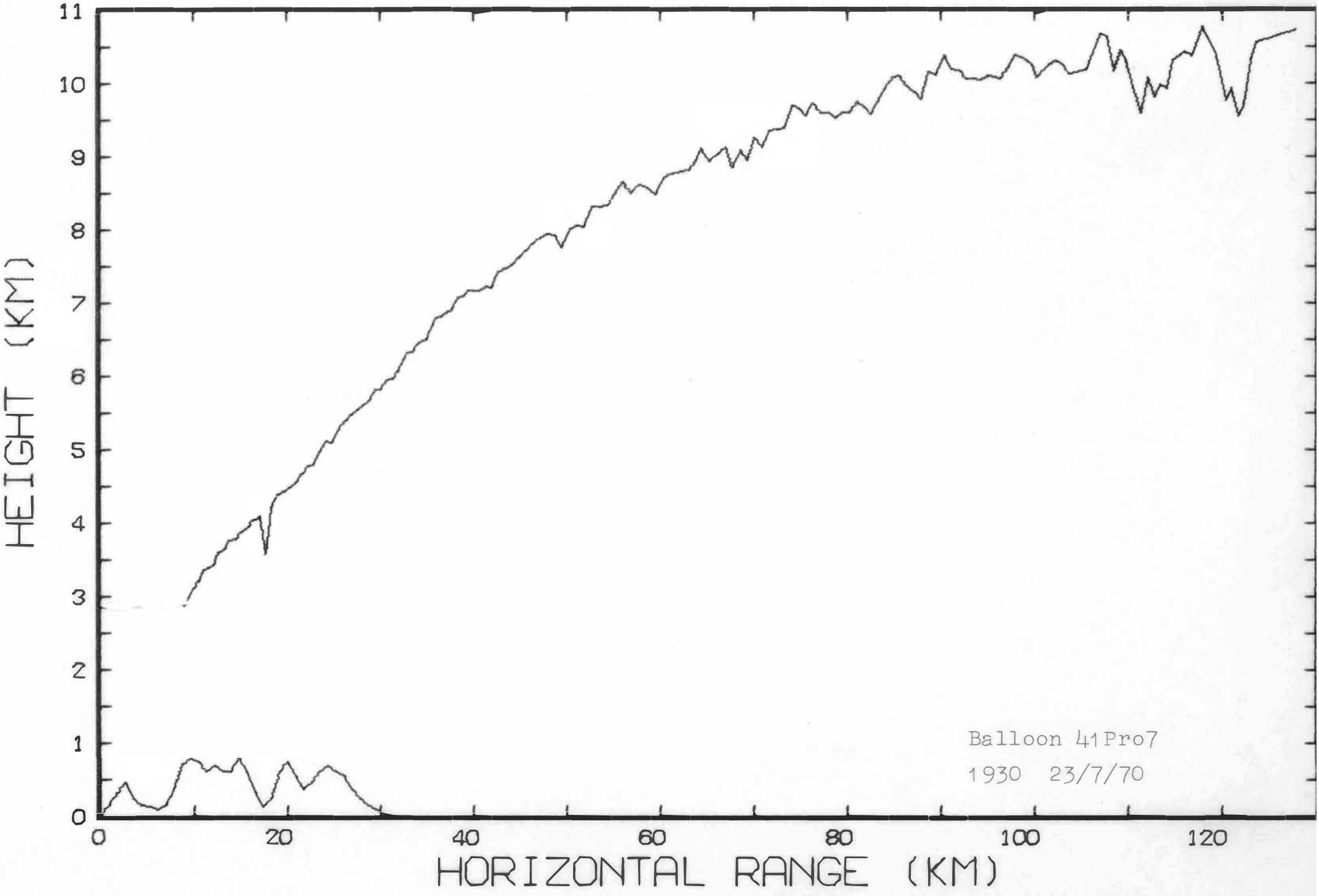
HEIGHT (KM)
0
1
2
3
4
5
6
7
8
9
10
11
0
20
40
60
80
100
120
HORIZONTAL RANGE (KM)
Balloon 41Pro7
1930 23/7/70

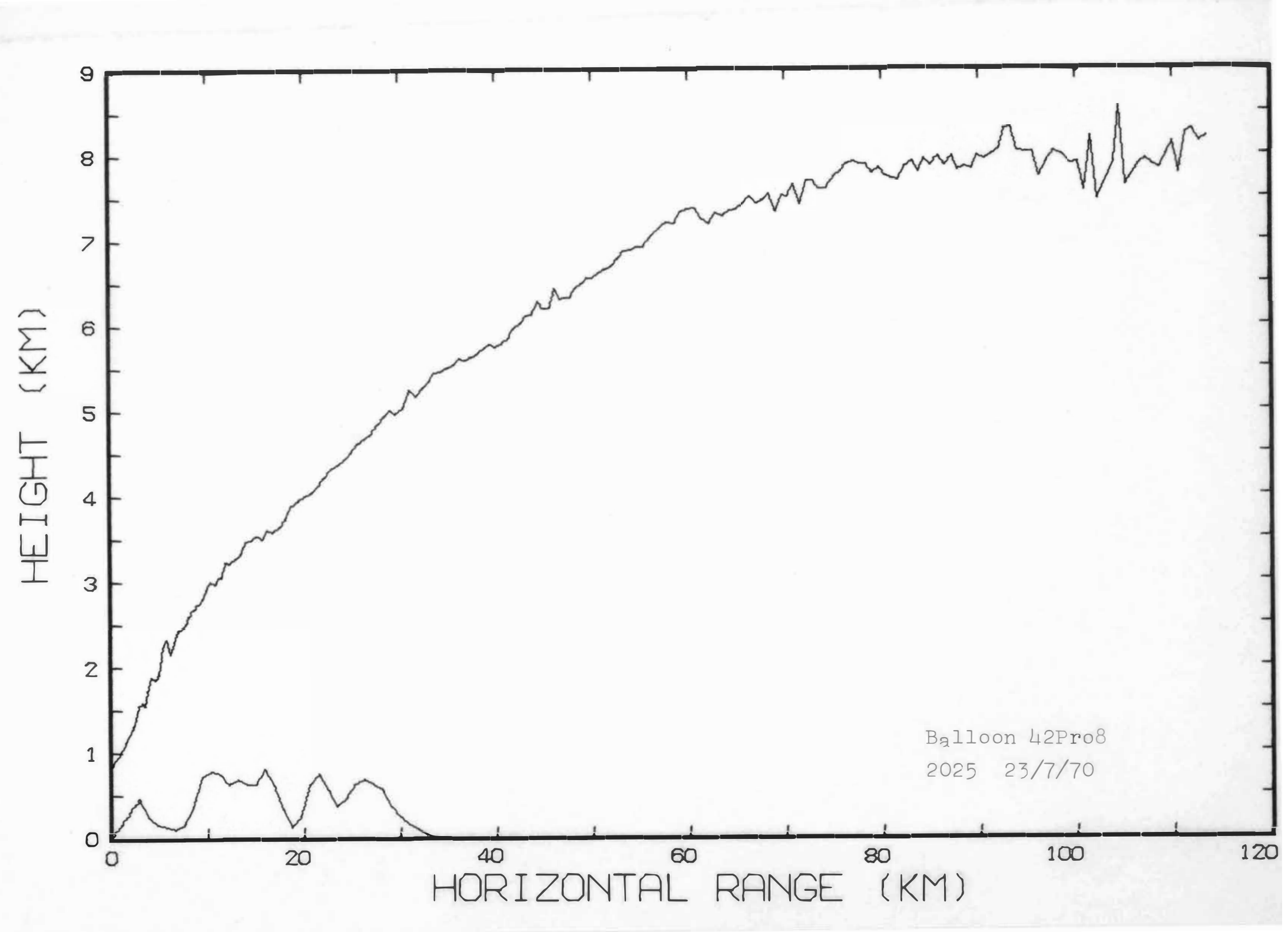
HEIGHT (KM)
0
1
2
3
4
5
6
7
8
9
0
20
40
60
80
100
120
HORIZONTAL RANGE (KM)
Balloon 42Pro8
2025 23/7/70

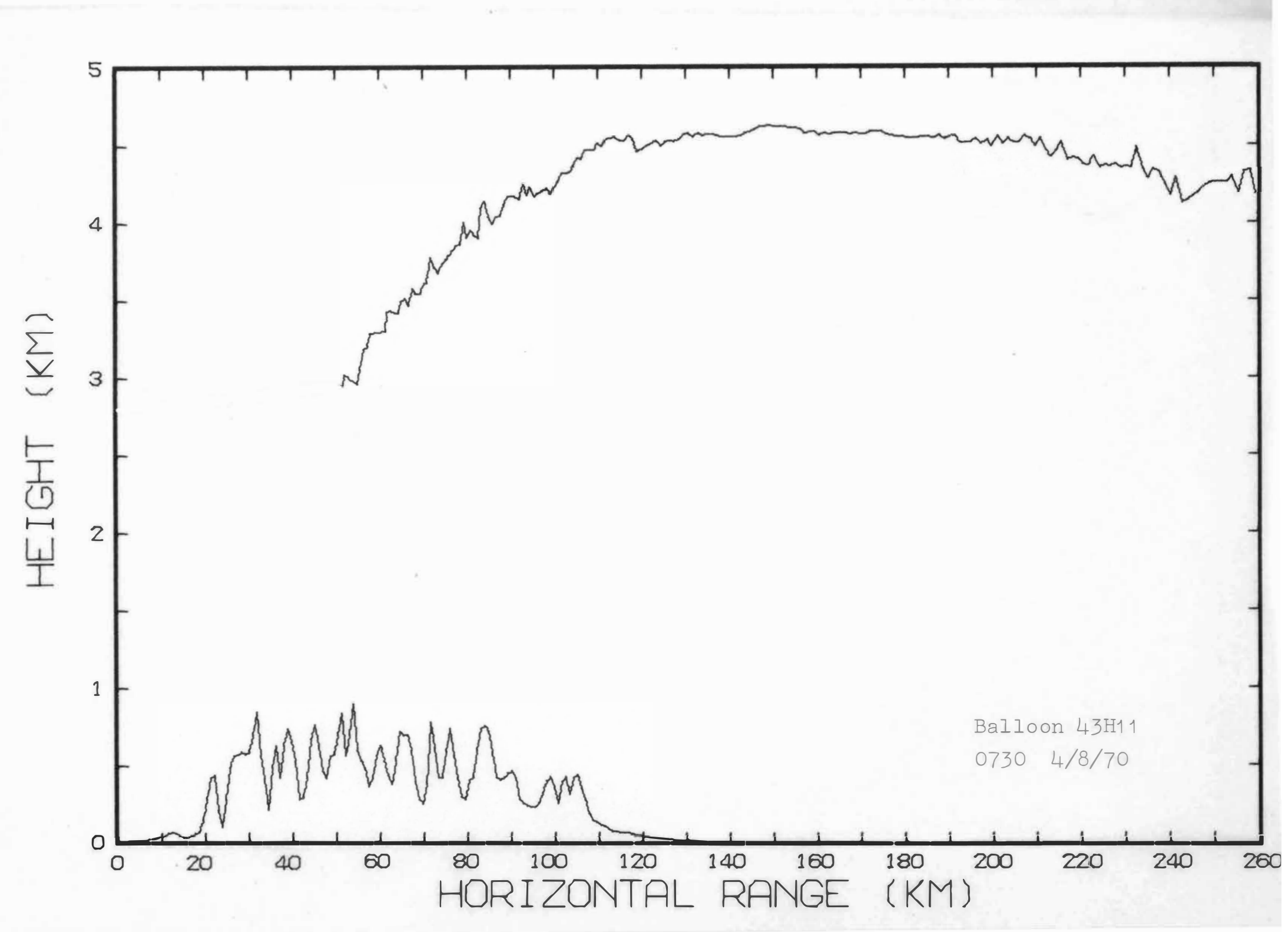
HEIGHT (KM)
0
1
2
3
4
5
0
20
40
60
80
100
120
140
160
180
200
220
240
260
HORIZONTAL RANGE (KM)
Balloon 43H11
0730 4/8/70

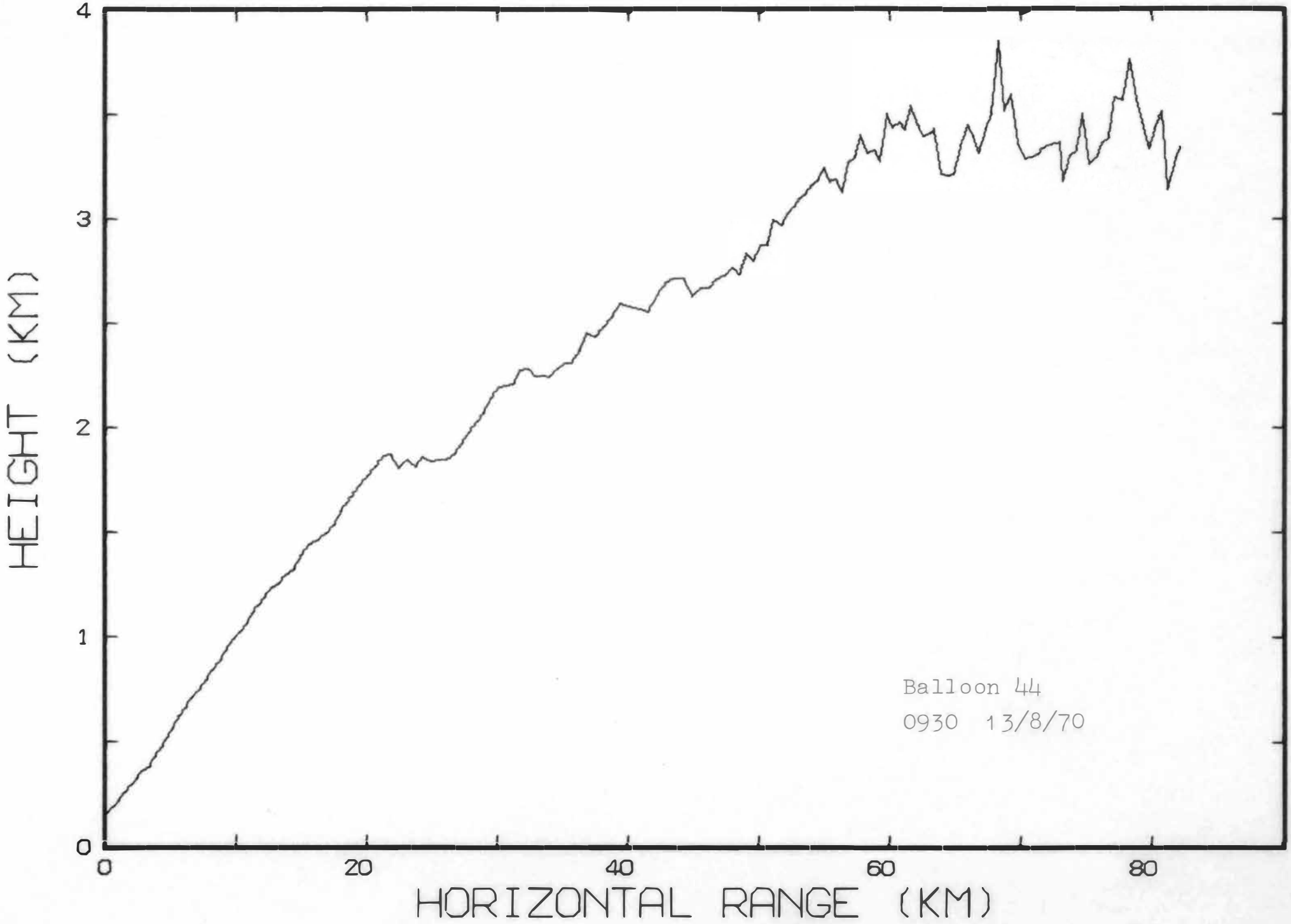
HEIGHT (KM)
4
3
2
1
0
0
20
40
60
80
HORIZONTAL RANGE (KM)
Balloon 44
0930 13/8/70

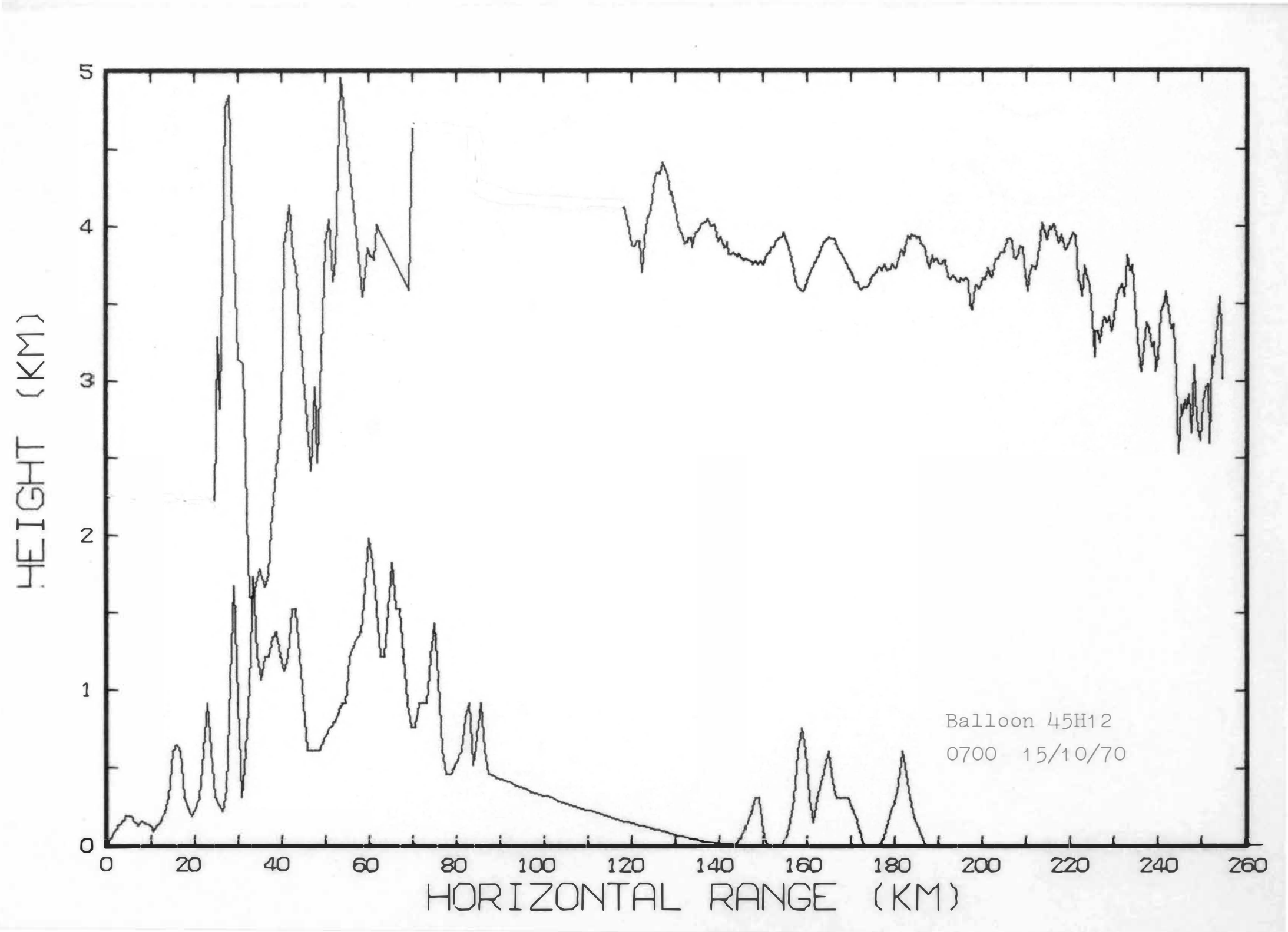
HEIGHT (KM)
0
1
2
3
4
5
0
20
40
60
80
100
120
140
160
180
200
220
240
260
HORIZONTAL RANGE (KM)
Balloon 45H12
0700 15/10/70

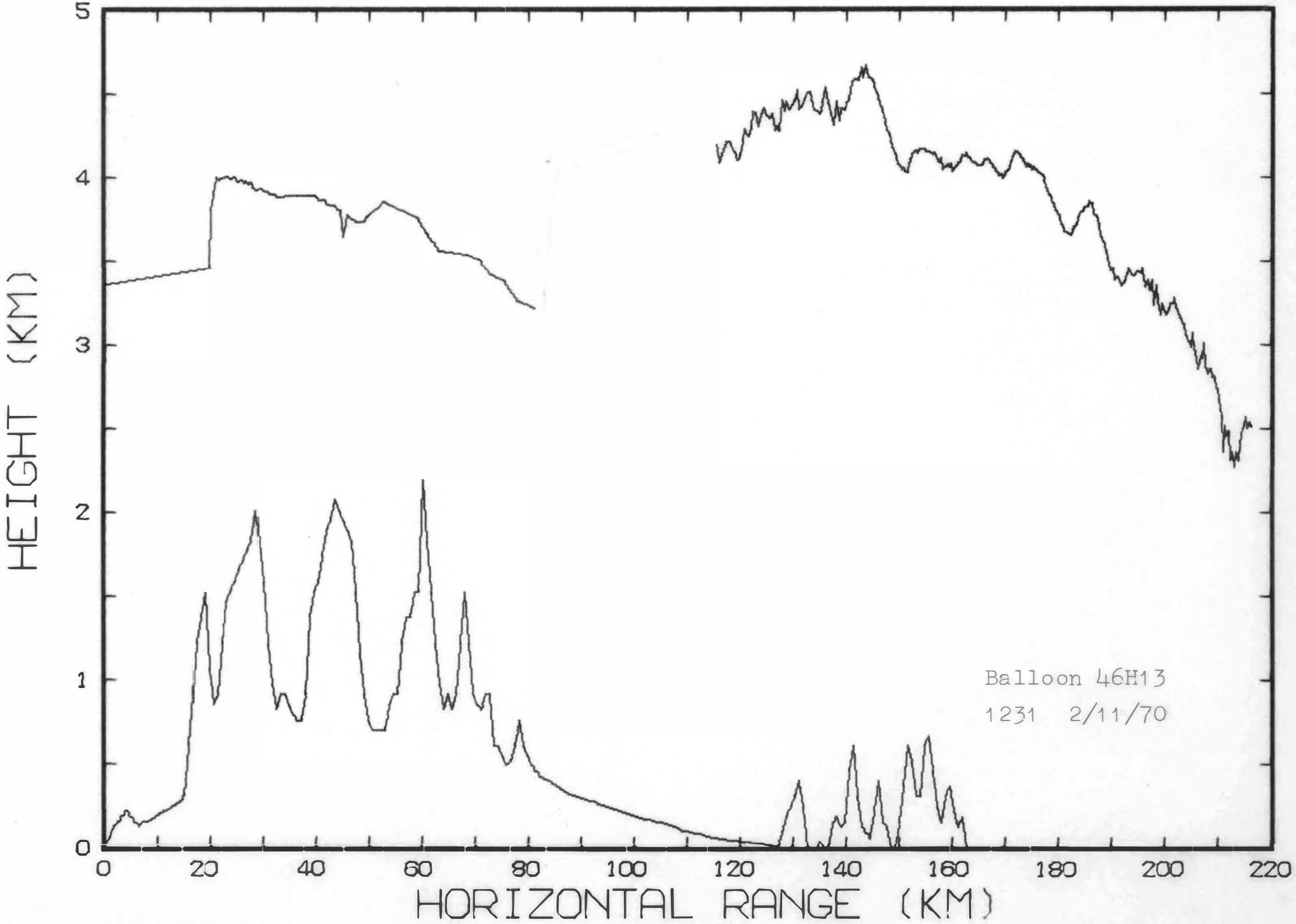
HEIGHT (KM)
0
1
2
3
4
5
0
20
40
60
80
100
120
140
160
180
200
220
HORIZONTAL RANGE (KM)
Balloon 46H13
1231 2/11/70

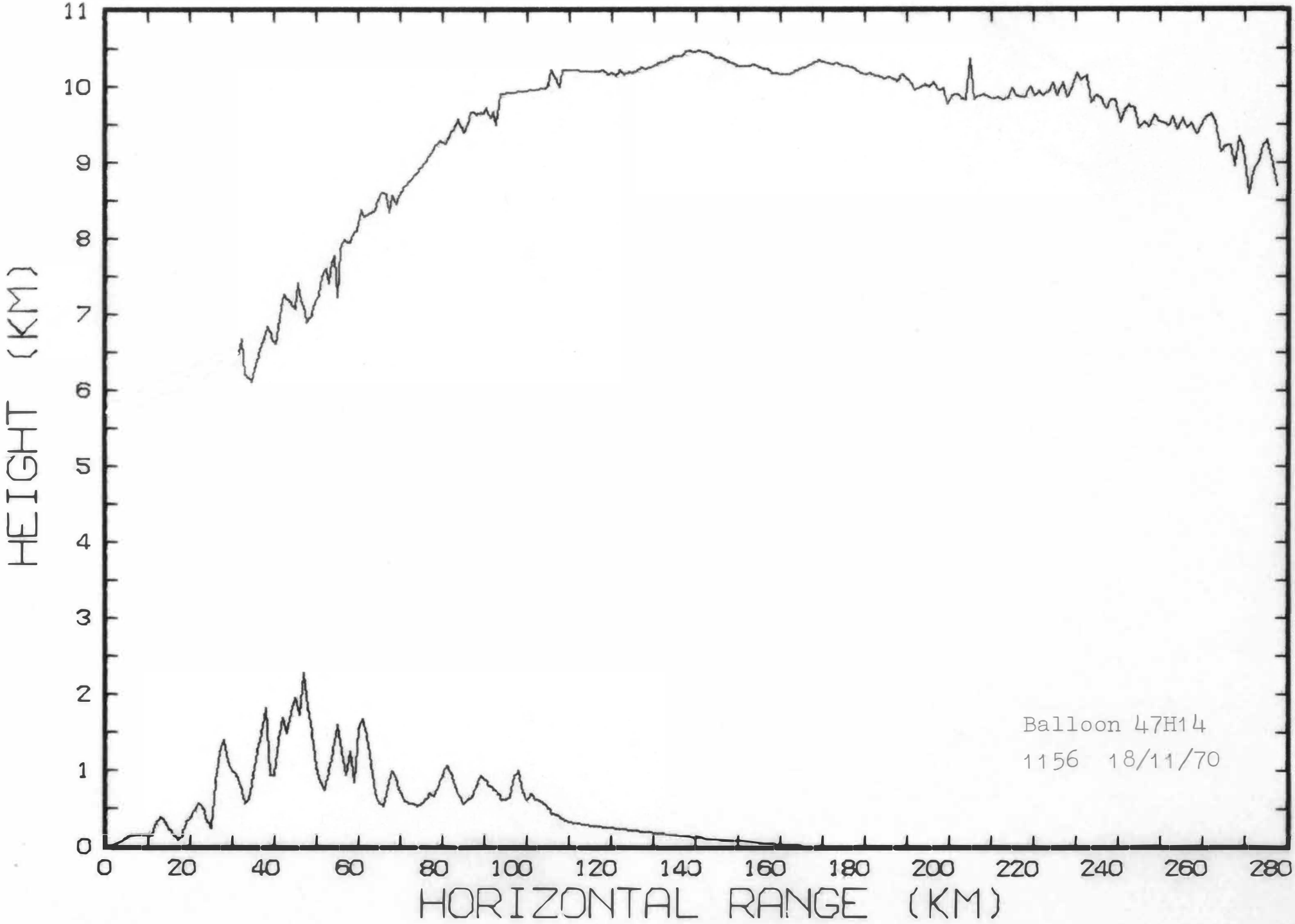
HEIGHT (KM)
0
1
2
3
4
5
6
7
8
9
10
11
0
20
40
60
80
100
120
140
160
180
200
220
240
260
280
HORIZONTAL RANGE (KM)
Balloon 47H14
1156 18/11/70

Appendix D

Airflow profile diagrams:-

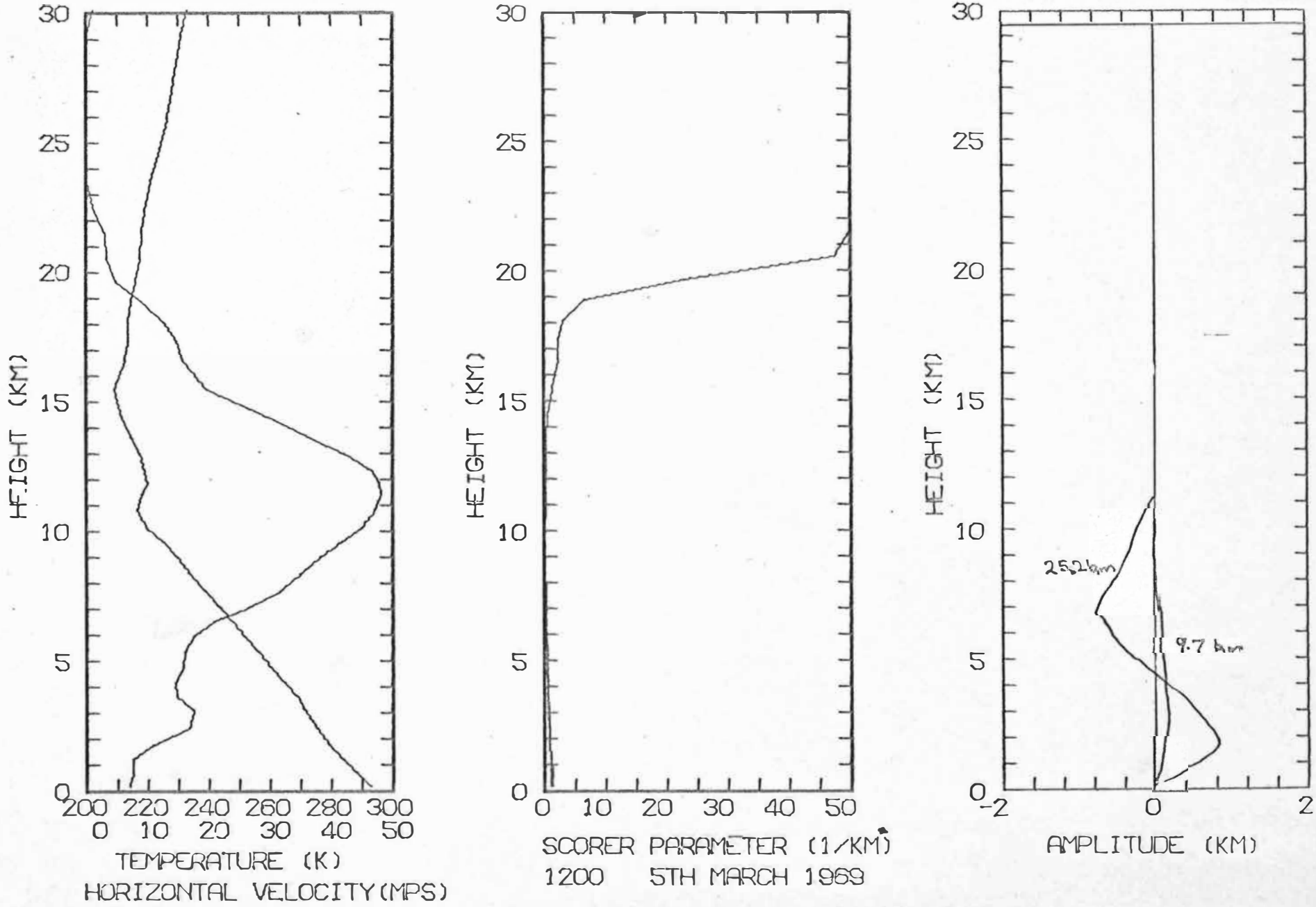
HEIGHT (KM)
30
25
20
15
10
5
0
200 220 240 260 280 300
0 10 20 30 40 50
TEMPERATURE (K)
HORIZONTAL VELOCITY (MPS)
0 10 20 30 40 50
SCORER PARAMETER (1/KM)
1200 5TH MARCH 1969
-2 0 2
AMPLITUDE (KM)
25.2 km
9.7 km

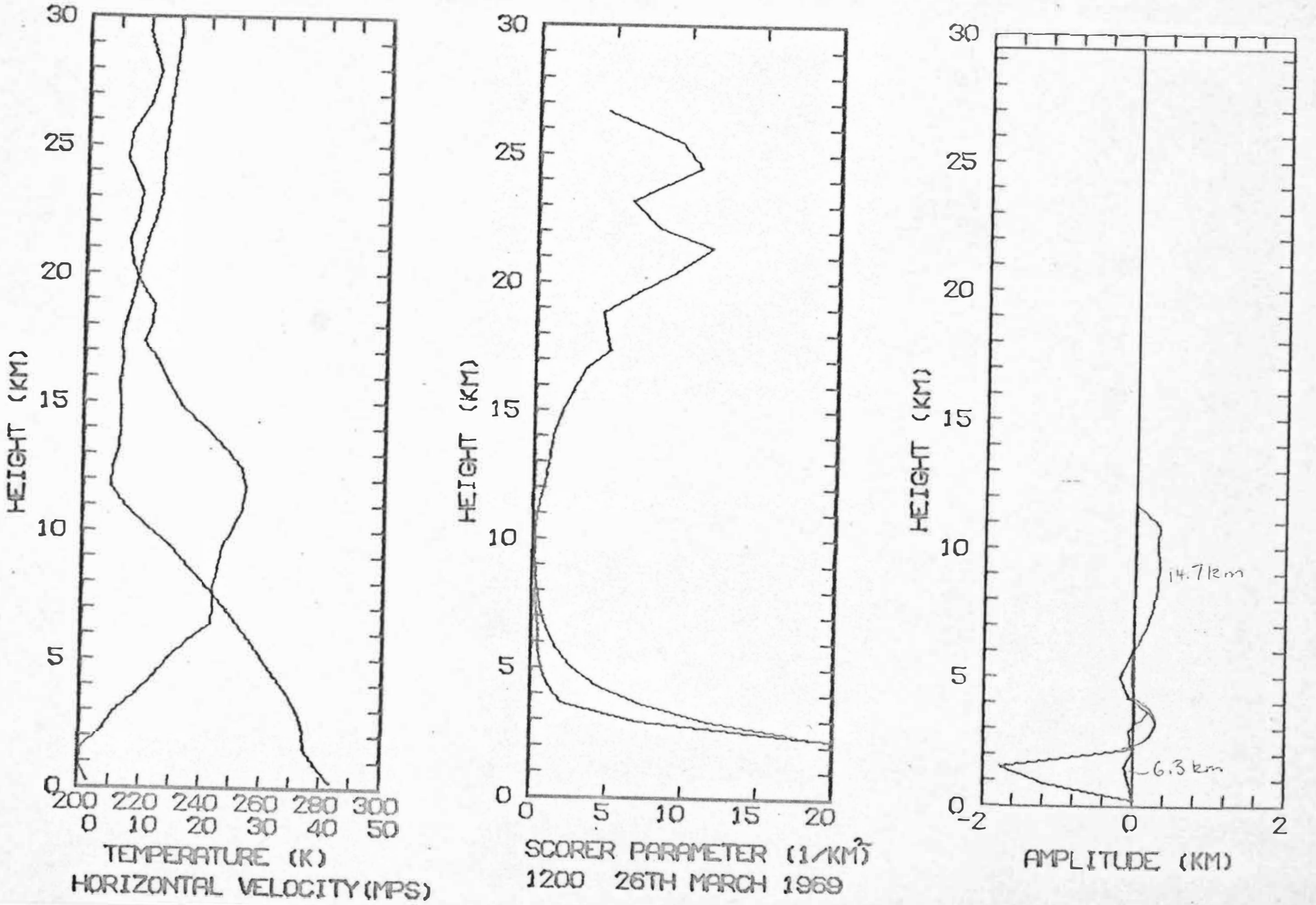
HEIGHT (KM)
30
25
20
15
10
5
0
200 220 240 260 280 300
0 10 20 30 40 50
TEMPERATURE (K)
HORIZONTAL VELOCITY (MPS)
HEIGHT (KM)
0 5 10 15 20
SCORER PARAMETER (1/KM²)
1200 26TH MARCH 1969
HEIGHT (KM)
-2 0 2
AMPLITUDE (KM)
14.7 km
6.3 km

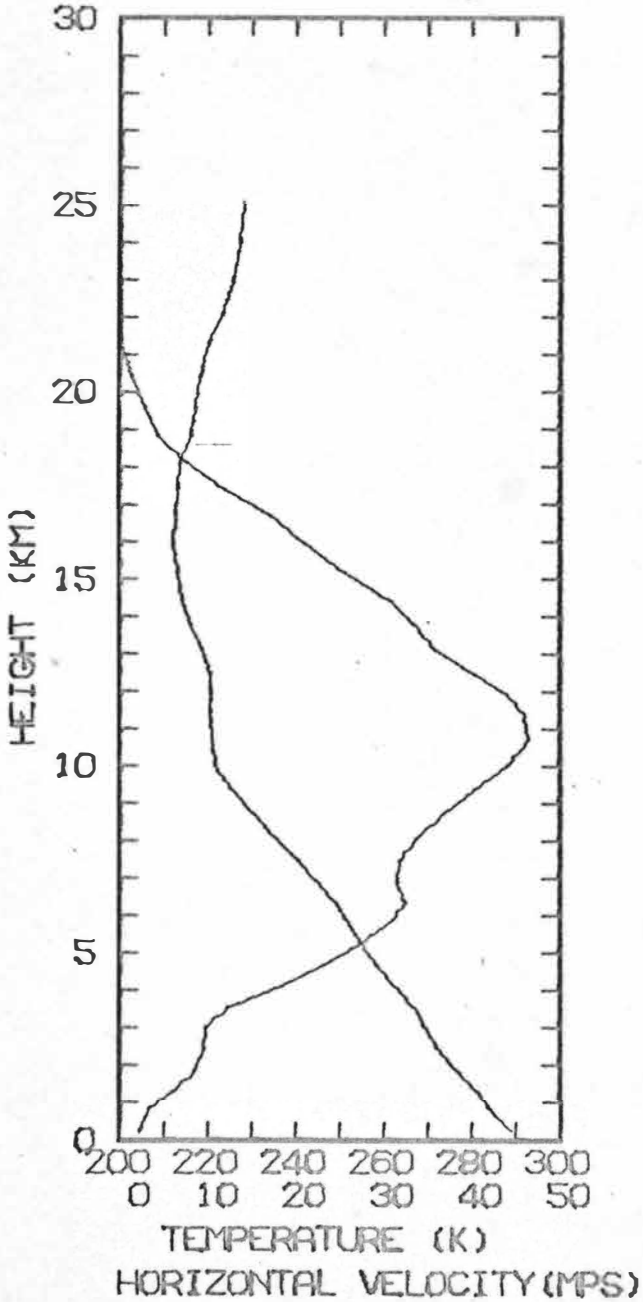
30
25
20
15
10
5
0
HEIGHT (KM)
200 220 240 260 280 300
0 10 20 30 40 50
TEMPERATURE (K)
HORIZONTAL VELOCITY (MPS)

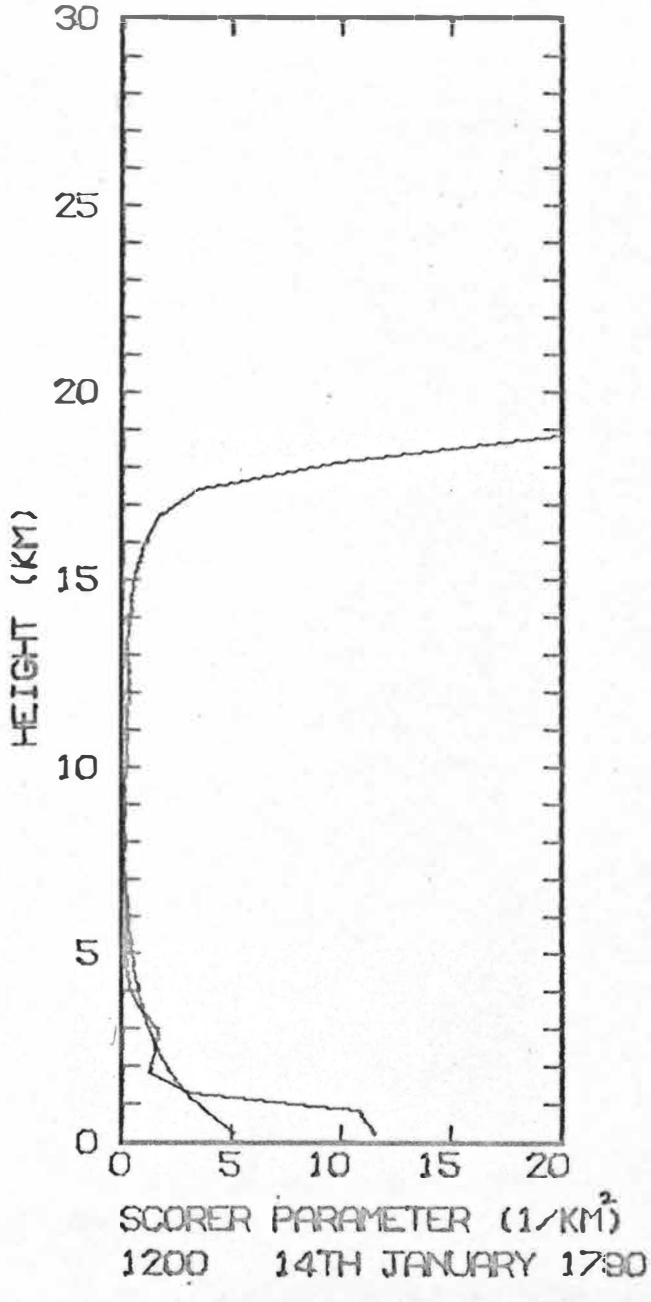
30
25
20
15
10
5
0
HEIGHT (KM)
0 5 10 15 20
SCORER PARAMETER (1/KM²)
1200 14TH JANUARY 1790

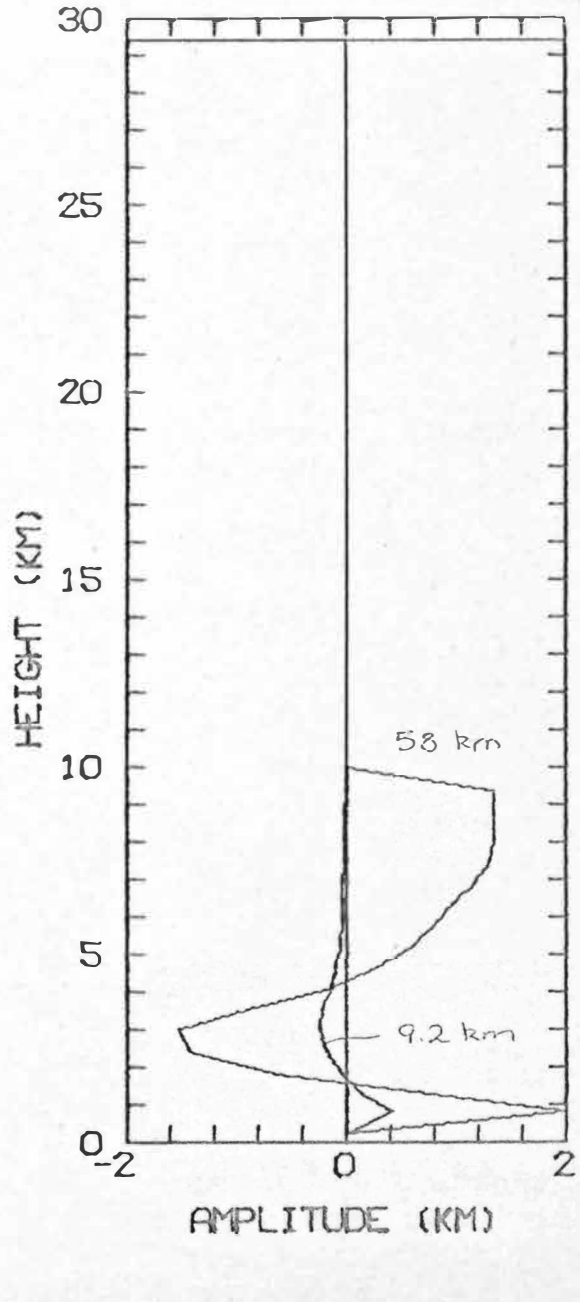
30
25
20
15
10
5
0
HEIGHT (KM)
58 km
9.2 km
-2 0 2
AMPLITUDE (KM)

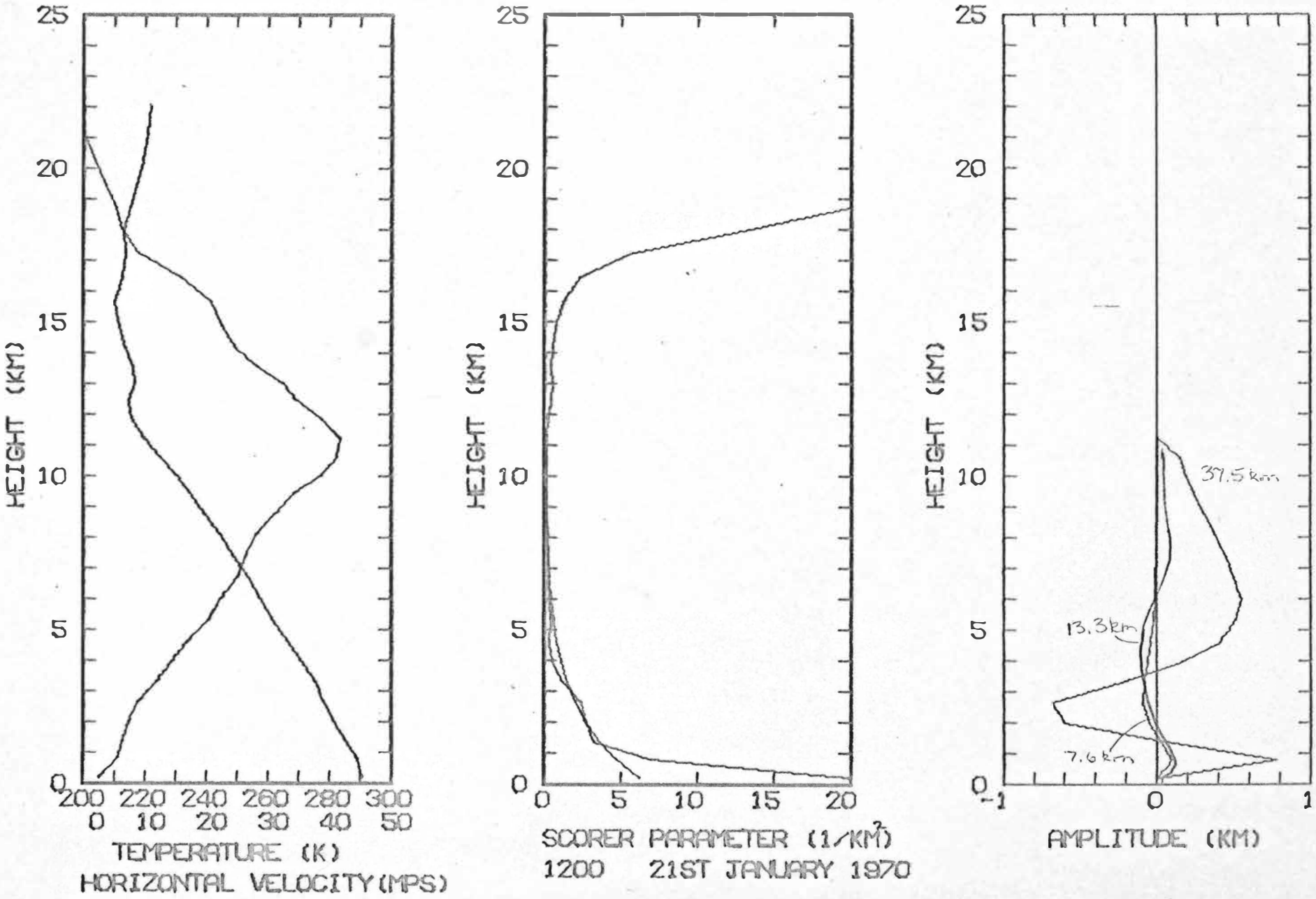
HEIGHT (KM)
25
20
15
10
5
0
200 220 240 260 280 300
0 10 20 30 40 50
TEMPERATURE (K)
HORIZONTAL VELOCITY (MPS)
0 5 10 15 20
SCORER PARAMETER (1/KM²)
1200 21ST JANUARY 1970
-1 0 1
AMPLITUDE (KM)
37.5 km
13.3km
7.6km

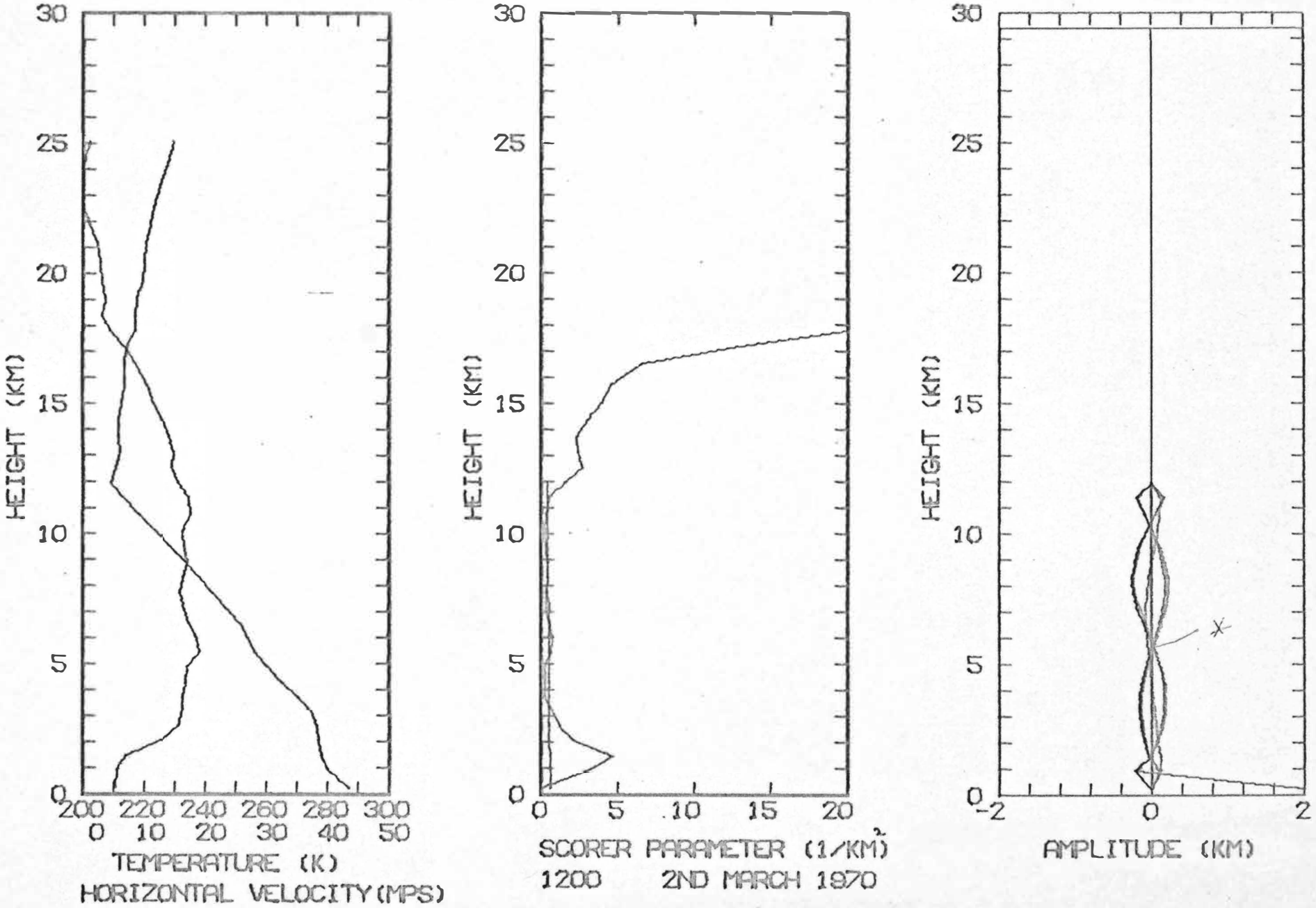
HEIGHT (KM)
30
25
20
15
10
5
0
200 220 240 260 280 300
0 10 20 30 40 50
TEMPERATURE (K)
HORIZONTAL VELOCITY (MPS)
HEIGHT (KM)
0 5 10 15 20
SCORER PARAMETER (1/KM²)
1200 2ND MARCH 1970
HEIGHT (KM)
-2 0 2
AMPLITUDE (KM)

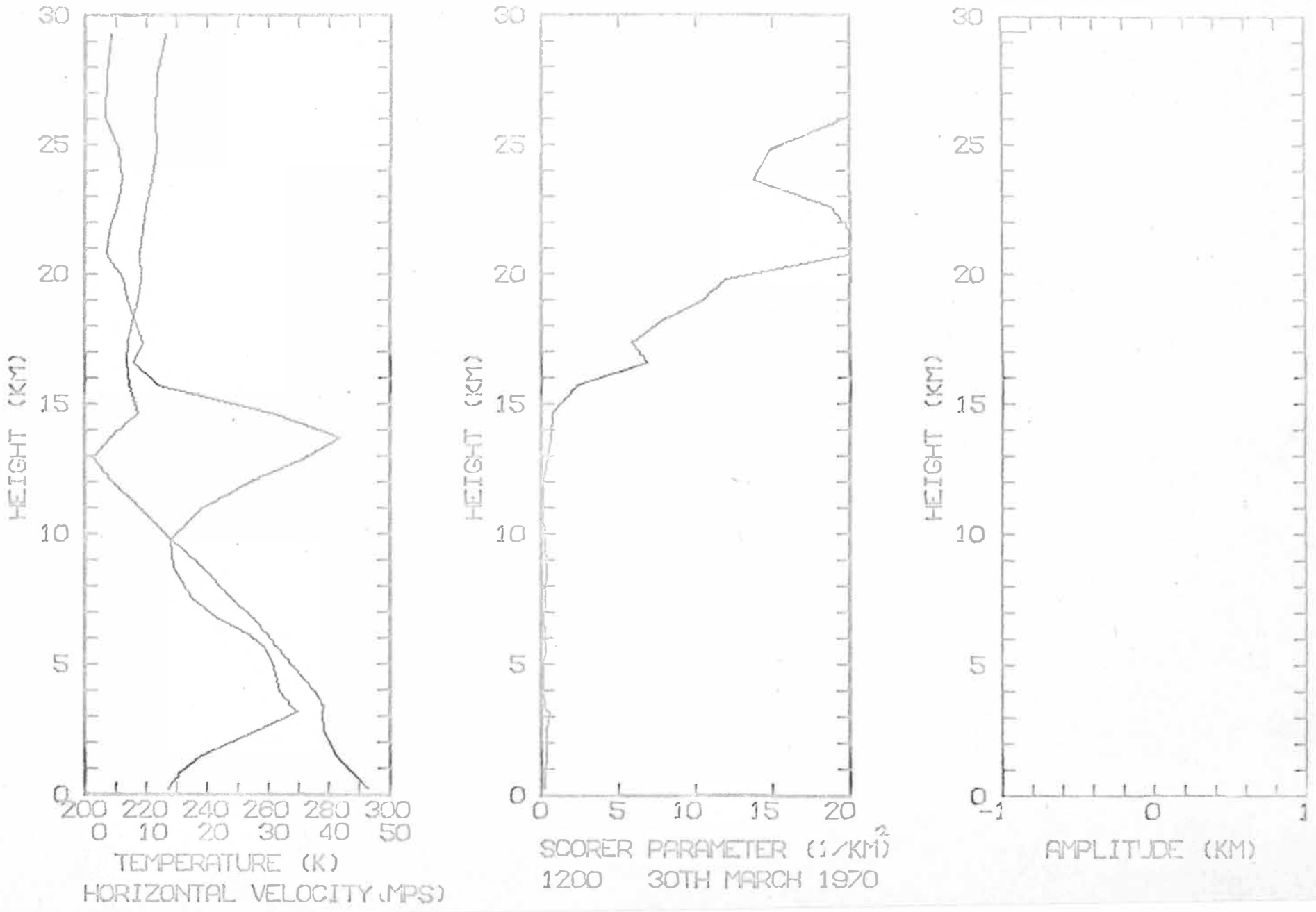
HEIGHT (KM)
30
25
20
15
10
5
0
200 220 240 260 280 300
0 10 20 30 40 50
TEMPERATURE (K)
HORIZONTAL VELOCITY (MPS)
HEIGHT (KM)
0 5 10 15 20
SCORER PARAMETER (1/KM)²
1200 30TH MARCH 1970
HEIGHT (KM)
-1 0 1
AMPLITUDE (KM)

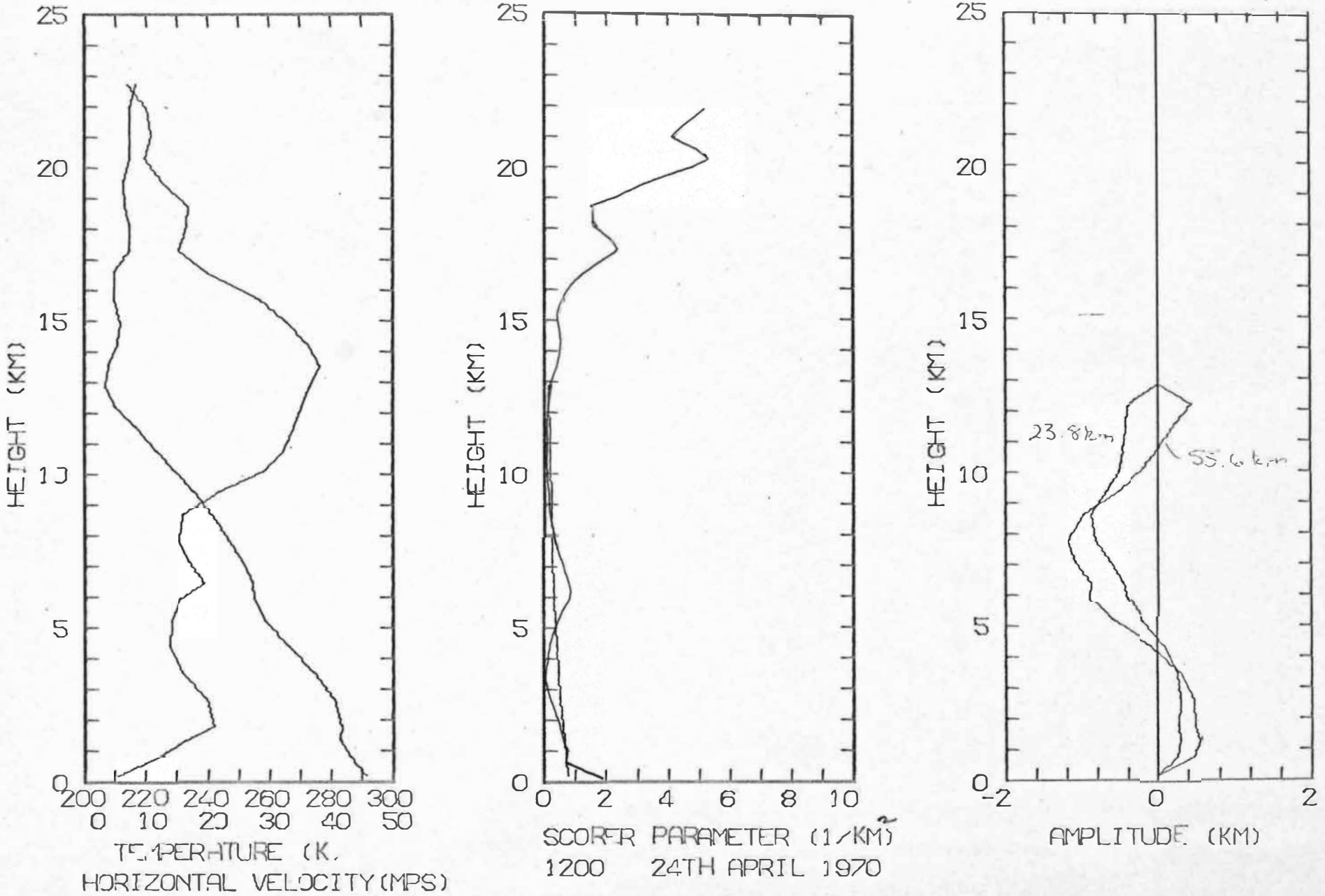
HEIGHT (KM)
25
20
15
10
5
0
200 220 240 260 280 300
0 10 20 30 40 50
TEMPERATURE (K.
HORIZONTAL VELOCITY (MPS)
0 2 4 6 8 10
SCORER PARAMETER (1/KM²)
1200 24TH APRIL 1970
-2 0 2
AMPLITUDE (KM)
23.8 km
55.6 km

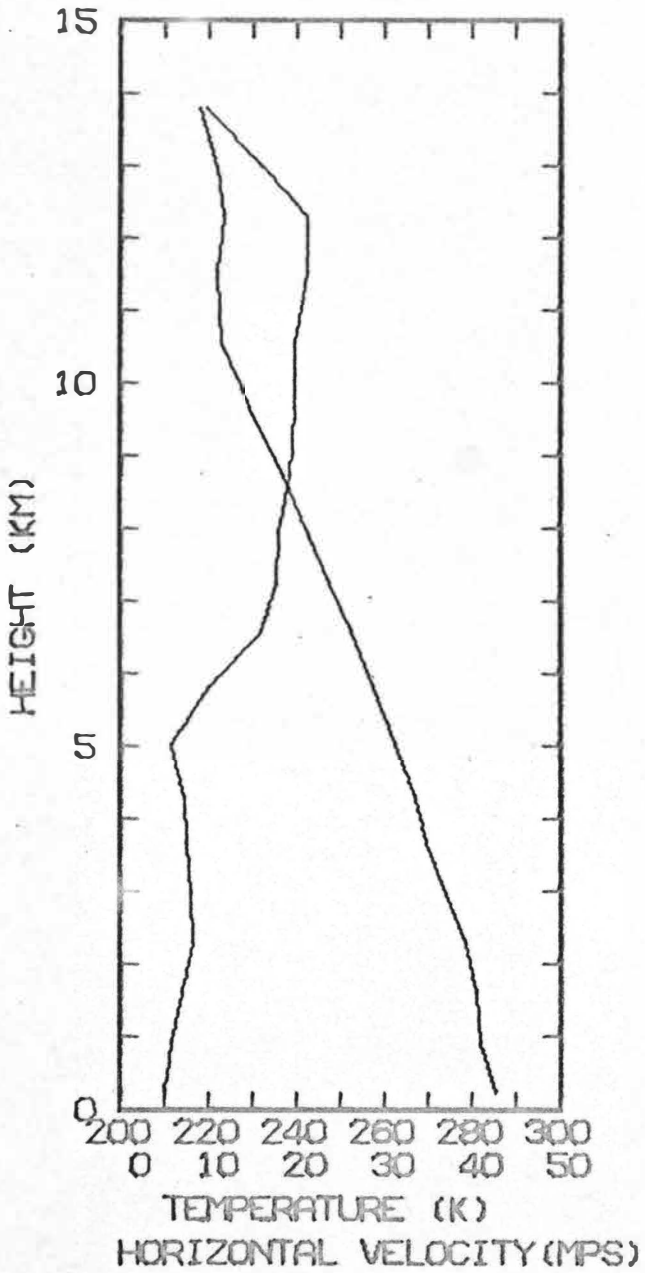
15
10
5
0
HEIGHT (KM)
200 220 240 260 280 300
0 10 20 30 40 50
TEMPERATURE (K)
HORIZONTAL VELOCITY (MPS)

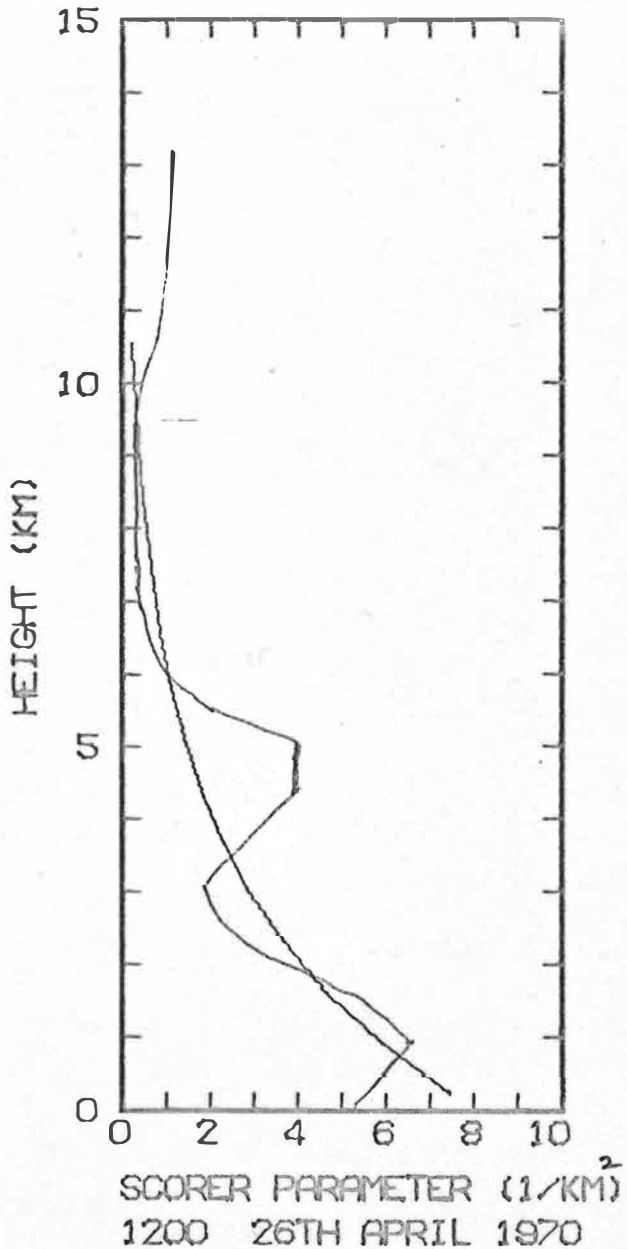
15
10
5
0
HEIGHT (KM)
0 2 4 6 8 10
SCORER PARAMETER (1/KM)²
1200 26TH APRIL 1970

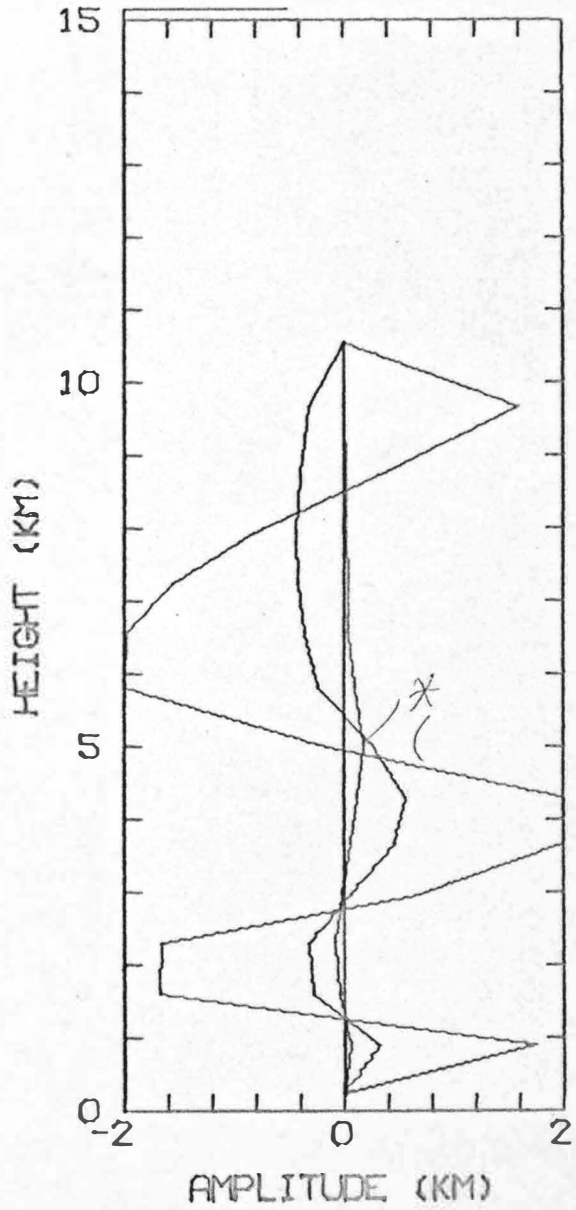
15
10
5
0
HEIGHT (KM)
-2 0 2
AMPLITUDE (KM)

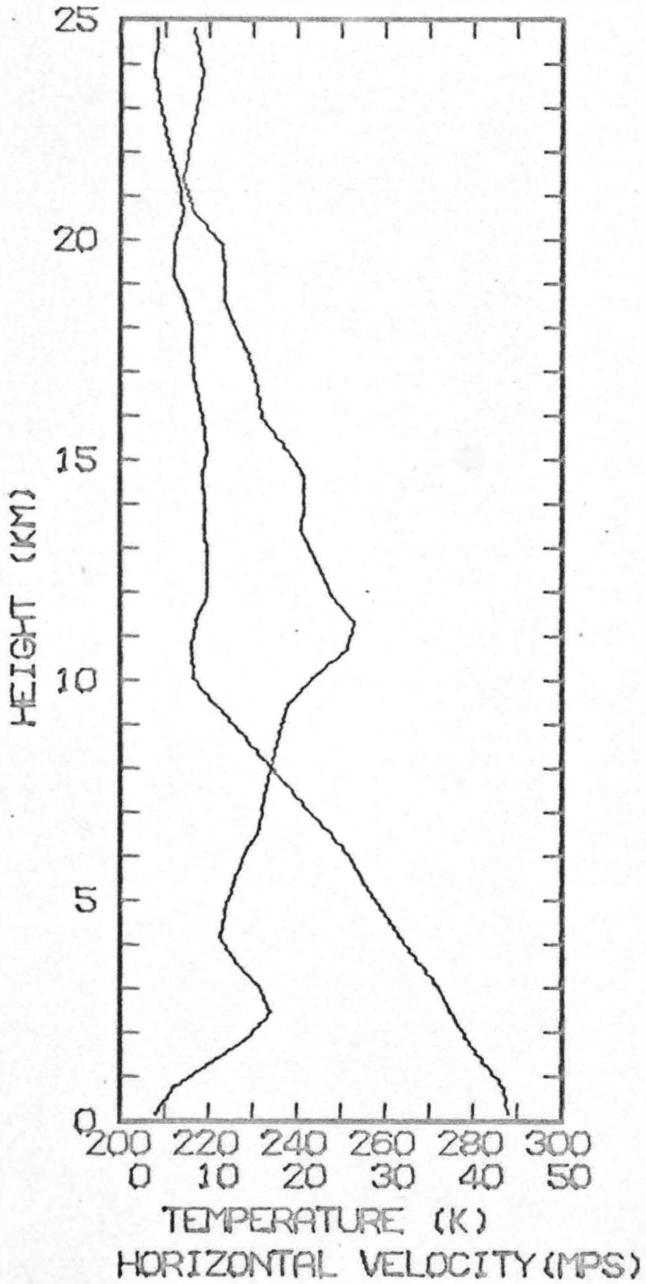
HEIGHT (KM)
25
20
15
10
5
0
200 220 240 260 280 300
0 10 20 30 40 50
TEMPERATURE (K)
HORIZONTAL VELOCITY (MPS)

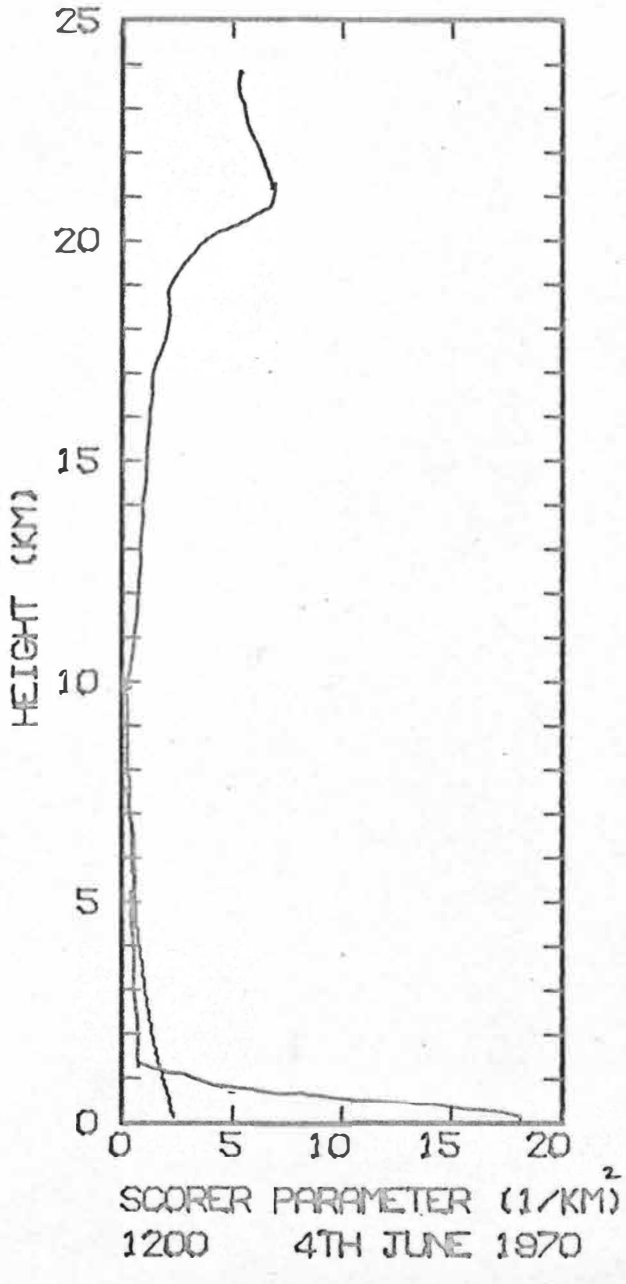
HEIGHT (KM)
25
20
15
10
5
0
0 5 10 15 20
SCORER PARAMETER (1/KM)²
1200 4TH JUNE 1970

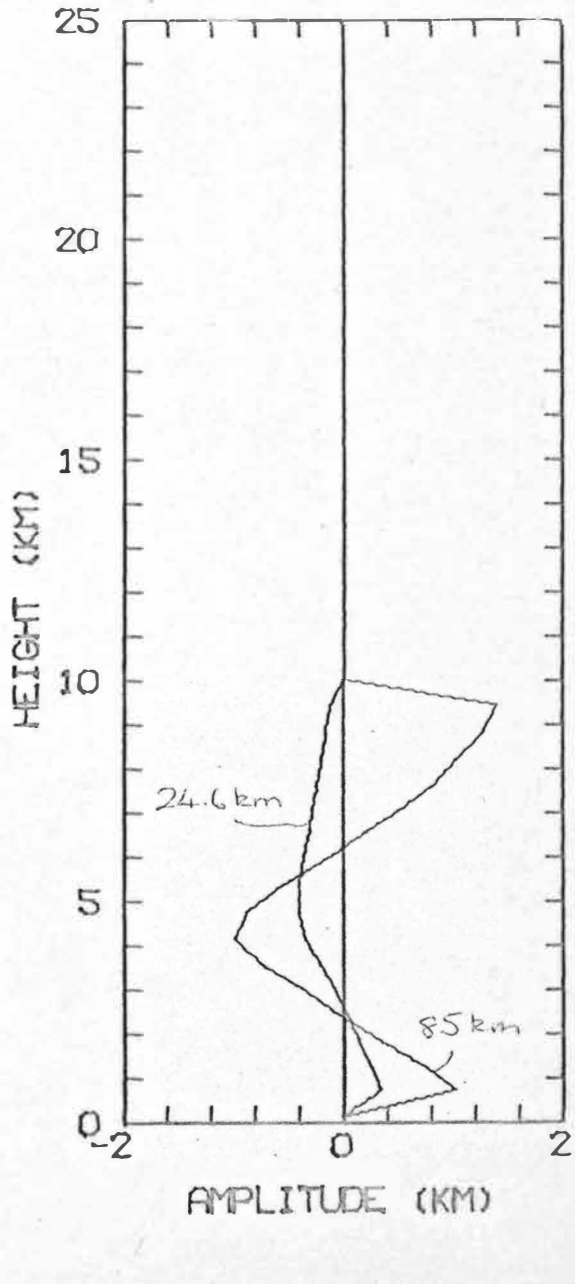
HEIGHT (KM)
25
20
15
10
5
0
-2 0 2
AMPLITUDE (KM)
24.6 km
8.5 km

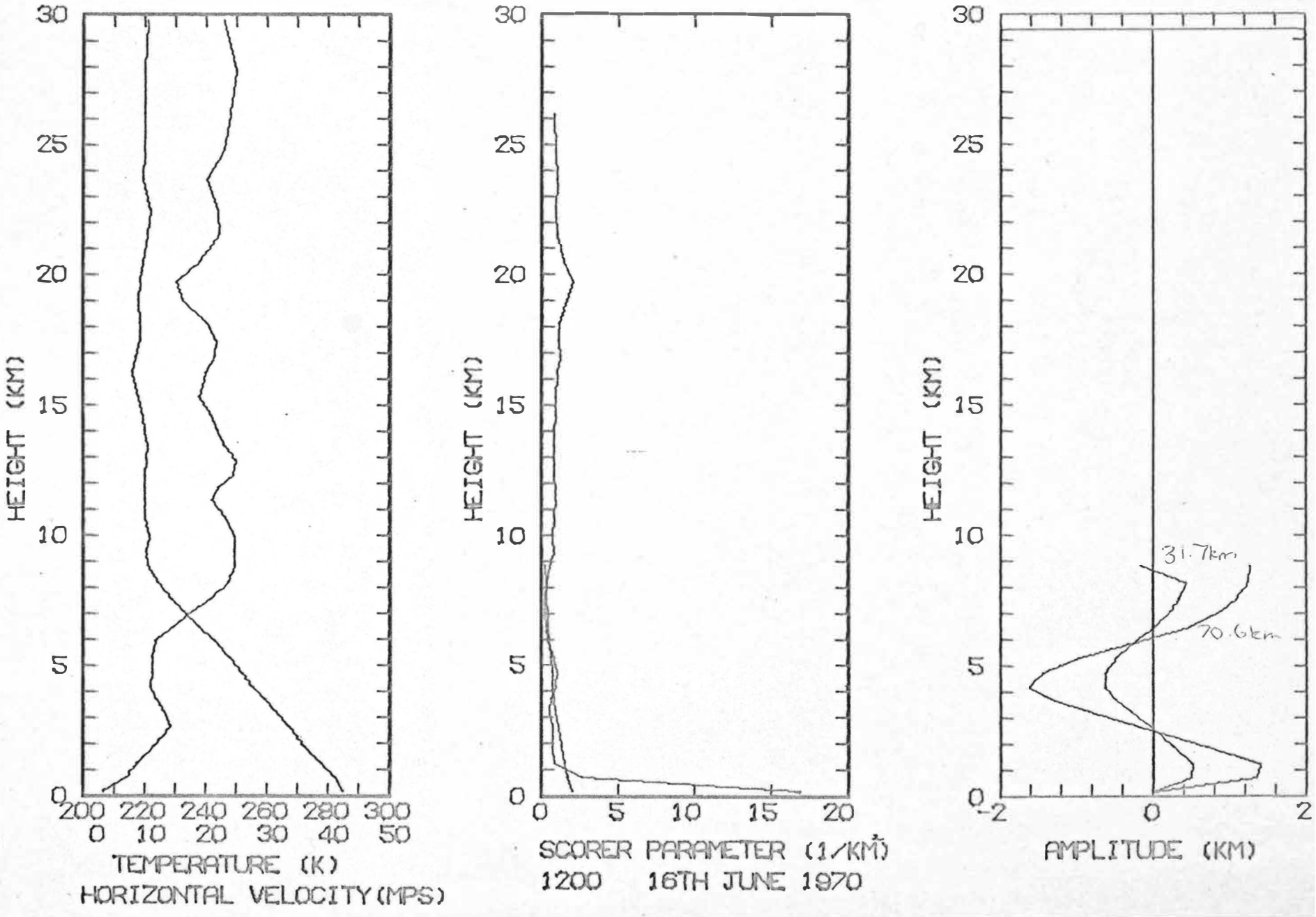
HEIGHT (KM)
30
25
20
15
10
5
0
200 220 240 260 280 300
0 10 20 30 40 50
TEMPERATURE (K)
HORIZONTAL VELOCITY (MPS)
HEIGHT (KM)
0 5 10 15 20
SCORER PARAMETER (1/KM²)
1200 16TH JUNE 1970
HEIGHT (KM)
-2 0 2
AMPLITUDE (KM)
31.7km
70.6km

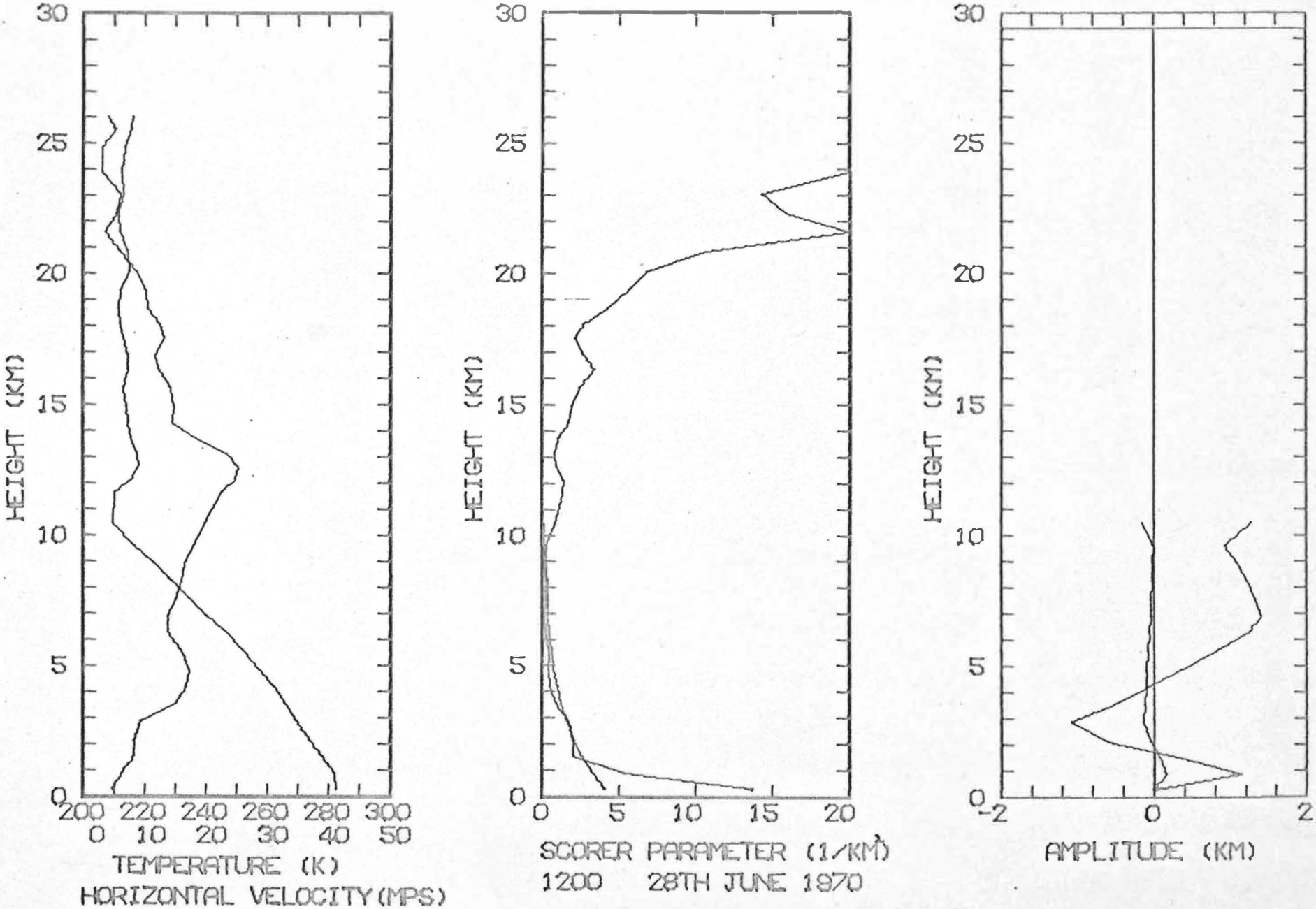
HEIGHT (KM)
30
25
20
15
10
5
0
200 220 240 260 280 300
0 10 20 30 40 50
TEMPERATURE (K)
HORIZONTAL VELOCITY (MPS)
HEIGHT (KM)
0 5 10 15 20
SCORER PARAMETER (1/KM)
1200 28TH JUNE 1970
HEIGHT (KM)
-2 0 2
AMPLITUDE (KM)

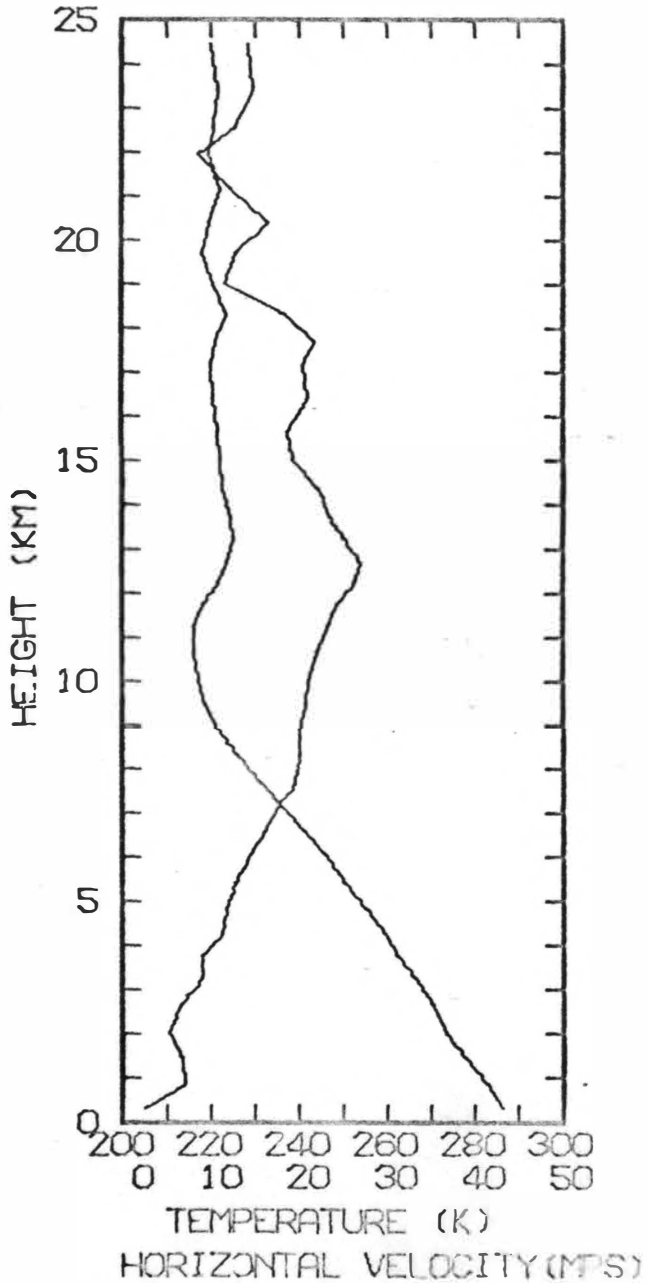
HEIGHT (KM)
25
20
15
10
5
0
200 220 240 260 280 300
0 10 20 30 40 50
TEMPERATURE (K)
HORIZONTAL VELOCITY (MPS)

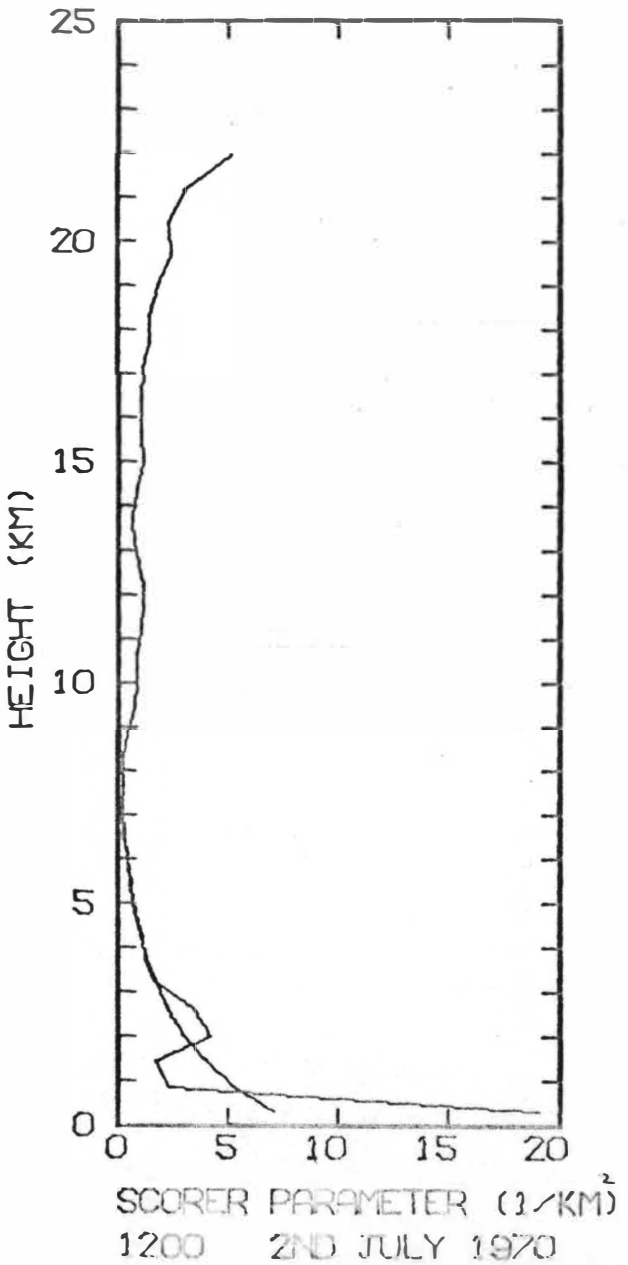
HEIGHT (KM)
25
20
15
10
5
0
0 5 10 15 20
SCORER PARAMETER (1/KM²)
1200 2ND JULY 1970

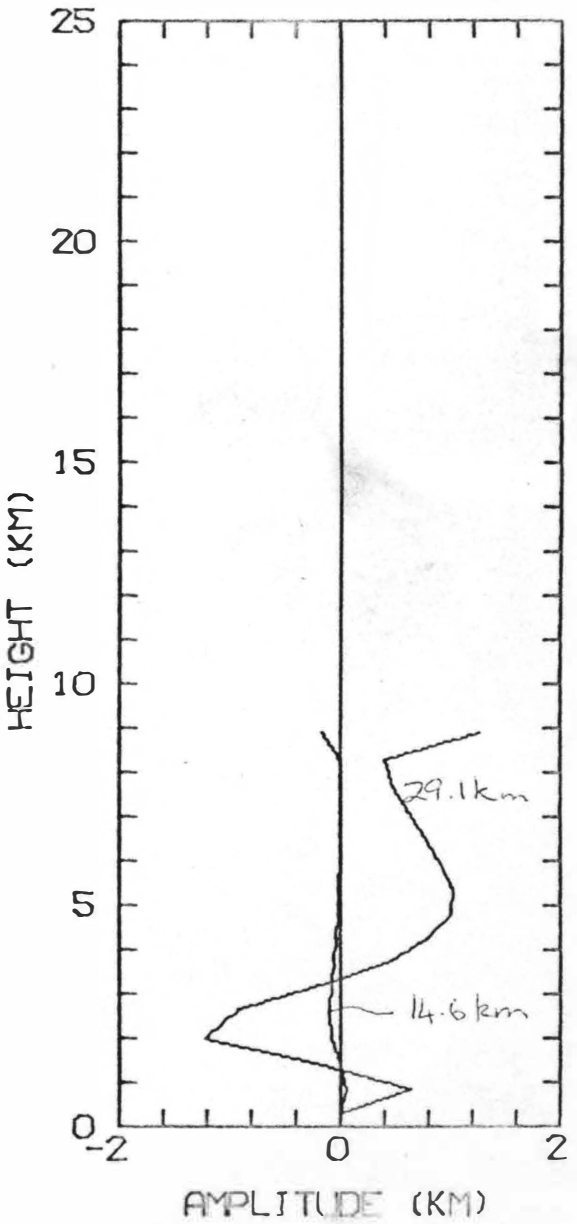
HEIGHT (KM)
25
20
15
10
5
0
-2 0 2
AMPLITUDE (KM)
29.1km
14.6km

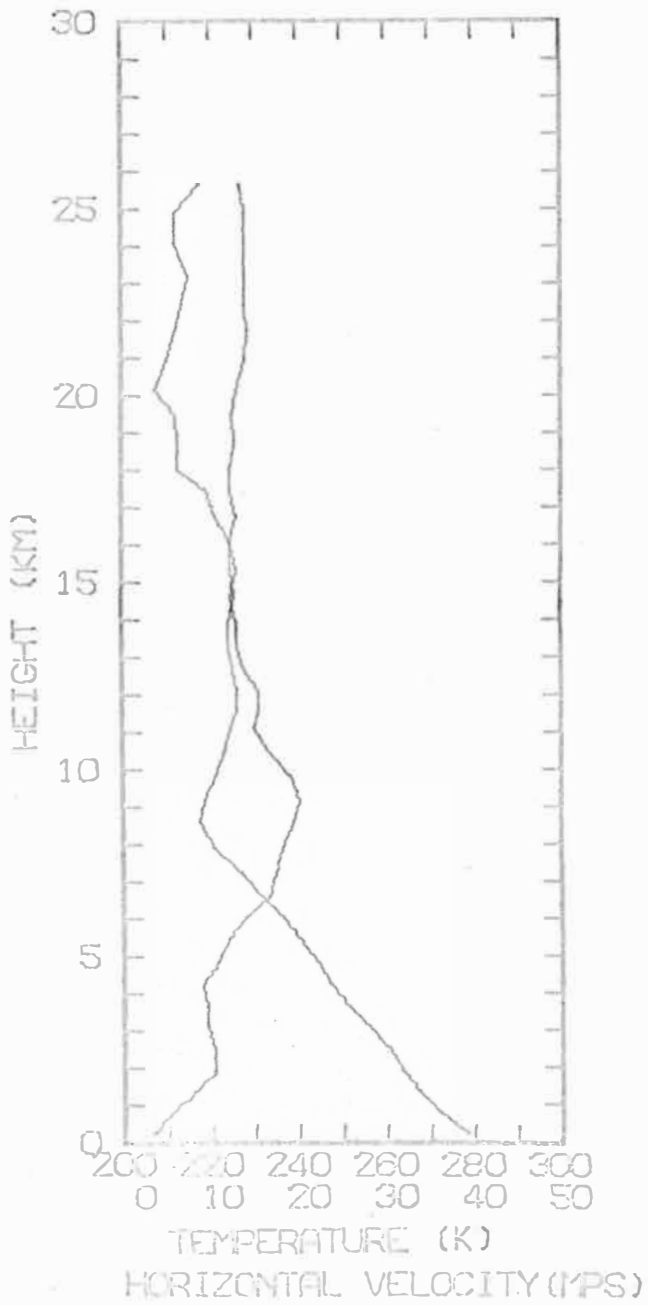
HEIGHT (KM)
30
25
20
15
10
5
0
200 220 240 260 280 300
0 10 20 30 40 50
TEMPERATURE (K)
HORIZONTAL VELOCITY(MPS)

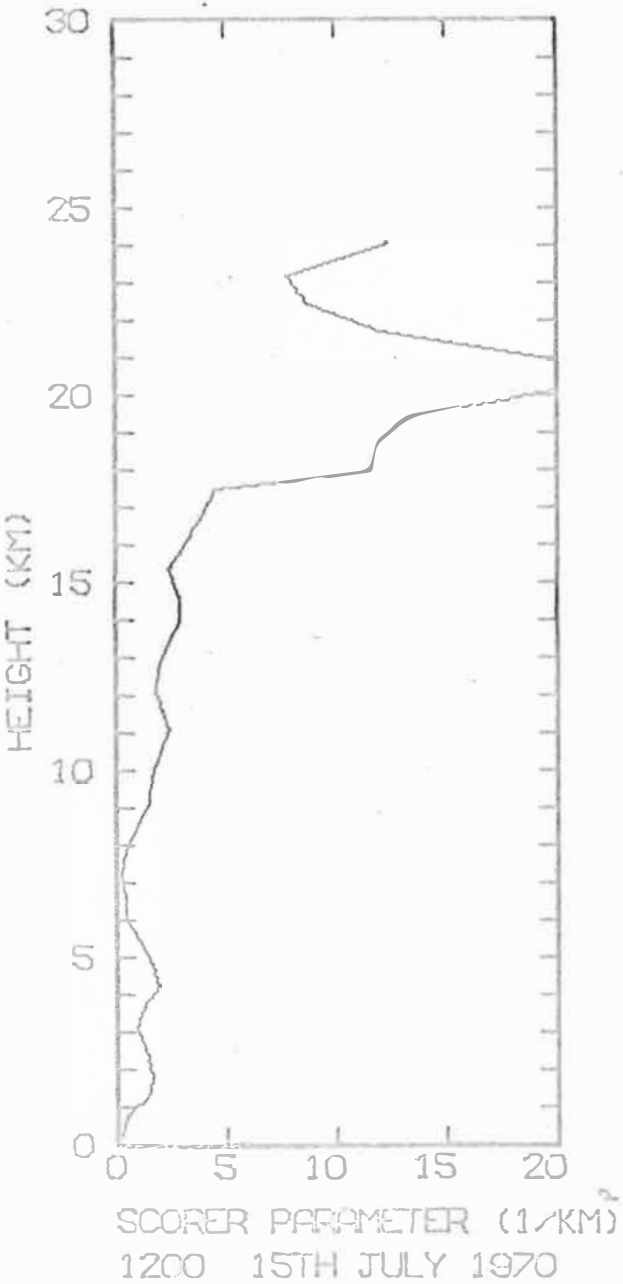
HEIGHT (KM)
30
25
20
15
10
5
0
0 5 10 15 20
SCORER PARAMETER (1/KM)²
1200 15TH JULY 1970

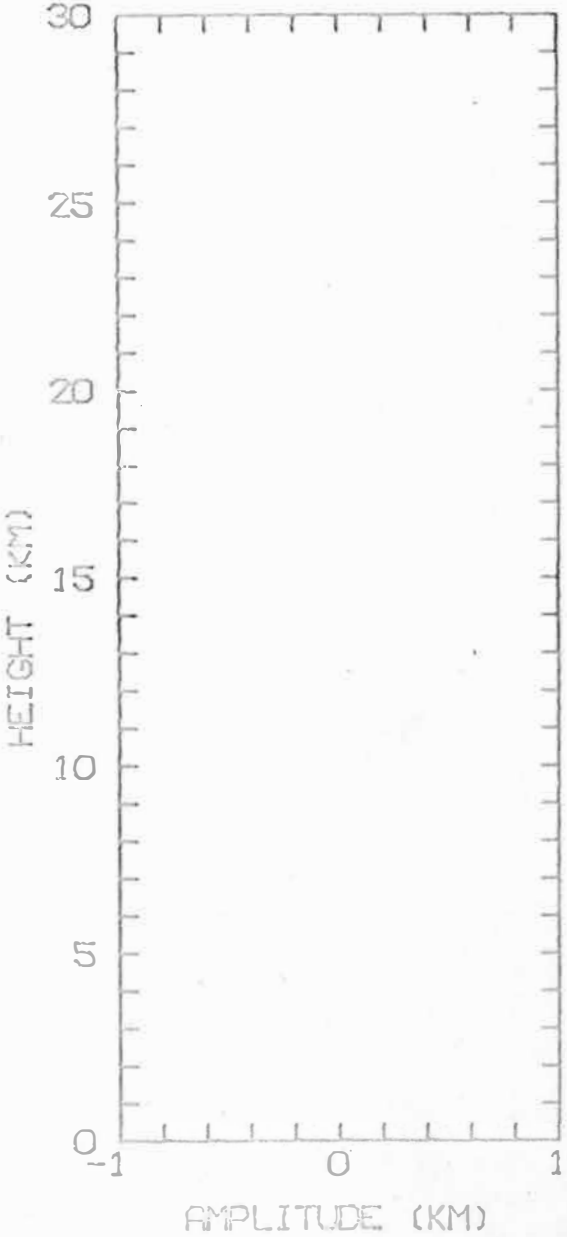
HEIGHT (KM)
30
25
20
15
10
5
0
-1 0 1
AMPLITUDE (KM)

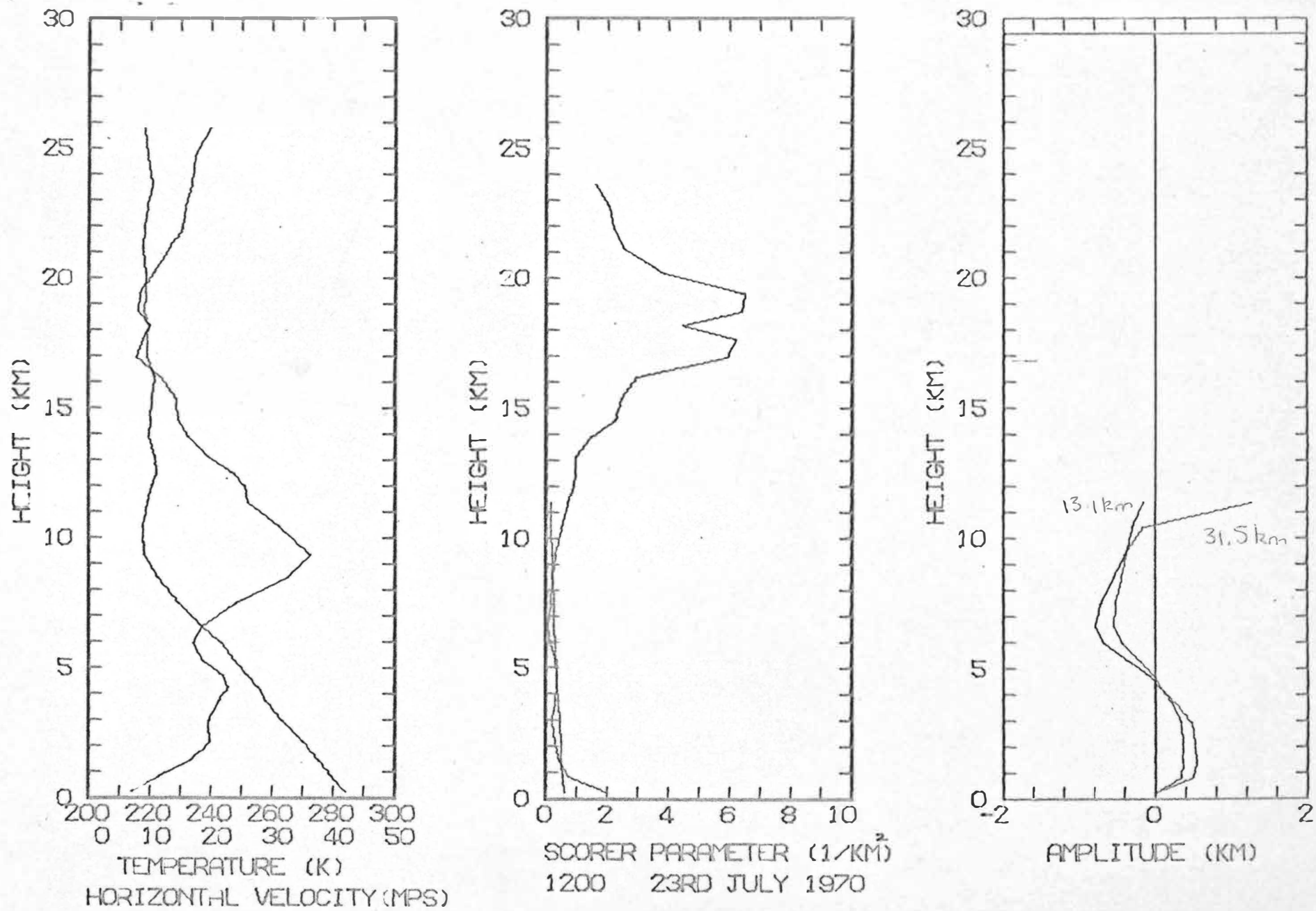
HEIGHT (KM)
30
25
20
15
10
5
0
200 220 240 260 280 300
0 10 20 30 40 50
TEMPERATURE (K)
HORIZONTAL VELOCITY (MPS)
0 2 4 6 8 10
SCORER PARAMETER (1/KM²)
1200 23RD JULY 1970
-2 0 2
AMPLITUDE (KM)
13.1km
31.5km

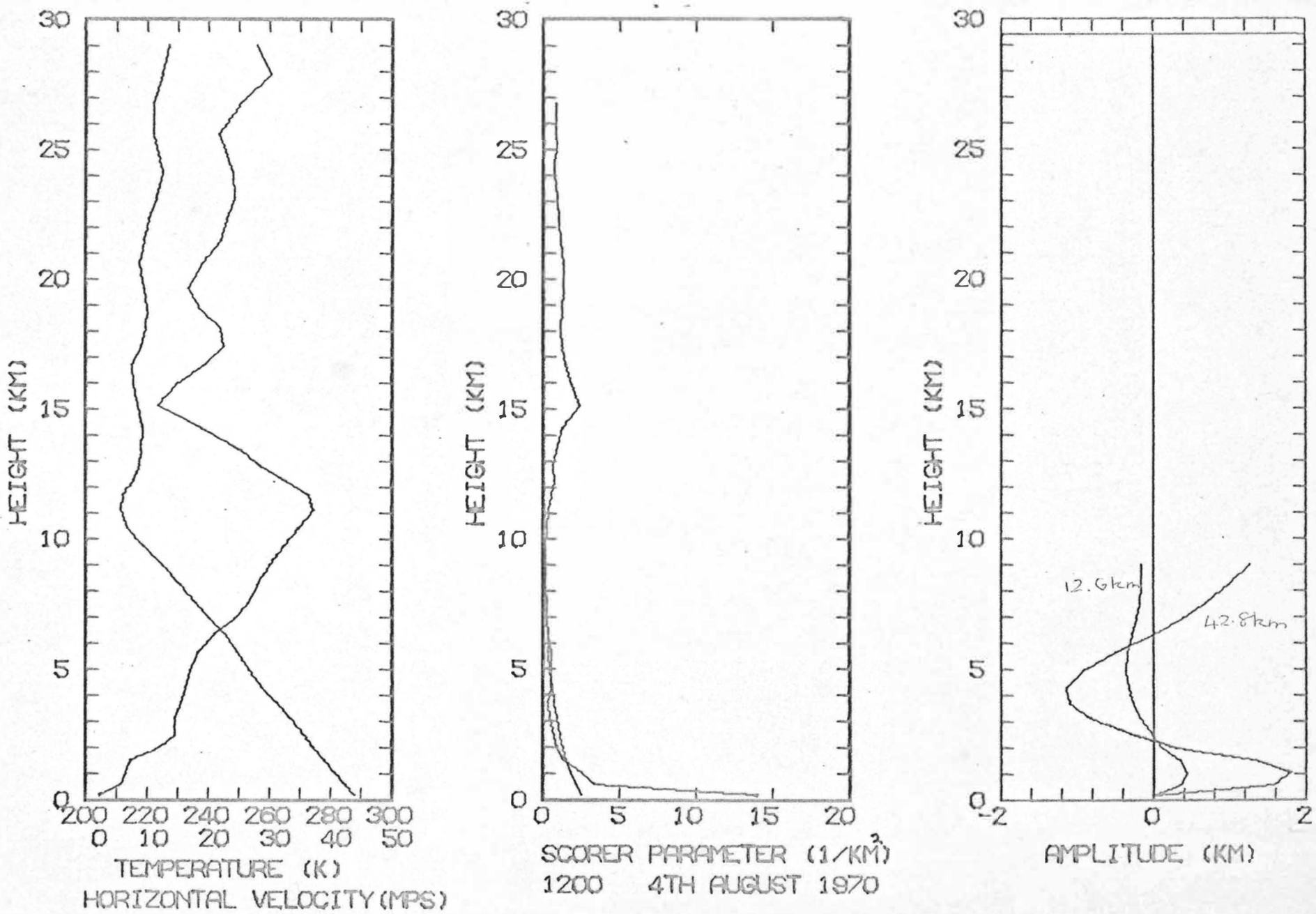
HEIGHT (KM)
30
25
20
15
10
5
0
200 220 240 260 280 300
0 10 20 30 40 50
TEMPERATURE (K)
HORIZONTAL VELOCITY (MPS)
0 5 10 15 20
SCORER PARAMETER (1/KM²)
1200 4TH AUGUST 1970
-2 0 2
AMPLITUDE (KM)
12.6km
42.8km

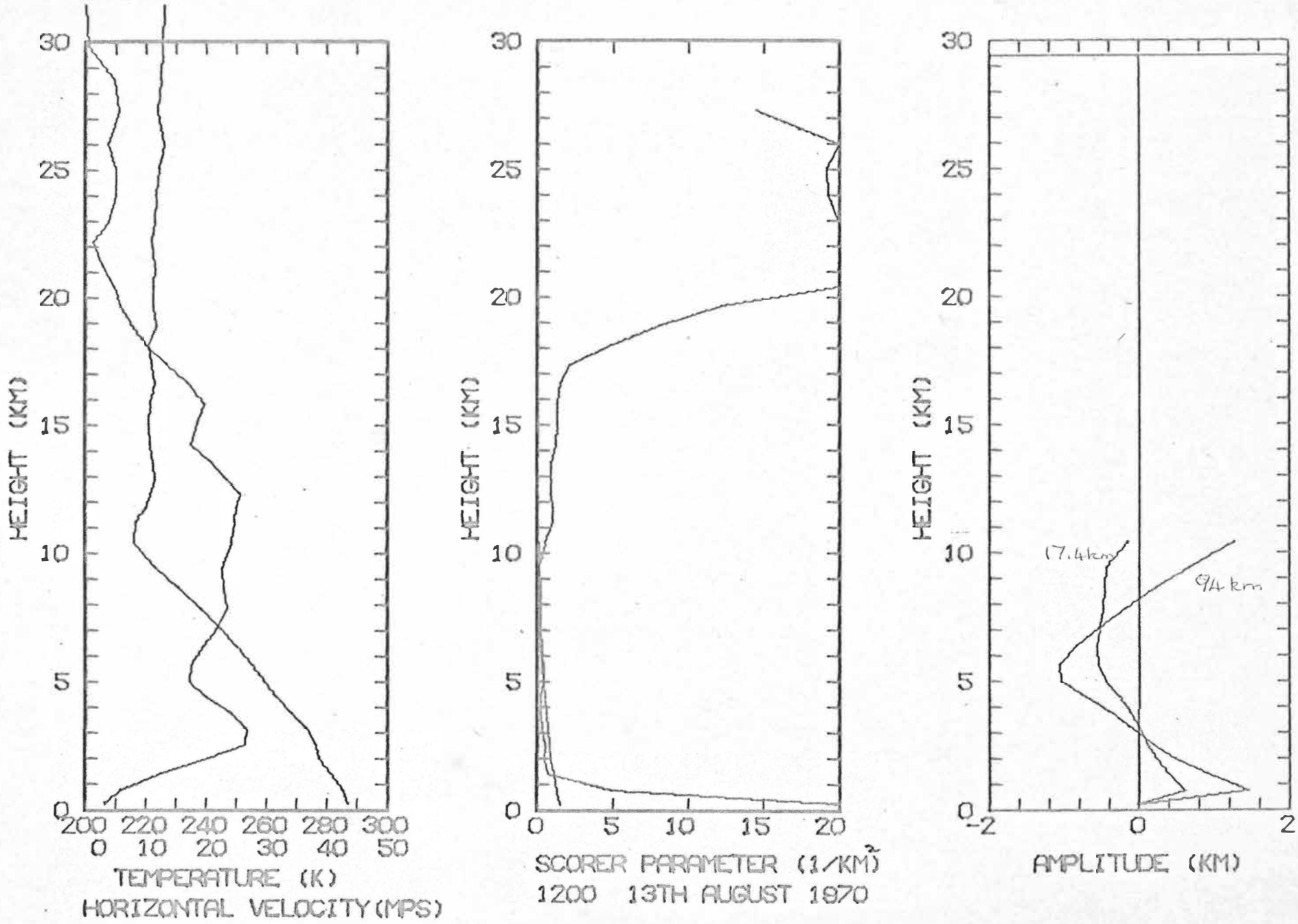
HEIGHT (KM)
30
25
20
15
10
5
0
200 220 240 260 280 300
0 10 20 30 40 50
TEMPERATURE (K)
HORIZONTAL VELOCITY (MPS)
0 5 10 15 20
SCORER PARAMETER (1/KM²)
1200 13TH AUGUST 1970
-2 0 2
AMPLITUDE (KM)
17.4km
9.4km

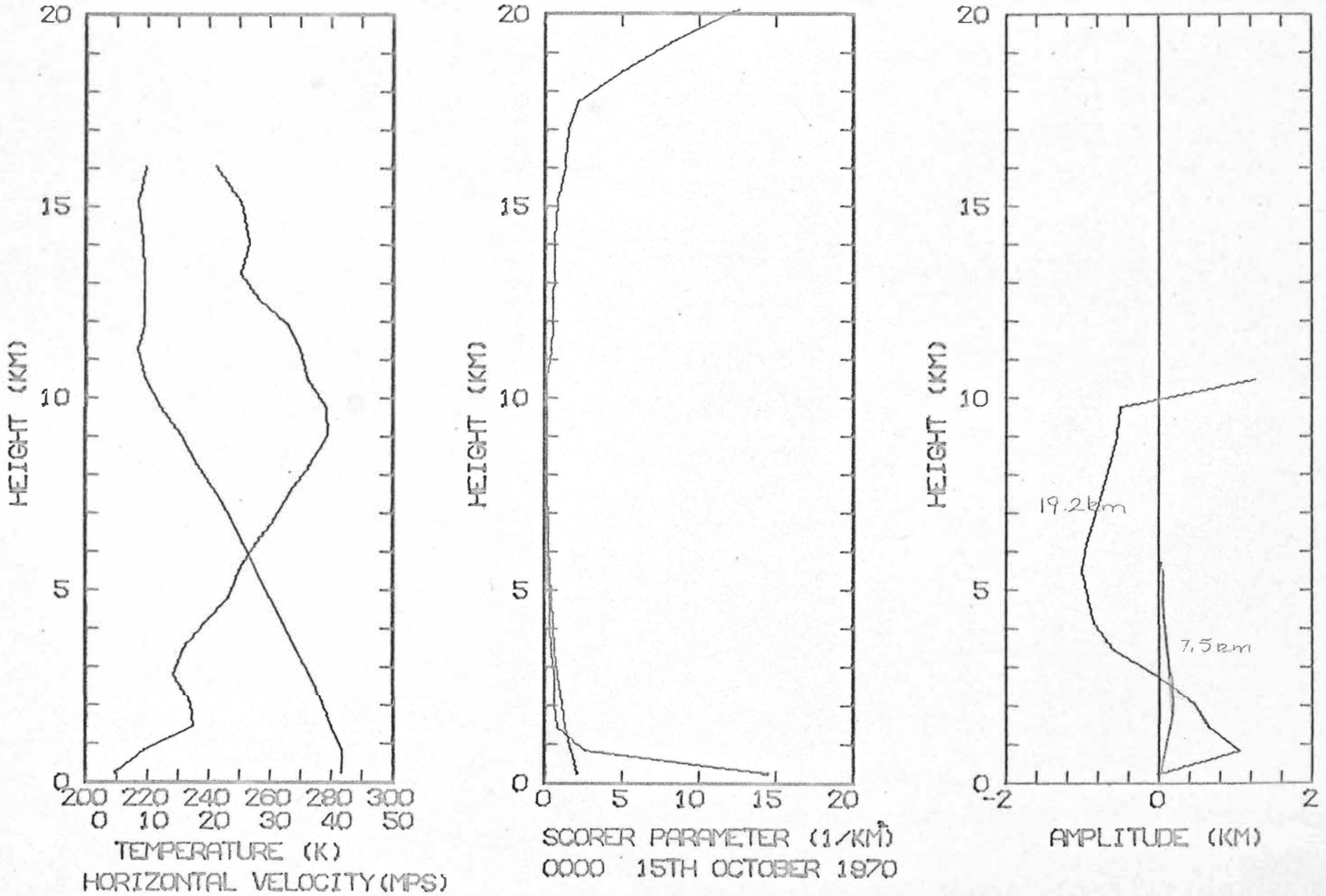
20
15
10
5
0
HEIGHT (KM)
200 220 240 260 280 300
0 10 20 30 40 50
TEMPERATURE (K)
HORIZONTAL VELOCITY (MPS)
0 5 10 15 20
SCORER PARAMETER (1/KM)
0000 15TH OCTOBER 1970
-2 0 2
AMPLITUDE (KM)
19.2km
7.5km

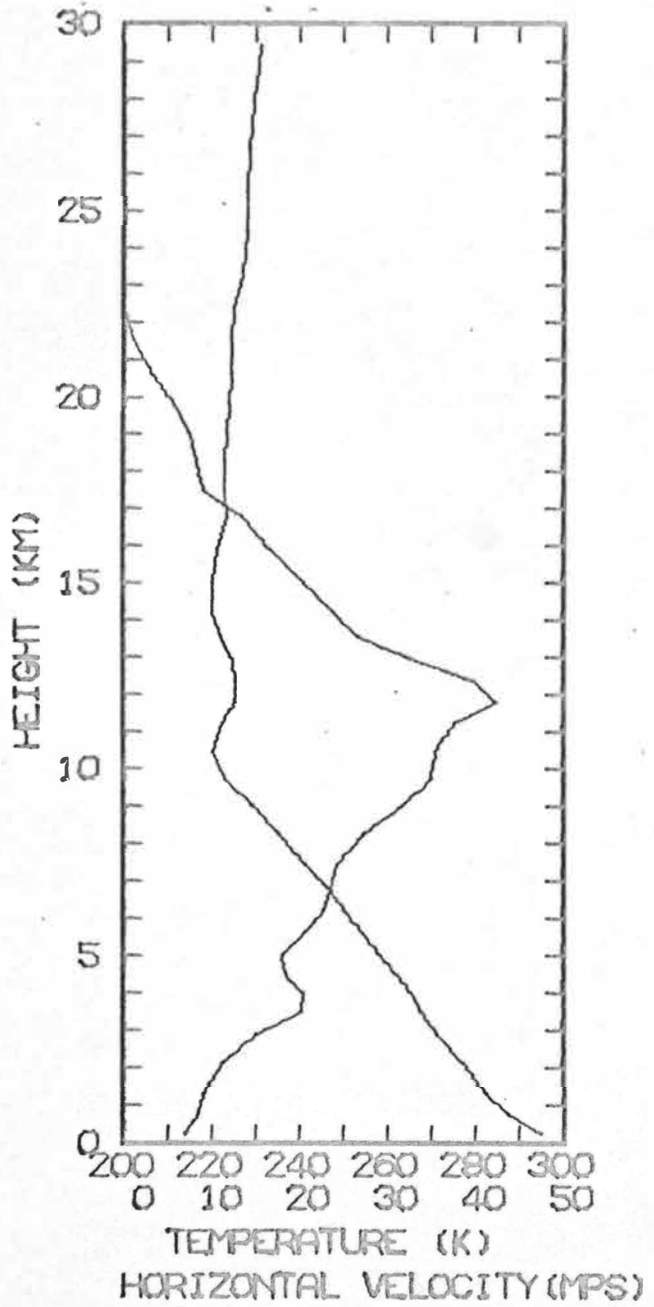
HEIGHT (KM)
30
25
20
15
10
5
0
200 220 240 260 280 300
0 10 20 30 40 50
TEMPERATURE (K)
HORIZONTAL VELOCITY (MPS)

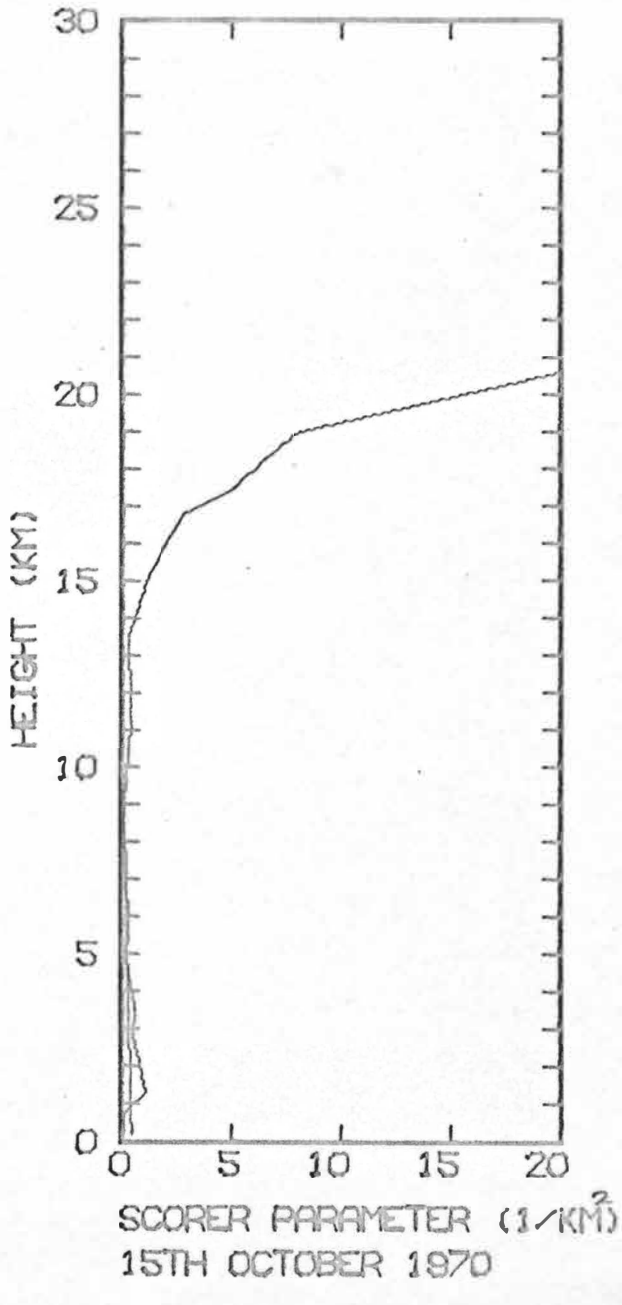
HEIGHT (KM)
30
25
20
15
10
5
0
0 5 10 15 20
SCORER PARAMETER (1/KM²)
15TH OCTOBER 1970

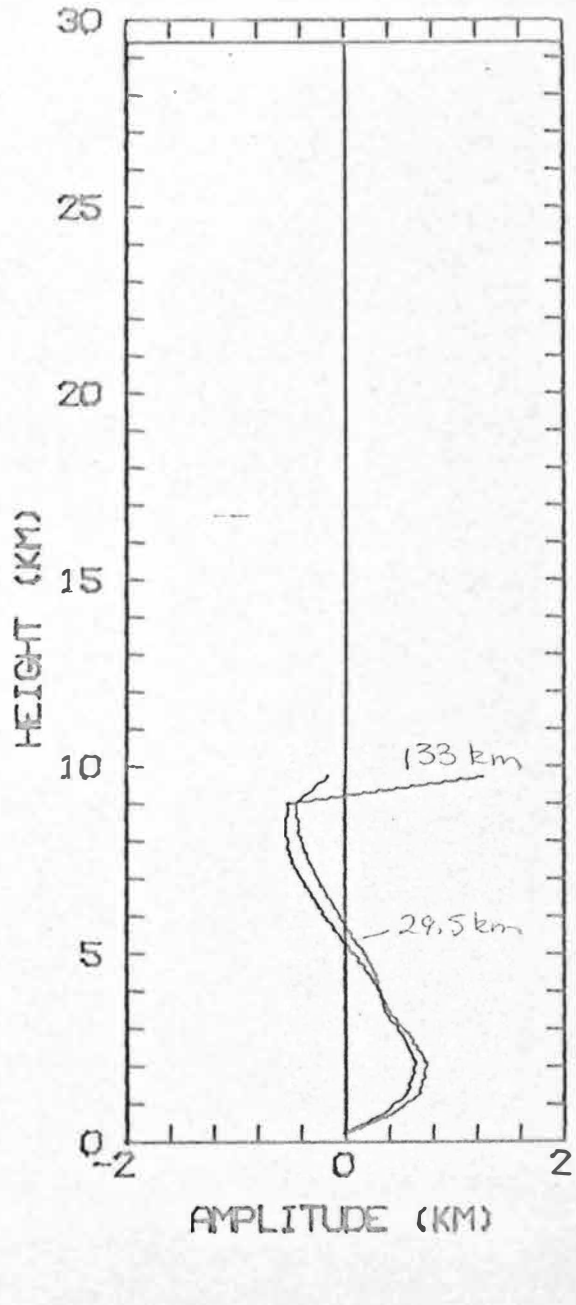
HEIGHT (KM)
30
25
20
15
10
5
0
-2 0 2
AMPLITUDE (KM)
13.3 km
9.5 km

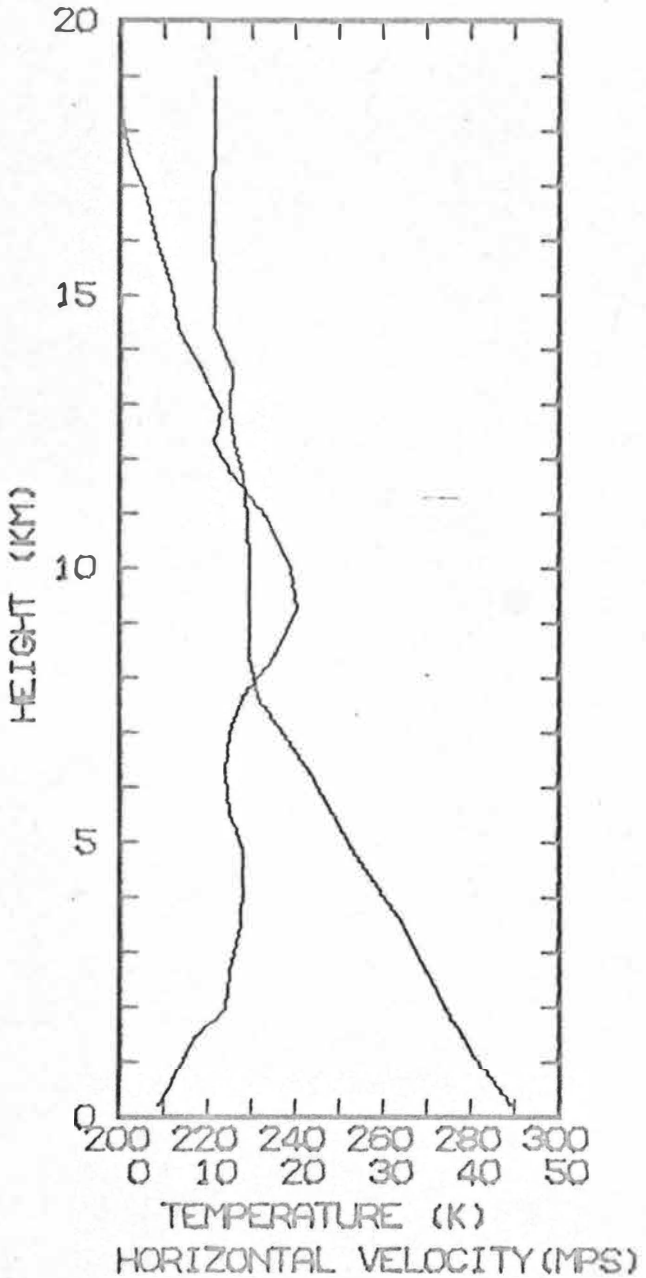
20
15
10
5
0
HEIGHT (KM)
200 220 240 260 280 300
0 10 20 30 40 50
TEMPERATURE (K)
HORIZONTAL VELOCITY (MPS)

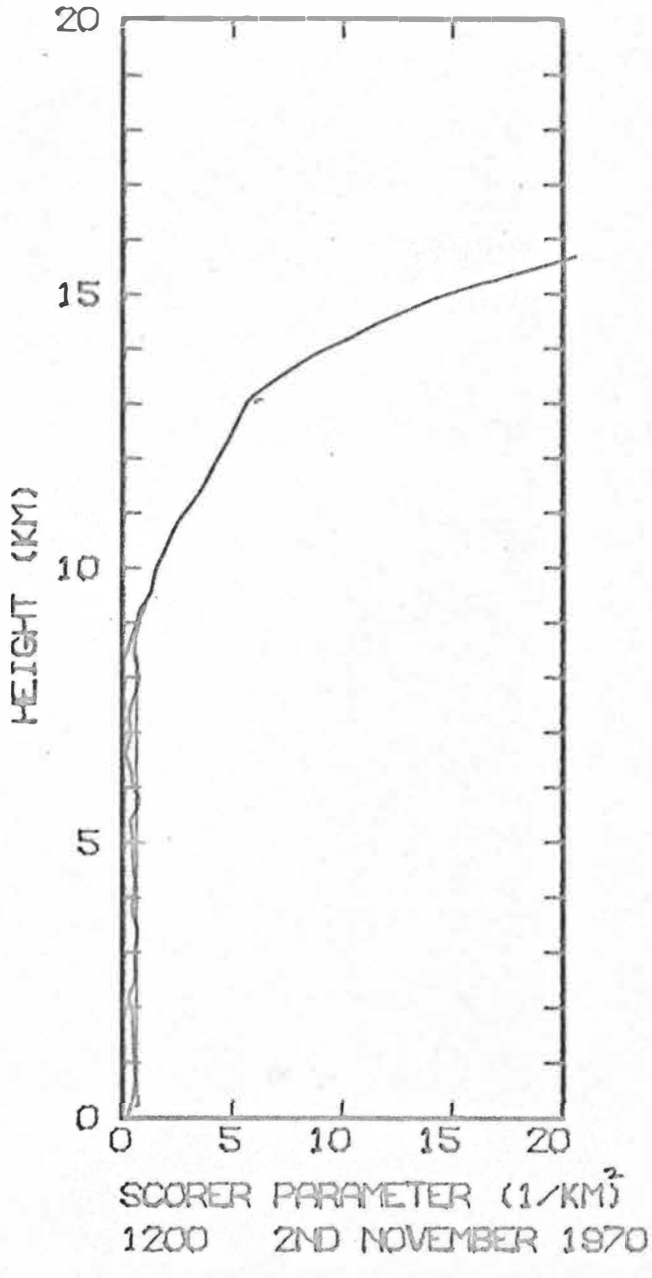
20
15
10
5
0
HEIGHT (KM)
0 5 10 15 20
SCORER PARAMETER (1/KM)²
1200 2ND NOVEMBER 1970

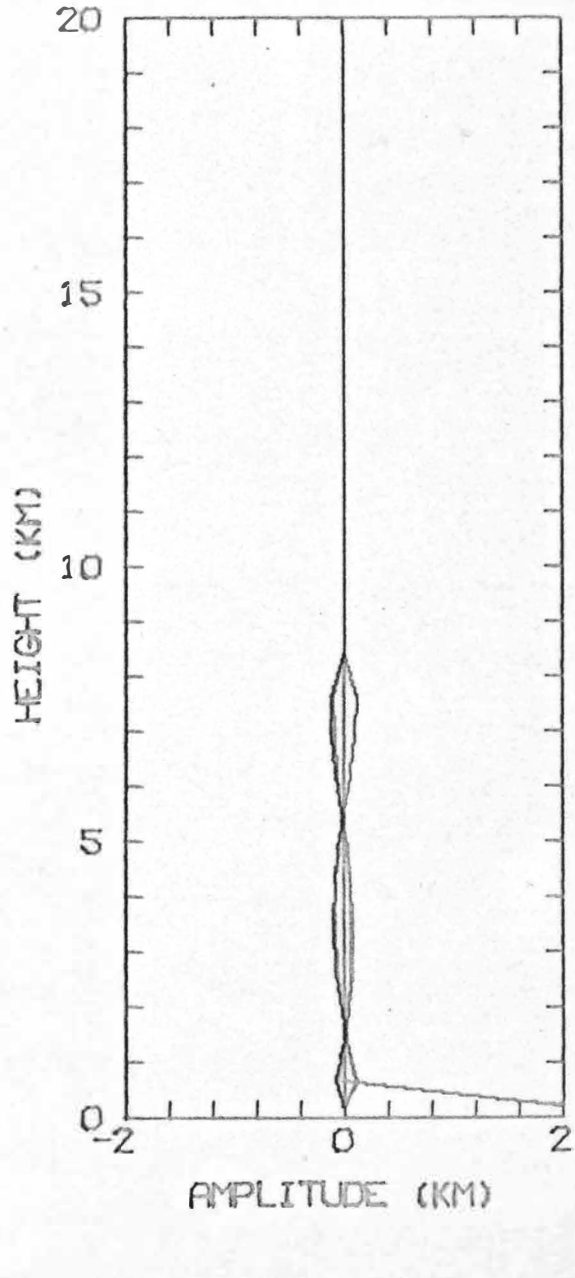
20
15
10
5
0
HEIGHT (KM)
-2 0 2
AMPLITUDE (KM)

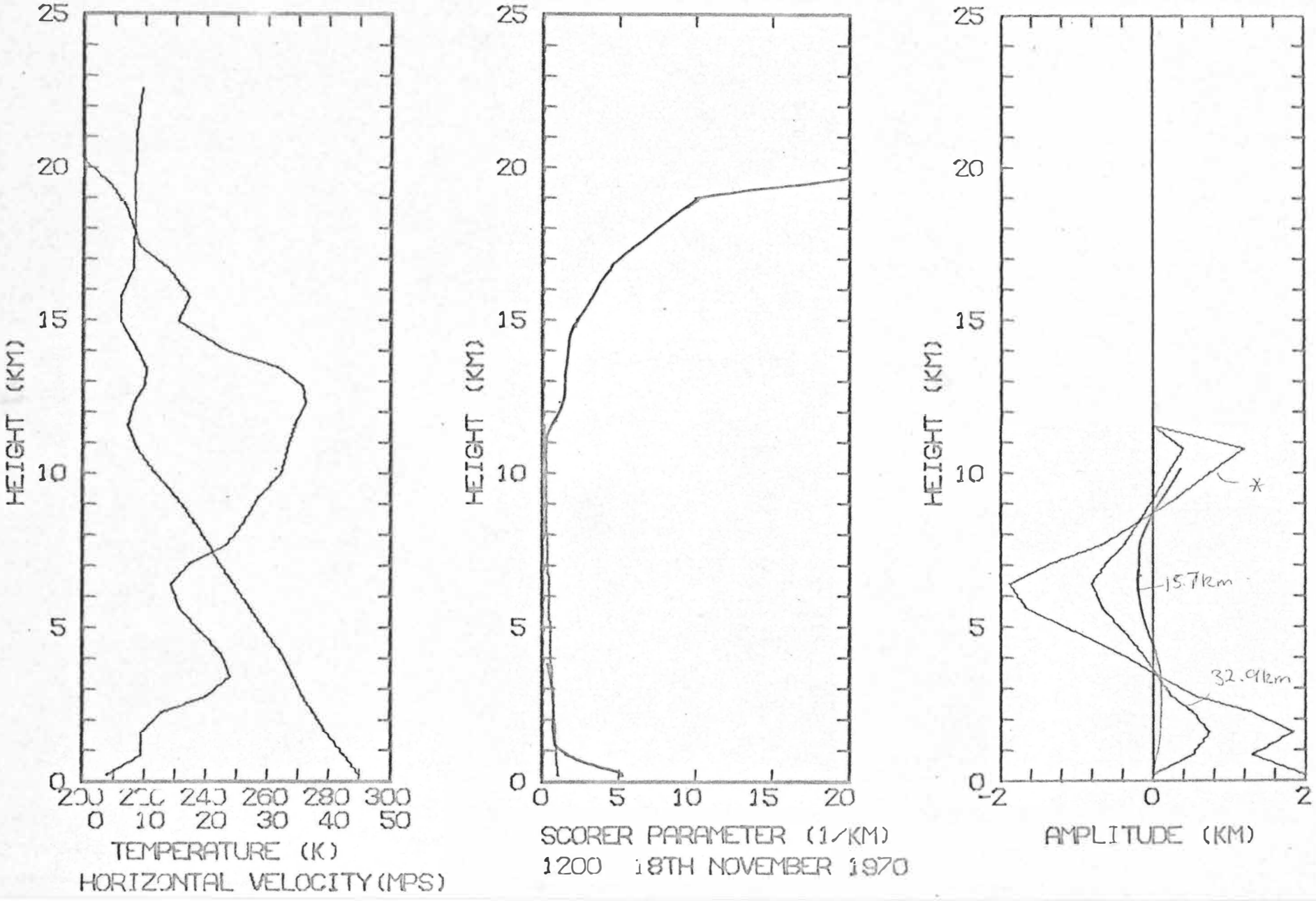
HEIGHT (KM)
25
20
15
10
5
0
200 220 240 260 280 300
0 10 20 30 40 50
TEMPERATURE (K)
HORIZONTAL VELOCITY (MPS)
0 5 10 15 20
SCORER PARAMETER (1/KM)
1200 18TH NOVEMBER 1970
-2 0 2
AMPLITUDE (KM)
15.7km
32.9km

REFERENCES

Alaka et al., 1960: W.M.O. Tech. Note 18, Aviation aspects of Mountain Waves.

Alexander, H., 1967: AFCRL-67-0075, Special Report No. 57 Proceedings, 4th AFCRL Scientific Balloon Symposium III.

Angell, J.K. and Pack, D.H., 1961: Mon. Wea. Rev., USWB, 89, p.273.

————————, 1962: J. Atm. Sci. 19, 87-98. Analysis of low level constant volume balloon (tetroon) flights.

Berkshire, F.H., 1969: NCAR-TN-43. Internal Gravity and Acoustic Waves - A colloquium. p.1, Mountain waves in the stratosphere.

Blackman, R.B. and Tukey, J.W., 1958: "The measurement of Power Spectra". Publ. Dover.

Booker, D.R., 1965: An unpublished Ph.D. thesis, Penn. State Univ., Dept Physics and Meteorology.

————————, Cooper, L.W., 1965: J. Appl. Met. 4, No.1, Feb. 1965,p.122. Superpressure Balloons for Weather Research.

————————, Cooper,L.W., Hart,H.E. and Cook,R.A., 1968: Improvements in Superpressure Balloon Transponder Systems for Meteorological Applications. Rept No. WR801. March 1968, Wea. Sci. Inc.

Cherry, N.J., 1969: Unpublished Departmental Report. Univ. of Canterbury, August 1969. Superpressure balloons

as tracers of Vertical Perturbations in Airflows.

Colquhoun, J.R., 1967: Austr. Met. Mag. 14, pp 158-171. Analysis of two occurrences of lee waves.

Corby, G.A., 1954: Quart. J. Roy. Met. Soc., 80, pp 491-521. The airflow over mountains. A review of the current state of knowledge.

Corby, G.A., 1957: Quart. J. Roy. Met. Soc. 83, pp 49-60. Preliminary study of atmospheric waves using radiosonde data.

Corby, G.A. and Sawyer, J.S., 1958: Quart. J. Roy. Met. Soc. 84, pp 25-37. The airflow over a ridge:- the effects of the upper boundary and high level conditions.

Crapper, G.D., 1959: J. Fluid Mech., 6, 51-76. A three dimensional solution for waves in the lee of mountains.

Danielson, E.F. and Bleck, R., 1970: J. Atm. Sci. 27, 5, 758-772. Tropospheric and stratospheric ducting of stationary mountain waves.

Doos, B.O., 1961: Tellus 13, 3, 305-319. A mountain wave theory including the effects of the vertical variation of the wind and stability.

Doos, B.O., 1962: Tellus 14, 3, 301-309. A theoretical analysis of lee waves observed by Tiros 1.

Förchtgott, J., 1949: Bull. Met. Czech, Prague, 3, p.49. Wave streaming in the lee of mountain ridges.

Fritz, S., 1965: J. Appl. Met., 4, 1, 31-37. Significance of mountain lee waves as seen from satellite pictures.

Georgii, W., 1969: Royal Aircraft Establishment LT. No.1334. Kinematics of lee wave flow.

Gerbier, N. and Berenger, M., 1960: Quart. J. Roy. Met. Soc. 86, 13-21. Experimental Studies of Lee Waves.

Harrison, H.T., 1965: NASA Contr. Rept. 315. The Mountain Wave. 56 pp.

Holmboe, J. and Klieforth, H., 1957: Final Rept. Contract No. AF 19(604) - 728. Investigations of mountain lee waves and the airflow over the Sierra Nevada.

Kelvin, Lord, 1886: Phil. Mag. 5 (22) 353-357, 445-452, 517-530. On stationary waves on the surface of running water.

Krishnamurti, T.N., 1964: Rev. of Geophys. 2, 4, 593-624. Theory of Two-dimensional Mountain Waves.

Lally, V.E., 1967: NCAR-TN-28. June 1967. Superpressure balloons for horizontal soundings of the atmosphere.

Lin, J.T. and Apelt, C.J., 1970: Project THEMIS. Tech. Rept. No. 7. College of Engineering, Colo. State Univ., Fort Collins, Colo.

Lyra, G., 1940: Beitr. Phys. frei Atmos 26, 197-206. Ueber den Einflus von Bodenerhebungen auf die Strömung einer Stabil geschichteten Atmosphäre.

Lyra, G., 1943: Z. angew. Math. Mech., 23, 1-28. Theorie der stationären Leewellenströmung in freier Atmosphäre.

Miles, J.W., 1968: Proc. 12th Intern. Congr. of Appl. Mech. Stanford Univ. August 1968. Wave and Wave Drag in Stratified Flows.

Pekelis, E.M., 1969: J. of Atmos. and Oceans 5, 1-7. A numerical method for calculating lee waves.

Pao, Y.H., 1969: Sc. Res. Lab. D1-82-0859. Spectra of internal waves and turbulence in stratified fluids. I.

———— and Hall, J.M., 1969: Sc. Res. Lab. D1-82-0860. Spectra of internal waves and turbulence in stratified fluids. II.

Queney, P., 1947: Misc. Rept 23. The univ. of Chicago Press. Theory of perturbations in stratified currents with application to airflow over mountain barriers.

———— et al., 1960: W.M.O. Tech. Note 34. The airflow over mountains.

Rayleigh, Lord, 1883: Proc. Lond. Math. Soc., 15, 69-78. The form of standing waves on the surface of running water.

Roper, R.D., 1952: Quart. J. Roy. Met. Soc., 75, p.415. Evening waves.

Scorer, R.S., 1949: Quart. J. Roy. Met. Soc., 57, 41-59. Theory of waves in the lee of mountains.

————————, 1951: Quart. J. Roy. Met. Soc. 79, 76-84. On the stability of stably stratified shearing layers.

————————, 1953: Quart. J. Roy. Met. Soc. 79, 70-83. Theory of airflow over mountains. II - The flow over a ridge.

————————, 1954: Quart. J. Roy. Met. Soc. 80, 417-428. Theory of airflow over mountains. III - Airstream characteristics.

————————, 1955: Quart. J. Roy. Met. Soc. 81, 340-350. Theory of airflow over mountains. IV - Separation of the flow from the surface.

————————, 1956: Quart. J. Roy. Met. Soc. 82, 75-81. Airflow over an isolated hill.

———————— and Wilkinson, M., 1956: Quart. J. Roy. Met. Soc. 82, 419-427. Waves in the lee of an isolated hill.

———————— and Kleiforth, H., 1959: Quart. J. Roy. Met. Soc. 85, 131-143. Theory of mountain waves of large amplitudes.

————————, 1969: NCAR-TN-43. Internal Gravity and Acoustic Waves - a colloquium p. 259. Present state of theory of large amplitude oscillations in stratified fluids.

Streeter, V.L., 1962: "Fluid Mechanics", published by McGraw-Hill.

Vergeiner, I. and Lilly, D.K., 1970: Mon. Wea. Rev. 98, 3, 219-232. The dynamic structure of lee wave flow as obtained from balloon and airplane observations.

Wallington, C.E., and Portnall, J., 1958: Quart. J. Roy. Met. Soc., 84, 38-45. A numerical study of the wavelength and amplitude of lee waves.

————————, 1970: Met. Mag. 99, 1175, 157-165. A computing aid to studies of airflow over mountains.

Wooldridge, G. and Lester, P.F., 1969: Dept Atm. Sci., Colo. State Univ. paper no. 138. Detailed observations of mountain lee waves and a comparison with theory.

Yih, C.S., 1965: "Dynamics of Nonhomogeneous Fluids" Published by MacMillan Co.